TUM School of Computation, Information and Technology
Technische Universität München

Early-Warning Signs for Bifurcation- and Noise-induced Tipping in Stochastic Partial Differential Equations

Applications to Climate Science and Degenerate Noise

Paolo Bernuzzi

Vollständiger Abdruck der von der TUM School of Computation, Information and Technology der Technischen Universität München zur Erlangung des akademischen Grades eines

Doktors der Naturwissenschaften (Dr. rer. nat.)

genehmigten Dissertation.

Vorsitz:
Prof. Dr. Johannes Zimmer

Prüfer der Dissertation:
1. Prof. Dr. Christian Kühn
2. Prof. Dr. Peter Ashwin
3. Prof. Dr. Niklas Boers

Die Dissertation wurde am 19.09.2025 bei der Technischen Universität München eingereicht und durch die TUM School of Computation, Information and Technology am 22.01.2026 angenommen.

To the friends that have cheered for me from Rome.
To the friends that have been by my side in Munich.
To the friends that have sheltered me when needed.

Acknowledgements

Acknowledgements:

I open this thesis expressing my gratitude to my supervisor, Christian Kuehn, for the support and invaluable guidance provided throughout my PhD career. He has been available for discussions, suggestions, and inputs from its beginning. Furthermore, I want to thank my co-supervisors, Freddy Bouchet and Henk A Dijkstra. Regardless of their busy schedule, they have always found time to guide me and discuss research directions. For equivalent reasons, I thank Tobias Grafke. Throughout these years, I had the luck to also have as collaborators Andreas Morr and Antonia Düx. Their precious support and teamwork have enabled the publication of this thesis. I am also grateful for the discussion with a large list of colleagues, among whom Alexandra Neamtu-Blessing, Reyk Börner, Ryan Deeley, Gianmarco Del Sarto, Maximilian Engel, Felix Hummel, Valérian Jacques-Dumas, Iacopo Longo, Kerstin Lux-Gottschalk, Raphael Römer and Sacha Sinet. I appreciate the support of my MSc supervisor, Paolo Buttà, for writing the reference letter that enabled my application to the project.

I am thankful to Christian Kuehn for making it possible for me to attend numerous conferences throughout Europe and America. I also want to thank Tobias Grafke for inviting me to collaborate multiple times at the University of Warwick. I thank Franco Flandoli for sponsoring my visit to Pisa for "Turbulence on the Banks of the Arno" and Alexandra Neamtu-Blessing for inviting me to participate in the minisymposium "Dynamics of Stochastic Partial Differential Equations" at SIAM DS, in May 2025.

I am deeply grateful to the M8 group at TUM for providing an excellent working environment. This has also been expressed in their support in the proofreading of this thesis by many of them. Namely, Tobias Böhle, Gideon Chiusole, Sara-Viola Kuntz, Giacomo Landi, Lucia Layritz, Jan Mölter, Chiara Piazzola, Elena Queirolo, and Jan-Eric Sulzbach. For similar reasons, I thank the groups whom I had the pleasure of visiting during my secondments: the Laboratoire de Physique ENS de Lyon and the Institute for Marine and Atmospheric Research Utrecht (IMAU).

Lastly, I am grateful to TUM and Marie Skłodowska-Curie Actions, which funded my PhD project and enabled me to carry out my projects and visit numerous institutions. Consequently, I also thank my ITN, CriticalEarth, for guiding me into the field of climate science.

Further recognitions:

Zuerst möchte ich meinem Supervisor Christian Kuehn danken. Danke für alles, Christian. Mit deiner Hilfe konnte ich der Mathematiker werden, der ich heute bin. Du bist nicht nur ein ausgezeichneter Supervisor, Forscher und Professor, sondern auch eine wundervolle Person. Ich werde dir immer dankbar sein dafür, dass du an mich geglaubt hast und für diese Jahre in München. Mein Dank gilt auch der M8 Gruppe. Ihr seid großartige Kolleginnen und Kollegen, und ich bin sehr dankbar für unsere gemeinsame Zeit. Besonders danken möchte ich Elena Queirolo, Kerstin Lux-Gottschalk, Pia Steinmeyer und Sara-Viola Kuntz, ohne den wäre diese Arbeit nicht möglich gewesen. Darüber hinaus danke ich anderen Kollegen, die die Geduld hatten, mir Deutsch zuzuhören. Um nur einige zu nennen Andreas Morr, Lucia Layritz, Oliver Mehling und Raphael Römer. Endlich, will ich meinen Studenten danken. Insbesondere denen, die bei mir ihre Thesis geschrieben haben. Allen Genannten wünsche ich das Beste.

My thanks also go to my co-supervisors, Freddy Bouchet and Henk A Dijkstra. With their patient instructions and collaborations, I have extended my research scope. I express my appreciation also to Tobias Grafke for our wonderful collaboration and for warmly welcoming me to Warwick. I am grateful to Paolo Buttà, my MSc supervisor, for supporting me at the start of the project.
I give special thanks to the whole CriticalEarth community, in particular Sacha Sinet and Valérian Jacques-Dumas, with whom I have shared secondments. I can't express how grateful I am for these years together. I wish you the best in your careers and lives, hoping to see you often. Luckily, I have many friends from Munich to thank for lightening the project with their support. Among them are Mohamad Omidi, Benedetta Casavecchia, Oskar Markkula, Deblina Sanyal, and Priyajit Ghosh. I warmly thank my family in Munich: Elena Queirolo, Ruben Boumans, Giacomo Queirolo and Paul Boumans. You have made me feel at home when I knew nobody.

Quiero agradecer a mi familia en Mexico por incluirme en todo no obstante la distancia. Están siempre en mi corazón. Entre todos quiero agradecer a mi primo Alejandro Dib Parada sobretodo por hospedarme en el momento de necesidad. Quiero agradecer también a la familia Mayer, en particular para ayudarme en mis primeros dias en Munich.

Un grande ringraziamento va ai miei genitori. Grazie per non esservi opposti alla mia scelta di fare questa esperienza. Grazie anche per essere sempre al mio fianco. Siete genitori e persone eccezionali. Un grandissimo ringraziamento va al mio coinquilino Kevin Mato. Sei una persona fantastica e dai mille talenti. Non dubitare mai di te stesso. Un enorme ringraziamento va a Simone Chiominto. Sei un amico prezioso e lo hai dimostrato ripetutamente in questi anni. Sono molto grato anche a Valeria Mascolo per aver riempito con la sua compagnia le mie giornate a Lyon. Un altro ringraziamento va ai miei italiani a Monaco: Matteo Sadun, Francesco Camilloni e Giada Colella. Abbiamo passato dei bellisimi momenti e spero continueremo a farlo. Ringrazio anche i miei amici di Roma, la mia grew. Siete una delle cose più preziose della mia vita. Voglio ringraziare infine la mia famiglia in Italia, in particolare mio cugino Lorenzo per avermi visitato piú di chiunque altro in questi anni.

Abstract

The study of tipping points in climate systems, such as within models of the Atlantic Meridional Overturning Circulation (AMOC), has become fundamental to our understanding of abrupt climate change. Tipping points indicate critical thresholds beyond which small perturbations can lead to large, often irreversible changes in systems. In the context of the AMOC, which plays a crucial role in global heat and salinity redistribution, surpassing such a threshold could drastically alter climate patterns across the globe. Due to the potential severity of these transitions, considerable research effort has been invested in constructing early-warning signals that might indicate an approaching tipping event. Methods such as critical slowing down, variance and autocorrelation analysis, and statistical indicators derived from data have been proposed. However, the inherent complexity and high-dimensionality of climate models, along with external noise influence, pose major challenges to the reliability and timeliness of these early warnings. Consequently, improving the theoretical and numerical tools to predict tipping events is the primary goal of this thesis.

A crucial conceptual setting to understand tipping phenomena is the study of fast-slow systems and critical transitions theory. In such an ansatz, the system displays a sudden qualitative change when a slow variable, or critical parameter, crosses a critical threshold. In this deterministic setting, tipping is often associated with bifurcations and labelled as B-tipping. Standard examples are saddle-node bifurcations, where a stable fixed point disappears as a parameter changes, resulting in a rapid transition to a distant attractor. B-tipping has been widely explored in simplified climate models, such as the Stommel-Cessi model. Nevertheless, real-world climate systems are subject to continuous fluctuations from internal variability and external forcings, which complicate the bifurcation picture. We rely on such a phenomenon to construct statistical observables that predict abrupt transitions. As an example, we extend classical early-warning signs for stochastic ordinary differential equations to models that include a spatial component. Consequently, we focus on the assumptions of space-heterogeneity and missing data. We define a hierarchy of early-warning signs and effects that perturb their observations.

Klaus Hasselmann's conjecture introduced the notion of stochastic climate modelling, emphasising the role of noise as a perturbation and, consequently, an input for critical transitions. This has led to the identification of N-tipping, or noise-induced tipping, wherein a system transitions from one metastable state to another due to rare, large fluctuations. In contrast with B-tipping, which depends on slow changes in system parameters, N-tipping can occur even when the system is far from a bifurcation point. This paradigm shift compels a change in how to anticipate climate transitions, especially under non-white stochastic forcing. The challenge lies in quantifying the probability and timescale of such noise-induced events. In this work, we employ large deviation theory, stochastic path integrals, and related probabilistic tools to compute corresponding estimates for coupled stochastic partial differential equations. Consequently, we address the complexity of practical application due to the high-dimensional nature and non-trivial structure of the noise of realistic climate models.

In order to gain insight into the stages that define a critical transition, contemporary research relies on numerical techniques to compute instantons, the most probable transition paths to display such an event under the setting of Freidlin-Wentzell theory. Computing them in realistic models often involves solving a constrained optimisation problem in path space, for which several numerical schemes have been developed, including the minimum action method, string method, and adaptive multilevel splitting. Such approaches allow for the estimation of escape rates, identification of dominant transition mechanisms, and even targeted early-warning signals that go beyond traditional linear stability analysis. In this thesis, we extend the discussed techniques to partial differential equations perturbed by degenerate noise. Such an assumption is relevant in numerous applications, as discussed in the work.

Overall, this thesis bridges deterministic and stochastic tipping mechanisms by developing early-warning signals for spatially extended models. By combining operator theory and stochastic analysis with advanced numerical methods, our work contributes both to the fundamental understanding of critical transitions and to the practical tools needed to anticipate them in high-dimensional noisy systems. In conclusion, these results offer new techniques for detecting and characterising tipping points in climate science, with implications for risk assessment and further applications.

Titel in deutscher Sprache: Frühwarnzeichen für durch Bifurkation und Rauschen induziertes Kippen in stochastischen partiellen Differentialgleichungen

Untertitel: Anwendungen in der Klimawissenschaft und auf degeneriertes Rauschen

Zusammenfassung

Die Untersuchung von Kipppunkten in Klimasystemen, beispielsweise in Modellen der Atlantischen Meridionalen Umwälzströmung (AMOC), ist für unser Verständnis des abrupten Klimawandels von grundlegender Bedeutung geworden. Kipppunkte bezeichnen kritische Schwellenwerte, bei deren Überschreitung bereits geringe Störungen zu großen, oft irreversiblen Veränderungen des Systemzustands führen können. Im Zusammenhang mit der AMOC, die eine entscheidende Rolle bei der globalen Umverteilung von Wärme und Salzgehalt spielt, könnte das Überschreiten eines solchen Schwellenwerts die Klimamuster weltweit drastisch verändern. Aufgrund der potenziellen Schwere dieser Übergänge wurden erhebliche Forschungsanstrengungen unternommen, um Frühwarnsignale zu entwickeln, die auf ein bevorstehendes Kippereignis hinweisen könnten. Es wurden Methoden wie kritische Verlangsamung, Varianz- und Autokorrelationsanalyse sowie aus Daten abgeleitete statistische Indikatoren vorgeschlagen. Die inhärente Komplexität und hohe Dimensionalität von Klimamodellen sowie der Einfluss externer Störgeräusche stellen jedoch große Herausforderungen für die Zuverlässigkeit und Rechtzeitigkeit dieser Frühwarnungen dar. Daher ist die Verbesserung der theoretischen und numerischen Methoden zur Vorhersage von Kippereignissen das Hauptziel dieser Arbeit.

Ein entscheidender konzeptioneller Ansatz zum Verständnis von Kippphänomenen ist die Untersuchung von Schnell-Langsam-Systemen und die Theorie kritischer Übergänge. In einem solchen Ansatz zeigt das System eine plötzliche qualitative Veränderung, wenn eine langsame Variable oder ein entscheidender Parameter einen kritischen Schwellenwert überschreitet. In diesem deterministischen Ansatz wird das Kippen oft mit Verzweigungen in Verbindung gebracht und als B-Kippen bezeichnet. Typische Beispiele sind Sattelpunkte Verzweigungen, bei denen ein stabiler Fixpunkt unter Änderung eines Parameters verschwindet, was zu einem schnellen Übergang zu einem entfernten Attraktor führt. B-Kipppunkte wurden in vereinfachten Klimamodellen wie dem Stommel-Cessi-Modell umfassend untersucht. Dennoch unterliegen reale Klimasysteme kontinuierlichen Schwankungen aufgrund interner Variabilität und externer Einflüsse, was das Bild der Verzweigung verkompliziert. Wir stützen uns auf ein solches Phänomen, um statistische Beobachtungsgrößen zu konstruieren, die abrupte Übergänge vorhersagen. Als Beispiel erweitern wir klassische Frühwarnzeichen für stochastische gewöhnlichen Differentialgleichungen auf Modelle, die eine räumliche Komponente enthalten. Anschließend konzentrieren wir uns auf die Annahmen der räumlichen Heterogenität und fehlender Daten. Wir definieren eine Hierarchie von Frühwarnzeichen und Effekten, die ihre Beobachtungen stören.

Klaus Hasselmanns Vermutung führte den Begriff der stochastischen Klimamodellierung ein und betonte die Rolle von Rauschen als Störung und damit als Auslöser für kritische Übergänge. Dies führte zur Identifizierung des N-Kippen-Effekts oder rauschinduzierten Kippens, bei dem ein System aufgrund seltener, großer Schwankungen von einem metastabilen Zustand in einen anderen übergeht. Im Gegensatz zum B-Kippen, das von langsamen Änderungen der Systemparameter abhängt, kann N-Kippen auch dann auftreten, wenn das System weit von einem Verzweigungspunkt entfernt ist. Dieser Paradigmenwechsel erfordert eine Änderung der Art und Weise, wie Klimawandelprognosen erstellt werden, insbesondere unter nicht-weißem stochastischem Rauschen. Die Herausforderung besteht darin, die Wahrscheinlichkeit und den Zeitrahmen solcher rauschinduzierter Ereignisse zu quantifizieren. In dieser Arbeit verwenden wir die Theorie der großen Abweichungen, stochastische Pfadintegrale und verwandte probabilistische Werkzeuge, um entsprechende Schätzungen für gekoppelte stochastische partielle Differentialgleichungen zu berechnen. Damit gehen wir auf die Komplexität der praktischen Anwendung ein, die sich aus der hochdimensionalen Natur und der nichttrivialen Struktur des Rauschens realistischer Klimamodelle ergibt. Um Einblicke in die Phasen zu gewinnen, die einen kritischen Übergang definieren, stützt sich die aktuelle Forschung auf numerische Techniken zur Berechnung von Instantonen, den wahrscheinlichsten Übergangspfaden, um ein solches Ereignis im Rahmen der Freidlin-Wentzell-Theorie darzustellen. Ihre Berechnung in realistischen Modellen erfordert oft die Lösung eines beschränktes Optimierungsproblems

im Pfadraum, für das mehrere numerische Schemata entwickelt wurden, darunter die Methode der minimalen Wirkung, die String-Methode und die adaptive mehrstufige Aufteilung. Diese Ansätze ermöglichen die Schätzung von Fluchtraten, die Identifizierung dominanter Übergangsmechanismen und sogar gezielte Frühwarnsignale, die über die traditionelle lineare Stabilitätsanalyse hinausgehen. In dieser Arbeit erweitern wir die diskutierten Techniken auf partielle Differentialgleichungen, die durch degeneriertes Rauschen gestört sind. Eine solche Annahme ist in zahlreichen Anwendungen relevant, wie in der Arbeit diskutiert wird.

Insgesamt schlägt diese Arbeit eine Brücke zwischen deterministischen und stochastischen Kippmechanismen, indem sie Frühwarnsignale für räumlich ausgedehnte Modelle entwickelt. Durch die Kombination von Operatorentheorie und stochastischer Analysis mit fortgeschrittenen numerischen Methoden trägt unsere Arbeit sowohl zum grundlegenden Verständnis kritischer Übergänge als auch zu den praktischen Werkzeugen bei, die erforderlich sind, um diese in hochdimensionalen, verrauschten Systemen zu antizipieren. Zusammenfassend bieten diese Ergebnisse neue Techniken zur Erkennung und Charakterisierung von Kipppunkten in der Klimawissenschaft, mit Implikationen für die Risikobewertung und weitere Anwendungen.

Contents

1 Introduction

The main objective of this thesis is to define, construct and extend indicators, referred to as observables or early-warning signs, that can anticipate qualitatively important and often sudden changes in applications. The main implementation considered throughout the work is climate science, which is associated with numerous events under this description. We achieve such a task through analytic and numerical methods in the study of mathematical systems. The properties of these models and a justification for our work are described further in this introductory chapter.
We first describe a variety of models in applied fields and then observe examples of multiscale models. As such, we list the most commonly studied bifurcations, which are related to the critical transition addressed throughout the thesis. Subsequently, we introduce stochastic models along with insights on the assumptions of the noise term. Then, we consider the different kinds of tipping and discuss the challenges in their prediction through standard early-warning signs. We finally introduce some of the most well-known models in climate science, such as Stommel-Cessi system and the Coupled Model Intercomparison Project (CMIP) model ensemble. We consider the effects of noise on the systems in view of Hasselmann's paradigm [104]. Lastly, we describe the structure of the thesis and the novelty of our work.

1.1 Deterministic models in applications

The use of mathematical models in applications is often meant to simulate corresponding phenomena. Naturally, in order for a system to be well-suited for such a task, it requires previous knowledge and assumptions from the implementer. The difficulty in choosing the structure of the model and fitting its parameters derives from the observations and understanding of the real inner forcings that define the events. As such, it is strongly related to the complexity of the application and to its observability. Moreover, the simplicity of a model can describe the main features of phenomena and enable an in-depth mathematical analysis, while sacrificing details of their realisation. Adequate simple mathematical models are capable of indicating and characterising the behaviours of the subjects studied. Among such systems are the widely studied Susceptible-Infected-Recovered (SIR) model, in medicine and epidemiology [201], and the Lotka-Volterra model, in biology [149]. These models are examples of coupled ordinary differential equations (ODEs) [131]. These types of equations include a time derivative of their solutions, which defines their evolution in time under given constraints. The solution is then a function to be interpreted as a descriptive and simplified simulation of the original event.

While the observation of a low-dimensional model may appear as an oversimplification of a problem, we need to consider the fact that its solution may not be easy to compute or trivial to describe. A prime example is the Lorenz-84 model [198], which aims to describe atmospheric circulation with four components. This is among the most well-known examples of a system characterised by the chaotic behaviour of its solution. Consequently, the computation of its solution is not only hard, but its numerical simulations are reliable only in relatively short time intervals.
More complex applied mathematical systems are defined by a large number of equations or constraints. Those arise either by the observation of the event along a large number of variables or by the consideration of the same component in different regions in space. These systems are called box models. This generalisation enables the observation of patterns and the pinpointing of variables that play a major role in the realisation of an event.
Models that consider a finer resolution in space and spatial derivatives are composed of partial differential equations (PDEs). These assume space as a continuous variable and observe finer patterns in their

solutions. Furthermore, local perspectives enable the construction of observables in the case of missing data. Standard PDE models can be found in physics, such as the heat equation and the Swift-Hohenberg equation [133]. Among the most renowned PDE models is the Navier-Stokes equations for fluid dynamics [75]. Standard techniques, such as diagonalisation or Koopman operators, enable the study of PDEs equivalently to an infinite-dimensional ODE [81]. Therefore, different approaches for simplified models can be extended to PDEs under sufficient conditions.

To the same degree as the phenomena represented, many systems are characterised by a multiscale behaviour. Specifically, trajectories are composed of distinct phases of fast transitions, opposed to intervals of slow evolution in time. This can result from the unbalanced influence of components on the resulting event or on their intrinsic timescales. As a consequence, multiscale dynamics, such as fast-slow systems, represent correctly different events and are associated with numerous applications. As an example among many, we can consider the Rosenzweig–MacArthur model [175] that explores the interaction between predator and prey in ecology. For a much extensive list of applications, we refer to [131].
The prediction of these changes in the trajectories of the solution of the models is justified by the profound impact that they represent in real-life scenarios. Consequently, the in-depth study of systems associated with such transitions is required.

1.2 Fast-slow systems

Multiscale dynamics are often represented by fast-slow systems. In the case of systems of ODEs, they are indicated as

$$\begin{cases} \frac{\mathrm{d}x}{\mathrm{d}t} &= f(x,q) \\ \frac{\mathrm{d}q}{\mathrm{d}t} &= \varepsilon g(x,q) \end{cases} \tag{1.2.1}$$

for $n \in \mathbb{N}_{>0}$, $m \in \mathbb{N}_{>0}$, $x : \mathbb{R} \to \mathbb{R}^n$, $q : \mathbb{R} \to \mathbb{R}^m$, $f : \mathbb{R}^n \times \mathbb{R}^m \to \mathbb{R}^n$, $g : \mathbb{R}^n \times \mathbb{R}^m \to \mathbb{R}^m$, $t \in \mathbb{R}$ and $0 < \varepsilon \ll 1$. We refer to x as the fast variable and q as the slow variable. Furthermore, t is the fast time, whereas $s = t\varepsilon$ is the slow time. In fact, the system can be equivalently observed, through rescaling, on the slow timescale:

$$\begin{cases} \varepsilon\frac{\mathrm{d}x}{\mathrm{d}s} &= f(x,q) \\ \frac{\mathrm{d}q}{\mathrm{d}s} &= g(x,q). \end{cases}$$

Due to the assumption of small parameter ε, it is natural to study the systems on the singular limit $\varepsilon = 0$. This results in the construction of the fast and slow subsystems. The first is

$$\begin{cases} \frac{\mathrm{d}x}{\mathrm{d}t} &= f(x,q) \\ \frac{\mathrm{d}q}{\mathrm{d}t} &= 0 \end{cases}$$

and is widely studied throughout this thesis. It assumes the slow variable to be constant, thus as a parameter. Consequently, it approximates the dynamics of the fast-slow system during fast transitions. The second is

$$\begin{cases} 0 &= f(x,q) \\ \frac{\mathrm{d}q}{\mathrm{d}s} &= g(x,q). \end{cases}$$

It examines the dynamics of the variable q along the critical set (or critical manifold, if it is a manifold) defined as

$$\{(x,q) \in \mathbb{R}^n \times \mathbb{R}^m \,|\, f(x,q) = 0\}.$$

The slow subsystem approximates the dynamics of the fast-slow system in slow transitions, i.e., when the first differential equation is close to zero and the fast variable is almost stationary.

We fix $0 < \varepsilon \ll 1$ and assume continuity of f and g. Setting $\mathcal{S}_0$, a compact uniformly hyperbolic submanifold of the critical manifold, then Fenichel's Theorem [17, 131, 83] implies the existence of a locally invariant (sub)manifold $\mathcal{S}_\varepsilon$ of Hausdorff distance of order $\mathcal{O}(\varepsilon)$ to $\mathcal{S}_0$ in the limit $\varepsilon \to 0$. This (sub)manifold $\mathcal{S}_\varepsilon$ can be non-unique and is referred to as slow manifold. In this case, local invariance refers to the fact that flows enter and exit the manifold only through its boundary. Smoothness and attractivity of the slow manifold are also obtained in the theorem [131]. Furthermore, Tikhonov's theorem [17, 131, 189] describes the approach to an attractive compact uniformly hyperbolic submanifold $\mathcal{S}_0$. In fact, sufficiently close states with distance of order $\mathcal{O}(1)$ reach any neighbourhood of order $\mathcal{O}(\varepsilon)$ in slow time of order $\mathcal{O}\left(\varepsilon\,|\log(\varepsilon)|\right)$.

While the slow manifold is tracked for long times, the deterministic system can display fast transitions due to the crossing of bifurcation thresholds. Examples of the simplest bifurcations are listed in the next subsection.

1.2.1 Bifurcations

By definition, we refer to bifurcation as the change of stability of one or more equilibria of a system and the appearance, or disappearance, of steady states [131]. Usually, they refer to nonlinear systems; in fact, the loss of hyperbolicity of an equilibrium in a linear model is not addressed as a bifurcation, although strictly related to the topic. As we study bifurcations, we consider a fast-slow system in the singular limit, with focus on the fast subsystem. In this subsection, we address the codimension-1 local bifurcations, i.e., caused by the change of a parameter q in (1.2.1) for $\varepsilon = 0$ and $m = 1$. This family of bifurcations has been fully categorised [5, 97, 131], although it does not cover all the possible types of critical transitions in a system. They are defined by specific properties of the vector field [131], nonetheless, we only provide the key concepts associated with these phenomena.

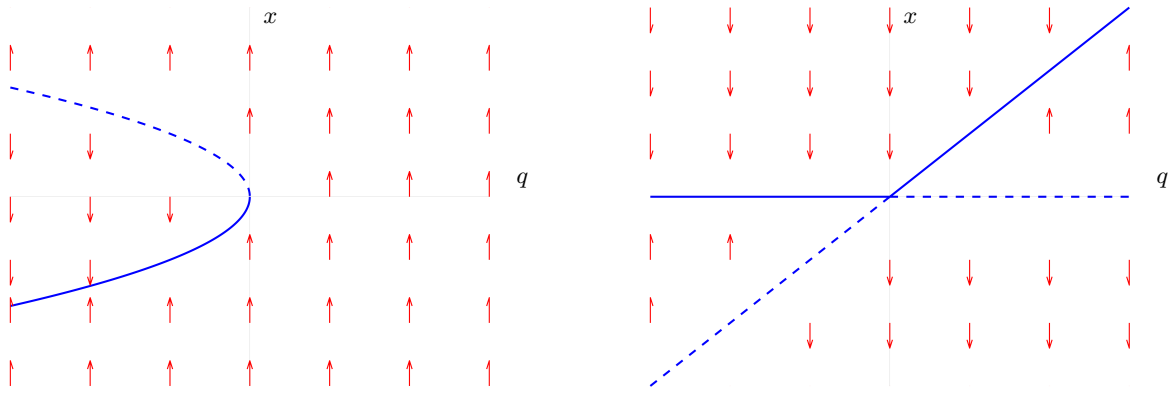

(a) Bifurcation diagram of a fold bifurcation

(b) Bifurcation diagram of a transcritical bifurcation

Fig. 1.1 Bifurcation diagram of a fold bifurcation, (a), and a transcritical bifurcation, (b). The solid blue lines refer to stable equilibria and the dashed blue lines to unstable steady states. The directions of the red arrows indicate the sign of the time derivative of x according to the state x. The lengths of the red arrows are normalised.

- The fold bifurcation indicates the collision and annihilation of two equilibria, generally of different attractivity properties. Its normal form, the canonical form, is

$$\frac{\mathrm{d}x}{\mathrm{d}t} = x^2 + q,$$

for the parameter $q \in \mathbb{R}$. The bifurcation diagram is displayed in Figure 1.1a. We can consider the model as the fast subsystem of

$$\begin{cases} \frac{\mathrm{d}x}{\mathrm{d}t} &= x^2 + q \\ \frac{\mathrm{d}q}{\mathrm{d}t} &= \varepsilon. \end{cases}$$

Then, the disappearance of the equilibria implies that orbits that follow the slow manifold display fast transitions after the bifurcation. This occurs for $0 < \varepsilon \ll 1$, however, the transition may happen far from the threshold, thus resulting in a canard [131].

- A transcritical bifurcation is associated with the instant collision of two equilibria that switch the stability. Its normal form is

$$\frac{\mathrm{d}x}{\mathrm{d}t} = x(q - x),$$

for the parameter $q \in \mathbb{R}$. The bifurcation diagram is shown in Figure 1.1b. Conversely to the previous case, the solutions of the fast-slow system

$$\begin{cases} \frac{\mathrm{d}x}{\mathrm{d}t} &= x(q - x) \\ \frac{\mathrm{d}q}{\mathrm{d}t} &= \varepsilon \end{cases}$$

with negative initial conditions of variable q display different behaviours once the bifurcation threshold is crossed, depending on the initial state of x.

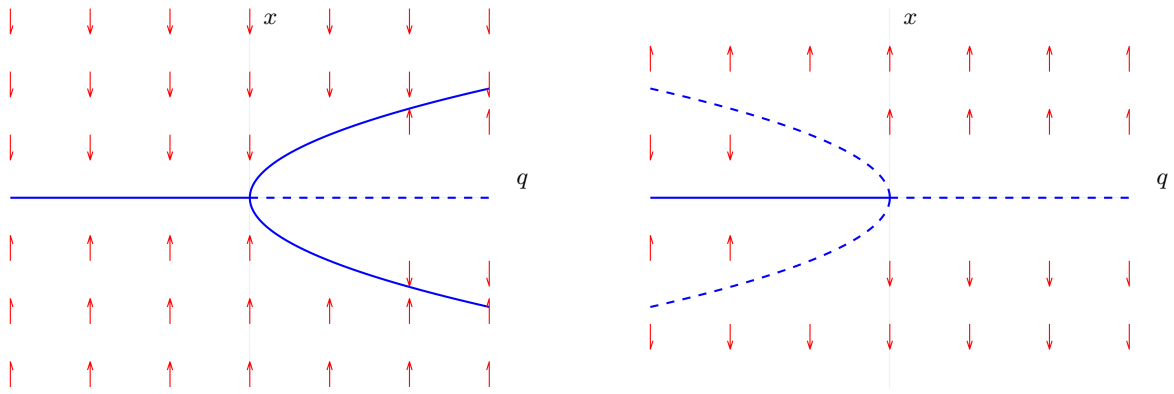

(a) Bifurcation diagram of a supercritical pitchfork bifurcation

(b) Bifurcation diagram of a subcritical pitchfork bifurcation

Fig. 1.2 Bifurcation diagram of the normal form of the supercritical pitchfork bifurcation, (a), and subcritical pitchfork bifurcation, (b). The legend of the lines is equivalent to Figure 1.1.

- The pitchfork bifurcation indicates the splitting of an equilibrium into three distinct steady states, or vice versa. There exist two types depending on the number of stable and unstable branches in the bifurcation diagram: the case of a single stable equilibrium forking into two unstable and a stable steady state is referred to as supercritical; assuming the attractivity of the equilibria involved to be reversed, then we refer to a subcritical pitchfork bifurcation. The normal forms are

$$\frac{\mathrm{d}x}{\mathrm{d}t} = x(q \mp x^2),$$

respectively. The bifurcation diagrams are shown in Figure 1.2. Similarly to the transcritical bifurcation, solutions of fast-slow systems that display pitchfork bifurcations show different behaviours after crossing the bifurcation threshold, in accordance to the initial conditions.

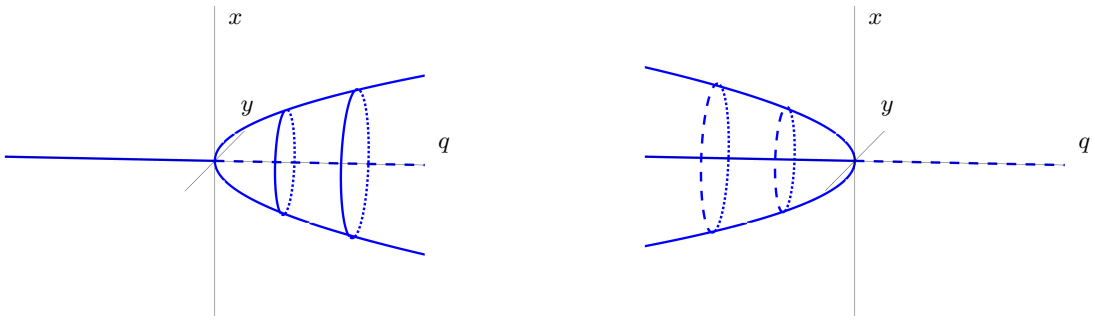

(a) Bifurcation diagram of a supercritical Hopf bifurcation

(b) Bifurcation diagram of a subcritical Hopf bifurcation

Fig. 1.3 Illustration of the bifurcation diagram corresponding to the supercritical Hopf bifurcation, (a), and subcritical Hopf bifurcation, (b). The solid blue lines refer to stable branches and the dashed lines to unstable equilibria. The solid-dotted lines in (a) indicate stable periodic orbits, whereas the dashed-dotted lines in (b) refer to unstable periodic orbits.

- A Hopf bifurcation is associated with the change in attractivity of an equilibrium, and the emergence of a new periodic orbit that arises from it. Similarly to the pitchfork bifurcation, we distinguish between the supercritical and subcritical cases. In real variables, the normal forms are

$$\begin{cases} \frac{\mathrm{d}x}{\mathrm{d}t} &= qx - y \mp x\left(x^2+y^2\right) \\ \frac{\mathrm{d}y}{\mathrm{d}t} &= x + qy \mp y\left(x^2+y^2\right), \end{cases}$$

  respectively. The bifurcation diagrams are shown in Figure 1.3. Such a bifurcation can be found in various models, including the Lotka-Volterra model, with applications in ecology, and the FitzHugh-Nagumo model, for medicine [131].

1.2.2 Multiple bifurcations

In this subsection, we include standard considerations to be taken in the interpretation of systems that display multiple bifurcations. The bifurcations listed in the previous subsection are called local bifurcations. In this sense, solutions of corresponding fast-slow systems may cross different bifurcation thresholds depending on the initial states, behaviour of the slow variable, and time interval considered. Consequently, the construction of observables that aim to predict the approach to a threshold may ignore the presence of distant equilibria. As a visual example, we consider the fast-slow system

$$\begin{cases} \frac{\mathrm{d}x}{\mathrm{d}t} &= q - 1.6x + 1.1x^3 - 0.11x^5 \\ \frac{\mathrm{d}q}{\mathrm{d}t} &= \varepsilon. \end{cases}$$

The corresponding fast system is multistable for fixed q in an interval. Moreover, the bifurcation diagram, in Figure 1.4a, displays multiple fold bifurcations. As observed in the panel, only a single fold bifurcation is crossed for specific initial conditions, although another threshold is traversed. This is also a clear example of how, in the case of several coexisting stable points, there can be a hierarchy of importance of branches implied by their position and stability. A related question is whether an observer should actually address the existence of all equilibria and bifurcations. While this usually depends on the application and model studied, the existence of minor bifurcations cannot be trivially ruled out in many models.

The fold bifurcation is the most recurrent in applications [97]. In fact, the transcritical and pitchfork bifurcations usually arise from symmetries of a physical model. In general, the presence of small perturbations in

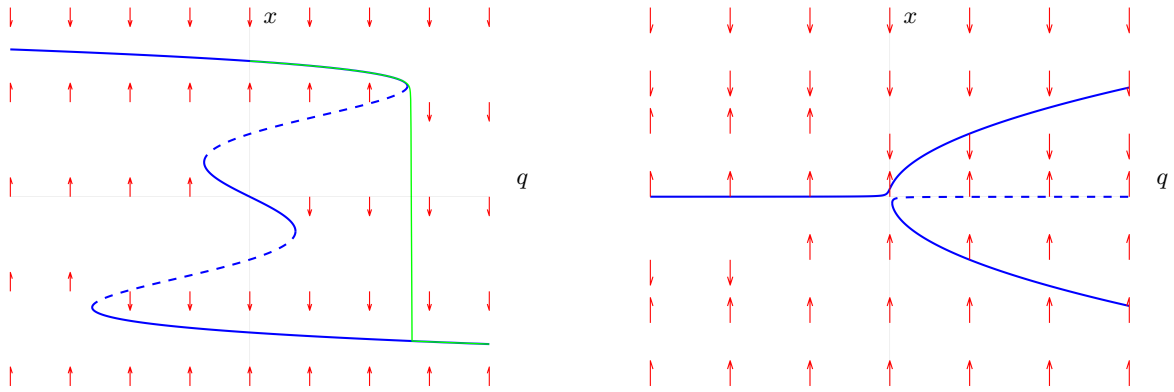

(a) Bifurcations ignored by a trajectory

(b) Bifurcation diagram of a false supercritical pitchfork bifurcation

Fig. 1.4 Panel (a) shows a trajectory (green) that crosses a fold bifurcation of the fast system. As it tracks the initial stable branch, it is virtually oblivious to the existence of another fold bifurcation since it refers to the disappearance of another stable solution. Panel (b) indicates the bifurcation diagram of the normal form of the supercritical pitchfork bifurcation under a minor perturbation. Then, the layout is replaced by a stable branch for all $q \in \mathbb{R}$ and a new fold bifurcation close to the original threshold. Furthermore, the stability of the solution corresponding to the first stable branch weakens close to $q = 0$. The legend of the blue and red lines is equivalent to Figure 1.1.

these systems implies the existence of close fold bifurcations or stationary branches. We consider, as an instance, the fast system

$$\frac{\mathrm{d}x}{\mathrm{d}t} = 0.002 + qx - x^3$$

and $q \in \mathbb{R}$. It resembles the normal form of the supercritical pitchfork bifurcation. Nonetheless, the bifurcation diagram in Figure 1.4b displays instead a fold bifurcation in the proximity to a stable branch. While this suggests that applied models could consider the wrong type of bifurcation, the possibility of (relatively) minor errors in the bifurcation diagram is less relevant in the case that further forcing were to be applied on trajectories of a fast-slow model. The simplest example is white noise (which is properly introduced further in the thesis) that establishes the possibility of a jump between two close stable solutions.

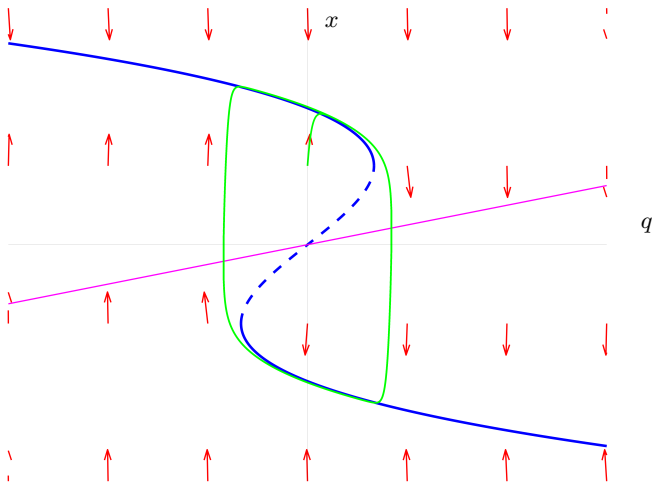

Fig. 1.5 An hysteresis loop (green) whose trajectory tracks the stable branch during slow transitions and enters fast transitions after crossing a fold bifurcation. The nullclines of the fast-slow system are shown in magenta and blue. As the orbit crosses the magenta nullcline, the derivative of q changes sign and the trajectory recovers from the fast transition. The dashed blue line refers to unstable steady states of the fast system. The direction of the red arrows corresponds to the time derivative of x and q. Their magnitude is normalised.

The importance of the construction of early-warning signs is related to the possibility of occurring in transitions that are difficult to reverse. A prime example is the hysteresis, which can be observed in a fast system with the first equation of the form

$$\frac{\mathrm{d}x}{\mathrm{d}t} = x - \frac{x^3}{3} - q.$$

In fact, once a fold bifurcation is crossed and a new stable point is reached, the slow variable needs to drive the trajectory towards another fold in order to return to the original steady state. This transition is slow by definition, therefore not as fast as the jump to the new steady state. A classic example that refers to the recurrent recovering from a fold bifurcation is the hysteresis loop [131]. This can be described, for instance, by the inclusion of the second equation

$$\frac{\mathrm{d}q}{\mathrm{d}t} = \varepsilon(x - 4y).$$

In Figure 1.5, we show a trajectory that satisfies such differential equations for $\varepsilon = 0.01$.

1.2.3 Bifurcations of PDEs

In this subsection, we address the extension of bifurcation theory to PDEs by considering a well-known model, the Chafee-Infante equation [50]. Its most standard form in the literature is

$$\frac{\mathrm{d}u}{\mathrm{d}t} = \Delta u + qu - u^3.$$

In this case, the function u assumes input in space and time. We indicate with Δ the second-order derivative in space, which is studied on an interval. In this example, we consider u to be null at the extremes. In Chapter 2, we address in detail operator theory, and we study the model in Chapter 3, Chapter 7 and Chapter 8. By fixing the parameter q, the study is equivalent to observing a fast system. The bifurcation diagram is illustrated in Figure 1.6. For $q < 0$, the system is monostable, and the null state is stable [50, 105]. Then, as $-q$ crosses each eigenvalue of Δ, it incurs into a pitchfork bifurcation. At each bifurcation, a pair of steady states emerges from the null state, and this becomes unstable along the corresponding eigenmode. The only stable states are those emerging from $q = 0$. All pitchfork bifurcations are supercritical in the correct space.

Equivalently to this example, the codimension-1 bifurcations can be carried over to PDEs. While they can be mathematically more complex, they correspond qualitatively to relative bifurcations for ODEs. Lastly, we underline that the bifurcations addressed are not the only known types and that in PDE theory further types are considered. An example is Turing bifurcations [115, 206] that indicate the emergence of spatial patterns.

1.3 Stochastic models in applications

Stochastic models can be interpreted as an extension of deterministic models with the inclusion of a noisy term meant to represent minor perturbations. Understanding and predicting systems influenced by uncertainty is usually achieved through observables. Among them, some rely on the fact that various types of noise induce intuitively ergodicity in the system [66], although not always trivial to prove [75]. The type of noise inserted is chosen in order to better replicate the underlying dynamics of the phenomenon. In this section, we do not provide mathematical definitions but include references to examples in which they are used in applications. In fact, these models are widely applied across diverse fields, offering insights that deterministic models cannot provide.

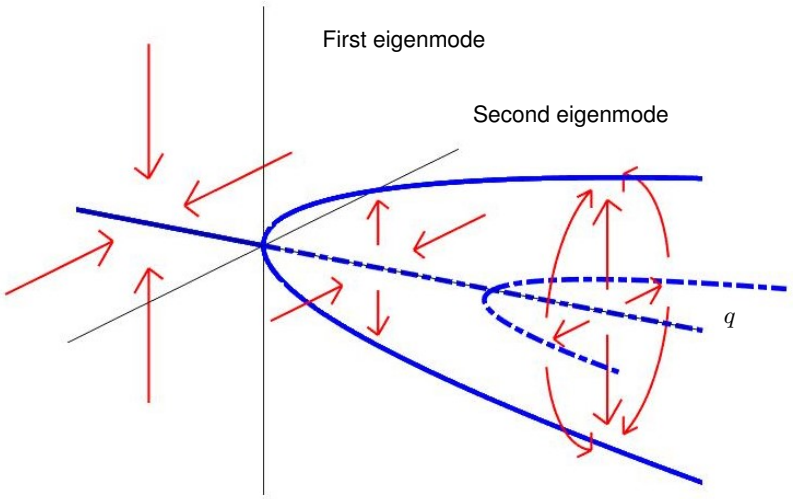

Fig. 1.6 Illustration of the bifurcation diagram of the Chafee-Infante equation. For negative q, there is only a stable equilibrium; for a small positive q, two stable solutions arise, and the null solution becomes unstable along the first eigenmode; for larger q, two other saddles emerge from the zero state. The rise of two new steady states through supercritical pitchfork bifurcations occurs each time $-q$ crosses an eigenvalue of the Laplace operator. At each iteration, the stable manifold of the new states possesses fewer dimensions than the previous. The trajectories between steady states are illustrated by red lines. The saddles are referred to by the dotted-dashed blue lines, while the bold blue lines indicate stable solutions.

- The first renowned type of noise is additive Gaussian noise [63]. It usually indicates external forcing and finds application in hydrodynamics [112], voltage collapses [59], environmental applications [140, 180], neuroscience [152, 154, 159] and signal theory [156].

- In fluid dynamics, multiplicative white noise has been used to indicate minor perturbations that originate from the components of the band-free plane Couette flow model [92]. Such a model captures the spreading of turbulence along a pipe.

- In active matter physics, models can include fractional Brownian motion, for instance, to study colloidal particles in plasma [128].

- In finance, stochastic models like Geometric Brownian Motion [150] are foundational to asset pricing and risk management. Used in the Black-Scholes formula, this model simulates the random movement of stock prices by capturing the volatility inherent in financial markets [88].

- In epidemiology, the stochastic (time-discrete) SIR model extends the traditional disease model by accounting for random variations in transmission and recovery [107]. This is particularly useful for modelling disease spread in small populations or during the early stages of an outbreak.

- In biology, gene expression is inherently noisy. While Gaussian noise models continuous fluctuations, Lévy noise captures burst-like behaviour, which is often observed in mRNA or protein production [147]. A similar type of noise finds application in the study of the foraging behaviour of animal groups and ecosystem dynamics [121].

- Queueing theory uses models such as the M/M/1 queue, a continuous time Markov chain, to analyse systems where entities (such as customers or data packets) arrive and are served at random intervals [1]. Moreover, in insurance and civil engineering, the Poisson process models the random occurrence of events like claims or accidents over time [52].

- Lastly, weather forecasting benefits from Markov weather models, which predict the likelihood of transitioning between weather states based on probabilistic patterns observed in past data [89].

In conclusion, by capturing the inherent uncertainty in complex systems, stochastic models provide a realistic approach to forecasting and system design in many fields [88]. In the case of fast-slow systems, the inclusion of a noise term usually can introduce a component evolving on a mesoscale in the system. In fact, we can consider the fast-slow system of stochastic differential equations (SDEs)

$$\begin{cases} \frac{\mathrm{d}x}{\mathrm{d}t} &= f(x,y) + \sigma\xi \\ \frac{\mathrm{d}y}{\mathrm{d}t} &= \varepsilon g(x,y), \end{cases} \tag{1.3.1}$$

for equivalent assumptions as in (1.2.1), $0 < \varepsilon \ll \sigma \ll 1$ and ξ noisy perturbations to be further defined in the next chapter. While the assumption on the magnitude of σ is not always enforced in applications, it is commonly used to represent small stochastic forcing or as a loose approximation of finite noise.

1.4 Tipping and early-warning signs

The stochastic term in (1.3.1) affects the behaviour of its solution and its trajectory. This is more relevant in neighbourhoods of bifurcation thresholds, which are regions where they are less resilient. The resulting critical transitions are often referred to as tipping [7]. In the next subsections, we address some of the types of transitions that they can undergo.

1.4.1 B-tipping

Bifurcation-induced tipping (B-tipping) arises when a deterministic bifurcation threshold is crossed, leading the trajectory to undergo a critical transition under deterministic forcing. This refers to the fact that the noise term in the system does not succeed in driving the orbit far from the stable branch, the slow manifold, and the corresponding basins of attraction until the bifurcation is reached. It is often associated with the case of monostability. Prime examples are then the supercritical pitchfork and supercritical Hopf bifurcations. Nonetheless, due to the stochastic nature of the system, it can be observed for other types of bifurcations, in particular under the assumption of small noise.

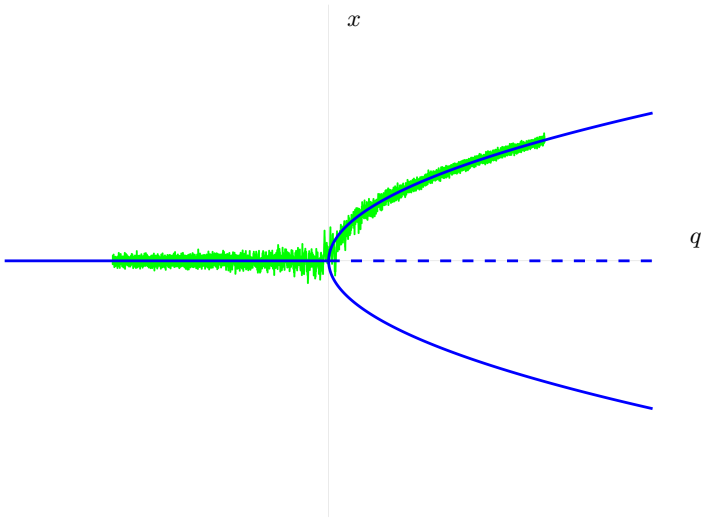

Fig. 1.7 Example of B-Tipping. We assume that q increases slowly and linearly in time. A trajectory (green) tracks a stable branch until crossing a bifurcation. The tipping is caused primarily by the properties of the fast system and there is no critical transition before q reaches 0.

Figure 1.7 displays, in green, a trajectory that incurs into B-tipping. It corresponds to the solution of the normal form of the supercritical pitchfork under small white noise perturbations and for variable q that satisfies $\frac{\mathrm{d}q}{\mathrm{d}t} = \varepsilon$.

A standard phenomenon related to B-tipping is critical slowing down (CSD) [25, 33, 39, 141], defined as the deceleration of the trajectory in the proximity of the bifurcation threshold. It is implied by the decreased attractivity of the stable branch due to the incoming loss of stability of the corresponding solution. In contrast, under the assumption of constant noise intensity, the stochastic perturbation overrules the drift term along certain modes. Such a phenomenon leads to the construction of standard early-warning signs, such as the increase of variance and autocorrelation in SDEs [73]. This is addressed further in the thesis to construct more complex observables.

1.4.2 N-tipping

Noise-induced tipping, or N-tipping, indicates the phenomenon in which a transition is noise-driven prior to a bifurcation crossing. Depending on the intensity of the noise, the critical jump is more likely to appear close to a bifurcation threshold, thus still facilitated by the deterministic forcing in the model. In the case of small noise, the transition is usually associated with fold and transcritical bifurcations, albeit subcritical bifurcations can also induce it. This is caused by the approach of the stable branch to a separatrix, or unstable branch in the one-dimensional case. For such a noise magnitude and under the assumption of multistability, it often corresponds to a metastable jump, i.e., a rapid transition between deterministic stable steady states between long periods of time fluctuating within the basins of attraction of each equilibrium.

Figure 1.8a shows a standard example of N-tipping. The trajectory in green satisfies

$$\begin{cases} \frac{\mathrm{d}x}{\mathrm{d}t} &= x - \frac{x^3}{3} - q + \sigma\xi \\ \frac{\mathrm{d}q}{\mathrm{d}t} &= \varepsilon, \end{cases}$$

for $\sigma = 0.4, \varepsilon = 0.001$ and ξ white noise. The trajectory follows the stable branch but performs a metastable jump prior to a fold bifurcation. Standard early-warning signs for N-tipping in SDEs are the analytic estimation for the probablity and for the average time of transition [17]. Alternatively, numerical computations of typical trajectories that display such events can reveal stages that preceed the phenomena and provide a statistical estimation of the average transition time [142].

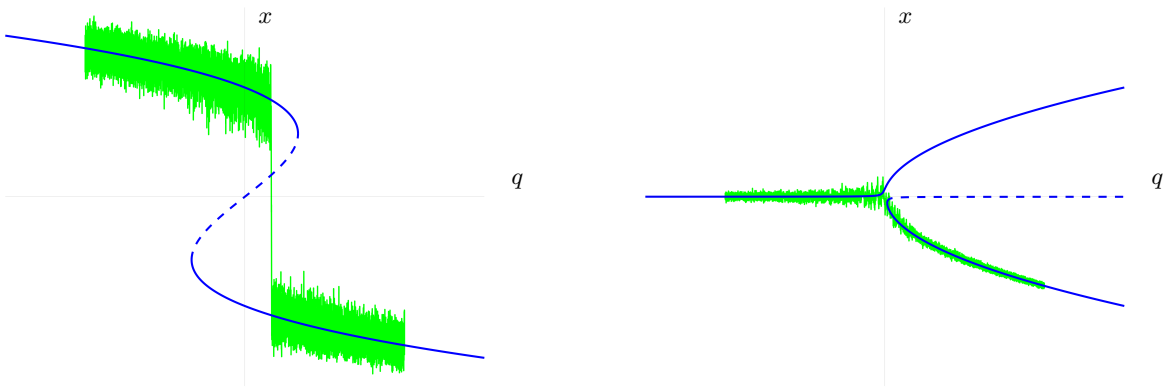

(a) An example of N-Tipping on an S-curve

(b) Tipping on a false supercritical pitchfork bifurcation

Fig. 1.8 In panel (a), we observe an example of N-Tipping. A green trajectory initially tracks a stable branch. Under the assumption that q increases linearly and slowly, the noise drives it into another stable steady state before crossing a fold bifurcation. The transition is then caused by the noise term and deterministic properties of the model, such as the proximity of the stable states. Panel (b) displays another example of N-Tipping. Under similar behaviour of q and initial conditions close to the origin, the transition would be impossible without the effect of the noise term. The tipping resembles the B-Tipping in Figure 1.7. As such, it is evident that there exist cases for which these phenomena can be mixed.

N-tipping and B-tipping refer, in principle, to opposite events. Nonetheless, they can be easily mixed in certain cases. In Figure 1.8b, we observe the trajectory of the solution of

$$\begin{cases} \frac{\mathrm{d}x}{\mathrm{d}t} &= 0.002 + qx - x^3 + \sigma\xi \\ \frac{\mathrm{d}q}{\mathrm{d}t} &= \varepsilon, \end{cases}$$

for $\sigma = 0.05$, $\varepsilon = 0.001$ and ξ white noise perturbation. As discussed in the bifurcation diagram in Figure 1.4b, a pitchfork bifurcation can be split into a stable branch and a fold bifurcation through small deterministic forcing. Nonetheless, the proximity of three branches implies that critical transitions driven by noise can be easily mistaken for B-tipping, as in Figure 1.7. As anticipated in the previous section, small errors can break a bifurcation but may not drastically change the simulations. In conclusion, it is reasonable to study pitchfork bifurcations even if unlikely in nature. An equivalent argument extends to transcritical bifurcations.

1.4.3 Other types of tipping

While the underlying dynamics during B-tipping and N-tipping are a focus of the thesis, the study of tipping is not limited to them. In this subsection, we briefly discuss other tipping mechanisms in the literature.

- State-tipping, or shock-tipping, or S-tipping, is defined by a forcing that drives the solution towards a different stable branch before crossing a bifurcation threshold [34]. In contrast to N-tipping, the perturbation is not stochastic in nature. Furthermore, it is assumed to be strong and rapid.
- Cascading tipping, or C-tipping, involves a cascade of local tipping events that propagate through an interconnected system, leading to a system-wide transition [8, 207]. It often indicates the domino effect of other types of tipping in coupled models.
- Fragmented tipping occurs when tipping is spatially or structurally localised, thus affecting only parts of a system. It is often related to spatially extended systems [15]. However, it can also be interpreted as the occurrence of a sequence of tipping points in spite of an achievable single critical transition. It can then happen for bifurcation diagrams such as the one discussed in Figure 1.4a, since multiple N-tipping can occur, and the Chafee-Infante equation, where a sequence of saddles can be crossed in a trajectory from the null solution to a heterogeneous stable state. While similar to C-tipping, it does not imply cascading.
- Rate-induced tipping, or R-tipping, is defined by a rate parameter that indicates how fast a non-autonomous forcing affects the solution [182, 203]. In the case that the drive is too fast, the trajectory is led out of an attractor. It is then the velocity of the forcing that causes the tipping, while no actual bifurcation is considered. It is relevant in various fields, among which the issue of zombie fires, in ecology [168].

1.5 Climate models and Hasselmann's Paradigm

Among applications, climate science is deeply connected to the topic of ergodicity and stochastic perturbations. A first renowned example is the Lorenz-63 system [145]. In 1963, it was originally envisioned as a simplified atmospheric convection model. It is a model composed of ODEs for three variables. Its most renowned property is the existence of a chaotic attractor for certain parameter values. This takes the name of Lorenz's butterfly, displayed in Figure 1.9, and it is usually regarded as the first step in chaos theory and a glimpse of the complex behaviour of the climate.[1]
In 1976, Klaus Hasselman theorised that the ergodic behaviour of climate models that studied the interactions between atmosphere, ocean, cryosphere, and land was induced by an external component [104].

[1] Curiously, chaos theory is cited extensively in media, such as in the novel and in the movie "Jurassic Park" [62, 185].

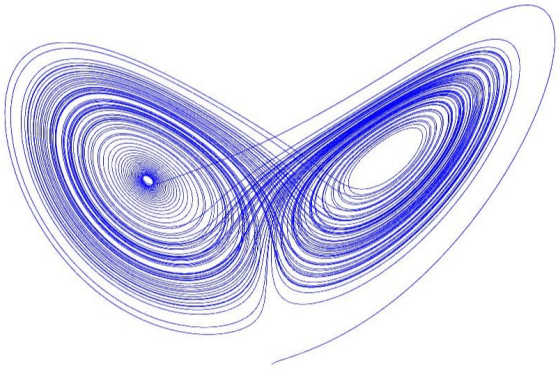

Fig. 1.9 The "butterfly" chaotic attractor from Lorenz-63 model [145]. It is considered the first insight into the complexity of climate and weather models.

He considered weather phenomena as minor perturbations in climate, which enforced a correlation associated with red noise-like behaviour, in accordance with observations. His groundbreaking work propelled the development of stochastic models for climate and led him to be awarded the Nobel Prize for Physics in 2021.
The inclusion of noise in climate models serves as a natural connection to the concept of tipping. In fact, climate models that display deterministic bifurcations can then be susceptible to noise-driven transitions. An example is the Stommel-Cessi model for buoyancy-driven ocean circulation. Stommel's two-box model [187] considers two regions of the ocean: the first box represents a low-latitude region in the North Atlantic Ocean; the second box is associated with a high-latitude part. Consequently, the first box is considered warmer than the second. In Figure 1.10a, we illustrate the main components of the model. Each box is characterised by the variables S and T, which indicate salinity and temperature, respectively. The water density ρ can then be obtained from the former through a linear equation. An external (inward and outward) forcing on the salinity ODEs is introduced as a flow ξ. Lastly, the exchange function g depends on the difference of density ρ between boxes.

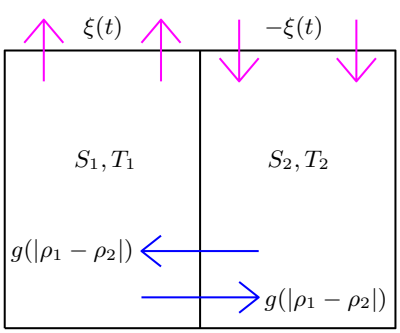

(a) Illustration of the two-box Stommel model

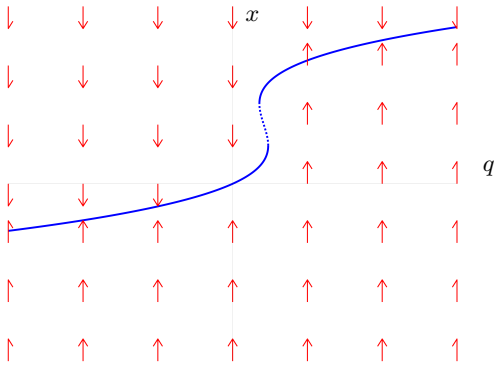

(b) Bifurcation diagram of the Stommel-Cessi model

Fig. 1.10 Panel (a) displays an illustration of the two-box model of Stommel [187]. The two boxes represent volumes of water of different sizes. Each box is characterised by a value of salinity and temperature. The magenta arrows indicate an external flux that affects salinity. The blue arrows represent the interchange between boxes caused by differences in (water mass) density. Panel (b) shows the bifurcation diagram of the fast system corresponding to the Stommel-Cessi model [48], i.e., under the assumption of a quadratic function g by Cessi. The diagram corresponds to a hysteresis, and the legend of the blue and red lines is equivalent to Figure 1.1.

The assumptions of Paola Cessi, in 1994 [48], bring the two-box model to a stochastic fast-slow system form. The flow ξ, induced by the melting of the Arctic ice sheet, is considered as minor (stationary) white

noise fluctuations. The noise was not assumed to be coloured, for simplicity. While Henry Stommel [187] assumed g to be of the form

$$g(|\rho_1 - \rho_2|) = c_1 + c_2|\rho_1 - \rho_2|,$$

she proposed an exchange function of the form

$$g(|\rho_1 - \rho_2|) = c_1 + c_2(\rho_1 - \rho_2)^2,$$

based on the properties of Boussinesq convection [49]. Rescaling the differences $S_1 - S_2$ and $T_1 - T_2$, she introduced respectively the variables y and x. On an adequate timescale, the two-box model can then be interpreted as

$$\begin{cases} \frac{\mathrm{d}x}{\mathrm{d}t} = -\alpha(x-1) - x\left(1 + \mu^2(x-y)^2\right) \\ \frac{\mathrm{d}y}{\mathrm{d}t} = \xi(t) - y\left(1 + \mu^2(x-y)^2\right), \end{cases}$$

for $1 < \mu^2 \ll \alpha$ and statistical properties of ξ obtained from observations [48]. The assumption of a large parameter α justifies the study of the (stochastic) fast subsystem

$$\begin{cases} x = 1 \\ \frac{\mathrm{d}y}{\mathrm{d}t} = \xi(t) - \left(1 + \mu^2(y-1)^2\right). \end{cases}$$

The corresponding (deterministic) bifurcation diagram is shown in Figure 1.10b. It displays two fold bifurcations and exhibits an hysteresis. As such, it indicates the possibility of critical transitions in the fast-slow system and highlights the importance of predicting tipping events.

The Stommel-Cessi is commonly employed to model tipping of the Atlantic Meridional Overturning Circulation (AMOC) [32, 72, 74]. It is a large system of ocean currents that transports warm, salty water from the tropics northward in the upper layers of the Atlantic and returns colder, denser water southward at deeper levels. Driven by differences in temperature and salinity (a process known as thermohaline circulation), the AMOC plays a key role in regulating climate, especially in the North Atlantic region. As warm surface water moves north, it cools and becomes denser, eventually sinking near Greenland and forming deep currents that flow southward. This circulation helps distribute heat across the globe and supports marine ecosystems. However, it is threatened by the melting of the Arctic ice sheet, which induces additional fresh water into its flow and could hinder the creation of deep currents. In fact, the AMOC is theorised to have multiple steady states under different climate regimes. The on-state is the present case, in which the current flows as discussed, whereas the off-state indicates the condition in which it halts, which would initiate deep changes in the global climate. In Figure 1.11, we show a simplified illustration of the AMOC on the Northern Hemisphere, from [85]. The figure highlights its behaviour in Greenland, Iceland, and Norwegian Seas (GIN), Labrador Sea Water (LSW), and Subtropical Mode Water (STMW).

A wide range of models has been developed to simulate the collapse of the AMOC. At the simplest level, box models, such as the Stommel-Cessi model, study their fundamental properties by dividing the system into a few large regions [49, 183]. In the thesis, we consider a two-dimensional Boussinesq model composed of stochastic partial differential equations (SPDEs) which accounts for a simplified treatment of density [10, 20, 184]. Among more complex models, we refer to Coupled Model Intercomparison Project (CMIP) models, which are sophisticated multi-component Earth models that simulate various interactions between the atmosphere, ocean, cryosphere, and land surface on a global three-dimensional grid [153]. Other phenomena in climate science to display critical transitions after minor perturbations are the end of the Younger Dryas in the tropical Atlantic [141], the melting of the Western Greenland Ice Sheet [33] and the loss of vegetation in West Sahara [160].

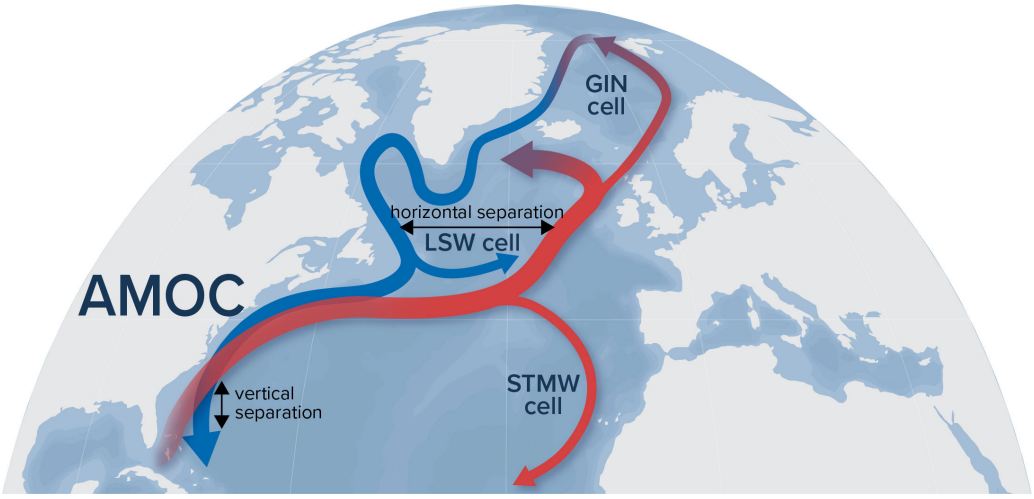

Fig. 1.11 Illustration of a component of the AMOC from [85]. The northward limb (red) represents the flow of warmer surface water, while the southward limb (blue) corresponds to the return flow of colder deep water. In northern regions, such as the subpolar gyre, the limbs are separated horizontally (by latitude), whereas in the subtropical Atlantic, such as along the Gulf Stream, they are separated vertically (by depth). The current active state of the AMOC, the on-state, is threatened by increased freshwater input from the melting Greenland Ice Sheet, which can reduce ocean water density and disrupt deepwater formation.

1.6 Structure of the thesis

This thesis is divided into three parts: Chapters 1-2 introduce the main topics with a discursive and then analytically formal approach; Chapters 3-7 focus on early-warning signs for SPDEs that display B-tipping under numerous types of stochastic perturbations and for different applications; Chapters 8-10 include the estimation of transition probability and the numerical computation of instantons for various SPDE applied models, thus addressing the time and stages of N-tipping. The thesis concludes with closing remarks and a general outlook. The majority of the appendices provide insights into operator theory and SPDEs to facilitate their comprehension. The remainder contain proofs of theorems discussed in the thesis.

In Chapter 2, we provide an introduction to Sobolev function spaces and operator theory, which are central topics in PDE theory. We then discuss standard arguments in probability theory and rigorously define Brownian motion and Gaussian noise. In the second section, we list theorems on the existence and uniqueness of solutions of SPDE under additive and multiplicative noise of different natures. These are employed throughout the thesis to assume the well-posedness of the studied objects. We also include fundamental properties of the Ornstein-Uhlenbeck process, which enable the construction of certain early-warning signs for B-tipping.

Chapter 3 focuses on the construction of early-warning signs in the form of time asymptotic covariance for SPDEs with discrete spectrum in the drift term and additive white Gaussian noise. We apply our results on a pitchfork bifurcation of the Chafee-Infante equation [105] under space-heterogeneous perturbations to address the non-uniform structure of climate models. As such, we initially describe its bifurcation diagrams and the existence of supercritical pitchfork bifurcations. We extend existing work on such an observable [93, 135] to synchronising noise frequencies. Furthermore, we obtain signals under the assumption of missing data in the sense of being constructed with limited knowledge of the trajectory of the solution. The early-warning sign is proven to be reliable even under the assumption of being limited by local and pointwise observations, aside from in the proximity to the bifurcation threshold. The observable is obtained through the Lyapunov equation and cross-validated by numerical simulation through the Euler-Maruyama scheme. The chapter is based on the work by the author [23].

In Chapter 4, we employ the time-asymptotic covariance as an early-warning sign for (linearised) SPDEs with purely continuous spectrum and additive white Gaussian noise. We observe a silencing effect on the observable caused by the peculiar nature of B-tipping. The signal is proven to be completely silenced for various analytic examples. Nonetheless, it is effective for renowned models such as a stochastic Swift-Hohenberg equation [112, 188], for hydrodynamics. An upper bound to the scaling law of the observable

is included for the one-, two-, and three-dimensional spatial domains and described through integration methods and estimations. We also provide an extensive list of further generalisations. The chapter includes insights into delayed early-warning signs under the assumption of purely discrete spectrum with small spectral gaps, such as in the case of a large domain and differential drift operators. The results presented are extracted from the paper [21].

Chapter 5 includes the application of the time-asymptotic autocovariance and autocorrelation as early-warning signs for specific models with constrained solutions. We focus on coupled SPDEs characterised by linear drift operators with purely generalised discrete spectrum and additive white boundary Gaussian noise. The scaling law of the time-asymptotic covariance is proven to be enhanced by the presence of generalised eigenfunctions. The time-asymptotic autocovariance is shown to be a reliable early-warning sign in the case of missing data, whereas the autocorrelation requires detailed knowledge of the system to predict B-tipping. The analytic results are applied through numerical methods on a Boussinesq model to study abrupt transitions in the AMOC [10]. The system is linearised through the analytic computation of the Schur complement. Part of its spectrum is obtained analytically, and the major spectral gaps are computed through discrete numerical approximations of the operator on different non-uniform grids. The material discussed is extracted from [20].

In Chapter 6, we extend the use of time-asymptotic covariance to the assumption of additive Gaussian red noise interpreted as a perturbed climate component. We employ the observable in the case of global knowledge of the corresponding trajectories, and then in the case of limited information. These results enable the prediction of B-tipping in climate models that are more consistent with Hasselmann's paradigm in comparison to those discussed in the previous chapters. Nonetheless, the signal is proven to be applicable to a wider range of application fields that account for memory in the stochastic component. The risk of false early warning is considered by including a limit on a second critical parameter. This highlights the need for previous knowledge of the structure of the system to properly anticipate critical transitions. The computation of the observable is achieved through the Lyapunov equation, taking into account the degeneracy of the noise in an extended model. The chapter results from the publication [25] and addresses the assumptions of purely discrete, generalised discrete, or continuous spectrum of the drift operator.

In Chapter 7, we introduce finite-time Lyapunov exponents to analytically construct a different early-warning sign for B-tipping. It observes the effect of critical slowing down on the supercritical pitchfork bifurcations of the space-heterogeneous Chafee-Infante equations with additive white Gaussian noise. We prove the existence of a singleton attractor with random dynamical systems theory and discuss the change of sign of the highest possible value assumed by the observable along such a trajectory. In fact, it is proven to change sign as the critical parameter crosses the primary bifurcation, thus indicating a type of stochastic bifurcation. Such a phenomenon is described through the computation of an upper and lower bound of the observable. The signal is also generalised to predict the crossing of the other pitchfork bifurcations through the use of wedge products. In such a case, the corresponding change of sign occurs previous to the transition. The chapter includes work from [23], which extends the results of [31].

Chapter 8 contains the estimation of transition probability for a non-autonomous space-heterogeneous Chafee-Infante equation perturbed by additive white Gaussian noise. In particular, we estimate the possibility of a jump prior to the crossing of the primary supercritical pitchfork bifurcation. As such, it describes the first stage of N-tipping: the noise-induced distancing from a deterministic, stable, steady state. The upper bound is analytically proven through a Young-type inequality on Sobolev spaces and a Bernstein-type inequality for a stochastic integral. Lastly, it enables the construction of further moment estimates. The original work is published in [23].

Chapter 9 focuses on the estimation of turbulence onset probability in a fluid dynamics model. We discuss plane Couette flow, or flow along a pipe, assuming as the initial state a virtually laminar condition. The model is introduced in [92], where it is observed via a numerical study. In this chapter, we obtain lower bounds to such a transition under different types of multiplicative noise. In fact, we discuss it from an Itô and Stratonovich perspective, accounting also for different interpretations of red noise. A first analytic method relies on the martingale properties of the mild solution following the techniques in [163]. A second estimate is obtained through the linearisation of the model and the comparison with further systems, such

as the Kardar–Parisi–Zhang (KPZ) equation [99]. Examples of the transition are obtained numerically through a stochastic rare event algorithm. These results are extracted from [24].
In Chapter 10, we construct instantons, the most likely orbits to describe a rare event, for numerous models under small noise intensity. The systems discussed include degenerate noise, i.e., stochastic perturbations do not affect some variables in certain regions of the domain. The spreading of stochastic driving throughout the different components of the models is then partially a result of their deterministic properties. The work is carried out through a numerical technique, the state adjoint method, which accounts for an interplay between the minimisation of an action, to limit the intervention of noise, summed to a penalty term that enforces the occurrence of the rare event. The phenomena addressed range from puff merging in a biology model, initiation of an impulse in a nerve axon, and splitting of a turbulent region of a fluid flowing along a pipe. The chapter includes material from [22].

2 Preliminaries

This chapter provides the necessary analytic foundation to discuss the topics in the parts to follow. It includes the definition of signals and observables that are central for the thesis, along with the theorems that define their existence and well-posedness. While we introduce topics that are relevant to all sections, the chapter provides an analytic background that is most directly applicable to the first part of the work (Chapters 3-7). In the second (Chapters 8-10), where the topics are more diverse, each chapter includes further introduction to its analytic content due to the diversity of the topics addressed.

2.1 Theoretical background

In this section, we introduce standard mathematical tools and notation required for a proper understanding of the thesis. We first describe the function spaces involved; then, we discuss basic topics in operator theory; lastly, we refer to stochastic analysis results. For a more detailed background on the subject, the reader is referred to [65, 105].

2.1.1 Function spaces

We fix the domain $\mathcal{X} \subset \mathbb{R}^N$ for $N \in \mathbb{N}_{>0}$ and assume $f : \mathcal{X} \to \mathbb{C}$. Then, we say that $f \in L^p(\mathcal{X}; \mathbb{C})$ if

$$\int_{\mathcal{X}} |f(x)|^p \, \mathrm{d}x < +\infty,$$

for $1 \leq p < \infty$ and $f \in L^\infty(\mathcal{X}; \mathbb{C})$ if

$$\operatorname*{ess\,sup}_{x \in \mathcal{X}} |f(x)| < \infty.$$

Unless otherwise specified, all L^p-spaces are taken with respect to Lebesgue measure. Two functions have the same representation in L^p if they are equal almost everywhere. Consequently, we define the L^p-norms as

$$||f||_p = \left(\int_{\mathcal{X}} |f(x)|^p \, \mathrm{d}x \right)^{\frac{1}{p}}$$

for $f \in L^p(\mathcal{X}; \mathbb{C})$ and $1 \leq p < \infty$. Furthermore,

$$||f||_\infty = \inf \left\{ C \geq 0 \,\middle|\, |f(x)| \leq C \quad \text{for almost every } x \right\}$$

for any $f \in L^\infty(\mathcal{X}; \mathbb{C})$. For any $a \in \mathbb{C}$, we denote its complex conjugate as $\overline{a} \in \mathbb{C}$. We also label as i the imaginary unit. We notice that $L^2(\mathcal{H}; \mathbb{C})$ is a Hilbert space, and its scalar product is defined as

$$\langle f, g \rangle = \int_{\mathcal{X}} f(x) \overline{g(x)} \mathrm{d}x.$$

For simplicity, we denote the L^2-norm as $||\cdot||$. In contrast, we refer to the scalar product of any other Hilbert space $\tilde{\mathcal{H}}$ as $\langle\cdot,\cdot\rangle_{\tilde{\mathcal{H}}}$ and to the corresponding norm as $||\cdot||_{\tilde{\mathcal{H}}}$. For $1 < p < \infty$, we employ the notation $L^p(\mathcal{X};\tilde{\mathcal{H}})$ to refer to the Bochner space of functions $f : \mathcal{X} \to \tilde{\mathcal{H}}$ such that

$$\left(\int_{\mathcal{X}} ||f(x)||^p_{\tilde{\mathcal{H}}} \, \mathsf{d}x\right)^{\frac{1}{p}} < \infty$$

and $\tilde{\mathcal{H}}$ is a Hilbert space. Furthermore, we use the notation $L^p(\mathcal{X})$ for any $1 \leq p \leq \infty$, to indicate the functions in $L^p(\mathcal{X};\mathbb{C})$ that assume real values. For $\alpha = (\alpha_1, \ldots, \alpha_N)$, we state that $g \in L^2(\mathcal{X})$ is the α-weak derivative of $f \in L^2(\mathcal{X})$ if

$$\langle g, \varphi\rangle = \left\langle f, \frac{\mathsf{d}}{\mathsf{d}x_1^{\alpha_1} \ldots \mathsf{d}x_N^{\alpha_N}}\varphi \right\rangle,$$

for any test function $\varphi \in C^\infty(\mathcal{X})$ in the set of functions that have continuous derivatives of all orders. We then indicate $g = \mathsf{D}^\alpha f$. We define the Sobolev space of degree $p = 2$ and integer order $s > 0$ as

$$\mathcal{W}^{s,p}(\mathcal{X}) := \left\{ f \in L^2(\mathcal{X}) \middle| \sum_{|\alpha|\leq s} ||\mathsf{D}^\alpha f||^2 < +\infty \right\}$$

with $|\alpha| = \sum_{i=1}^{N} \alpha_i$. For $0 < \delta < 1$, we define the Gagliardo seminorm

$$[f]_\delta := \int_{\mathcal{X}} \int_{\mathcal{X}} \frac{|f(x) - f(y)|^2}{|x - y|^{N+2\delta}} \mathsf{d}x\mathsf{d}y.$$

Then, the fractional Sobolev space $\mathcal{W}^{s,2}(\mathcal{X})$, for $s > 0$ such that $s \in \mathbb{R} \setminus \mathbb{N}$, is

$$\mathcal{W}^{s,2}(\mathcal{X}) := \left\{ f \in L^2(\mathcal{X}) \middle| \sum_{|\alpha|\leq n} ||\mathsf{D}^\alpha f||^2 + \sum_{|\alpha|=n} [\mathsf{D}^\alpha f]^2_\delta < +\infty \right\},$$

for $s = n+\delta$, $n \in \mathbb{N}$ and $0 < \delta < 1$. For positive s, we label as $\mathcal{W}^{s,2}_0(\mathcal{X})$, the functions in the corresponding Sobolev space that assume null value on the boundary. Lastly, we indicate as $\mathcal{W}^{-s,2}(\mathcal{X})$ the dual space (of distributions) of $\mathcal{W}^{s,2}(\mathcal{X})$ for any $s > 0$.

2.1.2 Operator theory

We introduce a linear operator such that $A : \mathcal{H}_a \to \mathcal{H}_b$ for the Hilbert spaces $\mathcal{H}_a$ and $\mathcal{H}_b$. Alternatively, its domain is indicated as $\mathcal{D}(A)$. It is bounded if there exists $M > 0$ such that

$$\sup_{f\in\mathcal{H}_a\setminus\{0\}} \frac{||Af||_{\mathcal{H}_b}}{||f||_{\mathcal{H}_a}} =: ||A||_{\mathcal{L}(\mathcal{H}_a,\mathcal{H}_b)} \leq M.$$

The inverse of the invertible operator A is labeled as $A^{-1} : \mathcal{H}_b \to \mathcal{H}_a$ and satisfies $AA^{-1} = A^{-1}A = \mathrm{Id}$, for Id that refers to the identity operator. The space of values $\lambda \in \mathbb{C}$ such that $A - \lambda\,\mathrm{Id}$ is not invertible is the spectrum of A. We distinguish such a set in three parts:

- $\lambda \in \mathbb{C}$ is in the point spectrum if $A - \lambda\,\mathrm{Id}$ is not injective;
- $\lambda \in \mathbb{C}$ is in the continuous spectrum if $A - \lambda\,\mathrm{Id}$ is injective, has dense range but is not surjective;
- $\lambda \in \mathbb{C}$ is in the residual spectrum if $A - \lambda\,\mathrm{Id}$ is injective but has no dense range.

An operator whose spectrum is solely composed of point spectrum is called purely discrete. Conversely, an operator with only continuous spectrum is defined as purely continuous. The resolvent set of A is the complementary set of its spectrum in $\mathbb{C}$. The resolvent operator of A on $\lambda \in \mathbb{C}$ in the resolvent set is indicated as $(A - \lambda \,\mathrm{Id})^{-1}$. More generally, for A that is non-negative linear diagonalisable and self-adjoint and $q \in \mathbb{R}$, we define as $A^q : \mathcal{D}(A^q) \to \mathcal{H}_b$, the operator that shares its eigenfunctions and, for any eigenvalue λ of A, the eigenvalue of A^q associated to the corresponding eigenfunction is λ^q. The adjoint operator of A is indicated by $A^* : \mathcal{H}_b \to \mathcal{H}_a$ and it satisfies

$$\langle Af, g\rangle_{\mathcal{H}_b} = \langle f, A^* g\rangle_{\mathcal{H}_a},$$

for any $f \in \mathcal{H}_a$ and $g \in \mathcal{H}_b$. Furthermore, an operator A is defined as sectorial if there exists $0 < \delta \leq \pi$ such that for every element $\lambda \neq 0$ in its spectrum it holds that $|\arg(\lambda)| \leq \delta$ and

$$\sup_{\lambda:\arg(\lambda)>\delta} |\lambda| \left|\left|(\lambda - A)^{-1}\right|\right|_{\mathcal{L}(\mathcal{H}_b,\mathcal{H}_a)} < +\infty.$$

A linear operator A is said to be trace-class if, for a basis $\{e_k\}_k$ of the separable Hilbert space $\mathcal{H}_a$, it holds

$$\mathsf{Tr}(A) := \sum_k \langle Ae_k, e_k\rangle_{\mathcal{H}_a} < +\infty.$$

Lastly, it is called Hilbert-Schmidt if A^*A is trace-class.
The next definitions introduce $\mathcal{C}_0$-semigroups, which are fundamental objects in the upcoming chapters.

Definition 2.1.1. *Let $\mathcal{H}_a$ be a Banach space. A $\mathcal{C}_0$-semigroup on $\mathcal{H}_a$ is defined as a family of operators $S = \{S(t)\}_{t\geq 0} = \left\{e^{At}\right\}_{t\geq 0}$ for $A : \mathcal{D}(A) \subset \mathcal{H}_a \to \mathcal{H}_a$ which are assumed continuous from X on itself and such that*

- $S(t_1)S(t_2) = S(t_1 + t_2)$ *for all* $t_1, t_2 \geq 0$,
- $S(0) = \mathrm{Id}$,
- *for each* $\phi \in \mathcal{H}_a$, $S(\cdot)\phi : [0, +\infty) \to \mathcal{H}_a$ *is continuous.*

Additionally, if $||S(t)||_{\mathcal{L}(\mathcal{H}_a)} \leq 1$ *for all* $t \geq 0$ *it is called a $\mathcal{C}_0$-contraction semigroup on $\mathcal{H}_a$.*
The infinitesimal generator of a $\mathcal{C}_0$-semigroup on $\mathcal{H}_a$ is the operator $A : \mathcal{D}(A) \to \mathcal{H}_a$ which satisfies

$$A = \lim_{t\to 0} \frac{S(t)\phi - \phi}{t}$$

for all $\phi \in \mathcal{D}(A)$.

The Hille-Yosida Theorem provides sufficient and necessary conditions for an operator to be the generator of a $\mathcal{C}_0$-contraction semigroup [105].

Theorem 2.1.2 (Hille-Yosida Theorem)**.** *An operator $A : \mathcal{D}(A) \to \mathcal{H}_a$, for which $\mathcal{D}(A) \subset \mathcal{H}_a$, is the generator of a $\mathcal{C}_0$-contraction semigroup on the Banach space $\mathcal{H}_a$ if and only if A is closed, densely defined and*

$$||(\lambda I - A)^{-1}||_{\mathcal{L}(\mathcal{H}_a)} \leq \frac{1}{\lambda}$$

for all $\lambda > 0$.

Through the thesis, we indicate as a Nemytskii operator a nonlinear operator $F : \mathcal{H}_a \to \mathcal{H}_b$ that is locally Lipschitz and Fréchet differentiable in a dense subset of $\mathcal{H}_a$. Its Fréchet derivative at $u_* \in \mathcal{H}_a$ is the linear and bounded (on the appropriate space) operator $A : \mathcal{H}_a \to \mathcal{H}_b$ such that

$$\lim_{||g||_{\mathcal{H}_a}\to 0} \frac{||F(u_* + g) - F(u_*) - Ag||_{\mathcal{H}_b}}{||g||_{\mathcal{H}_a}} = 0.$$

Consequently, we write $A = \mathsf{D}_{u_*} F$.

2.1.3 Stochastic analysis

In this subsection, we provide various definitions and tools from probability theory and stochastic analysis.

Definition 2.1.3. *A family of random variables $\{X_t\}_{t\in[0,T)} = \{X(\omega,t)\}_{t\in[0,T)}$ with time interval $[0,T)$ and $\omega \in \Omega$ is called a stochastic process. For a fixed $\omega_0 \in \Omega$, we call the function $X(\omega_0,\cdot) : T \to \mathbb{R}$ a sample path of X.*
A Gaussian process is a stochastic process $\{X_t\}_{t\in[0,T)}$ such that X_{t_0} for every $t_0 \in [0,T)$ is a Gaussian random variable.

The study of stochastic processes and their sample paths is fundamental to the work presented in the thesis. The next definitions enable the construction of martingales and Wiener processes.

Definition 2.1.4. *(i) A family of σ-fields $\{\mathcal{F}_t\}_{t\geq 0}$ such that $\mathcal{F}_t \subset \mathcal{F}$ for all $t \geq 0$ and $\mathcal{F}_{t_1} \subset \mathcal{F}_{t_2}$ for all $t_1 < t_2$ is called a filtration.*

(ii) We call a stochastic process $\{X_t\}_{t\geq 0}$ adapted to a filtration $\{\mathcal{F}_t\}_{t\geq 0}$ if X_t is $\mathcal{F}_t$-measurable for all $t \geq 0$.

(iii) Under the notation $(\Omega,\mathcal{F},\{\mathcal{F}_t\}_{t\geq 0},\mathbb{P})$, which combines a probability space $(\Omega,\mathcal{F},\mathbb{P})$ with a filtration $\{\mathcal{F}_t\}_{t\geq 0}$, we indicate a filtered probability space.

We now introduce the definition of a martingale, which is a specific type of stochastic process.

Definition 2.1.5. *A martingale is a sequence of random variables $\{X_t\}_{t\geq 0}$ such that*

(i) X_t is $\mathcal{F}_t$-measurable for all $t \geq 0$,

(ii) $\mathbb{E}[|X_t|] < \infty$ for all $t \geq 0$,

(iii) $\mathbb{E}[X_t|\mathcal{F}_s] = X_s$ for all $t > s$.

The scalar Brownian motion is a paramount martingale to this thesis and is introduced in the following definition.

Definition 2.1.6. *A scalar Brownian motion, or Wiener process, is a stochastic process $\{\beta(t)\}_{t\geq 0}$ that assumes real (or complex) values such that*

(i) $\beta(0) = 0$,

(ii) $\beta(t+s) - \beta(s)$ is independent of $\mathcal{F}_s^\beta$ for all $s,t \geq 0$,

(iii) $\beta(t+s) - \beta(s)$ has the distribution law $\mathcal{N}(0,t)$ for all $s,t \geq 0$, i.e., has a normal distribution with null mean and variance t,

(iv) $\{\beta(t)\}_{t\geq 0}$ have almost-surely continuous sample paths.

We extend the definition of Brownian motion to function spaces in the following.

Definition 2.1.7. *We introduce the operator $Q : \mathcal{H}_a \to \mathcal{H}_a$ that is assumed to be diagonalisable, non-negative, and self-adjoint. We label as $\{b_n\}_n$ a basis of $\mathcal{H}_a$ that diagonalises Q and as $\{\zeta_n\}_n$ its eigenvalues. A stochastic process $W(t)$ with values in $\mathcal{H}_a$ and for $t \geq 0$, is called a Q-Wiener process if it satisfies*

(i) $W(0) = 0$,

(ii) W has continuous trajectories,

(iii) W *has independent increments,*

(iv) $W(t) - W(s)$ *has the distribution law* $\mathcal{N}(0, (t-s)Q)$ *with* $t \geq s \geq 0$ *.*

If Q *is not trace-class but it is Hilbert-Schmidt for a larger space, then* $W(t)$ *is a generalised Wiener process. For the specific case* $Q = \mathrm{Id}$*, it is called a cylindrical Wiener process.*

Throughout the thesis, we also indicate a Wiener process as $W(t)$ or W_t in conformity with standard notation. We now list several properties for a Q-Wiener process, a central process that defines the noise term throughout the thesis.

Lemma 2.1.8 ([65, Chapter 4])**.** *Suppose* W *is a* Q*-Wiener process with* Q *trace-class for which we use the notation in Definition 2.1.7. Then, the following holds.*

(i) W *is a Gaussian process on* $\mathcal{H}_a$*. For* $t \geq 0$*, it holds that* $\mathbb{E}[W(t)] = 0$ *and the covariance operator of* $W(t)$ *is* tQ*.*

(ii) W *is of the form*

$$W(t) = \sum_{j=1}^{\infty} \sqrt{\zeta_j} \beta_j(t) b_j \tag{2.1.1}$$

for every t*, for real valued iid family of Brownian motions* $\{\beta_n(t)\}_n$ *on* $(\Omega, \mathcal{F}, \mathbb{P})$*. Further, the series* (2.1.1) *is convergent in* $L^2(\Omega, \mathcal{F}, \mathbb{P}; \mathcal{H}_a)$ *and* $\mathbb{P}$*-almost surely uniformly convergent on finite time intervals.*

Lastly, we define white noise in scalar and function space. Such a process is used to indicate singular stochastic perturbations on the boundary of a domain, as shown in the next section.

Definition 2.1.9. *Scalar white noise is defined as a scalar stochastic process* ξ*, such that* $\xi(s)$ *and* $\xi(t)$ *are iid for any* $s \neq t$*. White noise in a function space* $\mathcal{H}$ *can be constructed as*

$$\dot{W}(t) = \sum_{j=1}^{\infty} \xi_j(t) b_j, \tag{2.1.2}$$

for arbitrary t*, for* $\{b_n\}_n$ *a base of* $\mathcal{H}$ *and* $\{\xi_n\}_n$ *a collection of independent scalar white noise processes.*

For the rest of the thesis, we consider the distribution law of $\xi(t)$ in Definition 2.1.9 to be standard Gaussian for every t.

2.2 SPDE theory

In this section, we enclose different statements on the existence and uniqueness of solutions of stochastic partial differential equations (SPDEs) on a domain $\mathcal{X} \subset \mathbb{R}^N$. We consider first the case of additive noise, i.e., with a noise term that is not dependent on the realisation of the solution, and then, vice versa, the case of multiplicative noise. For a general SPDE of the form

$$u(x,t) = (Au(x,t) + F(u)(x,t))\,\mathsf{d}t + B(u)(x,t)Q^{\frac{1}{2}}\mathsf{d}W_t$$

with initial conditions

$$u(x,0) = u_0(x)$$

for $x \in \mathcal{X}$ and $t \in \mathbb{R}$, we distinguish between the mild solution and the more restrictive strong solution. We consider a linear operator $A : \mathcal{H}_a \subset \mathcal{H}_b \to \mathcal{H}_b$, the nonlinear operators $F : \mathcal{H}_a \to \mathcal{H}_b$ and $B : \mathcal{H}_a \to \mathcal{H}_b$ and Q as assumed in Definition 2.1.7. The mild solution satisfies the formula

$$u(\cdot,t) = \mathsf{e}^{At}u_0 + \int_0^t \mathsf{e}^{A(t-s)}F(u)(\cdot,s)\mathsf{d}s + \int_0^t \mathsf{e}^{A(t-s)}B(u)(\cdot,s)Q^{\frac{1}{2}}\mathsf{d}W_s,$$

whereas the strong solution is given as

$$u(\cdot,t) = u_0 + \int_0^t (Au(x,s) + F(u)(x,s))\,\mathsf{d}s + B(u)(x,t)Q^{\frac{1}{2}}W(t),$$

for any $t \in \mathbb{R}$ and $\mathbb{P}$-almost surely.

2.2.1 Additive noise

In the next theorem, we describe the properties of the stochastic convolution process therein defined. Such an object indicates the mild solution of a linearised SPDE with additive noise.

Theorem 2.2.1 ([65, Theorem 5.2])**.** *Assume that the linear operator $A : \mathcal{H}_a \to \mathcal{H}_b$ generates a $\mathcal{C}_0$-contraction semigroup on $\mathcal{H}_a$ and that $Q : \mathcal{H}_a \to \mathcal{H}_b$ is a bounded non-negative linear diagonalisable self-ajoint operator. If*

$$\int_0^t Tr\left(e^{As}Qe^{A^*s}\right) ds < +\infty,$$

then the process

$$W_A(t) := \int_0^t e^{A(t-s)}Q^{\frac{1}{2}}\,dW_s$$

is Gaussian and its trajectories are $\mathbb{P}$-almost surely in $\mathcal{H}_a$. Its covariance operator is

$$\int_0^t e^{As}Qe^{A^*s}ds.$$

In the next theorem, we state the required conditions for the existence of a mild solution of an SPDE with additive noise.

Theorem 2.2.2 ([65, Theorem 5.4])**.** *Under the assumptions of the previous theorem, the system*

$$\begin{aligned} du(x,t) &= Au(x,t)dt + Q^{\frac{1}{2}}dW_t,\\ u(x,0) &= u_0(x), \end{aligned}$$

for all $x \in \mathcal{X}$, $t > 0$ and $u_0 \in D(A)$, has a unique mild solution $\mathbb{P}$-almost surely in the form

$$u(x,t) = e^{At}u_0(x) + \int_0^t e^{A(t-s)}Q^{\frac{1}{2}}dW_s.$$

In the theorem below, we introduce a condition of well-posedness of the mild solution of a linearised SPDE. This is in the form of a stochastic convolution. Such a statement is also employed to establish the continuity in space of the solution.

Theorem 2.2.3 ([65, Theorem 5.20])**.** *Established the assumptions of the previous theorem, assume that A is negative and bounded from below. Assume also that A and Q share eigenfunctions $\{e_k\}_k$. The respective eigenvalues are $\{\lambda_k\}_k$ and $\{\zeta_k\}_k$. Furthermore, assume that there exists $C > 0$ such that, for any k and $x \in \mathcal{X}$, it holds*

$$|e_k(x)| \leq C \quad \textit{and} \quad |\nabla e_k(x)| \leq C(-\lambda_k)^{\frac{1}{2}}.$$

Consider the existence of $\gamma \in (0,1)$ such that

$$\sum_k \frac{\zeta_k}{(-\lambda_k)^{1-\gamma}} < +\infty.$$

Lastly, assume the existence of the Banach space $\mathcal{H}_c \subset \mathcal{H}_a$ that contains the set $\{e_k\}_k$ and is invariant under the action of e^{At} for any $t > 0$. Then, $W_A(t)$ has an $\mathcal{H}_c$-valued version with continuous trajectories.

In the next theorem, we discuss the existence of a strong solution of a linear SPDE with additive noise. Conversely to the previous assumptions, the noise perturbations are assumed only through finite modes.

Theorem 2.2.4 ([65, Theorem 5.29])**.** *Under the assumptions in Theorem 2.2.2, assume that A and Q share eigenfunctions $\{e_k\}_k$. Label the respective eigenvalues as $\{\lambda_k\}_k$ and $\{\zeta_k\}_k$, and assume that there exists an integer $n > 0$ such that $\zeta_k = 0$ for $n \leq k$. Then, the system*

$$\begin{aligned} du(x,t) &= Au(x,t)dt + Q^{\frac{1}{2}}dW_t, \\ u(x,0) &= u_0(x), \end{aligned}$$

for all $x \in \mathcal{X}$, $t > 0$ and $u_0 \in \mathcal{D}(A)$, admits a strong solution.

In the theorem below, we discuss the conditions for continuity in time and space of the strong solution of an SPDE with additive noise. Among them, we require the continuity in space of the stochastic convolution, as mentioned in Theorem 2.2.3.

Theorem 2.2.5 ([65, Theorem 7.13])**.** *Under the assumptions in Theorem 2.2.3, assume that A restricted to $C(\mathcal{X})$ generates a $\mathcal{C}_0$-semigroup $S_{C(\mathcal{X})}$ in $C(\mathcal{X})$. Also, assume that W_A has a $C(\mathcal{X})$-continuous version. Consider the existence of $\kappa > 0$ such that*

$$\left|\left|S_{C(\mathcal{X})}(t)\right|\right|_{\mathcal{L}(L^2(\mathcal{X}))} \leq e^{-\kappa t}$$

for all $t \geq 0$. Assume also that $F : \mathcal{H}_a \to \mathcal{H}_b$ is a dissipative Nemytskii operator. If the restriction of F to $C(\mathcal{X})$ is uniformly continuous on bounded sets of $C(\mathcal{X})$, then the system

$$\begin{aligned} du(x,t) &= \left(Au(x,t) + F(u)(x,t)\right)dt + Q^{\frac{1}{2}}dW_t, \\ u(\cdot,0) &= u_0 \in C(\mathcal{X}), \end{aligned}$$

for all $x \in \mathcal{X}$ and $t > 0$ has a unique mild solution $\mathbb{P}$-almost surely in $C([0,\infty), C(\mathcal{X}))$.

In the next theorem, we study the existence of a mild solution of an SPDE in the case of more general initial conditions compared to those in the previous theorems.

Theorem 2.2.6 ([65, Theorem 7.16])**.** *Under the assumptions of the previous theorem, assume that $A - a\,\mathrm{Id}$ and $F - b\,\mathrm{Id}$ are dissipative for certain $a, b \in \mathbb{R}$. Assume also that S has an extension $\tilde{S}$ to $L^2(\mathcal{X})$, that F has a continuous extension $\tilde{F}$ in $L^2(\mathcal{X})$ and that there exists $c > 0$ such that*

$$-\langle F(v) - F(w), v - w\rangle \geq c\,||v - w||^2$$

for all $v, w \in C(\mathcal{X})$. Moreover, consider the bounded function $f : [0,T] \to \mathbb{R}$ for $T > 0$. Then, the system

$$\begin{aligned} du(x,t) &= \left(Au(x,t) + F(u)(x,t) + f(t)u(x,t)\right)dt + Q^{\frac{1}{2}}dW_t, \\ u(\cdot,0) &= u_0 \in L^2(\mathcal{X}), \end{aligned}$$

has a unique mild solution for $T > 0$ that is $\mathbb{P}$-almost surely in

$$C([0,T]; L^2(\mathcal{X})) \cap L^2([0,T] \times \mathcal{X})$$

of the form

$$u(x,t) = S(t)u_0(x) + \int_0^t \tilde{S}(t-s)\left(\tilde{F}(u)(x,s) + f(s)u(x,s)\right)ds + \int_0^t e^{A(t-s)}Q^{\frac{1}{2}}dW_s,$$

for all $x \in \mathcal{X}$, $t \in [0,T]$ and $\mathbb{P}$-almost surely.

Theorem 2.2.6 concerns a non-autonomous SPDE. In Chapter 8, we apply this version of the theorem to analyse a fast–slow system, where we estimate the probability of leaving a neighborhood of a stable solution within a finite time interval. Such an event corresponds to the first stage of a critical transition.

2.2.2 Multiplicative noise

Under the definition of multiplicative noise, different typologies of stochastic perturbations are considered. Most cases assume the noise intensity to be state-dependent on the solution of an SPDE itself. In this thesis and in the theorems to follow, we restrict the study to our case of interest, in which the noise intensity scales linearly with the solution. In the next theorem, we discuss the existence and uniqueness of the mild solution of a linear SPDE with multiplicative noise of first degree.

Theorem 2.2.7 ([65, Theorem 6.24])**.** *Assume that the linear operator $A : \mathcal{H}_a \to \mathcal{H}_b$ generates a $\mathcal{C}_0$-contraction semigroup on $\mathcal{H}_a$ and that $Q : \mathcal{H}_a \to \mathcal{H}_a$ is a bounded non-negative linear diagonalisable self-ajoint operator. Then, the system*

$$\begin{aligned} \mathbf{d}u(x,t) &= Au(x,t)\mathbf{d}t + u(x,t)Q^{\frac{1}{2}}\mathbf{d}W_t, \\ u(\cdot,0) &= u_0 \in \mathcal{H}_a, \end{aligned}$$

for all $x \in \mathcal{X}$ and $t > 0$ admits a unique mild solution with continuous modification in $\mathcal{H}_a$.

In the theorem to follow, we discuss the existence of a strong solution for a linear SPDE with multiplicative noise of first degree. Similarly, to Theorem 2.2.4, the Q-Wiener process associated with the noise term perturbs the solution only along a finite number of modes.

Theorem 2.2.8 ([65, Theorem 6.29])**.** *Assume that the linear operator $A : \mathcal{H}_a \to \mathcal{H}_b$ generates a $\mathcal{C}_0$-contraction semigroup on $\mathcal{H}_a$ and that $Q : \mathcal{H}_a \to \mathcal{H}_a$ is a bounded non-negative linear diagonalisable self-ajoint operator with a finite number of positive operators. Then, the system*

$$\begin{aligned} \mathbf{d}u(x,t) &= Au(x,t)\mathbf{d}t + u(x,t)Q^{\frac{1}{2}}\mathbf{d}W_t, \\ u(\cdot,0) &= u_0 \in \mathcal{H}_a, \end{aligned}$$

for all $x \in \mathcal{X}$ and $t > 0$ has a strong solution in $\mathcal{H}_a$ in finite time intervals.

In the theorem below, we study the existence and uniqueness of a mild solution of a nonlinear SPDE. The nonlinear operator is assumed to be polynomial, thus restricting the family of models addressed.

Theorem 2.2.9 ([65, Theorem 7.19])**.** *Assume that the linear operator $A : \mathcal{H}_a \to \mathcal{H}_b$ generates a $\mathcal{C}_0$-contraction semigroup on $\mathcal{H}_a$, that $Q : \mathcal{H}_a \to \mathcal{H}_b$ is a bounded non-negative linear diagonalisable self-ajoint operator and that $F : \mathcal{H}_a \to \mathcal{H}_b$ is a polynomial operator of odd order and negative leading coefficient. If the stochastic convolution W_A has a $C(\mathcal{X})$-continuous version, then the system*

$$\begin{aligned} \mathbf{d}u(x,t) &= \left(Au(x,t) + F(u)(x,t)\right)\mathbf{d}t + u(x,t)Q^{\frac{1}{2}}\mathbf{d}W_t, \\ u(\cdot,0) &= u_0 \in \mathcal{H}_a, \end{aligned}$$

for all $x \in \mathcal{X}$ and $t > 0$ has a unique mild solution $\mathbb{P}$-almost surely in $L^2([0,T];\mathcal{H}_a)$ for any $T > 0$.

In this thesis, we rarely consider strong solutions of nonlinear SPDEs with multiplicative noise. An exception is in Chapter 9. For such a case, we refer to [65, Theorem 7.22] for the conditions for its existence.

2.2.3 Boundary noise

In the next theorem, we study the existence and construction of the mild solution of an SPDE perturbed by boundary additive noise. Therefore, we define $\mathcal{H}_1 = L^2(\mathcal{X})$ and $\mathcal{H}_0 = L^2(\partial\mathcal{X})$, which are the square-integrable space functions on the domain and on its boundary. For this example, we consider $Q : \mathcal{H}_0 \to \mathcal{H}_0$

and white noise $\dot{W}$ on the boundary and in time. For further background on the objects involved, see the next section.

Theorem 2.2.10 ([63, Theorem 2.3])**.** *Assume that the linear operator $A : \mathcal{H}_1 \to \mathcal{H}_1$ generates a $\mathcal{C}_0$-contraction semigroup on $\mathcal{H}_1$ and that $Q : \mathcal{H}_0 \to \mathcal{H}_0$ is a bounded non-negative linear diagonalisable self-ajoint operator. The boundary conditions operator is $\Gamma : \mathcal{H}_1 \to \mathcal{H}_0$ and the boundary continuous linear map $D : \mathcal{H}_0 \to \mathcal{H}_1$ is associated to A and Γ. This is meant in the sense that there exists a $q \in \mathbb{R}$ such that for any boundary value problem*

$$(A - q)w = 0 \quad , \quad \Gamma\, w = v \ ,$$

with $v \in \mathcal{H}_0$, there exists a unique solution $w = Dv \in \mathcal{D}(A) \subset \mathcal{H}_1$. We set $T > 0$ and $\alpha > 0$ such that

$$\int_0^T r^{-\alpha} \left|\left| Ae^{Ar} DQ \right|\right|^2_{\mathcal{L}(\mathcal{H}_0;\mathcal{H}_1)} dr < +\infty.$$

Then, the system

$$\begin{cases} du(x,t) &= Au(x,t)dt, \\ \Gamma u(\cdot,t) &= Q^{\frac{1}{2}}\dot{W}_t, \\ u(\cdot,0) &= u_0 \in \mathcal{H}_1, \end{cases}$$

has a mild solution in $\mathcal{H}_1$ in the form

$$u(\cdot,t) = e^{At}u_0 + (A_0 - q)\int_0^t e^{A(t-s)} DQ^{\frac{1}{2}} dW_s$$

for any $t \in [0,T]$ and $\mathbb{P}$-almost surely.

For an example of the construction of a solution of a nonlinear SPDE with additive boundary noise, we refer to [63, Section 4].

2.2.4 Itô-Stratonovich correction term

Throughout the majority of the thesis, we consider the noise in the Itô sense, i.e., the stochastic integral is defined by the limit

$$\int_0^t X_s \mathrm{d}W_s = \lim_{\delta \to 0} \sum_n X_{t_n} \left(W_{t_{n+1}} - W_{t_n} \right),$$

for $\{t_n\}_n$ that is a set of equidistant times of distance δ from 0 and to t. Such a form, while widely employed in applications, is not the only well-known interpretation in the literature [88]. One of the advantages of Itô calculus is the fact that the stochastic integral with respect to a Wiener process is a martingale. Nonetheless, a key property of deterministic calculus, the chain rule, is not satisfied. In fact, we introduce the Hilbert separable space $\mathcal{H}_a$, the linear operator $G_1 : \mathcal{H}_a \to \mathcal{H}_a$, the nonlinear operator $G_2 : \mathcal{H}_a \to \mathcal{H}_a$ and $u = u(x,t)$ the strong solution of

$$\mathrm{d}u(x,t) = G_1(u)(x,t)\mathrm{d}t + G_2(u)(x,t)Q^{\frac{1}{2}}\mathrm{d}W_t, \tag{2.2.1}$$

that assumes almost surely values in $\mathcal{H}_a$ for $t \in [0,T]$. Then, introducing $F : [0,T] \times \mathcal{H}_a \to \mathbb{R}$ and the uniform continuity on bounded sets of $\partial_t F, \partial_u F, \partial^2_{u^2} F$, the following equation holds:

$$F(t, u(\cdot,t)) = F(0, u(\cdot,0)) + \int_0^t \left\langle \partial_u F(s, u(\cdot,s)), G_2(u(\cdot,s))Q^{\frac{1}{2}}\mathrm{d}W_s \right\rangle_{\mathcal{H}_a}$$

$$+\int_0^t \partial_t F(s,u(\cdot,s)) + \langle \partial_u F(s,u(\cdot,s)), G_1(u(\cdot,s))\rangle_{\mathcal{H}_a}$$
$$+\frac{1}{2}\mathsf{Tr}\left(\partial^2_{u^2} F(s,u(\cdot,s)) G_2(u(\cdot,s))\left(G_2(u(\cdot,s))Q\right)^*\right)\mathsf{d}s.$$

This equation is often labelled as Itô's formula for SPDEs [65, Chapter 4]. In contrast, the Stratonovich interpretation, i.e.,

$$\int_0^t X_s \circ \mathsf{d}W_s = \lim_{\delta\to 0}\sum_n \frac{X_{t_{n+1}} - X_{t_n}}{2}\left(W_{t_{n+1}} - W_{t_n}\right),$$

satisfies the chain rule. This is to be interpreted in the sense that for u a strong solution of

$$\mathsf{d}u(x,t) = G_1(u)(x,t)\mathsf{d}t + G_2(u)(x,t)\circ Q^{\frac{1}{2}}\mathsf{d}W_t,$$

that assumes almost surely values in $\mathcal{H}_a$ for $t\in[0,T]$, then

$$F(t,u(\cdot,t)) = F(0,u(\cdot,0)) + \int_0^t \left\langle \partial_u F(s,u(\cdot,s)), G_2(u(\cdot,s))\circ Q^{\frac{1}{2}}\mathsf{d}W_s\right\rangle_{\mathcal{H}_a}$$
$$+\int_0^t \partial_t F(s,u(\cdot,s)) + \langle \partial_u F(s,u(\cdot,s)), G_1(u(\cdot,s))\rangle_{\mathcal{H}_a}\,\mathsf{d}s.$$

Although the interpretations differ, they can be translated through a correction term [192]. In fact, defining as $\{b_n\}_n$ an orthonormal base of $\mathcal{H}_a$ that diagonalizes Q with eigenvalues $\{\zeta_n\}_n$, the equation (2.2.1) is equivalent to

$$\mathsf{d}u = \left(G_1(u) - \frac{1}{2}\sum_n \zeta_n\left(\mathsf{D}_u G_2(u) G_2(u) b_n\right) b_n\right)\mathsf{d}t + G_2(u)\circ Q^{\frac{1}{2}}\mathsf{d}W_t,$$

for any $t\in[0,T]$. Consequently, the assumption of additive noise implies the equivalence of the Itô and Stratonovich interpretations. In Chapter 9, the noise term is characterised by $G_2(u) = u$. It follows then that the correction term is

$$-\frac{u}{2}\sum_n \zeta_n b_n^2.$$

We notice that the correction term assumes the opposite sign of u. In this chapter, the strong solution, which indicates turbulence along a pipe, is in fact defined as non-negative almost everywhere.

2.3 Further tools and notation

This section introduces the majority of the systems observed throughout the thesis and establishes further notation onward employed. The following framework allows for the modelling of spatially extended systems under the influence of stochastic perturbations. More concretely, we analyse the time evolution of a physical quantity u defined on a space domain under the influence of so-called white or red noise. We set the space domain $\mathcal{X}_1 \subset \mathbb{R}^N$ and the Hilbert space $\mathcal{H}_1 := L^2(\mathcal{X}_1)$ of possible solutions $u(x,t)$. We indicate the scalar product of this solution space as $\langle\cdot,\cdot\rangle$. The scalar product with respect to specific probing functions plays a central role in defining the concept of system variance, a potential early-warning sign of bifurcations. We focus on SPDEs on $\mathcal{X}_1$ with additive Gaussian noise or boundary Gaussian noise. As such, we define the boundary of $\mathcal{X}_1$ as $\mathcal{X}_0 := \partial\mathcal{X}_1$, and we label $\mathcal{H}_0 := L^2(\mathcal{X}_0)$. For $\kappa>0$, $\sigma>0$ and $j\in\{0,1\}$, we define the Ornstein-Uhlenbeck process $\xi_j = \xi_j(x,t)$ that solves

$$\mathsf{d}\xi_j(x,t) = -\kappa\xi_j(x,t)\mathsf{d}t + \sigma Q_j^{\frac{1}{2}}\mathsf{d}W_t^j, \tag{2.3.1}$$

for any $x \in \mathcal{X}_j$ and $t > 0$. Such a process is often referred to in the literature as red noise [101, 102, 143, 157, 166]. This is implied by the fact that its power spectral density is weighted most heavily in the low (red) frequencies. The constant $\kappa > 0$ controls the characteristic correlation time $1/\kappa$ of the noise. The smaller κ, the longer it takes for correlations in the noise to decay. For any $j \in \{0, 1\}$, i.e., either boundary or domain noise, the noise term is composed as follows: Q_j is a positive (unless stated otherwise) self-adjoint operator in $\mathcal{H}_j$ with real eigenvalues $\{\zeta_i\}_{i\in\mathbb{N}_{>0}}$ that are bounded from below by $c > 0$ and corresponding eigenbasis $\{b_i\}_{i\in\mathbb{N}_{>0}}$ of $\mathcal{H}_j$. The operator Q_j can be thought of as attributing varying finite noise amplitudes to all modes b_i on the domain of interest. The stochastic component itself is the cylindrical Wiener process W_t^j, which can be written as

$$W_t^j = W^j(x,t) = \sum_{n=1}^{\infty} b_n^j(x)\beta_n(t),$$

for the family of independent scalar Wiener processes $\{\beta_n\}_{n\in\mathbb{N}_{>0}}$. Its differential is then given as

$$\mathsf{d}W_t^j = \sum_{n=1}^{\infty} b_n^j(x)\mathsf{d}\beta_n(t).$$

The noise is induced by a Q_j-Wiener process [65]. Consequently, for every fixed $x \in \mathcal{X}_j$, $\xi_j(x,t)$ is a regular N-dimensional Ornstein-Uhlenbeck process. We study six SPDEs and their respective associated solution $u = u(x,t)$. In the case of red noise, the processes ξ_0 and ξ_1 are considered to be perturbations in the system that define u. Their intensity is indicated by $\sigma_{\mathsf{R}} > 0$.

(a) First, we consider $u^{(\mathsf{w,d})} = u^{(\mathsf{w,d})}(x,t)$, the mild solution of the following SPDE with white noise

$$\begin{cases} \mathsf{d}u^{(\mathsf{w,d})}(x,t) = A_0(p)u^{(\mathsf{w,d})}(x,t)\mathsf{d}t + \sigma Q_1^{\frac{1}{2}}\mathsf{d}W_t^1, \\ u^{(\mathsf{w,d})}(x,0) = u_0(x) \in \mathcal{H}_1, \end{cases} \tag{2.3.2}$$

for any $x \in \mathcal{X}_1$ and $t > 0$. The operators $A_0(p)$ and $A_0(p)^*$ are assumed to be closed and densely defined in $\mathcal{H}_1$. The linear and purely discrete operator $A_0(p)$ is assumed to be negative for $p < 0$ with eigenvalues

$$0 > \mathrm{Re}\left(\lambda_1^{(p)}\right) > \mathrm{Re}\left(\lambda_2^{(p)}\right) \geq \mathrm{Re}\left(\lambda_3^{(p)}\right) \geq \ldots,$$

which are assumed to be continuous in p. This constitutes a linearly stable system. A loss of linear stability occurs whenever at least one eigenvalue crosses the imaginary axis. This is a generic occurrence in bifurcating dynamical systems. We assume that the eigenvalue $\lambda_1^{(p)}$ is the only one to reach the imaginary axis at $p = 0$. We use m_a to indicate the algebraic multiplicity of an eigenvalue. For simplicity, their geometric multiplicity is set to 1.

(b) We consider the SPDE with domain noise ξ_1,

$$\begin{cases} \mathsf{d}u^{(\mathsf{r,d})}(x,t) = \left(A_0(p)u^{(\mathsf{r,d})}(x,t) + \sigma_{\mathsf{R}}\xi_1(x,t)\right)\mathsf{d}t, \\ u^{(\mathsf{r,d})}(x,0) = u_0(x) \in \mathcal{H}_1, \end{cases} \tag{2.3.3}$$

for any $x \in \mathcal{X}_1$ and $t > 0$. The purely discrete operator, linear $A_0(p)$, is assumed as in the previous case. The function $u^{(\mathsf{r,d})}$ is the mild solution of the linear equation under the influence of red noise that is added on every point x within the domain $\mathcal{X}_1$.

(c) As a third case, we consider $u^{(\mathsf{w,c})} = u^{(\mathsf{w,c})}(x,t)$, the mild solution of

$$\begin{cases} \mathsf{d}u^{(\mathsf{w,c})}(x,t) = f(x,p)u^{(\mathsf{w,c})}(x,t)\mathsf{d}t + \sigma Q_1^{\frac{1}{2}}\mathsf{d}W_t^1, \\ u^{(\mathsf{w,c})}(0,x) = u_0(x) \in \mathcal{H}_1, \end{cases} \tag{2.3.4}$$

for $x \in \mathcal{X}_1$ and $t > 0$. The function $f : \mathcal{X}_1 \times \mathbb{R}_{<0} \to \mathbb{R}_{<0}$ is assumed to be analytic. For a fixed x_*, the function satisfies

$$f(x,p) < 0 \quad \text{and} \quad f(x_*,0) = 0,$$

for any $(x,p) \in \mathcal{X}_1 \times \mathbb{R}_{\leq 0} \setminus \{(x_*,0)\}$. In contrast to $A_0(p)$, the multiplication operator $T_f = f$ can have a continuous spectrum. The implications of the assumptions on f are discussed further in the thesis.

(d) As a fourth case, we study $u^{(\mathsf{r,c})} = u^{(\mathsf{r,c})}(x,t)$, which is the mild solution of

$$\begin{cases} \mathsf{d}u^{(\mathsf{r,c})}(x,t) = \left(f(x,p)u^{(\mathsf{r,c})}(x,t) + \sigma_{\mathsf{R}}\xi_1(x,t)\right)\mathsf{d}t, \\ u^{(\mathsf{r,c})}(0,x) = u_0(x) \in \mathcal{H}_1, \end{cases} \tag{2.3.5}$$

for $x \in \mathcal{X}_1$ and $t > 0$. The function $f : \mathcal{X}_1 \times \mathbb{R}_{<0} \to \mathbb{R}_{<0}$ is assumed as above. In this case, we consider for simplicity values of $p < 0 < \kappa$ such that

$$f(x,p) + \kappa \neq 0$$

for any $x \in \mathcal{X}_1$.

(e) We study the SPDE of the form

$$\begin{cases} \mathsf{d}u^{(\mathsf{w,b})}(x,t) = A(p)u^{(\mathsf{w,b})}(x,t)\mathsf{d}t, \\ u^{(\mathsf{w,b})}(0,x) = u_0(x) \in \mathcal{H}_1, \end{cases} \tag{2.3.6}$$

for $x \in \mathcal{X}_1$ and

$$\Gamma(p)u^{(\mathsf{w,b})}(x,t) = \sigma Q_0^{\frac{1}{2}}\dot{W}_t^0,$$

on the boundary $x \in \mathcal{X}_0$ and $t > 0$. The deterministic versions of (2.3.2) and (2.3.6) are assumed to be equivalent. In this case, we are investigating the effect of setting noise on the boundary of the space domain. The linear operator

$$\Gamma(p) : \mathcal{D}\left(\Gamma(p)\right) \subset \mathcal{H}_1 \to \mathcal{H}_0$$

defines the boundary conditions. As stated in Theorem 2.2.10, this setting requires the use of a boundary map for the computation of its mild solution $u^{(\mathsf{w,b})} = u^{(\mathsf{w,b})}(x,t)$.

(f) Lastly, we study the mild solution $u^{(\mathsf{r,b})} = u^{(\mathsf{r,b})}(x,t)$ of

$$\begin{cases} \mathsf{d}u^{(\mathsf{r,b})}(x,t) = A(p)u^{(\mathsf{r,b})}(x,t)\mathsf{d}t, \\ u^{(\mathsf{r,b})}(0,x) = u_0(x) \in \mathcal{H}_1, \end{cases} \tag{2.3.7}$$

for $x \in \mathcal{X}_1$ and

$$\Gamma(p)u^{(\mathsf{r,b})}(x,t) = \sigma_{\mathsf{R}}\xi_0(x,t),$$

on the boundary $x \in \mathcal{X}_0$ and $t > 0$. The deterministic part and the boundary operators of (2.3.7) share the same properties as those of the previously considered case.

In order to simplify the notation, we indicate in the next chapter as Q, W and $\{b_n\}_n$ the components of the Q-Wiener process regardless of the space considered. The only exception is Chapter 6, wherein additive and boundary noise are considered.

Following [93, 135], we aim to construct early-warning signs for the approaches $p \to 0^-$ and $\kappa \to 0^+$, respectively. On such thresholds, the dissipativity in the linear system that defines u and ξ is lost, and the origin in $\mathcal{H}_1$, or $\mathcal{H}_1 \times \mathcal{H}_1$, including the red noise perspective, is not a stable deterministic equilibrium. However, the two limit cases have very different physical interpretations. While the $p \to 0^-$ limit is a stand-in for dynamical bifurcations of non-linear systems, $\kappa \to 0^+$ represents a change in the characteristics of the driving noise. In the context of, e.g., climate tipping points, only the former limit would be of interest. We aim to find an early-warning sign in the system variance with respect to different probing functions. For a probing function that is not orthogonal to a destabilising mode, we would conventionally expect variance to increase. We define the covariance as Cov. In cases (a), (c) and (e), we define the linear covariance operator as $V_t^{\mathsf{w}} : \mathcal{D}\left(V_t^{\mathsf{w}}\right) \subset \mathcal{H}_1 \to \mathcal{H}_1$ for which

$$\langle v, V_t^{\mathsf{w}} w \rangle = \mathsf{Cov}\left(\langle u(\cdot,t), v\rangle, \langle \xi_1(\cdot,t), w\rangle\right), \tag{2.3.8}$$

for $v, w \in \mathcal{H}_1$. In case (b) and (d), we set the linear covariance operator $V_t^{(\mathsf{r},1)} : \mathcal{D}\left(V_t^{(\mathsf{r},1)}\right) \subset \mathcal{H}_{(1,1)} \to \mathcal{H}_{(1,1)}$ and $\mathcal{H}_{(1,1)} := \mathcal{H}_1 \times \mathcal{H}_1$, such that

$$\left\langle \begin{pmatrix} v_1 \\ v_2 \end{pmatrix}, V_t^{(\mathsf{r},1)} \begin{pmatrix} w_1 \\ w_2 \end{pmatrix} \right\rangle_{\mathcal{H}_{(1,1)}} = \mathsf{Cov}\left(\left\langle \begin{pmatrix} u(\cdot,t) \\ \xi_1(\cdot,t) \end{pmatrix}, \begin{pmatrix} v_1 \\ v_2 \end{pmatrix} \right\rangle_{\mathcal{H}_{(1,1)}}, \left\langle \begin{pmatrix} u(\cdot,t) \\ \xi_1(\cdot,t) \end{pmatrix}, \begin{pmatrix} v_1 \\ v_2 \end{pmatrix} \right\rangle_{\mathcal{H}_{(1,1)}} \right), \tag{2.3.9}$$

for $v_1, v_2, w_1, w_2 \in \mathcal{H}_1$. Since we are solely interested in the covariance on variable u, we set $v_2 = w_2 \equiv 0$. In case (f), the boundary noise requires the different definition $V_t^{(\mathsf{r},0)} : \mathcal{D}\left(V_t^{(\mathsf{r},0)}\right) \subset \mathcal{H}_{(1,0)} \to \mathcal{H}_{(1,0)}$, for $\mathcal{H}_{(1,0)} := \mathcal{H}_1 \times \mathcal{H}_0$, and

$$\left\langle \begin{pmatrix} v_1 \\ v_2 \end{pmatrix}, V_t^{(\mathsf{r},0)} \begin{pmatrix} w_1 \\ w_2 \end{pmatrix} \right\rangle_{\mathcal{H}_{(1,0)}} = \mathsf{Cov}\left(\left\langle \begin{pmatrix} u(\cdot,t) \\ \xi_0(\cdot,t) \end{pmatrix}, \begin{pmatrix} v_1 \\ v_2 \end{pmatrix} \right\rangle_{\mathcal{H}_{(1,0)}}, \left\langle \begin{pmatrix} u(\cdot,t) \\ \xi_0(\cdot,t) \end{pmatrix}, \begin{pmatrix} v_1 \\ v_2 \end{pmatrix} \right\rangle_{\mathcal{H}_{(1,0)}} \right), \tag{2.3.10}$$

for $v_1, w_1 \in \mathcal{H}_1$ and $v_2, w_2 \in \mathcal{H}_0$. We define the time-asymptotic covariance operator as the limits $V_\infty^{\mathsf{w}} = \lim_{t\to\infty} V_t^{\mathsf{w}}$ and $V_\infty^{(\mathsf{r},\mathsf{j})} = \lim_{t\to\infty} V_t^{(\mathsf{r},\mathsf{j})}$ for $j \in \{0,1\}$. Such an observable is employed in the next section to construct early-warning signs, and its definition is extended for solutions of nonlinear SPDEs in equivalent spaces. They are defined as its rate of divergence in the limits $p \to 0^-$ and $\kappa \to 0^+$. As such, we recall the Landau notation

$$\begin{aligned}
r_1(p,\kappa) = \Theta_p\left(r_2(p,\kappa)\right) &\iff \lim_{p\to 0^-} \frac{r_1(p,\kappa)}{r_2(p,\kappa)} \in (0,+\infty), \\
r_1(p,\kappa) = \mathcal{O}_p\left(r_2(p,\kappa)\right) &\iff \lim_{p\to 0^-} \frac{r_1(p,\kappa)}{r_2(p,\kappa)} \in [0,+\infty), \\
r_1(p,\kappa) = \Theta_\kappa\left(r_2(p,\kappa)\right) &\iff \lim_{\kappa\to 0^+} \frac{r_1(p,\kappa)}{r_2(p,\kappa)} \in (0,+\infty), \\
r_1(p,\kappa) = \mathcal{O}_\kappa\left(r_2(p,\kappa)\right) &\iff \lim_{\kappa\to 0^+} \frac{r_1(p,\kappa)}{r_2(p,\kappa)} \in [0,+\infty), \\
r_1(p,\kappa) = \Theta\left(r_2(p,\kappa)\right) &\iff \lim_{(p,\kappa)\to(0,0)} \frac{r_1(p,\kappa)}{r_2(p,\kappa)} \in (0,+\infty), \\
r_1(p,\kappa) = \mathcal{O}\left(r_2(p,\kappa)\right) &\iff \lim_{(p,\kappa)\to(0,0)} \frac{r_1(p,\kappa)}{r_2(p,\kappa)} \in [0,+\infty),
\end{aligned}$$

for any pair of locally continuous functions $r_1 : \mathbb{R}_{<0} \times \mathbb{R}_{>0} \to \mathbb{R}_{>0}$ and $r_2 : \mathbb{R}_{<0} \times \mathbb{R}_{>0} \to \mathbb{R}_{>0}$. In essence, the Θ equivalence is a stronger asymptotic characteristic than the standard $\mathcal{O}$ equivalence, since it implies boundedness of the ratio and its inverse.

Part I

Bifurcation-induced Tipping: Early-Warning Signs for Loss of Stability

3 Time-asymptotic variance for purely discrete spectrum in drift operator

Stochastic dynamics are widely used in applied fields to model real-world systems. In this context, stochastic fluctuations can help identify early-warning signals for abrupt transitions. The content of this chapter is based on work presented in the publication [23] and extends a well-known early-warning sign for SDEs [73] to SPDEs of the type

$$\begin{cases} \mathrm{d}u(x,t) = (\Delta u(x,t) - g(x)u(x,t) + pu(x,t) - u(x,t)^3)\,\mathrm{d}t + \sigma\, Q^{\frac{1}{2}}\mathrm{d}W_t, \\ u(\cdot,0) = u_0 \in \mathcal{H}_1 = L^2(\mathcal{X}_1), \\ u(0,t) = u(L,t) = 0, \end{cases} \tag{3.0.1}$$

for all $t \in \mathbb{R}$, $x \in \mathcal{X}_1 = [0, L]$, critical parameter $p < 0$ and for a bounded and continuous almost everywhere positive function g. We consider the operator Q to be bounded. We define $A(p) = A + p$ and indicate the ordered eigenvalues of $A = \Delta - g$ as $\{\lambda_n\}_{n\in\mathbb{N}_{>0}}$ and the corresponding eigenfunctions as $\{e_n\}_{n\in\mathbb{N}_{>0}}$. The eigenfunctions of the operator Δ are $\{e'_n\}_{n\in\mathbb{N}_{>0}}$ and the corresponding eigenvalues $\left\{\lambda'_n := -\left(\frac{\pi n}{L}\right)^2\right\}_{n\in\mathbb{N}_{>0}}$. The observable takes the form of the increase of time-asymptotic variance along proxy functions. The reliability of such an indicator is proven on the linearised system on the null function, on which the observable diverges in the proximity to a bifurcation threshold. It is then numerically applied to the original system, and its application is justified by the comparison of its effectiveness on the models. This type of SPDEs, the stochastic Chafee-Infante equations [50], have been employed to model dynamics in numerous applications, e.g., in climate systems [69]. We include a heterogeneous term in space g to address the heterogeneity of applied models and to account for local minor effects in the phenomena addressed. While this does not qualitatively affect the structure of the bifurcation diagram, it shifts the sensitive modes and the bifurcation thresholds (see also Appendix A). In fact, the deterministic heterogeneous system (3.0.1), i.e., with $\sigma = 0$, inherits some properties from the classical spatially homogeneous PDE, as discussed below.

Proposition 3.0.1 ([105, Theorem 5.1.1])**.** *Set $u_* \in \mathcal{H}_1$. Suppose that $H : \mathcal{D}(H) \subset \mathcal{H}_1 \to \mathcal{H}_1$ is a sectorial linear operator and that $F : \mathcal{U} \to \mathcal{H}_1$ is a locally Lipschitz operator so that $\mathcal{U}$ is a neighbourhood of u_* and that*

$$F(u_* + v) = F(u_*) + Bv + G(v)$$

with $u_* + v \in \mathcal{U}$, $B \in \mathcal{L}_b(\mathcal{H}_1)$ with $\mathcal{L}_b(\mathcal{H}_1)$ denoting bounded linear operators on $\mathcal{H}_1$, $G : \mathcal{U} \to \mathcal{H}_1$ and $\|G(u)\| \le c\|u\|^{\gamma}_{\mathcal{W}^{1,2}(\mathcal{X}_1)}$ for $\gamma > 1$, any $u \in \mathcal{W}^{1,2}(\mathcal{X}_1)$ and a constant $c > 0$. Assume that $Hu_* = F(u_*)$ and that the spectrum of $B - H$ is in $\{\lambda \in \mathbb{C} : Re(\lambda) < -\epsilon\}$ for a $\epsilon > 0$, then u_* is a locally asymptotically stable steady state of the evolution equation $\dot{u} = F(u) - Hu$.

By Proposition 3.0.1, it is clear that the zero function is an asymptotically stable steady state of (3.0.1) with $\sigma = 0$ when $p < -\lambda_1$. In fact, for this parameter range, it is also the only steady state by the strict negativity of $A = \Delta - g$ and the strict dissipativity given by F. When $p > -\lambda_1$, the stability setting changes. The next proposition describes such a case.

Proposition 3.0.2 ([105, Corollary 5.1.6])**.** *Set u_*, H and F as in Proposition 3.0.1. Assume $Hu_* = F(u_*)$ and that the spectrum of $B - H$ has non-empty intersection with $\{\lambda \in \mathbb{C} : Re(\lambda) > \epsilon\}$ for an $\epsilon > 0$. Then, u_* is an unstable steady state of $\dot{u} = F(u) - Hu$.*

This latest result can be applied to show that the zero function is unstable for $p > -\lambda_1$. As such, the early warning sign aims to predict the approach of p to $-\lambda_1$ and the consequential loss of stability. Nonetheless, the global dissipativity still implies the existence of a compact attractor [105, Section 5.3]. The next theorem [60] establishes the bifurcation of near steady states from the trivial branch of zero solutions when p crosses a bifurcation point.

Theorem 3.0.3 (Crandall-Rabinowitz Theorem)**.** *Set $\mathcal{X}$ and $\mathcal{Y}$ Banach spaces, $u_* \in \mathcal{X}$ and $\mathcal{U}$ neighbourhood of $(u_*, 0)$ in $\mathcal{X} \times \mathbb{R}$. Let $F : \mathcal{U} \subset \mathcal{X} \times \mathbb{R} \to \mathcal{Y}$ be a C^3 function in $(u_*, 0)$ with $F(u_*, p_*) = 0$ for all $p_* \in (-\delta, \delta)$ for $\delta > 0$. Suppose the linearisation $G := \mathsf{D}_{u_*} F(\cdot, 0)$ is a Fredholm operator (with index zero). Assume that $\dim(\mathsf{Ker}(G)) = 1$, $\mathsf{Ker}(G) = \mathsf{Span}\{\phi_0\}$ and $\mathsf{D}_{p=0}\mathsf{D}_{u_*} F\phi_0 \notin \mathsf{Range}(G)$. Then, $(u_*, 0)$ is a bifurcation point and there exists a C^1 curve $s \mapsto (\phi(s), \tilde{p}(s))$, for s in a small interval, that passes through $(u_*, 0)$ so that*

$$F(\phi(s), \tilde{p}(s)) = 0. \tag{3.0.2}$$

In a sufficiently small neighbourhood $\mathcal{U}$ the only solutions to (3.0.2) *are the map $s \mapsto (\phi(s), \tilde{p}(s))$ and the trivial curve $\{(u_*, p) : (u_*, p) \in \mathcal{U}\}$.*

A proof of the last result can be found in [105, Lemma 6.3.1, Theorem 6.3.2] and [133, Theorem 5.1]. For $\mathcal{Y} = \mathcal{H}_1$, the space $\mathcal{X}$ generated by $\{e_k\}_{k \in \mathbb{N}_{>0}}$, the normalised eigenfunctions of $\Delta - g$, and given the nonlinear operator

$$F(u) = \Delta u - gu + pu - u^3,$$

then the Crandall-Rabinowitz theorem implies the existence of a bifurcation, which can be shown to be of pitchfork type, at $p + \lambda_k = 0$ and in $u_* \equiv 0$. It can also be proven similarly that the new steady states that arise at $k = 1$ are locally asymptotically stable. Furthermore, while the most important change in the system happens when p crosses $-\lambda_1$, the dimension of the unstable manifold associated with the null function increases by 1 at each $p = -\lambda_n$. This indicates a self-similarity in the bifurcations.
The spectrum of the drift operator is discrete, so we can find a set of basis functions (modes) of $\mathcal{H}_1$ composed of eigenfunctions to use as proxy functions along which the early-warning sign is studied. We notice that the boundary conditions, along with the deterministic components in the system, imply the existence of an optimal region of observation of the warning sign. Lastly, we obtain a family of observables that can predict sudden changes with limited knowledge of the system, e.g. missing data, following from to the completeness of $\mathcal{H}_1$.

3.1 Early-warning signs for the linearised system

The publications [93, 135] introduce early-warning signs for SPDEs that are based on the covariance operator of the linearised system, extending the employment of standard observables for SDEs [73]. The reliability of such an approximation is justified by estimates of the higher-order terms, which we consider further in the thesis. The linearised problem on the null solution is given by

$$\begin{cases} \mathsf{d}u^{(\mathsf{w},\mathsf{d})} = A(p)u^{(\mathsf{w},\mathsf{d})}\,\mathsf{d}t + \sigma\, Q^{\frac{1}{2}}\mathsf{d}W_t, \\ u^{(\mathsf{w},\mathsf{d})}(\cdot, 0) = u_0 \in \mathcal{H}_1, \end{cases} \tag{3.1.1}$$

for $t > 0$, $x \in \mathcal{X}_1$, $p < -\lambda_1$ and with Dirichlet boundary conditions. We note that $A(p)$ generates a $\mathcal{C}_0$-contraction semigroup (see Appendix B).
In order to prove the existence and uniqueness of the mild solution of (3.0.1), we employ Theorem 2.2.5. Moreover, to show that it is in $L^2(\Omega, \mathcal{F}, \mathbb{P}; \mathcal{H}_1)$ for any $t > 0$, we require continuity in $\mathcal{H}_1$ of the solution of (3.1.1). Hence, we assume the following conditions for Q (see Appendix B, Theorem 2.2.1 and Theorem 2.2.6):

(M1) there exists a constant $d_0 > 0$ such that the eigenfunctions of Q satisfy $b_j = e'_j$ for all $j > d_0$;

(M2) the eigenvalues $\{\zeta_j\}_{j\in\mathbb{N}_{>0}}$ corresponding to $\{b_j\}_{j\in\mathbb{N}_{>0}}$ are positive and satisfy $\sum_{j=1}^{\infty}\zeta_j(-\lambda_j')^{\gamma} < +\infty$ for a constant $\gamma > -1$.[1]

We can then conclude ([64, Theorem 2.34] and Theorem 2.2.1) that the transition semigroup of the system (3.1.1) has a unique invariant measure. Furthermore, it is Gaussian and has mean zero and covariance operator $V_\infty^{\mathsf{W}} := \lim_{t\to\infty} V_t^{\mathsf{W}}$. Such an operator is linear, self-adjoint, non-negative, and continuous in $\mathcal{H}_1$. Using the stated properties, it is possible to prove the following proposition and define a first early-warning sign through spectral analysis, building upon the paper [135].

Proposition 3.1.1. *Consider any pair of linear operators A and Q that satisfy the properties* (M1)*,* (M2)*, and assume $A(p) = A + p$ self-adjoint operator that generates a $\mathcal{C}_0$-contraction semigroup for a fixed $p \in \mathbb{R}$. Then, the covariance operator V_∞^{W} given by the first equation in* (3.1.1) *satisfies*

$$\langle V_\infty^{\mathsf{W}} e_{j_1}, e_{j_2}\rangle = \frac{-\sigma^2}{\lambda_{j_1}+\lambda_{j_2}+2p}\sum_{n=1}^{\infty}\zeta_n\langle e_{j_1}, b_n\rangle\langle e_{j_2}, b_n\rangle \tag{3.1.2}$$

for all $j_1, j_2 \in \mathbb{N}_{>0}$.

Proof. First, we consider the Lyapunov equation derived in [64, Lemma 2.45] and obtain

$$\langle A(p)V_\infty^{\mathsf{W}} f_1, f_2\rangle + \langle A(p)^* f_1, V_\infty^{\mathsf{W}} f_2\rangle = -\sigma^2\langle f_1, Q f_2\rangle \tag{3.1.3}$$

for all $f_1, f_2 \in \mathcal{H}_1$. From the self-adjointness of $A(p)$ and V_∞^{W}, for any $j_1, j_2 \in \mathbb{N}_{>0}$ we deduce that

$$\langle A(p)V_\infty^{\mathsf{W}} e_{j_1}, e_{j_2}\rangle + \langle A(p)e_{j_1}, V_\infty^{\mathsf{W}} e_{j_2}\rangle = (\lambda_{j_1}+\lambda_{j_2}+2p)\langle V_\infty^{\mathsf{W}} e_{j_1}, e_{j_2}\rangle.$$

We can then obtain the relation (see Appendix C)

$$\begin{aligned}
\langle V_\infty^{\mathsf{W}} e_{j_1}, e_{j_2}\rangle =& \frac{-\sigma^2}{\lambda_{j_1}+\lambda_{j_2}+2p}\langle e_{j_1}, Q e_{j_2}\rangle \\
=& \frac{-\sigma^2}{\lambda_{j_1}+\lambda_{j_2}+2p}\sum_{n=1}^{\infty}\langle e_{j_1}, b_n\rangle\langle b_n, Q e_{j_2}\rangle \\
=& \frac{-\sigma^2}{\lambda_{j_1}+\lambda_{j_2}+2p}\sum_{n=1}^{\infty}\langle e_{j_1}, b_n\rangle\sum_{m=1}^{\infty}\langle b_n, b_m\rangle\langle b_m, Q e_{j_2}\rangle \\
=& \frac{-\sigma^2}{\lambda_{j_1}+\lambda_{j_2}+2p}\sum_{n=1}^{\infty}\langle e_{j_1}, b_n\rangle\langle b_n, Q e_{j_2}\rangle \\
=& \frac{-\sigma^2}{\lambda_{j_1}+\lambda_{j_2}+2p}\sum_{n=1}^{\infty}\zeta_n\langle e_{j_1}, b_n\rangle\langle e_{j_2}, b_n\rangle,
\end{aligned}$$

which concludes the proof. □

The early-warning sign is qualitatively visible for $j_1 = j_2 = 1$ as (3.1.2) diverges in the limit $p + \lambda_1 \to 0$. In applications, this allows us to apply standard techniques (such as extracting a scaling law from a log-log plot) to estimate the bifurcation threshold, if sufficient data from the system is available. We also note that the statement can easily be extended to operators A that are not self-adjoint by studying, in that case, the real parts of their eigenvalues. Additionally, the strict positivity of Q can be substituted by non-negativity of the operator, although then the divergence by the $j_1 = j_2 = 1$ component is not implied. The early-warning sign in Proposition 3.1.1 is extended in the following theorem to a wider variety of proxy functions.

[1] From the order of divergence of $\{\lambda_j'\}_j$, the assumption is satisfied by bounded Q and $-1 < \gamma < -\frac{1}{2}$. Moreover, strict positivity of the $\{\zeta_j\}_j$ is not required but avoids further assumptions. A description of the case in which non-negativity of the spectrum is assumed is discussed separately in the relevant sections.

Theorem 3.1.2. *For any pair of linear operators A and Q that satisfy the properties stated in Proposition 3.1.1 and for A whose eigenfunctions $\{e_k\}_{k\in\mathbb{N}_{>0}}$ form a basis of $\mathcal{H}_1$, it holds*

$$\langle V_\infty^{\mathsf{w}} f_1, f_2\rangle = -\sigma^2 \sum_{j_1=1}^{\infty}\sum_{j_2=1}^{\infty} \frac{\langle f_1, e_{j_2}\rangle\langle f_2, e_{j_1}\rangle}{\lambda_{j_1}+\lambda_{j_2}+2p}\left(\sum_{n=1}^{\infty}\zeta_n\langle e_{j_1}, b_n\rangle\langle e_{j_2}, b_n\rangle\right), \tag{3.1.4}$$

for any $f_1, f_2 \in \mathcal{H}_1$.

Proof. Applying the splitting method described in Appendix C and the previous proposition, we obtain

$$\begin{aligned}\langle V_\infty^{\mathsf{w}} f_1, f_2\rangle &= \sum_{j_1=1}^{\infty}\langle V_\infty^{\mathsf{w}} f_1, e_{j_1}\rangle\langle e_{j_1}, f_2\rangle = \sum_{j_1=1}^{\infty}\langle f_1, V_\infty^{\mathsf{w}} e_{j_1}\rangle\langle e_{j_1}, f_2\rangle\\ &= \sum_{j_1=1}^{\infty}\sum_{j_2=1}^{\infty}\langle f_1, e_{j_2}\rangle\langle e_{j_2}, V_\infty^{\mathsf{w}} e_{j_1}\rangle\langle e_{j_1}, f_2\rangle\\ &= -\sigma^2 \sum_{j_1=1}^{\infty}\sum_{j_2=1}^{\infty} \frac{\langle f_1, e_{j_2}\rangle\langle f_2, e_{j_1}\rangle}{\lambda_{j_1}+\lambda_{j_2}+2p}\left(\sum_{n=1}^{\infty}\zeta_n\langle e_{j_1}, b_n\rangle\langle e_{j_2}, b_n\rangle\right).\end{aligned}$$

□

Theorem 3.1.2 implies that, given f_1 and f_2 that are not orthogonal to e_1, the resulting scalar product $\langle V_\infty^{\mathsf{w}} f_1, f_2\rangle$ diverges in $p = -\lambda_1$. Theorem 3.1.2 can describe local behaviour under the assumption that f_1 and f_2 have support on a small region of the interval. Moreover, it can also be used to study the effect of stochastic perturbations on a single point $x_0 \in \mathring{\mathcal{X}}_1$. This can be achieved by considering

$$f_1 = f_2 = f_\epsilon = \frac{1}{\epsilon}\mathbb{1}_{[x_0-\frac{\epsilon}{2}, x_0+\frac{\epsilon}{2}]}\Big|_{\mathcal{X}_1} \in \mathcal{H}_1 \text{ for } 0<\epsilon\ll 1, \tag{3.1.5}$$

for $\mathbb{1}_{[\cdot,\cdot]}$ meant as the indicator function on an interval. Clearly, f_ϵ is in $L^1(\mathcal{X}_1)$ and in $L^2(\mathcal{X}_1)$ for any $\epsilon > 0$. The L^1-norm is equal to 1 for small ϵ and the sequence $\{f_\epsilon\}_\epsilon$ converges weakly in $L^1(\mathcal{X}_1)$ to the Dirac delta in x_0 for $\epsilon \to 0$. Consequently, and recalling that $\{e_j\}_{j\in\mathbb{N}_{>0}} \subset \mathcal{W}_0^{1,2}(\mathcal{X}_1) \subset L^\infty(\mathcal{X}_1)$ by the Sobolev inequality, we compute $\lim_{\epsilon\to 0}\langle V_\infty^{\mathsf{w}} f_\epsilon, f_\epsilon\rangle$.

Corollary 3.1.3. *Consider any pair of linear operators A and Q with the same properties as required in Theorem 3.1.2 and $\{f_\epsilon\}$ defined in* (3.1.5)*. Then,*

$$\lim_{\epsilon\to 0}\langle V_\infty^{\mathsf{w}} f_\epsilon, f_\epsilon\rangle = -\sigma^2 \sum_{j_1=1}^{\infty}\sum_{j_2=1}^{\infty} \frac{e_{j_1}(x_0)e_{j_2}(x_0)}{\lambda_{j_1}+\lambda_{j_2}+2p}\left(\sum_{n=1}^{\infty}\zeta_n\langle e_{j_1}, b_n\rangle\langle e_{j_2}, b_n\rangle\right), \tag{3.1.6}$$

for all $x_0 \in \mathring{\mathcal{X}}_1$.

Proof. We fix $x_0 \in \mathring{\mathcal{X}}_1$. The goal of this proof is to show that the series in (3.1.4) satisfies the dominated convergence hypothesis for $f_1 = f_2 = f_\epsilon$ for all $0 < \epsilon$. In order to achieve it, we bound the series

$$\begin{aligned}\langle V_\infty^{\mathsf{w}} f_\epsilon, f_\epsilon\rangle &= \sum_{j_1=1}^{\infty}\sum_{j_2=1}^{\infty}\left|\frac{\langle f_\epsilon, e_{j_1}\rangle\langle f_\epsilon, e_{j_2}\rangle}{\lambda_{j_1}+\lambda_{j_2}+2p}\langle e_{j_1}, Qe_{j_2}\rangle\right| \\ &\le \frac{1}{2}\sum_{j=1}^{\infty}\left|\frac{\langle f_\epsilon, e_j\rangle^2}{\lambda_j+p}\langle e_j, Qe_j\rangle\right| + \sum_{j_1=1}^{\infty}\sum_{j_2\neq j_1}\left|\frac{\langle f_\epsilon, e_{j_1}\rangle\langle f_\epsilon, e_{j_2}\rangle}{\lambda_{j_1}+\lambda_{j_2}+2p}\langle e_{j_1}, Qe_{j_2}\rangle\right|.\end{aligned} \tag{3.1.7}$$

We then prove that the summands in the right-hand side are uniformly bounded in $p < 0$ in two corresponding parts.

Part 1. Following the synchronisation of modes (A.3) in Appendix A, we obtain the existence of $c, M > 0$ so that $||e_j - e'_j||_\infty \leq cj^{-1}$ and $||e_j||_\infty \leq M$. Furthermore, we note that $\{\lambda_j\}_j$ assumes the same order of divergence as $\{j^2\}_j$ for $j \to \infty$. For $j_1 = j_2$, we can use Hölder's inequality to study the series

$$\frac{1}{2}\sum_{j=1}^{\infty}\left|\frac{\langle f_\epsilon, e_j\rangle^2}{\lambda_j + p}\langle e_j, Qe_j\rangle\right| \leq -\frac{M^2}{2}\zeta_* \sum_{j=1}^{\infty}\frac{1}{\lambda_j} < +\infty, \tag{3.1.8}$$

for $\zeta_* = \sup_{j\in\mathbb{N}_{>0}}\{\zeta_j\}$.

Part 2. To prove the convergence of (3.1.7), we consider

$$\begin{aligned}
&\sum_{j_1=1}^{\infty}\sum_{j_2\neq j_1}\left|\frac{\langle f_\epsilon, e_{j_1}\rangle\langle f_\epsilon, e_{j_2}\rangle}{\lambda_{j_1}+\lambda_{j_2}+2p}\langle e_{j_1}, Qe_{j_2}\rangle\right| \leq M^2\sum_{j_1=1}^{\infty}\sum_{j_2\neq j_1}\left|\frac{\langle e_{j_1}, Qe_{j_2}\rangle}{\lambda_{j_1}+\lambda_{j_2}+2p}\right| \\
\leq & M^2\sum_{j_1=1}^{\infty}\sum_{j_2\neq j_1}\left|\frac{\langle e'_{j_1}, Qe'_{j_2}\rangle + \langle e_{j_1}, Q(e_{j_2}-e'_{j_2})\rangle + \langle e_{j_1}-e'_{j_1}, Qe_{j_2}\rangle + \langle e_{j_1}-e'_{j_1}, Q(e_{j_2}-e'_{j_2})\rangle}{\lambda_{j_1}+\lambda_{j_2}+2p}\right|.
\end{aligned}$$

We recall that $\langle e'_{j_1}, Qe'_{j_2}\rangle = \zeta_{j_1}\delta^{j_1}_{j_2}$ for $j_1, j_2 > d_0$ and δ meant as the Kronecker delta. Furthermore, the inclusion of $L^\infty(\mathcal{X}_1)$ with Dirichlet conditions in $\mathcal{H}_1$ implies that there exists $c_1 > 0$ such that, for all $w \in \mathcal{H}_1$, it holds $||w|| \leq c_1||w||_\infty$. Therefore, by Hölder's inequality and the min-max principle, it follows that

$$\begin{aligned}
&\sum_{j_1=1}^{\infty}\sum_{j_2\neq j_1}\left|\frac{\langle f_\epsilon, e_{j_1}\rangle\langle f_\epsilon, e_{j_2}\rangle}{\lambda_{j_1}+\lambda_{j_2}+2p}\langle e_{j_1}, Qe_{j_2}\rangle\right| \\
\leq & M^2\zeta_* d_0^2 + M^2\zeta_*\sum_{j_1=1}^{\infty}\sum_{j_2\neq j_1}\left|\frac{cc_1 j_2^{-1} + cc_1 j_1^{-1} + c^2c_1^2 j_1^{-1}j_2^{-1}}{\lambda_{j_1}+\lambda_{j_2}+2p}\right| \\
\leq & M^2\zeta_* d_0^2 + M^2\zeta_* cc_1\left(\sum_{j_1=1}^{\infty}\sum_{j_2\neq j_1}\frac{1}{|\lambda_{j_1}+\lambda_{j_2}|}\left(\left|j_2^{-1}\right| + \left|j_1^{-1}\right| + \left|cc_1 j_1^{-1}j_2^{-1}\right|\right)\right) < \infty.
\end{aligned} \tag{3.1.9}$$

From (3.1.8) and (3.1.9), we have proven the convergence of (3.1.7). By the weak convergence in $\mathcal{H}_1$ of f_ϵ to δ_{x_0}, the Dirac delta on x_0, and the dominated convergence theorem we can then calculate

$$\begin{aligned}
&\lim_{\epsilon\to 0}\langle V_\infty^{\mathsf{w}} f_\epsilon, f_\epsilon\rangle = -\sigma^2\lim_{\epsilon\to 0}\sum_{j_1=1}^{\infty}\sum_{j_2=1}^{\infty}\frac{\langle f_\epsilon, e_{j_1}\rangle\langle f_\epsilon, e_{j_2}\rangle}{\lambda_{j_1}+\lambda_{j_2}+2p}\left(\sum_{n=1}^{\infty}\zeta_n\langle e_{j_1}, b_n\rangle\langle e_{j_2}, b_n\rangle\right) \\
= & -\sigma^2\sum_{j_1=1}^{\infty}\sum_{j_2=1}^{\infty}\lim_{\epsilon\to 0}\frac{\langle f_\epsilon, e_{j_1}\rangle\langle f_\epsilon, e_{j_2}\rangle}{\lambda_{j_1}+\lambda_{j_2}+2p}\left(\sum_{n=1}^{\infty}\zeta_n\langle e_{j_1}, b_n\rangle\langle e_{j_2}, b_n\rangle\right) \\
= & -\sigma^2\sum_{j_1=1}^{\infty}\sum_{j_2=1}^{\infty}\frac{e_{j_1}(x_0)e_{j_2}(x_0)}{\lambda_{j_1}+\lambda_{j_2}+2p}\left(\sum_{n=1}^{\infty}\zeta_n\langle e_{j_1}, b_n\rangle\langle e_{j_2}, b_n\rangle\right),
\end{aligned}$$

which yields the aimed result. □

Corollary 3.1.3 enables the implementation of the observable in the case of limited knowledge of the trajectory. Its efficiency for any $x_0 \in \mathring{\mathcal{X}}_1$ is underlined by the following proposition.

Proposition 3.1.4 ([173, Theorem 2.6])**.** *Given the Schrödinger operator*

$$A = \Delta - g : \mathcal{W}^{2,2}(\mathcal{X}_1) \cap \mathcal{W}_0^{1,2}(\mathcal{X}_1) \to L^2(\mathcal{X}_1)$$

and $g \in L^2(\mathcal{X}_1)$, then each of its eigenfunctions, $\{e_k\}_{k\in\mathbb{N}_{>0}}$, admits exactly $k-1$ roots in $\mathring{\mathcal{X}}_1$.

From Proposition 3.1.4 and the strict positivity of Q, the influence of the divergence of (3.1.2) for $j_1 = j_2 = 1$ affects all interior points of $\mathcal{X}_1$. Hence, on each point $x_0 \in \mathring{\mathcal{X}}_1$ we observe divergence of (3.1.6) with hyperbolic scaling law. This is weighted by the constant $e_1(x_0)^2\left(\sum_{n=1}^{\infty}\zeta_n\langle e_1, b_n\rangle^2\right)$. Specifically, the point at which the divergence assumes highest magnitude is $x_0 \in \mathring{\mathcal{X}}_1$ such that $x_0 = \underset{x\in\mathring{\mathcal{X}}_1}{\text{argmax}}\{|e_1(x)|\}$. This is highly relevant for practical applications as it determines a good measurement location for the spatially heterogeneous SPDE.

Remark. The choice of g influences the early-warning signs described by (3.1.2), (3.1.4) and (3.1.6) in two aspects. By affecting the values of $\{\lambda_j\}_j$, it is related to the bifurcation thresholds. Furthermore, from its relation with the functions $\{e_j\}_j$, it influences the directions on $\mathcal{H}_1$ on which such a divergence assumes higher magnitude. By construction, the point $x_0 = \underset{x\in\mathring{\mathcal{X}}_1}{\text{argmax}}\{|e_1(x)|\}$ at which (3.1.6) assumes the highest values close to the bifurcation threshold, i.e., $x_0 \in \mathring{\mathcal{X}}_1$ that satisfies

$$\lim_{\epsilon\to 0}\frac{\langle V_\infty^{\mathtt{W}} f_\epsilon^{x_0}, f_\epsilon^{x_0}\rangle}{\langle V_\infty^{\mathtt{W}} f_\epsilon^{x}, f_\epsilon^{x}\rangle} \geq 1 \quad \text{for any} \quad x \in \mathring{\mathcal{X}}_1 \quad \text{and} \quad f_\epsilon^x = \frac{1}{\epsilon}\mathbb{1}_{[x-\frac{\epsilon}{2},x+\frac{\epsilon}{2}]}\Big|_{\mathcal{X}_1},$$

also depends on the choice of g.

3.2 Numerical simulations

In order to cross-validate and visualise the results obtained in the previous section, we rely on numerical simulations. We simulate (3.0.1) using a finite difference discretisation and the semi-implicit Euler-Maruyama method ([144, Chapter 10]). We introduce the following approximations through a different font for simplicity of notation.

- An integer $N \gg 1$ is chosen in order to split the interval $\mathcal{X}_1 = [0, L]$ into $N + 1$ subintervals, each of width $h = \dfrac{L}{N+1}$.
- The time interval of length $T \geq 5000$ is studied at the values $\{j\ dt\}_{j=0}^{nt}$ for $nt := \dfrac{T}{dt} \in \mathbb{N}$ and $nt \gg 0$.
- The Laplacian operator is approximated by $\mathtt{\Delta}$, the tridiagonal $N\times N$ matrix that assumes values $-\dfrac{2}{h^2}$ on the main diagonal and $\dfrac{1}{h^2}$ on the first off-diagonals. The operator $A(p)$ is then approximated by

  $$\mathtt{A}(p) := \mathtt{\Delta} - \mathtt{g} + p\mathtt{Id},$$

  for $\mathtt{g}$ the diagonal $N \times N$ matrix with elements $\mathtt{g}_{n,n} = g(n\ h)$ for any $n \in \{1, ..., N\}$ and $\mathtt{Id}$ as the $N \times N$ identity matrix.
- The values are taken by the solution u in $\mathring{\mathcal{X}}_1$ to be approximated by the $N \times (nt + 1)$ matrix $\mathtt{u}$. Set $j \in \{0, ..., nt\}$, the j^{th} column of $\mathtt{u}$ is labelled as $\mathtt{u}_j$.
- The noise is studied through the following:
  - the integer $0 < M \ll N$ is chosen in order to indicate the number of directions of interest in $\mathcal{H}_1$ on which the noise will be considered to have effect;
  - the $M \times N$ matrix $\mathtt{e}$ has elements $\mathtt{e}(m, n) := e_m(n\ h)$;
  - the $M \times M$ orthonormal matrix $\mathtt{O}$ is defined by $\mathtt{O}(j_1, j_2) := \langle b_{j_1}, e_{j_2}\rangle$;

– the vertical vector $\mathtt{q}$ is composed of the first M eigenvalues of Q ordered by index and $\mathtt{q}^{\frac{1}{2}}$, the element-wise squared root of $\mathtt{q}$.

– the random vertical vectors $\mathtt{W}_j$ with M elements are generated by independent standard Gaussian distributions each j^{th} iteration.

Such constructions enable the approximation

$$\mathtt{u}_{j+1} = (\mathtt{Id} - \mathtt{A}(p)dt)^{-1}(\mathtt{u}_j - \mathtt{u}_j^3 dt + \sigma \mathtt{q}^{\frac{1}{2}} \mathtt{W}_j \mathtt{0e}\sqrt{dt}) \tag{3.2.1}$$

for any $j \in \{0, ..., nt-1\}$. Figure 3.1 and Figure 3.2 show sample trajectories of (3.0.1) for the functions $g(x) = \cos(3x) + 1$ and $g(x) = \dfrac{x}{L}$, distinguishing the cases in which p is smaller or larger than $-\lambda_1$, the bifurcation threshold.[2] It is visible in Figure 3.1 that for $p < -\lambda_1$ the solution remains close to the null function and assumes no persistent shape. Figure 3.2 displays the change caused by the crossing of the bifurcation threshold. In particular, we notice that the solution leaves the null function and then remains in the proximity of an arising equilibrium. The perturbation generated by noise can then induce jumps to other stable deterministic stationary solutions whose shape is defined by the choice of g.

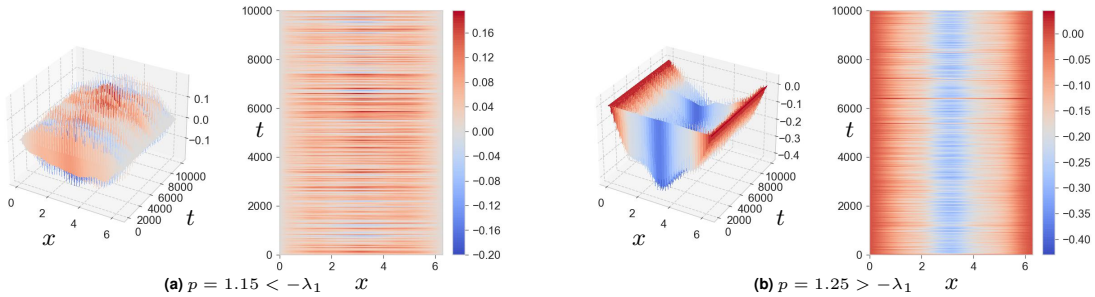

Fig. 3.1 Simulation of (3.0.1) with $g(x) = \cos(3x) + 1$ and $\lambda_1 \approx -1.188$. Each panel is composed of a surf plot and a contour plot obtained with (3.2.1) with the same noise sample. In (a), p is chosen to be smaller than the bifurcation value, and in (b) it is taken beyond the bifurcation threshold. Metastable behaviour is visible in the second case.

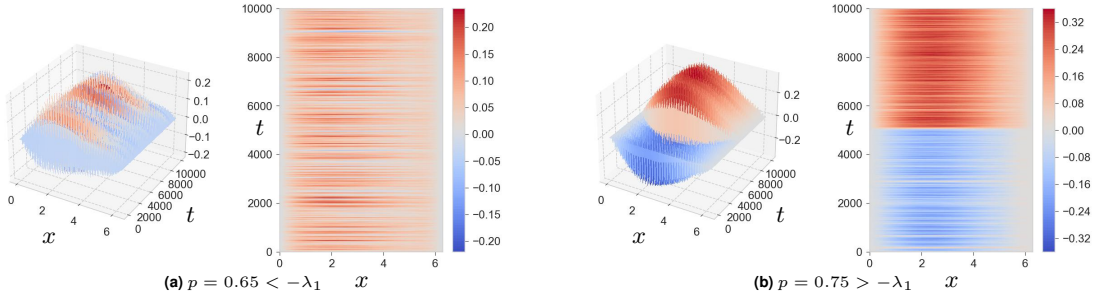

Fig. 3.2 Simulation of (3.0.1) with $g(x) = \dfrac{x}{L}$ and $\lambda_1 \approx -0.708$. The choice of p and the corresponding behaviour is the same as to Figure 3.1. The shape of g influences the value λ_1 and the equilibria of the deterministic system (3.0.1), i.e., for $\sigma = 0$. Therefore, g affects the behaviour of the solution and the value of the bifurcation threshold.

Simulation of early-warning signs.

As previously stated, linearisation is more reliable for p not in the proximity of $-\lambda_1$. The rest of this section is devoted to comparing numerically the early-warning signs interpreted as the left-hand side of (3.1.1),(3.1.2), and (3.1.3), applied to solutions of (3.0.1). Due to the linearisation, the increase of the observables is expected to be comparable to their applications to (3.1.1) prior to the approach to the bifurcation threshold. We show the effect on the early-warning signs of the dissipative nonlinear term present in (3.0.1) and that it hinders the divergence, in the $p \to -\lambda_1$ limit, of the right-hand side of

[2] $L = 2\pi$, $N = 200$, $T = 10000$, $nt = 100000$, $\sigma = 0.05$, $M = d_0 = 10$.
For different values of p, distinct random generated $\mathtt{0}$ and $\mathtt{q}$ are used. The maximum value in $\mathtt{q}$ is set to be 1.
The initial value has been chosen close to the null function because of its relevance in the theory.

(3.1.1),(3.1.2) and (3.1.3).
From Theorem 2.2.1, the invariant measure of the linear system (3.1.1), μ, is Gaussian with covariance operator $V_\infty^{\mathtt{w}}$ and mean equal to the null function. This implies that

$$\langle f_1, V_\infty^{\mathtt{w}} f_2\rangle = \int_{\mathcal{H}_1} \langle f_1, w\rangle\langle f_2, w\rangle \mathrm{d}\mu(w), \tag{3.2.2}$$

for all $f_1, f_2 \in \mathcal{H}_1$. Therefore, $\langle V_\infty^{\mathtt{w}} e_{k_1}, e_{k_2}\rangle$ from (3.1.2) can be compared with

$$\frac{1}{nt}\sum_{j=1}^{nt} \langle\!\langle \mathtt{u}_j, \mathtt{e}_{k_1}\rangle\!\rangle\langle\!\langle \mathtt{u}_j, \mathtt{e}_{k_2}\rangle\!\rangle - \left(\frac{1}{nt}\sum_{j_1=1}^{nt} \langle\!\langle \mathtt{u}_{j_1}, \mathtt{e}_{k_1}\rangle\!\rangle\right)\left(\frac{1}{nt}\sum_{j_2=1}^{nt} \langle\!\langle \mathtt{u}_{j_2}, \mathtt{e}_{k_2}\rangle\!\rangle\right), \tag{3.2.3}$$

that is the numerical covariance of the projection of the solution of (3.2.1) on the selected approximations of the eigenfunctions of $A(p)$. These are constructed as $\mathtt{e}_k(n) := e_k(nh)$ and obtained numerically through the "`quantumstates`" MATLAB function defined in [76]. The numerical scalar product $\langle\!\langle \cdot, \cdot \rangle\!\rangle$ is defined by $\langle\!\langle \mathtt{v}, \mathtt{w}\rangle\!\rangle = h\sum_{n=1}^{N} \mathtt{v}(n)\mathtt{w}(n)$, for any $\mathtt{v}, \mathtt{w} \in \mathbb{R}^N$.[3]
The plots in Figure 3.3 illustrate, for two examples of g, the scaling law of (3.2.3) for the indexes

$$k = k_1 = k_2 \in \{1, 2, 3, 4, 5\}$$

and p close to $-\lambda_1$. They are then compared with

$$\frac{-\sigma^2}{2(\lambda_1 + p)}\sum_{j=1}^{M} \mathtt{q}(j)\langle\!\langle \mathtt{e}_1, \mathtt{b}_j\rangle\!\rangle^2, \tag{3.2.4}$$

which is the numerical approximation of the right-hand side of (3.1.2) on $k = 1$. The row vectors of $\mathtt{0e}$, $\{\mathtt{b}_j\}_{j=1}^{M}$, are meant to replicate the eigenfunctions of Q.[4] It is clear from Figure 3.3 that the dissipativity by

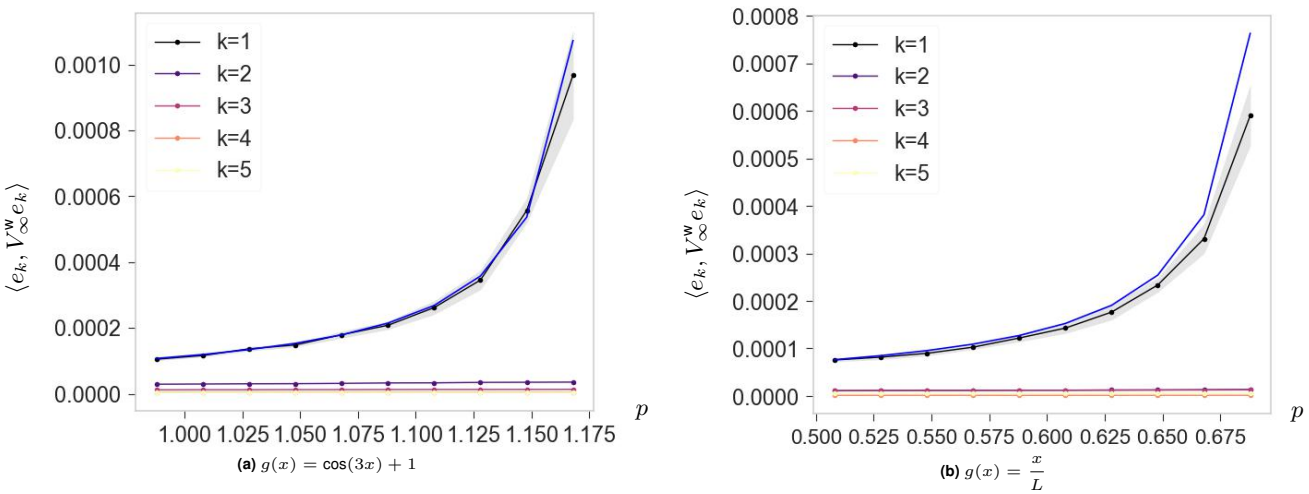

(a) $g(x) = \cos(3x) + 1$ **(b)** $g(x) = \frac{x}{L}$

Fig. 3.3 The results of (3.2.3) applied on the matrix $\mathtt{u}$, obtained through the iteration of (3.2.1), are displayed in the figure for parameters $k = k_1 = k_2 \in \{1, 2, 3, 4, 5\}$ and different choices of g. In (a), we assume $g(x) = \cos(3x) + 1$ and, in (b), we consider $g(x) = \frac{x}{L}$, for any $x \in [0, L]$. This implies that $\lambda_1 \approx -1.188$ and $\lambda_1 \approx -0.708$, for each respective panel. The dots indicate the mean of such values obtained from 10 simulations with the same parameters and initial conditions, but generated with different noise samples. The grey area has a width equal to twice the recorded numerical standard deviation, and it is centered on the mean results. The blue line displays the result (3.2.4) for the linear system. For p distant from $-\lambda_1$, the black and the blue lines show similar values.

the nonlinear term in the system (3.0.1) restrains the variance of the system for p close to $-\lambda_1$. Furthermore, the difference between early-warning sign on (3.1.1) and the average of (3.2.3) with $k_1 = k_2 = 1$ on

[3] The multiplication by h is justified by the fact that the functions involved have value 0 in $x = 0$ and $x = L$.

[4] $L = 2\pi$, $N = 100$, $T = 5000$, $nt = 100000$, $\sigma = 0.01$, $M = d_0 = 10$. The two plots show results for different $\mathtt{0}$ and $\mathtt{q}$ randomly generated as previously described.

solutions given by (3.2.1) with different noise samples grows with p. For p distant from $-\lambda_1$, the values of such results are close and the behaviour of the plots is similar.
A similar method can also be applied to compute the early-warning sign in (3.1.6). By Corollary 3.1.3, we can choose a function $f_0 \in L^\infty(\mathcal{X}_1)$ such that $f_0(0) = f_0(L) = 0$ and for which there exists an integer $0 < r < N + 2$ and a $x_0 = ph \in \mathcal{X}_1$ that satisfy

$$\langle V_\infty^{\mathtt{w}} f_0, f_0 \rangle \approx -\sigma^2 \sum_{j_1=1}^{\infty} \sum_{j_2=1}^{\infty} \frac{e_{j_1}(x_0) e_{j_2}(x_0)}{\lambda_{j_1} + \lambda_{j_2} + 2p} \left(\sum_{n=1}^{\infty} \zeta_n \langle e_{j_1}, b_n \rangle \langle e_{j_2}, b_n \rangle \right). \tag{3.2.5}$$

Proposition 3.1.4 implies that the observable displays a hyperbolic growth rate when p approaches $-\lambda_1$.

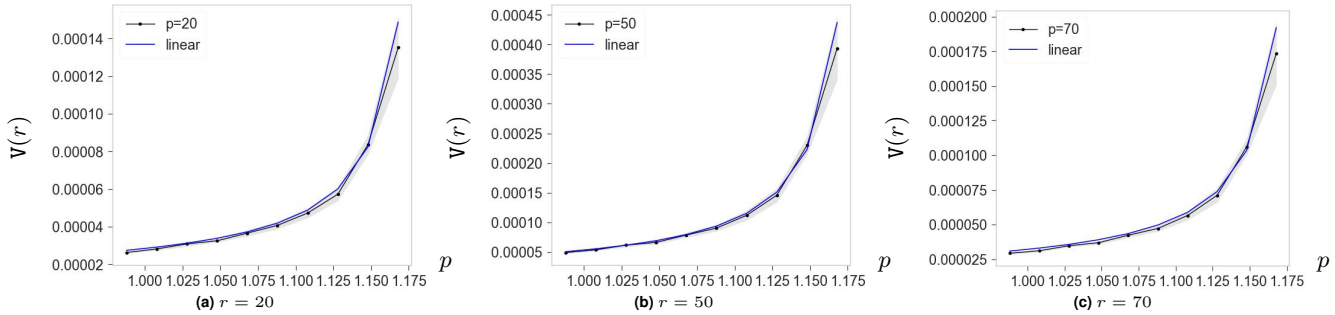

Fig. 3.4 Simulations of $\mathtt{V}(r)$ obtained from 10 sample solutions of (3.0.1) with $g(x) = \cos(3x) + 1$ and $\lambda_1 \approx -1.188$ obtained through the iteration (3.2.1). The black dots indicate the mean results, and the width of the grey area corresponds to twice the standard deviation for the relative p. It is clear that the early-warning sign resembles the expected result for the linear system until a neighbourhood of the bifurcation threshold, on which the nonlinear dissipative term prevents the divergence. The space discretisation is achieved by taking $N = 100$ equidistant internal points of $\mathcal{X}_1$ into account.

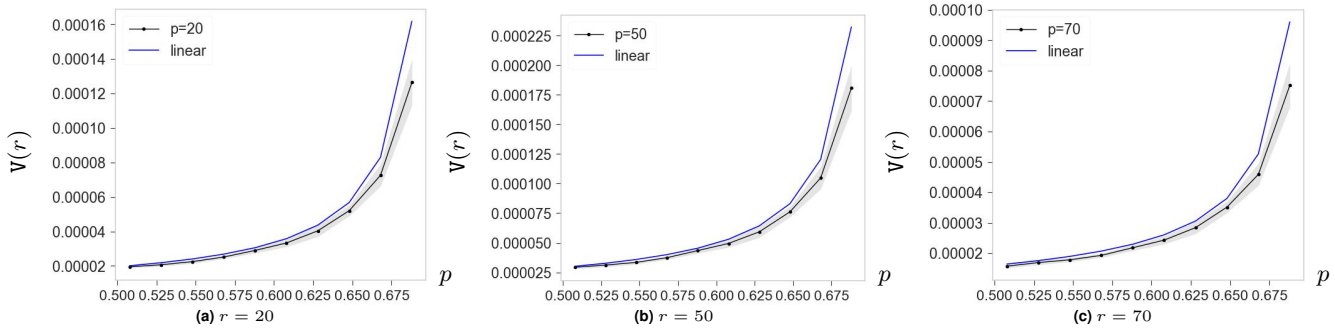

Fig. 3.5 Simulations of $\mathtt{V}(r)$ obtained from 10 sample solutions of (3.0.1) with $g(x) = \dfrac{x}{L}$ and $\lambda_1 \approx -0.708$. The results are similar to Figure 3.4 but the choice of g appears to influence the difference of the expected early-warning sign applied to the solution of the linear system (3.1.1) and its simulation applied to (3.0.1).

Figures 3.4 and 3.5 compare $\langle V_\infty^{\mathtt{w}} f_0, f_0 \rangle$ for different values of $p < -\lambda_1$ in the form

$$\mathtt{V}(r) := \frac{1}{nt} \sum_{j=1}^{nt} \mathtt{u}_j(r) \mathtt{u}_j(r) - \left(\frac{1}{nt} \sum_{j_1=1}^{nt} \mathtt{u}_{j_1}(r) \right) \left(\frac{1}{nt} \sum_{j_2=1}^{nt} \mathtt{u}_{j_2}(r) \right), \tag{3.2.6}$$

shown as black dots, and the approximation of the right-hand side in equation (3.2.5)

$$-\sigma^2 \sum_{j_1=1}^{m_1} \sum_{j_2=1}^{m_1} \frac{\mathtt{e}_{j_1}(r) \mathtt{e}_{j_2}(r)}{\lambda_{j_1} + \lambda_{j_2} + 2p} \left(\sum_{n=1}^{M} \mathtt{q}(n) \langle\!\langle \mathtt{e}_{j_1}, \mathtt{b}_n \rangle\!\rangle \langle\!\langle \mathtt{e}_{j_2}, \mathtt{b}_n \rangle\!\rangle \right), \tag{3.2.7}$$

in blue for a fixed integer $0 < m_1 \ll N$.[5] The subplots in Figure 3.4 and in Figure 3.5 are given by equivalent simulations to Figure 3.3 (a) and 3.3 (b) respectively. Each dot in the panels is the average of (3.2.6) obtained from 10 simulations which differ only by the sample noise observed. The numerical

[5] Such a truncation index is taken as $m_1 = 30$ in the figures.

standard deviation is represented by the grey area.
In Figure 3.3, the early-warning sign (3.2.6) on the linear system assumes higher values than the average numerical variance obtained on projections on chosen spaces (3.2.7) of solutions of the nonlinear system. The difference in the two results is more evident when the dissipative nonlinear term is more prominent, which is close to the bifurcation. For such values of p it seems also evident that the standard deviation on the simulations is wider. The cause of this behaviour is discussed in Chapter 7.

3.3 Summary

In this chapter, we investigate a spatially heterogeneous extension of the Chafee–Infante type PDE under additive noise and establish that the time-asymptotic variance offers a reliable early-warning signal for an impending bifurcation. We prove that, as the bifurcation threshold is approached from below, the variance of the linearised system diverges at a precise hyperbolic rate along almost any direction in the Hilbert space $\mathcal{H}_1$. An equivalent divergence rate is shown to hold from pointwise observations at any fixed spatial location. These results are obtained via different analytical techniques: spectral analysis for the infinite-dimensional covariance operator and direct estimation of pointwise variance. Furthermore, numerical simulations show that the early-warning signals for the linearised system remain predictive even for the nonlinear dynamics, provided the system is not too close to the bifurcation point. This consistency provides strong evidence that variance-based early-warning signals can serve as universal indicators in a broad class of SPDEs near classical codimension-1 bifurcations.

4 Time-asymptotic variance for purely continuous spectrum in drift operator

In this chapter, we discuss an early-warning sign based on the growth of the time-asymptotic variance along certain proxy functions of the solution of SPDE (2.3.4). Its content is the result of the supervision of the MSc thesis project of Antonia Düx [21]. Nonetheless, the material presented is primarily attributed to the author. In contrast to the previous chapter, the drift operator is not diagonalisable. As such, the observable can not be tracked along eigenmodes. Nonetheless, we find preferred directions that capture the loss of stability of the null solution and characterise their role in the signal. Furthermore, we observe that the shape of the spectrum of the linear operator can hinder or silence the early-warning sign. In the last sections, we discuss a more general type of SPDEs that find application in different fields. The systems are characterised by equations of the form

$$\mathsf{d}u^{(\mathsf{w},\mathsf{c})}(x,t) = A(p)u^{(\mathsf{w},\mathsf{c})}(x,t)\,\mathsf{d}t + \sigma\, Q^{\frac{1}{2}}\mathsf{d}W(t), \tag{4.0.1}$$

for any $x \in \mathcal{X}_1 \subset \mathbb{R}^N$ and $t > 0$. The drift operator is initially assumed to be of the form $A(p) = \mathrm{T}_f + p$, for T_f the multiplication operator for $f : \mathcal{X}_1 \subset \mathbb{R}^N \times \mathbb{R}_{<0} \to \mathbb{R}$ and $N \in \{1, 2, 3\}$, and later generalised to different operators with purely continuous spectrum. In the first case, the function f satisfies

$$f(x,p) < 0 \quad \text{and} \quad f(x_*, 0) = 0,$$

for a fixed x_* and any $(x,p) \in \mathcal{X}_1 \times \mathbb{R}_{\leq 0} \setminus \{(x_*, 0)\}$. It follows that for a linear, bounded, self-adjoint and diagonalisable operator Q, the mild solution of (4.0.1) can be computed pointwise in $\mathcal{X}_1$ for any $t > 0$. The definition of V_∞^{w} in (2.3.8) implies, through Fubini's Theorem, that

$$\begin{aligned}\langle g_1, V_\infty^{\mathsf{w}} g_2\rangle &= \int_{\mathcal{X}_1} g_1(x)\sigma^2 \lim_{t\to\infty}\int_0^t e^{(f(x)+p)r} Q e^{f(x,p)r} g_2(x)\,\mathsf{d}r\,\mathsf{d}x \\ &= \int_{\mathcal{X}_1} g_1(x)g_2(x)\frac{-\sigma^2}{2f(x,p)}\,\mathsf{d}x = -\frac{\sigma^2}{2}\left\langle f^{-1}(\cdot,p)g_1, g_2\right\rangle ,\end{aligned} \tag{4.0.2}$$

with $g_1, g_2 \in L^2(\mathcal{X}_1) = \mathcal{H}_1$.

4.1 One-dimensional case

In the current section, we assume $N = 1$ and obtain a precise rate of divergence of the time-asymptotic variance of the solution of (4.0.1) for different types of functions $f : \mathcal{X}_1 \subset \mathbb{R} \times \mathbb{R}_{\leq 0} \to \mathbb{R}$. Such a behaviour defines an early-warning sign for the approach to a bifurcation threshold of the system.
First, we choose a specific function type f to analyse. Afterwards, we expand our analysis by considering general analytic functions. Lastly, we discuss an example in which f is not analytic.

4.1.1 Tool function

Consider the function $f(x,p) = f_\alpha(x) + p$, for any $x \in \mathcal{X}_1$ and $p \leq 0$, defined by

$$f_\alpha(x) := -|x|^\alpha \quad \text{with } \alpha > 0 \tag{4.1.1}$$

with x in a neighbourhood of $x_* = 0$ and such that

$$f(x,p) < 0 \ \ \forall x \in \mathcal{X}_1 \setminus \{x_*\}, \quad \int_{\mathcal{X}_1} \frac{1}{|f(x,p)|} \mathrm{d}x < +\infty \text{ for any } p < 0, \text{ and } \quad f(x_*,0) = 0, \tag{4.1.2}$$

holds. This type of function is a useful tool for the study of system (4.0.1). Indeed, for f such that there exist $c_1, c_2, \varepsilon > 0$ and the bounds

$$c_1(f_\alpha(x) + p) \leq f(x,p) \leq c_2(f_\alpha(x) + p) \qquad \text{for all} \quad x \in [-\varepsilon, \varepsilon] \cap \mathcal{X}_1 \tag{4.1.3}$$

hold, we can transfer scaling laws obtained from the tool function directly to results for f. We note that up to rescaling of the spatial variable, we can assume $\varepsilon = 1$ and that $[0,1] \subset \mathcal{X}_1$. Therefore, employing T_{f_α} to analyse the covariance operator and by (4.0.2) we obtain

$$\langle g, V_\infty^{\mathsf{w}} g \rangle = -\left\langle g, \frac{\sigma^2}{2f(x,p)} g \right\rangle = -\int_0^1 \frac{\sigma^2}{2f(x,p)} \, \mathrm{d}x$$

and

$$\frac{1}{2c_1} \int_0^1 \frac{\sigma^2}{x^\alpha - p} \, \mathrm{d}x \leq -\int_0^1 \frac{\sigma^2}{2f(x,p)} \, \mathrm{d}x \leq \frac{1}{2c_2} \int_0^1 \frac{\sigma^2}{x^\alpha - p} \, \mathrm{d}x \tag{4.1.4}$$

for $g(x) = \mathbb{1}_{[0,1]}$ and certain constants $c_1 \geq 1 \geq c_2$.

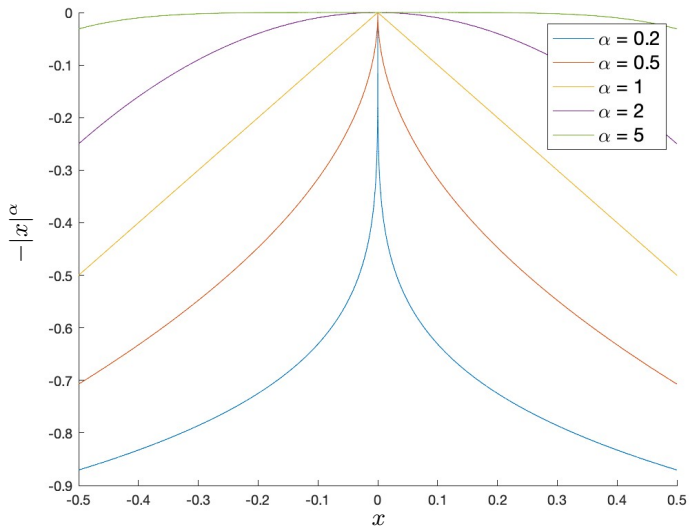

Fig. 4.1 Plot of function $-|x|^\alpha$ for different choices of α. For $\alpha > 1$ the function is C^1, with derivative equal to 0 at $x = 0$. Conversely, for $\alpha \leq 1$ the function is steep at $x = 0$.

The following theorem describes the rate of divergence assumed by $\langle g, V_\infty^{\mathsf{w}} g \rangle$ as $p \to 0^-$ for $f = f_\alpha + p$.

Theorem 4.1.1. *For $f = f_\alpha + p$ defined in* (4.1.1)*, $Q = \mathrm{Id}$ and $\varepsilon > 0$, the time-asymptotic covariance V_∞^{w} of the solution of* (4.0.1) *along $g(x) = \mathbb{1}_{[0,\varepsilon]}$, $\langle g, V_\infty^{\mathsf{w}} g \rangle$, assumes the scaling law, as $p \to 0^-$, described in Table 4.1.*

Proof. The scaling law of $\langle g, V_\infty^{\mathsf{w}} g \rangle$ for $p \to 0^-$ is equivalent to the one exhibited by $\int_0^1 \frac{1}{x^\alpha - p} \, \mathrm{d}x$, as described in (4.1.4). In such a limit in p we obtain

$$\lim_{p \to 0^-} \int_0^1 \frac{1}{x^\alpha - p} \, \mathrm{d}x = \int_0^1 \frac{1}{x^\alpha} \, \mathrm{d}x = \begin{cases} < \infty & \text{for } 0 < \alpha < 1, \\ = \infty & \text{for } \alpha \geq 1. \end{cases}$$

Table 4.1 Scaling law of the time-asymptotic variance in dimension $N = 1$ for the function $f(x,p) = f_\alpha(x) + p$ and $g = \mathbb{1}_{[0,\varepsilon]}$.

Case	Scaling law for $p \to 0^-$
$0 < \alpha < 1$	1
$\alpha = 1$	$-\log(-p)$
$\alpha > 1$	$(-p)^{-1+\frac{1}{\alpha}}$
$\alpha \to \infty$	$(-p)^{-1}$

For the case $\alpha = 1$, by substituting $y = x - p$ we find that

$$\int_0^1 \frac{1}{x-p}\,\mathrm{d}x = \int_{-p}^{1-p} \frac{1}{y}\,\mathrm{d}y = \log(1-p) - \log(-p) = \Theta_p(-\log(-p)) \quad \text{for } p \to 0^-.$$

We now consider the case $\alpha > 1$. Through the substitution $y = x(-p)^{-\frac{1}{\alpha}}$, we obtain

$$\int_0^1 \frac{1}{x^\alpha - p}\,\mathrm{d}x = \frac{1}{-p}\int_0^1 \frac{1}{\left(x(-p)^{-\frac{1}{\alpha}}\right)^\alpha + 1}\,\mathrm{d}x = (-p)^{-1+\frac{1}{\alpha}} \int_0^{(-p)^{-\frac{1}{\alpha}}} \frac{1}{y^\alpha + 1}\,\mathrm{d}y. \tag{4.1.5}$$

Since $\alpha > 1$, we find that

$$\lim_{p\to 0^-} \int_0^{(-p)^{-\frac{1}{\alpha}}} \frac{1}{y^\alpha + 1}\,\mathrm{d}y < \infty. \tag{4.1.6}$$

Therefore, in the limit of p to zero from below for the equation (4.1.5), we find divergence with the rate

$$(-p)^{-1+\frac{1}{\alpha}} \int_0^{(-p)^{-\frac{1}{\alpha}}} \frac{1}{y^\alpha + 1}\,\mathrm{d}y = \Theta_p\left((-p)^{-1+\frac{1}{\alpha}}\right).$$

Furthermore, we see that, for α approaching infinity, this expression is also well-defined with a rate of divergence $\Theta_p\left(\frac{1}{-p}\right)$. □

Theorem 4.1.1 states that, for the function f_α defined by (4.1.1) and $0 < \alpha < 1$, the time-asymptotic variance along g is converging in the limit $p \to 0^-$. Such function types f_α display a steep shape on $x = 0$, as seen in Figure 4.1. Alternatively, we observe that for $\alpha \geq 1$, the time-asymptotic variance along g diverges, indicating that a divergence appears as the function is flattened and smoothened, increasing α. The intuition behind such a difference is given by the fact that, although the solution $u^{(\mathsf{w,c})}$ of (4.0.1) for $A(p) = T_{f_\alpha} + p$ is less affected by the drift component on all $x \in \mathcal{X}_1$ as p approaches 0, the only region in space on which $u^{(\mathsf{w,c})}$ is solely driven by noise in the limit case is the set $\{x_* = 0\}$. In particular, while the time-asymptotic variance of $u^{(\mathsf{w,c})}(x,\cdot)$ increases for all $x \in \mathcal{X}_1$ in the limit $p \to 0^-$, it divergences only on $x = x_*$ due to the fact that $u^{(\mathsf{w,c})}(x_*,p)$ is the solution of an Orstein-Uhlenbeck equation for any $p \leq 0$. Analytically, it appears that, for steep structures of f_α on x_*, the divergence of the time-asymptotic variance of $u^{(\mathsf{w,c})}(x_*,\cdot)$ does not affect $\langle g, V_\infty^{\mathsf{w}} g\rangle$, as it is restricted by the dissipative effect of the drift component on $x \in (0,\varepsilon]$. Conversely, for smooth f_α on x_*, the dissipation induced by the multiplication operator on $u^{(\mathsf{w,c})}(x,\cdot)$, for $x \in (0,\varepsilon]$, is not sufficient to imply convergence of $\langle g, V_\infty^{\mathsf{w}} g\rangle$. Nonetheless, it affects its rate of divergence. It is interesting to note that a similar scaling law behaviour, associated with the intermittency scaling law of an ODE dependent on a parameter near a non-smooth fold bifurcation, has been found in [130, Table 1].

Remark 4.1.2. Under the assumptions of Theorem 4.1.1, the finite time $t > 0$ variance along a function g, $\langle g, V_t^{\mathsf{w}} g\rangle$, converges for $p \to 0^-$. Up to rescaling of x, we fix $\varepsilon = 1$ and note that

$$\begin{aligned}\langle g, V_t^{\mathsf{w}} g\rangle &= \int_0^\infty g(x)\sigma^2 \int_0^t \mathsf{e}^{(f_\alpha(x)+p)r} Q \mathsf{e}^{(f_\alpha(x)+p)r} g(x)\,\mathsf{d}r\,\mathsf{d}x \\ &= -\sigma^2 \int_0^1 \frac{1-\mathsf{e}^{(2(f_\alpha(x)+p))t}}{2(f_\alpha(x)+p)}\,\mathsf{d}x < +\infty\end{aligned}$$

for any $p \leq 0$. The growths of finite time variances are, therefore, early-warning signs which are hard to observe in finite time series due to the fact that they increase as p approaches 0 but do not diverge. For any fixed $p \leq 0$, longer times t imply that the variance attains higher values and, consequently, ease the prediction of the tipping point.

4.1.2 General analytic functions

We have found that $\langle g, V_\infty^{\mathsf{w}} g\rangle$ converges for $\alpha < 1$ and diverges for $\alpha \geq 1$ for the limit $p \to 0^-$ with the functions $f_\alpha(x) = -|x|^\alpha$ and $g = \mathbb{1}_{[0,\varepsilon]}$. Furthermore, we captured the corresponding scaling laws in the limit. Our aim in this subsection is to generalise these results considerably. In particular, we consider the analytic functions $f = f_{\mathsf{an}} + p$ such that (4.1.2) holds. Through Taylor's theorem and due to the fact that f vanishes at $x_* = 0$, the function f_{an} is of the form

$$f_{\mathsf{an}}(x) = -\sum_{n=1}^\infty a_n x^n$$

for any $x \in \mathcal{X}_1$ and with coefficients $\{a_n\}_{n\in\mathbb{N}} \subset \mathbb{R}$ such that (4.1.2) holds. Up to reparametrisation, we assume that $[0,\varepsilon] \subset \mathcal{X}_1$. The following theorem provides a scaling law, which can be interpreted as an early-warning sign, of the expression $\langle g, V_\infty^{\mathsf{w}} g\rangle$ for an analytic f and $g(x) = \mathbb{1}_{[0,\varepsilon]}$.

Theorem 4.1.3. *Set $f_{\mathsf{an}}(x) = -\sum_{n=1}^\infty a_n x^n$ for all $x \in \mathcal{X}_1 \subset \mathbb{R}$, that satisfies* (4.1.2)*, $\{a_n\}_{n\in\mathbb{N}} \subset \mathbb{R}$ and $Q = \mathrm{Id}$. Let $m \in \mathbb{N}$ denote the index for which $a_n = 0$ for any $n \in \{1,\dots,m-1\}$ and $a_m \neq 0$.[1] Then, the time-asymptotic variance of the solution of* (4.0.1) *along $g(x) = \mathbb{1}_{[0,\varepsilon]}$, $\langle g, V_\infty^{\mathsf{w}} g\rangle$, is characterised by the scaling law, as $p \to 0^-$, described in Table 4.1, now depending on the value of $m = \alpha > 0$.*[2]

Proof. As in the proof of Theorem 4.1.1, up to rescaling of the variable x, we can choose $\varepsilon = 1$. Analysing the variance along g, we obtain that

$$\langle g, V_\infty^{\mathsf{w}} g\rangle = \frac{\sigma^2}{2}\int_0^1 \frac{1}{\sum_{n=m}^\infty a_n x^n - p}\,\mathsf{d}x. \tag{4.1.7}$$

For positive x close to zero, the sum $\sum_{n=1}^\infty a_n x^n$ is dominated by the leading term $a_m x^m$, since

$$\lim_{x\to 0^+} \frac{\sum_{n=1}^\infty a_n x^n}{a_m x^m} = \lim_{x\to 0^+} \frac{\sum_{n=m}^\infty a_n x^n}{a_m x^m} = \lim_{x\to 0^+} \frac{a_m + \sum_{n=m+1}^\infty a_n x^{n-m}}{a_m} = 1.$$

[1] For odd m it is implied that $\mathcal{X}_1 \subset \mathbb{R}_{\geq 0} := \{x \in \mathbb{R} : x \geq 0\}$, or $\mathcal{X}_1 \subset \mathbb{R}_{\leq 0} := \{x \in \mathbb{R} : x \leq 0\}$ up to rescaling, due to the sign of f.

[2] Alternatively, we can assume to have a function $f_{\mathsf{an}} \in C^k$ such that $k \geq m$. This leads to the study of the Peano remainder instead of the whole series.

Therefore, there exists a constant $C > 1$ such that for any $x \in (0, 1]$

$$\frac{1}{C} a_m x^m \leq \sum_{n=1}^{\infty} a_n x^n \leq C a_m x^m$$

holds true. Hence, we obtain

$$\frac{\sigma^2}{C} \int_0^1 \frac{1}{a_m x^m - p} \, \mathsf{d}x \leq \sigma^2 \int_0^1 \frac{1}{\sum_{n=1}^{\infty} a_n x^n - p} \, \mathsf{d}x \leq C\sigma^2 \int_0^1 \frac{1}{a_m x^m - p} \, \mathsf{d}x$$

from (4.1.7). This result is equivalent to (4.1.4), in the sense that it implies that the rate of divergence of $\langle g, V_\infty^{\mathsf{w}} g \rangle$ is described in Table 4.1 with $m = \alpha$. □

Remark 4.1.4. In Theorem 4.1.3, we assume the functions g to be bounded. Through similar methods as the proof of Theorem 4.1.1, a scaling law can be obtained for more general families of functions in $\mathcal{H}_1$. For example, we consider $\varepsilon > 0$ such that $[0, \varepsilon] \subset \mathcal{X}_1$, $g = x^{-\gamma} \mathbb{1}_{[0,\varepsilon]}$, $\gamma < \frac{1}{2}$, $f = f_\alpha + p$ and $\alpha > 0$, which yields

$$\langle g, V_\infty^{\mathsf{w}} g \rangle = \frac{\sigma^2}{2} \int_0^\varepsilon \frac{1}{x^{2\gamma}} \frac{1}{x^\alpha - p} \mathsf{d}x.$$

For $0 < 2\gamma + \alpha < 1$, we obtain

$$\lim_{p \to 0^-} \langle g, V_\infty^{\mathsf{w}} g \rangle = \frac{\sigma^2}{2} \int_0^\varepsilon \frac{1}{x^{2\gamma+\alpha}} \mathsf{d}x < +\infty.$$

Setting instead $2\gamma + \alpha \geq 1$, we get

$$\begin{aligned}
\langle g, V_\infty^{\mathsf{w}} g \rangle &= \frac{\sigma^2}{2} \int_0^\varepsilon \frac{1}{x^{2\gamma}} \frac{1}{x^\alpha - p} \mathsf{d}x \\
&= \frac{\sigma^2}{2} (-p)^{-1-\frac{2\gamma}{\alpha}} \int_0^\varepsilon \frac{1}{\left(x(-p)^{-\frac{1}{\alpha}} \right)^{2\gamma}} \frac{1}{\left(x(-p)^{-\frac{1}{\alpha}} \right)^\alpha + 1} \mathsf{d}x \\
&= \frac{\sigma^2}{2} (-p)^{-1+\frac{1-2\gamma}{\alpha}} \int_0^{\varepsilon(-p)^{-\frac{1}{\alpha}}} \frac{1}{y^{2\gamma}} \frac{1}{y^\alpha + 1} \mathsf{d}y,
\end{aligned}$$

for $y = x(-p)^{-\frac{1}{\alpha}}$. The scaling law for $\langle g, V_\infty^{\mathsf{w}} g \rangle$ in $p \to 0^-$ is summarised in Table 4.2. This result generalises the statement in [135, Theorem 4.4] as an exact scaling law can be obtained for any analytic f_{an} that satisfies (4.1.2) and g in a dense subset of $\mathcal{H}_1$.

Table 4.2 Scaling law of the time-asymptotic variance in dimension $N = 1$ for the function $f(x, p) = f_\alpha(x) + p$ and $g = x^{-\gamma} \mathbb{1}_{[0,\varepsilon]}$.

Case	Scaling law for $p \to 0^-$
$0 < 2\gamma + \alpha < 1$	1
$2\gamma + \alpha = 1$	$-\log(-p)$
$2\gamma + \alpha > 1$	$(-p)^{-1+\frac{1-2\gamma}{\alpha}}$
$2\gamma \to 1 \quad \text{or} \quad \alpha \to \infty$	$(-p)^{-1}$

Remark 4.1.5. We found that the scaling law of the time-asymptotic variance, along an indicator function, of the solution of (4.0.1) is shown in Table 4.1 for every function f that satisfies (4.1.2) and (4.1.3) for $\alpha > 0$. Clearly, this does not include all possible functions f. We take as an example the case in which there exists $\delta \geq 1$ such that $[-\delta, \delta] \subset \mathcal{X}_1$ and functions f that converge for fixed p at two different rates as x approaches 0^- and 0^+. We consider

$$f(x,p) = \begin{cases} f_1(x) + p & \text{for } \ 0 \geq x \in \mathcal{X}_1, \\ f_2(x) + p & \text{for } \ 0 < x \in \mathcal{X}_1, \end{cases}$$

for smooth functions $f_1 : \mathcal{X}_1 \cap \mathbb{R}_{\leq 0} \to \mathbb{R}$ and $f_2 : \mathcal{X}_1 \cap \mathbb{R}_{\geq 0} \to \mathbb{R}$ and f that satisfies (4.1.2). We assume $g = \mathbb{1}_{[-1,1]}$ and by (4.0.2) we get

$$\langle g, V_\infty^{\mathsf{w}} g \rangle = \int_{-1}^{1} \frac{-\sigma^2}{2(f(x)+p)} \, \mathrm{d}x = \frac{\sigma^2}{2} \int_{-1}^{0} \frac{1}{-f_1(x) - p} \, \mathrm{d}x + \frac{\sigma^2}{2} \int_{0}^{1} \frac{1}{-f_2(x) - p} \, \mathrm{d}x. \tag{4.1.8}$$

We consider each summand separately and study the limit in p to zero from below. If $\lim\limits_{x \to 0^+} f_2(x) < 0$, then it holds that

$$\lim_{p \to 0^-} \int_0^1 \frac{1}{-f_2(x) - p} \, \mathrm{d}x < +\infty$$

and the scaling rate of $\langle g, V_\infty^{\mathsf{w}} g \rangle$ is equivalent to the one given by $\int_{-1}^{0} \frac{1}{-f_1(x)-p} \, \mathrm{d}x$. Otherwise, it is dictated by the highest rate associated with the two summands. Such rates are shown in Table 4.1, assuming that f_1 and f_2 are analytic or that they have the same order of convergence to 0 as f_α for any $\alpha > 0$.

4.2 Higher-dimensional cases

In the current section, we obtain upper bounds for the scaling of the time-asymptotic variance of the solutions of the system (4.0.1) along chosen functions g. In this case, we consider $N > 1$, therefore assuming that the system (4.0.1) is studied in higher spatial dimensions. We find that, for certain functions $f : \mathcal{X}_1 \subset \mathbb{R}^N \times \mathbb{R}_{\leq 0} \to \mathbb{R}$, the early-warning signs display convergence of the variance along the mentioned proxy function in the square-integrable function space, $\mathcal{H}_1$.

For the remainder of this section, we assume that $f(x,p) = f_{\mathsf{an}}(x) + p$ is analytic and satisfies (4.1.2) for $x_* = 0 \in \mathcal{X}_1 \subset \mathbb{R}^N$. Consequently, f_{an} is of the form

$$f_{\mathsf{an}}(x) = -\sum_{j \in \mathcal{C}} a_j x^j \quad \text{for } x = (x_1, \ldots, x_N) \in \mathcal{X}_1, \tag{4.2.1}$$

where j is a multi-index, i.e., $x^j = \prod\limits_{n=1}^{N} x_n^{i_n}$ with the collection $\mathcal{C}$ defined by the set

$$\mathcal{C} = \left\{ j = (i_1, \ldots, i_N) \in \mathbb{N}^N \right\}.$$

The coefficients a_j are real-valued, and their signs satisfy (4.1.2) as discussed further in the chapter. We assume that there exists $\varepsilon > 0$ such that $[0, \varepsilon]^N \subset \mathcal{X}_1$, up to rescaling of the space variable x. Properties (4.1.2) imply that equation (4.0.2) holds, hence for $g(x) = \mathbb{1}_{[0,\varepsilon]^N}(x)$ we find

$$\langle g, V_\infty^{\mathsf{w}} g \rangle = \sigma^2 \left\langle \frac{-1}{2(f_{\mathsf{an}} + p)} g, g \right\rangle = \frac{\sigma^2}{2} \int_0^\varepsilon \cdots \int_0^\varepsilon \frac{-1}{f_{\mathsf{an}}(x) + p} \, \mathrm{d}x = \frac{\sigma^2}{2} \int_0^\varepsilon \cdots \int_0^\varepsilon \frac{1}{\sum\limits_{j \in \mathcal{C}} a_j x^j - p} \, \mathrm{d}x.$$

In the next proposition, we prove that for any f in a dense subset of the analytic functions space that satisfies (4.1.2), the variance $\langle g, V_\infty^{\mathsf{w}} g\rangle$ converges for $p \to 0^-$.

Proposition 4.2.1. *Fix the dimension $N > 1$, and set the indices $\{i_k\}_{k\in\{1,\dots,N\}}$ as a permutation of $\{1,\dots,N\}$. Furthermore, suppose that there exist two multi-indices $j_1, j_2 \in \mathcal{C}$ such that $a_{j_1}, a_{j_2} > 0$ and that each of these multi-indices corresponds to the multiplication of only one x_{i_1}, resp. x_{i_2}, meaning that j_1, resp. j_2, has all elements equal to 0 with the exception of the component on the i_1-th, resp. i_2-th, position which assumes value 1. Then, it holds that*

$$\lim_{p\to 0^-} \langle g, V_\infty^{\mathsf{w}} g\rangle < \infty$$

for any $\varepsilon > 0$ and $g(x) = \mathbb{1}_{[0,\varepsilon]^N}(x)$.

Proof. Without loss of generality, we assume that $j_1 = (1, 0, 0\dots)$ and $j_2 = (0, 1, 0\dots)$. Then, we obtain

$$\begin{aligned}
\langle g, V_\infty^{\mathsf{w}} g\rangle &= \frac{\sigma^2}{2}\int_0^\varepsilon \cdots \int_0^\varepsilon \frac{1}{\sum_{j\in\mathcal{C}} a_j x^j - p}\,\mathsf{d}x_N \cdots \mathsf{d}x_1 \\
&= \frac{\sigma^2}{2}\int_0^\varepsilon \cdots \int_0^\varepsilon \frac{1}{a_{j_1}x_1 + a_{j_2}x_2 + \sum_{j\in\mathcal{C}\setminus\{j_1,j_2\}} a_j x^j - p}\,\mathsf{d}x_N \cdots \mathsf{d}x_1 \\
&\le C\frac{\sigma^2}{2}\int_0^\varepsilon \cdots \int_0^\varepsilon \frac{1}{x_1 + x_2 - p}\mathsf{d}x_N \cdots \mathsf{d}x_1
\end{aligned}$$

where the last inequality is satisfied by a constant $C > 0$ and follows from the values $a_{j_1}, a_{j_2} > 0 > p$, the continuity of f and the compactness of the support of g. This implies that

$$\begin{aligned}
&\lim_{p\to 0^-} \int_0^\varepsilon \cdots \int_0^\varepsilon \frac{1}{x_1 + x_2 - p}\mathsf{d}x_N \cdots \mathsf{d}x_1 \\
=&\varepsilon^{N-2} \lim_{p\to 0^-} \int_0^\varepsilon \int_0^\varepsilon \frac{1}{x_1 + x_2 - p}\mathsf{d}x_2\,\mathsf{d}x_1 \\
=&\varepsilon^{N-2} \lim_{p\to 0^-} \int_0^\varepsilon \mathsf{log}(\varepsilon + x_1 - p) - \mathsf{log}(x_1 - p)\,\mathsf{d}x_1 \\
=&\varepsilon^{N-2} \lim_{p\to 0^-} \Big((2\varepsilon - p)\mathsf{log}(2\varepsilon - p) - (2\varepsilon - p) - 2(\varepsilon - p)\mathsf{log}(\varepsilon - p) + 2(\varepsilon - p) - p\mathsf{log}(-p) + p\Big) \\
=&\varepsilon^{N-2} \lim_{p\to 0^-} \Big((2\varepsilon - p)\mathsf{log}(2\varepsilon - p) - 2(\varepsilon - p)\mathsf{log}(\varepsilon - p) - p\mathsf{log}(-p)\Big) < +\infty,
\end{aligned}$$

which concludes the proof. □

Example 4.2.2. In this example we study the trivial case in which we set $A(p) = T_f$ in (4.0.1) as $f(x, p) = f_\infty(x) + p$ with $f_\infty(x) := 0$ for any x in a neighbourhood of x_*, in order to exclude it from the following computations. Whereas the function f_∞ does not satisfy the assumptions on the sign of f in (4.1.2), it provides an interesting and easy-to-study limit case. The time-asymptotic variance along the function $g = \mathbb{1}_{[0,\varepsilon]^N}$ satisfies

$$\langle g, V_\infty^{\mathsf{w}} g\rangle = \frac{\sigma^2}{2}\int_0^\varepsilon \cdots \int_0^\varepsilon \frac{1}{f_\infty(x_1,\dots,x_N) - p}\,\mathsf{d}x_N \dots \mathsf{d}x_1 = \frac{\sigma^2}{2}\int_0^\varepsilon \cdots \int_0^\varepsilon \frac{1}{-p}\,\mathsf{d}x_N \dots \mathsf{d}x_1 = -\frac{\sigma^2}{2p}\varepsilon^N.$$

In the limit of p, we obtain that

$$\lim_{p\to 0^-} \langle g, V_\infty^{\mathsf{w}} g\rangle = \lim_{p\to 0^-} -\frac{\sigma^2}{2p}\varepsilon^N = \infty.$$

Then, we observe a divergence with rate $\Theta_p\left(-p^{-1}\right)$ for p approaching zero from below, if f in (4.0.1) is, locally, equal to the p.

4.2.1 Upper bounds

In the remainder of this section, we find upper bounds for the scaling law of $\langle g, V_\infty^{\mathsf{w}} g\rangle$ under the assumption that the dimension N of the domain of the function f_{an} is larger than 1. From the construction of f_{an} in (4.2.1), we define the set of multi-indices

$$\mathcal{C}^+ := \left\{ j = (i_1, \dots, i_N) \in \mathcal{C} \,\middle|\, \begin{array}{c} a_d = 0 \quad \forall d = (d_1, \dots, d_N) \in \mathcal{C} \quad \text{such that} \\ d_n \leq i_n \quad \forall n \in \{1, \dots, N\} \quad \text{and} \quad d \neq j \end{array} \right\}. \tag{4.2.2}$$

The following lemma introduces an upper bound of $\langle g, V_\infty^{\mathsf{w}} g\rangle$ as $p \to 0^-$. The scaling law induced by this upper bound is studied further below.

Lemma 4.2.3. *Set $f_{\mathsf{an}}(x) = -\sum_{j\in\mathcal{C}} a_j x^j$ for all $x \in \mathcal{X}_1 \subset \mathbb{R}^N$, that satisfies* (4.1.2)*, $\{a_j\}_{j\in\mathcal{C}} \subset \mathbb{R}$, $\varepsilon > 0$ and $Q = \mathrm{Id}$. Fix $j_* \in \mathcal{C}^+$, defined in* (4.2.2)*. Then, the time-asymptotic covariance of the solution of* (4.0.1)*, V_∞^{w}, satisfies,*

$$\langle g, V_\infty^{\mathsf{w}} g\rangle \leq \Theta_p \left(\int_0^\varepsilon \cdots \int_0^\varepsilon \frac{1}{a_{j_*} x^{j_*} - p} \, \mathsf{d}x_1 \dots \mathsf{d}x_N \right),$$

for $g(x) = \mathbb{1}_{[0,\varepsilon]^N}$.

Proof. Since we assume f_{an} to be negative in $\mathcal{X}_1 \setminus \{0\}$ and we consider the bounded domain $[0, \varepsilon]^N$, we know that $a_j > 0$ for any $j \in \mathcal{C}^+$. In particular, we note that for a constant $1 > C > 0$, dependent on ε, and any $x \in [0, \varepsilon]^N$, it holds

$$-f_{\mathsf{an}}(x) = \sum_{j\in\mathcal{C}} a_j x^j \geq C \sum_{j\in\mathcal{C}^+} a_j x^j \geq C a_{j_*} x^{j_*}$$

for $j_* \in \mathcal{C}^+$. In conclusion, we obtain that

$$\langle g, V_\infty^{\mathsf{w}} g\rangle = \frac{\sigma^2}{2} \int_0^\varepsilon \cdots \int_0^\varepsilon \frac{1}{\sum_{j\in\mathcal{C}} a_j x^j - p} \, \mathsf{d}x_1 \dots \mathsf{d}x_N \leq \frac{\sigma^2}{2C} \int_0^\varepsilon \cdots \int_0^\varepsilon \frac{1}{a_{j_*} x^{j_*} - p} \, \mathsf{d}x_1 \dots \mathsf{d}x_N. \tag{4.2.3}$$

□

Without loss of generality and for simplicity, we assume for the remainder of the section that $a_{j_*} = \frac{\sigma^2}{2} = 1$.

Remark 4.2.4. In case the multi-index j_* has $N > k \in \mathbb{N}$ indices with value 0, the analysis on the upper bound in (4.2.3) can be reduced to the case of $N - k$ spatial dimensions. In fact, assuming that $j_* = (i_1, \dots, i_{N-k}, 0, \dots, 0)$, we obtain

$$\int_0^\varepsilon \cdots \int_0^\varepsilon \frac{1}{x^{j_*} - p} \mathsf{d}x_1 \dots \mathsf{d}x_N = \varepsilon^k \int_0^\varepsilon \cdots \int_0^\varepsilon \left(\prod_{n=1}^{N-k} x_n^{i_n} - p \right)^{-1} \mathsf{d}x_1 \dots \mathsf{d}x_{N-k}.$$

We note that the case $N = k$ contradicts the assumption $f(x_*, 0) = 0$ and results in convergence of the upper bound as the bifurcation threshold is not reached for $p \to 0^-$.

As a consequence of Remark 4.2.4, we consider j_* with no elements equal to 0 in the upcoming subsections.

4.2.2 Two dimensions

In this subsection, we investigate an upper bound for the scaling law of $\langle g, V_\infty^{\mathsf{w}} g\rangle$ for $N = 2$. Therefore, we consider $j_* = (i_1, i_2) \in \mathbb{N}^2$. In the following theorem, we outline how to obtain such a bound according to the values of j_*. The proof is included in Appendix D.

Theorem 4.2.5. *We set $f_{an}(x) = -\sum_{j\in\mathcal{C}} a_j x^j$ for all $x \in \mathcal{X}_1 \subset \mathbb{R}^2$, that satisfies* (4.1.2)*, $\{a_j\}_{j\in\mathcal{C}} \subset \mathbb{R}$, $\varepsilon > 0$ and $Q = \mathrm{Id}$. We fix $j_* = (i_1, i_2) \in \mathcal{C}^+$ with $i_1, i_2 > 0$. Then, there exists an upper bound to the time-asymptotic variance of the solution of* (4.0.1) *along $g(x) = \mathbb{1}_{[0,\varepsilon]^2}$, $\langle g, V_\infty^{\mathsf{w}} g\rangle$, and its rate as $p \to 0^-$ is described in Table 4.3 in accordance to the value of i_1 and i_2.*

Table 4.3 Upper bounds to the scaling law of the time-asymptotic variance in dimension $N = 2$ for different choices of indices i_1, i_2, ordered for simplicity. We indicate as $\mathfrak{A}$ and $\mathfrak{B}$ two summands, discussed in Appendix D, whose sum corresponds to the upper bound.

Case	Scaling law for $p \to 0^-$		
	$\mathfrak{A}$	$\mathfrak{B}$	Upper bound
$\mathbf{1} : i_2 > i_1 > 1$	$(-p)^{-1+\frac{1}{i_1}}$	$(-p)^{-1+\frac{1}{i_2}}$	$(-p)^{-1+\frac{1}{i_2}}$
$\mathbf{2} : i_2 > i_1 = 1$	$-\log(-p)$	$(-p)^{-1+\frac{1}{i_2}}$	$(-p)^{-1+\frac{1}{i_2}}$
$\mathbf{3} : i_2 = i_1 > 1$	$(-p)^{-1+\frac{1}{i_1}}$	$-(-p)^{-1+\frac{1}{i_2}}\log(-p)$	$-(-p)^{-1+\frac{1}{i_2}}\log(-p)$
$\mathbf{4} : i_2 = i_1 = 1$	$-\log(-p)$	$\log^2(-p)$	$\log^2(-p)$

In Table 4.3, we establish that only the highest index i_2 affects directly the scaling law of the upper bound introduced in Theorem 4.2.5. However, its relation to the other index i_1 dictates the exact form. The limiting case for $i_1, i_2 \to \infty$ is discussed in Example 4.2.2. Lastly, we note that the bound may not indicate the exact scaling law of the observable, as described in Proposition 4.2.1 and as shown in the next figure. Figure 4.2 displays an intuition for the example $j_* = (2, 3)$ by illustrating the shapes of $-x_1 - x_2$ and $-x_1^2 x_2^3$, for $(x_1, x_2) \in [0, 0.1]^2$. Such functions can be assumed to be locally equal to f_{an} in Proposition 4.2.1 and Theorem 4.2.5, respectively. As displayed, the first function has a unique root on $(0, 0)$ and the second is null on the set (x_1, x_2) such that $x_1 = 0$ or $x_2 = 0$. The different dimensions of such sets are the reason for the fact that the time-asymptotic variance on an indicator function g, $\langle g, V_\infty^{\mathsf{w}} g\rangle$, is characterised by different scaling laws in the limit $p \to 0^-$. In particular, it converges in the first case and diverges with rate $(-p)^{-\frac{2}{3}}$ in the second.[3]

Example 4.2.6. We consider the function f such that it satisfies (4.1.2), $[0, 1]^2 \subset \mathcal{X}_1$ and there exists $C > 0$ for which

$$C^{-1}\left(-x_1^2 - x_2^2\right) \le f_{\mathsf{an}}(x) \le C\left(-x_1^2 - x_2^2\right),$$

for $0 \le x_1, x_2 \le 1$. This implies that

$$\langle g, V_\infty^{\mathsf{w}} g\rangle \le C^{-1}\int_0^1\int_0^1 \frac{1}{x_1^2 + x_2^2 - p}\,\mathrm{d}x_1\,\mathrm{d}x_2 \le C^{-1}\iint_D \frac{1}{x_1^2 + x_2^2 - p}\,\mathrm{d}x_1\,\mathrm{d}x_2,$$

where D denotes the circle of radius $\sqrt{2}$ centered at the origin. We study then the integral in polar coordinates and obtain

$$\iint_D \frac{1}{x_1^2 + x_2^2 - p}\,\mathrm{d}x_1\,\mathrm{d}x_2 = \int_0^{2\pi}\int_0^{\sqrt{2}} \frac{r}{r^2 - p}\,\mathrm{d}r\,\mathrm{d}\theta.$$

[3] We underline that, although $f_{\mathsf{an}}(x) = -x_1^2 x_2^3$ in a neighbourhood of 0 does not satisfy (4.1.2), the scaling law of its time-asymptotic variance is proven in the proof of Theorem 4.2.5.

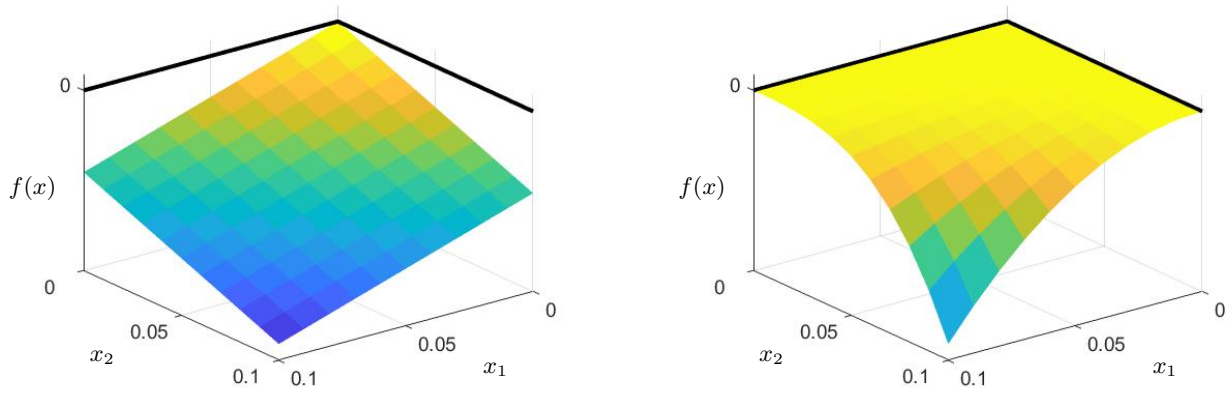

(a) $f_{\text{an}}(x) = -x_1 - x_2$, locally

(b) $f_{\text{an}}(x) = -x_1^2 x_2^3$, locally

Fig. 4.2 Illustration of functions $-x_1 - x_2$, in (a), and $-x_1^2 x_2^3$, in (b), for $x_1, x_2 \in [0, 0.1]$. We set an indicator function $g = \mathbb{1}_{[0,\varepsilon]^2}$, for $0 < \varepsilon \leq 0.1$. As discussed in Proposition 4.2.1 and in the proof of Theorem 4.2.5, the time-asymptotic variance $\langle g, V_\infty^{\mathsf{w}} g\rangle$ presents different scaling laws as $p \to 0^-$ under distinct assumptions of f_{an}. For f_{an} set as in (a), the variance converges in the limit, whereas for f_{an} as displayed in (b), it diverges. We note that the choice of f_{an} in the (a) presents only one value x_* such that $f_{\text{an}}(x_*) = 0$, in contrast with (b), for which $f_{\text{an}}(x_1, x_2) = 0$ for any (x_1, x_2) such that $x_1 = 0$ or $x_2 = 0$. Such lines are displayed in the figure for comparison.

Substituting $r' = r^2 - p$, we get

$$\int_0^{2\pi} \int_0^{\sqrt{2}} \frac{r}{r^2 - p} \,\mathrm{d}r \,\mathrm{d}\theta = \frac{1}{2} \int_0^{2\pi} \int_{-p}^{2-p} \frac{1}{r'} \,\mathrm{d}r' \,\mathrm{d}\theta = \pi \Big(\log(2 - p) - \log(-p) \Big) = \Theta_p \Big(-\log(-p) \Big).$$

A lower bound can be easily obtained through

$$\langle g, V_\infty^{\mathsf{w}} g\rangle \geq C \int_0^1 \int_0^1 \frac{1}{x_1^2 + x_2^2 - p} \,\mathrm{d}x_1 \,\mathrm{d}x_2 \geq C \iint_{\tilde{D}} \frac{1}{x_1^2 + x_2^2 - p} \,\mathrm{d}x_1 \,\mathrm{d}x_2 = \Theta_p \Big(-\log(-p) \Big),$$

for $\tilde{D} = \big\{(x, y) \big|\ x^2 + y^2 \leq 1,\ x, y > 0\big\}$. We find divergence of $\langle g, V_\infty^{\mathsf{w}} g\rangle$, for p approaching zero from below, of rate $\Theta_p \Big(-\log(-p) \Big)$, whereas the upper bounds in Theorem 4.2.5 assume scaling law $\Theta_p \Big((-p)^{-\frac{1}{2}} \Big)$.

4.2.3 Three dimensions

We now assume $N = 3$ and therefore $f_{\text{an}} : \mathcal{X}_1 \subset \mathbb{R}^3 \to \mathbb{R}$ and $g = \mathbb{1}_{[0,\varepsilon]^3}$. The following theorem provides an upper bound for the scaling law of the corresponding early-warning sign $\langle g, V_\infty^{\mathsf{w}} g\rangle$ and its proof is examined in Appendix E.

Theorem 4.2.7. *Set $f_{an}(x) = -\sum_{j \in \mathcal{C}} a_j x^j$ for all $x \in \mathcal{X}_1 \subset \mathbb{R}^3$, that satisfies* (4.1.2)*, $\{a_j\}_{j \in \mathcal{C}} \subset \mathbb{R}$, $\varepsilon > 0$ and $Q = \mathrm{Id}$. Fix $j_* = (i_1, i_2, i_3) \in \mathcal{C}^+$ with $i_1, i_2, i_3 > 0$. Then, there exists an upper bound to the time-asymptotic variance of the solution of* (4.0.1) *along $g(x) = \mathbb{1}_{[0,\varepsilon]^3}$, $\langle g, V_\infty^{\mathsf{w}} g\rangle$, and it has a scaling law bound as $p \to 0^-$ described in Table 4.4 depending upon the values of i_1, i_2 and i_3.*

We observe that if i_3 is strictly larger than the other indices, i_1 and i_2, we obtain a divergence of the upper bound to the signal of order $\Theta_p \Big((-p)^{-1+\frac{1}{i_3}} \Big)$. If the largest index value corresponds to two of the indices, i.e., $i_3 = i_2 > i_1$, then the upper bound to the scaling is $\Theta_p \Big(-(-p)^{-1+\frac{1}{i_3}} \log(-p) \Big)$. We see also that in the case all three indices are equal but larger than 1, i.e., $i_3 = i_2 = i_1 > 1$, then the upper bound is $\Theta_p \Big((-p)^{-1+\frac{1}{i_3}} \log^2(-p) \Big)$. Lastly, setting all the indices equal to 1, the corresponding rate is $\Theta_p \big(-\log^3(-p) \big)$. In Example 4.2.2, the limit case $i_1, i_2, i_3 \to \infty$ is covered.

Table 4.4 Upper bounds to the scaling law of the time-asymptotic variance in dimension $N = 3$ for different choices of indices i_1, i_2 and i_3, ordered for simplicity. We denote as $\mathfrak{C}$ and $\mathfrak{D}$ two values whose sum is the upper bound. These summands are discussed in Appendix E.

Case	Scaling law for $p \to 0^-$		
	$\mathfrak{C}$	$\mathfrak{D}$	Upper bound
$\mathbf{1}: i_3 > i_2 > i_1 > 1$	$(-p)^{-1+\frac{1}{i_2}}$	$(-p)^{-1+\frac{1}{i_3}}$	$(-p)^{-1+\frac{1}{i_3}}$
$\mathbf{2}: i_3 > i_2 = i_1 > 1$	$-(-p)^{-1+\frac{1}{i_2}}\log(-p)$	$(-p)^{-1+\frac{1}{i_3}}$	$(-p)^{-1+\frac{1}{i_3}}$
$\mathbf{3}: i_3 = i_2 > i_1 > 1$	$(-p)^{-1+\frac{1}{i_2}}$	$-(-p)^{-1+\frac{1}{i_3}}\log(-p)$	$-(-p)^{-1+\frac{1}{i_3}}\log(-p)$
$\mathbf{4}: i_3 = i_2 = i_1 > 1$	$-(-p)^{-1+\frac{1}{i_2}}\log(-p)$	$(-p)^{-1+\frac{1}{i_3}}\log^2(-p)$	$(-p)^{-1+\frac{1}{i_3}}\log^2(-p)$
$\mathbf{5}: i_3 > i_2 > i_1 = 1$	$(-p)^{-1+\frac{1}{i_2}}$	$(-p)^{-1+\frac{1}{i_3}}$	$(-p)^{-1+\frac{1}{i_3}}$
$\mathbf{6}: i_3 > i_2 = i_1 = 1$	$\log^2(-p)$	$(-p)^{-1+\frac{1}{i_3}}$	$(-p)^{-1+\frac{1}{i_3}}$
$\mathbf{7}: i_3 = i_2 > i_1 = 1$	$(-p)^{-1+\frac{1}{i_2}}$	$-(-p)^{-1+\frac{1}{i_3}}\log(-p)$	$-(-p)^{-1+\frac{1}{i_3}}\log(-p)$
$\mathbf{8}: i_3 = i_2 = i_1 = 1$	$\log^2(-p)$	$-\log^3(-p)$	$-\log^3(-p)$

4.3 Numerical simulations

In this section, we numerically investigate the analytic results from Section 4.1 and Section 4.2 to gain further insight and also to obtain an outlook on how they can be relevant in a more applied setting. The numerical methods used and discussed follow the theory of [109] and [144].
We simulate first a generalisation of the results obtained in Theorem 4.1.1 for the one-dimensional case and the tool function $f_\alpha(x) = -|x|^\alpha$ on an interval for $\alpha > 0$. In order to approximate the solution of the studied SPDE, we use the Euler-Maruyama method, which we introduce by considering the differential equation

$$\mathsf{d}u^{(\mathsf{w,c})}(x,t) = (f_\alpha(x) + p)\, u^{(\mathsf{w,c})}(x,t)\,\mathsf{d}t + \sigma Q^{\frac{1}{2}}\mathsf{d}W(t), \quad u^{(\mathsf{w,c})}(\cdot,0) = u_0, \quad 0 \le t \le T, \tag{4.3.1}$$

for $\sigma, T > 0 > p$, initial condition $u_0 \in \mathcal{H}_1$ and (further) condition $f_\alpha u^{(\mathsf{w,c})} \in \mathcal{H}_1$. We then discretise the time interval $[0,T]$ by defining the time step $\delta\mathtt{t} = \frac{T}{\mathtt{nt}}$ for a certain positive integer $\mathtt{nt}$, to be the number of steps in time, and $\tau_i := i\ \delta\mathtt{t}$, the time passed after i time steps. Furthermore, we discretise also the space interval $\mathcal{X}_1 = [-L, L]$ with its internal points $r_n = -L + 2\frac{n}{\mathtt{N}+1}L$ for $n \in \{1, \dots, \mathtt{N}\}$, with $\mathtt{N}$ that is an integer that defines the number of mesh points. The numerical approximations of $u^{(\mathsf{w,c})}(\cdot, \tau_i)$, f_α and $W(\cdot, \tau_i)$ are labelled respectively as $\mathtt{u}_i, \mathtt{f}_\alpha, \mathtt{W}_i \in \mathbb{R}^{\mathtt{N}+2}$ for any $i \in \{0, \dots, \mathtt{nt}\}$. Then, by the implicit Euler-Maruyama method, the numerical simulation takes the form

$$\mathtt{u}_i = \mathtt{u}_{i-1} + (\mathtt{f}_\alpha + p)\,\mathtt{u}_i\delta\mathtt{t} + \sigma(\mathtt{W}_i - \mathtt{W}_{i-1}), \quad i = 1, 2, \dots, \mathtt{nt}$$

which approximates the integral form of the SPDE. For fixed $i \in \{1, \dots, \mathtt{nt}\}$, the term $\mathtt{W}_i - \mathtt{W}_{i-1}$ can be expressed as

$$\mathtt{W}_i - \mathtt{W}_{i-1} = \sqrt{\delta\mathtt{t}} \sum_{m=1}^{M} \sqrt{\zeta_m} W_i^{(m)} \mathtt{b}_m$$

with $M \le \mathtt{N}$ being the number of directions in the space function on which the noise is taken numerically into account, $\left\{W_i^{(m)}\right\}_{m\in\{1,\dots,M\}}$ a collection of independent standard Gaussian random variables and the randomly generated $\{(\zeta_m, \mathtt{b}_m)\}_{m\in\{1,\dots,M\}}$, which are respectively the first M eigenvalues and approxima-

tions in $\mathbb{R}^{\mathtt{N}+2}$ of the eigenfunctions of the covariance operator Q of W in (4.3.1).[4]
We numerically simulate a generalisation of results from Theorem 4.1.1, as described in Section 4.4, for the function $f_\alpha = -|x|^\alpha$ for $\alpha > 0$ as defined by (4.1.1). We consider the case $g(x) = \mathbb{1}_{[-\varepsilon,\varepsilon]}$ for $|\{r_n \in [-\varepsilon,\varepsilon]|\ n \in \{1,\dots,\mathtt{N}\}\}| = M$.[5] Further, we assume Q and its inverse Q^{-1} to be bounded operators. The fact that Q is not assumed to be the identity operator implies that the random variables $u^{(\mathsf{w,c})}(x_1,t)$ and $u^{(\mathsf{w,c})}(x_2,t)$ are dependent for any $x_1, x_2 \in \mathcal{X}_1$ and $t > 0$. Hence, the simulation of $u^{(\mathsf{w,c})}$ must be studied as an SPDE rather than a collection of SDEs on the resolution points. As described in Section 4.4, such a choice of Q is expected to imply scaling laws, dependent on α, of the time-asymptotic variance as displayed in Table 4.1. We simulate the projection $\langle u^{(\mathsf{w,c})}(\cdot,\tau_i), g\rangle$ with $\mathrm{proj}_i = \sum_{n:r_n\in[-\varepsilon,\varepsilon]} \mathtt{u}_i(n)$

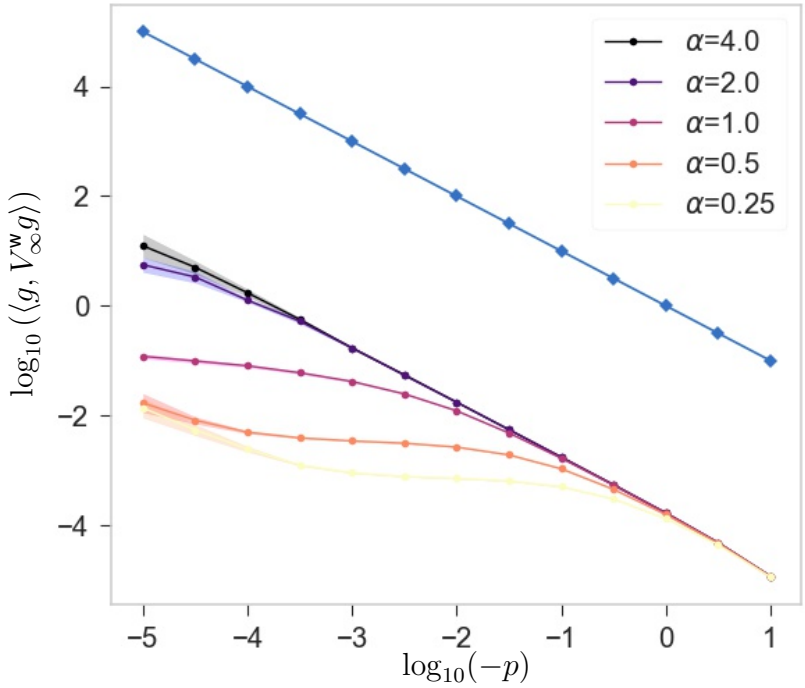

Fig. 4.3 Log-log plot that describes the behaviour of $\langle g, V_\infty^{\mathsf{w}} g\rangle$ as p approaches 0^- in accordance to the choice of the tool function f_α. The circles are obtained as the mean value of $\log_{10}(\langle g, V_\infty^{\mathsf{w}} g\rangle)$ given by 10 independent simulations. The width of the shaded areas scales linearly with the numerical standard deviation. Lastly, the blue line has a slope equal to -1 and is provided as a reference for the scaling law.
For $\alpha \geq 1$, the expected slope from Theorem 4.1.1 is shown close to $p = 10^{-5}$. The convergence is visible for $\alpha < 1$ until p assumes small values. In fact, for small $\mathtt{N}$, the log-log plot displays slope -1 induced by the divergence being only perceived on $x = 0$ and therefore leading to a behaviour similar to that of an Ornstein-Uhlenbeck process [131]. Conversely, this effect is a hint to the fact that under the case of purely discrete spectrum, such as discussed in Chapter 3, and small gaps, the early-warning is hindered before reaching the expected rate of divergence.

for any $i \in \{1,\dots,\mathtt{nt}\}$. We approximate the behaviour of the scalar product that defines the variance along g, $\langle g, V_\infty^{\mathsf{w}} g\rangle$, as the numerical variance in time i of proj_i. The results are displayed as a log-log plot in Figure 4.3. Since we are interested in the behaviour for p approaching zero from below, we focus on negative values of $\log_{10}(-p)$. Validating the analytic results in Table 4.1, for $\alpha > 1$ we observe $\log_{10}(\langle g, V_\infty^{\mathsf{w}} g\rangle)$ in order to assume a negative slope of $-1 + \frac{1}{\alpha}$ as $\log_{10}(-p)$ approaches $-\infty$. In the case $\alpha = 1$, we expect a logarithmic divergence to be displayed in the log-log plot as $\log_{10}(-p)$ decreases. Lastly, we expect convergence for $0 < \alpha < 1$, which is shown up to small values of p due to numerical errors.[6]

Next, we study the two-dimensional case and numerically simulate the asymptotic behaviour of the upper bound of $\langle g, V_\infty^{\mathsf{w}} g\rangle$ as described in Theorem 4.2.5. In particular, our goal is to illustrate the results analytically found for the indices i_1, i_2 such that $i_2 \geq i_1 \geq 1$. For this case, we have found the scal-

[4] The eigenvalues $\{(\zeta_m)\}_{m\in\{1,\dots,M\}}$ are generated uniformly in $[0.5, 2]$.

[5] The orthogonal matrix whose indices are $\{\mathtt{b}_m(n)|r_n \in [-\varepsilon,\varepsilon]\}_{m\in\{1,\dots,M\}}$ is generated through $\mathtt{O}(M)$ Haar distribution, for $\mathtt{O}(M)$ that indicates the space of orthogonal $M \times M$ matrices with real-valued elements [155]. The rest of the elements in $\{(\mathtt{b}_m)\}_{m\in\{1,\dots,M\}}$, which are irrelevant to the study of the time-asymptotic variance along g, can be obtained through Graham-Schmidt method.

[6] $L = 1$, $\mathtt{N} = 99999$, $\mathtt{nt} = 10000000$, $\delta\mathtt{t} = 0.1$, $\sigma = 0.1$, $\varepsilon = 0.01$, $M = 999$.

ing law of the upper bound as displayed in Table 4.3. Consequently, we compute the dependence of $\int_0^\varepsilon \int_0^\varepsilon \frac{1}{x_1^{i_1} x_2^{i_2} - p} \, \mathrm{d}x_1 \, \mathrm{d}x_2$ on $p < 0$ in a log-log plot.

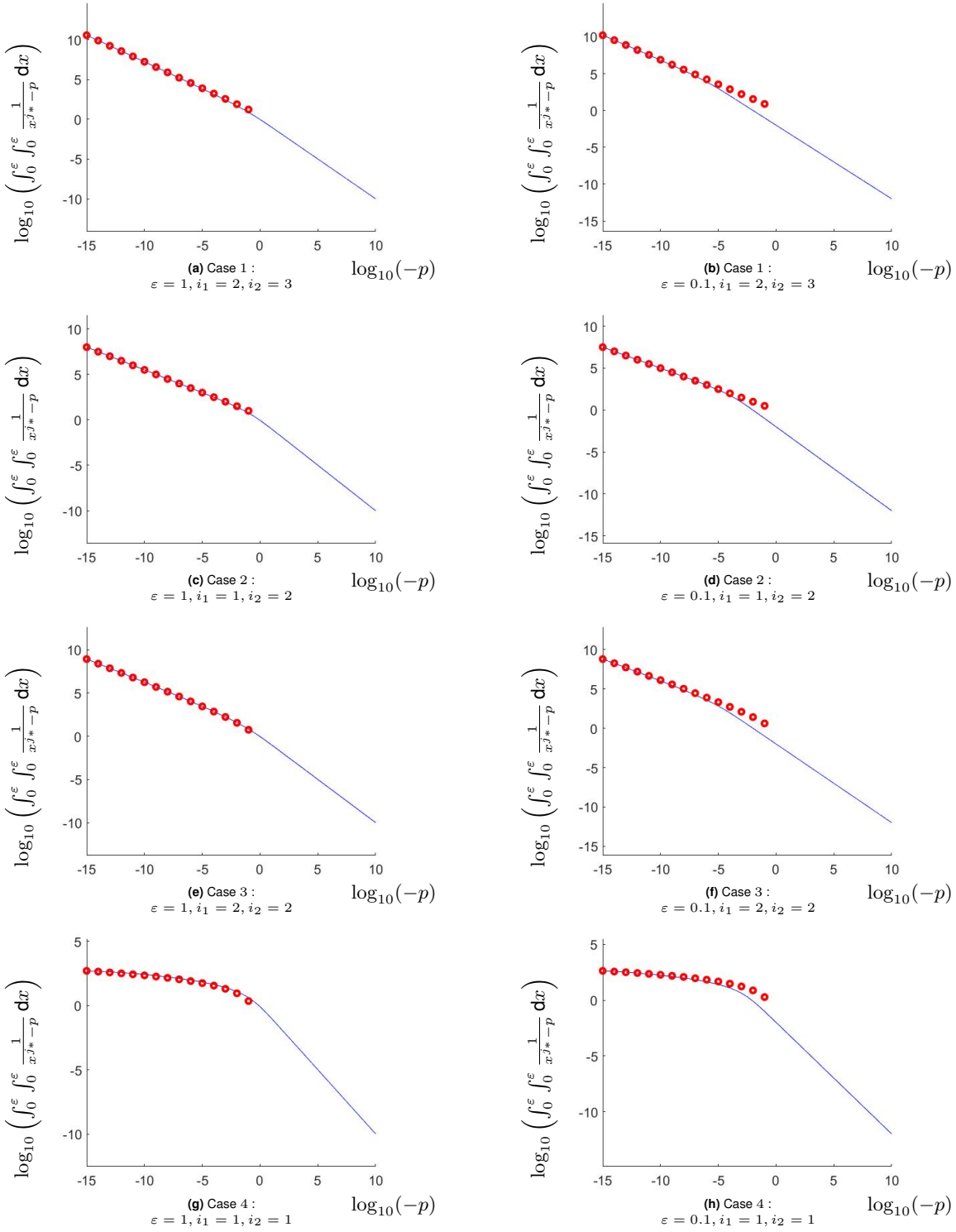

Fig. 4.4 The solid lines describe the scaling law of the upper bound for the two-dimensional problem, illustrated by $\log_{10}\left(\int_0^\varepsilon \int_0^\varepsilon \frac{1}{x^{j_*} - p} \, \mathrm{d}x\right)$ and decreasing $\log_{10}(-p)$ with $x = (x_1, x_2)$ and $j_* = (i_1, i_2)$. The numbering of the cases refers to Table 4.3. The circle lines are used as a comparison with the corresponding scaling law presented in the table as an argument of $\log_{10}$.

The subfigures shown in Figure 4.4 are obtained for different choices of ε and of $i_2 \geq i_1 \geq 1$. We see that the results are confirmed since the double integrals, displayed as solid lines, show a similar qualitative behaviour as the analytic result in Table 4.3, corresponding to the red circles, for small values of $-p$.

In particular, in the Figure 4.4a, Figure 4.4b, Figure 4.4c and Figure 4.4d, corresponding to Case 1 and Case 2 of the table, we obtain a slope equal to $-1+\frac{1}{i_2}$. The red circles in Figure 4.4e and Figure 4.4f, corresponding to Case 3, assume values $\log_{10}(-p)(-1+\frac{1}{i_2})+\log_{10}(-\log_{10}(-p))+c$ and the values in Figure 4.4g and Figure 4.4h, corresponding to Case 4, are equal to $2\log_{10}(-\log_{10}(-p))+c$, for different constants c. Decreasing the parameter $\varepsilon>0$ appears to imply a decrease of the lowest threshold $q_c>0$ such that for any $-p>q_c$ the slope of $\log_{10}\left(\int_0^\varepsilon\int_0^\varepsilon \frac{1}{x_1^{i_1}x_2^{i_2}-p}\,\mathrm{d}x_1\mathrm{d}x_2\right)$ in the log-log plot is approximately -1. Such a slope is implied by the fact that, for $p\ll 0$, the values of $x_1^{i_1}x_2^{i_2}-p$ present the same order of distance from 0 for any $x_1,x_2\in[0,\varepsilon]$ and, therefore, the early warning sign displays similar behaviour to those discussed in [93, 135] and Chapter 3 for such values of p.
Lastly, we illustrate the results of Theorem 4.2.7 by computing the values of $\int_0^\varepsilon\int_0^\varepsilon\int_0^\varepsilon \frac{1}{x_1^{i_1}x_2^{i_2}x_3^{i_3}-p}\,\mathrm{d}x_1\,\mathrm{d}x_2\,\mathrm{d}x_3$ on $p<0$ in a log-log plot for different values of $i_3\geq i_2\geq i_1\geq 1$. We then compare them to the corresponding scaling laws displayed in Table 4.4.
The plots shown in Figure 4.5 are obtained for the fixed value $\varepsilon=1$ and of the exponents $i_3\geq i_2\geq i_1\geq 1$. The triple integral displays a similar qualitative behaviour as the analytic results in Table 4.4, again denoted by red circles, for small values of $-p$. In fact, in Figure 4.5a, Figure 4.5b, Figure 4.5e and Figure 4.5f, corresponding to Case 1, Case 2, Case 5 and Case 6 of the mentioned table, they display a slope of value $-1+\frac{1}{i_3}$. The red circles in Figure 4.5c and Figure 4.5g, corresponding to Case 3 and Case 7, have values $\log_{10}(-p)(-1+\frac{1}{i_3})+\log_{10}(-\log_{10}(-p))+c$, for distinct constants c. The red circles shown in Figure 4.5d, corresponding to Case 4, are equal to $\log_{10}(-p)(-1+\frac{1}{i_3})+2\log_{10}(-\log_{10}(-p))+c$ and those displayed in Figure 4.5h, corresponding to Case 8, are $3\log_{10}(-\log_{10}(-p))+c$, for a different constant c each.

4.4 Generalisations and examples

4.4.1 Generalisations

In this subsection, we generalise and discuss the main results obtained above, focusing on the impact of relaxing the hypotheses in Chapter 2. In particular, similar results to those presented in Theorem 4.1.3, Theorem 4.2.5 and Theorem 4.2.7 can be obtained under more general choices of functions f,g and operator Q. We also study the theorems for $\mathrm{T}_{f_{\mathsf{an}}}$ with complex spectrum. Lastly, we discuss the case in which different linear operators $A(p)$ with continuous spectrum are assumed in the drift term of (4.0.1).

- The condition of the uniqueness of x_* such that $f(x_*,0)=0$ is required only in a local sense in $\mathcal{X}_1$. In fact, we could assume the existence of $\mathcal{Z}\subset\mathcal{X}_1$ which comprises the elements $x\in\mathcal{X}_1$ that satisfy $f(x)=0$ and that any $x\in\mathcal{Z}$ assures $|x_*-x|>\epsilon>0$. Such a choice would trivially leave unchanged the scaling laws described in Theorem 4.1.3, Theorem 4.2.5 and Theorem 4.2.7, for functions g such that the support of g has an empty intersection with $\mathcal{Z}$.
  The analytic behaviour of the non-positive function f presented in Theorem 4.1.3, Theorem 4.2.5 and Theorem 4.2.7 can be assumed only in a neighbourhood of the roots of the function, while f satisfies the integrability condition in (4.1.2) and the sign properties previously described.

- In Theorem 4.1.3, Theorem 4.2.5 and Theorem 4.2.7, the support of the function g is assumed to be $[0,\varepsilon]^N$ and g to be an indicator function. However, the scaling laws in Table 4.1, Table 4.3 and Table 4.4 are applicable for a more general choice of proxy functions.
  First, similarly to Remark 4.1.5, the upper bounds described in Theorem 4.2.5 and Theorem 4.2.7 can be shown to hold with $g=\mathbb{1}_{[-\varepsilon,\varepsilon]^N}$, in the sense that the hypercube $[-\varepsilon,\varepsilon]^N\subset\mathcal{X}_1$ that describes the support of g can be split in 2^N hypercubes on which such statements have been previously proven, up to reparametrisation and rescaling of the spatial variable x. In fact, the highest rate of divergence dictates the order assumed by the upper bound of $\langle g,V_\infty^{\mathsf{w}}g\rangle$.

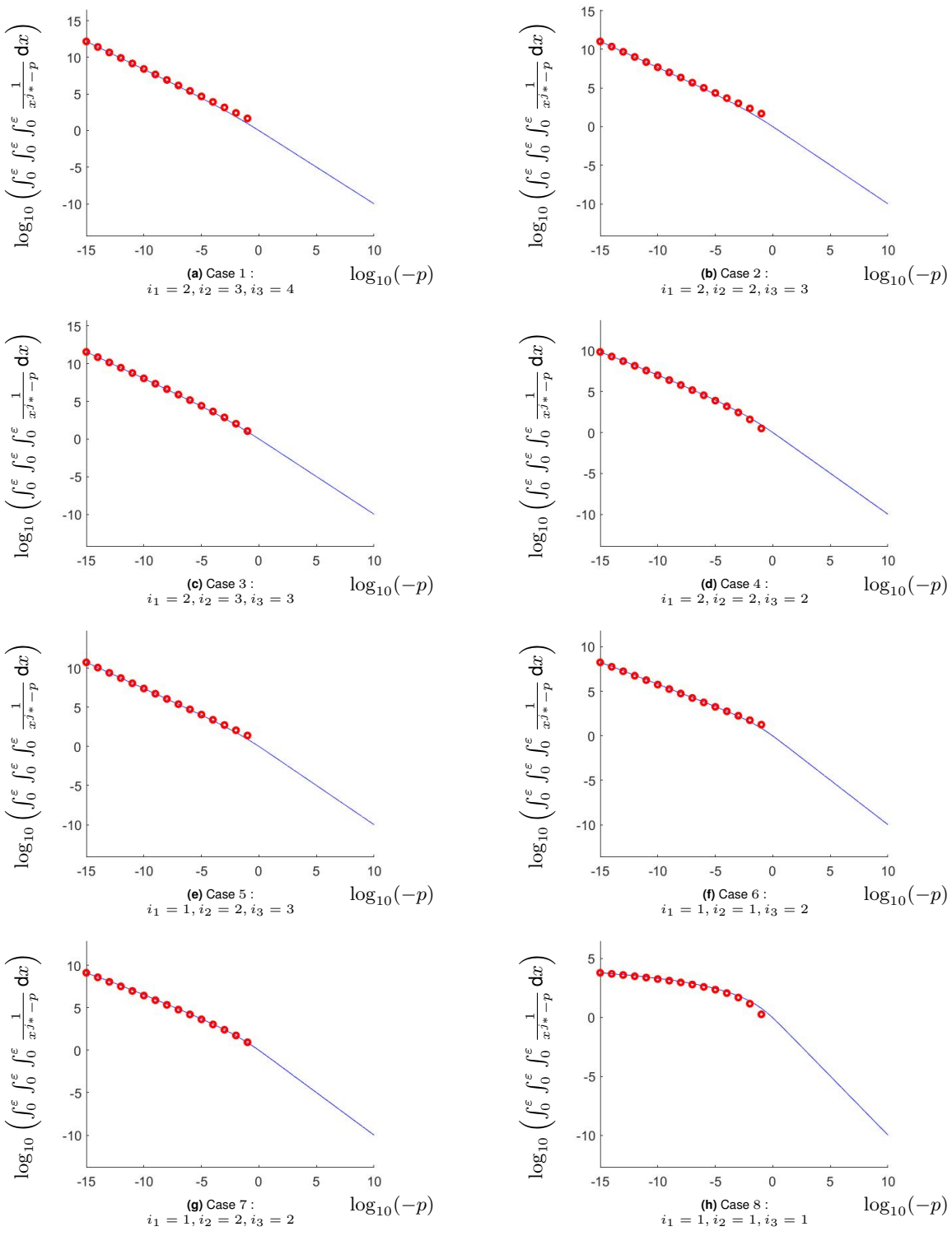

Fig. 4.5 The solid lines display the scaling law of the upper bound for the three-dimensional problem indicated by $\log_{10}\left(\int_0^\varepsilon \int_0^\varepsilon \int_0^\varepsilon \frac{1}{x^{j_*}-p}\,\mathrm{d}x\right)$ and decreasing $\log_{10}(-p)$ with $x = (x_1, x_2, x_3)$ and $j_* = (i_1, i_2, i_3)$. The numbering of cases is equivalent to Table 4.4. The circle lines serve as a comparison with the corresponding scaling law presented in the table as an argument of $\log_{10}$.

The shape of the support can also be generalised. Set $g = \mathbb{1}_{\mathcal{S}}$ for $[-\varepsilon, \varepsilon]^N \subset \mathcal{S} \subset \mathcal{X}_1$, then the integral

$$\langle g, V_\infty^{\mathsf{w}} g\rangle = \frac{\sigma^2}{2}\int_{\mathcal{S}} \frac{-1}{f_{\mathsf{an}}(x)+p}\,\mathrm{d}x = \frac{\sigma^2}{2}\int_{\mathcal{S}\setminus[-\varepsilon,\varepsilon]^N} \frac{-1}{f_{\mathsf{an}}(x)+p}\,\mathrm{d}x + \frac{\sigma^2}{2}\int_{[-\varepsilon,\varepsilon]^N} \frac{-1}{f_{\mathsf{an}}(x)+p}\,\mathrm{d}x$$

assumes an equivalent rate of divergence to the second summand on the right-hand side of the equation. That is implied by the fact that the first summand converges as $p \to 0^-$ by construction. The scaling law is also unchanged under the assumption of $g \in \mathcal{H}_1$ such that g and g^{-1} are bounded from above in a neighbourhood of x_* as, for any $p < 0$, it holds

$$C^{-1}\frac{\sigma^2}{2}\int_{\mathcal{S}} \frac{-1}{f_{\mathsf{an}}(x)+p}\,\mathrm{d}x \leq \langle g, V_\infty^{\mathsf{w}} g\rangle \leq C\frac{\sigma^2}{2}\int_{\mathcal{S}} \frac{-1}{f_{\mathsf{an}}(x)+p}\,\mathrm{d}x,$$

for a constant $C > 1$ depending on g and on the choice of $\mathcal{S}$.
Lastly, assume $g_1, g_2 \in \mathcal{H}_1$ which are continuous in a neighbourhood $\mathcal{S}$ of x_* and such that g_1, g_2, g_1^{-1} and g_2^{-1} are bounded from above in $\mathcal{S}$. We note that such a set of functions is dense in $\mathcal{H}_1$. For simplicity, we set $g_1(x_*)g_2(x_*) > 0$. The scaling law of the scalar product in (4.0.2) is obtained through

$$C^{-1}\frac{\sigma^2}{2}\int_{\mathcal{S}} \frac{-1}{f_{\mathsf{an}}(x)+p}\,\mathrm{d}x \leq \langle g_1, V_\infty^{\mathsf{w}} g_2\rangle \leq C\frac{\sigma^2}{2}\int_{\mathcal{S}} \frac{-1}{f_{\mathsf{an}}(x)+p}\,\mathrm{d}x,$$

for $C > 1$ and any p close to 0, thus enabling a study of the covariance operator V_∞^{w}.

- A third generalisation of Theorem 4.1.3, Theorem 4.2.5 and Theorem 4.2.7 is given by relaxation of the assumptions for Q. In particular, we can assume Q and its inverse on $\mathcal{H}_1$, Q^{-1}, to have bounded eigenvalues from above. The covariance operator takes the form

$$V_\infty^{\mathsf{w}} = \sigma^2 \int_0^\infty \mathrm{e}^{\tau(\mathrm{T}_{f_{\mathsf{an}}}+p)} Q \mathrm{e}^{\tau(\mathrm{T}_{f_{\mathsf{an}}}+p)}\,\mathrm{d}\tau.$$

Hence, we get

$$\langle g, V_\infty^{\mathsf{w}} g\rangle = \sigma^2 \int_0^\infty \langle Q^{\frac{1}{2}}\mathrm{e}^{t(\mathrm{T}_{f_{\mathsf{an}}}+p)} g, Q^{\frac{1}{2}}\mathrm{e}^{t(\mathrm{T}_{f_{\mathsf{an}}}+p)} g\rangle\,\mathrm{d}t = \sigma^2 \int_0^\infty \|Q^{\frac{1}{2}}\mathrm{e}^{t(\mathrm{T}_{f_{\mathsf{an}}}+p)} g\|^2\,\mathrm{d}t,$$

for any $g \in \mathcal{H}_1$. Since we have assumed that Q and its inverse have bounded eigenvalues from above, the scalar product is also bounded from below and above, as we have

$$\begin{aligned}&\inf_n \zeta_n \sigma^2 \int_0^\infty \|\mathrm{e}^{(\mathrm{T}_{f_{\mathsf{an}}}+p)t} g\|^2\,\mathrm{d}t \leq \sigma^2 \int_0^\infty \|Q^{\frac{1}{2}}\mathrm{e}^{(\mathrm{T}_{f_{\mathsf{an}}}+p)t} g\|^2\,\mathrm{d}t \\ &\leq \sup_n \zeta_n \sigma^2 \int_0^\infty \|\mathrm{e}^{(\mathrm{T}_{f_{\mathsf{an}}}+p)t} g\|^2\,\mathrm{d}t, \end{aligned} \tag{4.4.1}$$

with $\{\zeta_n\}_n$ referring to the eigenvalues of Q. This implies that we have found an upper and lower bound for $\langle g, V_\infty^{\mathsf{w}} g\rangle$ whose scaling law is controlled in accordance with the results in Theorem 4.1.3, Theorem 4.2.5 and Theorem 4.2.7. Therefore, the rate of divergence for the choices of f and g described in the theorems or in the previous generalisations is displayed in Tables 4.1, Table 4.3 and Table 4.4, in accordance to the value of dimension $N \in \{1, 2, 3\}$.
Assuming instead Q to be bounded, the validity of the rates of the upper bound in Theorem 4.2.5 and Theorem 4.2.7 is maintained as the second inequality in (4.4.1) holds.

- We now consider the case in which the spectrum of $A(p) = \mathrm{T}_{f_{\mathsf{an}}} + p$ in (4.0.1) has complex values, i.e., we choose a function $f_{\mathsf{an}} : \mathcal{X}_1 \subset \mathbb{R}^N \to \mathbb{C}$ and the solution of (4.0.1) as $u^{(\mathsf{w},\mathsf{c})} \in L^2(\mathcal{X}_1; \mathbb{C})$ for any $t > 0$ and $\mathbb{P}$-almost surely. We suppose also that $\mathrm{Re}(f)$ satisfies (4.1.2). The scalar product of the covariance operator takes the form

$$\langle g, V_\infty^{\mathsf{w}} g\rangle = \int_{\mathcal{X}_1} \overline{g(x)} \int_0^\infty \mathrm{e}^{(\overline{f_{\mathsf{an}}(x)}+p)t}\mathrm{e}^{(f_{\mathsf{an}}(x)+p)t} g(x)\,\mathrm{d}t\,\mathrm{d}x = -\int_{\mathcal{X}_1} |g(x)|^2 \frac{\sigma^2}{2(\mathrm{Re}(f_{\mathsf{an}}(x))+p)}\,\mathrm{d}x.$$

for any $g \in L^2(\mathcal{X}_1;\mathbb{C})$. Assuming that $\mathrm{Re}(f)$ is analytic, we conclude that the rate of divergence, or its upper bound if $N > 1$, of the studied time-asymptotic variance along almost any $g \in L^2(\mathcal{X}_1;\mathbb{C})$ behaves equivalently to those indicated by Theorem 4.1.3, Theorem 4.2.5 and Theorem 4.2.7 under the choices of real-valued functions $\mathrm{Re}(f)$, associated to the multiplication operator, and $|g(x)|$, as the direction along which the corresponding time-asymptotic variance is studied.

- Lastly, we study the system

$$\begin{cases} \mathsf{d}u^{(\mathsf{w,c})}(x,t) = (A+p)\,u^{(\mathsf{w,c})}(x,t)\,\mathsf{d}t + \sigma \mathsf{d}W(t) \\ u^{(\mathsf{w,c})}(\cdot,0) = u_0 \end{cases} \tag{4.4.2}$$

for A a linear self-adjoint operator in $\mathcal{H}_1$ with non-positive spectrum. The spectral theorem [100, Theorem 10.10] implies the existence of a σ-finite measure space $(\tilde{\mathcal{X}},\mu)$, a measurable function $\tilde{f} : \tilde{\mathcal{X}} \to \mathbb{R}$ and a unitary map $U : \mathcal{H}_1 \to L^2(\tilde{\mathcal{X}},\mu)$ such that

$$U(\mathcal{H}_1) = \left\{\tilde{g} \in L^2(\tilde{\mathcal{X}},\mu) |\ \tilde{f}\tilde{g} \in L^2(\tilde{\mathcal{X}},\mu)\right\}$$

and

$$UAU^{-1} = \mathrm{T}_{\tilde{f}},$$

for $\mathrm{T}_{\tilde{f}} : L^2(\tilde{\mathcal{X}},\mu) \to L^2(\tilde{\mathcal{X}},\mu)$ a multiplication operator for $\tilde{f}$. Assuming e^{A+p} to have finite trace, the time-asymptotic covariance operator for the solution of (4.4.2) is

$$\langle g, V_\infty^{\mathsf{w}} g\rangle = \sigma^2 \int_0^\infty \langle \mathsf{e}^{2t(A+p)} g, g\rangle\, \mathsf{d}t,$$

for $Q = \mathrm{Id}$ and $g \in \mathcal{H}_1$. Denoting $\tilde{g} = Ug$, we obtain through Fubini's Theorem that

$$\begin{aligned} \langle g, V_\infty^{\mathsf{w}} g\rangle &= \sigma^2 \int_0^\infty \langle U^{-1}\mathsf{e}^{2t(\mathrm{T}_{\tilde{f}}+p)} Ug, g\rangle\, \mathsf{d}t = \sigma^2 \int_0^\infty \langle \mathsf{e}^{2t(\mathrm{T}_{\tilde{f}}+p)}\tilde{g},\tilde{g}\rangle_{L^2(\tilde{\mathcal{X}},\mu)}\, \mathsf{d}t \\ &= \int_{\tilde{\mathcal{X}}} \tilde{g}(x) \int_0^\infty \mathsf{e}^{2t(\tilde{f}(x)+p)}\tilde{g}(x)\, \mathsf{d}t\, \mathsf{d}\mu(x) = -\int_{\tilde{\mathcal{X}}} \tilde{g}(x)^2 \frac{\sigma^2}{2(\tilde{f}(x)+p)}\, \mathsf{d}\mu(x). \end{aligned}$$

The operators A and $\mathrm{T}_{\tilde{f}}$ share the same spectrum. We can assume that there exists an interval $(-\delta, 0]$ in the continuous spectrum of A, which yields that $\mu(\{\tilde{f} = 0\}) = 0$ and that there exists at least a point $x_* \in \tilde{\mathcal{X}}$ such that $\tilde{f}(x_*) = 0$. From the Stone-Weierstrass theorem [100, Appendix A], we know that, for g in a dense subset of $\mathcal{H}_1$, the associated $\tilde{g} \in L^2(\tilde{\mathcal{X}},\mu)$ assumes bounded and non-null values μ-a.e. in a neighbourhood of each root x_*. The scaling law for the case $N = 1$ can be studied similarly to Remark 4.1.4, given insights about the measure μ and assuming $\tilde{f}$ analytic [100]. Such an assumption is not restrictive for A bounded since such a condition implies that $\tilde{f}$ is bounded [100, Theorem 7.20]. In fact, we fix x_*, a neighbourhood $\hat{\mathcal{X}} \subset \tilde{\mathcal{X}}$ and define

$$\begin{aligned} S_p &= \{\tilde{f} : \hat{\mathcal{X}} \to \mathbb{R} |\ \tilde{f} \quad \text{is polynomial},\ \tilde{f}(x_*) = 0\}, \\ S_a &= \{\tilde{f} : \hat{\mathcal{X}} \to \mathbb{R} |\ \tilde{f} \quad \text{is analytic},\ \tilde{f}(x_*) = 0\}, \\ S_c &= \{\tilde{f} : \hat{\mathcal{X}} \to \mathbb{R} |\ \tilde{f} \quad \text{is continuous},\ \tilde{f}(x_*) = 0\}, \\ S_b &= \{\tilde{f} : \hat{\mathcal{X}} \to \mathbb{R} |\ \tilde{f} \quad \text{is bounded},\ \tilde{f}(x_*) = 0\}, \\ S_l &= \{\tilde{f} : \hat{\mathcal{X}} \to \mathbb{R} |\ \tilde{f} \in L^2(\hat{\mathcal{X}}),\ \tilde{f}(x_*) = 0\}. \end{aligned}$$

Stone-Weierstrass Theorem states that S_p, and thus S_a, is dense in S_c. Also, S_c is dense in S_l, and therefore in S_b. Hence, elements in $S_a \cap \{\tilde{f} : \hat{\mathcal{X}} \to \mathbb{R} |\ \tilde{f}(x) < 0 \quad \text{for} \quad x \neq x_*\}$ can approximate functions in $S_b \cap \{\tilde{f} : \hat{\mathcal{X}} \to \mathbb{R} |\ \tilde{f}(x) < 0 \quad \text{for} \quad x \neq x_*\}$. Such sets of functions can be treated due to [100, Proposition 7.21].

4.4.2 Analytic examples

In the current subsection, we provide established examples of the previously introduced generalisations. The focus is on different operators observed in Fourier space. Such a choice is also justified by their significance in applications, in particular for the widely studied differential operators [31, 176]. Specific systems relevant to modelling real-life phenomena are described in Section 4.5.

Example 4.4.1. Fix a non-positive function $f : \mathbb{R} \to \mathbb{R}$ that satisfies (4.1.2). Consider the linear operator $A : \mathcal{D}(A) \to L^2(\mathbb{R})$ such that for any $g \in \mathcal{D}(A)$ it holds

$$Ag(x) = f_{\mathsf{an}} * g(x), \quad \mathcal{D}(A) := \left\{ g \quad \text{Lebesgue measurable} \;\middle|\; f_{\mathsf{an}} * g \in \mathcal{H}_1 \right\},$$

where $*$ denotes convolution. We want to study the variance of the solution of the system (4.4.2) for Q bounded with bounded inverse and $u_0 \in \mathcal{D}(A)$. We define the Fourier transform $\mathcal{F} : L^2(\mathbb{R}) \to L^2(\mathbb{R})$, which is a unitary map. Assume $g \in L^2(\mathbb{R})$, then

$$\begin{aligned}\langle g, V_\infty^{\mathsf{w}} g\rangle &= \sigma^2 \int_0^\infty \langle \mathsf{e}^{t(A+p)} Q \mathsf{e}^{t(A+p)} g, g\rangle \,\mathsf{d}t = \sigma^2 \int_0^\infty \|Q^{\frac{1}{2}} \mathsf{e}^{t(A+p)} g\|^2 \,\mathsf{d}t = \Theta_p\left(\int_0^\infty \|\mathsf{e}^{t(A+p)} g\|^2 \,\mathsf{d}t\right) \\ &= \Theta_p\left(\int_0^\infty \|\mathcal{F}^{-1} \mathsf{e}^{t(\mathrm{T}_{f_{\mathsf{an}}}+p)} \mathcal{F} g\|^2 \,\mathsf{d}t\right) = \Theta_p\left(\int_0^\infty \|\mathsf{e}^{t(\mathrm{T}_{f_{\mathsf{an}}}+p)} \mathcal{F} g\|^2 \,\mathsf{d}t\right).\end{aligned}$$

The scaling law of the variance can thus be computed, or compared, through Theorem 4.1.1 for f that satisfies (4.1.3) for $\alpha > 0$ and for g in a dense subset of $L^2(\mathbb{R})$. As an example, we consider

$$f(x,p) = \begin{cases} -|x| + p, & \text{for} \quad x \in [-1,1] \\ -x^2 + p, & \text{for} \quad x \in \mathbb{R} \setminus [-1,1] \end{cases}$$

and $g = \mathcal{F}^{-1}\mathbb{1}_{[-\varepsilon,\varepsilon]}$. The rate of divergence of the time-asymptotic variance is therefore $-\log(-p)$ as $p \to 0^-$.

Example 4.4.2. Consider the self-adjoint operator $A : \mathcal{W}^{2m,2}(\mathbb{R}) \to L^2(\mathbb{R})$ for $m \in \mathbb{N}$ such that

$$Ag(x) = (-1)^{(m-1)} \partial_x^{2m} g(x),$$

where ∂_x denotes the weak derivative on $\mathcal{W}^{1,2}(\mathbb{R})$, and assume $g \in \mathcal{W}^{2m,2}(\mathbb{R})$. We study the variance of the solution of (4.4.2) for $u_0 \in \mathcal{W}^{2m,2}(\mathbb{R})$, $p < 0$ and Q a bounded operator with bounded inverse. For $g \in \mathcal{W}^{2m,2}(\mathbb{R})$ and $f_{\mathsf{an}}(k) = -k^{2m}$ for any $k \in \mathbb{R}$, we find that

$$\begin{aligned}\langle g, V_\infty^{\mathsf{w}} g\rangle &= \sigma^2 \int_0^\infty \langle \mathsf{e}^{t(A+p)} Q \mathsf{e}^{t(A+p)} g, g\rangle \,\mathsf{d}t = \Theta_p\left(\int_0^\infty \|\mathsf{e}^{t(A+p)} g\|^2 \,\mathsf{d}t\right) \\ &= \Theta_p\left(\int_0^\infty \|\mathcal{F}^{-1} \mathsf{e}^{t(\mathrm{T}_{f_{\mathsf{an}}}+p)} \mathcal{F} g\|^2 \,\mathsf{d}t\right) = \Theta_p\left(\int_0^\infty \|\mathsf{e}^{t(\mathrm{T}_{f_{\mathsf{an}}}+p)} \mathcal{F} g\|^2 \,\mathsf{d}t\right).\end{aligned}$$

From Theorem 4.1.1, the scaling law as $p \to 0^-$ for g in a dense subset of $\mathcal{W}^{2m,2}(\mathbb{R})$ is $\Theta_p\left((-p)^{-1+\frac{1}{2m}}\right)$.

Example 4.4.3. We introduce the self-adjoint operator $A(p) : \mathcal{W}^{2,2}(\mathbb{R}) \to L^2(\mathbb{R})$ such that $A(p)$ has negative spectrum for $p < 0$. We assume the existence and uniqueness of $\lambda(p)$, an element in its spectrum that satisfies $\lambda(0) = 0$ and is continuous in p. The spectrum is assumed to be purely absolutely continuous for any $p \leq 0$ and supported in $(-\infty, \lambda(p)]$. The mentioned assumptions are satisfied, for instance, by certain Schrödinger operators $A(p) = \Delta - v(p,\cdot)$ for a bounded real potential $v(p,\cdot)$ with compact support

for any $p \leq 0$ [70]. For any $g \in \mathcal{H}_1$, $p \leq 0$ and any continuous function $\tilde{f}$, we define the absolutely continuous measure $\mu_{g,p}$ with respect to the Lebesgue measure, such that

$$\langle g, \tilde{f}(A(p))g \rangle = \int_{-\infty}^{\lambda(p)} \tilde{f}(x) \, \mathsf{d}\mu_{g,p}(x).$$

It follows that the time-asymptotic covariance operator associated with the solutions of

$$\begin{cases} \mathsf{d}u^{(\mathsf{w},\mathsf{c})}(x,t) = A(p)u^{(\mathsf{w},\mathsf{c})}(x,t) \, \mathsf{d}t + \sigma \mathsf{d}W(t) \\ u^{(\mathsf{w},\mathsf{c})}(\cdot,0) = u_0 \end{cases}$$

and $Q = \mathrm{Id}$ satisfies

$$\langle g, V_\infty^{\mathsf{w}} g \rangle = \sigma^2 \int_{-\infty}^{\lambda(p)} \int_0^\infty \mathsf{e}^{2tx} \, \mathsf{d}t \, \mathsf{d}\mu_{g,p}(x) = -\frac{\sigma^2}{2} \int_{-\infty}^{\lambda(p)} \frac{1}{x} \, \mathsf{d}\mu_{g,p}(x),$$

for any $p < 0$. We introduce the Radon–Nikodym derivative $r_{g,p}(x) = \frac{\mathsf{d}\mu_{g,p}(x)}{\mathsf{d}x}$. Under the assumption of continuity of $r_{g,p}$ on p, we obtain that

$$\langle g, V_\infty^{\mathsf{w}} g \rangle = -\frac{\sigma^2}{2} \int_{-\infty}^{\lambda(p)} \frac{r_{g,p}(x)}{x} \, \mathsf{d}x$$

and the scaling law of the early-warning sign.

Remark 4.4.4. The early-warning sign in the form of the divergence of the time-asymptotic variance of the solution of a linearised system (4.4.2) has been studied in the case of the linear non-positive self-adjoint operator A with discrete spectrum [23, 93, 135]. An example of such an operator is

$$\partial_x^2 : \mathcal{W}^{2,2}([-L, L]) \to L^2([-L, L])$$

with Neumann boundary conditions. Its eigenvalues are known to be $\{\lambda_i\}_{i \in \mathbb{N}}$ for $\lambda_i = -\left(\frac{i\pi}{L}\right)^2$ and corresponding eigenfunctions $e_i(\cdot) := \cos(\lambda_i \cdot)$. For $g \in \mathcal{W}^{2,2}([-L, L])$, the time-asymptotic variance of the solution of (4.4.2) is

$$\langle g, V_\infty^{\mathsf{w}} g \rangle = -\frac{\sigma^2}{2} \sum_{i \in \mathbb{N}} \frac{\langle g, e_i \rangle^2}{\lambda_i + p}, \tag{4.4.3}$$

which is proven in [23]. Under the assumption that $\langle g, e_0 \rangle \neq 0$, the rate of divergence of the variance is of order $\Theta_p\left((-p)^{-1}\right)$ as $p \to 0^-$. This property is shared with the case $\alpha \to \infty$ in Table 4.1.
In the limit $L \to \infty$, the spectrum of the operator $\partial_x^2 : \mathcal{W}^{2,2}(\mathbb{R}) \to L^2(\mathbb{R})$ is continuous and the rate of the divergence of time-asymptotic variance of the solution of the linearised system (4.4.2) can be obtained as described in Example 4.4.2. In detail,

$$\begin{aligned} \langle g, V_\infty^{\mathsf{w}} g \rangle &= \sigma^2 \int_0^\infty \langle \mathsf{e}^{t2(\partial_x^2 + p)} g, g \rangle \, \mathsf{d}t = \sigma^2 \int_0^\infty \langle \mathcal{F}^{-1} \mathsf{e}^{t2(\partial_x^2 + p)} \mathcal{F} g, g \rangle \, \mathsf{d}t \\ &= \sigma^2 \int_0^\infty \int_{\mathbb{R}} \mathsf{e}^{2t(-k^2 + p)} \mathcal{F}g(k)^2 \, \mathsf{d}k \, \mathsf{d}t = \frac{\sigma^2}{2} \int_{\mathbb{R}} \frac{\mathcal{F}g(k)^2}{k^2 - p} \, \mathsf{d}k. \end{aligned} \tag{4.4.4}$$

We define the functions $d_k(x) = \mathsf{e}^{-2\pi \mathsf{i} k x}$ for $x, k \in \mathbb{R}$ and the imaginary unit i. Under the assumption that $\mathcal{F}g$ assumes bounded nonzero values in a neighbourhood of $k = 0$, i.e., the projections of function g along the most sensible functions in $\{d_k\}_{k \in \mathbb{R}}$ are bounded and nonzero, the rate of divergence of such variance is of order $\Theta_p\left((-p)^{-\frac{1}{2}}\right)$ as proven in Example 4.4.2.
Intuitively, the difference of the rates of (4.4.3) and (4.4.4) is implied by the different shape of the spectrum

of ∂_x^2 for the finite or infinite value of L. In particular, as p crosses 0 from below in the case $L < \infty$, the solution of (4.4.2) is repelled by the linear term along e_0. Conversely, for $p \to 0^-$ in the case $L = \infty$, the most unstable direction d_0, the constant function, is not in the domain of the drift operator.

4.5 Applications

The early-warning signs introduced in Theorem 4.1.3, Theorem 4.2.5 and Theorem 4.2.7 can be applied to a wide range of applications. As described in Example 4.4.2, the study of reaction-diffusion equations can be achieved through Fourier transforms. We conclude the chapter by studying linearisations of reaction-diffusion systems in the form (4.0.1), thus showing the applicability of the results. In fact, for a distance $-p$ to the bifurcation threshold, the solution of the linearised system on a stable solution $u_*(p)$ behaves similarly to the solution of the original equation [93]. As such, the observables are particularly reliable on systems with a unique stable solution prior to the approach.
The current section examines the relevance of our results to different models. Moreover, their implementation in the prediction of real-life scenarios is discussed.

▷ First, we consider the Ginzburg-Landau, Allen-Cahn, or Chafee-Infante equation,

$$\mathsf{d}u = \left(\partial_x^2 u + pu - u^3\right)\mathsf{d}t,$$

in the domain $\mathcal{X}_1 = [-L, L]$ and Dirichlet boundary conditions. It finds applications in phase-ordering kinetic [37], quantum mechanics [82] and climate science [111]. The model is known to present a pitchfork supercritical bifurcation threshold at the parameter value $p = 0$ [50]. The introduction of additive Gaussian noise is justified by the presence of lesser components in the physical model that can be treated as small stochastic perturbations [31, 176]. We also consider the domain in the limit $L \to \infty$, in order to consider large intervals. In such a limit, the spectrum of ∂_x^2 is continuous and the only stable solution for $p < 0$ is the null function $u_* = 0$.
The linearised system (4.0.1) is characterised by the drift operator

$$A(p) = \partial_x^2 + p. \tag{4.5.1}$$

Example 4.4.2 implies that the time-asymptotic variance along almost any function $g \in \mathcal{W}^{2,2}(\mathbb{R})$ yields a rate of divergence of order $\Theta_p\left((-p)^{\frac{1}{2}}\right)$ as $p \to 0^-$. In Figure 4.6a, a numerical approximation of the time-asymptotic variance of a solution of (4.4.2) for (4.5.1) is displayed. The observable is considered along $g = \mathcal{F}^{-1}\mathbb{1}_{[-0.25,0.25]}$ and exhibits a slope of $-\frac{1}{2}$ in a logarithmic scale, for p close to 0.

▷ We now consider the one-dimensional complex Ginzburg-Landau equation,

$$\mathsf{d}u = \left(\partial_x^2 u + (p + \mathsf{i})u - \left(-1 + \frac{\mathsf{i}}{10}\right)|u|^2 u - |u|^4 u\right)\mathsf{d}t,$$

for i the imaginary unit and $|\cdot|$ the absolute value, in the domain $\mathcal{X}_1 = [-L, L]$ and Neumann boundary conditions. Similar to its real counterpart, the introduction of white additive noise is justified by minor components in the system [114]. For finite values of L, it is known that a supercritical Hopf bifurcation occurs at the stable solution $u_* = 0$ in the limit $p \to 0^-$ [193]. The assumption of the limit $L \to +\infty$ follows from the observation of large domains in relevant applications and via the justification of the Ginzburg-Landau equation as an amplitude/modulation equation. The linearised system on $u_* = 0$, (4.0.1) with linear operator

$$A(p) = \partial_x^2 + p + \mathsf{i}, \tag{4.5.2}$$

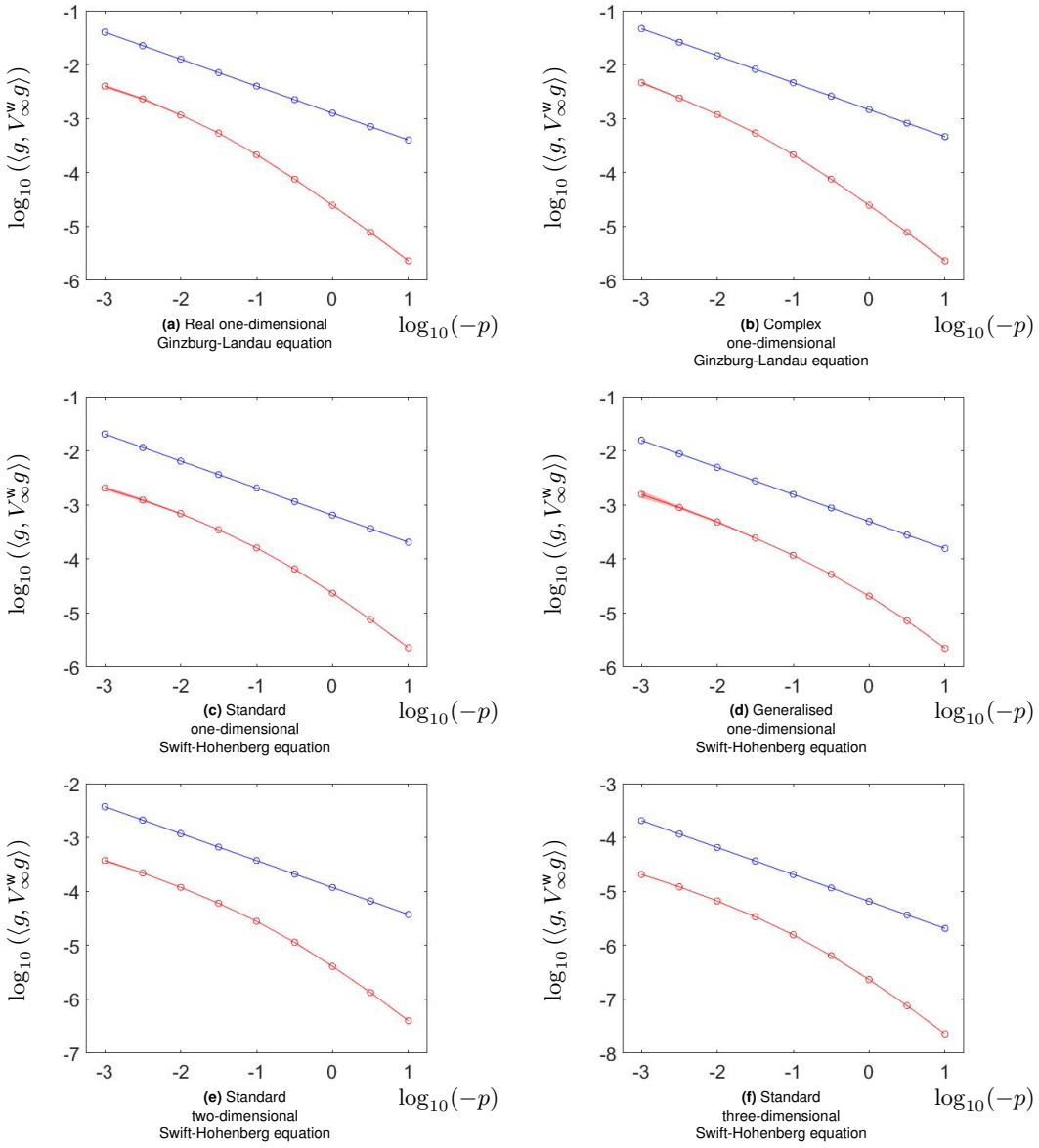

Fig. 4.6 A numerical approximation of the time-asymptotic variance of the solution of (4.4.2) along the function g is displayed for different models discussed in Section 4.5 in a log-log plot. The figures are obtained following the method in Section 4.3 in Fourier space, for $T = 10^4$, $\delta\mathfrak{t} = 0.01$ and $Q = \mathrm{Id}$. The red lines refer to the mean values of the observable for 10 sample solutions, different for noise realisations. The width of the areas are linear to the corresponding numerical standard deviation. In (a), the drift term is described by (4.5.1); in (b), it is associated to (4.5.2); in (c), to (4.5.3); in (d), to (4.5.4); in (e), to (4.5.5); in (f), to (4.5.6). The respective functions g are introduced in Section 4.5. In blue, a line with a slope equal to $-\frac{1}{2}$ is included as a comparison. In all panels, the lines appear to align for small values of p.

can be treated in Fourier space following Example 4.4.2 and the fourth generalisation in Section 4.4. In detail, for any $g \in \mathcal{W}^{2,2}(\mathbb{R};\mathbb{C})$ it holds

$$\begin{aligned}\langle g, V_\infty^{\mathsf{w}} g\rangle &= \sigma^2 \int_0^\infty \langle \mathsf{e}^{tA(p)} \mathsf{e}^{tA(p)^*} g, g\rangle \,\mathsf{d}t = \sigma^2 \int_0^\infty \int_{\mathbb{R}} \overline{g(x)} \mathsf{e}^{t(\partial_x^2+p-\mathrm{i})} \mathsf{e}^{t(\partial_x^2+p+\mathrm{i})} g(x) \,\mathsf{d}x \,\mathsf{d}t \\ &= \sigma^2 \int_0^\infty ||\mathsf{e}^{t(\partial_x^2+p)} g||^2 \,\mathsf{d}t = \sigma^2 \int_0^\infty ||\mathcal{F}^{-1} \mathsf{e}^{t(T_{-k^2}+p)} \mathcal{F} g||^2 \,\mathsf{d}t \\ &= \Theta_p\left(\int_0^\infty ||\mathsf{e}^{t(T_{-k^2}+p)} \mathcal{F} g||^2 \,\mathsf{d}t \right) = \Theta_p\left(- \int_{\mathbb{R}} |\mathcal{F} g(k)|^2 \frac{1}{2(-k^2+p)} \,\mathsf{d}k \right).\end{aligned}$$

The time-asymptotic variance of the solution of the linearised system along almost any $g \in \mathcal{W}^{2,2}(\mathbb{R};\mathbb{C})$ is therefore characterised by rate $\Theta_p\Big((-p)^{-\frac{1}{2}} \Big)$ as $p \to 0^-$. In Figure 4.6b, an approximation of the

observable along $g = \mathcal{F}^{-1}\mathbb{1}_{[-0.25,0.25]}$ displays a slope of $-\frac{1}{2}$ in a logarithmic scale, as p approaches 0 from below.
An example of fields with which the complex Ginzburg-Landau equation is associated is the research on thin superconductors [158]. The stochastic non-linear Ginzburg-Landau equation in dimension $N > 1$ is ill-defined in the classical sense under the assumption of perturbation by white noise and requires renormalisation; however, the linearised SPDEs considered in this work are well-defined, also under the perturbation of space-time white noise. Assuming the covariance operator Q such that a solution for such an equation exists (Theorem 2.2.3 and Theorem 2.2.5), an upper bound to the rate of divergence of the time-asymptotic variance of the solution of the linearised system can be obtained following Theorem 4.2.5, Theorem 4.2.7 and the third generalisation in Section 4.4.

▷ Another equation of interest is the (standard) one-dimensional Swift-Hohenberg equation [41, 42, 123],

$$\mathsf{d}u = \big(-(1+\partial_x^2)^2 u + pu - u^3 \big)\mathsf{d}t,$$

with domain $\mathcal{X}_1 = \mathbb{R}$. Such a deterministic equation is known to display Turing bifurcations [115, 122]. We include a white-noise term to simulate the effect of minor physical components in the system [106]; in fact, the stochastic Swift-Hohenberg equation has been studied in multiple works in the context of amplitude equations. The linearisation of such an SPDE on the trivial solution $u_*(x) = 0$, for any $x \in \mathbb{R}$, takes the form of (4.4.2) with $u_0 \in \mathcal{W}^{4,2}(\mathbb{R})$, $Q = \mathrm{Id}$ and $A : \mathcal{W}^{4,2}(\mathbb{R}) \to L^2(\mathbb{R})$ such that

$$Ag(x) = -\left(1+\partial_x^2\right)^2 g(x), \tag{4.5.3}$$

for any $g \in \mathcal{W}^{4,2}(\mathbb{R})$. Example 4.4.2 can easily be generalised to such self-adjoint linear differential operators through Theorem 4.1.3. The scaling law of the variance of such a solution along g in a dense subset of $\mathcal{W}^{4,2}(\mathbb{R})$ is given, therefore, by

$$\langle g, V_\infty^{\mathsf{w}} g\rangle = \sigma^2 \int_0^\infty \langle \mathsf{e}^{t(A+p)}\mathsf{e}^{t(A+p)}g, g\rangle \,\mathsf{d}t = \Theta_p\left(\int_0^\infty \|\mathsf{e}^{t(\mathrm{T}_{f_{\mathsf{an}}}+p)}\mathcal{F}g\|^2 \,\mathsf{d}t\right),$$

with $f(k) = -\left(1-k^2\right)^2$ for any $k \in \mathbb{R}$. From the Taylor expansion of f at $k = \pm 1$, it follows that the rate of divergence presents order $\Theta_p\left((-p)^{-\frac{1}{2}}\right)$.
The time-asymptotic variance of the linearised model is displayed in red in the log-log plot in Figure 4.6c. As described in Section 4.4, the variance along $g = \mathcal{F}^{-1}\mathbb{1}_{[0.75,1.25]}$ displays the rate of divergence $\Theta_p\left((-p)^{-\frac{1}{2}}\right)$ as $p \to 0^-$. The Swift-Hohenberg equation on large or unbounded domains [29] can be obtained from the Boussinesq approximation for fluid dynamics [188]. In such an application, the ergodic theory states that the figure displays the rate of divergence of the time-asymptotic variance of the projection of the rescaled fluid velocity u on the function g up to the proximity to a bifurcation threshold. In particular, Theorem 4.1.3 asserts that an equivalent order of divergence is assumed for g in a large set of indicator functions in $\mathcal{H}_1$. Consequently, it validates the study of the variance restricted to observations in bounded regions of space.

As an example from [103], another practical use of the corresponding early-warning sign is the prediction of sudden changes in the electric field in crystal optical fibre resonators implied by the change of a bifurcation parameter. In this case, the generalised Swift-Hohenberg equation linearised on $u_* = 0$ yields

$$A = -\frac{\beta^2}{4} + \beta\partial_x^2 + \beta'\partial_x^3 - \partial_x^4 \tag{4.5.4}$$

and the variable u represents the deviation of the electric field from its value at the bifurcation threshold. Upon consideration of the variational equation, i.e., $\beta' = 0$, the rate of the early-warning sign can be obtained from Example 4.4.2. Set $\beta < 0$ and $g(x) = \mathcal{F}^{-1}\mathbb{1}_{[a,b]}$ for $a < b$, the scaling law

of the time-asymptotic variance of the solution of the linearised system (4.0.1) on $u_* = 0$ along g is given by

$$\langle g, V_\infty^{\mathsf{w}} g\rangle = \sigma^2 \int_0^\infty \langle \mathsf{e}^{t(A+p)} \mathsf{e}^{t(A+p)} g, g\rangle \,\mathsf{d}t = \Theta_p\left(\int_0^\infty \|\mathsf{e}^{t(\mathrm{T}_{f\mathsf{an}}+p)}\mathcal{F}g\|^2 \,\mathsf{d}t\right),$$

with $f(k) = -k^2(\beta+k^2) - \frac{\beta^2}{4}$ for any $k \in \mathbb{R}$. The function f has multiple roots, and the corresponding equation presents an example of the first generalisation in Section 4.4. The values $k_* = \pm\left(-\frac{\beta}{2}\right)^{\frac{1}{2}}$ are global maxima of f and solutions of order 2. Therefore, the scaling law of the time-asymptotic variance of the solution of the linearised equation along g is

$$\langle g, V_\infty^{\mathsf{w}} g\rangle = \begin{cases} \Theta_p\left((-p)^{-\frac{1}{2}}\right), & \text{for} \quad a < -\left(-\frac{\beta}{2}\right)^{\frac{1}{2}} < b \quad \text{or} \quad a < \left(-\frac{\beta}{2}\right)^{\frac{1}{2}} < b, \\ \Theta_p\left(1\right), & \text{otherwise,} \end{cases}$$

for $p \to 0^-$. In Figure 4.6d, the time-asymptotic variance of the solution of (4.4.2) along the function $g = \mathcal{F}^{-1}\mathbb{1}_{\left[\left(-\frac{\beta}{2}\right)^{\frac{1}{2}} - 0.25, \left(-\frac{\beta}{2}\right)^{\frac{1}{2}} + 0.25\right]}$ is displayed in red on logarithmic scale. Under the assumption $\beta = -1$, the variance appears to diverge with order $\Theta_p\left((-p)^{-\frac{1}{2}}\right)$ in the limit $p \to 0^-$. Among other instances, the (standard) Swift-Hohenberg equation finds further applications in chemistry [148] and in hydrodynamics [170].

▷ We also consider the application of Theorem 4.1.3 to the standard two-dimensional Swift-Hohenberg equation. For more general versions whose linearisation includes a self-adjoint drift operator, Theorem 4.2.5 and Example 4.4.2 provide an upper bound to the rate of the time-asymptotic variance of the solution of the linearised system. Such equations hold particular interest in the field of hydrodynamics as they enable a simulation of the Rayleigh-Bénard convection phenomena in non-Boussinesq fluids [188, 208] and of the Taylor-Couette flow [112, 170]. A generalisation of the two-dimensional Swift-Hohenberg equation has also been employed in optics [138, 139].
The standard two-dimensional Swift-Hohenberg equation is of the form

$$\mathsf{d}u = \big(-(1+\partial_{x_1}^2+\partial_{x_2}^2)^2 u + pu - u^3\big)\mathsf{d}t,$$

on domain $\mathcal{X}_1 = \mathbb{R}^2$ and can be studied similarly to its one-dimensional equivalent. Again, we insert an additive noise component [106] and consider only the linearised SPDE along the deterministic stable solution $u_* = 0$, which presents a valid approximation of the standard equation for values of the bifurcation parameter suitably distant to the bifurcation threshold. We set $A : \mathcal{W}^{4,2}(\mathbb{R}^2) \to L^2(\mathbb{R}^2)$ as the Swift-Hohenberg operator on two spatial dimensions, i.e.,

$$Ag(x) = -\left(1+\partial_{x_1}^2+\partial_{x_2}^2\right)^2 g(x), \tag{4.5.5}$$

for any $g \in \mathcal{W}^{4,2}(\mathbb{R}^2)$ and $x = (x_1, x_2)$. We study the time-asymptotic variance of the solution of (4.4.2) for $u_0 \in \mathcal{W}^{4,2}(\mathbb{R}^2)$, $p < 0$ and Q a bounded operator with bounded inverse. We consider $g \in \mathcal{W}^{4,2}(\mathbb{R}^2)$ and $f_i(k) = k_i$ for $i \in \{1,2\}$ and $k = (k_1, k_2) \in \mathbb{R}^2$. We also denote by $\mathcal{F}$ the Fourier transform on $L^2(\mathbb{R}^2)$ and $\hat{g} = \mathcal{F}g$. It follows that

$$\begin{aligned}\langle g, V_\infty^{\mathsf{w}} g\rangle &= \sigma^2 \int_0^\infty \langle \mathsf{e}^{t(A+p)} Q \mathsf{e}^{t(A+p)} g, g\rangle \,\mathsf{d}t = \Theta_p\left(\int_0^\infty \|\mathsf{e}^{t(A+p)} g\|^2 \,\mathsf{d}t\right) \\ &= \Theta_p\left(\int_0^\infty \left\| \mathcal{F}^{-1} \mathsf{e}^{t\left(\mathrm{T}_{-\left(1-f_1^2-f_2^2\right)^2}+p\right)} \mathcal{F}g \right\|^2 \mathsf{d}t\right)\end{aligned}$$

$$= \Theta_p \left(\int_0^\infty \left\| \mathsf{e}^{t\left(\mathrm{T}_{-\left(1-f_1^2-f_2^2\right)^2+p} \right)} \hat{g} \right\|^2 \mathsf{d}t \right).$$

We know that the scaling law as $p \to 0^-$ of such a scalar product is equivalent for a dense set of functions g in $\mathcal{W}^{4,2}(\mathbb{R}^2)$. From such a set we can choose g such that $\hat{g} = \mathbb{1}_D$, where D denotes the circle of radius $\sqrt{2}$ centered at the origin in $\mathbb{R}^2$. Through Fubini's Theorem, we can study the integral on polar spatial coordinates as

$$\int_0^\infty \iint_D \mathsf{e}^{t\left(-\left(1-k_1^2-k_2^2\right)^2+p\right)} \mathsf{d}k \, \mathsf{d}t = \iint_D \frac{1}{\left(1-k_1^2-k_2^2\right)^2 - p} \mathsf{d}k = \int_0^{2\pi} \int_0^{\sqrt{2}} \frac{r}{(1-r^2)^2 - p} \mathsf{d}r \, \mathsf{d}\theta.$$

Introducing $r' = 1 - r^2$ and $r'' = r'(-p)^{-\frac{1}{2}}$ we can use the substitution method and obtain

$$\begin{aligned} \int_0^{2\pi} \int_0^{\sqrt{2}} \frac{r}{(1-r^2)^2 - p} \mathsf{d}r \, \mathsf{d}\theta &= \pi \int_{-1}^{1} \frac{1}{r'^2 - p} \mathsf{d}r' \\ =(-p)^{-\frac{1}{2}} \int_{-(-p)^{-\frac{1}{2}}}^{(-p)^{-\frac{1}{2}}} \frac{1}{r''^2+1} \mathsf{d}r'' &= \Theta_p \left((-p)^{-\frac{1}{2}} \right). \end{aligned}$$

Figure 4.6e displays the time-asymptotic variance of a solution of (4.4.2) along a function g in red on a logarithmic scale. In such a case we consider $g = \mathcal{F}^{-1}\mathbb{1}_{\hat{D}}$, for $\hat{D} \subset \mathbb{R}^2$ such that

$$\hat{D} = \left\{ (k_1, k_2) \in \mathbb{R}^2 \middle| k_1 = r\mathsf{sin}(\theta), \quad k_2 = r\mathsf{cos}(\theta), \quad r \in [0.75, 1.25] \quad \text{and} \quad \theta \in \left[-\frac{\pi}{36}, \frac{\pi}{36} \right] \right\}.$$

The observable exhibits the scaling law $\Theta_p\left((-p)^{-\frac{1}{2}}\right)$ as p approaches the bifurcation threshold.

▷ Similarly to the previous application, we consider the three-dimensional Swift-Hohenberg equation. It is employed in numerous applications, including hydrodynamics [112, 188]. For solutions of generalised versions whose linearisation includes a self-adjoint operator in the drift component, upper bounds to the time-asymptotic variance of the solution of the linearised equation can be obtained through Theorem 4.2.7 and Example 4.4.2.
The standard three-dimensional Swift-Hohenberg equation is of the form

$$\mathsf{d}u = \big(-(1 + \partial_{x_1}^2 + \partial_{x_2}^2 + \partial_{x_3}^2)^2 u + pu - u^3 \big) \mathsf{d}t,$$

on the domain $\mathcal{X}_1 = \mathbb{R}^3$. The linearised SPDE on $u_* = 0$ with additive Gaussian noise is characterised by the drift operator $A : \mathcal{W}^{4,2}(\mathbb{R}^3) \to L^2(\mathbb{R}^3)$ of the form

$$Ag(x) = -\left(1 + \partial_{x_1}^2 + \partial_{x_2}^2 + \partial_{x_3}^2\right)^2 g(x), \tag{4.5.6}$$

for any $g \in \mathcal{W}^{4,2}(\mathbb{R}^3)$ and $x = (x_1, x_2, x_3)$. We study the time-asymptotic variance of the solution of (4.4.2) for initial condition $u_0 \in \mathcal{W}^{4,2}(\mathbb{R}^3)$, $p < 0$ and Q a bounded operator with bounded inverse. We consider $g \in \mathcal{W}^{4,2}(\mathbb{R}^3)$ and $f_i(k) = k_i$ for $i \in \{1, 2, 3\}$ and $k = (k_1, k_2, k_3) \in \mathbb{R}^3$. We refer by $\mathcal{F}$ to the Fourier transform on $L^2(\mathbb{R}^3)$ and indicate $\hat{g} = \mathcal{F}g$. It follows that

$$\begin{aligned} \langle g, V_\infty^{\mathsf{w}} g \rangle &= \sigma^2 \int_0^\infty \langle \mathsf{e}^{t(A+p)} Q \mathsf{e}^{t(A+p)} g, g \rangle \, \mathsf{d}t = \Theta_p \left(\int_0^\infty \| \mathsf{e}^{t(A+p)} g \|^2 \, \mathsf{d}t \right) \\ &= \Theta_p \left(\int_0^\infty \left\| \mathcal{F}^{-1} \mathsf{e}^{t\left(\mathrm{T}_{-\left(1-f_1^2-f_2^2-f_3^2\right)^2+p} \right)} \mathcal{F}g \right\|^2 \mathsf{d}t \right) \end{aligned}$$

$$= \Theta_p \left(\int_0^\infty \left\| \mathsf{e}^{t\left(\mathrm{T}_{-\left(1-f_1^2-f_2^2-f_3^2\right)^2+p} \right)} \hat{g} \right\|^2 \mathsf{d}t \right).$$

We know that the scaling law as $p \to 0^-$ of such scalar product is equivalent for a dense set of functions g in $\mathcal{W}^{4,2}(\mathbb{R}^3)$. We can choose g from such a set such that $\hat{g} = \mathbb{1}_S$, where S denotes the sphere of radius $\sqrt{2}$ centered at the origin in $\mathbb{R}^3$. Through Fubini's Theorem, we can study the integral on spherical spatial coordinates as

$$\int_0^\infty \iiint_S \mathsf{e}^{t\left(-\left(1-k_1^2-k_2^2-k_3^2\right)^2+p\right)} \mathsf{d}k\, \mathsf{d}t = \iiint_S \frac{1}{\left(1-k_1^2-k_2^2-k_3^2\right)^2 - p} \mathsf{d}k$$
$$= \int_0^\pi \int_0^{2\pi} \int_0^{\sqrt{2}} \frac{r^2 \mathsf{sin}(\phi)}{\left(1-r^2\right)^2 - p} \mathsf{d}r\, \mathsf{d}\theta\, \mathsf{d}\phi = 4\pi \int_0^{\sqrt{2}} \frac{r^2}{\left(1-r^2\right)^2 - p} \mathsf{d}r = \Theta_p \left((-p)^{-\frac{1}{2}} \right).$$

Figure 4.6f displays the time-asymptotic variance of a solution of (4.4.2) along a function g in red on a logarithmic scale. We consider $g = \mathcal{F}^{-1}\mathbb{1}_{\hat{S}}$, for $\hat{S} \subset \mathbb{R}^3$ such that

$$\hat{S} = \left\{ (k_1, k_2) \in \mathbb{R}^2 \middle| \begin{array}{c} k_1 = r\mathsf{sin}(\theta)\mathsf{sin}(\phi), \quad k_2 = r\mathsf{sin}(\theta)\mathsf{cos}(\phi), \quad k_3 = r\mathsf{cos}(\theta), \\ r \in [0.75, 1.25] \quad \text{and} \quad \theta, \phi \in \left[-\tfrac{\pi}{36}, \tfrac{\pi}{36}\right] \end{array} \right\}.$$

Then, the observable shows a slope of $-\frac{1}{2}$ in logarithmic scale for $p \to 0^-$.

▷ A renowned example of reaction-diffusion equations is the (one-dimensional) FitzHugh-Nagumo model [6] (see also Chapter 10). Among the applications to such a model is the study of activators and inhibitors in anisotropic systems [11], with interest in fluid mechanics [129] and medicine [204]. Recently, the inclusion of an additive stochastic term in the system and its reduced version, the Nagumo equation in the form

$$\mathsf{d}u = \left(\Delta u + pu + u(1-u)(u-a) + v\right)\mathsf{d}t$$

with Δ the Laplace operator and v a space-heterogeneous term, has been examined [55, 56, 79, 190] along with the assumption of unbounded domain $\mathcal{X}_1 = \mathbb{R}$ [197]. As an example, the inclusion of noise is justified in the application of neurophysiology by the effect of random input current in neurons of synaptic or external nature [190]. Under such assumptions, the reduced equation is of a generalised space-heterogeneous Ginzburg-Landau form, which can be treated similarly. In fact, Theorem 4.1.3 provides the corresponding rate of the time-asymptotic variance of the solution of the linearised equation previous to a pitchfork [50] or saddle-node [132] bifurcation. Given the stable solution $u_*(p)$, such an equation is of the form (4.0.1) and also displays a Schrödinger operator

$$A(p) = \Delta + p - a + 2(1+a)u_*(p) - 3u_*(p)^2.$$

The dependence of u_* on p affects the spectrum of $A(p)$ because it introduces heterogeneity in space. The scaling law is described analytically in Example 4.4.3. Unless u_* is the null function, $A(p)$ is not diagonalised in Fourier space, which leads to substantial additional numerical difficulties. For the case $a = v(x) = u_*(x) = 0$ for any $x \in \mathbb{R}$, we refer to Figure 4.6a, where the time-asymptotic variance along $g = \mathbb{1}_{[-0.25,0.25]}$ displays a rate of divergence of order $\Theta_p\left((-p)^{\frac{1}{2}}\right)$ as p approaches 0.

▷ As discussed in Section 4.4, the generalizations of Theorem 4.1.3, Theorem 4.2.5 and Theorem 4.2.7 are not restricted to unbounded domains. This is the case for certain more complex models with linear operators $A(p)$, such as certain Schrödinger operators with electric and magnetic potentials [127]. We also note that, for large domains and $N = 1$, the proximity of eigenvalues of differential

operators with discrete spectrum, such as the Laplace operator, can delay the hyperbolic divergence of the early-warning sign in reaction-diffusion equations discussed in Remark 4.4.4. An example of an application to such a case can be found in climate science in different two-dimensional ocean models which display supercritical pitchfork and saddle-node bifurcations [10, 72] (see also Chapter 5).

4.6 Summary

In this chapter, we justify the use of the time-asymptotic covariance along certain types of functions $g \in \mathcal{H}_1$ as an early-warning sign for SPDEs with purely continuous spectrum of the linear drift operator. A critical role for the behaviour of the signal is attributed to the structure of the spectrum in the proximity to the imaginary axis.

We compute sharp scaling laws for locally analytic spectra on a one-dimensional domain through the use of tool functions. For the two- and three-dimensional cases, we study the asymptotic behaviour of upper bounds of $\langle g, V_\infty^{\mathsf{w}} g\rangle$. For general dimensions N, we prove the convergence of the variance for certain choices of drift operators. In these cases, the search for a finer early-warning sign that captures this more subtle approach to the bifurcation threshold is required. Our results can be extended to a wide range of models that include critical transitions and bifurcations. An extensive list of generalisations and applications is discussed throughout the chapter.

5 Time-asymptotic variance for boundary noise

In this chapter, we extend the prediction of critical transitions to SPDEs with boundary additive noise. The novel work presented here is based on the content in [20]. The author of the thesis is its main contributor, while the research was carried out under the supervision of Christian Kuehn and Henk A Dijkstra. Similarly to the previous chapters, we rely on linearisation techniques and focus on the fast component of the fast-slow model. We study the mild solution $u^{(\mathsf{w,b})} = u^{(\mathsf{w,b})}(x,t)$ of

$$\begin{cases} \mathsf{d}u^{(\mathsf{w,b})}(x,t) = A(p)u^{(\mathsf{w,b})}(x,t)\mathsf{d}t, \\ u^{(\mathsf{w,b})}(0,x) = u_0(x) \in \mathcal{H}_1, \end{cases} \tag{5.0.1}$$

for $x \in \mathcal{X}_1$ and

$$\Gamma(p)u^{(\mathsf{w,b})}(x,t) = \sigma Q^{\frac{1}{2}}\dot{W}_t,$$

on the boundary $x \in \mathcal{X}_0 = \partial\mathcal{X}_1$ and $t > 0$. The linear operator

$$\Gamma(p) : \mathcal{D}\left(\Gamma(p)\right) \subset \mathcal{H}_1 \to \mathcal{H}_0$$

defines the boundary conditions from $\mathcal{H}_1 = L^2(\mathcal{X}_1)$ to $\mathcal{H}_0 = L^2(\mathcal{X}_0)$. The operator $Q : \mathcal{H}_0 \to \mathcal{H}_0$ is assumed to be self-adjoint, bounded and with bounded inverse. We assume that, for fixed $p \leq 0$, there exists a continuous $q = q(p) \in \mathbb{R}$ such that for any boundary value problem

$$(A(p) - q)w = 0 \quad , \quad \Gamma(p)\, w = v \ ,$$

with $v \in \mathcal{H}_0$, there exists a unique solution $w = D(p)v \in \mathcal{D}(A(p)) \subset \mathcal{H}_1$. For any $p \leq 0$, we indicate $D(p)^*$ as the adjoint operator of $D(p)$ with respect to the scalar products on the Hilbert spaces $\mathcal{H}_1$ and $\mathcal{H}_0$. We assume the operator $D(p)^*$ to be uniformly bounded in $L^2(\mathcal{H}_1;\mathcal{H}_0)$ for any $p \leq 0$. We set

$$A_0(p)v = A(p)v$$

for any $v \in \mathcal{H}_1$ such that $\Gamma(p)v = 0$. The operators $A_0(p)$ and $A_0(p)^*$ are assumed to be closed and densely defined in $\mathcal{H}_1$. The purely discrete operator, linear $A_0(p)$ is assumed to be negative for $p < 0$ with eigenvalues

$$0 > \mathrm{Re}\left(\lambda_1^{(p)}\right) > \mathrm{Re}\left(\lambda_2^{(p)}\right) \geq \mathrm{Re}\left(\lambda_3^{(p)}\right) \geq \dots,$$

which are continuous in p. We assume that the eigenvalue $\lambda_1^{(p)}$ is the only one to reach the imaginary axis at $p = 0$. The geometric multiplicity of each eigenvalue is set for simplicity as 1. For any $i \in \mathbb{N}_{>0}$, $p \leq 0$ and $k \in \left\{1, \dots, m_a\left(\lambda_i^{(p)}\right)\right\}$, the generalised eigenfunctions of $A_0(p)$ and $A_0(p)^*$ corresponding to $\lambda_i^{(p)}$ and $\overline{\lambda_i^{(p)}}$, respectively, are labelled as $e_{i,k}^{(p)}$ and ${e_{i,k}^{(p)}}^*$ and satisfy

$$\begin{aligned} &A_0(p)e_{i,k}^{(p)} = \lambda_i^{(p)}e_{i,k}^{(p)}, && A_0(p)^*{e_{i,k}^{(p)}}^* = \overline{\lambda_k^{(p)}}{e_{i,1}^{(p)}}^*, && \text{for } k = 1, \\ &A_0(p)e_{i,k}^{(p)} = \lambda_i^{(p)}e_{i,k}^{(p)} + e_{i,k-1}^{(p)}, && A_0(p)^*{e_{i,k}^{(p)}}^* = \overline{\lambda_i^{(p)}}{e_{i,k}^{(p)}}^* + {e_{i,k-1}^{(p)}}^*, && \text{for } k \neq 1. \end{aligned}$$

We assume that such functions are continuous in $\mathcal{H}_1$ with regard to p. The deterministically invariant subspaces generated by the generalised eigenfunctions of $A_0(p)$ and $A_0(p)^*$ associated to the eigenvalue $\lambda_i^{(p)}$ and $\overline{\lambda_i^{(p)}}$ are denoted respectively as $E_i(p)$ and $E_i(p)^*$. Their dimensions, the algebraic multiplicities of the corresponding eigenvalues, are labelled as $\mathcal{M}_i = m_a\left(\lambda_i^{(p)}\right)$ and are assumed to be independent of p. For each $i \in \mathbb{N}_{>0}$, the sets $\left\{e_{i,k}^{(p)}\right\}_{k\in\{1,\dots,\mathcal{M}_i\}}$ and $\left\{e_{i,\mathcal{M}_i-k+1}^{(p)^*}\right\}_{k\in\{1,\dots,\mathcal{M}_i\}}$ are scaled to form a biorthogonal system. Each family is assumed to be complete [211] in $\mathcal{H}_1$. For $i \in \mathbb{N}_{>0}$, we label $e_i^{(p)} = e_{i,1}^{(p)}$ and $e_i^{(p)^*} = e_{i,1}^{(p)^*}$ if $\mathcal{M}_i = 1$. Lastly, we set $e_{i,0}^{(p)} = e_{i,0}^{(p)^*} \equiv 0$ for all $i \in \mathbb{N}_{>0}$. Moreover, we consider values of q that are not in the spectrum of $A_0(p)$ and $A_0(p)^*$ for p close to 0.
We construct an early-warning sign for the system (5.0.1) on the limit $p \to 0^-$ and the loss of stability of the null solution. Then, we extend these results to a Boussinesq model, a nonlinear ocean model whose solution is subject to a constraint equation. In this case, we predict the approach to a pitchfork and saddle-node bifurcation, observing the reliability of the signal up to proximity to the bifurcation. In detail, the observable displays a rate of divergence similar to the case discussed in Chapter 3. Nonetheless, in order to ensure a proper analytic justification for such a scaling law, further assumptions need to be enforced. While these are not restrictive, they are difficult to assess in real-life applications. Due to the study of different bifurcations in an applied model, we do not enforce the bifurcation to occur at $p = 0$, but rather at a general value $\lambda \in \mathbb{R}$. Consequently, the Landau notation Θ_p refers to such a limit.

5.1 Construction of the early-warning signs

In this section, we assume that

$$\int_0^t \left|(A_0(p) - q)e^{A_0(p)s}D(p)Q^{\frac{1}{2}}\right|^2_{L^2(\mathcal{X}_0;\mathcal{H}_1)} \mathsf{d}s < +\infty \tag{5.1.1}$$

holds for any $t_{\mathsf{end}} > 0$, operators A_0, D, Q as considered in (5.0.1) and $p \leq \lambda$. Then, from Theorem 2.2.10 follows the existence of the mild solution of (5.0.1) for any $p \leq \lambda$. We construct early-warning signs able to predict the approach of p to λ and the corresponding changes ensuing in (5.0.1). For any $p < \lambda$, we define the autocovariance operator of lag time $\tau \geq 0$ as $V_t^{\tau,\mathsf{w}} : \mathcal{D}(A_0(p)^*) \to \mathcal{H}_1$ that satisfies

$$\left\langle v, V_t^{\tau,\mathsf{w}} w\right\rangle = \mathsf{Cov}\left(\left\langle u^{(\mathsf{w},\mathsf{b})}(\cdot, t+\tau), v\right\rangle, \left\langle u^{(\mathsf{w},\mathsf{b})}(\cdot, t), w\right\rangle\right)$$

for any $v, w \in \mathcal{D}\left(A_0(p)^*\right)$ and $t \geq 0$. In the next proposition, we address the equivalent definitions of the time-asymptotic autocovariance operator.

Proposition 5.1.1. *For any $p < \lambda$, the time-asymptotic autocovariance operator of lag time $\tau \geq 0$, defined by the solution of* (5.0.1)*,*

$$\lim_{t\to\infty} V_t^{\tau,\mathsf{w}},$$

is the linear operator

$$V_\infty^{\tau,\mathsf{w}} = \mathsf{e}^{A_0(p)\tau} V_\infty^{\mathsf{w}} : \mathcal{D}(A_0(p)^*) \to \mathcal{H}_1, \tag{5.1.2}$$

for V_∞^{w} defined in (2.3.8)*.*

Proof. Set $v, w \in \mathcal{D}\left(A_0(p)^*\right)$, then

$$\mathsf{Cov}\left(\left\langle u^{(\mathsf{w},\mathsf{b})}(\cdot, t+\tau), v\right\rangle, \left\langle u^{(\mathsf{w},\mathsf{b})}(\cdot, t), w\right\rangle\right)$$

$$
\begin{aligned}
&=\mathbb{E}\left(\left\langle\int_0^{t+\tau}(q-A_0(p))\mathsf{e}^{A_0(p)(t+\tau-s)}D(p)Q^{\frac{1}{2}}\mathsf{d}W_s,v\right\rangle\overline{\left\langle\int_0^{t}(q-A_0(p))\mathsf{e}^{A_0(p)(t-s)}D(p)Q^{\frac{1}{2}}\mathsf{d}W_s,w\right\rangle}\right)\\
&=\mathbb{E}\left(\left\langle\int_0^{t}(q-A_0(p))\mathsf{e}^{A_0(p)(t-s)}D(p)Q^{\frac{1}{2}}\mathsf{d}W_s,\mathsf{e}^{A_0(p)^*\tau}v\right\rangle\overline{\left\langle\int_0^{t}(q-A_0(p))\mathsf{e}^{A_0(p)(t-s)}D(p)Q^{\frac{1}{2}}\mathsf{d}W_s,w\right\rangle}\right)\\
&=\int_0^t\left\langle D(p)^*\mathsf{e}^{A_0(p)^*(t-s)}(A_0(p)^*-q)\mathsf{e}^{A_0(p)^*\tau}v,QD(p)^*\mathsf{e}^{A_0(p)^*(t-s)}(A_0(p)^*-q)w\right\rangle_{\mathcal{H}_0}\mathsf{d}s\\
&=\left\langle v,\mathsf{e}^{A_0(p)\tau}V_tw\right\rangle.
\end{aligned}
$$

Through the limit $t\to\infty$ the proof is concluded. □

Having constructed the time-asymptotic autocovariance operator, we prove that it satisfies a generalised Lyapunov equation [64].

Lemma 5.1.2. *Set $\tau\geq 0$. For any $p<\lambda$, the time-asymptotic autocovariance operator $V_\infty^{\tau,\mathsf{W}}$ is a solution in $\mathcal{L}_b(\mathcal{H}_1)$, the space of bounded linear operators in $\mathcal{H}_1$, of the generalised Lyapunov equation*

$$
\langle v,A_0(p)V_\infty^{\tau,\mathsf{W}}w\rangle+\langle v,V_\infty^{\tau,\mathsf{W}}A_0(p)^*w\rangle=-\left\langle v,\mathsf{e}^{A_0(p)\tau}(A_0(p)-q)D(p)QD(p)^*(A_0(p)^*-q)w\right\rangle,\quad(5.1.3)
$$

with $v,w\in\mathcal{D}(A_0(p)^*)$.

Proof. The proof follows the method described in [64, Lemma 2.45]. We fix $p<\lambda$. We prove that $V_\infty^{\tau,\mathsf{W}}$ solves the generalised Lyapunov equation for any $v,w\in\mathcal{D}(A_0(p)^*)$. Through integration by parts and the fact that $A_0(p)^*$ and $A_0(p)^*-q$ commute for any $q\in\mathbb{R}$ we obtain

$$
\begin{aligned}
&\langle v,A_0(p)V_\infty^{\tau,\mathsf{W}}w\rangle\\
&=\int_0^\infty\left\langle A_0(p)^*v,\mathsf{e}^{A_0(p)\tau}(A_0(p)-q)\mathsf{e}^{A_0(p)s}D(p)QD(p)^*\mathsf{e}^{A_0(p)^*s}(A_0(p)^*-q)w\right\rangle\mathsf{d}s\\
&=\int_0^\infty\left\langle\frac{\mathsf{d}}{\mathsf{d}s}\mathsf{e}^{A_0(p)^*s}v,\mathsf{e}^{A_0(p)\tau}(A_0(p)-q)D(p)QD(p)^*\mathsf{e}^{A_0(p)^*s}(A_0(p)^*-q)w\right\rangle\mathsf{d}s\\
&=\left\langle\mathsf{e}^{A_0(p)^*s}v,\mathsf{e}^{A_0(p)\tau}(A_0(p)-q)D(p)QD(p)^*\mathsf{e}^{A_0(p)^*s}(A_0(p)^*-q)w\right\rangle\Big|_0^\infty\\
&\quad-\int_0^\infty\left\langle\mathsf{e}^{A_0(p)^*s}v,\mathsf{e}^{A_0(p)\tau}(A_0(p)-q)D(p)QD(p)^*\mathsf{e}^{A_0(p)^*s}A_0(p)^*(A_0(p)^*-q)w\right\rangle\mathsf{d}s\\
&=-\left\langle v,\mathsf{e}^{A_0(p)\tau}(A_0(p)-q)D(p)QD(p)^*(A_0(p)^*-q)w\right\rangle-\langle v,V_\infty^{\tau,\mathsf{W}}A_0(p)^*w\rangle.
\end{aligned}
$$

Therefore, we have proven that $V_\infty^{\tau,\mathsf{W}}$ is a solution of (5.1.3). □

The following theorem introduces an early-warning sign for $p\to\lambda^-$, and hence for the change of sign of an eigenvalue of $A_0(p)$. This is considered as the divergence of $V_\infty^{\tau,\mathsf{W}}$ along certain directions in $\mathcal{H}_1$. The proof follows methods described in [21, 23, 93, 135] and Chapter 2.

Theorem 5.1.3. *Set $\tau\geq 0$.*

a) For any $i,j\in\mathbb{N}_{>0}$, it holds that

$$
\begin{aligned}
\left\langle e_{i,1}^{(p)^*},V_\infty^{\tau,\mathsf{W}}e_{j,1}^{(p)^*}\right\rangle&=-\frac{\left(\overline{\lambda_i^{(p)}}-q\right)\left(\lambda_j^{(p)}-q\right)}{\left(\overline{\lambda_i^{(p)}}+\lambda_j^{(p)}\right)}\mathsf{e}^{\overline{\lambda_i^{(p)}}\tau}\left\langle e_{i,1}^{(p)^*},D(p)QD(p)^*e_{j,1}^{(p)^*}\right\rangle\\
&=\mathsf{e}^{\overline{\lambda_i^{(p)}}\tau}\left\langle e_{i,1}^{(p)^*},V_\infty^{\mathsf{W}}e_{j,1}^{(p)^*}\right\rangle.
\end{aligned}\quad(5.1.4)
$$

b) For $i,j \in \mathbb{N}_{>0}$, assume that there exist $C^- > 0$ and $q = q(p)$ that satisfy

$$|\lambda_i - q| > C^-,\ |\lambda_j - q| > C^- \tag{5.1.5}$$

and

$$\left|\left\langle e_{i,1}^{(p)^*}, D(p)QD(p)^* e_{j,1}^{(p)^*}\right\rangle\right| > C^- \tag{5.1.6}$$

for any $p \leq \lambda$. Then, for $i = j = 1$, it holds that

$$\lim_{p\to\lambda^-}\left|\left\langle e_{1,1}^{(p)^*}, V_\infty^{\tau,\mathsf{w}} e_{1,1}^{(p)^*}\right\rangle\right| = +\infty,$$

and for $(i,j) \in \mathbb{N}_{>0}\times\mathbb{N}_{>0}\setminus(1,1)$, it follows that

$$\left|\left\langle e_{i,1}^{(p)^*}, V_\infty^{\tau,\mathsf{w}} e_{j,1}^{(p)^*}\right\rangle\right| = \Theta_p(1), \tag{5.1.7}$$

as $p \to \lambda^-$.

c) Denoting $e_{i,0} = e_{j,0} \equiv 0$ and $k_1 \in \{1,\dots,\mathcal{M}_i\}, k_2 \in \{1,\dots,\mathcal{M}_j\}$, it holds that

$$\left\langle e_{i,k_1}^{(p)\ *}, V_\infty^{\tau,\mathsf{w}} e_{j,k_2}^{(p)\ *}\right\rangle = -\frac{\left\langle e_{i,k_1}^{(p)\ *}, V_\infty^{\tau,\mathsf{w}} e_{j,k_2-1}^{(p)\ *}\right\rangle + \left\langle e_{i,k_1-1}^{(p)\ *}, V_\infty^{\tau,\mathsf{w}} e_{j,k_2}^{(p)\ *}\right\rangle}{\left(\overline{\lambda_i^{(p)}} + \lambda_j^{(p)}\right)}$$
$$-\frac{e^{\overline{\lambda_i^{(p)}}\tau}\sum_{k=1}^{k_1}\frac{\tau^{k_1-k}}{(k_1-k)!}\left\langle\left(\left(\overline{\lambda_i^{(p)}}-q\right)e_{i,k_1}^{(p)\ *}+e_{i,k_1-1}^{(p)\ *}\right), D(p)QD(p)^*\left(\left(\overline{\lambda_j^{(p)}}-q\right)e_{j,k_2}^{(p)\ *}+e_{j,k_2-1}^{(p)\ *}\right)\right\rangle}{\left(\overline{\lambda_i^{(p)}} + \lambda_j^{(p)}\right)}$$

for any $i,j \in \mathbb{N}_{>0}$.

d) Fix $i,j \in \mathbb{N}_{>0}$, $k_1 \in \{1,\dots,\mathcal{M}_i\}$ and $k_2 \in \{1,\dots,\mathcal{M}_j\}$. Assume that there exists $C^- > 0$ and $q = q(p)$ that satisfy (5.1.5) *and* (5.1.6) *for any $p \leq \lambda$. Then, it holds that*

$$\left|\left\langle e_{i,k_1}^{(p)\ *}, V_\infty^{\tau,\mathsf{w}} e_{j,k_2}^{(p)\ *}\right\rangle\right| = \Theta_p\left(\left|\left(\overline{\lambda_i^{(p)}} + \lambda_j^{(p)}\right)^{-k_1-k_2+1}\right|\right) \tag{5.1.8}$$

as $p \to \lambda^-$.

Proof. a) We fix the pair of indexes $i,j \in \mathbb{N}_{>0}$. Equation (5.1.3) implies that

$$\begin{aligned}&\left\langle e_{i,1}^{(p)^*}, A_0(p)V_\infty^{\tau,\mathsf{w}} e_{j,1}^{(p)}\right\rangle + \left\langle e_{i,1}^{(p)^*}, V_\infty^{\tau,\mathsf{w}} A_0(p)^* e_{j,1}^{(p)^*}\right\rangle \\ &= -\left\langle e_{i,1}^{(p)^*}, \mathsf{e}^{A_0(p)\tau}(A_0(p)-q)D(p)QD(p)^*(A_0(p)^*-q)e_{j,1}^{(p)^*}\right\rangle.\end{aligned} \tag{5.1.9}$$

The left-hand side and the right-hand side of (5.1.9) satisfy

$$\left\langle e_{i,1}^{(p)^*}, A_0(p)V_\infty^{\tau,\mathsf{w}} e_{j,1}^{(p)^*}\right\rangle + \left\langle e_{i,1}^{(p)^*}, V_\infty^{\tau,\mathsf{w}} A_0(p)^* e_{j,1}^{(p)^*}\right\rangle = \left(\overline{\lambda_i^{(p)}} + \lambda_j^{(p)}\right)\left\langle e_{i,1}^{(p)^*}, V_\infty^{\tau,\mathsf{w}} e_{j,1}^{(p)^*}\right\rangle$$

and

$$\begin{aligned}&-\left\langle e_{i,1}^{(p)^*}, \mathsf{e}^{A_0(p)\tau}(A_0(p)-q)D(p)QD(p)^*(A_0(p)^*-q)e_{j,1}^{(p)^*}\right\rangle \\ &= -\left\langle (A_0(p)^*-q)\mathsf{e}^{A_0(p)^*\tau}e_{i,1}^{(p)^*}, D(p)QD(p)^*(A_0(p)^*-q)e_{j,1}^{(p)^*}\right\rangle\end{aligned}$$

$$= - \left(\overline{\lambda_i^{(p)}} - q \right) \left(\overline{\lambda_j^{(p)}} - q \right) \mathrm{e}^{\overline{\lambda_i^{(p)}} \tau} \left\langle e_{i,1}^{(p)^*}, D(p) Q D(p)^* e_{j,1}^{(p)^*} \right\rangle,$$

respectively. In conclusion, equation (5.1.4) is proven.

b) The rate in (5.1.7) follows from (5.1.3), (5.1.5),the uniform boundedness of D and the fact that $A_0(p)$ has a purely discrete spectrum for any $p \leq \lambda$. In the case $i = j = 1$, the divergence is implied by (5.1.6).

c) The construction of the generalised eigenfunctions implies that

$$\begin{aligned} &\left\langle e_{i,k_1}^{(p)\ *}, A_0(p) V_\infty^{\tau,\mathsf{w}} e_{j,k_2}^{(p)\ *} \right\rangle + \left\langle e_{i,k_1}^{(p)\ *}, V_\infty^{\tau,\mathsf{w}} A_0(p)^* e_{j,k_2}^{(p)\ *} \right\rangle \\ &= \left(\overline{\lambda_i^{(p)}} + \lambda_j^{(p)} \right) \left\langle e_{i,k_1}^{(p)\ *}, V_\infty^{\tau,\mathsf{w}} e_{j,k_2}^{(p)\ *} \right\rangle + \left\langle e_{i,k_1}^{(p)\ *}, V_\infty^{\tau,\mathsf{w}} e_{j,k_2-1}^{(p)\ *} \right\rangle + \left\langle e_{i,k_1-1}^{(p)\ *}, V_\infty^{\tau,\mathsf{w}} e_{j,k_2}^{(p)\ *} \right\rangle. \end{aligned}$$

It also holds that

$$\begin{aligned} &- \left\langle e_{i,k_1}^{(p)\ *}, \mathrm{e}^{A_0(p)\tau} (A_0(p) - q) D(p) Q D(p)^* (A_0(p)^* - q) e_{j,k_2}^{(p)\ *} \right\rangle \\ &= - \left\langle \mathrm{e}^{A_0(p)^*\tau} (A_0(p)^* - q) e_{i,k_1}^{(p)\ *}, D(p) Q D(p)^* (A_0(p)^* - q) e_{j,k_2}^{(p)\ *} \right\rangle \\ &= - \left\langle \mathrm{e}^{A_0(p)^*\tau} \left(\left(\overline{\lambda_i^{(p)}} - q \right) e_{i,k_1}^{(p)\ *} + e_{i,k_1-1}^{(p)\ *} \right), D(p) Q D(p)^* \left(\left(\overline{\lambda_j^{(p)}} - q \right) e_{j,k_2}^{(p)\ *} + e_{j,k_2-1}^{(p)\ *} \right) \right\rangle \\ &= - \mathrm{e}^{\overline{\lambda_i^{(p)}}\tau} \sum_{k=1}^{k_1} \frac{\tau^{k_1-k}}{(k_1-k)!} \left\langle \left(\overline{\lambda_i^{(p)}} - q \right) e_{i,k}^{(p)^*}, D(p) Q D(p)^* \left(\overline{\lambda_j^{(p)}} - q \right) e_{j,k_2}^{(p)\ *} \right\rangle \\ &\quad - \mathrm{e}^{\overline{\lambda_i^{(p)}}\tau} \sum_{k=1}^{k_1} \frac{\tau^{k_1-k}}{(k_1-k)!} \left\langle \left(\overline{\lambda_i^{(p)}} - q \right) e_{i,k}^{(p)^*}, D(p) Q D(p)^* e_{j,k_2-1}^{(p)\ *} \right\rangle \\ &\quad - \mathrm{e}^{\overline{\lambda_i^{(p)}}\tau} \sum_{k=1}^{k_1} \frac{\tau^{k_1-k}}{(k_1-k)!} \left\langle e_{i,k-1}^{(p)\ *}, D(p) Q D(p)^* \left(\overline{\lambda_j^{(p)}} - q \right) e_{j,k_2}^{(p)\ *} \right\rangle \\ &\quad - \mathrm{e}^{\overline{\lambda_i^{(p)}}\tau} \sum_{k=1}^{k_1} \frac{\tau^{k_1-k}}{(k_1-k)!} \left\langle e_{i,k-1}^{(p)\ *}, D(p) Q D(p)^* e_{j,k_2-1}^{(p)\ *} \right\rangle. \end{aligned}$$

The equality follows from (5.1.3).

d) The rate can be proven by induction. For $k_1 = k_2 = 1$, the equality (5.1.4), assumptions (5.1.5), (5.1.6) and the uniform boundedness of D imply that

$$\left| \left\langle e_{i,1}^{(p)^*}, V_\infty^{\tau,\mathsf{w}} e_{j,1}^{(p)^*} \right\rangle \right| = \Theta_p \left(\left| \left(\overline{\lambda_i^{(p)}} + \lambda_j^{(p)} \right)^{-1} \right| \right).$$

The uniform boundedness of D implies the existence of $C_+ > 0$ from which the induction step follows directly. From induction, the scaling law is given by the fact that the unique term with the leading absolute value in

$$\left\langle e_{i,k_1}^{(p)\ *}, V_\infty^{\tau,\mathsf{w}} e_{j,k_2}^{(p)\ *} \right\rangle$$

is

$$(-1)^{k_1+k_2} \binom{k_1+k_2-2}{k_1-1} \left\langle e_{i,1}^{(p)^*}, V_\infty^{\tau,\mathsf{w}} e_{j,1}^{(p)^*} \right\rangle \left(\overline{\lambda_i^{(p)}} + \lambda_j^{(p)} \right)^{-k_1-k_2+2}.$$

This concludes the proof.

□

Theorem 5.1.3 introduces an early-warning sign in the form of the qualitative behaviour of the time-asymptotic autocovariance of the solution of system (5.0.1) along certain directions in $\mathcal{H}_1$. Of particular importance is the case $i = j = 1$ under assumptions (5.1.5) and (5.1.6), which establishes the divergence of the early-warning sign, whose scaling law can be observed under the assumption of uniform boundedness of D. The restriction on the choice of space on which the autocovariance is studied limits the use of such theory in practical applications. In the following theorem, the use of the time-asymptotic autocovariance operator as an early-warning sign is extended to a bigger subspace of functions in $\mathcal{H}_1$. To prove such a generalisation, we introduce the projection operators $\Pi_{1,k}(p)^*$, $\Pi_1(p)^*$ and $\Pi_{-1}(p)^*$ in $\mathcal{H}_1$ as

$$\Pi_{1,k}(p)^* v = \left\langle v, e^{(p)}_{1,\mathcal{M}_1-k+1} \right\rangle e^{(p)^*}_{1,k}, \quad \Pi_1(p)^* v = \sum_{k=1}^{\mathcal{M}_1} \Pi_{1,k}(p)^* v \quad \text{and} \quad \Pi_{-1}(p)^* v = v - \Pi_1(p)^* v,$$

for any $v \in \mathcal{H}$ and $k \in \{1, \dots, \mathcal{M}_1\}$. We define also $O_M(p)^* := \bigoplus_{i=1}^{M} E_i(p)^*$.

Theorem 5.1.4. *Set $\tau \geq 0$ and $M \in \mathbb{N}_{>0}$. Then, the following items hold.*

a) For any $f_1, f_2 \in O_M(p)^*$ it holds

$$\begin{aligned} &\langle f_1, V_\infty^{\tau,\mathsf{w}} f_2 \rangle \\ &= \sum_{i,j\in\{1,\dots,M\}} \sum_{k_1\in\{1,\dots,\mathcal{M}_i\}} \sum_{k_2\in\{1,\dots,\mathcal{M}_j\}} \left\langle f_1, e^{(p)}_{i,\mathcal{M}_i-k_1+1} \right\rangle \left\langle e^{(p)^*}_{i,k_1}, V_\infty^{\tau,\mathsf{w}} e^{(p)^*}_{j,k_2} \right\rangle \overline{\left\langle f_2, e^{(p)}_{j,\mathcal{M}_j-k_2+1} \right\rangle}. \end{aligned} \tag{5.1.10}$$

b) Assume the existence of $C^- > 0$ and $q = q(p)$ that satisfy (5.1.5) *for all $i, j \in \{1, \dots, M\}$ and* (5.1.6) *for $i, j = 1$. Set the sequences $\left\{f_1^{(p)}\right\}, \left\{f_2^{(p)}\right\}$ which are continuous in $\mathcal{H}_1$, for $p \leq \lambda$, such that $\Pi_1(\lambda)^* f_1^{(\lambda)} \not\equiv 0 \not\equiv \Pi_1(\lambda)^* f_2^{(\lambda)}$ and $f_1^{(p)}, f_2^{(p)} \in O_M(p)^*$ for any $p \leq \lambda$. Then, it holds that*

$$\lim_{p\to\lambda^-} \left| \left\langle f_1^{(p)}, V_\infty^{\tau,\mathsf{w}} f_2^{(p)} \right\rangle \right| = +\infty.$$

c) Under the assumption of the previous item and for fixed $k_1, k_2 \in \{1, \dots, \mathcal{M}_1\}$ such that

$$k_m = \underset{i\in\{1,\dots,\mathcal{M}_1\}}{\textit{argmax}} \left\{ \Pi_{1,j}(\lambda)^* f_m^{(\lambda)} \not\equiv 0 \right\}, \tag{5.1.11}$$

for $m \in \{1, 2\}$, it holds that

$$\left| \left\langle f_1^{(p)}, V_\infty^{\tau,\mathsf{w}} f_2^{(p)} \right\rangle \right| = \Theta_p \left(\mathrm{Re}\left(-\lambda_1^{(p)}\right)^{-k_1-k_2+1} \right). \tag{5.1.12}$$

Proof. a) The construction of $O_M(p)^*$ implies that f_1 and f_2 are linear combinations of the generalised eigenfunctions of $A_0(p)^*$ associated to $\overline{\lambda_i^{(p)}}$ for $i \in \{1, \dots, M\}$. The coefficients in such a sum follow from the fact that the generalised eigenfunctions are chosen to satisfy the Jordan block structure. It therefore holds that

$$\begin{aligned} &\langle f_1, V_\infty^{\tau,\mathsf{w}} f_2 \rangle \\ &= \sum_{i,j\in\{1,\dots,M\}} \left\langle \sum_{k_1\in\{1,\dots,\mathcal{M}_i\}} \left\langle f_1, e^{(p)}_{i,\mathcal{M}_i-k_1+1} \right\rangle e^{(p)^*}_{i,k_1}, V_\infty^{\tau,\mathsf{w}} \sum_{k_2\in\{1,\dots,\mathcal{M}_j\}} \left\langle f_2, e^{(p)}_{j,\mathcal{M}_j-k_2+1} \right\rangle e^{(p)^*}_{j,k_2} \right\rangle \end{aligned}$$

$$= \sum_{i,j\in\{1,\dots,M\}} \sum_{k_1\in\{1,\dots,\mathcal{M}_i\}} \sum_{k_2\in\{1,\dots,\mathcal{M}_j\}} \left\langle f_1, e^{(p)}_{i,\mathcal{M}_i-k_1+1}\right\rangle \left\langle e^{(p)}_{i,k_1}{}^*, V^{\tau,\mathsf{w}}_\infty e^{(p)}_{j,k_2}{}^*\right\rangle \overline{\left\langle f_2, e^{(p)}_{j,\mathcal{M}_j-k_2+1}\right\rangle}.$$

b) The uniform boundedness of D implies that, for any $p \le \lambda$, it holds

$$\int_0^\infty \left|\left|Q^{\frac{1}{2}} D(p)^* \mathsf{e}^{A_0(p)^* s} \left(A_0(p)^* - q\right) \Pi_{-1}(p)^* f\right|\right|^r_{L^2(\mathcal{X}_0)} \mathsf{d}s < +\infty, \tag{5.1.13}$$

for any $f \in O_M(p)^*$ and $r > 0$. Since $f_1^{(p)}, f_2^{(p)} \in \mathcal{H}$, it holds for any $p \le \lambda$ that

$$\begin{aligned}\left\langle f_1^{(p)}, V^{\tau,\mathsf{w}}_\infty f_2^{(p)}\right\rangle &= \left\langle (\Pi_{-1}(p)^* + \Pi_1(p)^*) f_1^{(p)}, V^{\tau,\mathsf{w}}_\infty (\Pi_{-1}(p)^* + \Pi_1(p)^*) f_2^{(p)}\right\rangle \\ &= \left\langle \Pi_{-1}(p)^* f_1^{(p)}, V^{\tau,\mathsf{w}}_\infty \Pi_{-1}(p)^* f_2^{(p)}\right\rangle + \left\langle \Pi_{-1}(p)^* f_1^{(p)}, V^{\tau,\mathsf{w}}_\infty \Pi_1(p)^* f_2^{(p)}\right\rangle \\ &\quad + \left\langle \Pi_1(p)^* f_1^{(p)}, V^{\tau,\mathsf{w}}_\infty \Pi_{-1}(p)^* f_2^{(p)}\right\rangle + \left\langle \Pi_1(p)^* f_1^{(p)}, V^{\tau,\mathsf{w}}_\infty \Pi_1(p)^* f_2^{(p)}\right\rangle.\end{aligned}$$

From (5.1.13) it is implied that

$$\left|\left\langle \Pi_{-1}(p)^* f_1^{(p)}, V^{\tau,\mathsf{w}}_\infty \Pi_{-1}(p)^* f_2^{(p)}\right\rangle\right| < +\infty \tag{5.1.14}$$

for any $p \le \lambda$. In the following we use the fact that, for any $i \in \mathbb{N}_{>0}$, $E_i(p)^*$ is an invariant subspace of $\mathcal{D}(A_0(p)^*)$ under the action of $A_0(p)^*$ and that $A_0(p)^*|_{E_i}$ is a bounded non-positive operator in $\mathcal{D}(A_0(p)^*)$ by construction. Moreover, condition (5.1.1) and (5.1.13) imply that, for p approaching λ from below,

$$\begin{aligned}&\left|\left\langle \Pi_{-1}(p)^* f_1^{(p)}, V^{\tau,\mathsf{w}}_\infty \Pi_1(p)^* f_2^{(p)}\right\rangle\right| \qquad (5.1.15)\\ \le& C \int_0^\infty \left|\left|Q^{\frac{1}{2}} D(p)^* \mathsf{e}^{A_0(p)^* s} (A_0(p)^* - q) \Pi_{-1}(p)^* \mathsf{e}^{A_0(p)^* \tau} f_1^{(p)}\right|\right|_{L^2(\mathcal{X}_0)} \mathsf{d}s \sum_{k=1}^{\mathcal{M}_1} \left|\left|Q^{\frac{1}{2}} D(p)^* e^{(p)}_{1,k}{}^*\right|\right|_{L^2(\mathcal{X}_0)} \\ =& \Theta_p(1).\end{aligned}$$

Equivalently,

$$\left|\left\langle \Pi_1(p)^* f_1^{(p)}, V^{\tau,\mathsf{w}}_\infty \Pi_{-1}(p)^* f_2^{(p)}\right\rangle\right| = \Theta_p(1) \tag{5.1.16}$$

for $p \to \lambda^-$. Lastly, from (5.1.10) we obtain that

$$\begin{aligned}&\left|\left\langle \Pi_1(p)^* f_1^{(p)}, V^{\tau,\mathsf{w}}_\infty \Pi_1(p)^* f_2^{(p)}\right\rangle\right| \qquad (5.1.17)\\ =& \left|\sum_{k_1,k_2\in\{1,\dots,\mathcal{M}_1\}} \left\langle f_1^{(p)}, e^{(p)}_{1,k_1}\right\rangle \left\langle e^{(p)}_{1,k_1}{}^*, V^{\tau,\mathsf{w}}_\infty e^{(p)}_{1,k_2}{}^*\right\rangle \left\langle f_2^{(p)}, e^{(p)}_{1,k_2}\right\rangle\right|.\end{aligned}$$

From (5.1.8) and the continuity of the generalised eigenfunctions on variable p, the divergence follows.

c) The previous item and (5.1.17) imply

$$\left|\left\langle \Pi_1(p)^* f_1^{(p)}, V^{\tau,\mathsf{w}}_\infty \Pi_1(p)^* f_2^{(p)}\right\rangle\right| = \Theta_p\left(\mathrm{Re}\left(-\lambda_1^{(p)}\right)^{-k_1-k_2+1}\right)$$

and the conclusion of the proof.

□

In Theorem 5.1.4 we construct an early-warning sign whose numerical approximation (see Section 5.2) does not rely on the precise computation of the elements in $E_1(p)$ and $E_1(p)^*$ for $p \leq \lambda$. As an implication, simulations and implementations of such results are more practical than the early-warning signs obtained in Theorem 5.1.3.

Remark 5.1.5. The assumption of boundary noise can affect the rate of divergence of the autocovariance along certain directions in $\mathcal{D}(A_0(p))^*$. Furthermore, the omission of assumption (5.1.6) can silence the early-warning sign. For example, in the case

$$\left\langle {e_{1,k_1}^{(p)}}^*, D(p)QD(p)^* {e_{1,k_2}^{(p)}}^* \right\rangle = 0$$

for any $p \leq \lambda$ and $k_1, k_2 \in \{1, \dots, \mathcal{M}_1\}$, it is implied that the observable $\left|\left\langle f_1^{(p)}, V_\infty^{\tau,\mathsf{w}} f_2^{(p)} \right\rangle\right|$, for $\left\{f_1^{(p)}\right\}$ and $\left\{f_2^{(p)}\right\}$ that satisfy the assumptions in Theorem 5.1.4, does not display divergence as $p \to \lambda^-$. This is caused by the interplay of the linear operator $A(p)$ that defines the drift component, the boundary operator $\Gamma(p)$ and the operator Q associated to the diffusion. In detail, the first two define $A_0(p)$, $A_0(p)^*$ and their eigenfunctions, along with the operators $D(p)$ and $D(p)^*$. The observable can display convergence also in the case $\left\{f_1^{(p)}\right\}$ or $\left\{f_2^{(p)}\right\}$ are orthogonal to $E_1(p)$, as implied by (5.1.10). A similar property is employed in Section 5.2.3.

For $p < \lambda$, we define the autocorrelation nonlinear operator at time $t > 0$ and lag $\tau \geq 0$ as

$$\hat{V}_t^{\tau,\mathsf{w}}(v, w) := \frac{\langle v, V_t^{\tau,\mathsf{w}} w \rangle}{\langle v, V_\infty^{\mathsf{w}} w \rangle}$$

for any $v, w \in \mathcal{D}(A_0(p)^*)$ such that $\langle v, V_\infty^{\mathsf{w}} w \rangle \neq 0$ and V_∞^{w} defined in (2.3.8). Then, the role of the choice of proxy functions in $\mathcal{H}_1$, along which the time-asymptotic autocovariance is studied, is discussed further in the following corollary.

Corollary 5.1.6. *Set $\tau \geq 0$.*

a) Assume the existence of $C^- > 0$ and $q = q(p)$ that satisfy (5.1.5) *for all $i, j \in \mathbb{N}_{>0}$ and* (5.1.6) *for $i, j = 1$. Assume also that the generalised eigenfunctions of $A_0(p)^*$ are complete in $\mathcal{D}(A_0(p)^*)$ for any $p \leq \lambda$. Lastly, set the sequences $\left\{f_1^{(p)}\right\}, \left\{f_2^{(p)}\right\}$ continuous in $\mathcal{H}_1$ for $p \leq \lambda$. Then, for any $\delta > 0$ there exist two sequences $\left\{g_1^{(p)}\right\}, \left\{g_2^{(p)}\right\}$ that are continuous in $\mathcal{H}_1$ such that $g_1^{(p)}, g_2^{(p)} \in \mathcal{D}(A_0(p)^*)$,*

$$\left|\left| f_1^{(p)} - g_1^{(p)} \right|\right| < \delta \quad , \quad \left|\left| f_2^{(p)} - g_2^{(p)} \right|\right| < \delta, \tag{5.1.18}$$

for any $p \leq \lambda$, and

$$\left|\left\langle g_1^{(p)}, V_\infty^{\tau,\mathsf{w}} g_2^{(p)} \right\rangle\right| = \Theta_p\left(\mathrm{Re}\left(-\lambda_1^{(p)}\right)^{-2\mathcal{M}_1+1}\right)$$

for $p \to \lambda^-$.

b) We set $p < \lambda$ and assume that the generalised eigenfunctions of $A_0(p)^*$ are complete in $\mathcal{D}(A_0(p)^*)$. The time-asymptotic autocorrelation nonlinear operator of lag $\tau \geq 0$, labelled $\hat{V}_\infty^{\tau,\mathsf{w}}$ and defined as

$$\hat{V}_\infty^{\tau,\mathsf{w}}(v, w) = \lim_{t \to \infty} \hat{V}_t^{\tau,\mathsf{w}}(v, w)$$

for any $v, w \in \mathcal{D}(A_0(p)^*)$ such that $\langle v, V_\infty^{\mathsf{w}} w \rangle \neq 0$, satisfies

$$\hat{V}_\infty^{\tau,\mathsf{w}}\left({e_{i,1}^{(p)}}^*, f\right) = e^{\overline{\lambda_i^{(p)}}\tau}, \tag{5.1.19}$$

for any $i \in \mathbb{N}_{>0}$ and f in a dense subset $\mathcal{H}'$ of $\mathcal{H}_1$ such that $\left\langle {e_{i,1}^{(p)}}^*, V_\infty^{\mathsf{w}} f \right\rangle \neq 0$.

Proof. a) For $p \leq \lambda$, the fact that the generalised eigenfunctions of $A_0(p)^*$ are complete in its domain implies that the set of finite linear combinations of such functions, called $\tilde{\mathcal{H}}(p)$, is dense in $\mathcal{D}(A_0(p)^*)$. We also denote the set of functions $f \in \mathcal{H}_1$ such that $\Pi_{1,\mathcal{M}_1}(p)^* f \not\equiv 0$ as $\hat{\mathcal{H}}(p)$. By construction, $\hat{\mathcal{H}}(p)$ is dense in $\mathcal{H}_1$ and open. Therefore, $\mathcal{H}'(p) := \tilde{\mathcal{H}}(p) \cap \hat{\mathcal{H}}(p)$ is dense in $\mathcal{D}(A_0(p)^*)$, which in return is dense in $\mathcal{H}_1$.
From the continuity of $\left\{f_1^{(p)}\right\}, \left\{f_2^{(p)}\right\}$ and the generalised eigenfunctions of $A_0(p)$ and $A_0(p)^*$, we can construct $\left\{g_1^{(p)}\right\}, \left\{g_2^{(p)}\right\}$ continuous in $\mathcal{H}$ such that $g_1^{(p)}, g_2^{(p)} \in \mathcal{H}'(p)$ for any $p \leq \lambda$. In particular, there exists M, dependent on δ, such that $g_1^{(p)}, g_2^{(p)} \in O_M(p)^*$ for any $p \leq \lambda$. The conclusion is obtained from Theorem 5.1.4.

b) We construct $\mathcal{H}' = \tilde{\mathcal{H}}(p)$, as in the previous part of the proof, for the chosen $p < \lambda$. The conclusion holds directly from (5.1.2) and (5.1.10), fixing $f_1 = {e_{i,1}^{(p)}}^*$ and $f_2 = f \in \mathcal{H}'$.

□

Corollary 5.1.6 introduces an early-warning sign for the approach to the bifurcation threshold λ as the time-asymptotic autocorrelation with lag time $\tau > 0$, along ${e_{1,1}}^{(p)^*}$ and another general function. This observable reaches the value 1 with an exponential rate. The behaviour of the autocorrelation is not trivial to observe numerically since such a sign is given by a quantitative property, in contrast to the divergence of the time-asymptotic autocovariance, whose corresponding sign is defined by a qualitative property. Moreover, such a divergence is observed for a wide variety of directions in $\mathcal{H}_1$. This is implied by the assumption that the generalised eigenfunctions of $A_0(\lambda)^*$ are dense in $\mathcal{H}_1$. Such a property has been proven for different non-self-adjoint operators with compact resolvent [2, 117, 211].

Remark 5.1.7. The time-asymptotic autocorrelation is a well-known early-warning sign for systems in finite dimensions [73]. Setting $\tau > 0$ and assuming $\mathcal{M}_1 = 1$, then the autocorrelation $\hat{V}_\infty^{\tau,\mathsf{w}}\left(f_1^{(p)}, f_2^{(p)}\right)$, for functions $f_1^{(p)}, f_2^{(p)} \in O_M(p)^*$ as in Theorem 5.1.4 and $M \in \mathbb{N}_{>0}$, is yet not a straightforward object to determine analytically. From the sum in (5.1.10), we know that, assuming $\Pi_1(p)^* f_1^{(p)} \not\equiv 0 \not\equiv \Pi_1(p)^* f_2^{(p)}$, the leading term in the outer sum as $p \to \lambda^-$ is the component associated to $i = j = 1$. This implies that for values of p such that the mentioned element assumes a higher order of magnitude than the rest, and consequently the rates in Theorem 5.1.4 (c) are observed, the time-asymptotic autocorrelation behaves similarly to $\mathrm{e}^{\overline{\lambda_1^{(p)}}\tau}$ and assumes absolute value equal to 1 on the threshold.

Remark 5.1.8. In Theorem 5.1.3, Theorem 5.1.4 and Corollary 5.1.6, we assume the operator $A_0(p)$ to have discrete spectrum and $\lambda_1^{(p)}$ to be the only eigenvalue whose real part changes sign as $p \to \lambda^-$. Such properties can be generalised by considering that the set of eigenvalues $\Lambda_0 = \left\{\lambda_i^{(p)}\right\}_i$ such that

$$\mathrm{Re}\left(\lambda_i^{(p)}\right) \to 0 \qquad \text{as} \qquad p \to \lambda^-$$

is finite and isolated. This implies an asymptotic gap between the elements of such a set and the rest of the spectrum. Under such an assumption, the divergence in Theorem 5.1.3 (b) is observed along the corresponding simple eigenfunctions of any element in Λ_0 and the divergence in Theorem 5.1.4 (b) is obtained along $\left\{f_1^{(p)}\right\}$ and $\left\{f_2^{(p)}\right\}$ whose projection on the generalised eigenspace of any element in Λ_0 is not null for $p = \lambda$. The scaling laws in Theorem 5.1.4 (c) and Corollary 5.1.6 (a) depend on the rate of convergence of the real part of the elements in Λ_0. Certain elliptic (differential) operators are known to display discrete spectrum and completeness of the generalised eigenfunctions [2, 117]. For the property of boundedness of $D(p)$ for such operators, we refer to [137]. We emphasise that Theorem 5.1.4 (b) and (c) do not require the spectrum of $A_0(p)^*$ to be discrete, but rely on the fact that the set $\left\{\overline{\lambda_i^{(p)}}\right\}_i$ is composed by isolated points from the rest of the spectrum. This is in contrast with the case studied in the previous chapter and avoids the corresponding hindrance in the signal.

5.2 Examples and applications

The current section provides several examples of models on which the constructed early-warning signs are applicable. Unless stated otherwise, the figures displayed are obtained in MATLAB [151].

5.2.1 The heat equation with noise boundary conditions

Example 5.2.1. We set $\mathcal{X}_1 = [0, L]^N$, for $N \in \{1, 2, 3\}$, and $\Gamma(p) = \Gamma_{\mathsf{N}}$ in (5.0.1) that defines homogeneous Neumann boundary conditions on $\mathcal{X}_1$. We also consider $A(p) = \Delta + p$ and $A_0(p) = \Delta_{\mathsf{N}} + p$ for Δ the Laplace operator on $\mathcal{X}_1$ and Δ_{N} the Laplace operator with homogeneous Neumann boundary conditions, i.e.,

$$\Delta_{\mathsf{N}} f = \Delta f, \text{ for any } f \in \mathcal{D}(\Delta_{\mathsf{N}}) := \left\{ v \in \mathcal{W}^{2,2}(\mathcal{X}_1) : \ \Gamma_{\mathsf{N}}\, v(x) = 0, \ x \in \mathcal{X}_0 \right\}.$$

It is well known that the non-positive self-adjoint operator Δ_{N} has discrete spectrum $\left\{ \hat{\lambda}_i \right\}_{i \in \mathbb{N}_{>0}}$ and that its eigenfunctions form a basis in $\mathcal{H}_1$. Due to the construction of $A_0(p)$, the domain $\mathcal{D}(A_0(p))$ does not depend on p. We note that the smallest value in $\left\{ -\hat{\lambda}_i \right\}_{i \in \mathbb{N}_{>0}}$ is $-\hat{\lambda}_1 = 0$ and that it has multiplicity 1, hence in this case $\lambda = 0$ and $\mathcal{M}_1 = 1$. Furthermore, for any $p < 0$ we set $q = q(p) = p + c$ for a fixed $c > 0$. Such a choice implies that $A(p) - q = \Delta_{\mathsf{N}} - c$ and that the operator D is independent of p. From the structure of $\mathcal{X}_1$ we know that D is also bounded [66].
It is also known, from [66, Theorem 13.3.6], that, for certain operators Q, the conditions (5.1.1) and (5.1.13) hold. It follows that the solution of (5.0.1) assumes values in $\mathcal{H}_1$. We can then write the covariance operator at time $t > 0$, defined in (2.3.8), as

$$V_\infty^{\mathsf{W}} := \int_0^t (\Delta_{\mathsf{N}} - c)\mathsf{e}^{(\Delta_{\mathsf{N}} + p)s} D(p) Q D(p)^* \mathsf{e}^{(\Delta_{\mathsf{N}} + p)s} (\Delta_{\mathsf{N}} - c)\mathsf{d}s.$$

We can also state that Theorem 5.1.3, Theorem 5.1.4 and Corollary 5.1.6 hold. In particular for any $f_1, f_2 \in \mathcal{D}(\Delta_{\mathsf{N}})$ such that $\Pi_1(\lambda)^* f_1 \not\equiv 0 \not\equiv \Pi_1(\lambda)^* f_2$ and $\tau \geq 0$,

$$|\langle f_1, V_\infty^{\tau,\mathsf{W}} f_2 \rangle| = \Theta_p\left(-\frac{1}{p} \right)$$

as $p \to 0^-$.

Example 5.2.2. We fix $\mathcal{X}_1 = [0, L]$ and $\Gamma(p) = \Gamma_{\mathsf{D}}$ in (5.0.1) such that Γ_{D} requires the solutions of the system to satisfy homogeneous Dirichlet boundary conditions on the interval. Similarly to the previous example, we set $A(p) = \Delta + p$ and $A_0(p) = \Delta_{\mathsf{D}} + p$, for

$$\Delta_{\mathsf{D}} f = \Delta f, \text{ for any } f \in \mathcal{D}(\Delta_{\mathsf{D}}) := \left\{ v \in \mathcal{W}^{2,2}(\mathcal{X}_1) : \Gamma_{\mathsf{D}}\, v(x) = 0, \ x \in \mathcal{X}_0 \right\}.$$

The negative self-adjoint operator Δ_{D} has discrete spectrum $\left\{ \hat{\lambda}_i \right\}_{i \in \mathbb{N}_{>0}}$ coupled to the eigenbasis $\{\hat{e}_i\}_{i \in \mathbb{N}_{>0}}$ in $\mathcal{H}_1$. The domain $\mathcal{D}(A_0(p))$ is independent of p. We label the highest value in $\left\{ \hat{\lambda}_i \right\}_{i \in \mathbb{N}_{>0}}$ as $\hat{\lambda}_1$, which has multiplicity 1. Hence, in this case, the threshold is $\lambda = -\hat{\lambda}_1$ and $\mathcal{M}_1 = 1$. For any $p < -\hat{\lambda}_1$ we set $q = q(p) = p + c$ for a fixed $c > 0$, which implies that $A(p) - q = \Delta_{\mathsf{D}} - c$ and that the operator D is independent of p. We know from [63] that D is bounded, yet (5.0.1) does not have solutions in $\mathcal{H}_1$. The system admits nevertheless solutions in $\mathcal{W}^{\alpha,2}(\mathcal{X}_1)$, the Sobolev space of degree α, for $\alpha < -\frac{1}{2}$. The fact that α is required to be negative implies that (5.1.1) does not hold. Following the same step as the proof of Lemma 5.1.2, a generalised Lyapunov equation of the form

$$\langle (-A_0(p))U(p)v, V_\infty^{\tau,\mathsf{W}} U(p)w \rangle + \langle U(p)v, V_\infty^{\tau,\mathsf{W}} (-A_0(p))U(p)w \rangle$$

$$= -\left\langle U(p)v, \mathsf{e}^{A_0(p)\tau}(A_0(p)-q)D(p)QD(p)^*(A_0(p)-q)U(p)w\right\rangle,$$

can be proven for weight $U(p) = (-A_0(p))^{\frac{\alpha}{2}}$, functions $U(p)v, U(p)w \in \mathcal{D}(A_0(p))$ and any $\tau \geq 0$. We can then obtain

$$\langle U(p)\hat{e}_i, V_\infty^{\tau,\mathsf{w}}U(p)\hat{e}_j\rangle = -\frac{\mathsf{e}^{\hat{\lambda}_i\tau}\left(\hat{\lambda}_i - c\right)\left(\hat{\lambda}_i - c\right)\left((\hat{\lambda}_i+p)(\hat{\lambda}_j+p)\right)^{\frac{\alpha}{2}}}{\left(\hat{\lambda}_i+\hat{\lambda}_i+2p\right)}\langle \hat{e}_i, D(p)QD(p)^*\hat{e}_j\rangle\,.$$

From the steps in Theorem 5.1.3 and Theorem 5.1.4, it follows that

$$|\langle U(p)\hat{e}_i, V_\infty^{\tau,\mathsf{w}}U(p)\hat{e}_j\rangle| = \Theta_p\left(\left|\frac{\left((\hat{\lambda}_i+p)(\hat{\lambda}_j+p)\right)^{\frac{\alpha}{2}}}{\left(\hat{\lambda}_i+\hat{\lambda}_i+2p\right)}\right|\right) \tag{5.2.1}$$

and, for any $U(p)f_1, U(p)f_2 \in \mathcal{D}(A_0(p))$ such that $\Pi_1(\lambda)^*f_1 \not\equiv 0 \not\equiv \Pi_1(\lambda)^*f_2$, f_1 and f_2 are finite linear combinations of eigenfunctions $\{\hat{e}_i\}_{i\in\mathbb{N}_{>0}}$ and $\tau \geq 0$,

$$|\langle U(p)f_1, V_\infty^{\tau,\mathsf{w}}U(p)f_2\rangle| = \Theta_p\left(\left|\left(\hat{\lambda}_1+p\right)^{-1+\alpha}\right|\right) \tag{5.2.2}$$

as $p \to -\hat{\lambda}_1$.

Remark 5.2.3. Introducing a weighting of the norm in $\mathcal{H}_1$ through the operator $U(p) = (-A_0(p))^{\frac{\alpha}{2}}$ leads to early-warning signs in (5.2.1) and (5.2.2) with a larger rate of divergence than those established in Theorem 5.1.3 and Theorem 5.1.4. This increased divergence is attributed to the convergence of the dominant eigenvalue of $A_0(p)$ to the imaginary axis. To circumvent this effect, it is preferable to employ $(-A_0(p)+q)^{\frac{\alpha}{2}} = (-\Delta_{\mathsf{D}}+c)^{\frac{\alpha}{2}} = U$ as a weighting operator. From [63] and assuming

$$g_1 \in \mathcal{H}_1, \quad f_1 = (-\Delta_{\mathsf{D}}+c)^{-\frac{1}{4}}g_1 \in \mathcal{D}(A_0(p)), \quad g_2 \in \mathcal{H}_1 \quad \text{and} \quad f_2 = (-\Delta_{\mathsf{D}}+c)^{-\frac{1}{4}}g_2 \in \mathcal{D}(A_0(p)),$$

it holds that $\left\langle f_1, V_\infty^{\tau,\mathsf{w}}f_2\right\rangle < \infty$ for any $p < \lambda$. A numerical analysis of the early-warning signs is possible as the functions f_1 and f_2 can be assumed to approximate elements in $O_M(p)^*$, for a sufficiently large $M \in \mathbb{N}_{>0}$ and any $p < \lambda$, due to the completeness of the eigenfunctions of $A_0(p)$ in $\mathcal{H}_1$.

5.2.2 From theory to practical applications

The early-warning signs discussed in Corollary 5.1.6 generalise the tools employed in finite-dimensional models as they consider the effect of spatial components and noise on the boundary of the domain. As an example, such early-warning signs are employed in climate science. Specific models study the collapse of the Atlantic Meridional Overturning Circulation [32, 74, 202] and the melting of the Western Greenland Ice Sheet [33]. Such tipping points are often associated with fold bifurcations.

Similarly to the previous chapters, the application of the time-asymptotic autocovariance and autocorrelation as early-warning signs on real-life models relies on Birkhoff's Ergodic Theorem, which states that, for fixed $p < \lambda$ and ergodic solutions $u^{(\mathsf{w},\mathsf{b})}$ of (5.0.1), the time-asymptotic autocovariance equals the asymptotic temporal autocovariance, i.e.,

$$\langle f_1, V_\infty^{\tau,\mathsf{w}}f_2\rangle = \int_0^\infty \left\langle u^{(\mathsf{w},\mathsf{b})}(\cdot, s+\tau), f_1\right\rangle\left\langle u^{(\mathsf{w},\mathsf{b})}(\cdot, s), f_2\right\rangle \mathsf{d}s,$$

and the time-asymptotic autocorrelation corresponds to the asymptotic temporal autocorrelation, i.e.,

$$\hat{V}_{\infty}^{\tau,\mathsf{w}}(f_1,f_2)=\frac{\int_0^{\infty}\left\langle u^{(\mathsf{w},\mathsf{b})}(\cdot,s+\tau),f_1\right\rangle\left\langle u^{(\mathsf{w},\mathsf{b})}(\cdot,s),f_2\right\rangle \mathrm{d}s}{\int_0^{\infty}\left\langle u^{(\mathsf{w},\mathsf{b})}(\cdot,s),f_1\right\rangle\left\langle u^{(\mathsf{w},\mathsf{b})}(\cdot,s),f_2\right\rangle \mathrm{d}s},$$

for any $f_1, f_2 \in \mathcal{D}(A_0(p)^*)$ such that $\langle f_1, V_{\infty}^{\mathsf{w}} f_2\rangle \neq 0$. The temporal autocovariance and autocorrelation along functions f_1 and f_2 provide practical observables, as such quantities can be extracted from time series and real-life data. As an example, the choice of f_1 and f_2 as indicator functions implies the correlation and autocorrelation of the average of some of the components in $u^{(\mathsf{w},\mathsf{b})}$ on the supports of the observed functions [21]. A concrete example of this approach is described in Section 5.2.3. For any fixed $p \leq \lambda$ and under the assumption of completeness of the generalised eigenfunctions of $A_0(p)$, the functions f_1 and f_2 can also be assumed to be in $O_M(p)^*$, for a sufficiently large $M \in \mathbb{N}_{>0}$.

5.2.3 A Boussinesq model with noise boundary conditions

The Boussinesq model, studied in [72], describes flows in a two-dimensional region of the ocean. Such an area is defined by the spatial variables $(x_1, x_2) \in [-H, 0] \times [0, L]$, for depth H and latitude length L. The scaled and non-dimensionalised variables that define the model are the salinity S, the temperature T, the vorticity ω and the streamfunction ψ. The two-dimensional model is described as follows:

$$\begin{aligned}
Pr^{-1}\left(\frac{\partial\omega}{\partial t}+v\frac{\partial\omega}{\partial x_2}+w\frac{\partial\omega}{\partial x_1}\right)&=\Delta\omega+Ra\left(\frac{\partial T}{\partial x_2}-\frac{\partial S}{\partial x_2}\right),\\
\omega=-\Delta\psi \quad , \quad v=\frac{\partial\psi}{\partial x_1} \quad , \quad w&=-\frac{\partial\psi}{\partial x_2},\\
\frac{\partial T}{\partial t}+v\frac{\partial T}{\partial x_2}+w\frac{\partial T}{\partial x_1}&=\Delta T,\\
\frac{\partial S}{\partial t}+v\frac{\partial S}{\partial x_2}+w\frac{\partial S}{\partial x_1}&=Le^{-1}\Delta S;
\end{aligned} \tag{5.2.3}$$

lateral boundary conditions for any $x_1 \in (-H, 0)$ and $t \geq 0$ as

$$x_2=0,L: \qquad \psi(x_1,x_2,t)=\omega(x_1,x_2,t)=\frac{\partial S}{\partial x_2}(x_1,x_2,t)=\frac{\partial T}{\partial x_2}(x_1,x_2,t)=0; \tag{5.2.4}$$

conditions at the ocean floor for any $x_2 \in (0, L)$ and $t \geq 0$ as

$$x_1=-H: \qquad \psi(x_1,x_2,t)=\omega(x_1,x_2,t)=\frac{\partial S}{\partial x_1}(x_1,x_2,t)=\frac{\partial T}{\partial x_1}(x_1,x_2,t)=0; \tag{5.2.5}$$

conditions at the surface for any $x_2 \in (0, L)$ and $t \geq 0$ as

$$\begin{aligned}
&\psi(x_1,x_2,t)=\omega(x_1,x_2,t)=0,\\
x_1=0: \qquad &\frac{\partial S}{\partial x_1}(x_1,x_2,t)=p\left(Q_S(x_2)+\nu V_S(x_2)\right)+\sigma Q_S(x_2)\dot{W}(x_2,t),\\
&\frac{\partial T}{\partial x_1}(x_1,x_2,t)=-\kappa(T(x_1,x_2,t)-T_S(x_2)+\delta).
\end{aligned} \tag{5.2.6}$$

The initial conditions of the model are denoted as

$$u_0(x_1,x_2)=\left(\psi(x_1,x_2,0),\omega(x_1,x_2,0),T(x_1,x_2,0),S(x_1,x_2,0)\right),$$

for any $x_1 \in [-H, 0]$ and $x_2 \in [0, L]$. The term $\dot{W}$ indicates Gaussian white noise, in space and time, on the surface boundary, which is physically justified by minor external forcing in the region. In the following SPDEs, the noise intensity is set as $\sigma = 0.01$, unless stated otherwise. The Prandtl number Pr and the

Lewis number Le are fixed as $Pr = 2.25$ and $Le = 1$. Following [72], we set $H = 1$. We use Δ to denote the two-dimensional Laplace operator on $[-H, 0] \times [0, L]$. For clarity, Figure 5.1 displays the model set-up. The forcing functions are

$$Q_S(x_2) = 3\cos\left(2\pi\left(\frac{x_2}{L} - \frac{1}{2}\right)\right),$$
$$V_S(x_2) = -\sin\left(\pi\left(\frac{x_2}{L} - \frac{1}{2}\right)\right),$$

and

$$T_S(x_2) = \frac{1}{2}\left(\cos\left(2\pi\left(\frac{x_2}{L} - \frac{1}{2}\right)\right) + 1\right)$$

for $x_2 \in [0, L]$. The shape of functions Q_S, V_S and T_S are shown in Figure 5.1.

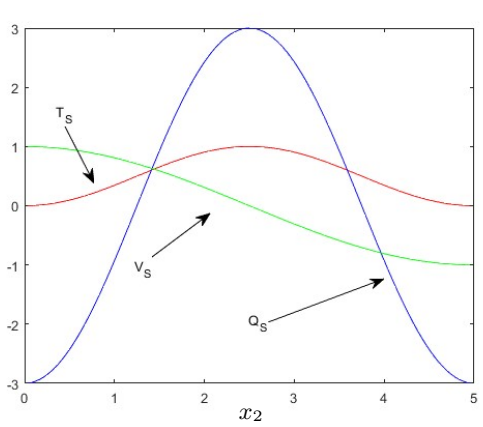

(a) Functions defining surface conditions in model (S1)

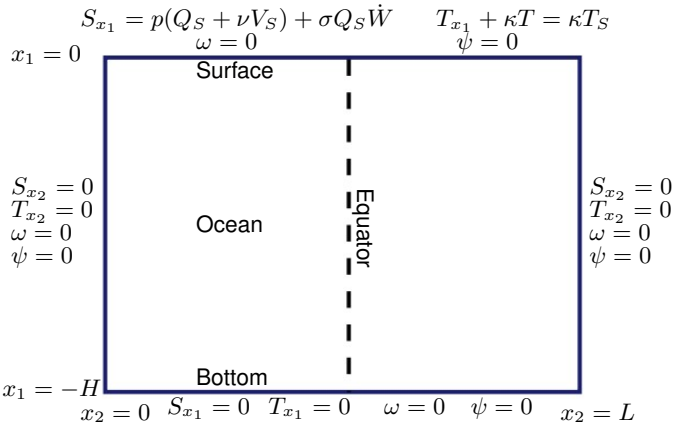

(b) Boundary conditions and visual interpretation of model (S1)

Fig. 5.1 Panel (a) shows the shape of the forcing functions as functions of x_2 for $L = 5$. The choice of function T_S affects the temperature forcing, and the freshwater flux forcing is related to Q_S and V_S. The function V_S provides asymmetry in x_2 on the boundary conditions.
The Boussinesq model (S1) setup and its boundary conditions are displayed in panel (b). The partial derivatives are indicated as $S_{x_1}, T_{x_1}, S_{x_2}, T_{x_2}$. The boundary condition for the temperature at the surface is a Newtonian cooling condition, or Robin condition. Following [10], we insert white noise on the surface boundary condition of the salinity variable.

We set a bifurcation threshold λ. For fixed $p < \lambda$ we pick a deterministically stable equilibrium solution $(\psi_*, \omega_*, T_*, S_*)$ of (5.2.3), (5.2.4), (5.2.5) and (5.2.6) with $\sigma = 0$. We can then linearise the system locally, thus obtaining

$$\begin{pmatrix} 0 \\ \frac{\partial \omega}{\partial t} \\ \frac{\partial T}{\partial t} \\ \frac{\partial S}{\partial t} \end{pmatrix} = A(\psi_*, \omega_*, T_*, S_*) \begin{pmatrix} \psi \\ \omega \\ T \\ S \end{pmatrix} \tag{5.2.7}$$

and linearised boundary conditions (5.2.4), (5.2.5) and

$$x_1 = 0: \quad \begin{aligned} &\psi(x_1, x_2, t) = \omega(x_1, x_2, t) = 0, \\ &\frac{\partial S}{\partial x_1}(x_1, x_2, t) = \sigma Q_S(x_2)\dot{W}(x_2, t), \\ &\frac{\partial T}{\partial x_1}(x_1, x_2, t) + \kappa T(x_1, x_2, t) = 0. \end{aligned} \tag{5.2.8}$$

for any $x_2 \in (0, L)$ and $t \geq 0$. The original system (5.2.3) with boundary conditions (5.2.4), (5.2.5) and (5.2.6) is called (S0) under the assumption $\sigma = 0$ and (S1) for the initial condition $u_0 = (\psi_*, \omega_*, T_*, S_*)$.

The linearised system (5.2.7) with boundary conditions (5.2.4), (5.2.5), (5.2.8) and initial condition in the null function $u_0 \equiv 0$ is denoted as (S2). The operator $A(\psi_*, \omega_*, T_*, S_*)$ is of the form

$$A(\psi_*, \omega_*, T_*, S_*) = \left(\begin{array}{c|c} A_{11} & A_{12} \\ \hline A_{21}(\omega_*, T_*, S_*) & A_{22}(\psi_*) \end{array} \right),$$

for: $A_{11} = \Delta$, the Laplace operator;

$$A_{12} = \begin{pmatrix} \mathrm{Id} & 0 & 0 \end{pmatrix},$$

with Id, the identity operator, and 0, the null operator;

$$A_{21}(\omega_*, T_*, S_*) = \begin{pmatrix} -\frac{\partial \omega_*}{\partial x_2}\frac{\partial}{\partial x_1} + \frac{\partial \omega_*}{\partial x_1}\frac{\partial}{\partial x_2} \\ -\frac{\partial T_*}{\partial x_2}\frac{\partial}{\partial x_1} + \frac{\partial T_*}{\partial x_1}\frac{\partial}{\partial x_2} \\ -\frac{\partial S_*}{\partial x_2}\frac{\partial}{\partial x_1} + \frac{\partial S_*}{\partial x_1}\frac{\partial}{\partial x_2} \end{pmatrix};$$

for the operator

$$A_{22}(\psi_*) = \begin{pmatrix} -\frac{\partial \psi_*}{\partial x_1}\frac{\partial}{\partial x_2} + \frac{\partial \psi_*}{\partial x_2}\frac{\partial}{\partial x_1} + Pr\Delta & Pr\ Ra\frac{\partial}{\partial x_2} & -Pr\ Ra\frac{\partial}{\partial x_2} \\ 0 & -\frac{\partial \psi_*}{\partial x_1}\frac{\partial}{\partial x_2} + \frac{\partial \psi_*}{\partial x_2}\frac{\partial}{\partial x_1} + \Delta & 0 \\ 0 & 0 & -\frac{\partial \psi_*}{\partial x_1}\frac{\partial}{\partial x_2} + \frac{\partial \psi_*}{\partial x_2}\frac{\partial}{\partial x_1} + Le^{-1}\Delta \end{pmatrix}.$$

Solutions (ψ, ω, T, S) of (5.2.7) satisfy

$$\begin{cases} -A_{11}\psi = A_{12}\begin{pmatrix} \omega \\ T \\ S \end{pmatrix}, \\ \frac{\partial}{\partial t}\begin{pmatrix} \omega \\ T \\ S \end{pmatrix} = A_{21}(\omega_*, T_*, S_*)\psi + A_{22}(\psi_*)\begin{pmatrix} \omega \\ T \\ S \end{pmatrix}. \end{cases}$$

Under boundary conditions (5.2.4), (5.2.5) and (5.2.8), A_{11} is invertible and the Schur complement of $A(\psi_*, \omega_*, T_*, S_*)$ is defined as

$$A_{\mathsf{S}}(\psi_*, \omega_*, T_*, S_*) := A_{22}(\psi_*) - A_{21}(\omega_*, T_*, S_*)A_{11}^{-1}A_{12}. \tag{5.2.9}$$

We introduce also

$$A_0(\psi_*, \omega_*, T_*, S_*) = A_{\mathsf{S}}(\psi_*, \omega_*, T_*, S_*) \tag{5.2.10}$$

for

$$\mathcal{D}\left(A_0(\psi_*, \omega_*, T_*, S_*)\right) = \mathcal{D}\left(A_S(\psi_*, \omega_*, T_*, S_*)\right) \cap \left\{ \begin{array}{c} (\omega, T, S) \quad \text{that satisfy} \\ \text{(5.2.4), (5.2.5) and (5.2.8) for } \sigma = 0 \end{array} \right\}, \tag{5.2.11}$$

and any steady solution $(\psi_*, \omega_*, T_*, S_*)$ of (S0). We can then consider the linearised problem

$$\frac{\partial}{\partial t}\begin{pmatrix}\omega\\T\\S\end{pmatrix} = A_{\mathsf{S}}(\psi_*, \omega_*, T_*, S_*)\begin{pmatrix}\omega\\T\\S\end{pmatrix}$$

with boundary conditions (5.2.4), (5.2.5) and (5.2.8). Setting an initial condition in $\mathcal{D}(A_{\mathsf{S}}(\psi_*, \omega_*, T_*, S_*))$, the system is of the form (5.0.1). In particular, we can now apply Theorem 5.1.3, Theorem 5.1.4 and Corollary 5.1.6. The results are discussed and compared to numerical methods in the examples to follow.

The variable S appears in the model (S1) only under the application of derivative operators, thus indicating the invariance of the time derivatives and boundary conditions under shifting by a constant along the S component. For all stable solutions of system (S0), $(\psi_*, \omega_*, T_*, S_*)$, the eigenvalue with highest real part of $A_0(\psi_*, \omega_*, T_*, S_*)$ is $\lambda_1^{(p)} = 0$ for any $p < \lambda$. Its corresponding eigenfunction $e_{1,1}^{(p)}$ is characterised by

$$e_{1,1}^{(p)}(x_1, x_2) = \begin{pmatrix}0\\0\\c\end{pmatrix}, \tag{5.2.12}$$

for $c \in \mathbb{R}$, for any $p \leq \lambda$ and $(x_1, x_2) \in [-H, 0] \times [0, L]$. In the following examples, we ensure that the early-warning sign is not affected by the presence of an eigenvalue with zero real part.

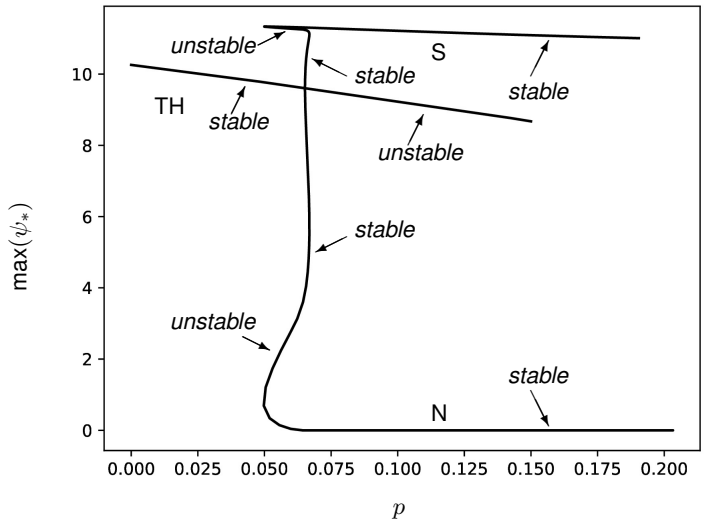

Fig. 5.2 Section of the bifurcation diagram of (S0) under the assumptions $Ra = 10^4$, $\kappa = 10^2$, $L = 10$ and $\nu = \delta = 0$, for the parameter p. The thermally dominated 2-cell state, TH-solution, is stable for $p < \lambda \approx 0.0638$ and unstable for $p > \lambda$. The value λ indicates a supercritical pitchfork threshold. The system is multistable for $p > \tilde{\lambda} \approx 0.049$, as two saddle-node bifurcations indicate the presence of the southward sinking solution, S-solution, and the northward sinking solution, N-solution.
The diagram is obtained with the Python library Transiflow [9] through a pseudo-arclength continuation method and uniform resolution grid $(\mathtt{M}, \mathtt{N}) = (30, 100)$, similar as [72].

Example 5.2.4. In this example, we assume that $L = 10$, $\nu = \delta = 0$, and $Ra = 10^4$. The value κ, a ratio of the diffusive timescale of vertical heat transfer and the relaxation timescale, is assumed as $\kappa = 100$. The bifurcation diagram of system (S0) is displayed in Figure 5.2. It is shown that a supercritical pitchfork bifurcation threshold is located at $p = \lambda \approx 0.0638$, where a stable solution with components T and S symmetric along the equator $x_2 = \frac{L}{2}$, the thermally dominated 2-cell state, loses its stability.

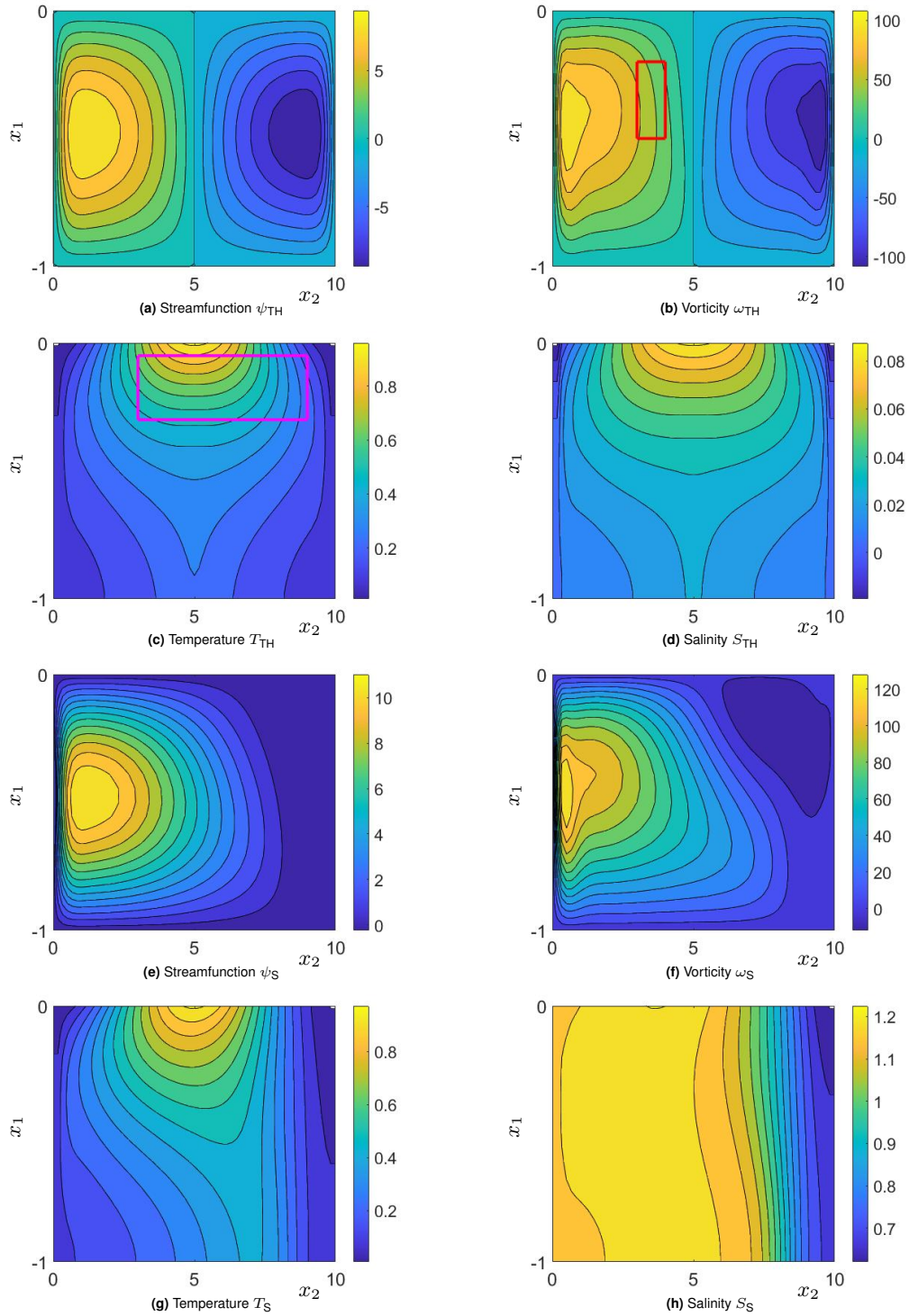

Fig. 5.3 The panels (a)-(d) display the simulation of a stable solution $(\psi_{\mathsf{TH}}, \omega_{\mathsf{TH}}, T_{\mathsf{TH}}, S_{\mathsf{TH}})$ of the system defined by (S0) and assumptions $Ra = 10^4$, $\kappa = 10^2$, $L = 10$ and $\nu = \delta = 0$. The parameter leading to a pitchfork bifurcation is taken as $p = 0.055$, hence less than the threshold value λ. The coloured boxes delimit supports of indicator functions, chosen further in the example as $f_1^{(p)}$ and $f_2^{(p)}$, for any $p < \lambda$, in (5.1.12) in Theorem 5.1.4. The red box, in the plot of ω_{TH}, defines the rectangle $[-0.5, -0.2] \times [3, 4] \subset [-H, 0] \times [0, L]$ on the domain of ω_{TH}. Such a shape delimits the support of the indicator function $\mathbb{1}_\omega$. Similarly, the magenta box, in the plot of T_{TH}, defines the rectangle $[-0.3, -0.05] \times [3, 9] \subset [-H, 0] \times [0, L]$ on the domain of T_{TH}, which indicates the support of the indicator function $\mathbb{1}_T$.
The panels (e)-(h) show the southward sinking steady solution $(\psi_{\mathsf{S}}, \omega_{\mathsf{S}}, T_{\mathsf{S}}, S_{\mathsf{S}})$ at $p = 0.055$, under equivalent assumptions. Such a stable solution arises from a saddle-node bifurcation at $p = \tilde{\lambda} \approx 0.049$.

We label the thermally dominated 2-cell state as $(\psi_{\mathsf{TH}}, \omega_{\mathsf{TH}}, T_{\mathsf{TH}}, S_{\mathsf{TH}})$, which is chosen as $(\psi_*, \omega_*, T_*, S_*)$ and shown in the panels (a)-(d) of Figure 5.3 for $p = 0.055$. At $p = \tilde{\lambda} \approx 0.049$, two pairs of solutions appear from saddle-node bifurcations, inducing multistability in the system for $\tilde{\lambda} < p \leq \lambda$. One of the

stable solutions that arises from such a threshold, the southward sinking solution, is displayed in panels (e)-(h) from Figure 5.3. The northward sinking solution can be constructed from the latter. Proof of such a statement is provided in [20].
The solutions of the original system (S1) and of the linearised system (S2) are obtained through an implicit Euler finite difference method with time step 10^{-2} and final time t_{end}. Similarly to [72], $\mathtt{M} = 29$ and $\mathtt{N} = 59$ internal resolution points have been considered for the intervals $(-H, 0)$ and $(0, L)$ respectively. The grid is built by assuming the resolution coordinates $\{\mathtt{x}_i\}_{i\in\{1,\dots,\mathtt{N}\}} = \left\{\frac{i\,A}{\mathtt{N}+1}\right\}_{i\in\{1,\dots,\mathtt{N}\}}$, along the x_2 direction, and $\{\mathtt{z}_i\}_{i\in\{1,\dots,\mathtt{M}\}}$, along the x_1 direction, for

$$\mathtt{z}_i := -\frac{1}{2} - \frac{\tanh\left(-3\left(\mathtt{y}_i + \frac{1}{2}\right)\right)}{2\tanh\left(\frac{3}{2}\right)}$$

and $\{\mathtt{y}_i\}_{i\in\{1,\dots,\mathtt{M}\}} = \left\{-1 + \frac{i}{\mathtt{M}+1}\right\}_{i\in\{1,\dots,\mathtt{M}\}}$. Such a choice of grid, similar to the one described in [71], is selected to achieve a higher resolution in the proximity to the surface and ocean floor boundary. The numerical techniques employed to obtain first- and second-order derivatives in a non-equidistant grid are described in [195].

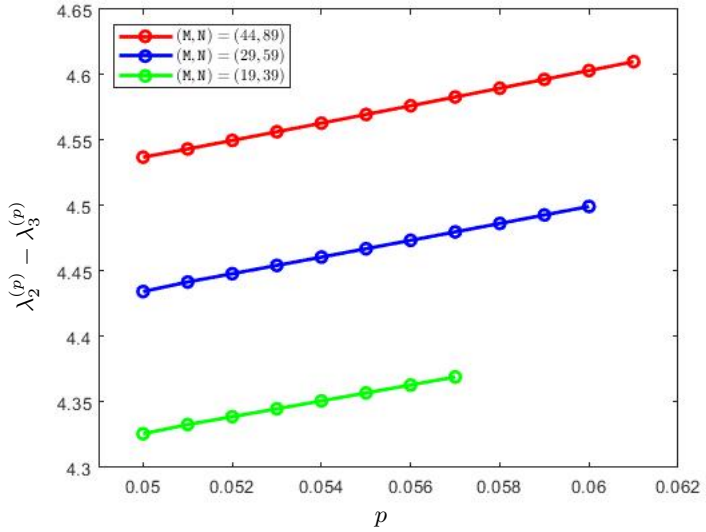

Fig. 5.4 Plot of $\lambda_2^{(p)} - \lambda_3^{(p)}$, the difference between the second and third eigenvalues of $A_0(\psi_{\text{TH}}, \omega_{\text{TH}}, T_{\text{TH}}, S_{\text{TH}})$ with highest real part, for various resolution grid choices. In green the resolution is assumed to be $(\mathtt{M}, \mathtt{N}) = (19, 39)$, in blue $(\mathtt{M}, \mathtt{N}) = (29, 59)$ and in red $(\mathtt{M}, \mathtt{N}) = (44, 89)$. The differences appear to increase in the proximity of the bifurcation threshold, which assumes lower values for coarse resolution grids, as discussed in [72].

We consider $(\psi_{\text{TH}}, \omega_{\text{TH}}, T_{\text{TH}}, S_{\text{TH}})$ as a family of stable steady solutions of (S0) as p approaches a super-critical pitchfork bifurcation at λ. The structure of the spectrum of the operator $A_0(\psi_{\text{TH}}, \omega_{\text{TH}}, T_{\text{TH}}, S_{\text{TH}})$ is not known explicitly; in particular, its discreteness is not trivial to prove through analytic methods. Following Remark 5.1.8, we study the behaviour of the spectrum region with the highest real part as p approaches the bifurcation threshold. The threshold value is obtained numerically with more precision for increased grid resolution of the space. We show in Figure 5.4 the difference between the second and third eigenvalues with highest real part of the numerical approximation, by finite difference method, of $A_0(\psi_{\text{TH}}, \omega_{\text{TH}}, T_{\text{TH}}, S_{\text{TH}})$ previous to the registered bifurcation threshold, for different values of $\mathtt{N}$ and $\mathtt{M}$. The difference appears to be steadily distant from 0, indicating a gap between such eigenvalues, and increasing as p approaches the detected bifurcation point. We can, therefore, compare the results of Corollary 5.1.6 with simulations obtained from the model.
In Figure 5.5a, we observe in blue the behaviour of $\log_{10}\left(-\frac{1}{\lambda_2^{(p)}}\right)$, for $\lambda_2^{(p)}$ being the second eigenvalue of $A_0(\psi_{\text{TH}}, \omega_{\text{TH}}, T_{\text{TH}}, S_{\text{TH}})$ with largest real part. Depending on the grid resolution, such a value increases as p approaches the registered bifurcation threshold in $p \approx 0.0618$. On the circles shown along the red

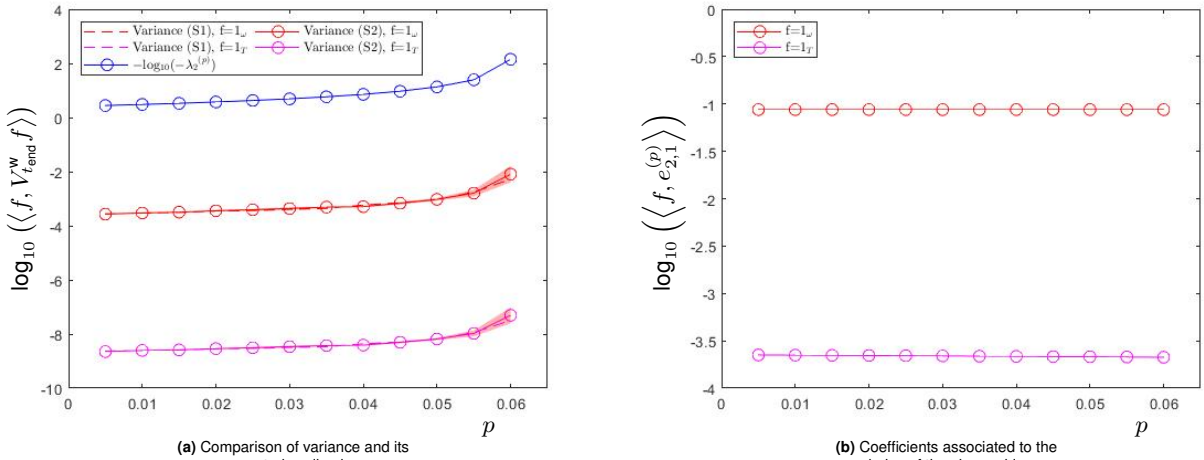

(a) Comparison of variance and its expected scaling law

(b) Coefficients associated to the choice of the observables

Fig. 5.5 The blue line shows the behaviour of $\log_{10}\left(-\frac{1}{\lambda_2^{(p)}}\right)$, for $\lambda_2^{(p)}$ the second eigenvalue of $A_0(\psi_{\mathsf{TH}}, \omega_{\mathsf{TH}}, T_{\mathsf{TH}}, S_{\mathsf{TH}})$ with highest real part.
In (a), the red and magenta lines refer to means of observables obtained from 5 run samples, differing from noise realisations. Such lines display respectively the mean of the logarithm of the temporal autocovariance, for time $t_{\mathsf{end}} = 10^3$ and $\tau = 0$, of solutions of a numerically approximated system projected on indicator functions. The red lines indicate projection on $f = \mathbb{1}_\omega$ and the magenta lines on $f = \mathbb{1}_T$. Such functions are defined in the caption of Figure 5.3. The solutions in (a) associated with the dashed lines satisfy (S1), and those related to the solid lines solve (S2).
In (a), the circles on the red and magenta solid lines indicate the mean values of observables from the linearised systems. The shaded areas have widths equal to double the corresponding standard deviations. The stable solutions are obtained through the natural parameter continuation method, and their stability is observed by solving the eigenvalue problem corresponding to the numerical approximation of $A_0(\psi_{\mathsf{TH}}, \omega_{\mathsf{TH}}, T_{\mathsf{TH}}, S_{\mathsf{TH}})$ through the finite difference method. For $p > \tilde{\lambda} \approx 0.049$, the sampled solutions of (S1) do not present a jump to a neighbourhood of another stable solution before t_{end}, which suggests that they remain in the basin of attraction of $(\psi_{\mathsf{TH}}, \omega_{\mathsf{TH}}, T_{\mathsf{TH}}, S_{\mathsf{TH}})$ for such interval of time.
Panel (b) displays the scalar product in $\mathcal{H}_1$ of $f = \mathbb{1}_\omega$, in red, and $f = \mathbb{1}_T$, in magenta, with $e_{2,1}^{(p)}$. The values are not heavily dependent on p and do not affect the observation of the rate in (a).

and magenta solid lines in Figure 5.5a, we observe the mean logarithm of the temporal variance, for time $t_{\mathsf{end}} = 10^3$, of 5 solutions, differing from noise realisations, of the numerically approximated linearised system (S2), projected respectively on the indicator functions $\mathbb{1}_\omega$ and $\mathbb{1}_T$ with supports defined by the boxes in Figure 5.3. From ergodicity, implied by the additive noise term and the diffusion of the system, we can expect the time-asymptotic temporal variance of an observable of a simulation to be equal to the time-asymptotic variance in function space of the solution of the system along the function that defines the observable [66, 93]. On the red and magenta dashed lines in Figure 5.5a, we display the mean logarithm of the temporal variance in time t_{end} for 5 solutions, under different noise samples, of the numerically approximated original system (S1), projected on $\mathbb{1}_\omega$ and $\mathbb{1}_T$ respectively.

The behaviour of the solid and dashed lines of the same colour is similar, as expected up to proximity to the bifurcation. They also resemble, as p approaches the approximated bifurcation threshold, the blue line with the difference of a constant, suggesting an order of divergence as presented in (5.1.12). Such a resemblance is affected, however, by the choices of functions $\mathbb{1}_\omega$ and $\mathbb{1}_T$. As described in Corollary 5.1.6, the time-asymptotic autocovariance with $\tau = 0$, diverges for a dense set of functions in $\mathcal{H}_1$ as $\mathrm{Re}\left(-\lambda_1^{(p)}\right)^{-2\mathcal{M}_1+1}$, but the chosen direction functions are orthogonal to the unique generalised eigenfunction, $e_{1,1}^{(p)}$, of $A_0(\psi_{\mathsf{TH}}, \omega_{\mathsf{TH}}, T_{\mathsf{TH}}, S_{\mathsf{TH}})$ associated to $\lambda_1^{(p)}$, as described in (5.2.12). The leading term in the series (5.1.10) is therefore associated to $\lambda_2^{(p)}$ and the corresponding generalised eigenfunctions of $A_0(\psi_{\mathsf{TH}}, \omega_{\mathsf{TH}}, T_{\mathsf{TH}}, S_{\mathsf{TH}})$ and its adjoint. The rate displayed by the solid lines in Figure 5.5a is, in fact, $\mathrm{Re}\left(-\lambda_2^{(p)}\right)^{-2\mathcal{M}_2+1}$. In Figure 5.5b, the scalar products in $\mathcal{H}_1$ of $\mathbb{1}_\omega$ and $\mathbb{1}_T$ with the second simple eigenfunction, $e_{2,1}^{(p)}$, of $A_0(\psi_{\mathsf{TH}}, \omega_{\mathsf{TH}}, T_{\mathsf{TH}}, S_{\mathsf{TH}})$ are displayed. Such a value does not appear to be highly dependent on p; therefore, the choice of observables does not greatly impact the rate of the early-warning sign. For each observed value p, there exists only a simple eigenfunction related to $\lambda_2^{(p)}$, which is displayed

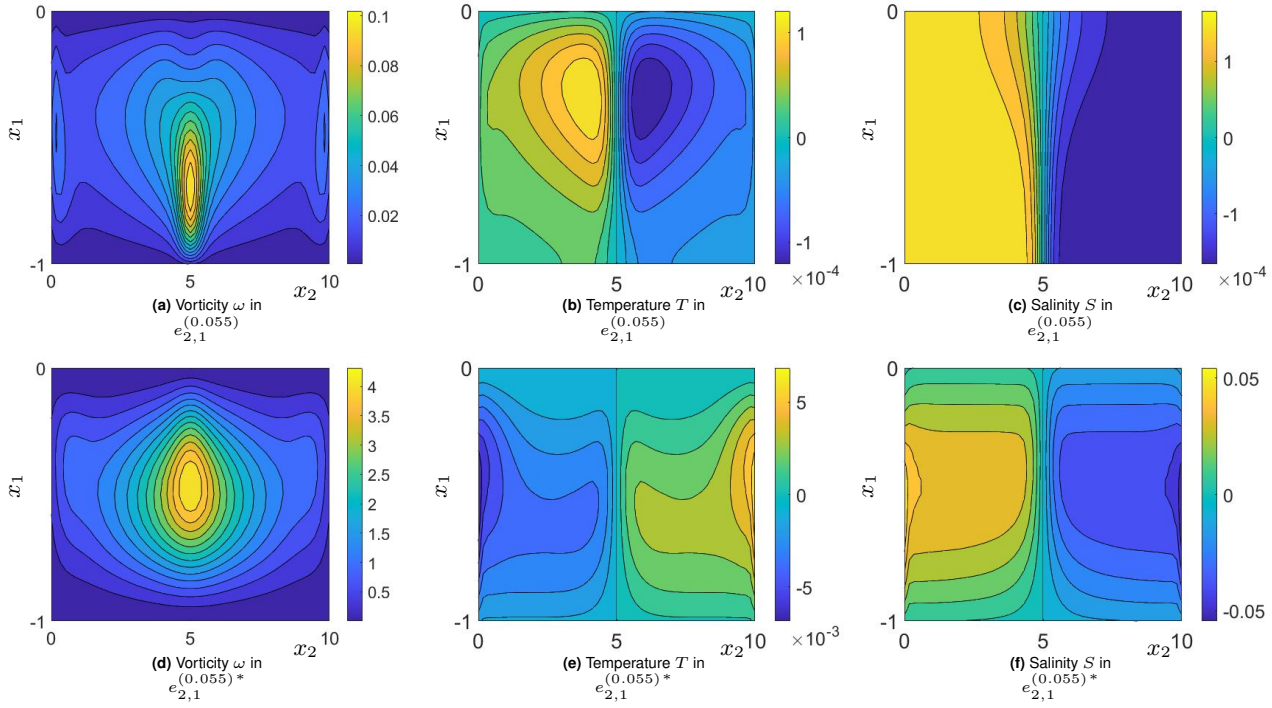

Fig. 5.6 Panels (a)-(c) and (d)-(f) display the components of the approximations of $e_{2,1}^{(0.055)}$ and $e_{2,1}^{(0.055)*}$, which are respectively the (unique) eigenfunctions of $A_0(\psi_{\mathsf{TH}}, \omega_{\mathsf{TH}}, T_{\mathsf{TH}}, S_{\mathsf{TH}})$ and $A_0(\psi_{\mathsf{TH}}, \omega_{\mathsf{TH}}, T_{\mathsf{TH}}, S_{\mathsf{TH}})^*$ associated to the second eigenvalues with highest real part.

in Figure 5.6 for $p = 0.055$, and $\mathcal{M}_2 = 1$.
The divergences in Figure 5.5a can also be affected by the term

$$\left| \left\langle e_{2,1}^{(p)*}, D(p)QD(p)^* e_{2,1}^{(p)*} \right\rangle \right|.$$

The multistability of the system (S0) for p close to the pitchfork bifurcation threshold λ requires a careful choice of t_{end}. Such a time needs to capture the time-asymptotic property of Lemma 5.1.2 and still has to be associated with a small probability of jumping from $(\psi_{\mathsf{TH}}, \omega_{\mathsf{TH}}, T_{\mathsf{TH}}, S_{\mathsf{TH}})$ to another stable solution for any $p < \lambda$ observed. If the second property is not fulfilled, attracting properties in other basins of attraction can be observed, affecting the results in Figure 5.5. The small intensity of the noise in the simulations of the solution of the system (S1) makes such an occurrence rare and not observed in the simulations for $\tilde{\lambda} < p < \lambda$.

Example 5.2.5. We consider the model (S1) for parameters $L = 5$, $\nu = -0.2$, $\delta = 0.5$, $Ra = 4 \times 10^4$. For such values, the surface boundary conditions (5.2.6) on S are not symmetric with respect to the mid-axis. We also consider the limit case $\kappa = +\infty$, thus enforcing heterogeneous Dirichlet boundary conditions on T. Under such an assumption, the bifurcation diagram in Figure 5.7 shows a saddle-node bifurcation at $L_1 = \lambda \approx 1.03$.
Similarly to the previous example, we study a stable solution of (S0), the skewed sinking southward solution $(\psi_{\mathsf{SS}}, \omega_{\mathsf{SS}}, T_{\mathsf{SS}}, S_{\mathsf{SS}})$ displayed in the first row of Figure 5.8, as $(\psi_*, \omega_*, T_*, S_*)$. We also observe early-warning signs able to predict the approach of p to λ from the behaviour of solutions of the corresponding linearised system (S2). The salinity-dominated solution [72], shown in the second row of Figure 5.8, is another stable solution for p in a neighbourhood of λ. The early-warning signs are, therefore, able to predict the jump of a solution of the system (S1) to the proximity of such an equilibrium. Nonetheless, the fact that the bifurcation is of saddle-node type implies that, under the effect of noise, the transition may happen before the threshold approach. The reliability of the signs is consequently dependent on the noise intensity, which is known to affect the probability of metastable jump before a given time [19, 23].

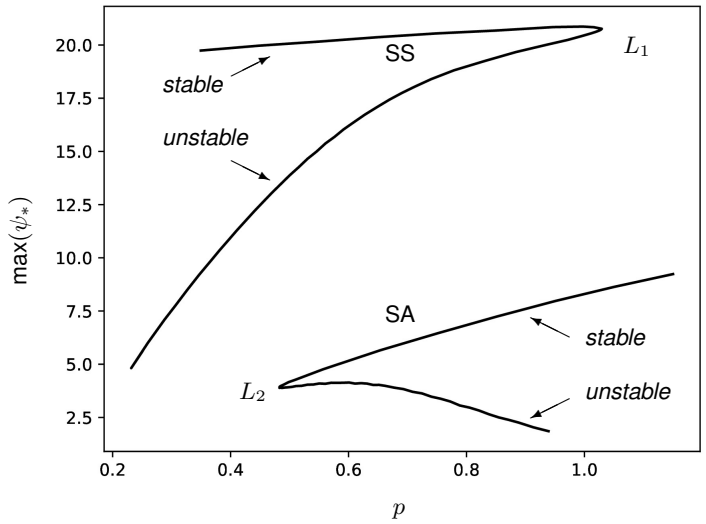

Fig. 5.7 Section of the bifurcation diagram of system (S0) under the assumptions $Ra = 4 \times 10^4$, $\kappa = +\infty$, $L = 5$, $\nu = -0.2$ and $\delta = 0.5$, for parameter p. The skewed southward sinking solution, SS-solution, exists and is stable for $p < \lambda \approx 1.03$. The bifurcation threshold on $p = \lambda$ is associated to a saddle-node bifurcation.
The system is multistable for p close to λ. In the figure we indicate the salinity-dominated stable solution, SA-solution. The lines are obtained with the Python library Transiflow [9] through the pseudo-arclength continuation method and uniform resolution grid $(\mathtt{M}, \mathtt{N}) = (30, 60)$.

The four eigenvalues of the matrix $A_0(\psi_{\mathsf{SS}}, \omega_{\mathsf{SS}}, T_{\mathsf{SS}}, S_{\mathsf{SS}})$ with largest real part, for the studied values of p, are $\lambda_1^{(p)} = 0$, $\lambda_2^{(p)} \neq \overline{\lambda_2^{(p)}} = \overline{\lambda_3^{(p)}}$ and $\lambda_4^{(p)} \in \mathbb{R}$. Figure 5.9 displays $\mathrm{Re}\left(\lambda_2^{(p)} - \lambda_4^{(p)}\right)$ for different non-uniform resolution grids, constructed as in the previous example. It is apparent that for $p > 0.4$, the difference increases with p and the resolution of the chosen grids. In particular, the difference strays from 0. This justifies the application of the results of Theorem 5.1.3, Theorem 5.1.4, and Corollary 5.1.6 on the linearised stochastic system (S2) and the observation of its temporal autocovariance and temporal autocorrelation for long time intervals [93].
Figure 5.10 is obtained from 5 sample solutions of the approximated linearised system (S2), final time $t_{\mathsf{end}} = 10^4$ and the implicit Euler finite difference method, as in the previous example. Figure 5.10a and Figure 5.10b display in blue respectively $\log_{10}\left(-\frac{1}{\mathrm{Re}(\lambda_2^{(p)})}\right)$ and $\log_{10}\left(-\frac{1}{\mathrm{Re}(\lambda_4^{(p)})}\right)$. Such lines are compared with the mean logarithm of the temporal variance of the solutions projected on the corresponding eigenfunctions of $A_0(\psi_{\mathsf{SS}}, \omega_{\mathsf{SS}}, T_{\mathsf{SS}}, S_{\mathsf{SS}})^*$, in red.

Figure 5.10a indicates a similar behaviour of the two lines for p close to λ, aside from the difference of a constant. Such a similarity is affected by the shape of the noise and of the corresponding eigenfunction, as described in (5.1.4). This effect can be observed in Figure 5.10b. In such a case, the red line does not indicate divergence of the early-warning sign, similarly to the blue line.

In Figure 5.11, the shape of the simple eigenfunction $e_{2,1}^{(p)^*}$ of $A_0(\psi_{\mathsf{SS}}, \omega_{\mathsf{SS}}, T_{\mathsf{SS}}, S_{\mathsf{SS}})^*$ is displayed for $p = 1$. It generates the corresponding generalised eigenspace $E_2(p)^*$, for the observed p, and $\mathcal{M}_2 = 1$. For any $p \leq \lambda$, we assume the sequences $\left\{f_1^{(p)}\right\}, \left\{f_2^{(p)}\right\}$ continuous in $\mathcal{H}_1$ and such that the integral of the component on S is 0, i.e., it is orthogonal to the only generalised eigenfunction, $e_{1,1}^{(p)}$, of $A_0(\psi_{\mathsf{SS}}, \omega_{\mathsf{SS}}, T_{\mathsf{SS}}, S_{\mathsf{SS}})$ correspondent to $\lambda_1^{(p)}$, as defined in (5.2.12). Under the assumptions of Corollary 5.1.6, there exist for any $\delta > 0$ the sequences $\left\{g_1^{(p)}\right\}$ and $\left\{g_2^{(p)}\right\}$, generated by a finite number of generalised eigenfunctions of $A_0(\psi_{\mathsf{SS}}, \omega_{\mathsf{SS}}, T_{\mathsf{SS}}, S_{\mathsf{SS}})^*$, that satisfy (5.1.18) and

$$\left|\left\langle g_1^{(p)}, V_\infty^{\tau,\mathbf{w}} g_2^{(p)} \right\rangle\right| = \Theta_p\left(\mathrm{Re}\left(-\lambda_2^{(p)}\right)^{-1}\right) \tag{5.2.13}$$

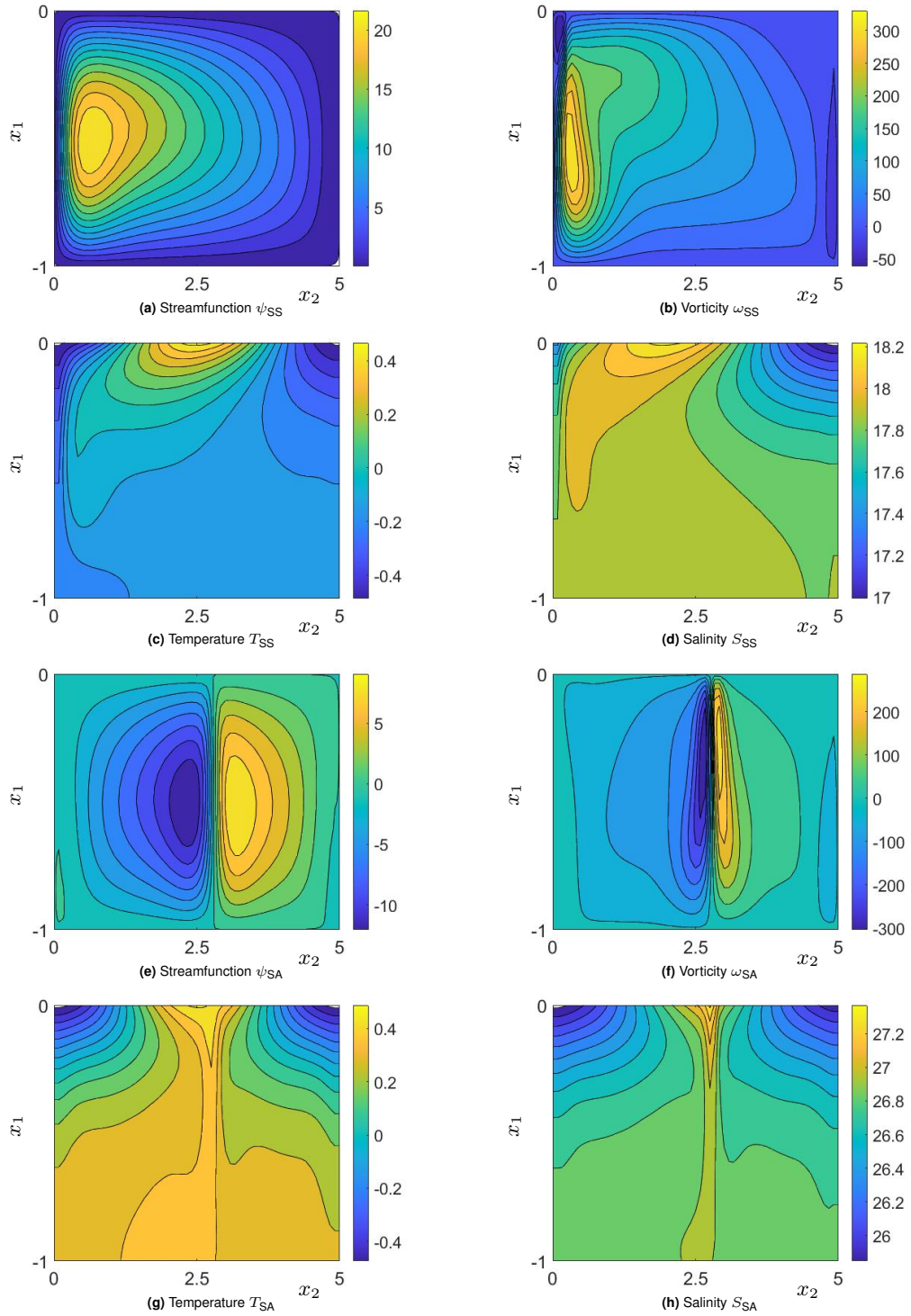

Fig. 5.8 Panels (a)-(d) present the simulation of the skewed sinking southward solution $(\psi_{SS}, \omega_{SS}, T_{SS}, S_{SS})$ of the system (S0) and assumptions $Ra = 4 \times 10^4$, $\kappa = +\infty$, $L = 5$, $\nu = -0.2$ and $\delta = 0.5$. We fix $p = 1$, therefore less than the saddle-node bifurcation value. Panels (e)-(h) display the salinity-dominated stable solution $(\psi_{SA}, \omega_{SA}, T_{SA}, S_{SA})$ at $p = 1$, under equivalent assumptions.

for p that approaches the bifurcation threshold. We can therefore conclude that, although the shape of the function $e_{2,1}^{(p)^*}$ is non-trivial, the simple shape of $e_{1,1}^{(p)}$, described in (5.2.12), facilitates the search of other sequences $\left\{g_1^{(p)}\right\}$ and $\left\{g_2^{(p)}\right\}$ that satisfy

$$\left\langle g_1^{(p)}, e_{1,1}^{(p)} \right\rangle = 0, \quad \left\langle g_2^{(p)}, e_{1,1}^{(p)} \right\rangle = 0, \quad \left\langle g_1^{(p)}, e_{2,1}^{(p)} \right\rangle \neq 0 \quad \text{and} \quad \left\langle g_2^{(p)}, e_{2,1}^{(p)} \right\rangle \neq 0, \tag{5.2.14}$$

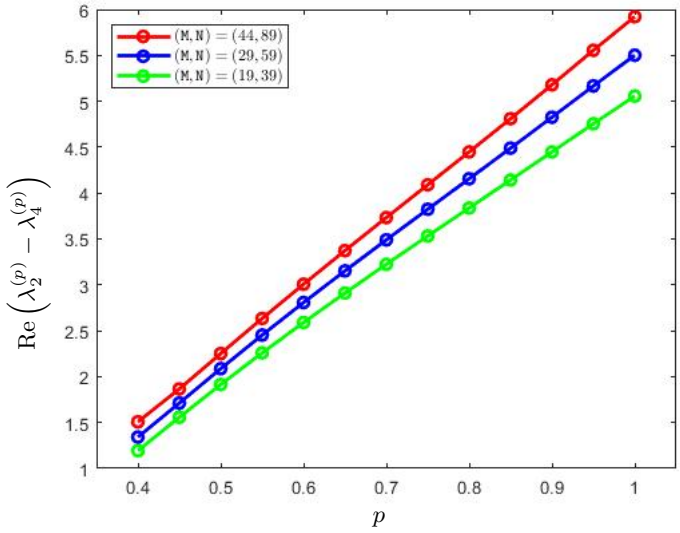

Fig. 5.9 Plot of $\mathrm{Re}\left(\lambda_2^{(p)} - \lambda_4^{(p)}\right)$, for $\lambda_2^{(p)}$ and $\lambda_4^{(p)}$ respectively the second and fourth eigenvalues of $A_0(\psi_{\mathrm{SS}}, \omega_{\mathrm{SS}}, T_{\mathrm{SS}}, S_{\mathrm{SS}})$ with highest real part for various resolution grid choices. In green the resolution is assumed to be $(\mathtt{M}, \mathtt{N}) = (19, 39)$, in blue to be $(\mathtt{M}, \mathtt{N}) = (29, 59)$ and in red to be $(\mathtt{M}, \mathtt{N}) = (44, 89)$.

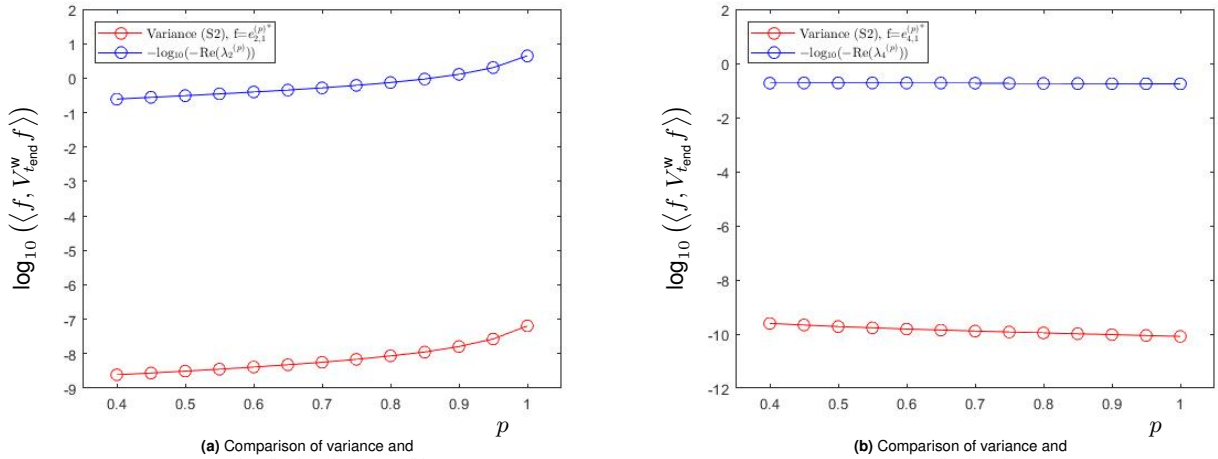

(a) Comparison of variance and expected scaling law along a sensible direction

(b) Comparison of variance and expected scaling law along a not sensible direction

Fig. 5.10 The panels (a) and (b) show in blue $\log_{10}\left(-\frac{1}{\mathrm{Re}\left(\lambda_2^{(p)}\right)}\right)$ and $\log_{10}\left(-\frac{1}{\mathrm{Re}\left(\lambda_4^{(p)}\right)}\right)$ respectively, for $\lambda_2^{(p)}$ and $\lambda_4^{(p)}$ the second and fourth eigenvalue of $A_0(\psi_{\mathrm{SS}}, \omega_{\mathrm{SS}}, T_{\mathrm{SS}}, S_{\mathrm{SS}})$ with highest real part. The red lines refer to the mean logarithm of the temporal variance, for time $t_{\mathrm{end}} = 10^4$ and $\tau = 0$, of solutions of the numerically approximated linearised system (S2), projected on $e_{2,1}^{(p)*}$, in (a), and on $e_{4,1}^{(p)*}$, in (b). Such lines are obtained from 5 run samples, which are different from noise realisation.

for any $p \leq \lambda$, and, consequently, imply (5.2.13).

In Figure 5.12, the mean temporal autocorrelation of 5 solutions of the linearised system (S2) in time $t_{\mathrm{end}} = 10^4$ is studied in relation to the lag $0 \leq \tau \leq 10$ and fixed parameter values p. For $i \in \{2, 4\}$, the figures refer to the absolute values of the numerical approximation of $\hat{V}_{t_{\mathrm{end}}}^{\tau,\mathtt{W}}\left(e_{i,1}^{(p)*}, e_{i,1}^{(p)*}\right)$, in solid lines, and the absolute values of the function $\mathrm{e}^{\overline{\lambda_i^{(p)}}\tau}$, denoted by circles. Corollary 5.1.6 expects the L^2-norm of the differences of $\hat{V}_{\infty}^{\tau,\mathtt{W}}\left(e_{i,1}^{(p)*}, e_{i,1}^{(p)*}\right)$ and $\mathrm{e}^{\overline{\lambda_i^{(p)}}\tau}$ on the interval $\tau \in [0, 10]$ to be 0 for any $0.4 \leq p \leq 1$. Such numerical errors are of order 10^{-3} for all values $i \in \{2, 4\}$ and $p \in \{0.4, 0.6, 0.8, 1\}$, as reported in the figure.

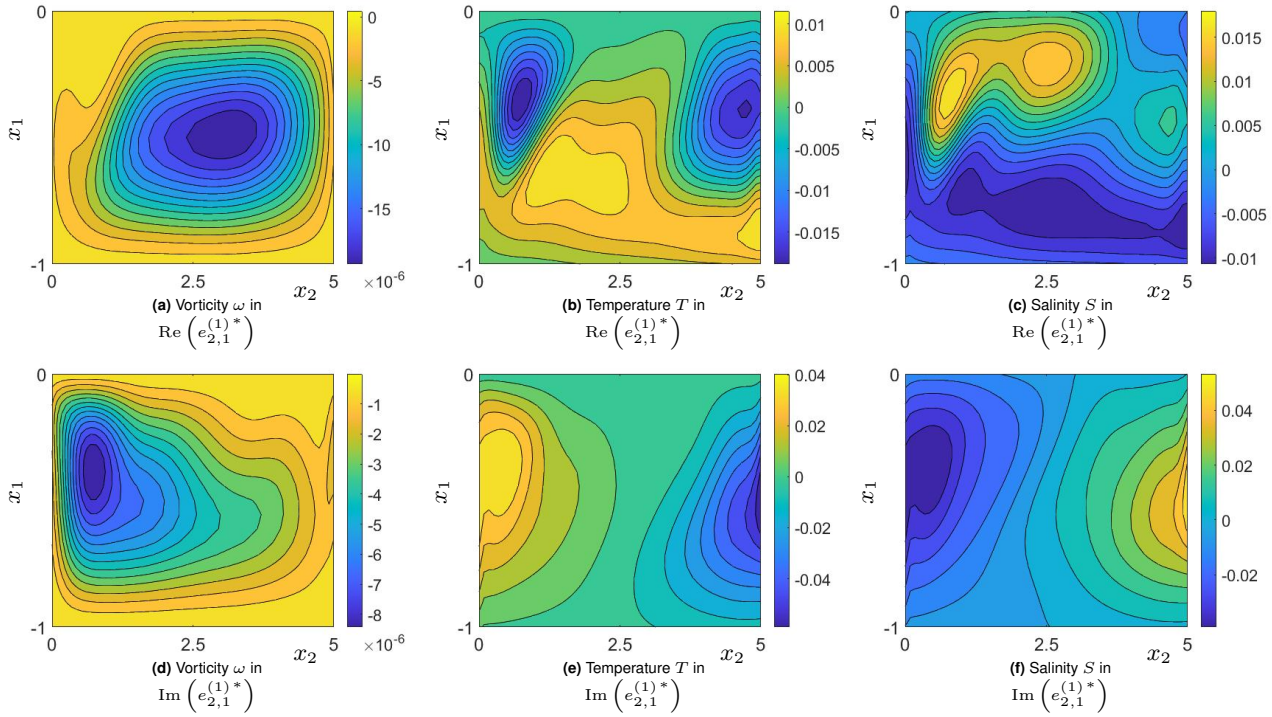

Fig. 5.11 The panels (a)-(c) and (d)-(f) display respectively the real and imaginary parts of the components of the numerical approximations of $e_{2,1}^{(1)*}$. Such a function is the unique generalised eigenfunction of $A_0(\psi_{\mathrm{SS}}, \omega_{\mathrm{SS}}, T_{\mathrm{SS}}, S_{\mathrm{SS}})^*$ associated to $\overline{\lambda_2^{(p)}}$. We label its real and imaginary parts as $\mathrm{Re}\left(e_{2,1}^{(1)*}\right)$ and $\mathrm{Im}\left(e_{2,1}^{(1)*}\right)$.

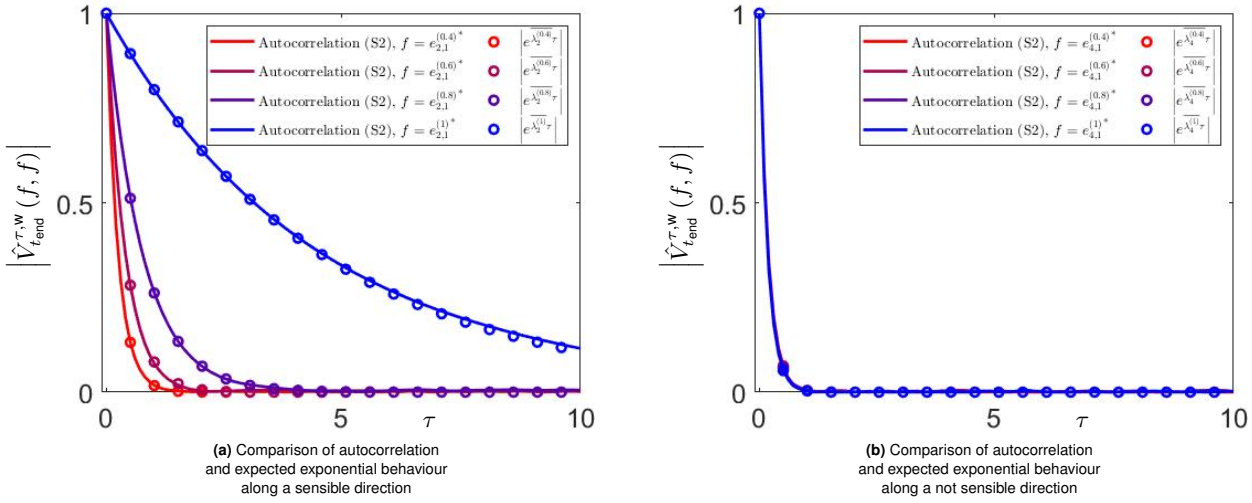

Fig. 5.12 The plots are obtained from 5 solutions, differing from noise samples, of the numerically approximated linearised system (S2) until $t_{\mathrm{end}} = 10^4$. The solid lines indicate the absolute value of the mean temporal autocorrelation of the solutions projected on $e_{i,1}^{(p)*}$. In contrast, the circles display the absolute value of $\mathrm{e}^{\overline{\lambda_i^{(p)}}\tau}$. The functions are shown with the fixed parameter p and under the dependence of the lag time τ.

5.3 Summary

In this chapter, we focus on systems affected by white noise on the boundary. We construct two early-warning signs as the time-asymptotic autocovariance and autocorrelation of the solution of the corresponding linearised fast system. We also provide a description of the directions in the square-integrable functions space along which such objects can predict the crossing of a bifurcation threshold, and discuss the observation of the signs in several examples. In detail, under the referred assumptions, we prove that the divergent time-asymptotic autocovariance, along a general choice of functions, is able to forecast the

bifurcation in the linearised fast system. Conversely, the time-asymptotic autocorrelation provides a more precise prediction if observed along a restrictive set of direction functions.

Particular focus is given to applying the tools to a Boussinesq ocean model, such as examining the projection of the solution on certain eigendirections in the proximity of bifurcation thresholds and the rates adopted by the observables. The study is carried out on a supercritical pitchfork bifurcation and a saddle-node bifurcation. The role of multistability and linearisation in the warning of the bifurcation event is examined. The simulations cross-validate the analytic results and provide further insight into the correct practical use of the tools.

6 Time-asymptotic variance for red noise

In this chapter, we study the scaling law of the time-asymptotic covariance of the mild solutions associated with the three (linear) SPDEs perturbed by red noise. Its content is the result of the contribution by the author in [25].

We define a red noise term through the perturbation induced by an Ornstein-Uhlenbeck process on an SPDE, as described in Chapter 2. We introduce the domain $\mathcal{X}_1 \subset \mathbb{R}^N$ and its boundary $\mathcal{X}_0 = \partial\mathcal{X}_1$, along with the corresponding Hilbert spaces $\mathcal{H}_1 = L^2(\mathcal{X}_1)$ and $\mathcal{H}_0 = L^2(\mathcal{X}_0)$. For $\kappa > 0$, $\sigma > 0$ and $j \in \{0, 1\}$, we define red noise as the mild solution $\xi_j = \xi_j(x,t)$ of

$$\mathsf{d}\xi_j(x,t) = -\kappa\xi_j(x,t)\mathsf{d}t + \sigma Q_j^{\frac{1}{2}}\mathsf{d}W_t^j, \tag{6.0.1}$$

for any $x \in \mathcal{X}_j$ and $t > 0$. In (6.0.1), we assume $Q_j : \mathcal{H}_j \to \mathcal{H}_j$ to be a linear self-adjoint operator and W_t^j to be a cylindrical Wiener process in $\mathcal{X}_j$. The operator Q_j is also assumed to be bounded with a bounded inverse.

First, we study $u^{(\mathsf{r},\mathsf{d})} = u^{(\mathsf{r},\mathsf{d})}(x,t)$, the mild solution of the following SPDE with domain noise ξ_1,

$$\begin{cases} \mathsf{d}u^{(\mathsf{r},\mathsf{d})}(x,t) = \left(A_0(p)u^{(\mathsf{r},\mathsf{d})}(x,t) + \sigma_{\mathsf{R}}\xi_1(x,t)\right)\mathsf{d}t, \\ u^{(\mathsf{r},\mathsf{d})}(x,0) = u_0(x) \in \mathcal{H}_1, \end{cases} \tag{6.0.2}$$

for any $x \in \mathcal{X}_1$ and $t > 0$. The operators $A_0(p)$ and $A_0(p)^*$ are closed and densely defined in $\mathcal{H}_1$. Furthermore, the linear purely discrete operator $A_0(p)$ is negative for $p < 0$ with eigenvalues

$$0 > \mathrm{Re}\left(\lambda_1^{(p)}\right) > \mathrm{Re}\left(\lambda_2^{(p)}\right) \geq \mathrm{Re}\left(\lambda_3^{(p)}\right) \geq \dots,$$

which are assumed to be continuous in p. We assume that the eigenvalue $\lambda_1^{(p)}$ is the only one to reach the imaginary axis at $p = 0$. The geometric multiplicity of each eigenvalue is set as 1. For any $i \in \mathbb{N}_{>0}$, $p \leq 0$ and $k \in \left\{1, \dots, m_a\left(\lambda_i^{(p)}\right)\right\}$, the generalised eigenfunctions of $A_0(p)$ and $A_0(p)^*$ corresponding to $\lambda_i^{(p)}$ and $\overline{\lambda_i^{(p)}}$, respectively, are labelled as $e_{i,k}^{(p)}$ and ${e_{i,k}^{(p)}}^*$ and satisfy

$$\begin{aligned} &A_0(p)e_{i,k}^{(p)} = \lambda_i^{(p)}e_{i,k}^{(p)}, && A_0(p)^*{e_{i,k}^{(p)}}^* = \overline{\lambda_k^{(p)}}{e_{i,1}^{(p)}}^*, && \text{for } k = 1, \\ &A_0(p)e_{i,k}^{(p)} = \lambda_i^{(p)}e_{i,k}^{(p)} + e_{i,k-1}^{(p)}, && A_0(p)^*{e_{i,k}^{(p)}}^* = \overline{\lambda_i^{(p)}}{e_{i,k}^{(p)}}^* + {e_{i,k-1}^{(p)}}^*, && \text{for } k \neq 1. \end{aligned} \tag{6.0.3}$$

Such functions are assumed to be continuous in $\mathcal{H}_1$ with regard to p. The deterministically invariant subspaces generated by the generalised eigenfunctions of $A_0(p)$ and $A_0(p)^*$ associated to the eigenvalue $\lambda_i^{(p)}$ and $\overline{\lambda_i^{(p)}}$ are indicated respectively as $E_i(p)$ and $E_i(p)^*$. Their dimension is called $\mathcal{M}_i = m_a\left(\lambda_i^{(p)}\right)$ and is independent of p. For each $i \in \mathbb{N}_{>0}$, the sets $\left\{e_{i,k}^{(p)}\right\}_{k\in\{1,\dots,\mathcal{M}_i\}}$ and $\left\{{e_{i,\mathcal{M}_i-k+1}^{(p)}}^*\right\}_{k\in\{1,\dots,\mathcal{M}_i\}}$ are scaled to form a biorthogonal system. We assume each family to be complete in $\mathcal{H}_1$ [20, 211]. For any $i \in \mathbb{N}_{>0}$, we label $e_i^{(p)} = e_{i,1}^{(p)}$ and ${e_i^{(p)}}^* = {e_{i,1}^{(p)}}^*$ if the algebraic multiplicity of the corresponding eigenvalue

is 1. Lastly, we set $e_{i,0}^{(p)} = e_{i,0}^{(p)^*} \equiv 0$ for all $i \in \mathbb{N}_{>0}$. For simplicity, we assume that $-\kappa$ is not in the spectrum of $A_0(p)$ for any small $p \leq 0$ and fixed $\kappa > 0$. Such an assumption implies the construction of the functions

$$\mathrm{R}\left(A_0(p)^* + \kappa\right) e_{i,k}^{(p)^*} = -\sum_{j=1}^{k} \left(-\overline{\lambda_i^{(p)}} - \kappa\right)^{-k+j-1} e_{i,j}^{(p)^*} =: \mu_{i,k}^{(p,\kappa)} \tag{6.0.4}$$

for any $i \in \mathbb{N}_{>0}$ and $k \in \{1, \ldots, \mathcal{M}_i\}$, which are used in the theorems to follow.

Secondly, we consider $u^{(\mathsf{r,c})} = u^{(\mathsf{r,c})}(x,t)$, the mild solution of

$$\begin{cases} \mathsf{d}u^{(\mathsf{r,c})}(x,t) = \left(f(x,p)u^{(\mathsf{r,c})}(x,t) + \sigma_{\mathsf{R}}\xi_1(x,t)\right)\mathsf{d}t, \\ u^{(\mathsf{r,c})}(0,x) = u_0(x) \in \mathcal{H}_1, \end{cases} \tag{6.0.5}$$

for $x \in \mathcal{X}_1$ and $t > 0$. The function $f : \mathcal{X}_1 \times \mathbb{R}_{<0} \to \mathbb{R}_{<0}$ is assumed to be analytic and such that, for a fixed x_*, it satisfies

$$f(x,p) < 0 \quad \text{and} \quad f(x_*,0) = 0,$$

for any $(x,p) \in \mathcal{X}_1 \times \mathbb{R}_{\leq 0} \setminus \{(x_*,0)\}$. In contrast to the linear operator in (6.0.2), the multiplication operator associated with f can have a purely continuous spectrum. In this case, we consider for simplicity values of $p < 0 < \kappa$ such that

$$f(x,p) + \kappa \neq 0$$

for any $x \in \mathcal{X}_1$.

Lastly, we study the mild solution $u^{(\mathsf{r,b})} = u^{(\mathsf{r,b})}(x,t)$ of

$$\begin{cases} \mathsf{d}u^{(\mathsf{r,b})}(x,t) = A(p)u^{(\mathsf{r,b})}(x,t)\mathsf{d}t, \\ u^{(\mathsf{r,b})}(0,x) = u_0(x) \in \mathcal{H}_1, \end{cases} \tag{6.0.6}$$

for $x \in \mathcal{X}_1$ and

$$\Gamma(p)u^{(\mathsf{r,b})}(x,t) = \sigma_{\mathsf{R}}\xi_0(x,t),$$

on the boundary $x \in \mathcal{X}_0$ and $t > 0$. The deterministic versions of (6.0.2) and (6.0.6) are assumed to share equivalent assumptions. In this setting, we are investigating the effect of setting noise on the boundary of the space domain. The linear operator

$$\Gamma(p) : \mathcal{D}\left(\Gamma(p)\right) \subset \mathcal{H}_1 \to \mathcal{H}_0$$

defines the boundary conditions. Furthermore, we assume that, for fixed $p \leq 0$, there exists a continuous $q = q(p) \in \mathbb{R}$ such that for any boundary value problem

$$(A(p) - q)w = 0 \quad , \quad \Gamma(p)\, w = v\ ,$$

with $v \in \mathcal{H}_0$, there exists a unique solution $w = D(p)v \in \mathcal{D}(A(p)) \subset \mathcal{H}_1$. For any $p \leq 0$, we indicate $D(p)^*$ as the adjoint operator of $D(p)$ with respect to the scalar products on the Hilbert spaces $\mathcal{H}_1$ and $\mathcal{H}_0$. We assume the operator $D(p)^*$ to be uniformly bounded in $L^2(\mathcal{H}_1; \mathcal{H}_0)$ for any $p \leq 0$. We set

$$A_0(p)v = A(p)v$$

for any $v \in \mathcal{D}(A(p))$ such that $\Gamma(p)v = 0$, which satisfies the spectral properties described above for (6.0.2). Lastly, we consider values of q that are not in the spectrum of $A_0(p)$ and $A_0(p)^*$ for p close to 0. We obtain then that

$$\Lambda(p) := (A_0(p) - q)\, D(p)Q_0D(p)^*\, (A_0(p)^* - q) \tag{6.0.7}$$

depends on operator Γ.
The scaling laws of the observable are considered in the limits $p \to 0^-$ and $\kappa \to 0^+$, where the dissipativity of the models is lost. The early-warning signs for the first limit, considered as "real", are characterised by an equivalent scaling law to the corresponding systems with white noise. Namely, these are the SPDEs (2.3.2), (2.3.4) and (2.3.6) in Chapter 2. The "false" early-warning signs, referring to the second limit, are hyperbolic in κ due to the nature of the noise in time. The SPDEs (6.0.2), (6.0.5) and (6.0.6) are studied, respectively, in the following sections, whereas the results are cross-validated numerically in the last section.

6.1 Discrete Spectrum

We first consider $u^{(\mathsf{r,d})} = u^{(\mathsf{r,d})}(x,t)$ that solves (6.0.2). Its existence is implied by Theorem 2.2.2. In the case of a linear drift term in the system associated with an operator of purely discrete spectrum, the scaling law of the time-asymptotic covariance depends on the functions along which it is observed. The following theorem indicates these sensible modes and the corresponding relation.

Theorem 6.1.1. *Let $\xi_1 = \xi_1(x,t)$ and $u^{(\mathsf{r,d})} = u^{(\mathsf{r,d})}(x,t)$ be the mild solutions of* (6.0.1) *and* (6.0.2)*, respectively, with initial conditions in $\mathcal{H}_1$, $x \in \mathcal{X}_1$, $p < 0$ and $t > 0$. Then, the scaling laws*

$$\left| \left\langle \begin{pmatrix} e^{(p)}_{i_1,k_1} \end{pmatrix}^* \\ 0 \end{pmatrix}, V^{(\mathsf{r},1)}_\infty \begin{pmatrix} \begin{pmatrix} e^{(p)}_{i_2,k_2} \end{pmatrix}^* \\ 0 \end{pmatrix} \right\rangle_{\mathcal{H}_1 \times \mathcal{H}_1} \right| = \Theta_\kappa\left(\kappa^{-1}\right) \quad \textit{for any} \quad p < 0$$

and

$$\left| \left\langle \begin{pmatrix} e^{(p)}_{i_1,k_1} \end{pmatrix}^* \\ 0 \end{pmatrix}, V^{(\mathsf{r},1)}_\infty \begin{pmatrix} \begin{pmatrix} e^{(p)}_{i_2,k_2} \end{pmatrix}^* \\ 0 \end{pmatrix} \right\rangle_{\mathcal{H}_1 \times \mathcal{H}_1} \right| = \Theta_p\left(\left| \overline{\lambda^{(p)}_{i_1}} + \lambda^{(p)}_{i_2} \right|^{-(k_1+k_2-1)} \right) \quad \textit{for any} \quad \kappa > 0$$

hold for any $i_1, i_2 \in \mathbb{N}_{>0}$, $k_1 \in \{1, \dots, \mathcal{M}_{i_1}\}$, $k_2 \in \{1, \dots, \mathcal{M}_{i_2}\}$ and for $V^{(\mathsf{r},1)}_\infty$ introduced in (2.3.9)*.*

Proof. We define the operator

$$B_0(p) = \begin{pmatrix} A_0(p) & \sigma_{\mathsf{R}} \\ 0 & -\kappa \end{pmatrix} \tag{6.1.1}$$

and its adjoint in respect to $\mathcal{H}_1 \times \mathcal{H}_1$

$$B_0(p)^* = \begin{pmatrix} A_0(p)^* & 0 \\ \sigma_{\mathsf{R}} & -\kappa \end{pmatrix}.$$

They generate the $\mathcal{C}_0$-semigroups

$$\mathsf{e}^{B_0(p)t} = \begin{pmatrix} \mathsf{e}^{A_0(p)t} & \sigma_{\mathsf{R}}\left(\mathsf{e}^{A_0(p)t} - \mathsf{e}^{-\kappa t}\right) \mathrm{R}\left(A_0(p) + \kappa\right) \\ 0 & \mathsf{e}^{-\kappa t} \end{pmatrix}$$

and

$$\left(\mathsf{e}^{B_0(p)t}\right)^* = \mathsf{e}^{B_0(p)^*t} = \begin{pmatrix} \mathsf{e}^{A_0(p)^*t} & 0 \\ \sigma_{\mathsf{R}}\,\mathrm{R}\left(A_0(p)^* + \kappa\right)\left(\mathsf{e}^{A_0(p)^*t} - \mathsf{e}^{-\kappa t}\right) & \mathsf{e}^{-\kappa t} \end{pmatrix}$$

for $t > 0$, respectively. The time-asymptotic covariance operator is

$$V_\infty^{(\mathsf{r},1)} = \int_0^\infty \mathsf{e}^{B_0(p)t} \begin{pmatrix} 0 & 0 \\ 0 & \sigma^2 Q_1 \end{pmatrix} \mathsf{e}^{B_0(p)^*t} \mathsf{d}t.$$

The first element in the diagonal of the integrand is then

$$\sigma_{\mathsf{R}}^2 \left(\mathsf{e}^{A_0(p)t} - \mathsf{e}^{-\kappa t}\right) \mathrm{R}\left(A_0(p) + \kappa\right) Q_1 \,\mathrm{R}\left(A_0(p)^* + \kappa\right) \left(\mathsf{e}^{A_0(p)^*t} - \mathsf{e}^{-\kappa t}\right).$$

In the next steps, we employ

$$\mathsf{e}^{A_0(p)^*t} e_{i,k}^{(p)^*}(x) = \mathsf{e}^{\overline{\lambda_i^{(p)}}t} \sum_{j=1}^{k} \frac{t^{k-j}}{(k-j)!} e_{i,j}^{(p)^*}(x).$$

Setting $i_1, i_2 \in \mathbb{N}_{>0}$, $k_1 \in \{1, \ldots, \mathcal{M}_{i_1}\}$ and $k_2 \in \{1, \ldots, \mathcal{M}_{i_2}\}$, we use the construction (6.0.4), to obtain that

$$\begin{aligned}
&\left\langle \begin{pmatrix} {e_{i_1,k_1}^{(p)}}^* \\ 0 \end{pmatrix}, V_\infty^{(\mathsf{r},1)} \begin{pmatrix} {e_{i_2,k_2}^{(p)}}^* \\ 0 \end{pmatrix} \right\rangle_{\mathcal{H}_1 \times \mathcal{H}_1} \\
=&\sigma^2 \int_0^\infty \left\langle {e_{i_1,k_1}^{(p)}}^*, \sigma_{\mathsf{R}}^2 \left(\mathsf{e}^{A_0(p)t} - \mathsf{e}^{-\kappa t}\right) \mathrm{R}\left(A_0(p) + \kappa\right) Q_1 \,\mathrm{R}\left(A_0(p)^* + \kappa\right) \left(\mathsf{e}^{A_0(p)^*t} - \mathsf{e}^{-\kappa t}\right) {e_{i_2,k_2}^{(p)}}^* \right\rangle \mathsf{d}t \\
=&\sigma^2\sigma_{\mathsf{R}}^2 \int_0^\infty \left\langle \mathsf{e}^{\overline{\lambda_{i_1}^{(p)}}t} \sum_{j_1=1}^{k_1} \frac{t^{k_1-j_1}}{(k_1-j_1)!} \mu_{i_1,j_1}^{(p,\kappa)} - \mathsf{e}^{-\kappa t} \mu_{i_1,k_1}^{(p,\kappa)}, Q_1 \left(\mathsf{e}^{\overline{\lambda_{i_2}^{(p)}}t} \sum_{j_2=1}^{k_2} \frac{t^{k_2-j_2}}{(k_2-j_2)!} \mu_{i_2,j_2}^{(p,\kappa)} - \mathsf{e}^{-\kappa t} \mu_{i_2,k_2}^{(p,\kappa)} \right) \right\rangle \mathsf{d}t \\
=&\sigma^2\sigma_{\mathsf{R}}^2 \Bigg(\sum_{j_1=1}^{k_1} \sum_{j_2=1}^{k_2} \binom{k_1 - j_1 + k_2 - j_2}{k_1 - j_1} \left(-\overline{\lambda_{i_1}^{(p)}} - \lambda_{i_2}^{(p)}\right)^{-k_1+j_1-k_2+j_2-1} \left\langle \mu_{i_1,j_1}^{(p,\kappa)}, Q_1 \mu_{i_2,j_2}^{(p,\kappa)} \right\rangle \qquad (6.1.2) \\
&- \sum_{j_2=1}^{k_2} \left(-\lambda_{i_2}^{(p)} + \kappa\right)^{-k_2+j_2-1} \left\langle \mu_{i_1,k_1}^{(p,\kappa)}, Q_1 \mu_{i_2,j_2}^{(p,\kappa)} \right\rangle \\
&- \sum_{j_1=1}^{k_1} \left(-\overline{\lambda_{i_1}^{(p)}} + \kappa\right)^{-k_1+j_1-1} \left\langle \mu_{i_1,j_1}^{(p,\kappa)}, Q_1 \mu_{i_2,k_2}^{(p,\kappa)} \right\rangle + (2\kappa)^{-1} \left\langle \mu_{i_1,k_1}^{(p,\kappa)}, Q_1 \mu_{i_2,k_2}^{(p,\kappa)} \right\rangle \Bigg),
\end{aligned}$$

which is the covariance of $u^{(\mathsf{r},\mathsf{d})}$ along the modes ${e_{i_1,k_1}^{(p)}}^*$ and ${e_{i_2,k_2}^{(p)}}^*$. Since $-\kappa$ is not in the spectrum of $A_0(p)^*$ and at most one term in the sum diverges in the limits $p \to 0^-$ and $\kappa \to 0^+$, it follows that the scaling laws are

$$\left| \left\langle \begin{pmatrix} {e_{i_1,k_1}^{(p)}}^* \\ 0 \end{pmatrix}, V_\infty^{(\mathsf{r},1)} \begin{pmatrix} {e_{i_2,k_2}^{(p)}}^* \\ 0 \end{pmatrix} \right\rangle_{\mathcal{H}_1 \times \mathcal{H}_1} \right| = \Theta_p \left(\left| \overline{\lambda_{i_1}^{(p)}} + \lambda_{i_2}^{(p)} \right|^{-(k_1+k_2-1)} \right)$$

and

$$\left| \left\langle \begin{pmatrix} e_{i_1,k_1}^{(p)} \\ 0 \end{pmatrix}^*, V_\infty^{(\mathsf{r},1)} \begin{pmatrix} e_{i_2,k_2}^{(p)} \\ 0 \end{pmatrix}^* \right\rangle_{\mathcal{H}_1 \times \mathcal{H}_1} \right| = \Theta_\kappa \left(\kappa^{-1} \right).$$

□

In Theorem 6.1.1, the early-warning sign is associated with the divergence of the observable and its rate. In $p \to 0^-$, this occurs only for $i_1 = i_2 = 1$ since a single mode loses stability on such a limit. The fact that the generalised eigenfunctions of $A_0(p)^*$ are complete in $\mathcal{H}_1$ for any $p < 0$ enables the extension of the early-warning sign to a set of functions dense in $\mathcal{H}_1$.

Corollary 6.1.2. *Let $\xi_1 = \xi_1(x,t)$ and $u^{(r,d)} = u^{(r,d)}(x,t)$ be the mild solutions of* (6.0.1) *and* (6.0.2)*, respectively, with initial conditions in $\mathcal{H}_1$, $x \in \mathcal{X}_1$, $p < 0$ and $t > 0$. For $M \in \mathbb{N}_{>0}$, set*

$$h_1^{(p)}, h_2^{(p)} \in \bigoplus_{i=1}^{M} E_i(p)^* \setminus \bigoplus_{i=2}^{M} E_i(p)^* \subset \mathcal{H}_1.$$

Then,

$$\left| \left\langle \begin{pmatrix} h_1^{(p)} \\ 0 \end{pmatrix}, V_\infty^{(r,1)} \begin{pmatrix} h_2^{(p)} \\ 0 \end{pmatrix} \right\rangle_{\mathcal{H}_1 \times \mathcal{H}_1} \right| = \Theta_\kappa \left(\kappa^{-1} \right) \quad \text{for any} \quad p < 0$$

holds for $V_\infty^{(r,1)}$ defined in (2.3.9)*. Furthermore, if $h_1^{(p)}$ and $h_2^{(p)}$ satisfy*

$$a_{1,\mathcal{M}_1,1} := \left\langle h_1^{(p)}, e_{1,1}^{(p)} \right\rangle \neq 0 \neq \left\langle h_2^{(p)}, e_{1,1}^{(p)} \right\rangle =: a_{1,\mathcal{M}_1,2} \tag{6.1.3}$$

for any $p \leq 0$, then

$$\left| \left\langle \begin{pmatrix} h_1^{(p)} \\ 0 \end{pmatrix}, V_\infty^{(r,1)} \begin{pmatrix} h_2^{(p)} \\ 0 \end{pmatrix} \right\rangle_{\mathcal{H}_1 \times \mathcal{H}_1} \right| = \Theta_p \left(\mathit{Re} \left(-\lambda_1^{(p)} \right)^{-(2\mathcal{M}_1 - 1)} \right) \quad \text{for any} \quad \kappa > 0$$

stands.

Proof. We define the families $\left\{ a_{i,k,1}^{(p)} \right\} \subset \mathbb{C}$ and $\left\{ a_{i,k,2}^{(p)} \right\} \subset \mathbb{C}$ for $i \in \{1, \ldots, M\}$ and $k \in \{1, \ldots, \mathcal{M}_i\}$, such that

$$h_1^{(p)} = \sum_{\substack{i \in \{1,\ldots,M\} \\ k \in \{1,\ldots,\mathcal{M}_i\}}} a_{i,k,1}^{(p)} e_{i,k}^{(p)*} \qquad \text{and} \qquad h_2^{(p)} = \sum_{\substack{i \in \{1,\ldots,M\} \\ k \in \{1,\ldots,\mathcal{M}_i\}}} a_{i,k,2}^{(p)} e_{i,k}^{(p)*}$$

for any $p \leq 0$. It follows that

$$\begin{aligned} &\left\langle \begin{pmatrix} h_1^{(p)} \\ 0 \end{pmatrix}, V_\infty^{(\mathsf{r},1)} \begin{pmatrix} h_2^{(p)} \\ 0 \end{pmatrix} \right\rangle_{\mathcal{H}_1 \times \mathcal{H}_1} \\ &= \sum_{\substack{i_1 \in \{1,\ldots,M\} \\ k_1 \in \{1,\ldots,\mathcal{M}_{i_1}\}}} \sum_{\substack{i_2 \in \{1,\ldots,M\} \\ k_2 \in \{1,\ldots,\mathcal{M}_{i_2}\}}} a_{i_1,k_1,1}^{(p)} \overline{a_{i_2,k_2,2}^{(p)}} \left\langle \begin{pmatrix} e_{i_1,k_1}^{(p)} \\ 0 \end{pmatrix}^*, V_\infty^{(\mathsf{r},1)} \begin{pmatrix} e_{i_2,k_2}^{(p)} \\ 0 \end{pmatrix}^* \right\rangle_{\mathcal{H}_1 \times \mathcal{H}_1}. \end{aligned}$$

From the form (6.1.2) in Theorem 6.1.1, this implies that

$$\begin{aligned}
&\left|\left\langle \begin{pmatrix} h_1^{(p)} \\ 0 \end{pmatrix}, V_\infty^{(\mathsf{r},1)} \begin{pmatrix} h_2^{(p)} \\ 0 \end{pmatrix} \right\rangle_{\mathcal{H}_1\times\mathcal{H}_1}\right| \\
=&\Theta_\kappa\left(\left|(2\kappa)^{-1} \sum_{\substack{i_1\in\{1,\dots,M\}\\ k_1\in\{1,\dots,\mathcal{M}_{i_1}\}}} \sum_{\substack{i_2\in\{1,\dots,M\}\\ k_2\in\{1,\dots,\mathcal{M}_{i_2}\}}} a_{i_1,k_1,1}^{(p)} \overline{a_{i_2,k_2,2}^{(p)}} \left\langle \mu_{i_1,k_1}^{(p,\kappa)}, Q_1 \mu_{i_2,k_2}^{(p,\kappa)} \right\rangle\right|\right) \\
=&\Theta_\kappa\left(\kappa^{-1}\left|\left\langle \sum_{\substack{i_1\in\{1,\dots,M\}\\ k_1\in\{1,\dots,\mathcal{M}_{i_1}\}}} a_{i_1,k_1,1}^{(p)} \mu_{i_1,k_1}^{(p,\kappa)}, Q_1 \sum_{\substack{i_2\in\{1,\dots,M\}\\ k_2\in\{1,\dots,\mathcal{M}_{i_2}\}}} a_{i_2,k_2,2}^{(p)} \mu_{i_2,k_2}^{(p,\kappa)} \right\rangle\right|\right) \\
=&\Theta_\kappa\left(\kappa^{-1}\right).
\end{aligned}$$

In the limit $p \to 0^-$, the covariance

$$\left|\left\langle \begin{pmatrix} {e_{i_1,k_1}^{(p)}}^* \\ 0 \end{pmatrix}, V_\infty^{(\mathsf{r},1)} \begin{pmatrix} {e_{i_2,k_2}^{(p)}}^* \\ 0 \end{pmatrix} \right\rangle_{\mathcal{H}_1\times\mathcal{H}_1}\right| = \Theta_p\left(\left|\overline{\lambda_{i_1}^{(p)}} + \lambda_{i_2}^{(p)}\right|^{-(k_1+k_2-1)}\right)$$

diverges only for $i_1 = i_2 = 1$. Furthermore, its scaling law is defined by the choice of $k_1, k_2 \in \{1, \dots, \mathcal{M}_1\}$, and the highest rate of divergence is associated with $k_1 = k_2 = \mathcal{M}_1$. Equation (6.1.2) and condition (6.1.3) imply that

$$\begin{aligned}
&\left|\left\langle \begin{pmatrix} h_1^{(p)} \\ 0 \end{pmatrix}, V_\infty^{(\mathsf{r},1)} \begin{pmatrix} h_2^{(p)} \\ 0 \end{pmatrix} \right\rangle_{\mathcal{H}_1\times\mathcal{H}_1}\right| \\
=&\Theta_p\left(\left|\sum_{\substack{i_1\in\{1,\dots,M\}\\ k_1\in\{1,\dots,\mathcal{M}_{i_1}\}}} \sum_{\substack{i_2\in\{1,\dots,M\}\\ k_2\in\{1,\dots,\mathcal{M}_{i_2}\}}} a_{i_1,k_1,1}^{(p)} \overline{a_{i_2,k_2,2}^{(p)}} \left\langle \begin{pmatrix} {e_{i_1,k_1}^{(p)}}^* \\ 0 \end{pmatrix}, V_\infty^{(\mathsf{r},1)} \begin{pmatrix} {e_{i_2,k_2}^{(p)}}^* \\ 0 \end{pmatrix} \right\rangle_{\mathcal{H}_1\times\mathcal{H}_1}\right|\right) \\
=&\Theta_p\left(\left|\sum_{k_1=1}^{\mathcal{M}_1}\sum_{k_2=1}^{\mathcal{M}_1} a_{1,k_1,1}^{(p)} \overline{a_{1,k_2,2}^{(p)}} \left\langle \begin{pmatrix} {e_{1,k_1}^{(p)}}^* \\ 0 \end{pmatrix}, V_\infty^{(\mathsf{r},1)} \begin{pmatrix} {e_{1,k_2}^{(p)}}^* \\ 0 \end{pmatrix} \right\rangle_{\mathcal{H}_1\times\mathcal{H}_1}\right|\right) \\
=&\Theta_p\left(\left|\sum_{k_1=1}^{\mathcal{M}_1}\sum_{k_2=1}^{\mathcal{M}_1} a_{1,k_1,1}^{(p)} \overline{a_{1,k_2,2}^{(p)}} \mathsf{Re}\left(-\lambda_1^{(p)}\right)^{-(k_1+k_2-1)}\right|\right) \\
=&\Theta_p\left(\mathsf{Re}\left(-\lambda_1^{(p)}\right)^{-(2\mathcal{M}_1-1)}\right).
\end{aligned}$$

□

6.2 Continuous Spectrum

We study $u^{(\mathsf{r},\mathsf{c})} = u^{(\mathsf{r},\mathsf{c})}(x,t)$, the mild solution of (6.0.5) for any $x \in \mathcal{X}_1$, $p < 0$ and $t > 0$. In fact, its existence can be proven pointwise in $\mathcal{X}_1$ for any $t > 0$. Since the spectrum of the considered linear drift

operator is not discrete, the observation of the time-asymptotic covariance along favoured modes is not viable. Hence, we search for other functions in $\mathcal{H}_1$ that enable the construction of the early-warning signs.

Theorem 6.2.1. *Let $\xi_1 = \xi_1(x,t)$ and $u^{(r,c)} = u^{(r,c)}(x,t)$ be the mild solutions of* (6.0.1) *and* (6.0.5)*, respectively, with initial conditions in $\mathcal{H}_1$, $x \in \mathcal{X}_1$, $p < 0$ and $t > 0$. For any $g_1, g_2 \in \mathcal{H}_1$, it holds*

$$\left\langle \begin{pmatrix} g_1 \\ 0 \end{pmatrix}, V_\infty^{(r,1)} \begin{pmatrix} g_2 \\ 0 \end{pmatrix} \right\rangle_{\mathcal{H}_1 \times \mathcal{H}_1} = \sigma^2 \sigma_R^2 \int_0^\infty \left\langle \frac{e^{f(\cdot,p)t} - e^{-\kappa t}}{f(\cdot,p)+\kappa} g_1, Q_1 \frac{e^{f(\cdot,p)t} - e^{-\kappa t}}{f(\cdot,p)+\kappa} g_2 \right\rangle dt, \tag{6.2.1}$$

with $V_\infty^{(r,1)}$ introduced in (2.3.9)*.*

Proof. We define the operators

$$B_0(p) = \begin{pmatrix} f(\cdot,p) & \sigma_R \\ 0 & -\kappa \end{pmatrix} \tag{6.2.2}$$

and its adjoint in $\mathcal{H}_1 \times \mathcal{H}_1$,

$$B_0(p)^* = \begin{pmatrix} f(\cdot,p) & 0 \\ \sigma_R & -\kappa \end{pmatrix}.$$

They generate the $\mathcal{C}_0$-semigroups in t,

$$e^{B_0(p)t} = \begin{pmatrix} e^{f(\cdot,p)t} & \sigma_R \frac{e^{f(\cdot,p)t} - e^{-\kappa t}}{f(\cdot,p)+\kappa} \\ 0 & e^{-\kappa t} \end{pmatrix}$$

and

$$\left(e^{B_0(p)t}\right)^* = e^{B_0(p)^* t} = \begin{pmatrix} e^{f(\cdot,p)t} & 0 \\ \sigma_R \frac{e^{f(\cdot,p)t} - e^{-\kappa t}}{f(\cdot,p)+\kappa} & e^{-\kappa t} \end{pmatrix},$$

respectively. It follows from the construction of the covariance operator (Section 2.3) that

$$\begin{aligned} V_\infty^{(r,1)} &= \int_0^\infty e^{B_0(p)t} \begin{pmatrix} 0 & 0 \\ 0 & \sigma^2 Q_1 \end{pmatrix} e^{B_0(p)^* t} dt \\ &= \int_0^\infty \begin{pmatrix} e^{f(\cdot,p)t} & \sigma_R \frac{e^{f(\cdot,p)t} - e^{-\kappa t}}{f(\cdot,p)+\kappa} \\ 0 & e^{-\kappa t} \end{pmatrix} \begin{pmatrix} 0 & 0 \\ 0 & \sigma^2 Q_1 \end{pmatrix} \begin{pmatrix} e^{f(\cdot,p)t} & 0 \\ \sigma_R \frac{e^{f(\cdot,p)t} - e^{-\kappa t}}{f(\cdot,p)+\kappa} & e^{-\kappa t} \end{pmatrix} dt \\ &= \sigma^2 \int_0^\infty \begin{pmatrix} \sigma_R^2 \frac{e^{f(\cdot,p)t} - e^{-\kappa t}}{f(\cdot,p)+\kappa} Q_1 \frac{e^{f(\cdot,p)t} - e^{-\kappa t}}{f(\cdot,p)+\kappa} & \sigma_R \frac{e^{f(\cdot,p)t} - e^{-\kappa t}}{f(\cdot,p)+\kappa} Q_1 \\ \sigma_R Q_1 \frac{e^{f(\cdot,p)t} - e^{-\kappa t}}{f(\cdot,p)+\kappa} & e^{-2\kappa t} Q_1 \end{pmatrix} dt. \end{aligned}$$

Setting $g_1, g_2 \in \mathcal{H}_1$, the time-asymptotic covariance along those functions is then

$$\left\langle \begin{pmatrix} g_1 \\ 0 \end{pmatrix}, V_\infty^{(r,1)} \begin{pmatrix} g_2 \\ 0 \end{pmatrix} \right\rangle_{\mathcal{H}_1 \times \mathcal{H}_1} = \sigma^2 \sigma_R^2 \int_0^\infty \left\langle \frac{e^{f(\cdot,p)t} - e^{-\kappa t}}{f(\cdot,p)+\kappa} g_1, Q_1 \frac{e^{f(\cdot,p)t} - e^{-\kappa t}}{f(\cdot,p)+\kappa} g_2 \right\rangle dt,$$

for $p < 0$. □

We set $\alpha > 0$ and we also consider the case $\mathcal{X}_1 \subset \mathbb{R}$. We then focus on $f(x,p) = -|x|^\alpha + p$ for any $x \in \mathbb{R}$, $p \leq 0$. This type of function enables further construction of early-warning signs in the case of f analytic. We define $g = \mathbb{1}_{\mathcal{S}}$, the indicator function on the Lebesgue-measurable set $\mathcal{S} \subset \mathcal{X}_1$ and assume $0 = x_* \in \mathcal{S}$.

Corollary 6.2.2. *Let $\xi_1 = \xi_1(x,t)$ and $u^{(r,c)} = u^{(r,c)}(x,t)$ be the mild solutions of* (6.0.1) *and* (6.0.5)*, respectively, with initial conditions in $\mathcal{H}_1$, $x \in \mathcal{X}_1$, $p < 0$ and $t > 0$.*

(a) Let $f(x,p) = -|x|^\alpha + p$ in (6.0.5) *for $x \in \mathcal{X}_1$, $\alpha > 0$, $p < 0$ and $t > 0$. Then, for any $g = \mathbb{1}_{\mathcal{S}}$, the scaling law of the time-asymptotic variance along g is given by*

$$\left\langle \begin{pmatrix} g \\ 0 \end{pmatrix}, V_\infty^{(r,1)} \begin{pmatrix} g \\ 0 \end{pmatrix} \right\rangle_{\mathcal{H}_1 \times \mathcal{H}_1} = \Theta_\kappa\left(\kappa^{-1}\right)$$

for the limit $\kappa \to 0^+$ and for $V_\infty^{(r,1)}$ defined in (2.3.9)*. It also entails that, for $p \to 0^-$, the following holds:*

- $$\left\langle \begin{pmatrix} g \\ 0 \end{pmatrix}, V_\infty^{(r,1)} \begin{pmatrix} g \\ 0 \end{pmatrix} \right\rangle_{\mathcal{H}_1 \times \mathcal{H}_1} = \Theta_p\left((-p)^{-1+\frac{1}{\alpha}}\right), \quad \textit{for} \quad \alpha > 1;$$
- $$\left\langle \begin{pmatrix} g \\ 0 \end{pmatrix}, V_\infty^{(r,1)} \begin{pmatrix} g \\ 0 \end{pmatrix} \right\rangle_{\mathcal{H}_1 \times \mathcal{H}_1} = \Theta_p\left(\textit{log}(-p)\right), \qquad \textit{for} \quad \alpha = 1;$$
- $$\left\langle \begin{pmatrix} g \\ 0 \end{pmatrix}, V_\infty^{(r,1)} \begin{pmatrix} g \\ 0 \end{pmatrix} \right\rangle_{\mathcal{H}_1 \times \mathcal{H}_1} = \Theta_p\left(1\right), \qquad \textit{for} \quad 0 < \alpha < 1.$$

(b) Let $f(x,p) = f_{an}(x) + p$ in (6.0.5) *for $x \in \mathcal{X}_1$, $\alpha > 0$, $p < 0$ and $t > 0$. Assume that*

$$f_{an}(x) = \sum_{n=1}^{\infty} a_n x^n$$

for any $x \in \mathcal{X}_1$ and for the family $\{a_n\}_{n \in \mathbb{N}_{>0}} \subset \mathbb{R}$. It follows that for any $g = \mathbb{1}_{\mathcal{S}}$, the scaling law of the time-asymptotic variance along g is

$$\left\langle \begin{pmatrix} g \\ 0 \end{pmatrix}, V_\infty^{(r,1)} \begin{pmatrix} g \\ 0 \end{pmatrix} \right\rangle_{\mathcal{H}_1 \times \mathcal{H}_1} = \Theta_\kappa\left(\kappa^{-1}\right)$$

for the limit $\kappa \to 0^+$. Moreover, fix n_* such that

$$n_* = \underset{n \in \mathbb{N}_{>0}}{\textit{argmin}} \{a_n \neq 0\}.$$

Then, for any $g = \mathbb{1}_{\mathcal{S}}$, the rate of divergence of the time-asymptotic variance along g for the limit $p \to 0^-$ is given by

$$\left\langle \begin{pmatrix} g \\ 0 \end{pmatrix}, V_\infty^{(r,1)} \begin{pmatrix} g \\ 0 \end{pmatrix} \right\rangle_{\mathcal{H}_1 \times \mathcal{H}_1} = \Theta_p\left((-p)^{-1+\frac{1}{n_*}}\right), \quad \textit{if} \quad n_* > 1,$$

or

$$\left\langle \begin{pmatrix} g \\ 0 \end{pmatrix}, V_{\infty}^{(r,1)} \begin{pmatrix} g \\ 0 \end{pmatrix} \right\rangle_{\mathcal{H}_1 \times \mathcal{H}_1} = \Theta_p \left(\textit{log}(-p) \right), \quad \textit{if} \quad n_* = 1.$$

Proof. The assumption of Q_1 bounded and bounded from below far from zero and the formula (6.2.1) imply that the rates of divergence of the time-asymptotic variance are equivalent to the integral

$$\int_0^{\infty} \left\langle \frac{\mathsf{e}^{f(\cdot,p)t} - \mathsf{e}^{-\kappa t}}{f(\cdot,p)+\kappa} g, \frac{\mathsf{e}^{f(\cdot,p)t} - \mathsf{e}^{-\kappa t}}{f(\cdot,p)+\kappa} g \right\rangle \mathsf{d}t = \int_0^{\infty} \int_{\mathcal{X}_1} \left(\frac{\mathsf{e}^{f(x,p)t} - \mathsf{e}^{-\kappa t}}{f(x,p)+\kappa} g \right)^2 \mathsf{d}x \, \mathsf{d}t$$
$$= \int_0^{\infty} \int_{\mathcal{S}} \left(\frac{\mathsf{e}^{f(x,p)t} - \mathsf{e}^{-\kappa t}}{f(x,p)+\kappa} \right)^2 \mathsf{d}x \, \mathsf{d}t = \int_{\mathcal{S}} \left(-\frac{1}{2f(x,p)} - \frac{2}{f(x,p)-\kappa} + \frac{1}{2\kappa} \right) \frac{1}{\left(f(x,p)+\kappa\right)^2} \mathsf{d}x.$$

From the negative sign of the analytic function f for any $p < 0$, it follows that

$$\left\langle \begin{pmatrix} g \\ 0 \end{pmatrix}, V_{\infty}^{(\mathsf{r},1)} \begin{pmatrix} g \\ 0 \end{pmatrix} \right\rangle_{\mathcal{H}_1 \times \mathcal{H}_1} = \Theta_{\kappa} \left(\kappa^{-1} \right).$$

In part (a), we assume $f(x,p) = -|x|^{\alpha} + p$ for any $x \in \mathcal{X}_1$ and $p < 0$. As such, it entails that

$$\left\langle \begin{pmatrix} g \\ 0 \end{pmatrix}, V_{\infty}^{(\mathsf{r},1)} \begin{pmatrix} g \\ 0 \end{pmatrix} \right\rangle_{\mathcal{H}_1 \times \mathcal{H}_1} = \Theta_p \left(-\int_{\mathcal{S}} \frac{1}{f(x,p)} \mathsf{d}x \right) = \Theta_p \left(\int_{\mathcal{S}} \frac{1}{|x|^{\alpha} - p} \mathsf{d}x \right). \tag{6.2.3}$$

The rate depends on the parameter α and can be obtained as described in Theorem 4.1.3. From the construction of n_*, it follows that there exists $c > 0$ such that

$$c x^{n_*} \leq f_{\mathsf{an}}(x) \leq c^{-1} x^{n_*}$$

for x in a neighbourhood of $x_* = 0$. Then, the rate in the limit $p \to 0^-$ described in (6.2.3) entails the remainder of statement (b). □

6.3 Boundary Noise

In this section, we study the behaviour of $u^{(\mathsf{r},\mathsf{b})} = u^{(\mathsf{r},\mathsf{b})}(x,t)$, the mild solution of (6.0.6), in the limits $p \to 0^-$ and $\kappa \to 0^+$. The existence of such a solution follows from Theorem 2.2.10. As in the previous sections, we employ the scaling law of the time-asymptotic covariance as an early-warning sign. Since the linear operator associated with the drift term in (6.0.6) has a purely discrete spectrum, the time-asymptotic covariance can be studied as an observable along favoured modes. Nonetheless, the structure of the noise requires a different approach to its construction in comparison to the other examples in the chapter.

Theorem 6.3.1. *Let $\xi_0 = \xi_0(x,t)$ be the mild solution of* (6.0.1) *with $x \in \mathcal{X}_0$, for initial conditions in $\mathcal{H}_0$ and $t > 0$. Let also $u^{(r,b)} = u^{(r,b)}(x,t)$ be the mild solution of* (6.0.6) *with $x \in \mathcal{X}_1$, for initial conditions in $\mathcal{H}_1$, $p < 0$ and $t > 0$. Then, the scaling laws*

$$\left| \left\langle \begin{pmatrix} e_{i_1,k_1}^{(p)\,*} \\ 0 \end{pmatrix}, V_{\infty}^{(r,0)} \begin{pmatrix} e_{i_2,k_2}^{(p)\,*} \\ 0 \end{pmatrix} \right\rangle_{\mathcal{H}_1 \times \mathcal{H}_0} \right| = \mathcal{O}_{\kappa} \left(\kappa^{-1} \right) \quad \textit{for any} \quad p < 0$$

and

$$\left|\left\langle \begin{pmatrix} e^{(p)}_{i_1,k_1} \\ 0 \end{pmatrix}^*, V_\infty^{(r,0)} \begin{pmatrix} e^{(p)}_{i_2,k_2} \\ 0 \end{pmatrix}^* \right\rangle_{\mathcal{H}_1\times\mathcal{H}_0}\right| = \mathcal{O}_p\left(\left|\overline{\lambda^{(p)}_{i_1}} + \lambda^{(p)}_{i_2}\right|^{-(k_1+k_2-1)}\right) \quad \textit{for any} \quad \kappa > 0$$

hold for any $i_1, i_2 \in \mathbb{N}_{>0}$*,* $k_1 \in \{1,\dots,\mathcal{M}_{i_1}\}$*,* $k_2 \in \{1,\dots,\mathcal{M}_{i_2}\}$ *and for* $V_\infty^{(r,0)}$ *defined in* (2.3.10)*.*

Proof. We define the operator

$$B_0(p) = \begin{pmatrix} A_0(p) & \sigma_{\mathsf{R}}\left(A_0(p)-q\right)D(p) \\ 0 & -\kappa \end{pmatrix} \tag{6.3.1}$$

and its adjoint on $\mathcal{H}_1 \times \mathcal{H}_0$

$$B_0(p)^* = \begin{pmatrix} A_0(p)^* & 0 \\ \sigma_{\mathsf{R}} D(p)^*\left(A_0(p)^* - q\right) & -\kappa \end{pmatrix}.$$

Since the second term in the diagonal of $B_0(p)$ is a multiplication operator by a scalar, they generate the $\mathcal{C}_0$-semigroups

$$\mathsf{e}^{B_0(p)t} = \begin{pmatrix} \mathsf{e}^{A_0(p)t} & \sigma_{\mathsf{R}}\left(\mathsf{e}^{A_0(p)t} - \mathsf{e}^{-\kappa t}\right)\mathrm{R}\left(A_0(p)+\kappa\right)\left(A_0(p)-q\right)D(p) \\ 0 & \mathsf{e}^{-\kappa t} \end{pmatrix}$$

and

$$\left(\mathsf{e}^{B_0(p)t}\right)^* = \mathsf{e}^{B_0(p)^*t} = \begin{pmatrix} \mathsf{e}^{A_0(p)^*t} & 0 \\ \sigma_{\mathsf{R}} D(p)^*\left(A_0(p)^*-q\right)\mathrm{R}\left(A_0(p)^*+\kappa\right)\left(\mathsf{e}^{A_0(p)^*t} - \mathsf{e}^{-\kappa t}\right) & \mathsf{e}^{-\kappa t} \end{pmatrix}$$

for $t > 0$, respectively. The time-asymptotic covariance operator is then

$$V_\infty^{(\mathsf{r},0)} = \int_0^\infty \mathsf{e}^{B_0(p)t} \begin{pmatrix} 0 & 0 \\ 0 & \sigma^2 Q_0 \end{pmatrix} \mathsf{e}^{B_0(p)^*t}\mathsf{d}t$$

and the first element in the integrand corresponds to

$$\sigma^2\sigma_{\mathsf{R}}^2\left(\mathsf{e}^{A_0(p)t} - \mathsf{e}^{-\kappa t}\right)\mathrm{R}\left(A_0(p)+\kappa\right)\Lambda(p)\,\mathrm{R}\left(A_0(p)^*+\kappa\right)\left(\mathsf{e}^{A_0(p)^*t} - \mathsf{e}^{-\kappa t}\right),$$

for $\Lambda(p)$ defined in (6.0.7). Following equivalent steps to (6.1.2), we obtain

$$\begin{aligned}
&\left\langle \begin{pmatrix} e^{(p)}_{i_1,k_1} \\ 0 \end{pmatrix}^*, V_\infty^{(\mathsf{r},0)} \begin{pmatrix} e^{(p)}_{i_2,k_2} \\ 0 \end{pmatrix}^* \right\rangle_{\mathcal{H}_1\times\mathcal{H}_0} \\
=&\sigma^2\sigma_{\mathsf{R}}^2\int_0^\infty \left\langle \mathsf{e}^{\overline{\lambda^{(p)}_{i_1}}t}\sum_{j_1=1}^{k_1}\frac{t^{k_1-j_1}}{(k_1-j_1)!}\mu^{(p,\kappa)}_{i_1,j_1} - \mathsf{e}^{-\kappa t}\mu^{(p,\kappa)}_{i_1,k_1}, \Lambda(p)\left(\mathsf{e}^{\overline{\lambda^{(p)}_{i_2}}t}\sum_{j_2=1}^{k_2}\frac{t^{k_2-j_2}}{(k_2-j_2)!}\mu^{(p,\kappa)}_{i_2,j_2} - \mathsf{e}^{-\kappa t}\mu^{(p,\kappa)}_{i_2,k_2}\right)\right\rangle \mathsf{d}t \\
=&\sigma^2\sigma_{\mathsf{R}}^2\left(\sum_{j_1=1}^{k_1}\sum_{j_2=1}^{k_2}\binom{k_1-j_1+k_2-j_2}{k_1-j_1}\left(-\overline{\lambda^{(p)}_{i_1}} - \lambda^{(p)}_{i_2}\right)^{-k_1+j_1-k_2+j_2-1}\left\langle \mu^{(p,\kappa)}_{i_1,j_1}, \Lambda(p)\mu^{(p,\kappa)}_{i_2,j_2}\right\rangle\right.
\end{aligned}$$

$$- \sum_{j_2=1}^{k_2} \left(-\lambda_{i_2}^{(p)} + \kappa\right)^{-k_2+j_2-1} \left\langle \mu_{i_1,k_1}^{(p,\kappa)}, \Lambda(p)\mu_{i_2,j_2}^{(p,\kappa)} \right\rangle \tag{6.3.2}$$
$$- \sum_{j_1=1}^{k_1} \left(-\overline{\lambda_{i_1}^{(p)}} + \kappa\right)^{-k_1+j_1-1} \left\langle \mu_{i_1,j_1}^{(p,\kappa)}, \Lambda(p)\mu_{i_2,k_2}^{(p,\kappa)} \right\rangle + (2\kappa)^{-1} \left\langle \mu_{i_1,k_1}^{(p,\kappa)}, \Lambda(p)\mu_{i_2,k_2}^{(p,\kappa)} \right\rangle \Bigg),$$

We notice that

$$\left|\lambda_i^{(p)} + \kappa\right| = \Theta(1) \qquad \text{and} \qquad \left|\lambda_i^{(p)} - \kappa\right| = \Theta(1)$$

for any $i \in \mathbb{N}_{>0}$. Furthermore, it holds that

$$\left|\overline{\lambda_{i_1}^{(p)}} + \lambda_{i_2}^{(p)}\right| = \Theta(1)$$

for any $(i_1, i_2) \in \mathbb{N}_{>0} \times \mathbb{N}_{>0} \setminus \{(1,1)\}$. Lastly, since the functions $\mu_{i,k}^{(p,\kappa)}$ are finite combinations of generalised eigenfunctions of $A_0(p)^*$, the property

$$A_0(p)^* \mu_{i,j}^{(p,\kappa)} = \overline{\lambda_i^{(p)}} \mu_{i,k}^{(p,\kappa)} - \left(\overline{\lambda_i^{(p)}} + \kappa\right)^{-1} \mu_{i,k-1}^{(p,\kappa)},$$

follows for any $i \in \mathbb{N}_{>0}$, $k \in \{1, \dots, \mathcal{M}_i\}$, $p < 0$ and $\kappa > 0$, and from the uniform boundedness of $D(p)^*$, we obtain that

$$\left\langle \mu_{i_1,k_1}^{(p,\kappa)}, \Lambda(p)\mu_{i_2,k_2}^{(p,\kappa)} \right\rangle = \mathcal{O}(1),$$

for any $(i_1, i_2) \in \mathbb{N}_{>0} \times \mathbb{N}_{>0} \setminus \{(1,1)\}$, $k_1 \in \{1, \dots, \mathcal{M}_{i_1}\}$ and $k_2 \in \{1, \dots, \mathcal{M}_{i_2}\}$. The early-warning signs are consequently defined by the scaling laws of the observable in (6.3.2). The rate of divergence in $\kappa \to 0^+$ is implied by the last term in (6.3.2); whereas for the limit $p \to 0^-$, it is induced by the behaviour of the term in the first sum in the righthand-side of (6.3.2) corresponding to $j_1 = j_2 = 1$. As such, the theorem is proven. □

Theorem 6.3.1 describes the rates of the time-asymptotic covariance operator along chosen modes. The next corollary extends the use of such an early-warning sign to a larger set of proxy functions. Due to the completeness of the generalised eigenfunction of $A_0(p)^*$ in $\mathcal{H}_1$ for any $p \leq 0$, such a set is dense in $\mathcal{H}_1$.

Corollary 6.3.2. *Let $\xi_0 = \xi_0(x,t)$ be the mild solution of* (6.0.1) *with $x \in \mathcal{X}_0$, for initial conditions in $\mathcal{H}_0$ and $t > 0$. Let also $u^{(r,b)} = u^{(r,b)}(x,t)$ be the mild solution of* (6.0.6) *with $x \in \mathcal{X}_1$, for initial conditions in $\mathcal{H}_1$, $p < 0$ and $t > 0$. For $M \in \mathbb{N}_{>0}$, set*

$$h_1^{(p)}, h_2^{(p)} \in \bigoplus_{i=1}^{M} E_i(p)^* \setminus \bigoplus_{i=2}^{M} E_i(p)^* \subset \mathcal{H}_1$$

such that

$$a_{1,\mathcal{M}_1,1} := \left\langle h_1^{(p)}, e_{1,1}^{(p)} \right\rangle \neq 0 \neq \left\langle h_2^{(p)}, e_{1,1}^{(p)} \right\rangle =: a_{1,\mathcal{M}_1,2} \tag{6.3.3}$$

for any $p \leq 0$. Then,

$$\left| \left\langle \begin{pmatrix} h_1^{(p)} \\ 0 \end{pmatrix}, V_\infty^{(r,0)} \begin{pmatrix} h_2^{(p)} \\ 0 \end{pmatrix} \right\rangle_{\mathcal{H}_1 \times \mathcal{H}_0} \right| = \mathcal{O}_\kappa\left(\kappa^{-1}\right) \quad \textit{for any} \quad p < 0$$

and

$$\left|\left\langle \begin{pmatrix} h_1^{(p)} \\ 0 \end{pmatrix}, V_\infty^{(r,0)} \begin{pmatrix} h_2^{(p)} \\ 0 \end{pmatrix} \right\rangle_{\mathcal{H}_1\times\mathcal{H}_0}\right| = \mathcal{O}_p\left(Re\left(-\lambda_1^{(p)}\right)^{-(2\mathcal{M}_1-1)}\right) \quad \textit{for any} \quad \kappa > 0$$

hold for $V_\infty^{(r,0)}$ defined in (2.3.10)*.*

Proof. We set the families $\left\{a_{i,k,1}^{(p)}\right\} \subset \mathbb{C}$ and $\left\{a_{i,k,2}^{(p)}\right\} \subset \mathbb{C}$ for $i \in \{1,\dots,M\}$ and $k \in \{1,\dots,\mathcal{M}_i\}$, such that

$$h_1^{(p)} = \sum_{\substack{i\in\{1,\dots,M\}\\ k\in\{1,\dots,\mathcal{M}_i\}}} a_{i,k,1}^{(p)} e_{i,k}^{(p)*} \qquad \text{and} \qquad h_2^{(p)} = \sum_{\substack{i\in\{1,\dots,M\}\\ k\in\{1,\dots,\mathcal{M}_i\}}} a_{i,k,2}^{(p)} e_{i,k}^{(p)*},$$

for any $p \leq 0$. We obtain then

$$\begin{aligned}
&\left\langle \begin{pmatrix} h_1^{(p)} \\ 0 \end{pmatrix}, V_\infty^{(r,0)} \begin{pmatrix} h_2^{(p)} \\ 0 \end{pmatrix} \right\rangle_{\mathcal{H}_1\times\mathcal{H}_0} \\
&= \sum_{\substack{i_1\in\{1,\dots,M\}\\ k_1\in\{1,\dots,\mathcal{M}_{i_1}\}}} \sum_{\substack{i_2\in\{1,\dots,M\}\\ k_2\in\{1,\dots,\mathcal{M}_{i_2}\}}} a_{i_1,k_1,1}^{(p)} \overline{a_{i_2,k_2,2}^{(p)}} \left\langle \begin{pmatrix} e_{i_1,k_1}^{(p)\,*} \\ 0 \end{pmatrix}, V_\infty^{(r,0)} \begin{pmatrix} e_{i_2,k_2}^{(p)\,*} \\ 0 \end{pmatrix} \right\rangle_{\mathcal{H}_1\times\mathcal{H}_0}.
\end{aligned}$$

The form (6.3.2) in Theorem 6.3.1 entails that

$$\begin{aligned}
&\left|\left\langle \begin{pmatrix} h_1^{(p)} \\ 0 \end{pmatrix}, V_\infty^{(r,0)} \begin{pmatrix} h_2^{(p)} \\ 0 \end{pmatrix} \right\rangle_{\mathcal{H}_1\times\mathcal{H}_0}\right| \\
=&\Theta_\kappa\left(\left|(2\kappa)^{-1} \sum_{\substack{i_1\in\{1,\dots,M\}\\ k_1\in\{1,\dots,\mathcal{M}_{i_1}\}}} \sum_{\substack{i_2\in\{1,\dots,M\}\\ k_2\in\{1,\dots,\mathcal{M}_{i_2}\}}} a_{i_1,k_1,1}^{(p)} \overline{a_{i_2,k_2,2}^{(p)}} \left\langle \mu_{i_1,k_1}^{(p,\kappa)}, \Lambda(p)\mu_{i_2,k_2}^{(p,\kappa)} \right\rangle\right|\right) \\
=&\Theta_\kappa\left(\kappa^{-1}\left|\left\langle \sum_{\substack{i_1\in\{1,\dots,M\}\\ k_1\in\{1,\dots,\mathcal{M}_{i_1}\}}} a_{i_1,k_1,1}^{(p)} \mu_{i_1,k_1}^{(p,\kappa)}, \Lambda(p) \sum_{\substack{i_2\in\{1,\dots,M\}\\ k_2\in\{1,\dots,\mathcal{M}_{i_2}\}}} a_{i_2,k_2,2}^{(p)} \mu_{i_2,k_2}^{(p,\kappa)} \right\rangle\right|\right) \\
=&\mathcal{O}_\kappa\left(\kappa^{-1}\right).
\end{aligned}$$

In the limit $p \to 0^-$, the covariance

$$\left|\left\langle \begin{pmatrix} e_{i_1,k_1}^{(p)\,*} \\ 0 \end{pmatrix}, V_\infty^{(r,0)} \begin{pmatrix} e_{i_2,k_2}^{(p)\,*} \\ 0 \end{pmatrix} \right\rangle_{\mathcal{H}_1\times\mathcal{H}_0}\right| = \mathcal{O}_p\left(\left|\overline{\lambda_{i_1}^{(p)}} + \lambda_{i_2}^{(p)}\right|^{-(k_1+k_2-1)}\right)$$

displays divergence only for the indexes $i_1 = i_2 = 1$. Moreover, its rate of divergence is associated with the values $k_1, k_2 \in \{1,\dots,\mathcal{M}_1\}$. Consequently, equation (6.3.2) and condition (6.3.3) imply that

$$\left|\left\langle \begin{pmatrix} h_1^{(p)} \\ 0 \end{pmatrix}, V_\infty^{(r,0)} \begin{pmatrix} h_2^{(p)} \\ 0 \end{pmatrix} \right\rangle_{\mathcal{H}_1\times\mathcal{H}_0}\right|$$

$$
\begin{aligned}
=&\Theta_p\left(\left|\sum_{\substack{i_1\in\{1,\dots,M\}\\ k_1\in\{1,\dots,\mathcal{M}_{i_1}\}}}\sum_{\substack{i_2\in\{1,\dots,M\}\\ k_2\in\{1,\dots,\mathcal{M}_{i_2}\}}} a^{(p)}_{i_1,k_1,1}\overline{a^{(p)}_{i_2,k_2,2}}\left\langle\begin{pmatrix} {e^{(p)}_{i_1,k_1}}^* \\ 0\end{pmatrix}, V_\infty^{(\mathsf{r},0)}\begin{pmatrix} {e^{(p)}_{i_2,k_2}}^* \\ 0\end{pmatrix}\right\rangle_{\mathcal{H}_1\times\mathcal{H}_0}\right|\right)\\
=&\Theta_p\left(\left|\sum_{k_1=1}^{\mathcal{M}_1}\sum_{k_2=1}^{\mathcal{M}_1} a^{(p)}_{1,k_1,1}\overline{a^{(p)}_{1,k_2,2}}\left\langle\begin{pmatrix} {e^{(p)}_{1,k_1}}^* \\ 0\end{pmatrix}, V_\infty^{(\mathsf{r},0)}\begin{pmatrix} {e^{(p)}_{1,k_2}}^* \\ 0\end{pmatrix}\right\rangle_{\mathcal{H}_1\times\mathcal{H}_0}\right|\right)\\
=&\mathcal{O}_p\left(\left|\sum_{k_1=1}^{\mathcal{M}_1}\sum_{k_2=1}^{\mathcal{M}_1} a^{(p)}_{1,k_1,1}\overline{a^{(p)}_{1,k_2,2}}\mathsf{Re}\left(-\lambda_1^{(p)}\right)^{-(k_1+k_2-1)}\right|\right)\\
=&\mathcal{O}_p\left(\mathsf{Re}\left(-\lambda_1^{(p)}\right)^{-(2\mathcal{M}_1-1)}\right).
\end{aligned}
$$

□

6.4 Considerations on scaling laws and comparison with other signals

In the previous sections, the scaling laws of the time-asymptotic covariance along various modes are considered for $p\to 0^-$ and $\kappa\to 0^+$. In such limits, the early-warning signs are shown to display different behaviours depending on the assumption of the spectrum of the linear drift operator in the SPDE that defines u. The degeneracy of the noise and the correlation of u and ξ_j for $j\in\{0,1\}$ imply that the effect of the stochastic perturbation on ξ_j on u is not trivial. Nonetheless, the simple form of the linear operator $B_0(p)$ in (6.1.1), (6.2.2) and (6.3.1) enables the study of the problem along its eigenmodes. We consider first the limit $p\to 0^-$. In (6.0.2), the spectrum of $A_0(p)$ is discrete for any $p\le 0$ and the early-warning sign is shown to display a hyperbolic rate of divergence along the sensible eigenfunction ${e^{(p)}_1}^*$ of its adjoint in Theorem 6.1.1. Furthermore, the observables along the sensible generalised eigenfunctions ${e^{(p)}_{1,k}}^*$ of $A_0(p)^*$ indicate a faster scaling law depending on their rank k. Through the biorthogonality of the generalised eigenfunctions of $A_0(p)$ and $A_0(p)^*$ we know that the the projection of $g\in\mathcal{H}_1$ on ${e^{(p)}_{1,k}}^*$ is equivalent to the coefficient of g on the $e^{(p)}_{1,\mathcal{M}_1-k+1}$, for any $k\in\{1,\dots,\mathcal{M}_1\}$. This is meant in the sense that for $M\in\mathbb{N}_{>0}$ and

$$
g=\sum_{i=1}^{M}\sum_{k=1}^{\mathcal{M}_i} c_{i,k}e^{(p)}_{i,k},
$$

then it holds

$$
\left\langle g, {e^{(p)}_{i,k}}^*\right\rangle = c_{i,\mathcal{M}_i-k+1}
$$

for any $i\in\{1,\dots,M\}$, $k\in\{1,\dots,\mathcal{M}_i\}$ and $p\le 0$. As a result, the time-asymptotic covariance along ${e^{(p)}_{1,k_1}}^*$ and ${e^{(p)}_{1,k_2}}^*$ refers to the time-asymptotic covariance of the oscillations of the coefficients of $u^{(\mathsf{r},\mathsf{d})}$, the solution of (6.0.2), along $e^{(p)}_{1,\mathcal{M}_1-k_1+1}$ and $e^{(p)}_{1,\mathcal{M}_1-k_2+1}$. This observable collects also the oscillations along $e^{(p)}_{1,j_1}$ and $e^{(p)}_{1,j_2}$ for $j_1\in\{\mathcal{M}_1-k_1+2,\dots,\mathcal{M}_1\}$ and $j_2\in\{\mathcal{M}_2-k_2+2,\dots,\mathcal{M}_2\}$. This is implied by the fact that oscillations along $e^{(p)}_{1,k}$ imply further perturbations along the mode $e^{(p)}_{1,k-1}$ for any $k\in\{2,\dots,\mathcal{M}_1\}$, as shown in (6.0.3).

The limit in (6.0.5) is different in nature from the previous case. The absence of eigenfunctions entails that there are no preferred directions along which the early-warning sign captures the bifurcation. As shown in Corollary 6.2.2, the shape of the spectrum can dampen the observable and hinder the scaling law of the time-asymptotic covariance. Furthermore, for a non-differentiable f, it is silenced or assumes a logarithmic

rate of divergence. In applications, the first case corresponds to the crossing of the bifurcation threshold being unrecognised by the early-warning sign.

The system (6.0.6) shows a similar scaling law to (6.0.2). Nonetheless, the noise perturbation is filtered by $(A_0 - q)D(p)$, an operator often unknown in applications. As such, its dependence on p can affect the scaling law of the early-warning sign and hinder the divergence of the observable. Conversely, the operator $D(p)$ is known for simple models (Chapter 5 and [63]) and may not be dependent on p. A related example is described in the section to follow.

The limit $\kappa \to 0^+$ implies the (at most) hyperbolic divergence of the early-warning sign in (6.0.2), (6.0.5) and (6.0.6). Such a behaviour is entailed by the shape of $B_0(p)$ in (6.1.1), (6.2.2) and (6.3.1), respectively. While in the limit $p \to 0^-$, at most only one eigenvalue tends to the imaginary axis, in this case, an infinite number of real eigenvalues tend simultaneously to 0^- along an equivalent number of eigenfunctions. The assumptions of Q_1, or $\Lambda(p)$ in the case of (6.0.6), imply that the corresponding scaling law is captured along a large set of modes in $\mathcal{H}_1$.

The resemblance of the scaling laws in the limit $p \to 0^-$ of the time-asymptotic covariance of the models (6.0.2), (6.0.5) and (6.0.6) compared to the corresponding deterministic models perturbed by white noise ((2.3.2), (2.3.4) and (2.3.6) respectively) invites the construction of further well-known early-warning signs proven for the latter. Under the assumption of a purely discrete spectrum, a natural example is the time-asymptotic autocorrelation, which is known to behave as an exponential function if studied along eigenmodes. We consider the case of (6.0.2). Then, we construct the time-asymptotic autocovariance with lag time $\tau > 0$ as the operator $V_\infty^{\tau,(\mathsf{r},1)}$ in $\mathcal{H}_1 \times \mathcal{H}_1$ such that

$$V_\infty^{\tau,(\mathsf{r},1)} = \lim_{t\to\infty} V_t^{\tau,(\mathsf{r},1)}$$

and

$$\left\langle \begin{pmatrix} v_1 \\ v_2 \end{pmatrix}, V_t^{\tau,(\mathsf{r},1)} \begin{pmatrix} w_1 \\ w_2 \end{pmatrix} \right\rangle_{\mathcal{H}_1\times\mathcal{H}_1} = \mathsf{Cov}\left(\langle u(\cdot,t+\tau), v_1\rangle + \langle \xi_1(\cdot,t+\tau), v_2\rangle, \langle u(\cdot,t), w_1\rangle + \langle \xi_1(\cdot,t), w_2\rangle\right),$$

for any $v_1, v_2, w_1, w_2 \in \mathcal{H}_1$. Following the reasoning in Proposition 5.1.1, such an operator satisfies the equality

$$V_\infty^{\tau,(\mathsf{r},1)} = \mathsf{e}^{B_0(p)\tau} V_\infty^{(\mathsf{r},1)}. \tag{6.4.1}$$

A standard approach to employ the time-asymptotic autocorrelation as an early-warning sign is to consider it as a nonlinear operator

$$\hat{V}_\infty^{\tau,(\mathsf{r},1)}\left(\begin{pmatrix} v_1 \\ v_2 \end{pmatrix}, \begin{pmatrix} w_1 \\ w_2 \end{pmatrix}\right) = \frac{\left\langle \begin{pmatrix} v_1 \\ v_2 \end{pmatrix}, V_\infty^{\tau,(\mathsf{r},1)} \begin{pmatrix} w_1 \\ w_2 \end{pmatrix} \right\rangle_{\mathcal{H}_1\times\mathcal{H}_1}}{\left\langle \begin{pmatrix} v_1 \\ v_2 \end{pmatrix}, V_\infty^{(\mathsf{r},1)} \begin{pmatrix} w_1 \\ w_2 \end{pmatrix} \right\rangle_{\mathcal{H}_1\times\mathcal{H}_1}}$$

for any v_1, v_2, w_1, w_2 such that $\left\langle \begin{pmatrix} v_1 \\ v_2 \end{pmatrix}, V_\infty^{(\mathsf{r},1)} \begin{pmatrix} w_1 \\ w_2 \end{pmatrix} \right\rangle_{\mathcal{H}_1\times\mathcal{H}_1} \neq 0$. From (6.1.1) we define $\beta_i^{(p)^*} \in \mathcal{H}_1 \times \mathcal{H}_1$ as the eigenfunction of $B_0(p)^*$ corresponding to the eigenvalue $\overline{\lambda_i^{(p)}}$ for any $i \in \mathbb{N}_{>0}$. It can then be proven from (6.4.1) that

$$\hat{V}_\infty^{\tau,(\mathsf{r},1)}\left(\beta_i^{(p)^*}, w\right) = \mathsf{e}^{\overline{\lambda_i^{(p)}}\tau}$$

holds for any $i \in \mathbb{N}_{>0}$ and $w \in \mathcal{H}_1 \times \mathcal{H}_1$. A key consideration of this result is the fact that, while

$$\beta_i^{(p)} := \begin{pmatrix} e_i^{(p)} \\ 0 \end{pmatrix} \in \mathcal{H}_1 \times \mathcal{H}_1$$

is the eigenfunction of $B_0(p)$ corresponding to $\lambda_i^{(p)}$, the eigenfunctions

$$\beta_i^{(p)^*} = \begin{pmatrix} e_i^{(p)^*} \\ d_i^{(p)^*} \end{pmatrix} \in \mathcal{H}_1 \times \mathcal{H}_1$$

of $B_0(p)^*$ are characterised by $d_i^{(p)^*} \neq 0$. This follows from (6.1.1) and, as a consequence, the sole knowledge of the mild solution $u^{(\mathsf{r,d})}$ of (6.0.2) is not sufficient to describe the autocorrelation as an exponential function to be employed as an early-warning sign in the limit $p \to 0^-$. Then, the structure of the stochastic perturbation ξ_1 in (6.0.1) is required to obtain such a construction. In contrast, the time-asymptotic autocorrelation $\hat{V}_\infty^{\tau,(\mathsf{r,1})}(v,w)$ for

$$v = \begin{pmatrix} v_1 \\ 0 \end{pmatrix} \in \mathcal{H}_1 \times \mathcal{H}_1,$$

any $v_1 \in \mathcal{H}_1$ and $w \in \mathcal{H}_1 \times \mathcal{H}_1$ shows a more complex structure in function of τ. This can be computed explicitly from (6.4.1), depends on κ, and is deferred for future studies. Conversely, any

$$v = \begin{pmatrix} 0 \\ v_2 \end{pmatrix} \in \mathcal{H}_1 \times \mathcal{H}_1$$

for $v_2 \in \mathcal{H}_1$ is an eigenfunction of $B_0(p)^*$ with eigenvalue $-\kappa$. Hence,

$$\hat{V}_\infty^{\tau,(\mathsf{r,1})}(v,w) = \mathsf{e}^{-\kappa\tau}$$

holds for any $w \in \mathcal{H}_1 \times \mathcal{H}_1$ such that $\left\langle v, V_\infty^{(\mathsf{r,1})} w \right\rangle_{\mathcal{H}_1 \times \mathcal{H}_1} \neq 0$. In conclusion, the knowledge of the behaviour of ξ_1 in time is sufficient to construct another (false) early-warning sign in the limit $\kappa \to 0^+$ for any $\tau > 0$.

6.5 Numerical Analysis

In this section, we discuss numerical simulations to cross-validate our findings. We solve numerically different types of SPDEs and study the variance of projections along specific modes over a large time interval. By ergodicity, such a value approximates the time-asymptotic variance on the corresponding functions in $\mathcal{H}_1$. As such, we substitute the observable with the time variance of the solutions in the time interval $[0,T]$, for $T = 10^5$. As discussed in the previous sections, we observe different scaling in the early-warning signs in accordance with the assumptions of the systems. Figure 6.1 and Figure 6.2 encompass our results by displaying the rate of the observables in log-log plots in the limits $p \to 0^-$ and $\kappa \to 0^+$, respectively. In Figure 6.1 we fix the value $\kappa = 2$, whereas in Figure 6.2 we consider $p = 0.5$.
In the following examples, the red noise term is the solution of (6.0.1) for $\sigma = 0.1$ and $Q_j = \mathrm{Id}$, the identity operator in $\mathcal{H}_j$ for $j \in \{0,1\}$. The systems are solved through the discretisation of the mild solution formula (Section 2.2), unless stated otherwise. The time step is chosen as $\delta t = 0.1$ and the spatial step δx is fixed in each example. The projections along different modes are computed through the discrete scalar product that approximates the product in $\mathcal{H}_1$. In the corresponding figures, the values are obtained as the average of 10 independent run samples, and the initial conditions are set near the null function. The shaded grey

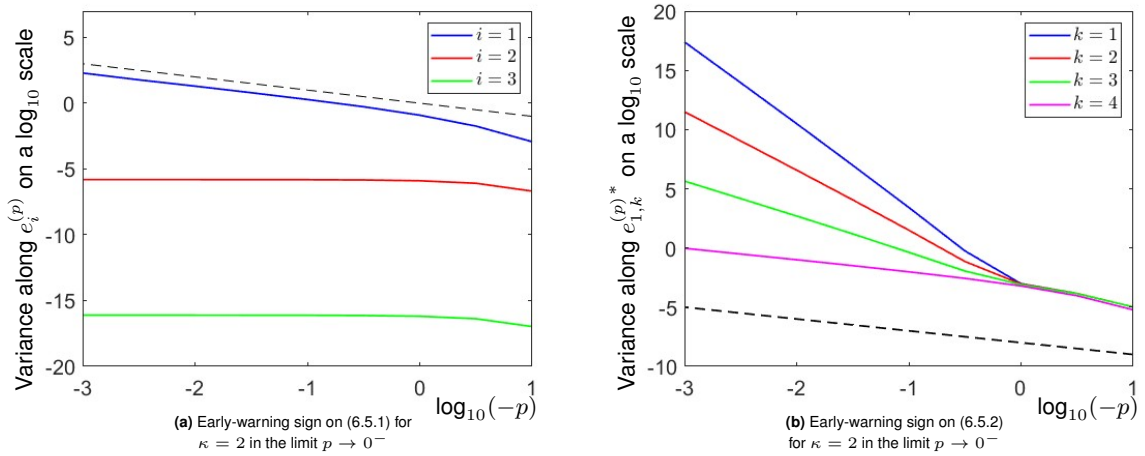

(a) Early-warning sign on (6.5.1) for $\kappa = 2$ in the limit $p \to 0^-$

(b) Early-warning sign on (6.5.2) for $\kappa = 2$ in the limit $p \to 0^-$

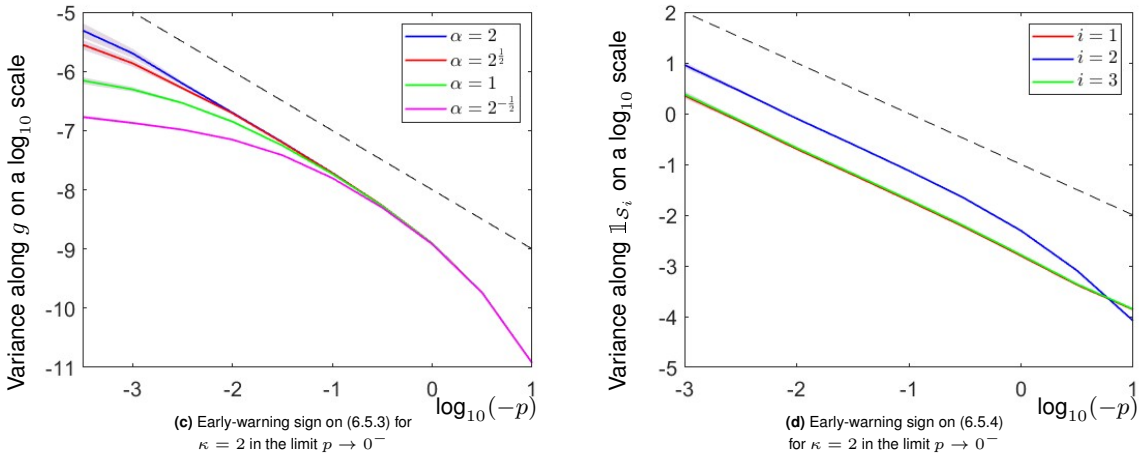

(c) Early-warning sign on (6.5.3) for $\kappa = 2$ in the limit $p \to 0^-$

(d) Early-warning sign on (6.5.4) for $\kappa = 2$ in the limit $p \to 0^-$

Fig. 6.1 Log-log plots of the time variance of the solution projected along different modes in the limit $p \to 0^-$. Each panel corresponds to a different system: (a) the cable equation on an interval with periodic boundary conditions; (b) an SDE with linear drift displaying generalised eigenvectors; (c) an SPDE with a linear drift term with purely continuous spectrum; (d) a boundary-driven system with red Dirichlet noise at the extremes of an interval. The values refer to the average of 10 run samples. The dashed black lines indicate reference hyperbolic scaling laws, while the shaded grey regions represent twice the numerical standard deviation. The increase of variance in the projected modes is the manifestation of critical slowing down in this destabilising SPDE.

areas have a width equal to double the numerical standard deviation in a logarithmic scale to indicate sensitivities in the algorithm. As a reference, we display a dashed black line in each figure that indicates the hyperbolic rate of divergence.

First, we solve the cable equation with periodic boundary conditions:

$$\begin{cases} \mathrm{d}u^{(\mathrm{r,d})}(x,t) = \Big((\Delta + p)u^{(\mathrm{r,d})}(x,t) + \xi_1(x,t)\Big)\,\mathrm{d}t, \\ u^{(\mathrm{r,d})}(0,t) = u^{(\mathrm{r,d})}(1,t), \\ u^{(\mathrm{r,d})}(x,0) = 0, \end{cases} \tag{6.5.1}$$

for $x \in [0,1]$ and $0 < t < T$. The spatial step is $\delta x = 0.005$. We denote as $\left\{e_i^{(p)}\right\}_{i\in\mathbb{N}_{>0}}$, the eigenfunctions of the self-adjoint differential operator $\Delta + p$ with periodic boundary conditions. We notice then that $\lambda_1^{(p)} = p$. In Figure 6.1a, we display the variance of $\left\langle u^{(\mathrm{r,d})}, f\right\rangle$ for $f = e_i^{(p)}$ and $i \in \{0,1,2\}$ in correspondence to $-p$. Those values are scaled on a logarithmic scale to capture the scaling law in the limit $p \to 0^-$. Of such, only the variance along $f = e_1^{(p)}$ assumes a hyperbolic rate of divergence, while the rest converge in the limit. In contrast, in Figure 6.2a, the scaling law of the variance in the limit $\kappa \to 0^+$ is hyperbolic regardless of the eigenmode along which the early-warning sign is observed, since $Q = \mathrm{Id}$. This behaviour is visible through the comparison to the dashed reference line.

In the next case, we study an SDE with a linear drift component characterised by the existence of generalised eigenvectors. Our example is

$$\begin{cases} \mathsf{d}u^{(\mathsf{r},\mathsf{g})}(x,t) = \left(\begin{pmatrix} p & 1 & 0 & 0 \\ 0 & p & 1 & 0 \\ 0 & 0 & p & 1 \\ 0 & 0 & 0 & p \end{pmatrix} u^{(\mathsf{r},\mathsf{g})}(x,t) + \xi_1(x,t) \right) \mathsf{d}t, \\ u^{(\mathsf{r},\mathsf{g})}(x,0) = 0, \end{cases} \tag{6.5.2}$$

for $x \in \mathbb{R}^4$ and $0 < t < T$. In Figure 6.1b, we observe the time variance of the solution along the left generalised eigenvectors of the matrix that defines the drift component, or the generalised eigenvectors of its transpose. The only eigenvalue is $\lambda_1^{(p)} = p$ and its corresponding left generalised eigenvectors are

$$e_{1,1}^{(p)^*} = \begin{pmatrix} 1 \\ -1 \\ 0 \\ 0 \end{pmatrix}, \quad e_{1,2}^{(p)^*} = \begin{pmatrix} 0 \\ 1 \\ -1 \\ 0 \end{pmatrix}, \quad e_{1,3}^{(p)^*} = \begin{pmatrix} 0 \\ 0 \\ 1 \\ -1 \end{pmatrix}, \quad e_{1,4}^{(p)^*} = \begin{pmatrix} 0 \\ 0 \\ 0 \\ 1 \end{pmatrix}.$$

As described in Theorem 6.1.1, the scaling laws in the limit $p \to 0^-$ of the time-asymptotic variances are $\Theta_p\left((-p)^{-1}\right)$ along $e_{1,1}^{(p)^*}$, $\Theta_p\left((-p)^{-3}\right)$ along $e_{1,2}^{(p)^*}$, $\Theta_p\left((-p)^{-5}\right)$ along $e_{1,3}^{(p)^*}$ and $\Theta_p\left((-p)^{-7}\right)$ along $e_{1,4}^{(p)^*}$. This behaviour is reflected in Figure 6.1b where only the time variance along the first mode is hyperbolic. Conversely, the rate of divergence in the limit $\kappa \to 0^+$ is $\Theta_\kappa\left(\kappa^{-1}\right)$ along each mode, as shown in Figure 6.2b.

In Figure 6.1c and Figure 6.2c, we study the time variance of the numerical approximation of the mild solution associated with

$$\begin{cases} \mathsf{d}u^{(\mathsf{r},\mathsf{c})}(x,t) = \Big((-|x|^\alpha + p)\, u^{(\mathsf{r},\mathsf{c})}(x,t) + \sigma_{\mathsf{R}} \xi_1(x,t) \Big)\, \mathsf{d}t, \\ \quad \mathsf{d}\xi_1(x,t) = -\kappa \xi_1(x,t) \mathsf{d}t + \sigma Q_1^{\frac{1}{2}} \mathsf{d}W_t^1, \\ u^{(\mathsf{r},\mathsf{c})}(x,0) = 0, \end{cases} \tag{6.5.3}$$

for all $x \in \mathbb{R}$ and $0 < t < T$. The spatial step is set as $\delta x = 10^{-5}$. In this case, we fix the function along which we project $u^{(\mathsf{r},\mathsf{c})}$, which is $g = \mathbb{1}_{\mathcal{S}}$ for $\mathcal{S} = [-0.01, 0.01]$. However, we consider different values of α that define the system, specifically $\alpha \in \left\{2^{-\frac{1}{2}}, 1, 2^{\frac{1}{2}}, 2\right\}$. As described in Corollary 6.2.2, the time-asymptotic variance of the solution along g shows a rate of divergence less than hyperbolic in the limit $p \to 0^-$. In Figure 6.1c, the lines associated with $\alpha = 2^{\frac{1}{2}}$ and $\alpha = 2$ approach for small values of $-p$ their expected scaling law, which correspond to the slopes $-1 + \frac{1}{\alpha}$ in the log-log scale. For the rest, the slope decreases steadily as p approaches 0, indicating lower rates of divergence. In Figure 6.2c, the scaling law is equivalent for each value of α and it is hyperbolic in the limit $\kappa \to 0^+$.

Lastly, in Figure 6.1d and Figure 6.2d, we consider the mild solution of

$$\begin{cases} \mathsf{d}u^{(\mathsf{r},\mathsf{b})}(x,t) = \Big((\Delta + \pi^2 + p) u^{(\mathsf{r},\mathsf{b})}(x,t) \Big)\, \mathsf{d}t, \\ u^{(\mathsf{r},\mathsf{b})}(0,t) = \xi_0(0,t), \\ u^{(\mathsf{r},\mathsf{b})}(1,t) = \xi_0(1,t), \\ u^{(\mathsf{r},\mathsf{b})}(x,0) = 0, \end{cases} \tag{6.5.4}$$

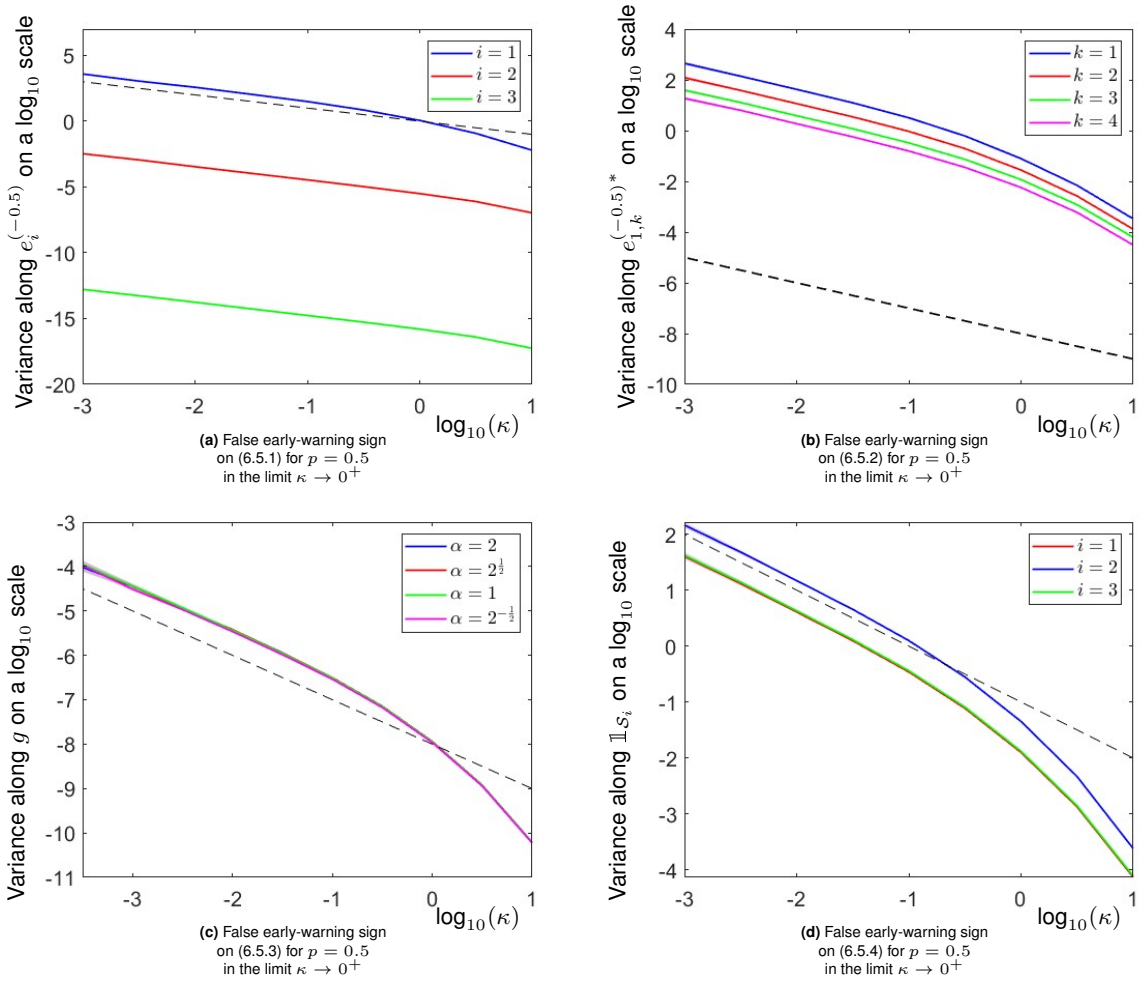

(a) False early-warning sign on (6.5.1) for $p = 0.5$ in the limit $\kappa \to 0^+$

(b) False early-warning sign on (6.5.2) for $p = 0.5$ in the limit $\kappa \to 0^+$

(c) False early-warning sign on (6.5.3) for $p = 0.5$ in the limit $\kappa \to 0^+$

(d) False early-warning sign on (6.5.4) for $p = 0.5$ in the limit $\kappa \to 0^+$

Fig. 6.2 Log-log plots of the time variance of the solution projected along different modes in the limit $\kappa \to 0^+$. The panels (a)-(d) correspond to the same systems as in Figure 6.1 and their values refer to the average of 10 run samples. In contrast to the limit $p \to 0^-$, the variance exhibits hyperbolic divergence across all modes due to the noise structure. This is indicated by the alignment of all lines to the dashed black lines, which serve as a reference slope. The grey-shaded regions depict numerical uncertainties. The observed increase in variance, which only depends on the increase in the noise correlation time $1/\kappa$, represents a false early-warning sign in the context of critical slowing down.

for all $x \in [0,1]$ and $0 < t < T$. The spatial step is fixed as $\delta x = 0.005$ and the numerical solution is obtained through the implicit Euler method. The space interval $\mathcal{X}_1 = [0,1]$ is partitioned into $\mathcal{S}_1 = \left[0, \frac{1}{3}\right]$, $\mathcal{S}_2 = \left[\frac{1}{3}, \frac{2}{3}\right]$ and $\mathcal{S}_3 = \left[\frac{2}{3}, 1\right]$. In the figure, we observe the log-log plot of the time variance of the solution along $f = \mathbb{1}_{\mathcal{S}_i}$, for $i \in \{1,2,3\}$. For such a system, we know the Dirichlet map $D(p) : \mathcal{H}_0 \to \mathcal{H}_1$ explicitly [63] and that it does not depend on p. This implies the statement of Corollary 6.3.2, which is corroborated by the findings in the figures. In fact, for each $i \in \{1,2,3\}$ we consider $h_1^{(p)} = h_2^{(p)} = \mathbb{1}_{\mathcal{S}_i}$ for any $p < 0$. Then, the time-asymptotic variance along such families of functions displays hyperbolic divergence in the limit $p \to 0^-$, as shown in Figure 6.1d, and in the limit $\kappa \to 0^+$, as displayed in Figure 6.2d.

6.6 Summary

In this chapter, we derive expressions for system covariance in linear SPDEs under the influence of red noise. The dependence of covariance on a critical eigenvalue suggests that in such systems, covariance diverges when linear stability is lost. This is also the case for generic probing functions in the solution space. In this sense, it is reasonable to expect the occurrence of critical slowing down in bifurcating SPDEs with red noise. However, we find that a similar divergence takes place when the correlation time of the noise increases. This is problematic, as there is no way to tell the genuine source of an increase in covariance in an application setting [213]. The possibility of non-stationary noise characteristics would

need to be carefully considered before assuming critical slowing down for the detection of approaching bifurcations. We also discuss a second early-warning sign for bifurcations, an exponential increase in the autocorrelation. We show that such an effect indeed occurs with respect to some specific probing functions. However, we emphasise, also for this early-warning sign, the potential for false indications resulting from non-stationary noise.

We perform numerical experiments for the same class of SPDEs. We introduce red noise either as a dynamic term or as a boundary condition. The observed divergence of variance corresponding to critical slowing down is reproduced in these simulations. The performed statistical assessment resembles the setting of an applied time series analysis in a real-world system suspected of bifurcating. Furthermore, we have reproduced the effect of an increase in variance as a response to an increase in the correlation time of the noise, which results in a false early warning. This underscores the need for specific knowledge of the system to properly employ such observables.

7 Finite time Lyapunov exponents

In this chapter, we construct early-warning signs for the pitchfork bifurcations in the SPDE

$$\begin{cases} \mathrm{d}u(x,t) = (\Delta u(x,t) - g(x)u(x,t) + pu(x,t) - u(x,t)^3)\,\mathrm{d}t + \sigma\, Q^{\frac{1}{2}}\mathrm{d}W_t, \\ u(\cdot,0) = u_0 \in \mathcal{H}_1, \\ u(0,t) = u(L,t) = 0, \end{cases} \tag{7.0.1}$$

for all $t \in \mathbb{R}$, $x \in \mathcal{X}_1 = [0, L]$, $p < 0$. We also assume g to be a bounded and continuous almost everywhere positive function and consider the operator Q to be bounded and strictly positive. Consequently, we follow the work in [23] and employ an equivalent notation to the one adopted for (3.0.1) in the introduction of Chapter 3. Specifically, we define the operator $A = \Delta - g$. Its ordered eigenvalues are $\{\lambda_n\}_{n\in\mathbb{N}_{>0}}$ and their eigenfunctions are called $\{e_n\}_{n\in\mathbb{N}_{>0}}$. Similarly, the eigenfunctions of Δ are $\{e'_n\}_{n\in\mathbb{N}_{>0}}$ and the corresponding eigenvalues $\left\{\lambda'_n := -\left(\frac{\pi n}{L}\right)^2\right\}_{n\in\mathbb{N}_{>0}}$. Nonetheless, in contrast to Chapter 3, we assume the linear operators to satisfy the properties:

(M1') there exists an $d_0 > 0$ such that the eigenfunctions of Q satisfy $b_j = e'_j$ for all $j > d_0$;

(M2') the eigenvalues $\{\zeta_j\}_{j\in\mathbb{N}_{>0}}$ associated with $\{b_j\}_{j\in\mathbb{N}_{>0}}$ are positive and satisfy $\sum_{j=1}^{\infty}\zeta_j(-\lambda'_j)^\gamma < +\infty$ for a constant $\gamma > 0$.

As stated in Section 2.2 and Appendix B, such assumptions imply the continuity of the solutions of (7.0.1) in $\mathcal{W}^{1,2}(\mathcal{X}_1)$ if $u_0 \in \mathcal{W}^{1,2}(\mathcal{X}_1)$ and that, for $u_0 \in \mathcal{H}_1 = L^2(\mathcal{X}_1)$, there exists a unique mild solution

$$u \in L^2(\Omega \times (0,T); \mathcal{W}^{1,2}(\mathcal{X}_1)) \cap L^2(\Omega, \mathcal{F}, \mathbb{P}; C((0,T); \mathcal{H}_1)).$$

The observables are in the form of the change of sign of the possible highest value assumed by the finite-time Lyapunov exponents. Consequently, they predict the change of different eigenvalues of the drift operator, albeit critical transitions are likely to occur primarily before the second threshold is crossed.

7.1 Random dynamical system and attractor

We consider the probability space $(\Omega, \mathcal{F}, \mathbb{P})$ with $\Omega := C_0(\mathbb{R}; \mathcal{H}_1)$ composed of the functions $\omega : \mathbb{R} \to \mathcal{H}_1$ such that $\omega(0) = 0$ and endowed with the compact-open topology, which has as a basis the finite intersections of the sets $\{\omega \in C_0(\mathbb{R}; \mathcal{H}_1) |\ \omega(K) \subset \mathcal{U}\}$ such that K is a compact and $\mathcal{U}$ is a open. With $\mathcal{F}$ we denote the Borel sigma-algebra on Ω and with $\mathbb{P}$ a Wiener measure generated by a two-sided Wiener process. As in [31], we consider $\omega_t = W_t(\omega)$ and the two-sided filtration $(\mathcal{F}_{t_1}^{t_2})_{t_1<t_2}$ defined as $\mathcal{F}_{t_1}^{t_2} := \sigma(\omega_{t_2} - \omega_{t_1})$, the coarsest σ-algebra on which such a difference is measurable. We can then obtain

$$\begin{aligned} \mathcal{F}_{-\infty}^{t} &= \sigma(\mathcal{F}_{t_1}^{t} : t_1 < t), \\ \mathcal{F}_{t}^{\infty} &= \sigma(\mathcal{F}_{t}^{t_1} : t < t_1), \end{aligned}$$

as the coarsest σ-algebras to contains such sets. We also introduce the Wiener shift for all $t > 0$

$$(\theta^t\omega)_{t_1} := \omega_{t+t_1} - \omega_{t_1}, \quad \text{for any } \ t_1 \in \mathbb{R}, \omega \in \Omega\ .$$

Thus $(\theta^t)_{t\in\mathbb{R}}$ is a family of $\mathbb{P}$-preserving transformations that satisfies the flow property and $(\Omega, \mathcal{F}, \mathbb{P}, (\theta^t)_{t\in\mathbb{R}})$ is an ergodic metric dynamical system [54]. The next properties are described in [43]; nonetheless, we summarise them here to simplify the results discussed in the chapter.

Proposition 7.1.1. *There exists a θ^t-invariant subset $\Omega' \subset \Omega$ of full probability measure such that for all $\omega \in \Omega'$ and $t \geq 0$ there is a Fréchet differentiable C^1-semiflow on $\mathcal{H}_1$*

$$u_0 \longmapsto \varphi(t, \omega, u_0) =: \varphi^t_\omega(u_0)$$

that satisfies the following for any $\omega \in \Omega'$:

(P1) for all $T > 0$ and $u_0 \in \mathcal{H}_1$, the mapping $(\omega, t) \mapsto \varphi^t_\omega(u_0)$ in $\Omega \times [0, T] \mapsto \mathcal{H}_1$ is the unique pathwise mild solution of (7.0.1)*;*

(P2) it satisfies the cocycle property, i.e., for any $t_1, t_2 > 0$,

$$\varphi^{t_1+t_2}_\omega = \varphi^{t_2}_{\theta^{t_1}\omega} \circ \varphi^{t_1}_\omega;$$

(P3) fixing $t_2 > t_1 > 0$, then the $\mathcal{H}_1$-valued random variable $\varphi^{t_2-t_1}_{\theta^{t_1}\omega}(u)$ is $\mathcal{F}^{t_2}_{t_1}$-measurable for any $u \in \mathcal{H}_1$.

The pair of mappings (θ, φ) is the random dynamical system (RDS) generated by (7.0.1). Moreover, property (P3) implies that the process u_t, defined by $u_t := \varphi^t_\omega(u_0)$ for generic $\omega \in \Omega'$, is $\mathcal{F}^t_0$-adapted. The next proposition is obtained by [68, Lemma 4.4].

Proposition 7.1.2. *For all $T > 0$ and $u_0, v_0 \in \mathcal{H}_1$ and given the Fréchet-differentiable C^1-semiflow described in Proposition 7.1.1, it follows that the mapping $\Omega \times [0, T] \mapsto \mathcal{H}_1$ given by $(\omega, t) \mapsto D_{u_0}\varphi^t_\omega(v_0)$ is the unique solution of the first variation evolution equation along u with initial conditions set on u_0 and v_0:*

$$\begin{cases} dv = (\Delta v - gv + pv - 3u^2 v)\, dt, \\ u(\cdot, 0) = u_0, \\ v(\cdot, 0) = v_0, \\ v(0, t) = v(L, t) = 0, \end{cases} \tag{7.1.1}$$

for any $t \in [0, T]$.

Next, we present the relevant result for the existence and uniqueness of an invariant measure. We define the transition semigroup of the system (7.0.1) as

$$P_t\phi := \mathbb{E}(\phi(\varphi^t_\cdot(u_0))),$$

for all $\phi \in B_b(\mathcal{H}_1)$, the set of bounded Borel-measurable functions that assume real values, and $t \geq 0$ [64]. It is said that it satisfies the strong Feller property if continuous for $\phi \in B_b(\mathcal{H}_1)$ and $t > 0$. It is irreducible if positive for all $t \geq 0$ and ϕ indicator function on open sets in $\mathcal{H}_1$. The next lemma and proposition [47, Chapter 8] are employed to prove the following results and are implied by Lemma B.1 and the strict positivity of the eigenvalues of Q.

Lemma 7.1.3. *The transition semigroup of the system* (7.0.1) *satisfies the strong Feller property and irreducibility.*

By Krylov-Bogoliubov Theorem, for the existence, Doob's Theorem and by Khas'minskii's Theorem [66, 125] we obtain the next proposition.

Proposition 7.1.4. *There exists a unique stationary measure μ for the process u_t which is equivalent to any transition probability measure $\mathfrak{P}_t(u_0, \cdot)$ for all $t > 0$ and $u_0 \in \mathcal{H}_1$, in the sense that they are mutually absolutely continuous. It is defined as*

$$\mathfrak{P}_t(u_0, \mathcal{B}) := P_t\mathbb{1}_\mathcal{B} = \mathbb{P}(\varphi^t_\cdot(u_0) \in \mathcal{B}) \quad \textit{for} \quad u_0 \in \mathcal{H}_1,\ t > 0,$$

for any $\mathcal{B} \in \mathfrak{B}(\mathcal{H}_1)$, the sigma-algebra of Borelian sets in $\mathcal{H}_1$, and it is concentrated on $\mathcal{W}^{1,2}(\mathcal{X}_1)$.

Finally, we can consider the random attractor itself.

Definition 7.1.5. *A global random attractor of an RDS (φ, θ) is a compact random set $\mathcal{A} \subset \mathcal{H}_1$, i.e., it depends on $\omega \in \Omega'$ and satisfies:*

- *it is invariant under the RDS, which means $\varphi^t_\omega(\mathcal{A}(\omega)) = \mathcal{A}(\theta^t\omega)$;*
- *it is attracting so that for every bounded set $\mathcal{B} \subset \mathcal{H}_1$, i.e.,*

$$\lim_{t\to\infty} \|\varphi^t_{\theta^{-t}\omega}(\mathcal{B}) - \mathcal{A}(\omega)\| = 0$$

for $\mathbb{P}$-a.s. in ω.

We can use Proposition 7.1.4 to prove a strong property of the random attractor.

Proposition 7.1.6. *For any $p \in \mathbb{R}$, the random dynamical system generated by* (7.0.1) *has a global random attractor $\mathcal{A}$ that is a singleton, i.e., there exists a random variable $a : \Omega \to \mathcal{H}_1$ such that $\mathcal{A}(\omega) = a(\omega)$ $\mathbb{P}$-a.s., and it is $\mathcal{F}^0_{-\infty}$-measurable. The law of the attractor a is the unique invariant measure of the system.*

The proof of this proposition follows the steps of [44, Theorem 6.1]. In particular, the existence of the global random attractor $\mathcal{A}$ is the result of [68, Theorem 4.5] and its $\mathcal{F}^0_{-\infty}$-measurability can be derived from [61, Theorem 3.3]. Another important property is the order-preservation of the system (7.0.1), i.e., for two initial conditions $u_1(x, 0) \leq u_2(x, 0)$ for almost all $x \in \mathcal{X}_1$ the solutions satisfy $u_1(x, t) \leq u_2(x, t)$ for almost all $x \in \mathcal{X}_1$ and $t > 0$. This is a consequence of [191, Theorem 5.1] and [53, Theorem 5.8].

The main result of the paper [31] is the description of the possible influences of the attractor a on close solutions, for different values of p. This can be expressed by the sign of the leading finite-time Lyapunov exponent (FTLE).

Definition 7.1.7. *The (leading) finite-time Lyapunov exponents, at a time $t > 0$ and sample $\omega \in \Omega$, of an RDS (φ, θ) with Fréchet differentiable semiflow φ is defined by the following equation:*

$$\mathfrak{L}_1(t; \omega, u) := \frac{1}{t} log \|D_u\varphi^t_\omega\|$$

for any $u \in \mathcal{H}_1$.

The FTLE describes the influence of the linear operator $\mathrm{D}_u\varphi^t_\omega$, for given $\omega \in \Omega$, $u \in \mathcal{H}_1$ and $t > 0$, on elements of $\mathcal{H}_1$ close to u. A positive FTLE indicates that close functions in $\mathcal{H}_1$, that are near u, tend to separate in time t. Conversely, a negative FTLE indicates the distance between elements in a neighbourhood of u tends to be smaller after time t. Of great interest is the FTLE on the attractor, defined as

$$\mathfrak{L}_1(t; \omega) := \mathfrak{L}_1(t; \omega, a(\omega)).$$

By the subadditive ergodic theorem [186] there exists a limit $t \to \infty$ of $\mathfrak{L}_1(t; \omega)$ for $\omega - \mathbb{P}$-a.s., referred to as the Lyapunov exponent of $a(\omega)$.[1]

Next, we discuss the extension to further bifurcations beyond the first pitchfork bifurcation point. As previously described, any $p \in \{-\lambda_j\}_{j\in\mathbb{N}_{>0}}$ is a deterministic bifurcation threshold of the system on which, when crossed, two new steady states appear and the origin in $\mathcal{H}_1$ increases dimension of its unstable manifold by one. We make use of wedge products to study this case by addressing the loss of stability on volumes and, consequently, along multiple modes. For a separable Hilbert space $\mathcal{H}_1$ and for $v_1, ..., v_k \in \mathcal{H}_1$, the wedge product ($k$-blade) is denoted by

$$v_1 \wedge ... \wedge v_k.$$

[1] From the synchronisation of the system it would be expected that the Lyapunov exponent is non-positive with probability 1. This is still an open problem.

We define the following scalar product for all $v_1, ..., v_k, w_1, ..., w_k \in \mathcal{H}_1$,

$$(v_1 \wedge ... \wedge v_k, w_1 \wedge ... \wedge w_k) := \det[(v_{j_1}, w_{j_2})_{j_1,j_2}] \tag{7.1.2}$$

with $(v_{j_1}, w_{j_2})_{j_1,j_2}$ denoting the $k \times k$ matrix with j_1, j_2-th element (v_{j_1}, w_{j_2}). The set $\wedge^k \mathcal{H}_1$ is the closure of finite linear combinations of k-blades under the norm defined by such an inner product. Given $\{e_j\}_{j \in \mathbb{N}_{>0}}$ as a basis of $\mathcal{H}_1$, we can define a basis for $\wedge^k \mathcal{H}_1$ whose elements are the k-blades

$$\mathbf{e_i} := e_{i_1} \wedge ... \wedge e_{i_k}$$

with $\mathbf{i} = (i_1, ..., i_k)$ for $0 < i_1 < ... < i_k$. Given $B \in \mathcal{L}(\mathcal{H}_1)$, we can obtain an operator in $\mathcal{L}(\wedge^k \mathcal{H}_1)$ by the following operation:

$$\wedge^k B(v_1 \wedge ... \wedge v_k) := Bv_1 \wedge ... \wedge Bv_k,$$

for all $v_1, ..., v_k \in \mathcal{H}_1$. Such operators satisfy the property[2]

$$\| \wedge^k B\|_{\wedge^k \mathcal{H}_1} = \max\{|\det(B|_E)| : \ E \subset \mathcal{H}_1, \ \mathsf{dim}(E) = k\}.$$

The last definitions allow us to introduce

$$\mathfrak{L}_k(t; \omega, u) := \frac{1}{t} \mathsf{log} \| \wedge^k \mathsf{D}_u \varphi_\omega^t \|_{\wedge^k \mathcal{H}_1},$$
$$\mathfrak{L}_k(t; \omega) := \mathfrak{L}_k(t; \omega, a(\omega)).$$

Such functions describe the behaviour of volumes defined by the position of elements of $\mathcal{H}_1$ in a neighbourhood of $u \in \mathcal{H}_1$ or of the attractor.

7.2 Bounds for FTLEs

We illustrate the construction of the observables for the prediction of the approach to a bifurcation threshold in (7.0.1). The proofs of the theorems considered in this section build upon the approach described in [31]. The main results are Theorems 7.2.1 and 7.2.4. Theorem 7.2.1 constructs an upper bound to $\mathfrak{L}_k$ for any value of p. It follows from this result that for $k = 1$ and $p < -\lambda_1$ the FTLE is almost surely negative. Theorem 7.2.4 provides a lower bound to the highest admissible value that $\mathfrak{L}_k$ can assume. Specifically, it shows that there is a positive probability of $\mathfrak{L}_k$ to be positive for p beyond the k-th bifurcation.

7.2.1 Upper bound

Theorem 7.2.1. *For any $k \geq 1$, the inequality*

$$\mathfrak{L}_k(t; \omega) \leq \sum_{j=1}^{k} \big(p + \lambda_j\big)$$

holds with probability 1 for all $t > 0$.

Proof. Given $\mathbf{v}_t = v_t^1 \wedge ... \wedge v_t^k = \wedge^k \mathsf{D}_{a(\omega)} \varphi_\omega^t(\mathbf{v}_0)$, with $\mathbf{v}_0 \in \wedge^k \mathcal{H}_1$, we obtain by [31, Lemma 3.5] and the min-max principle that

$$\frac{1}{2} \frac{\mathsf{d}}{\mathsf{d}t} ||\mathbf{v}_t||^2_{\wedge^k \mathcal{H}_1} = \sum_{j=1}^{k} (\mathbf{v}_t, v_t^1 \wedge ... \wedge v_t^{j-1} \wedge (\Delta - g + p + B_\omega^t) v_t^j \wedge v_t^{j+1} \wedge ... \wedge v_t^k)$$

[2] The operator $B|_E : E \to B(E)$ is assumed to be a linear operator on a finite-dimensional inner product space and we set $\det(B|_E) = 0$ for E such that $\mathsf{dim}(E) < k$.

$$\leq \sum_{j=1}^{k} (\mathbf{v}_t, v_t^1 \wedge ... \wedge v_t^{j-1} \wedge (\Delta - g + p) v_t^j \wedge v_t^{j+1} \wedge ... \wedge v_t^k)$$

$$= \frac{\mathsf{d}}{\mathsf{d}r}\bigg|_{r=0} (\mathbf{v}_t, \wedge^k \mathsf{e}^{(\Delta - g + p)r} \mathbf{v}_t) \leq \frac{\mathsf{d}}{\mathsf{d}r}\bigg|_{r=0} \mathsf{e}^{\sum_{j=1}^{k} (p+\lambda_j) r} ||\mathbf{v}_t||^2_{\wedge^k \mathcal{H}_1} = \sum_{j=1}^{k} \big(p + \lambda_j\big) ||\mathbf{v}_t||^2_{\wedge^k \mathcal{H}_1}$$

for $B^t_\omega := -3a(\theta^t\omega)^2$. □

7.2.2 Lower bound

Lemma 7.2.2. *With probability* 1*, it holds that* $a(\theta^t\omega) \in \mathcal{W}^{1,2}(\mathcal{X}_1)$ *for all* $p \in \mathbb{R}$ *and* $t \in \mathbb{R}$*. Also, for any* $T, \epsilon > 0$*, there exists an* $\mathcal{F}^T_{-\infty}$*-measurable set* $\Omega_0 \subset \Omega$ *such that* $\mathbb{P}(\Omega_0) > 0$ *and*

$$||a(\theta^t\omega)||_{\mathcal{W}^{1,2}(\mathcal{X}_1)} \in (0, \epsilon) \quad \textit{for all} \quad p \in \mathbb{R},\ t \in [0, T] \quad \textit{and} \quad \omega \in \Omega_0.$$

Proof. We begin the proof assuming for the initial condition $u_0 \in \mathcal{W}^{1,2}(\mathcal{X}_1)$. From Proposition 7.1.4 and the continuity of the solution in $\mathcal{W}^{1,2}(\mathcal{X}_1)$ we get for the singleton attractor that $a(\omega) \in \mathcal{W}^{1,2}(\mathcal{X}_1)$ for all $\omega \in \Omega$. Additionally, from Lemma 7.1.3 and Proposition 7.1.4 we know that the invariant measure that describes the law of the attractor is locally positive on $\mathcal{W}^{1,2}(\mathcal{X}_1)$. As a result it follows that $||a(\omega)||_{\mathcal{W}^{1,2}(\mathcal{X}_1)} \in (0, \eta)$, for all $\omega \in \Omega_1$ with Ω_1 that is $\mathcal{F}^0_{-\infty}$-measurable ([54, Proposition 3.1]) and $\mathbb{P}(\Omega_1) > 0$ and for a constant $\eta > 0$ dependent on Ω_1. We now define the family of operators $S(t) := \mathsf{e}^{(A+p)t}$ in order to study the solutions of

$$\mathsf{d}u = (\Delta u - gu + pu - u^3)\, \mathsf{d}t + \sigma\, Q^{\frac{1}{2}} \mathsf{d}W_t.$$

From this SPDE we subtract the Orstein-Uhlenbeck process which is solution of

$$\begin{cases} \mathsf{d}z = (\Delta z - gz + pz)\, \mathsf{d}t + \sigma\, Q^{\frac{1}{2}} \mathsf{d}W_t, \\ z(x, 0) = 0,\ \forall x \in \mathcal{X}_1, \end{cases}$$

with zero Dirichlet boundary conditions and takes the form

$$z(t) = \sigma \int_0^t S(t - t_1) Q^{\frac{1}{2}} \mathsf{d}W_{t_1},$$

to introduce $\tilde{u} := u - z$. Consequently, we obtain the random PDE

$$\mathsf{d}\tilde{u} = (\Delta \tilde{u} - g\tilde{u} + p\tilde{u})\, \mathsf{d}t - (\tilde{u} + z)^3\, \mathsf{d}t,$$

whose mild solution is

$$\tilde{u}(t) = S(t)\tilde{u}_0 + \int_0^t S(t - t_1) \iota(\tilde{u}(t_1) + z(t_1)) \mathsf{d}t_1 \tag{7.2.1}$$

with $\tilde{u}_0 := \tilde{u}(0) = u_0$ and $\iota(x) = -x^3$ for all $x \in \mathcal{X}_1$. From [2, 67] we obtain that $S(t)$ is an analytic semigroup. The norms $||\cdot||_{\mathcal{W}^{1,2}(\mathcal{X}_1)} = ||(-\Delta)^{\frac{1}{2}} \cdot||$ and $||\cdot||_A = ||(-A)^{\frac{1}{2}} \cdot||$ are equivalent in $\mathcal{W}^{1,2}(\mathcal{X}_1)$ as proven in Appendix A. Therefore, we obtain the following inequalities from [105]:

$$\begin{aligned} ||S(t)||_{\mathcal{L}(\mathcal{W}^{1,2}(\mathcal{X}_1))} &\leq \mathsf{e}^{(\lambda_1 + p)t}, \text{ for all } t > 0, \\ ||S(t)||_{\mathcal{L}(\mathcal{H}_1, \mathcal{W}^{1,2}(\mathcal{X}_1))} &\leq c t^{-\frac{1}{2}} \mathsf{e}^{(\lambda_1 + p)t}, \text{ for all } t > 0 \end{aligned} \tag{7.2.2}$$

for a certain constant $c > 0$. Another important estimate is obtained by the fact that the nonlinear term $\iota : \mathcal{W}^{1,2}(\mathcal{X}_1) \to \mathcal{H}_1$ is locally Lipschitz and thus for any $u_1, u_2 \in \mathcal{U} \subset \mathcal{W}^{1,2}(\mathcal{X}_1)$ there exists a constant $\ell > 0$ such that

$$||\iota(u_1) - \iota(u_2)|| \leq \ell ||u_1 - u_2||_{\mathcal{W}^{1,2}(\mathcal{X}_1)}$$

with $\mathcal{U}$ being a bounded subset of $\mathcal{W}^{1,2}(\mathcal{X}_1)$. Using a cut-off technique, we can truncate ι outside of a ball in $\mathcal{W}^{1,2}(\mathcal{X}_1)$ of radius $R>0$ and center in the null function and obtain the globally Lipschitz function

$$\tilde{\iota}(u) := -\Theta\left(\frac{||u||_{\mathcal{W}^{1,2}(\mathcal{X}_1)}}{R}\right)u^3,$$

with $\Theta : \mathbb{R}^+ \to [0,1]$, a C^1 cut-off function. As for ι, the Lipschitz inequality takes the form, for a certain $\tilde{\ell} > 0$,

$$||\tilde{\iota}(u_1) - \tilde{\iota}(u_2)|| \leq \tilde{\ell}||u_1 - u_2||_{\mathcal{W}^{1,2}(\mathcal{X}_1)} \text{ for all } u_1, u_2 \in \mathcal{W}^{1,2}(\mathcal{X}_1).$$

From (7.2.1), the estimates (7.2.2) and the fact that $\tilde{\iota}(u) = \iota(u)$ on the ball with center in the null function and radius R in $\mathcal{W}^{1,2}(\mathcal{X}_1)$, we can obtain the following inequality

$$\begin{aligned} ||\tilde{u}(t)||_{\mathcal{W}^{1,2}(\mathcal{X}_1)} &\leq ||S(t)\tilde{u}_0||_{\mathcal{W}^{1,2}(\mathcal{X}_1)} + \int_0^t ||S(t-t_1)||_{\mathcal{L}(\mathcal{H}_1,\mathcal{W}^{1,2}(\mathcal{X}_1))}||\tilde{\iota}(\tilde{u}(t_1)+z(t_1))||\mathsf{d}t_1 \qquad (7.2.3)\\ &\leq \mathsf{e}^{(\lambda_1+p)t}||\tilde{u}_0||_{\mathcal{W}^{1,2}(\mathcal{X}_1)} + c\int_0^t \mathsf{e}^{(\lambda_1+p)(t-t_1)}(t-t_1)^{-\frac{1}{2}}(\tilde{\ell}||\tilde{u}(t_1)+z(t_1)||_{\mathcal{W}^{1,2}(\mathcal{X}_1)})\mathsf{d}t_1, \end{aligned}$$

for which we have assumed R large enough to have $\sup_{t\in[0,T]} ||\tilde{u}(t)+z(t)||_{\mathcal{W}^{1,2}(\mathcal{X}_1)} < R$. By [54, Proposition 3.1] we can consider the set

$$\Omega_2 := \left\{\omega \in \Omega : \sup_{t\in[0,T]} ||z(t)||_{\mathcal{W}^{1,2}(\mathcal{X}_1)} \leq \eta\right\} \in \mathcal{F}_0^T,$$

which has positive probability. Since $\Omega_1 \in \mathcal{F}_{-\infty}^0$ and $\Omega_2 \in \mathcal{F}_0^T$, they are independent and the set

$$\Omega_0 := \Omega_1 \cap \Omega_2 \in \mathcal{F}_{-\infty}^T$$

has also positive probability measure. We therefore fix $\omega \in \Omega_0$ and derive from (7.2.3)

$$\begin{aligned} ||\tilde{u}(t)||_{\mathcal{W}^{1,2}(\mathcal{X}_1)} \leq& \mathsf{e}^{(\lambda_1+p)t}||\tilde{u}_0||_{\mathcal{W}^{1,2}(\mathcal{X}_1)} + \tilde{\ell}\eta c\int_0^t \mathsf{e}^{(\lambda_1+p)(t-t_1)}(t-t_1)^{-\frac{1}{2}}\mathsf{d}t_1\\ &+ \tilde{\ell}c\int_0^t \mathsf{e}^{(\lambda_1+p)(t-t_1)}(t-t_1)^{-\frac{1}{2}}||\tilde{u}(t_1)||_{\mathcal{W}^{1,2}(\mathcal{X}_1)}\mathsf{d}t_1, \end{aligned}$$

and then

$$\begin{aligned} \mathsf{e}^{-(\lambda_1+p)t}||\tilde{u}(t)||_{\mathcal{W}^{1,2}(\mathcal{X}_1)} \leq& ||\tilde{u}_0||_{\mathcal{W}^{1,2}(\mathcal{X}_1)} + \tilde{\ell}\eta c\int_0^t \mathsf{e}^{-(\lambda_1+p)t_1}(t-t_1)^{-\frac{1}{2}}\mathsf{d}t_1\\ &+ \tilde{\ell}c\int_0^t \mathsf{e}^{-(\lambda_1+p)t_1}(t-t_1)^{-\frac{1}{2}}||\tilde{u}(t_1)||_{\mathcal{W}^{1,2}(\mathcal{X}_1)}\mathsf{d}t_1. \qquad (7.2.4) \end{aligned}$$

The rest of the proof is equivalent to the steps in [31, Proposition 2.7], where it is proven that the right-hand side in (7.2.4) is bounded by $c_1\eta$, for $c_1 > 0$ that does not depend on t but is dependent on T, by assuming $\tilde{u}_0 = a(\omega)$. □

We define now, for $\mathbf{v} = v_1 \wedge ... \wedge v_k$ and $\mathbf{w} = w_1 \wedge ... \wedge w_k \in \wedge^k\mathcal{H}_1$,

$$\mathfrak{D}_\delta^{(k)}(\mathbf{v},\mathbf{w}) := \delta\big(\Pi_{\mathbf{i}_0}\mathbf{v},\mathbf{w}\big) - \big(\Pi_{\mathbf{i}_0}^{\perp}\mathbf{v},\mathbf{w}\big)$$

with $\Pi_{\mathbf{i}}$ denoting the projection on $\mathbf{e}_{\mathbf{i}} := e_{i_1} \wedge ... \wedge e_{i_k}$, $\mathbf{i} = \{i_1, ..., i_k\}$ and $\mathbf{i}_0 = \{1, ..., k\}$ aside from permutations. The scalar product present in such a construction is defined in (7.1.2). In the next proof we make use of $\Lambda_{\mathbf{i}_0} := \sum_{j=1}^{k}(p + \lambda_{i_j})$.

Lemma 7.2.3. *Let $T > 0$, $0 < \epsilon \ll \frac{1}{k}(\lambda_k - \lambda_{k+1})$ be fixed, and $\omega \in \Omega$ be an event with the property that the nonlinear term $B^t_\omega := -3a(\theta^t\omega)^2$ satisfies*

$$||B^t_\omega||_{\mathcal{W}^{1,2}(\mathcal{X}_1)} \leq \epsilon$$

for all $t \in [0,T]$. Finally, assume that $\boldsymbol{v}_0 = v^1_0 \wedge ... \wedge v^k_0 \in \wedge^k\mathcal{H}_1$ satisfies $\mathfrak{D}^{(k)}_\delta(\boldsymbol{v}_0) > 0$ for $\delta > 0$ for which

$$\epsilon(1+\delta)k \leq \Lambda_{\boldsymbol{i}_0} - \Lambda_{\boldsymbol{i}} - \frac{\epsilon(1+\delta)k}{\delta},$$

for all $\boldsymbol{i} \neq \boldsymbol{i}_0$. Under these conditions, the k-blade $\boldsymbol{v}_t := \wedge^k D_{a(\omega)}\varphi^t_\omega(\boldsymbol{v}_0)$, corresponding to the solutions $v^j_t = D_{a(\omega)}\varphi^t_\omega(v^j_0)$ of the first variation equation with initial condition set at v^j_0 for $j \in \{1,...,k\}$ and assumed at time $t > 0$, satisfies the inequality

$$\frac{1}{2}\frac{d}{dt}\mathfrak{D}^{(k)}_\delta(\boldsymbol{v}_t) \geq \left(\Lambda_{\boldsymbol{i}_0} - \frac{(1+\delta)k\epsilon}{\delta}\right)\mathfrak{D}^{(k)}_\delta(\boldsymbol{v}_t). \tag{7.2.5}$$

Proof. We know that

$$|\mathfrak{D}^{(k)}_\delta(\mathbf{v},\mathbf{w})| \leq (1+\delta)||\mathbf{v}||_{\wedge^k\mathcal{H}_1}||\mathbf{w}||_{\wedge^k\mathcal{H}_1}.$$

We then denote $v_j = v^j_t = \mathsf{D}_{a(\omega)}\varphi^t_\omega(v^j_0)$. For the multiplication operator B^t_ω we use the hypothesis $||B^t_\omega||_{\mathcal{W}^{1,2}(\mathcal{X}_1)} \leq \epsilon$ which implies that $||B^t_\omega v|| \leq \epsilon||v||$ for any $v \in \mathcal{H}_1$. Therefore, we obtain

$$\begin{aligned}
&\frac{1}{2}\frac{\mathsf{d}}{\mathsf{d}t}\mathfrak{D}^{(k)}_\delta(v_1\wedge...\wedge v_k, v_1\wedge...\wedge v_k)\\
=&\sum_{j=1}^k \mathfrak{D}^{(k)}_\delta(v_1\wedge...\wedge v_k, v_1\wedge...\wedge v_{j-1}\wedge\dot{v}_j\wedge v_{j+1}\wedge...\wedge v_k)\\
=&\sum_{j=1}^k \mathfrak{D}^{(k)}_\delta(v_1\wedge...\wedge v_k, v_1\wedge...\wedge v_{j-1}\wedge(\Delta - g + p + B^t_\omega)v_j\wedge v_{j+1}\wedge...\wedge v_k)\\
\geq&\sum_{j=1}^k \mathfrak{D}^{(k)}_\delta(v_1\wedge...\wedge v_k, v_1\wedge...\wedge v_{j-1}\wedge(\Delta - g + p)v_j\wedge v_{j+1}\wedge...\wedge v_k)\\
&-\epsilon(1+\delta)k||v_1\wedge...\wedge v_k||^2_{\wedge^k\mathcal{H}_1}.
\end{aligned}$$

We know the existence of some coefficients $\rho_{\mathbf{i}}$ such that

$$v_1\wedge...\wedge v_k = \sum_{\mathbf{i}}\rho_{\mathbf{i}}\mathbf{e}_{\mathbf{i}}$$

holds. This entails that

$$\mathfrak{D}^{(k)}_\delta(v_1\wedge...\wedge v_k, v_1\wedge...\wedge v_{j-1}\wedge(\Delta-g+p)v_j\wedge v_{j+1}\wedge...\wedge v_k) = \sum_{\mathbf{i},\mathbf{i}'}\rho_{\mathbf{i}}\rho_{\mathbf{i}'}(p+\lambda_{i'_j})\mathfrak{D}^{(k)}_\delta(\mathbf{e}_{\mathbf{i}},\mathbf{e}_{\mathbf{i}'}),$$

for which

$$\mathfrak{D}^{(k)}_\delta(\mathbf{e}_{\mathbf{i}},\mathbf{e}_{\mathbf{i}'}) = \begin{cases} 0, & \text{if} \quad \mathbf{i} \neq \mathbf{i}', \\ \delta, & \text{if} \quad \mathbf{i} = \mathbf{i}' = \mathbf{i}_0, \\ -1, & \text{if} \quad \mathbf{i} = \mathbf{i}' \neq \mathbf{i}_0. \end{cases}$$

We can obtain, therefore,

$$\mathfrak{D}_\delta^{(k)}(v_1\wedge...\wedge v_k, v_1\wedge...\wedge v_{j-1}\wedge(\Delta-g+p)v_j\wedge v_{j+1}\wedge...\wedge v_k) = \delta(p+\lambda_j)\rho_{\mathbf{i}_0}^2 - \sum_{\mathbf{i}\neq\mathbf{i}_0}\rho_{\mathbf{i}}^2(p+\lambda_{i_j})$$

and

$$\sum_{j=1}^{k}\mathfrak{D}_\delta^{(k)}(v_1\wedge...\wedge v_k, v_1\wedge...\wedge v_{j-1}\wedge(\Delta-g+p)v_j\wedge v_{j+1}\wedge...\wedge v_k) = \delta\Lambda_{\mathbf{i}_0}\rho_{\mathbf{i}_0}^2 - \sum_{\mathbf{i}\neq\mathbf{i}_0}\Lambda_{\mathbf{i}}\rho_{\mathbf{i}}^2.$$

This gives us the following result:

$$\begin{aligned}\frac{1}{2}\frac{\mathsf{d}}{\mathsf{d}t}\mathfrak{D}_\delta^{(k)}(v_1\wedge...\wedge v_k, v_1\wedge...\wedge v_k) &\geq \delta\Lambda_{\mathbf{i}_0}\rho_{\mathbf{i}_0}^2 - \sum_{\mathbf{i}\neq\mathbf{i}_0}\Lambda_{\mathbf{i}}\rho_{\mathbf{i}}^2 - \epsilon(1+\delta)k\sum_{\mathbf{i}}\rho_{\mathbf{i}}^2\\ &= \delta\left(\Lambda_{\mathbf{i}_0} - \frac{\epsilon(1+\delta)k}{\delta}\right)\rho_{\mathbf{i}_0}^2 - \sum_{\mathbf{i}\neq\mathbf{i}_0}(\Lambda_{\mathbf{i}}+\epsilon(1+\delta)k)\rho_{\mathbf{i}}^2.\end{aligned}$$

Hence, for parameters that satisfy

$$\epsilon(1+\delta)k \leq \Lambda_{\mathbf{i}_0} - \Lambda_{\mathbf{i}} - \frac{\epsilon(1+\delta)k}{\delta}$$

holds for all $\mathbf{i}\neq\mathbf{i}_0$, or equivalently,

$$\epsilon k\frac{(1+\delta)^2}{\delta} \leq \lambda_k - \lambda_{k+1},$$

we can deduce that

$$\frac{1}{2}\frac{\mathsf{d}}{\mathsf{d}t}\mathfrak{D}_\delta^{(k)}(v_1\wedge...\wedge v_k, v_1\wedge...\wedge v_k) \geq \delta\left(\Lambda_{\mathbf{i}_0} - \frac{\epsilon(1+\delta)k}{\delta}\right)\mathfrak{D}_\delta^{(k)}(v_1\wedge...\wedge v_k, v_1\wedge...\wedge v_k).$$

□

Theorem 7.2.4. *For any $k\geq 1$, $0<\eta\ll\lambda_k-\lambda_{k+1}$ and $T>0$, there exists $\Omega_0\subset\Omega$, a probability event of positive measure $\mathbb{P}$, such that*

$$\mathfrak{L}_k(t;\omega) \geq \sum_{j=1}^{k}\big(p+\lambda_j\big) - \eta$$

for all $\omega\in\Omega_0,\ t\in[0,T]$.

Proof. Lemma 7.2.2 proves for any $\epsilon>0$ the existence of a set $\Omega_0\subset\Omega$ so that for all $\omega\in\Omega_0$ we have the bound $||a(\theta^t\omega)||_{\mathcal{W}^{1,2}(\mathcal{X}_1)}<\epsilon$ for $t\in[0,T]$. Such a result, along with the fact that $\mathcal{W}^{1,2}(\mathcal{X}_1)$ is a Banach algebra and a subset of $L^2(\mathcal{X}_1)$, satisfies the first hypothesis of Lemma 7.2.3. Precisely, for any $\epsilon>0$ we obtain $\mathbb{P}\Big(\{||B_\omega^t||_{\mathcal{W}^{1,2}(\mathcal{X}_1)}<\epsilon, \text{for all } t\in[0,T]\}\Big)>0$.

From Lemma 7.2.3, we know that $\mathfrak{D}_\delta^{(k)}(\mathbf{v}_0)>0$ implies $\mathfrak{D}_\delta^{(k)}(\mathbf{v}_t)>0$ for all $t\in[0,T]$ and, assuming $\delta=\sqrt{\epsilon}\ll 1$ in (7.2.5),

$$\frac{1}{2}\frac{\mathsf{d}}{\mathsf{d}t}\mathfrak{D}_\delta^{(k)}(\mathbf{v}_t) \geq (\Lambda_{\mathbf{i}_0}-2k\delta)\mathfrak{D}_\delta^{(k)}(\mathbf{v}_t).$$

This result gives

$$\mathfrak{D}_\delta^{(k)}(\mathbf{v}_t) \geq \exp\{(\Lambda_{\mathbf{i}_0}-2k\delta)t\}\mathfrak{D}_\delta^{(k)}(\mathbf{v}_0). \tag{7.2.6}$$

We take $\mathbf{v}_0 \in \wedge^k \mathcal{H}_1$ and $M > 1$ such that $\mathfrak{D}^{(k)}_{\frac{\delta}{M}}(\mathbf{v}_0) \geq 0$.[3] It follows that

$$\mathfrak{D}^{(k)}_{\delta}(\mathbf{v}_0) = \delta||\Pi_{\mathbf{i}_0}\mathbf{v}_0||^2_{\wedge^k\mathcal{H}_1} - ||\Pi^{\perp}_{\mathbf{i}_0}\mathbf{v}_0||^2_{\wedge^k\mathcal{H}_1} = \delta\Big(1-\frac{1}{M}\Big)||\Pi_{\mathbf{i}_0}\mathbf{v}_0||^2_{\wedge^k\mathcal{H}_1} + \mathfrak{D}^{(k)}_{\frac{\delta}{M}}(\mathbf{v}_0) \geq \frac{\delta(M-1)}{M}||\Pi_{\mathbf{i}_0}\mathbf{v}_0||^2_{\wedge^k\mathcal{H}_1}.$$

Since $\mathfrak{D}^{(k)}_{\frac{\delta}{M}}(\mathbf{v}_0) \geq 0$ we know that $||\mathbf{v}_0||^2_{\wedge^k\mathcal{H}_1} \leq (1+\frac{\delta}{M})||\Pi_{\mathbf{i}_0}\mathbf{v}_0||^2_{\wedge^k\mathcal{H}_1}$ and, therefore,

$$\mathfrak{D}^{(k)}_{\delta}(\mathbf{v}_0) \geq \frac{\delta(M-1)}{M\big(1+\frac{\delta}{M}\big)}||\mathbf{v}_0||^2_{\wedge^k\mathcal{H}_1} = \frac{\delta(M-1)}{M+\delta}||\mathbf{v}_0||^2_{\wedge^k\mathcal{H}_1}. \tag{7.2.7}$$

From $\mathfrak{D}^{(k)}_{\delta}(\mathbf{v}_t) \leq \delta||\mathbf{v}_t||^2_{\wedge^k\mathcal{H}_1}$, and using (7.2.6) and (7.2.7), we obtain

$$||\mathbf{v}_t||^2_{\wedge^k\mathcal{H}_1} \geq \frac{M-1}{M+\delta}\exp\{(\Lambda_{\mathbf{i}_0} - 2k\delta)t\}||\mathbf{v}_0||^2_{\wedge^k\mathcal{H}_1}.$$

The proof is complete considering Lemma 7.2.2, the fact that the prefactor can be close to 1 for $M \to +\infty$ and taking $\eta = 2k\delta \ll \lambda_k - \lambda_{k+1}$ with $\delta = \sqrt{\epsilon}$. □

Remark. Theorems $7.2.1$ and $7.2.4$ prove that the right extreme of the interval of the possible values assumed by $\mathfrak{L}_k$ is $\Lambda_{\mathbf{i}_0}$. In particular for $k = 1$ it is $p + \lambda_1$.

For $k > 1$ the value of p that satisfies $\Lambda_{\mathbf{i}_0} = 0$ is not corresponding to $-\lambda_k$, therefore the change of sign of the highest possible value assumed by $\mathfrak{L}_k$ is not associated with a bifurcation event. The fact that $\frac{1}{k}\sum_{j=1}^{k}\lambda_j > \lambda_k$ implies that $\Lambda_{\mathbf{i}_0} = 0$ is satisfied for $p < -\lambda_k$, i.e., before the k-th bifurcation threshold.

Remark. The introduction of the heterogeneous term g in (7.0.1) induces a change of value in the bifurcation thresholds $\{-\lambda_k\}_{k\in\mathbb{N}_{>0}}$ but maintains their existence. For any $k \in \mathbb{N}_{>0}$ there is a dependence on $\Lambda_{\mathbf{i}_0}$ of g for all $p \in \mathbb{R}$ and, moreover, the choice of g shifts the values of p at which the highest possible value of $\mathfrak{L}_k$ changes sign.

7.3 Summary

Complementing the variance-based early-warning indicators discussed in Chapter 3, we analyse the behaviour of the highest extreme of FTLEs as the critical parameter in a space-heterogeneous Chafee-Infante approach that approaches the bifurcation point under perturbations driven by additive noise. Our results show that such extremes reach zero at a rate that is precisely the reciprocal of the variance divergence rate described in Chapter 3. This inverse relationship emerges despite the fundamentally different techniques used in each study: variational analysis for the corresponding FTLE and stochastic linearisation for the time-asymptotic variance. This underscores a deep mathematical connection between dynamical sensitivity and statistical fluctuations.

The convergence of observable to zero signals a loss of exponential stability and is tightly coupled to the increase in noise-induced variance. These insights motivate the conjecture that similar relationships hold across a wide range of bifurcation scenarios, especially where the deterministic system features a single-eigenvalue crossing instability, in contrast with the setting in Chapter 4.

[3] Note that for any $\frac{\delta}{M} > 0$ this can be satisfied in a neighborhood of $\mathbf{v}_0 = \mathbf{e}_{\mathbf{i}_0}$.

Part II

Noise-induced Tipping: Prediction of Transitions and Metastable Jumps

8 Upper bound to Transition Probability

In the this chapter we study the non-autonomous system

$$\begin{cases} \mathsf{d}u(x,t) = (\Delta u(x,t) + p(\epsilon t)u(x,t) - g(x)u(x,t) - u(x,t)^3)\,\mathsf{d}t + \sigma\, Q^{\frac{1}{2}}\mathsf{d}W_t, \\ u(\cdot,0) = u_0 \in \mathcal{H}_1 = L^2(\mathcal{X}_1), \\ u(0,t) = u(L,t) = 0,\ \forall t \geq 0 \end{cases} \tag{8.0.1}$$

with the noise intensity $\sigma > 0$ and g a continuous almost everywhere positive function in $\mathcal{X}_1 = [0, L]$ as defined in (3.0.1). We use an equivalent notation as the one employed in the introduction of Chapter 3. In particular, we label the operator $A = \Delta - g$. Its ordered eigenvalues are $\{\lambda_n\}_{n\in\mathbb{N}_{>0}}$ and the eigenvalues of Δ are $\left\{\lambda'_n := -\left(\frac{\pi n}{L}\right)^2\right\}_{n\in\mathbb{N}_{>0}}$. We refer to the corresponding eigenfunctions with $\{e_n\}_{n\in\mathbb{N}_{>0}}$ and $\{e'_n\}_{n\in\mathbb{N}_{>0}}$, respectively. Furthermore, the eigenvalues $\{\zeta_j\}_{j\in\mathbb{N}_{>0}}$ and eigenfunctions $\{b_j\}_{j\in\mathbb{N}_{>0}}$ of the covariance operator Q are assumed to satisfy the properties (M1) and (M2) to obtain the existence and uniqueness in $L^2(\Omega, \mathcal{F}, \mathbb{P}; \mathcal{H}_1)$ of the mild solution of (8.0.1) for any $t > 0$ through Theorem 2.2.1, Theorem 2.2.6 and Appendix B. However, we assume $p \in C([0, \tau])$ for a given $\tau > 0$ and $0 < \epsilon \ll 1$. The slow dependence on time is in accordance with the fact that in simulations of realistic applications, the previous parameter p in (3.0.1) is not constant but slowly changing; see also [90]. For a fixed ϵ, we assume $p(\epsilon t) < -\lambda_1$ in $0 \leq \epsilon t \leq \tau$. Therefore, we study the system before the first non-autonomous bifurcation. The content of this chapter is an excerpt of [23]. First, following the methods used in [17, 19] we aim to gain insight on the probabilistic properties of the first time in which the solutions of (8.0.1), with u_0 close to the null function, get driven apart from a chosen solution of the equivalent deterministic system, i.e., (8.0.1) with $\sigma = 0$. This is achieved by taking as a metric the distance induced by a fractional Sobolev norm of small degree. Lastly, we use the obtained bound to briefly construct moment estimates of such an aleatory time.

In this chapter we use the Landau notation on scalars $\rho_1 \in \mathbb{R},\ \rho_2 > 0$ as $\rho_1 = O(\rho_2)$ if there exists a constant $c > 0$ that satisfies $|\rho_1| \leq c\rho_2$. Such a constant is independent of ϵ and σ; however, it depends on g and p. We also employ the relation symbol $\sim$ to indicate that the positive scalars ρ_1 and ρ_2 satisfy $0 < \lim_{\rho_2\to\infty} \frac{\rho_1}{\rho_2} < \infty$ and that two the sequences $\{\rho^1_k\}_{k\in\mathbb{N}\setminus\{0\}} \subset \mathbb{R}$ and $\{\rho^2_k\}_{k\in\mathbb{N}\setminus\{0\}} \subset \mathbb{R}_{>0}$ satisfy $0 < \lim_{k\to\infty} \frac{\rho^1_k}{\rho^2_k} < \infty$. Furthermore, the symbol $\propto$ refers to proportionality of the terms for a constant dependent on g.

The first equation in (8.0.1) can be studied for the slow time ϵt setting, named again for convenience t, giving the form

$$\mathsf{d}u(x,t) = \frac{1}{\epsilon}(\Delta u(x,t) + p(t)u(x,t) - g(x)u(x,t) - u(x,t)^3)\,\mathsf{d}t + \frac{\sigma}{\sqrt{\epsilon}}\, Q^{\frac{1}{2}}\mathsf{d}W_t$$

through rescaling of time.

We denote the A^s-norm of power $s \geq 0$ of any function $\phi = \sum_{k=1}^{\infty} \rho_k e_k \in \mathcal{H}_1$ with $\{\rho_k\}_{k\in\mathbb{N}_{>0}} \subset \mathbb{R}$ as

$$||\phi||^2_{A^s} := \sum_{k=1}^{\infty} (-\lambda_k)^s \rho_k^2.$$

The functions in $\mathcal{H}_1$ that present finite A^s-norm define the space $\mathcal{W}^{s,2}(\mathcal{X}_1)$. In fact, the A^s-norm is equivalent to the fractional Sobolev norm on $\mathcal{W}^{s,2}(\mathcal{X}_1)$ under Dirichlet conditions,

$$||\phi||^2_{\mathcal{W}^{s,2}(\mathcal{X}_1)} := \sum_{k=1}^{\infty}(-\lambda'_k)^s\langle\phi, e'_k\rangle^2.$$

Such a result follows from the fact that, as shown in Appendix A, $\mathcal{D}((-\Delta)^{\frac{1}{2}}) = \mathcal{D}((-A)^{\frac{1}{2}})$ and from the characterisation of interpolation spaces described by [146, Theorem 4.36]. In particular, it implies that

$$\mathcal{W}_0^{s,2}(\mathcal{X}_1) := \mathcal{D}((-A)^{\frac{s}{2}}).$$

For simplicity, we assume $g(x) \geq 1$ for all $x \in \mathcal{X}_1$, so that for any couple of parameters $0 \leq s < s_1$ and $\phi \in \mathcal{W}^{s_1,2}(\mathcal{X}_1)$, $||\phi||_{A^s} \leq ||\phi||_{A^{s_1}}$. The following lemma shows an important property, a Young-type inequality, of the A^s-norms, which we exploit further in the chapter.

Lemma 8.0.1. *Set* $0 < r, s$ *and* $0 < q < \frac{1}{2}$ *so that* $q + \frac{1}{2} < r + s$*. Then, there exists* $c(r, s, q) > 0$ *for which*

$$||\phi_1\phi_2||_{A^q} \leq c(r, s, q)||\phi_1||_{A^r}||\phi_2||_{A^s}, \tag{8.0.2}$$

for any $\phi_1 \in \mathcal{W}^{r,2}(\mathcal{X}_1)$ *and* $\phi_2 \in \mathcal{W}^{s,2}(\mathcal{X}_1)$*.*

Proof. The equivalence of the A^{s_1}-norm and the $\mathcal{W}^{s_1,2}$-norm for any $0 \leq s_1 \leq 1$ justifies the study of (8.0.2) for the $\mathcal{W}^{s_1,2}$-norms. Then, for any $\phi \in \mathcal{H}_1$ we can rewrite the series

$$\phi(x) = \sum_{k=1}^{\infty}\langle\phi, e'_k\rangle e'_k(x) = \sum_{k=-\infty}^{\infty}\tilde{\rho}_k\frac{1}{\sqrt{L}}\mathsf{e}^{\mathsf{i}\frac{\pi k}{L}x}$$

for $\tilde{\rho}_k := -\dfrac{\mathrm{sign}(k)\mathsf{i}}{\sqrt{2}}\langle\phi, e'_k\rangle$, $\tilde{\rho}_0 = 0$.[1] Furthermore, it is easy to prove that for any $0 \leq s_1 \leq 1$

$$||\phi||^2_{\mathcal{W}^{s_1,2}(\mathcal{X}_1)} = \sum_{k=-\infty}^{\infty}(-\lambda'_k)^{s_1}|\tilde{\rho}_k|^2.$$

Since the product of any couple of elements in $\left\{\frac{1}{\sqrt{L}}\mathsf{e}^{\mathsf{i}\frac{\pi k}{L}x}\right\}_{k\in\mathbb{Z}}$ is proportional to another member of the set, we can apply the Young-type inequality in [18, Lemma 4.3] which implies the existence of a constant $c'(r, s, q)$ that satisfies

$$||\phi_1\phi_2||_{\mathcal{W}^{q,2}(\mathcal{X}_1)} \leq c'(r, s, q)||\phi_1||_{\mathcal{W}^{r,2}(\mathcal{X}_1)}||\phi_2||_{\mathcal{W}^{s,2}(\mathcal{X}_1)},$$

for any $\phi_1 \in \mathcal{W}^{r,2}(\mathcal{X}_1)$ and $\phi_2 \in \mathcal{W}^{s,2}(\mathcal{X}_1)$. From the equivalence of the A^s-norms and the $\mathcal{W}^{s,2}$-norms, we can state that there exists $c(r, s, q) > 0$ that satisfies the aimed inequality. □

From the fact that $p(t) < -\lambda_1$ for $t < \tau$, we know that any mild solution $\bar{u}$ of the deterministic problem

$$\begin{cases}\mathsf{d}\bar{u}(x,t) = \dfrac{1}{\epsilon}(\Delta\bar{u}(x,t) + p(t)\bar{u}(x,t) - g(x)\bar{u}(x,t) - \bar{u}(x,t)^3)\,\mathsf{d}t,\\ \bar{u}(0,t) = \bar{u}(L,t) = 0,\ \forall t \geq 0,\end{cases} \tag{8.0.3}$$

with initial conditions in $\mathcal{H}_1$, approaches the null function exponentially in $\mathcal{H}_1$ in time $0 \leq t \leq \tau$. Furthermore, following the proof of [19, Proposition 2.3], we prove equivalent results for the A^1-norm in the next Proposition.

[1] Note that $\left\{\frac{1}{\sqrt{L}}\mathsf{e}^{\mathsf{i}\frac{\pi k}{L}x}\right\}_{k\in\mathbb{Z}}$ is not a basis of $\mathcal{H}_1$, therefore it is not a Parseval identity on such a space.

Proposition 8.0.2. *Given $\bar{u}$, a mild solution of* (8.0.3) *such that* $||\bar{u}(\cdot,0)||_A := ||\bar{u}(\cdot,0)||_{A^1} \leq \delta$*, then*

$$||\bar{u}(\cdot,t)||_A \leq \delta$$

holds for all $0 \leq t \leq \tau$*. Furthermore,* $||\bar{u}(\cdot,t)||_A$ *approaches* 0 *exponentially in* $0 \leq t \leq \tau$*.*

Proof. We define the Lyapunov function

$$F_{\mathsf{L}}(\phi) := \frac{1}{2}\Big(||\nabla\phi||^2_{\mathcal{W}^{1,2}(\mathcal{X}_1)} + ||g^{\frac{1}{2}}\phi||^2_{\mathcal{W}^{1,2}(\mathcal{X}_1)}\Big) = \frac{1}{2}\langle -A\phi, \phi\rangle$$

for any $\phi \in \mathcal{W}^{1,2}(\mathcal{X}_1)$. Therefore, we obtain

$$\begin{aligned}
&\frac{\mathsf{d}}{\mathsf{d}t}F_{\mathsf{L}}(\bar{u}) = -\langle A\bar{u}, \partial_t\bar{u}\rangle = \frac{1}{\epsilon}\Big(- ||A\bar{u}||^2_{\mathcal{W}^{1,2}(\mathcal{X}_1)} - p(t)\langle A\bar{u}, \bar{u}\rangle + \langle A\bar{u}, \bar{u}^3\rangle\Big)\\
=&\frac{1}{\epsilon}\Big(- \langle (A-\lambda_1)\bar{u}, A\bar{u}\rangle - (p(t)+\lambda_1)\langle A\bar{u}, \bar{u}\rangle + \langle A\bar{u}, \bar{u}^3\rangle\Big)\\
\leq&\frac{1}{\epsilon}\Big(- (p(t)+\lambda_1)\langle A\bar{u}, \bar{u}\rangle + \langle A\bar{u}, \bar{u}^3\rangle\Big) = \frac{2}{\epsilon}(p(t)+\lambda_1)F_{\mathsf{L}}(\bar{u}) + \frac{1}{\epsilon}\langle A\bar{u}, \bar{u}^3\rangle\\
=&\frac{2}{\epsilon}(p(t)+\lambda_1)F_{\mathsf{L}}(\bar{u}) - \frac{3}{\epsilon}\langle \nabla\bar{u}, \bar{u}^2\nabla\bar{u}\rangle - \frac{1}{\epsilon}||g^{\frac{1}{2}}\bar{u}^2||^2_{\mathcal{W}^{1,2}(\mathcal{X}_1)} \leq \frac{2}{\epsilon}(p(t)+\lambda_1)F_{\mathsf{L}}(\bar{u})
\end{aligned}$$

by using the min-max principle in

$$-\langle (A-\lambda_1)\bar{u}, A\bar{u}\rangle = \langle -A(A-\lambda_1)\bar{u}, \bar{u}\rangle \leq 0.$$

We have then shown that, given initial condition $\bar{u}(\cdot,0) = u_0 \in \mathcal{H}_1$,

$$F_{\mathsf{L}}(\bar{u}(\cdot,t)) \leq F_{\mathsf{L}}(u_0)\mathsf{e}^{-\frac{2c_1}{\epsilon}t}$$

holds for a constant $c_1 > 0$. The result follows since the norm defined by F_{L} is equivalent to $||\cdot||_A$. □

Given a function $\bar{u}$ that satisfies Proposition 8.0.2 for a fixed $\delta > 0$, we define the set in $\mathcal{W}^{1,2}(\mathcal{X}_1)$,

$$\mathcal{B}(h) := \{(t,\phi) \in [0,\tau] \times \mathcal{W}^{1,2}(\mathcal{X}_1) : \ ||\phi - \bar{u}||_{A^s} < h\}$$

for $s, h > 0$. The first-exit time from $\mathcal{B}(h)$ is the stopping time

$$\tau_{\mathcal{B}(h)} := \mathsf{inf}\{t > 0 : (t, u(\cdot,t)) \notin \mathcal{B}(h)\}.$$

With these definitions, we obtain an estimate for the probability of transition outside of the defined neighbourhood $\mathcal{B}(h)$ over a finite timescale.

Theorem 8.0.3. *We set* $\zeta_* = \sup_{j\in\mathbb{N}_{>0}}\{\zeta_j\}$*. Then, for any* $0 < s < \frac{1}{2}$ *and* $\epsilon, \nu > 0$ *there exist the positive constants and parameters* $\delta_0, \kappa = \kappa(s), h_1$ *and* $C_{\frac{h^2}{\zeta_*\sigma^2}}(\kappa, T, \epsilon, s)$ *for which, given* $0 < \sqrt{\zeta_*}\sigma \ll h < h_1\epsilon^\nu$ *and a function* $\bar{u}$ *that solves* (8.0.3) *and* $||\bar{u}(\cdot,0)||_A \leq \delta_0$*, the solution of* (8.0.1) *with* $u_0 = \bar{u}(\cdot,0)$ *satisfies*

$$\mathbb{P}\Big(\tau_{\mathcal{B}(h)} < T\Big) \leq C_{\frac{h^2}{\zeta_*\sigma^2}}(\kappa, T, \epsilon, s)\mathsf{exp}\Bigg\{ - \kappa\frac{h^2}{\zeta_*\sigma^2}\Big(1 - O\Big(\frac{h}{\epsilon^\nu}\Big)\Big)\Bigg\},$$

for any $0 \leq T \leq \tau$*.*

The inequality obtained in the previous theorem does not require $h^2 \gg \zeta_*\sigma^2$, but such an assumption simplifies the dependence of $C_{\frac{h^2}{\zeta_*\sigma^2}}(\kappa, T, \epsilon, s)$ on $\frac{h^2}{\zeta_*\sigma^2}$, otherwise nontrivial, and enables further study of the moments of the exit-time.

The proof of such an error estimate is based on [19, Proposition 2.4]. It is comprised of the study of the linear problem obtained from (8.0.1) and the extension of the results to the nonlinear cases. These steps are discussed in the following section.

8.1 Proof of error estimate

We define $\psi := u - \bar{u}$ for u the mild solution of (8.0.1) and $\bar{u}$ the mild solution of (8.0.3) with initial conditions

$$\bar{u}(\cdot, 0) = u(\cdot, 0) = u_0.$$

Then, ψ is the mild solution of

$$\begin{cases} \mathrm{d}\psi(x,t) = \dfrac{1}{\epsilon}\big(\Delta\psi(x,t) + p(t)\psi(x,t) - g(x)\psi(x,t) - (u(x,t)^3 - \bar{u}(x,t)^3)\big)\,\mathrm{d}t + \dfrac{\sigma}{\sqrt{\epsilon}}\,Q^{\frac{1}{2}}\mathrm{d}W_t, \\ \psi(x,0) = 0,\ \forall x \in \mathcal{X}_1 \\ \psi(0,t) = \psi(L,t) = 0,\ \forall t \geq 0. \end{cases} \tag{8.1.1}$$

The first equation of the system (8.1.1) is equivalent, by Taylor's formula, to

$$\mathrm{d}\psi(x,t) = \Big(\Delta\psi(x,t) + p(\epsilon t)\psi(x,t) - g(x)\psi(x,t) - 3\bar{u}(x,t)^2\psi(x,t) + G(\psi(x,t))\Big)\,\mathrm{d}t + \sigma\,Q^{\frac{1}{2}}\mathrm{d}W_t,$$

with

$$G(\psi) := \frac{1}{2}\partial_\phi^2\Big(-\phi^3\Big)\Big|_{\bar{u}+\eta\psi}\psi^2 = -3(\bar{u} + \eta\psi)\psi^2 \tag{8.1.2}$$

for a certain $0 < \eta < 1$.

8.1.1 Linear case

We call ψ_0 the mild solution of

$$\begin{cases} \mathrm{d}\psi_0(x,t) = \dfrac{1}{\epsilon}(\Delta\psi_0(x,t) + p(t)\psi_0(x,t) - g(x)\psi_0(x,t))\,\mathrm{d}t + \dfrac{\sigma}{\sqrt{\epsilon}}\,Q^{\frac{1}{2}}\mathrm{d}W_t, \\ \psi_0(\cdot,0) \equiv 0 \in \mathcal{H}_1, \\ \psi_0(0,t) = \psi_0(L,t) = 0,\ \forall t \geq 0. \end{cases} \tag{8.1.3}$$

Then, $\psi_k := \langle \psi_0, e_k \rangle$ satisfies

$$\begin{aligned} \mathrm{d}\psi_k(t) &= \frac{1}{\epsilon}(\lambda_k\psi_k(t) + p(t)\psi_k(t))\,\mathrm{d}t + \frac{\sigma}{\sqrt{\epsilon}}\,\mathrm{d}\langle W_t, e_k\rangle \\ &= \frac{1}{\epsilon}(\lambda_k\psi_k(t) + p(t)\psi_k(t))\,\mathrm{d}t + \frac{\sigma}{\sqrt{\epsilon}}\,\mathrm{d}\Big(\sum_{j=1}^{\infty}\sqrt{\zeta_j}\beta_j(t)\langle b_j, e_k\rangle\Big), \end{aligned} \tag{8.1.4}$$

for a family of independent Wiener processes $\{\beta_j\}_{j\in\mathbb{N}_{>0}}$. We can now prove the following lemmas.

Lemma 8.1.1. *There exists a constant $c_0 > 0$ such that*

$$\mathrm{Var}(\psi_k(t)) \leq -c_0\zeta_*\frac{\sigma^2}{\lambda_k},$$

for $\zeta_* := \sup_j\{\zeta_j\}$, all $0 \leq t \leq \tau$ and $k \in \mathbb{N}_{>0}$.

Proof. By definition,

$$\begin{aligned}
&\mathsf{Var}(\psi_k(t)) = \frac{\sigma^2}{\epsilon}\int_0^t \Big\langle e_k, \mathsf{e}^{\frac{1}{\epsilon}\left(A(t-t_1)+\int_{t_1}^t p(t_2)\mathsf{d}t_2\right)} Q \mathsf{e}^{\frac{1}{\epsilon}\left(A(t-t_1)+\int_{t_1}^t p(t_2)\mathsf{d}t_2\right)} e_k \Big\rangle \mathsf{d}t_1 \\
=&\frac{\sigma^2}{\epsilon}\int_0^t \Big\langle \mathsf{e}^{\frac{1}{\epsilon}\left(\lambda_k(t-t_1)+\int_{t_1}^t p(t_2)\mathsf{d}t_2\right)} e_k, Q \mathsf{e}^{\frac{1}{\epsilon}\left(\lambda_k(t-t_1)+\int_{t_1}^t p(t_2)\mathsf{d}t_2\right)} e_k \Big\rangle \mathsf{d}t_1 \\
=&\frac{\sigma^2}{\epsilon}\int_0^t \mathsf{e}^{\frac{2}{\epsilon}\left(\lambda_k(t-t_1)+\int_{t_1}^t p(t_2)\mathsf{d}t_2\right)} \langle e_k, Q e_k\rangle \mathsf{d}t_1 \leq \frac{\sigma^2}{\epsilon}\zeta_* \int_0^t \mathsf{e}^{\frac{2}{\epsilon}\left(\lambda_k + \max\limits_{0\leq t_2\leq\tau}\{p(t_2)\}\right)(t-t_1)} \mathsf{d}t_1 \\
=&-\zeta_* \frac{\sigma^2}{2\left(\lambda_k + \max\limits_{0\leq t_1\leq\tau}\{p(t_1)\}\right)}\left(1 - \mathsf{e}^{\frac{2}{\epsilon}\left(\lambda_k + \max\limits_{0\leq t_1\leq\tau}\{p(t_1)\}\right)t}\right) \leq -c_0\zeta_*\frac{\sigma^2}{\lambda_k},
\end{aligned}$$

for $0 \leq t \leq \tau$ and $k \in \mathbb{N}_{>0}$. □

The subsequent lemma relies on methods presented in [19] and part of the proof follows [16, Theorem 2.4]. Additional steps are required due to the fact that the eigenfunctions of A do not diagonalise Q.

Lemma 8.1.2. *Given $c^+ > 0$ and $0 \leq T \leq \tau$ for which $\lambda_k + \min\limits_{0\leq t\leq T}\{p(t)\} \geq c^+\lambda_k$ for all $k \in \mathbb{N}_{>0}$, then there exists a constant $\gamma_0 > 0$ that satisfies*

$$\mathbb{P}\left(\sup_{0\leq t\leq T}|\psi_k(t)| \geq h\right) \leq -\frac{2c^+\lambda_k T}{\gamma\epsilon}\exp\left\{\frac{\mathsf{e}^{-2\gamma}}{2c_0}\lambda_k\frac{h^2}{\zeta_*\sigma^2}\right\} \tag{8.1.5}$$

for any $0 < \gamma \leq \gamma_0$, for $\zeta_* := \sup\limits_j\{\zeta_j\}$ and c_0 obtained in Lemma 8.1.1.

Proof. For a fixed $k \in \mathbb{N}_{>0}$, the solution ψ_k of (8.1.4) is a Gaussian process. In fact, we have

$$\sum_{j=1}^{\infty}\sqrt{\zeta_j}\langle b_j, e_k\rangle\beta_j(t) = \sqrt{\sum_{j=1}^{\infty}\zeta_j\langle b_j, e_k\rangle^2}\beta(t) \tag{8.1.6}$$

for a Wiener process β and $0 \leq t \leq \tau$. The equation (8.1.6) can be proven with the following considerations.

- For any $0 \leq t \leq \tau$ and $n \in \mathbb{N}_{>0}$, we define $\Xi_n(t) = \sum\limits_{j=1}^{n}\sqrt{\zeta_j}\langle b_j, e_k\rangle\beta_j(t)$. Given the integers $n_1 > n_2 > 0$, it follows that

  $$\mathbb{E}\big(|\Xi_{n_1}(t) - \Xi_{n_2}(t)|^2\big) = t\sum_{j=n_2+1}^{n_1}\zeta_j\langle b_j, e_k\rangle^2 \leq \tau\sup_j\{\zeta_j\} = \tau\zeta_*.$$

  Hence, $\{\Xi_n(t)\}_n$ converges to a random variable $\Xi(t)$ in $L^2(\Omega, \mathcal{F}, \mathbb{P})$ for all $0 \leq t \leq \tau$.

- It is clear that

  $$\Xi(0) = 0$$

  and that the series has independent increments.

- The time increments of Ξ from t_1 to t_2 with $t_1 < t_2 \leq \tau$ are normally distributed with mean 0 and with variance $(t_2 - t_1)\sum\limits_{j=1}^{\infty}\zeta_j\langle b_j, e_k\rangle^2$. This can be proven through the Lévy continuity Theorem [27, Section 26] and the pointwise convergence in time of the characteristic functions of $\Xi_n(t)$.

- The almost sure continuity of Ξ is implied by the Borel-Cantelli Lemma [27, Section 4] and by the almost sure continuity of all elements in $\{\Xi_n\}_{n\in\mathbb{N}_{>0}}$.

From (8.1.4) and (8.1.6) we can state that ψ_k is represented by Duhamel's formula,

$$\psi_k(t) = \frac{\sigma}{\sqrt{\epsilon}} \sqrt{\sum_{j=1}^{\infty} \zeta_j \langle b_j, e_k \rangle^2} \int_0^t \mathsf{e}^{\frac{1}{\epsilon}\left(\lambda_k(t-t_1) + \int_{t_1}^t p(t_2)\mathsf{d}t_2\right)} \mathsf{d}\beta(t_1).$$

Due to the dependence on time t of $\lambda_k(t-t_1) + \int_{t_1}^t p(t_2)\mathsf{d}t_2$, ψ_k is not a martingale. Nonetheless, following [17, Proposition 3.1.5], we study the martingale $\mathsf{e}^{-\frac{1}{\epsilon}\left(\lambda_k t + \int_0^t p(t_1)\mathsf{d}t_1\right)}\psi_k$ and split the time interval through the times $0 = s_0 < s_1 < ... < s_N = T$. For convenience, we define for all $0 \leq t \leq T$, $D(t) := \lambda_k t + \int_0^t p(t_1)\mathsf{d}t_1$. We obtain that

$$\begin{aligned}
&\mathbb{P}\bigg(\sup_{0\leq t\leq T} |\psi_k(t)| \geq h \bigg) \\
=&\mathbb{P}\bigg(\sup_{0\leq t\leq T} \left| \frac{\sigma}{\sqrt{\epsilon}} \sqrt{\sum_{j=1}^{\infty} \zeta_j \langle b_j, e_k \rangle^2} \int_0^t \mathsf{e}^{\frac{1}{\epsilon}\left(\lambda_k(t-t_1) + \int_{t_1}^t p(t_2)\mathsf{d}t_2\right)} \mathsf{d}\beta(t_1) \right| \geq h \bigg) \\
=&\mathbb{P}\bigg(\exists j \in \{1,...,N\} : \sup_{s_{j-1}<t<s_j} \left| \frac{\sigma}{\sqrt{\epsilon}} \langle e_k, Qe_k \rangle^{\frac{1}{2}} \int_0^t \mathsf{e}^{\frac{1}{\epsilon}\left(D(t)-D(t_1)\right)} \mathsf{d}\beta(t_1) \right| \geq h \bigg) \\
\leq& \sum_{j=1}^{N} \mathbb{P}\bigg(\frac{\sigma}{\sqrt{\epsilon}} \langle e_k, Qe_k \rangle^{\frac{1}{2}} \sup_{s_{j-1}<t<s_j} \left| \int_0^t \mathsf{e}^{\frac{1}{\epsilon}\left(D(t)-D(t_1)\right)} \mathsf{d}\beta(t_1) \right| \geq h \bigg) \\
=&2\sum_{j=1}^{N} \mathbb{P}\bigg(\frac{\sigma}{\sqrt{\epsilon}} \langle e_k, Qe_k \rangle^{\frac{1}{2}} \sup_{s_{j-1}<t<s_j} \int_0^t \mathsf{e}^{\frac{1}{\epsilon}\left(D(t)-D(t_1)\right)} \mathsf{d}\beta(t_1) \geq h \bigg) \\
\leq&2\sum_{j=1}^{N} \mathbb{P}\bigg(\langle e_k, Qe_k \rangle^{\frac{1}{2}} \sup_{s_{j-1}<t<s_j} \int_0^t \mathsf{e}^{-\frac{1}{\epsilon}D(t_1)} \mathsf{d}\beta(t_1) \geq \inf_{s_{j-1}<t<s_j} \mathsf{e}^{-\frac{1}{\epsilon}D(t)} \frac{\sqrt{\epsilon}}{\sigma} h \bigg) \\
=&2\sum_{j=1}^{N} \mathbb{P}\bigg(\langle e_k, Qe_k \rangle^{\frac{1}{2}} \sup_{s_{j-1}<t<s_j} \int_0^t \mathsf{e}^{-\frac{1}{\epsilon}D(t_1)} \mathsf{d}\beta(t_1) \geq \mathsf{e}^{-\frac{1}{\epsilon}D(s_{j-1})} \frac{\sqrt{\epsilon}}{\sigma} h \bigg).
\end{aligned}$$

We can now apply a Bernstein-type inequality [17]. Therefore, it follows that

$$\begin{aligned}
&\mathbb{P}\bigg(\sup_{0\leq t\leq T} |\psi_k(t)| \geq h \bigg) \leq 2\sum_{j=1}^{N} \mathbb{P}\bigg(\sup_{0<t<s_j} \int_0^t \mathsf{e}^{-\frac{1}{\epsilon}D(t_1)} \mathsf{d}\beta(t_1) \geq \langle e_k, Qe_k \rangle^{-\frac{1}{2}} \mathsf{e}^{-\frac{1}{\epsilon}D(s_{j-1})} \frac{\sqrt{\epsilon}}{\sigma} h \bigg) \\
\leq& 2\sum_{j=1}^{N} \exp\bigg\{ -\frac{\epsilon h^2 \mathsf{e}^{-\frac{2}{\epsilon}D(s_{j-1})}}{2\sigma^2 \langle e_k, Qe_k \rangle \int_0^{s_j} \mathsf{e}^{-\frac{2}{\epsilon}D(t_1)} \mathsf{d}t_1} \bigg\} = 2\sum_{j=1}^{N} \exp\bigg\{ -\frac{\epsilon h^2 \mathsf{e}^{\frac{2}{\epsilon}(D(s_j)-D(s_{j-1}))}}{2\sigma^2 \langle e_k, Qe_k \rangle \int_0^{s_j} \mathsf{e}^{\frac{2}{\epsilon}(D(s_j)-D(t_1))} \mathsf{d}t_1} \bigg\} \\
=& 2\sum_{j=1}^{N} \exp\bigg\{ -\frac{h^2 \mathsf{e}^{\frac{2}{\epsilon}(D(s_j)-D(s_{j-1}))}}{2\mathsf{Var}(\psi_k(s_j))} \bigg\} \leq 2\sum_{j=1}^{N} \exp\bigg\{ \frac{h^2 \lambda_k \mathsf{e}^{\frac{2}{\epsilon}(D(s_j)-D(s_{j-1}))}}{2c_0\zeta_* \sigma^2} \bigg\},
\end{aligned}$$

for which we use Lemma 8.1.1 in the last inequality. By assumption, we know that $\lambda_k + p(t) < 0$ for all $k \in \mathbb{N}_{>0}$ and $0 \leq t \leq T$. We can set the sequence of times $\{s_j\}_{j=0}^N$ so that there exists $\gamma_0 > 0$ for which $-\dfrac{\lambda_k T + \int_0^T p(t_1)\mathsf{d}t_1}{\gamma_0 \epsilon} = N \in \mathbb{N}_{>0}$ and

$$\lambda_k(s_{j+1} - s_j) + \int_{s_j}^{s_{j+1}} p(t_1)\mathsf{d}t_1 = -\gamma_0 \epsilon \qquad \forall j \in \{0,...,N-1\}.$$

In conclusion, for $\gamma_0 > 0$ small enough, such a choice leads to

$$\mathbb{P}\Big(\sup_{0\le t\le T} |\psi_k(t)| \ge h \Big) \le -2\frac{\lambda_k T \int_0^T p(t_1)\mathsf{d}t_1}{\gamma_0 \epsilon} \mathsf{exp}\Big\{ \frac{h^2\lambda_k \mathsf{e}^{-2\gamma_0}}{2c_0\zeta_*\sigma^2} \Big\} \le -\frac{2c^+\lambda_k T}{\gamma\epsilon} \mathsf{exp}\Big\{ \frac{h^2\lambda_k \mathsf{e}^{-2\gamma}}{2c_0\zeta_*\sigma^2} \Big\}$$

for any $\gamma_0 \ge \gamma$.

□

The inequality (8.1.5) can be treated as follows for assumptions equivalent to the previous lemma:

$$\begin{aligned} \mathbb{P}\Big(\sup_{0\le t\le T} |\psi_k(t)| \ge h \Big) &\le -\frac{2c^+\lambda_k T}{\gamma\epsilon} \mathsf{exp}\Big\{ \frac{h^2\lambda_k \mathsf{e}^{-2\gamma}}{2c_0\zeta_*\sigma^2} \Big\} \\ \le -\frac{2c^+\lambda_k T}{\gamma\epsilon} \mathsf{exp}\Big\{ \frac{h^2\lambda_k}{2c_0\zeta_*\sigma^2} \Big\} &\mathsf{exp}\Big\{ -\frac{h^2\lambda_k\gamma}{c_0\zeta_*\sigma^2} \Big\}. \end{aligned} \tag{8.1.7}$$

Moreover, for large enough $\dfrac{h^2}{\zeta_*\sigma^2}$, (8.1.7) can be optimised on γ at $\gamma = -\dfrac{c_0\zeta_*\sigma^2}{h^2\lambda_k}$, resulting in

$$\mathbb{P}\Big(\sup_{0\le t\le T} |\psi_k(t)| \ge h \Big) \le \frac{h^2}{\zeta_*\sigma^2} \frac{2c^+\lambda_k^2 eT}{c_0\epsilon} \mathsf{exp}\Big\{ \frac{h^2}{\zeta_*\sigma^2} \frac{\lambda_k}{2c_0} \Big\}. \tag{8.1.8}$$

The previous lemmas are sufficient to prove the subsequent theorem, whose proof follows the steps of [19, Theorem 2.4 in the linear case].

Theorem 8.1.3. *For any* $0 < s < \dfrac{1}{2}$, $0 < \epsilon$, $\zeta_*\sigma^2 \ll h^2$ *and* $0 \le T \le \tau$ *there exist constants* $0 < \kappa(s), C_{\frac{h^2}{\zeta_*\sigma^2}}(\kappa, T, \epsilon, s)$ *such that the solution* ψ_0 *of* (8.1.3) *satisfies*

$$\mathbb{P}\Big(\sup_{0\le t\le T} ||\psi_0(\cdot,t)||_{A^s} \ge h \Big) \le C_{\frac{h^2}{\zeta_*\sigma^2}}(\kappa, T, \epsilon, s) \mathsf{e}^{-\kappa(s)\frac{h^2}{\zeta_*\sigma^2}}.$$

Proof. We set $\eta, \rho > 0$ such that $\rho = \dfrac{1}{2} - s$. Then, for any sequence $\{h_k\}_{k\in\mathbb{N}_{>0}} \subset \mathbb{R}_{>0}$ that satisfies $h^2 = \sum\limits_{k=1}^{\infty} h_k^2$, it holds

$$\begin{aligned} &\mathbb{P}\Big\{ \sup_{0\le t\le T} ||\psi_0(\cdot,t)||_{A^s} \ge h \Big\} = \mathbb{P}\Big\{ \sup_{0\le t\le T} ||\psi_0(\cdot,t)||_{A^s}^2 \ge h^2 \Big\} = \mathbb{P}\Big\{ \sup_{0\le t\le T} \sum_{k=1}^{\infty} (-\lambda_k)^s |\psi_k(t)|^2 \ge h^2 \Big\} \\ \le &\sum_{k=1}^{\infty} \mathbb{P}\Big\{ \sup_{0\le t\le T} |\psi_k(t)|^2 \ge \frac{h_k^2}{(-\lambda_k)^s} \Big\} = \sum_{k=1}^{\infty} \mathbb{P}\Big\{ \sup_{0\le t\le T} |\psi_k(t)| \ge \frac{h_k}{(-\lambda_k)^{\frac{s}{2}}} \Big\} \\ \le &\sum_{k=1}^{\infty} \frac{h_k^2}{\zeta_*\sigma^2} \frac{2c^+(-\lambda_k)^{2-s} eT}{c_0\epsilon} \mathsf{exp}\Big\{ -\frac{h_k^2}{\zeta_*\sigma^2} \frac{(-\lambda_k)^{1-s}}{2c_0} \Big\}, \end{aligned}$$

for which we used (8.1.8) in the last inequality. We can assume $h_k = C(\eta, s) h^2 (-\lambda_k)^{-1+s+\frac{\eta}{2}}$ with

$$C(\eta, s) := \frac{1}{\sum_{k=1}^{\infty} (-\lambda_k)^{-1+s+\frac{\eta}{2}}}.$$

Since $-\lambda_k \sim k^2$ holds from (A.3), we can use the Riemann Zeta function $\xi(\nu) := \sum_{k=1}^{\infty} k^{-\nu}$ to prove that $C(\eta, s) > 0$ for any $\eta > 0$. In fact, we have $\xi(2 - 2s - \eta) < \infty$ for any $0 < \eta < 2\rho$ and

$$C(\eta, s) = \frac{1}{\sum_{k=1}^{\infty} (-\lambda_k)^{-1+s+\frac{\eta}{2}}} \propto \frac{1}{\sum_{k=1}^{\infty} k^{-2+2s+\eta}} = \xi(2 - 2s - \eta)^{-1}.$$

For $0 < \eta < 2\rho$, we write

$$\mathbb{P}\Big\{ \sup_{0\leq t\leq T} ||\psi_0(\cdot,t)||_{A^s} \geq h \Big\} \leq \sum_{k=1}^{\infty} \frac{h_k^2}{\zeta_*\sigma^2} \frac{2c^+(-\lambda_k)^{2-s}eT}{c_0\epsilon} \mathsf{exp}\Big\{ -\frac{h_k^2}{\zeta_*\sigma^2}\frac{(-\lambda_k)^{1-s}}{2c_0} \Big\}$$
$$\leq \frac{h^2}{\zeta_*\sigma^2}\frac{2c^+eT}{c_0\epsilon}\sum_{k=1}^{\infty}\lambda_k^2 \mathsf{exp}\Big\{ -\frac{h^2}{\zeta_*\sigma^2}\frac{C(\eta,s)(-\lambda_k)^{\frac{\eta}{2}}}{2c_0} \Big\} \leq \ell_T \sum_{k=1}^{\infty}(1+k^2)^2\mathsf{e}^{-\ell(1+k^2)^{\frac{\eta}{2}}}$$

for $\ell_T \propto \dfrac{h^2}{\zeta_*\sigma^2}\dfrac{c^+eT}{c_0\epsilon}$ and $\ell \propto \dfrac{h^2}{\zeta_*\sigma^2}\dfrac{C(\eta,s)}{c_0}$. We define

$$\iota(x) := (1+x^2)^2\mathsf{e}^{-\ell(1+x^2)^{\frac{\eta}{2}}}$$

for which we know that

$$\frac{\mathsf{d}}{\mathsf{d}x}\iota(x) = 2x(1+x^2)\Big(2-\ell\frac{\eta}{2}(1+x^2)^{\frac{\eta}{2}}\Big)\mathsf{e}^{-\ell(1+x^2)^{\frac{\eta}{2}}}.$$

We can therefore bound

$$\sum_{k=1}^{\infty}\iota(k) \leq \int_0^{\infty}\iota(x)\mathsf{d}x$$

by assuming ι decreasing in $[0,\infty)$. Such a case is satisfied for $\dfrac{h^2}{\zeta_*\sigma^2}$ larger than a constant of order 1 dependent on the choice of η and on s. Conversely, the theorem would be trivially proven.
Setting $x' = \ell(1+x^2)^{\frac{\eta}{2}}$ and $y = -\ell + x'$, we can state that

$$\int_0^{\infty}\iota(x)\mathsf{d}x = \int_0^{\infty}(1+x^2)^2\mathsf{e}^{-\ell(1+x^2)^{\frac{\eta}{2}}}\mathsf{d}x = \frac{1}{\ell^{\frac{6}{\eta}}\eta}\int_{\ell}^{\infty}\frac{x'^{\frac{6}{\eta}-1}}{\sqrt{\Big(\frac{x'}{\ell}\Big)^{\frac{2}{\eta}}-1}}\mathsf{e}^{-x'}\mathsf{d}x'$$
$$= \frac{\mathsf{e}^{-\ell}}{\ell^{\frac{6}{\eta}}\eta}\int_0^{\infty}\frac{(\ell+y)^{\frac{6}{\eta}-1}}{\sqrt{\Big(1+\frac{y}{\ell}\Big)^{\frac{2}{\eta}}-1}}\mathsf{e}^{-y}\mathsf{d}y \leq \frac{\mathsf{e}^{-\ell}}{\ell^{\frac{6}{\eta}}\eta}\int_0^{\infty}\frac{(\ell+y)^{\frac{6}{\eta}-1}}{\sqrt{\frac{2y}{\eta\ell}}}\mathsf{e}^{-y}\mathsf{d}y$$
$$= \frac{\mathsf{e}^{-\ell}}{\ell^{\frac{6}{\eta}}\eta}\sqrt{\frac{\eta\ell}{2}}\int_0^{\ell}\frac{(\ell+y)^{\frac{6}{\eta}-1}}{\sqrt{y}}\mathsf{e}^{-y}\mathsf{d}y + \frac{\mathsf{e}^{-\ell}}{\ell^{\frac{6}{\eta}}\eta}\sqrt{\frac{\eta\ell}{2}}\int_{\ell}^{\infty}\frac{(\ell+y)^{\frac{6}{\eta}-1}}{\sqrt{y}}\mathsf{e}^{-y}\mathsf{d}y$$
$$\leq \frac{\mathsf{e}^{-\ell}}{\ell^{\frac{6}{\eta}}\eta}(2\ell)^{\frac{6}{\eta}-1}\sqrt{\frac{\eta\ell}{2}}\int_0^{\ell}\frac{1}{\sqrt{y}}\mathsf{e}^{-y}\mathsf{d}y + \frac{\mathsf{e}^{-\ell}}{\ell^{\frac{6}{\eta}}\eta}\sqrt{\frac{\eta\ell}{2}}\int_{\ell}^{\infty}\frac{(2y)^{\frac{6}{\eta}-1}}{\sqrt{y}}\mathsf{e}^{-y}\mathsf{d}y$$
$$\leq c_1(\eta)\ell^{-\frac{1}{2}}\mathsf{e}^{-\ell} + c_2(\eta)\ell^{-\frac{6}{\eta}+\frac{1}{2}}\mathsf{e}^{-\ell},$$

for which we used $\Big(1+\frac{y}{\ell}\Big)^{\frac{2}{\eta}} - 1 \geq \frac{2y}{\eta\ell}$ and took the constants $c_1(\eta), c_2(\eta) > 0$ that are uniformly bounded in ℓ since $\eta < 12$. Such results lead to

$$\mathbb{P}\Big\{ \sup_{0\leq t\leq T} ||\psi_0(\cdot,t)||_{A^s} \geq h \Big\} \leq \ell_T\sum_{k=1}^{\infty}f(k) \leq \ell_T\Big(c_1(\eta)\ell^{-\frac{1}{2}}\mathsf{e}^{-\ell} + c_2(\eta)\ell^{-\frac{6}{\eta}+\frac{1}{2}}\mathsf{e}^{-\ell}\Big)$$
$$\propto \frac{h^2}{\zeta_*\sigma^2}\frac{c^+T}{c_0\epsilon}\Big(c_1(\eta)\Big(\frac{h^2}{\zeta_*\sigma^2}\frac{C(\eta,s)}{c_0}\Big)^{-\frac{1}{2}} + c_2(\eta)\Big(\frac{h^2}{\zeta_*\sigma^2}\frac{C(\eta,s)}{c_0}\Big)^{-\frac{6}{\eta}+\frac{1}{2}}\Big)\mathsf{e}^{-\ell}.$$

The proof is concluded assuming $\eta = \rho = \frac{1}{2} - s$, such that $C(\eta, s) \propto \xi\Big(\frac{3}{2} - s\Big)^{-1}$, $\kappa(s) \propto \dfrac{C(\eta, s)}{c_0}$ and

$$C_{\frac{h^2}{\zeta_*\sigma^2}}(\kappa, T, \epsilon, s) \propto \frac{h^2}{\zeta_*\sigma^2}\frac{c^+T}{c_0\epsilon}\left(c_1(\eta)\left(\frac{h^2}{\zeta_*\sigma^2}\frac{C(\eta,s)}{c_0}\right)^{-\frac{1}{2}} + c_2(\eta)\left(\frac{h^2}{\zeta_*\sigma^2}\frac{C(\eta,s)}{c_0}\right)^{-\frac{6}{\eta}+\frac{1}{2}}\right).$$

□

Remark. The dependence of $C_{\frac{h^2}{\zeta_*\sigma^2}}(\kappa, \tau, \epsilon, s)$ on τ and ϵ is well known. In fact, $C_{\frac{h^2}{\zeta_*\sigma^2}}(\kappa, \tau, \epsilon, s) \sim \dfrac{\tau}{\epsilon}$ is a property employed to obtain moment estimates further in the chapter. Such a proportionality is inherited from (8.1.8). Additionally, for $\zeta_*\sigma^2 \ll h^2$, the relation $C_{\frac{h^2}{\zeta_*\sigma^2}}(\kappa, \tau, \epsilon, s) \sim \Big(\dfrac{h^2}{\zeta_*\sigma^2}\Big)^{\frac{1}{2}}$ holds. Furthermore, the constants $C_{\frac{h^2}{\zeta_*\sigma^2}}(\kappa, \tau, \epsilon, s)$ and κ depend on the choice of g and p from construction and the definition of c_0 in Lemma 8.1.1.

We now study the error estimate given by ψ_*, mild solution of

$$\begin{cases} \mathsf{d}\psi_*(x,t) = \dfrac{1}{\epsilon}(\Delta\psi_*(x,t) + p(t)\psi_*(x,t) - g(x)\psi_*(x,t) - \bar{u}(x,t)^2\psi_*(x,t))\,\mathsf{d}t + \dfrac{\sigma}{\sqrt{\epsilon}}\,Q^{\frac{1}{2}}\mathsf{d}W_t \\ \psi_*(x,0) = 0, \quad \forall x \in \mathcal{X}_1 \\ \psi_*(0,t) = \psi_*(L,t) = 0, \quad \forall t \geq 0, \end{cases} \tag{8.1.9}$$

for the function $\bar{u}$ assumed in the construction of ψ in (8.1.1). In particular, $\bar{u}$ satisfies the hypothesis in Proposition 8.0.2. The proof of the next corollary adapts the method used in [16, Proposition 3.7] and makes use of the Young-type inequality proven in Lemma 8.0.1.

Corollary 8.1.4. *For any $0 < s < \dfrac{1}{2}$ and $0 < \epsilon$, $\zeta_*\sigma^2 \ll h^2$, there exist $m, \delta_0 > 0$ such that for any $\delta \leq \delta_0$ and $\bar{u}$ solution of* (8.0.3) *for which $||\bar{u}(\cdot,0)||_A \leq \delta$, the constants $0 < \kappa(s), C_{\frac{h^2}{\zeta_*\sigma^2}}(\kappa, \tau, \epsilon, s)$ obtained in Theorem 8.1.3 satisfy*

$$\mathbb{P}\left(\sup_{0\leq t\leq T}||\psi_*(\cdot,t)||_{A^s} \geq mh\right) \leq C_{\frac{h^2}{\zeta_*\sigma^2}}(\kappa, \tau, \epsilon, s)\mathsf{e}^{-\kappa\frac{h^2}{\zeta_*\sigma^2}} \tag{8.1.10}$$

for the solution ψ_* of (8.1.9) *and any $0 \leq T \leq \tau$.*

Proof. We define, for $m > 0$,

$$\tilde{\tau} = \inf\{0 \leq t \quad \text{such that} \quad ||\psi_*(\cdot,t)||_{A^s} \geq mh\} \in [0,\tau] \cup \infty$$

and the event

$$\tilde{\Omega} := \left\{\sup_{0\leq t\leq T}||\psi_0(\cdot,t)||_{A^s} \leq h\right\} \cap \{\tilde{\tau} < \infty\}.$$

We denote then the norm $||\cdot||_{A^s}$ norm as

$$||\phi||_{A^s}^2 = \langle(-A)^s\phi, \phi\rangle,$$

for $\phi \in \mathcal{W}_0^{s,2}(\mathcal{X}_1)$, the fractional Sobolev space of order 2 and degree $0 < s < \dfrac{1}{2}$ with Dirichlet conditions. Taking ψ_0 the solution of (8.1.3), we can state from Duhamel's formula that

$$\begin{aligned}\psi_*(x,t) &= \int_0^t \mathsf{e}^{\frac{1}{\epsilon}\left(A(t-t_1)+\int_{t_1}^t p(t_2)\mathsf{d}t_2\right)}Q^{\frac{1}{2}}\mathsf{d}W_{t_1} - \int_0^t \mathsf{e}^{\frac{1}{\epsilon}\left(A(t-t_1)+\int_{t_1}^t p(t_2)\mathsf{d}t_2\right)}\bar{u}(x,t_1)^2\psi_*(x,t_1)\mathsf{d}t_1 \\ &= \psi_0(x,t) - \int_0^t \mathsf{e}^{\frac{1}{\epsilon}\left(A(t-t_1)+\int_{t_1}^t p(t_2)\mathsf{d}t_2\right)}\bar{u}(x,t_1)^2\psi_*(x,t_1)\mathsf{d}t_1,\end{aligned}$$

for all $0 \leq t \leq \tau$. Therefore, for $t < \tilde{\tau}$ and for $\omega \in \tilde{\Omega}$, it holds that

$$
\begin{aligned}
&||\psi_*(\cdot,t)||^2_{A^s} = \langle (-A)^s \psi_*(\cdot,t), \psi_*(\cdot,t)\rangle \\
\leq &\langle (-A)^s \psi_0(\cdot,t), \psi_0(\cdot,t)\rangle + 2\left|\left\langle (-A)^s \int_0^t \mathsf{e}^{\frac{1}{\epsilon}\left(A(t-t_1)+\int_{t_1}^t p(t_2)\mathsf{d}t_2\right)} \bar{u}(\cdot,t_1)^2 \psi_*(\cdot,t_1)\mathsf{d}t_1, \psi_0(\cdot,t)\right\rangle\right| \\
+ &\left|\left\langle (-A)^s \int_0^t \mathsf{e}^{\frac{1}{\epsilon}\left(A(t-t_1)+\int_{t_1}^t p(t_2)\mathsf{d}t_2\right)} \bar{u}(\cdot,t_1)^2 \psi_*(\cdot,t_1)\mathsf{d}t_1, \int_0^t \mathsf{e}^{\frac{1}{\epsilon}\left(A(t-t_1')+\int_{t_1'}^t p(t_2')\mathsf{d}t_2'\right)} \bar{u}(\cdot,t_1')^2 \psi_*(\cdot,t_1')\mathsf{d}t_1'\right\rangle\right| \\
\leq &||\psi_0(\cdot,t)||^2_{A^s} + 2\int_0^t ||\mathsf{e}^{\frac{1}{\epsilon}\left(A(t-t_1)+\int_{t_1}^t p(t_2)\mathsf{d}t_2\right)} \bar{u}(\cdot,t_1)^2 \psi_*(\cdot,t_1)||_{A^s} ||\psi_0(\cdot,t)||_{A^s}\mathsf{d}t_1 \\
&+ \int_0^t \int_0^t ||\mathsf{e}^{\frac{1}{\epsilon}\left(A(t-t_1)+\int_{t_1}^t p(t_2)\mathsf{d}t_2\right)} \bar{u}(\cdot,t_1)^2 \psi_*(\cdot,t_1)||_{A^s} \\
&\times ||\mathsf{e}^{\frac{1}{\epsilon}\left(A(t-t_1')+\int_{t_1'}^t p(t_2')\mathsf{d}t_2'\right)} \bar{u}(\cdot,t_1')^2 \psi_*(\cdot,t_1')||_{A^s}\mathsf{d}t_1\, \mathsf{d}t_1' \\
\leq &||\psi_0(\cdot,t)||^2_{A^s} + 2\int_0^t \mathsf{e}^{\frac{1}{\epsilon}\left(\lambda_1 + \max\limits_{0\leq t_2\leq t} p(t_2)\right)(t-t_1)} ||\bar{u}(\cdot,t_1)^2 \psi_*(\cdot,t_1)||_{A^s} ||\psi_0(\cdot,t)||_{A^s}\mathsf{d}t_1 \\
&+ \int_0^t \int_0^t \mathsf{e}^{\frac{1}{\epsilon}\left(\lambda_1 + \max\limits_{0\leq t_2\leq t} p(t_2)\right)(t-t_1)} ||\bar{u}(\cdot,t_1)^2 \psi_*(\cdot,t_1)||_{A^s} \\
&\times \mathsf{e}^{\frac{1}{\epsilon}\left(\lambda_1 + \max\limits_{0\leq t_2'\leq t} p(t_2')\right)(t-t_1')} ||\bar{u}(\cdot,t_1')^2 \psi_*(\cdot,t_1')||_{A^s}\mathsf{d}t_1\, \mathsf{d}t_1',
\end{aligned}
\tag{8.1.11}
$$

for which we used Cauchy-Schwarz inequality and the min-max principle on $||\cdot||_{A^s}$. From the Young-type inequality in Lemma 8.0.1 and the control over the deterministic solution in Propostion $8.0.2$ we obtain

$$
\begin{aligned}
&||\bar{u}(\cdot,t_1)^2 \psi_*(\cdot,t_1)||_{A^s} \leq c(r,s)||\bar{u}(\cdot,t_1)^2||_A ||\psi_*(\cdot,t_1)||_{A^s} \\
\leq &c(r,s)||\bar{u}(\cdot,t_1)||^2_A ||\psi_*(\cdot,t_1)||_{A^s} \leq mc(r,s)\delta^2 h,
\end{aligned}
\tag{8.1.12}
$$

for any $||\bar{u}(\cdot,0)||_A \leq \delta$.[2] Labelling $\eta = -\lambda_1 - \max\limits_{0\leq t_1\leq T} p(t_1) > 0$, we obtain from (8.1.11) and (8.1.12) that

$$
\begin{aligned}
||\psi_*(\cdot,t)||^2_{A^s} \leq &h^2 + 2mc(r,s)\delta^2 h^2 \int_0^t \mathsf{e}^{-\frac{\eta}{\epsilon}(t-t_1)}\mathsf{d}t_1 \\
&+ m^2 c(r,s)^2 \delta^4 h^2 \int_0^t \int_0^t \mathsf{e}^{-\frac{\eta}{\epsilon}(t-t_1)} \mathsf{e}^{-\frac{\eta}{\epsilon}(t-t_1')}\mathsf{d}t_1\, \mathsf{d}t_1' \\
\leq &h^2 + 2m\frac{\epsilon c(r,s)}{\eta}\delta^2 h^2 + m^2 \frac{\epsilon^2 c(r,s)^2}{\eta^2}\delta^4 h^2 = \left(1 + m\frac{\epsilon c(r,s)}{\eta}\delta^2\right)^2 h^2.
\end{aligned}
\tag{8.1.13}
$$

For any $0 < s < \dfrac{1}{2}$, we can find a pair of parameters $\delta_0, m > 0$ such that $m^2 > \left(1 + m\dfrac{\epsilon c(r,s)}{\eta}\delta^2\right)^2$ for any $\delta \leq \delta_0$. From the definition of $\tilde{\tau}$, it holds that $||\psi_*(\cdot,\tilde{\tau})||^2_{A^s} = m^2 h^2$, which contradicts (8.1.13). In conclusion, we infer that $\mathbb{P}(\tilde{\Omega}) = 0$ and

$$
\mathbb{P}\left(\sup_{0\leq t\leq T} ||\psi_*(\cdot,t)||_{A^s} \geq mh\right) \leq \mathbb{P}\left(\sup_{0\leq t\leq T} ||\psi_0(\cdot,t)||_{A^s} \geq h\right).
$$

The inequality (8.1.10) follows from Theorem 8.1.3. □

[2] The exponential decay of $||\bar{u}(\cdot,t)||_A$, proven in Proposition $8.0.2$, can be used in (8.1.12) to achieve more freedom on the choice of δ.

Notation. For the sake of notation, we omit m from (8.1.10) since it can be absorbed in the construction of the constants $C_{\frac{h^2}{\zeta_* \sigma^2}}(\kappa, \tau, \epsilon, s)$ and κ. We note that the constants m and δ_0 are dependent on g and p.

8.1.2 Nonlinear case

In order to study the estimate error for (8.1.1) the following lemmas are required.

Lemma 8.1.5. *Set $0 \leq t \leq \tau$. For G defined as in* (8.1.2) *and a function $\psi(\cdot, t) \in \mathcal{W}^{s,2}(\mathcal{X}_1)$ with $\frac{1}{3} < s < \frac{1}{2}$, the inequality*

$$||G(\psi(\cdot,t))||_{A^r} \leq c(r,s) \max\{||\psi(\cdot,t)||^2_{A^s}, ||\psi(\cdot,t)||^3_{A^s}\} \tag{8.1.14}$$

holds when $0 < r < \frac{1}{2} - 3\Big(\frac{1}{2} - s\Big)$ and for a certain $c(r,s) < \infty$.

Proof. The current proof relies on Lemma 8.0.1. By definition of the function G, (8.1.2), and Theorem 8.0.2,

$$\begin{aligned}
&||G(\psi(\cdot,t))||_{A^r} \leq 3||\bar{u}(\cdot,t)\psi(\cdot,t)^2||_{A^r} + 3||\psi(\cdot,t)^3||_{A^r} \\
\leq& c(r,s)\Big(||\bar{u}(\cdot,t)||_{A^s}||\psi(\cdot,t)||^2_{A^s} + ||\psi(\cdot,t)||^3_{A^s}\Big) \leq c(r,s)\Big(||\bar{u}(\cdot,t)||_A||\psi(\cdot,t)||^2_{A^s} + ||\psi(\cdot,t)||^3_{A^s}\Big) \\
\leq& c(r,s)\Big(||\bar{u}(\cdot,0)||_A||\psi(\cdot,t)||^2_{A^s} + ||\psi(\cdot,t)||^3_{A^s}\Big) \leq c(r,s)\max\{||\psi(\cdot,t)||^2_{A^s}, ||\psi(\cdot,t)||^3_{A^s}\}.
\end{aligned}$$

In the last inequality, we have rewritten for simplicity $(1+\delta)c(r,s)$ as $c(r,s)$ for $||\bar{u}(\cdot,0)||_A \leq \delta$. □

The next lemma can be proven following the same steps as [19, Lemma 3.5, Corollary 3.6].

Lemma 8.1.6. *Given ψ mild solution of* (8.1.1)*, the parameter $0 < r < \frac{1}{2}$ such that $G(\psi(\cdot,t)) \in \mathcal{W}^{r,2}(\mathcal{X}_1)$ for all $0 \leq t \leq \tau$ and chosen $q < r + 2$, then there exists $\tilde{m}(r,q) < \infty$ that satisfies, for all $0 \leq t \leq \tau$,*

$$\begin{aligned}
&\Big|\Big|\int_0^t \mathrm{e}^{\frac{1}{\epsilon}\left((A+p(t))(t-t_1) - \int_{t_1}^t \bar{u}(\cdot,t_2)^2 dt_2\right)} G(\psi(\cdot,t_1))dt_1\Big|\Big|_{A^q} \\
=&||\psi(\cdot,t) - \psi_*(\cdot,t)||_{A^q} \leq \tilde{m}(r,q)\epsilon^{\frac{q-r}{2}-1} \sup_{0\leq t_1\leq t} ||G(\psi(\cdot,t))||_{A^r},
\end{aligned} \tag{8.1.15}$$

with ψ_* mild solution of (8.1.9)*.*

We can then prove Theorem 8.0.3 according to a similar method to the one used in the proof of [19, Theorem 2.4].

Proof of Theorem 8.0.3. Assume $h_1, h_2 > 0$ such that $h = h_1 + h_2$ and set $\frac{1}{3} < s < \frac{1}{2}$. Then,

$$\begin{aligned}
&\mathbb{P}\Big(\tau_{\mathcal{B}(h)} < T\Big) = \mathbb{P}\Big(\sup_{0\leq t\leq \min\{T,\tau_{\mathcal{B}(h)}\}} ||\psi(\cdot,t)||_{A^s} \geq h\Big) \\
\leq&\mathbb{P}\Big(\sup_{0\leq t\leq T} ||\psi_*(\cdot,t)||_{A^s} + \sup_{0\leq t\leq \min\{T,\tau_{\mathcal{B}(h)}\}} ||\psi(\cdot,t) - \psi_*(\cdot,t)||_{A^s} \geq h\Big) \\
\leq&\mathbb{P}\Big(\sup_{0\leq t\leq T} ||\psi_*(\cdot,t)||_{A^s} \geq h_1\Big) + \mathbb{P}\Big(\sup_{0\leq t\leq \min\{T,\tau_{\mathcal{B}(h)}\}} ||\psi(\cdot,t) - \psi_*(\cdot,t)||_{A^s} > h_2\Big).
\end{aligned}$$

For $t < \tau_{\mathcal{B}(h)}$ and since $h = O(1)$, the inequalities (8.1.14) and (8.1.15) imply

$$||\psi(\cdot,t) - \psi_*(\cdot,t)||_{A^q} \leq \tilde{m}(r,q)\epsilon^{\frac{q-r}{2}-1} \sup_{0\leq t_1\leq t} ||G(\psi(\cdot,t))||_{A^r}$$

$$\leq \tilde{m}(r,q)\epsilon^{\frac{q-r}{2}-1}c(r,s)||\psi(\cdot,t)||^2_{A^s} \leq \tilde{m}(r,q)\epsilon^{\frac{q-r}{2}-1}c(r,s)h^2,$$

for $0 < r < \frac{1}{2} - 3\Big(\frac{1}{2} - s\Big)$ and $0 < q < r + 2$. Assuming $q \geq s$ and setting $h_2 = \tilde{m}(r,q)\epsilon^{\frac{q-r}{2}-1}c(r,s)h^2$, we obtain

$$\mathbb{P}\Big(\sup_{0\leq t\leq \min\{T,\tau_{\mathcal{B}(h)}\}} ||\psi(\cdot,t) - \psi_*(\cdot,t)||_{A^s} > h_2\Big) \leq \mathbb{P}\Big(\sup_{0\leq t\leq \min\{T,\tau_{\mathcal{B}(h)}\}} ||\psi(\cdot,t) - \psi_*(\cdot,t)||_{A^q} > h_2\Big) = 0.$$

We can then estimate $\mathbb{P}\Big(\tau_{\mathcal{B}(h)} < T\Big) \leq \mathbb{P}\Big(\sup_{0\leq t\leq T} ||\psi_*(\cdot,t)||_{A^s} \geq h_1\Big)$ with Corollary 8.1.4 for

$$h_1 = h - h_2 = h\Big(1 - O\Big(\frac{h}{\epsilon^\nu}\Big)\Big)$$

and $\nu = 1 - \frac{q-r}{2}$. The choice of $s \leq q < r + 2$ implies that the inequality (8.1.15) holds for any $\nu > 0$. Setting $0 < s < \frac{1}{3}$, the inclusion $\mathcal{W}^{s_1,2}(\mathcal{X}_1) \subset \mathcal{W}^{s,2}(\mathcal{X}_1)$ for $s < s_1$ entails that

$$\mathbb{P}\Big(\tau_{\mathcal{B}(h)} < T\Big) = \mathbb{P}\Big(\sup_{0\leq t\leq \min\{T,\tau_{\mathcal{B}(h)}\}} ||\psi(\cdot,t)||_{A^s} \geq h\Big) \leq \mathbb{P}\Big(\sup_{0\leq t\leq \min\{T,\tau_{\mathcal{B}(h)}\}} ||\psi(\cdot,t)||_{A^{s_1}} \geq h\Big), \quad (8.1.16)$$

for which the last term can be controlled as before by choosing $\frac{1}{3} < s_1 < \frac{1}{2}$. The inequality (8.1.16) holds since we assume $g \geq 1$ and, therefore, $\lambda_1 < -1$. □

8.2 Moment estimates

The inequality presented in Theorem 8.0.3 enables an estimation of the moments of $\tau_{\mathcal{B}(h)}$. In particular, it provides a bound on the expected transition time, corresponding to the first moment. The proof of the next corollary relies on the step described in [17, Proposition 3.1.12].

Corollary 8.2.1. *For any $k \in \mathbb{N}_{>0}$, $0 < s < \frac{1}{2}$, $\sigma\sqrt{\zeta_*} \ll h$ and the same assumptions in Theorem 8.0.3, the following estimate holds:*

$$\mathbb{E}\Big(\tau^k_{\mathcal{B}(h)}\Big) \geq \frac{1}{(k+1)}\left(\frac{\epsilon}{c}\Big(\frac{h^2}{\zeta_*\sigma^2}\Big)^{-\frac{1}{2}}\exp\left\{\tilde{\kappa}\frac{h^2}{\zeta_*\sigma^2}\right\}\right)^k \quad (8.2.1)$$

for a constant $c = c_{\kappa,s} > 0$ and $\tilde{\kappa} = \kappa\Big(1 - O\Big(\frac{h}{\epsilon^\nu}\Big)\Big)$, given $h, \kappa, \nu > 0$ from Theorem 8.0.3.

Proof. The $k^{\text{th}}-$moment can be estimated by

$$\begin{aligned}\mathbb{E}\Big(\tau^k_{\mathcal{B}(h)}\Big) &= \int_0^\infty kt^{k-1}\mathbb{P}\Big(\tau_{\mathcal{B}(h)} \geq t\Big)\mathrm{d}t \geq \int_0^T kt^{k-1}\Big(1 - \mathbb{P}\Big(\tau_{\mathcal{B}(h)} < t\Big)\Big)\mathrm{d}t \\ &\geq \int_0^T kt^{k-1}\left(1 - C_{\frac{h^2}{\zeta_*\sigma^2}}(\kappa,t,\epsilon,s)\exp\left\{-\kappa\frac{h^2}{\sigma^2}\left(1 - O\Big(\frac{h}{\epsilon^\nu}\Big)\right)\right\}\right)\mathrm{d}t\end{aligned}$$

for any $T > 0$. From the hypothesis we know that $C_{\frac{h^2}{\zeta_*\sigma^2}}(\kappa, t, \epsilon, s) \sim \frac{t}{\epsilon}\Big(\frac{h^2}{\zeta_*\sigma^2}\Big)^{\frac{1}{2}}$ by construction. Therefore, there exists $c > 0$ such that $C_{\frac{h^2}{\zeta_*\sigma^2}}(\kappa, t, \epsilon, s) < c\frac{t}{\epsilon}\Big(\frac{h^2}{\zeta_*\sigma^2}\Big)^{\frac{1}{2}}$ and

$$\begin{aligned}\mathbb{E}\Big(\tau^k_{\mathcal{B}(h)}\Big) &\geq \int_0^T kt^{k-1}\left(1 - c\frac{t}{\epsilon}\Big(\frac{h^2}{\zeta_*\sigma^2}\Big)^{\frac{1}{2}}\exp\left\{-\tilde{\kappa}\frac{h^2}{\zeta_*\sigma^2}\right\}\right)\mathrm{d}t \\ &= T^k - \frac{kc}{(k+1)\epsilon}T^{k+1}\Big(\frac{h^2}{\zeta_*\sigma^2}\Big)^{\frac{1}{2}}\exp\left\{-\tilde{\kappa}\frac{h^2}{\zeta_*\sigma^2}\right\}.\end{aligned}$$

The last term on the right-hand side can be optimised in T at $T = \frac{\epsilon}{c}\Big(\frac{h^2}{\zeta_*\sigma^2}\Big)^{-\frac{1}{2}}\exp\left\{\tilde{\kappa}\frac{h^2}{\zeta_*\sigma^2}\right\}$, from which the corollary is proven. □

The right-hand side in (8.2.1) depends on g and p due to the presence of c and $\tilde{\kappa}$. While the nature of the dependence is not trivial, it is apparent that it also affects the bound in an exponential scale.

8.3 Summary

In this chapter, we analyse the probability of noise-induced transitions in the space-heterogeneous Chafee-Infante equation with additive noise. Specifically, we study the first exit-time from a small neighbourhood of the deterministic solution and derive an upper bound on its distribution function, which leads to lower bounds on its moments. These bounds provide insight into how noise can trigger transitions departing from the metastable null state, and how close the system can be brought to bifurcation before such transitions become likely. In fact, although the system is monostable for the assumed conditions, the addressed phenomenon describes the first stage of N-tipping.

9 Lower bound to Transition Probability

The flow of a fluid is known to display different behaviour depending on its physical properties and the shape of the geometry traversed. In this chapter, we use the material from [24] to study the plane Couette flow, or flow along a pipe, and the transition to turbulence starting from an initially laminar state [136]. Recently, this area has been connected to directed percolation, a classical topic of probability theory. It is known that the transition to turbulence crucially depends upon the Reynolds number, i.e., on the ratio between inertial and viscous forces in a fluid. From a mathematical perspective, studying the transition to turbulence directly in the Euler or Navier-Stokes equations turns out to be extremely difficult. Nonetheless, quite recently, other simplified models have been proposed and directly validated against experiments.
The first model proposed in [12, 13] is defined by two coupled SPDEs that include second-order dissipation, an advection term, and multiplicative degenerate Itô noise [165]. The solution of this system may display structures referred to as slugs for high Reynolds numbers, and the turbulent state covers the whole pipe in finite time with a high probability. Conversely, for low values of the corresponding parameter, the turbulent regions are absorbed in the laminar state in finite time with high probability. Lastly, travelling structures called puffs indicate a fluctuating transition for intermediate values. In such cases, metastable transitions between turbulent and laminar states are observed in the pipe. The study of the rise and the splitting of puffs is relevant to describe the transition to turbulence as a rare event [91]. The steps involved in such an occurrence can be described through the computation of instantons, most likely paths to display rare occurrences [142, 199] (see also Chapter 10).
The complex structure provided by the model discussed above is not observed for all fluids and is in contrast with the perspective of [171, 172]. In this case, the turbulent state is seen as a fluctuating state able to decay spontaneously. Conversely, the laminar state is an absorbing state, which is unable to induce turbulence into the system. The alternative model proposed in [92] is a one-dimensional SPDE lacking advection. Furthermore, this simplified model does not show well-defined travelling states such as puffs and slugs. For this reason, the flow is labelled as band-free. In particular, the transition to turbulence is primarily driven by noise and occurs more rarely than in the previously discussed cases. The transition mechanism can be studied numerically through the adjoint state method (Chapter 10), which captures the instanton for various types of noise. Alternatively, the Trajectory-Adaptive Multilevel Sampling algorithm (TAMS) computes different trajectories that display such an event [142, 199]. Along with the description of such an occurrence, the analytic estimation of the probability of jumps provides a valuable tool to predict the likelihood of this phenomenon.
The metastable jump to turbulence is rare under the assumption of initial conditions close to the laminar state. Under such conditions, we label this transition as turbulence initiation, or turbulence onset, to indicate that it is primarily induced by noise. Therefore, the linearisation of the model near such a steady state is a natural simplification. The linearised system resembles the cable equation [196], or a heat equation with a second linear dissipative term, with multiplicative noise. The literature regarding such a model is vast. These types of SPDEs have been studied in a theoretical context to understand the influence of noise on potential finite-time blow-up of the solution. In particular, for standard white noise multiplied by a multiplicative term of order $\gamma > \frac{3}{2}$, the mild solution is proven to diverge in finite time [164, 163]. Conversely, for a multiplicative term of order $0 \leq \gamma \leq \frac{3}{2}$, the mild solution of the linear system does not explode in finite time [162, 177]. Although the band-free plane Couette flow model considers noise of order $\gamma = 1$, we show in this chapter that analytic techniques employed in the proof of blow-up of the mild solution, in [163], can be applied to our case of interest to describe turbulence initiation under Itô white Gaussian noise.
In [13], different types of noise are admitted to perturb the system, although only Itô noise is addressed, to simplify numerical simulations. In this work, we study the onset of turbulence for various Gaussian noise

terms. For instance, Stratonovich noise is a natural alternative to Itô noise in physical applications and fluid dynamics, particularly due to the chain rule property [84, 113]. The computation of higher bounds for the probability of metastable transitions has already been achieved for cable equations under the assumption of additive Itô noise ([19] and Chapter 8). Under such assumptions, the solution to the problem displays a qualitatively different behaviour from the multiplicative noise case: first, its sign can change in contrast to the cable equation with multiplicative noise; furthermore, the laminar state is not an absorbing state, which is a fundamental property of the original system. Nevertheless, the Cole-Hopf transformation reveals structural parallels between the systems. In fact, the study of the strong solution of the original system under Stratonovich noise on a logarithmic scale, in the form of the Kardar–Parisi–Zhang (KPZ) equation, displays an additive noise term [14, 57, 99]. Standard techniques enable the construction of a lower bound to the probability of transition to turbulence in specific domain regions. This method is then extended to the case of red noise in order to introduce memory in the noise component. We discuss two different interpretations of red (Stratonovich) noise, which are known to find applications in climate science [134, 161].

In conclusion, our methods prove the possibility of transition to turbulent states under different types of noise assumptions in simplified fluid dynamics models that have been suggested in applications. These results are implied by the stochastic perturbations in the system despite the non-trivial nature of the noise involved. Furthermore, they advance the analytic study of SPDEs, particularly with (multiplicative) Stratonovich noise.

9.1 Turbulence model and linearisation

We introduce the spatial interval $\mathcal{X}_1 = [0, L]$ for $L > 0$, to be interpreted as the width of a pipe. For $x \in \mathcal{X}_1$ and $t > 0$, we define a variable $q = q(x, t)$ modelling the turbulence level of a fluid along the plane Couette flow as discussed in [13, 92]. We study a family of stochastic partial differential equations (SPDEs) used as simplified transition-to-turbulence models, for which we provide a mathematical and physical interpretation below. The SPDEs are given by

$$\begin{cases} \mathrm{d}q(x,t) = \left(\partial_{xx}^2 q(x,t) - q(x,t) + (r+1)q(x,t)^2\left(2 - q(x,t)\right) + \sigma_{\mathsf{R}} q(x,t) \circ F(\xi)(x,t)\right)\mathrm{d}t \\ \qquad\qquad + \sigma_{\mathsf{I}} q(x,t) Q^{\frac{1}{2}} \mathrm{d}W_t + \sigma_{\mathsf{S}} q(x,t) \circ Q^{\frac{1}{2}} \mathrm{d}W_t, \\ \partial_x q(0,t) = \partial_x q(L,t) = 0, \\ q(x,0) = q_0(x). \end{cases} \tag{9.1.1}$$

We interpret $r > 0$ as a value related to the Reynolds number, which defines the behaviour of the solution. The family of models (9.1.1) includes noises of different forms to consider different interpretations of the small stochastic forcing. Therefore, the following parameters are to be interpreted as intensities of the noise term and are justified by models describing turbulence: $\sigma_{\mathsf{I}} \geq 0$ as the intensity of white noise interpreted in the Itô sense [92]; $\sigma_{\mathsf{S}} \geq 0$ as the intensity of white noise interpreted in the Stratonovich perspective [84], labelled with $\circ$; $\sigma_{\mathsf{R}} \geq 0$ as a correlation intensity which can induce perturbations in the system [134, 161] in Stratonovich sense. The Itô and Stratonovich assumptions are mathematically equivalent, as they can be converted by including the Itô-Stratonovich correction term ([88, 192] and Subsection 2.2.4). As such, we always assume $\sigma_{\mathsf{I}}\sigma_{\mathsf{S}} = 0$. Then, under the assumption of red noise, we introduce the adapted Ornstein-Uhlenbeck process $\xi = \xi(x, t)$ in $\mathcal{H}_1 = L^2(\mathcal{X}_1)$ and assume $\sigma_{\mathsf{R}} > 0$. The operator F is interpreted as a differential operator that maps the Ornstein-Uhlenbeck process to $\mathcal{H}_1$. Examples are provided in Subsection 9.3.2. Conversely, the noise is interpreted in Section 9.2 as Itô white noise in time, i.e., $\sigma_{\mathsf{I}} > \sigma_{\mathsf{S}} = \sigma_{\mathsf{R}} = 0$, and in Subsection 9.3.1 as Stratonovich white noise in time, i.e., $\sigma_{\mathsf{S}} > \sigma_{\mathsf{I}} = \sigma_{\mathsf{R}} = 0$. The systems discussed in the chapter are converted to the Itô noise form in Appendix G. We introduce the cylindrical Wiener process W, as defined in Chapter 2. The noise $Q^{\frac{1}{2}}W$, considered as minor fluctuations in the fluid, is then assumed to be a Q-Wiener process. We define the eigenvalues of Q as $\{\zeta_i\}_{i\in\mathbb{N}}$ with corresponding eigenbasis $\{b_i\}_{i\in\mathbb{N}}$ of $\mathcal{H}_1$, described further below in each section.

The operator also assumes at least one of the following properties: it is trace-class, or it is bounded with eigenfunctions that converge to the eigenfunctions of the Laplacian in L^∞-norm with rate sufficient to imply the existence of the solution (Theorem 2.2.9 and Appendix B). The boundary conditions are specified as homogeneous Neumann, although our methods also extend to periodic boundary conditions. Lastly, the initial condition q_0 is assumed to be non-negative on $[0, L]$ and a positive function almost everywhere on the interval. Therefore, we consider q to be non-negative for any $t > 0$ and to not be initiated in the laminar state. Under these assumptions, the solution of (9.1.1) is proven in Theorem 2.2.9 to be in the Hilbert space $\mathcal{H}_1$ almost surely for $t > 0$ (see also Appendix B for the regularity of the diffusion term).
The deterministic system, i.e., $\sigma_{\mathsf{I}} = \sigma_{\mathsf{S}} = \sigma_{\mathsf{R}} = 0$, displays three steady states: $q_1 \equiv 0$, $q_2 \equiv q_-$ and $q_3 \equiv q_+$, for

$$q_\pm = 1 \pm \sqrt{\frac{r}{r+1}} \in [0, 2].$$

The deterministically stable states q_1 and q_3 are identified as the laminar and the turbulent state, respectively. The state q_2 is a saddle for the deterministic model. Lastly, we define τ_J as the first time $t \geq 0$, such that $||q(\cdot, t)||_\infty > J$. In Figure 9.1, we observe two examples of turbulence onset under Itô white noise and Stratonovich white noise assumptions, respectively. In each case, the initial state lies below the saddle, $0 < q_0 < q_2$, and $\tau_{q_3} < T = 10$. The initiation of turbulence is attributed to the growth of an L^p-norm. The paths are obtained through the TAMS algorithm [142].
In order to observe the behaviour of q in the proximity of the laminar state, we study the mild solution $u_\alpha = u_\alpha(x, t)$ of the linear system with corresponding noise,

$$\begin{cases} \mathsf{d}u_\alpha(x,t) = \left(\partial^2_{xx} u_\alpha(x,t) - \alpha u_\alpha(x,t) + \sigma_{\mathsf{R}} u_\alpha(x,t) \circ F(\xi)(x,t)\right) \mathsf{d}t \\ \qquad\qquad + \sigma_{\mathsf{I}} u_\alpha(x,t) Q^{\frac{1}{2}} \mathsf{d}W_t + \sigma_{\mathsf{S}} u_\alpha(x,t) \circ Q^{\frac{1}{2}} \mathsf{d}W_t, \\ \partial_x u_\alpha(0,t) = \partial_x u_\alpha(L,t) = 0, \\ u_\alpha(x,0) = q_0(x), \end{cases} \tag{9.1.2}$$

for $\alpha = 1$. We refer to the solution of the system following the noise assumptions, i.e., the values of $\sigma_{\mathsf{I}}, \sigma_{\mathsf{S}}, \sigma_{\mathsf{R}}$: we denote by $u^{\mathsf{I}}_\alpha = u^{\mathsf{I}}_\alpha(x, t)$ the mild solution of (9.1.2) under Itô white noise; $u^{\mathsf{S}}_\alpha = u^{\mathsf{S}}_\alpha(x, t)$ is the strong solution under Stratonovich white noise; $u^{\mathsf{R}}_\alpha = u^{\mathsf{R}}_\alpha(x, t)$ refers to the strong solution under Stratonovich red noise. The existence of such solutions follows from Theorem 2.2.7 and Theorem 2.2.8. We focus on the case for which $q \leq 2$, as $0 \equiv q_1 < q_2 < q_3 < 2$. We define υ^{S}_J as the first time $t \geq 0$, such that $||u^{\mathsf{S}}_\alpha(\cdot, t)||_\infty > J$. Equivalently, υ^{I}_J is the first time t, such that $||u^{\mathsf{I}}_\alpha(\cdot, t)||_\infty > J$. Therefore, we can prove the lemma to follow.

Lemma 9.1.1. *Consider q, the mild solution of* (9.1.1)*, and u_1, the mild solution of* (9.1.2) *for $\alpha = 1$, $x \in [0, L]$ and $t \in [0, T]$. Moreover, assume that $q(x, t) \leq 2$ for any $x \in [0, L]$ and $t \in [0, T]$. Then, the conclusions are:*

(a) the inequality $q(x, t) \geq u_1(x, t)$ holds under the same sample W and for almost every $x \in [0, L]$ and $t \in [0, T]$;

(b) for $J \leq 2$ and $\sigma_S > \sigma_I = 0$, the inequality $\tau_J \leq \upsilon^S_J$ holds;

(c) for $J \leq 2$ and $\sigma_I > \sigma_S = 0$, the inequality $\tau_J \leq \upsilon^I_J$ holds.

Proof. We study $\tilde{u} = q - u_1$ under the assumptions $\sigma_{\mathsf{I}} \geq 0$, $\sigma_{\mathsf{S}} \geq 0$ and $\sigma_{\mathsf{R}} \geq 0$. The difference $\tilde{u}$ is the mild solution of

$$\begin{cases} \mathsf{d}\tilde{u}(x,t) = \left(\partial^2_{xx}\tilde{u}(x,t) - \tilde{u}(x,t) + (r+1)q(x,t)^2\left(2 - q(x,t)\right) + \sigma_{\mathsf{R}}\tilde{u}(x,t) \circ F(\xi)(x,t)\right) \mathsf{d}t \\ \qquad\qquad + \sigma_{\mathsf{I}}\tilde{u}(x,t) Q^{\frac{1}{2}} \mathsf{d}W_t + \sigma_{\mathsf{S}}\tilde{u}(x,t) \circ Q^{\frac{1}{2}} \mathsf{d}W_t, \\ \partial_x \tilde{u}(0,t) = \partial_x \tilde{u}(L,t) = 0, \\ \tilde{u}(x,0) \equiv 0. \end{cases}$$

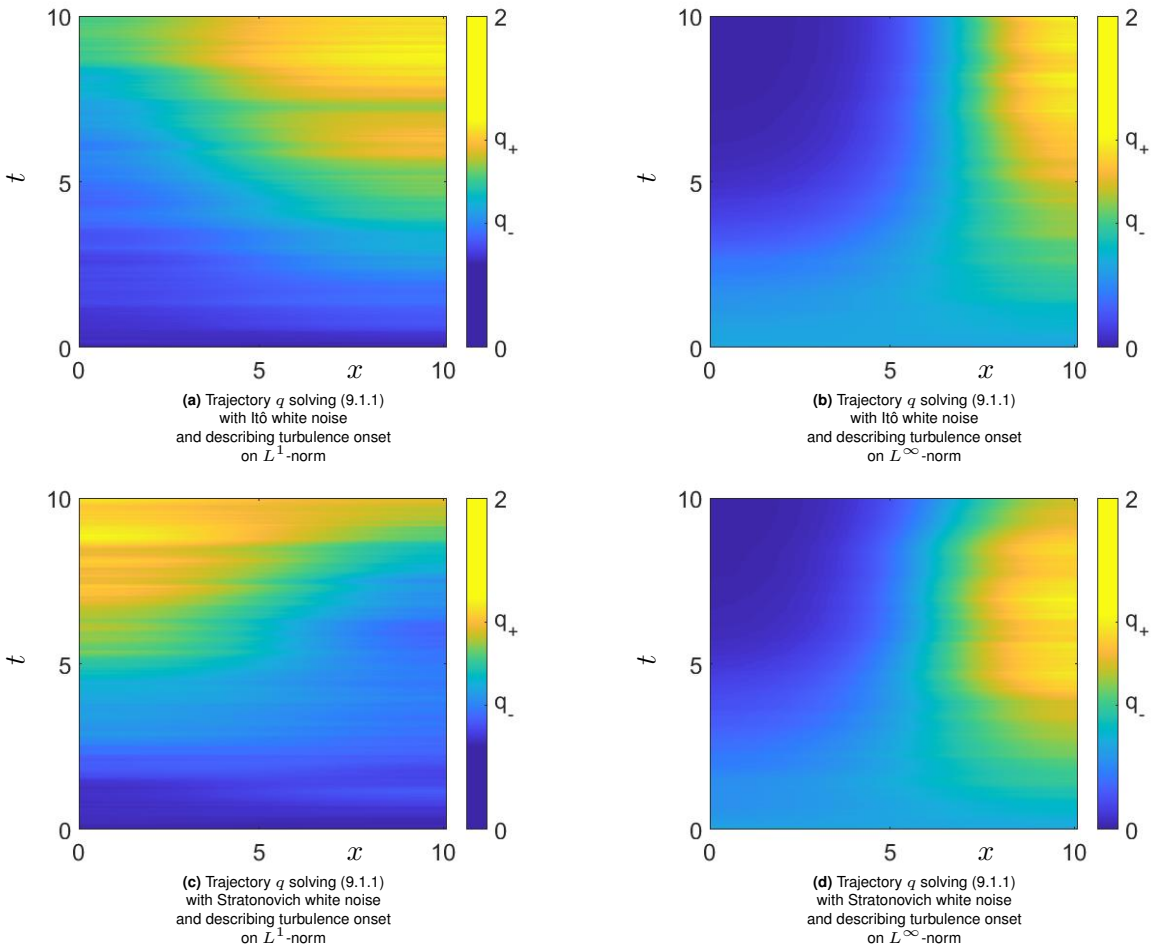

(a) Trajectory q solving (9.1.1) with Itô white noise and describing turbulence onset on L^1-norm

(b) Trajectory q solving (9.1.1) with Itô white noise and describing turbulence onset on L^∞-norm

(c) Trajectory q solving (9.1.1) with Stratonovich white noise and describing turbulence onset on L^1-norm

(d) Trajectory q solving (9.1.1) with Stratonovich white noise and describing turbulence onset on L^∞-norm

Fig. 9.1 Panels (a) and (b) show trajectories of q, solution of (9.1.1), indicating the onset of turbulence under Itô noise, $0.5 = \sigma_{\mathsf{I}} > \sigma_{\mathsf{S}} = \sigma_{\mathsf{R}} = 0$; whereas in (c) and (d) it is associated with Stratonovich noise, $0.5 = \sigma_{\mathsf{S}} > \sigma_{\mathsf{R}} = \sigma_{\mathsf{R}} = 0$. The interpretation of turbulence initiation is associated with an L^p-norm described below.
We consider $\{e_i\}_{i\in\mathbb{N}}$ the normalised eigenfunctions of the Laplace operator on $[0, L]$ under Neumann boundary conditions. We assume the noise perturbation on the solution along 101 modes, $b_i = e_i$ for $i \in \{0, \dots, 100\}$, with intensity $\zeta_i = \exp\left(-(i-1)^2\right)$. The initial solution is set at $q_0 \equiv 0.5$. The Reynolds parameter is $r = \frac{1}{15}$, which implies that $q_- = 0.75$ and $q_+ = 1.25$. We set $L = T = 10$ and space and time step as 0.1 and 0.01, respectively. In (a) and (c) we observe the rise of $||q||_1$ to the value q_+L, while in (b) and (d) we capture the rise of $||q||_\infty$ to the value q_+. These rare events are computed via the TAMS algorithm, for which we run 50 simulations each and use the respective norm as a score function. The simulations are achieved through the discretised mild solution formula. As described in Appendix G, the systems differ in view of the Itô-Stratonovich correction term, which implies an additional heterogeneous positive drift term in the case of Stratonovich white noise.

Therefore, it solves,

$$\begin{aligned}\tilde{u}(x,t) =&(r+1)\int_0^t \mathsf{e}^{(t-s)\left(\partial_{xx}^2-1\right)}\left(q(x,s)^2\left(2-q(x,s)\right)\right)\mathsf{d}s\\ &+\sigma_{\mathsf{R}}\int_0^t \mathsf{e}^{(t-s)\left(\partial_{xx}^2-1\right)}\tilde{u}(x,s)\circ F(\xi)(x,s)\mathsf{d}s\\ &+\sigma_{\mathsf{I}}\int_0^t \mathsf{e}^{(t-s)\left(\partial_{xx}^2-1\right)}\tilde{u}(x,s)Q^{\frac{1}{2}}\mathsf{d}W_s+\sigma_{\mathsf{S}}\int_0^t \mathsf{e}^{(t-s)\left(\partial_{xx}^2-1\right)}\tilde{u}(x,s)\circ Q^{\frac{1}{2}}\mathsf{d}W_s.\end{aligned} \tag{9.1.3}$$

Due to the Neumann boundary conditions, the continuous semigroup $\mathsf{e}^{(t-s)\left(\partial_{xx}^2-1\right)}$ does not affect the sign of the argument function. Since the first term in the right-hand side of (9.1.3) is positive and by the fact that the other terms are multiplicative in $\tilde{u}$, it follows that $q(x,t) \geq u_1^{\mathsf{S}}(x,t)$ for any $x \in [0, L]$ and $t \in [0, T]$.

We set $\sigma_{\mathsf{S}} > \sigma_{\mathsf{I}} = 0$. If $\upsilon_J^{\mathsf{S}} \leq \tau_2$, then we obtain $\tau_J \leq \upsilon_J^{\mathsf{S}}$. Conversely, for $\tau_2 \leq \upsilon_J^{\mathsf{S}}$, it follows that $\tau_J \leq \upsilon_J^{\mathsf{S}}$, since $\tau_J \leq \tau_2$. The Itô noise perspective, i.e., case (c), can be proven through equivalent reasoning. □

The linearisation enables the construction of the following results and further justifies the study of the fundamental solution of the cable equation. We denote the fundamental solution by G_α, which solves the system

$$\begin{cases} \mathsf{d}G_\alpha(x,y,t,[0,L]) = \left(\partial_{xx}^2 - \alpha\right) G_\alpha(x,y,t,[0,L])\mathsf{d}t, \\ \partial_x G_\alpha(0,y,t,[0,L]) = \partial_x G_\alpha(L,y,t,[0,L]) = 0, \\ G_\alpha(x,y,0,[0,L]) = \delta_0(y-x), \end{cases} \tag{9.1.4}$$

where δ_0 is the Dirac delta. The solution G_α can be obtained through different methods [196]. For the purposes of this chapter, we consider solely the form

$$G_\alpha(x,y,t,[0,L]) = \mathsf{e}^{-t\alpha}\left(\sum_{n=0}^{\infty} e_n(x)e_n(y)\mathsf{e}^{t\lambda_n}\right),$$

for $\{e_i\}_{i\in\mathbb{N}}$ the eigenbasis of the Laplacian operator in $\mathcal{H}_1$ and for $\{\lambda_i\}_{i\in\mathbb{N}}$ the corresponding eigenfunctions. Under Neumann boundary conditions, they are defined as

$$\begin{aligned} e_0 &\equiv \frac{1}{\sqrt{L}}, \\ e_n(x) &= \sqrt{\frac{2}{L}}\cos\left(\frac{n\pi x}{L}\right), \text{ for any } n \in \mathbb{N}_{>0}, \\ \lambda_n &= -\left(\frac{n\pi}{L}\right)^2, \qquad \text{for any } n \in \mathbb{N}, \end{aligned}$$

for $x \in [0,L]$. Finally, it is easy to observe that the fundamental solution satisfies

$$\int_0^L G_\alpha(x,y,t,[0,L])G_\alpha(y,z,s,[0,L])\mathsf{d}y = G_\alpha(x,z,t+s,[0,L]), \tag{9.1.5}$$

for $t>0$, $s>0$ and $z \in [0,L]$.

9.2 Itô noise: Countering the drift component

In this section, we study white noise in Itô sense, interpreted as the assumption $\sigma_\mathsf{I} > \sigma_\mathsf{S} = \sigma_\mathsf{R} = 0$ in (9.1.1) and in (9.1.2). We assume $b_0 = e_0$ and that $\zeta_0 > 0$. We consider $u_\alpha^\mathsf{I} = u_\alpha^\mathsf{I}(x,t)$, the mild solution of (9.1.2) for $\alpha > 0$ as

$$u_\alpha^\mathsf{I}(x,t) = \int_0^L G_\alpha(x,y,t,[0,L])q_0(y)\mathsf{d}y + \sigma_\mathsf{I}\int_0^L\int_0^t G_\alpha(x,y,t-s,[0,L])u_\alpha^\mathsf{I}(y,s)Q^{\frac{1}{2}}\mathsf{d}W_s\mathsf{d}y. \tag{9.2.1}$$

For the fixed time $T>0$ and any $y \in [0,L]$, we define

$$\phi_\alpha(x,y,t,[0,L]) := G_\alpha(x,y,T-t,[0,L]),$$

where $x \in [0,L]$ and $t \in [0,T]$. By construction of (9.1.4), we have that ϕ_α solves

$$\begin{cases} \mathsf{d}\phi_\alpha(x,y,t,[0,L]) = \left(-\partial_{xx}^2 + \alpha\right)\phi_\alpha(x,y,t,[0,L])\mathsf{d}t, \\ \partial_x\phi_\alpha(0,y,t,[0,L]) = \partial_x\phi_\alpha(L,y,t,[0,L]) = 0, \\ \phi_\alpha(x,y,T,[0,L]) = \delta_0(y-x), \end{cases}$$

for $x \in [0, L]$ and $t \in [0, T)$. In the following lemma, we use ϕ_α to define an observable, which we prove to be a martingale.

Lemma 9.2.1. *For any $x \in [0, L]$ and $t \in [0, T]$, the process X defined as*

$$X_t = \int_0^L \int_0^L \phi_\alpha(x, y, t, [0, L]) u_\alpha^I(y, t) \, \mathrm{d}y\mathrm{d}x = \mathrm{e}^{-(T-t)\alpha} ||u_\alpha^I(\cdot, t)||_1, \tag{9.2.2}$$

with u_α^I denoting the mild solution of (9.1.2)*, is a non-negative $\mathcal{F}_t^W$-martingale. Its quadratic variation, $\langle X \rangle$, satisfies*

$$\langle X \rangle (t) \geq \zeta_0 \frac{\sigma_I^2}{L^2} \int_0^t X_s^2 \, \mathrm{d}s, \tag{9.2.3}$$

for any $t \in [0, T]$.

Proof. In the first part of the proof, we follow a similar approach to [164, Lemma 2.3] to prove that X is a $\mathcal{F}_t^W$-martingale. From its construction in (9.2.2), we consider the mild solution form of u_α^I in (9.2.1). Then, we employ property (9.1.5) to obtain

$$\begin{aligned} X_t = &\int_0^L \int_0^L \phi_\alpha(x, y, 0, [0, L]) q_0(y) \mathrm{d}y\mathrm{d}x \\ &+ \sigma_\mathsf{I} \int_0^L \int_0^L \int_0^t \phi_\alpha(x, y, s, [0, L]) u_\alpha^\mathsf{I}(y, s) Q^{\frac{1}{2}} \mathrm{d}W_s \mathrm{d}y\mathrm{d}x. \end{aligned} \tag{9.2.4}$$

The observable X is an $\mathcal{F}_t^W$-martingale since it is the sum of a constant and an $\mathcal{F}_t^W$-martingale, which is a stochastic integral with integrand independent of t. Its quadratic variation is

$$\langle X \rangle (t) = \sigma_\mathsf{I}^2 \int_0^L \int_0^L \int_0^t \left(Q^{\frac{1}{2}} \left(\phi_\alpha(x, y, s, [0, L]) u_\alpha^\mathsf{I}(y, s) \right) \right)^2 \mathrm{d}s\mathrm{d}y\mathrm{d}x. \tag{9.2.5}$$

Inequality (9.2.3) follows from similar steps to those included in the proof of [163, Lemma 2], which we adapt here to our setting. Through Jensen's inequality, we obtain

$$\begin{aligned} &\sigma_\mathsf{I}^2 \int_0^L \int_0^L \left(Q^{\frac{1}{2}} \left(\phi_\alpha(x, y, s, [0, L]) u_\alpha^\mathsf{I}(y, s) \right) \right)^2 \mathrm{d}y\mathrm{d}x \\ =&\sigma_\mathsf{I}^2 L^2 \int_0^L \int_0^L \left(Q^{\frac{1}{2}} \left(\phi_\alpha(x, y, s, [0, L]) u_\alpha^\mathsf{I}(y, s) \right) \right)^2 \frac{1}{L^2} \mathrm{d}y\mathrm{d}x \\ \geq&\sigma_\mathsf{I}^2 L^2 \left(\int_0^L \int_0^L Q^{\frac{1}{2}} \left(\phi_\alpha(x, y, s, [0, L]) u_\alpha^\mathsf{I}(y, s) \right) \frac{1}{L^2} \mathrm{d}y\mathrm{d}x \right)^2 \\ =&\sigma_\mathsf{I}^2 L^2 \left(\zeta_0^{\frac{1}{2}} \int_0^L \int_0^L \left(\phi_\alpha(x, y, s, [0, L]) u_\alpha^\mathsf{I}(y, s) \right) \frac{1}{L^2} \mathrm{d}y\mathrm{d}x \right)^2 = \zeta_0 \frac{\sigma_\mathsf{I}^2}{L^2} X_s^2. \end{aligned}$$

The proof is concluded by integrating the left-hand side and right-hand side over the time interval $s \in [0, t]$, for $t \in [0, T]$. □

As indicated in (9.2.2), the observable X is equivalent to the L^1-norm of u_α^I rescaled in time through an exponential weight. The weight increases with time t, and its effect balances the dissipative term in the cable equation in (9.1.2) for $\alpha > 0$. Consequently, the integrands in (9.2.4) do not depend on t, and X is a martingale. The simplicity of the formula is a consequence of the fact that $\lambda_0 = 0$ and that the corresponding eigenfunction e_0 is constant.
We set $J_1 = \frac{||q_0||_1}{L}$ and $J_0 \mathrm{e}^{-T\alpha} < J_1 \mathrm{e}^{-T\alpha} < J_1 < J_2$. From construction, we obtain $X_0 = L J_1 \mathrm{e}^{-T\alpha}$. The values J_0, J_1 and J_2 are chosen to guarantee the correctness of the studied inequalities upon rescaling

of $L, \sigma_{\mathsf{I}}, \alpha$ and T. Lastly, we define the stopping time τ as the first time at which X_t assumes the values $LJ_0\mathsf{e}^{-T\alpha}$ or LJ_2.

Lemma 9.2.2. *For any $\alpha > 0$, $\sigma_I > 0$, $T > 0$, we assume J_0, J_1 and J_2 as defined above. Then, the following result holds:*

$$\mathbb{P}\left(X_\tau = LJ_2\right) = \frac{J_1 - J_0}{J_2 e^{T\alpha} - J_0}. \tag{9.2.6}$$

Furthermore, the bound

$$\mathbb{P}\left(X_{\tau\wedge T} = LJ_2\right) \geq \frac{J_1 - J_0}{J_2 e^{T\alpha} - J_0} - \left(\frac{J_2}{J_0} e^{T\alpha} - \frac{J_1}{J_0}\right) \frac{L}{\zeta_0^{\frac{1}{2}} \sigma_I} T^{-\frac{1}{2}}, \tag{9.2.7}$$

holds for $\tau \wedge T = min\{\tau, T\}$.

Proof. Since X is a martingale, we can apply Doob's optional sampling theorem [27, Section 35] to obtain that

$$\mathbb{E}(X_\tau) = \mathbb{E}(X_0) = LJ_1\mathsf{e}^{-T\alpha}.$$

The definition of the stopping time τ implies that

$$\mathbb{E}(X_\tau) = LJ_2\mathbb{P}\left(X_\tau = LJ_2\right) + LJ_0\mathsf{e}^{-T\alpha}\left(1 - \mathbb{P}\left(X_\tau = LJ_2\right)\right),$$

from which equality (9.2.6) follows. The Dambis-Dubins-Schwarz theorem [174, Theorem V.1.6] and the fact that X is a continuous martingale entail that

$$X_t = LJ_1\mathsf{e}^{-T\alpha} + \tilde{W}\left(\langle X\rangle(t)\right),$$

for some scalar Wiener process $\tilde{W}(t)$ and any $t \in [0, T]$. Setting the martingale in such a form implies

$$\begin{aligned}
\mathbb{P}\left(T < \tau\right) &= \mathbb{P}\left(T < t, LJ_0\mathsf{e}^{-T\alpha} < X_t < LJ_2, \text{for } t \in [0, T]\right) \\
&\leq \mathbb{P}\left(T < t, X_t < LJ_2, \text{for } t \in [0, T]\right) \\
&= \mathbb{P}\left(T < t, LJ_1\mathsf{e}^{-T\alpha} + \tilde{W}\left(\langle X\rangle(t)\right) < LJ_2, \text{ for } t \in [0, T]\right).
\end{aligned} \tag{9.2.8}$$

In the case $t < \tau$, it follows from (9.2.3) that

$$\langle X\rangle(t) \geq \zeta_0\sigma_{\mathsf{I}}^2 J_0^2\mathsf{e}^{-2T\alpha}t$$

and, from (9.2.8), that

$$\begin{aligned}
\mathbb{P}\left(T < \tau\right) &\leq \mathbb{P}\left(T < t, LJ_1\mathsf{e}^{-T\alpha} + \tilde{W}\left(\langle X\rangle(t)\right) < LJ_2, \text{ for } t \in [0, T]\right) \\
&\leq \mathbb{P}\left(T < t, LJ_1\mathsf{e}^{-T\alpha} + \tilde{W}(t) < LJ_2, \text{ for } t \in [0, \langle X\rangle(T)]\right) \\
&\leq \mathbb{P}\left(T < t, LJ_1\mathsf{e}^{-T\alpha} + \tilde{W}(t) < LJ_2, \text{ for } t \in \left[0, \zeta_0\sigma_{\mathsf{I}}^2 J_0^2\mathsf{e}^{-2T\alpha}T\right]\right).
\end{aligned}$$

Subsequently, we get

$$\begin{aligned}
\mathbb{P}\left(T < \tau\right) &\leq \mathbb{P}\left(T < t, LJ_1\mathsf{e}^{-T\alpha} + \tilde{W}(t) < LJ_2, \text{ for } t \in \left[0, \zeta_0\sigma_{\mathsf{I}}^2 J_0^2\mathsf{e}^{-2T\alpha}T\right]\right) \\
&\leq \mathbb{P}\left(\sup_{t\in\left[0,\zeta_0\sigma_{\mathsf{I}}^2 J_0^2\mathsf{e}^{-2T\alpha}T\right]} \tilde{W}(t) < LJ_2 - LJ_1\mathsf{e}^{-T\alpha}\right) \\
&= 1 - \mathbb{P}\left(\sup_{t\in\left[0,\zeta_0\sigma_{\mathsf{I}}^2 J_0^2\mathsf{e}^{-2T\alpha}T\right]} \tilde{W}(t) \geq LJ_2 - LJ_1\mathsf{e}^{-T\alpha}\right).
\end{aligned}$$

Then, through the reflection principle, we obtain

$$\begin{aligned}\mathbb{P}\left(T<\tau\right) &\leq 1-\mathbb{P}\left(\sup_{t\in\left[0,\zeta_0\sigma_{\mathsf{I}}^2J_0^2\mathsf{e}^{-2T\alpha}T\right]}\tilde{W}\left(t\right)\geq LJ_2-LJ_1\mathsf{e}^{-T\alpha}\right)\\ &=1-2\mathbb{P}\left(\tilde{W}\left(\zeta_0\sigma_{\mathsf{I}}^2J_0^2\mathsf{e}^{-2T\alpha}T\right)\geq LJ_2-LJ_1\mathsf{e}^{-T\alpha}\right)\\ &=\mathbb{P}\left(\left|\tilde{W}\left(\zeta_0\sigma_{\mathsf{I}}^2J_0^2\mathsf{e}^{-2T\alpha}T\right)\right|\leq LJ_2-LJ_1\mathsf{e}^{-T\alpha}\right)\\ &=\left(2\pi\zeta_0\sigma_{\mathsf{I}}^2J_0^2\mathsf{e}^{-2T\alpha}T\right)^{-\frac{1}{2}}\int_{-LJ_2+LJ_1\mathsf{e}^{-T\alpha}}^{LJ_2-LJ_1\mathsf{e}^{-T\alpha}}\exp\left(-\frac{x^2}{2\zeta_0\sigma_{\mathsf{I}}^2J_0^2\mathsf{e}^{-2T\alpha}T}\right)\mathrm{d}x\\ &\leq\left(\frac{J_2}{J_0}\mathsf{e}^{T\alpha}-\frac{J_1}{J_0}\right)\frac{L}{\zeta_0^{\frac{1}{2}}\sigma_{\mathsf{I}}}T^{-\frac{1}{2}}.\end{aligned}\tag{9.2.9}$$

From (9.2.6) and (9.2.9), it follows that

$$\begin{aligned}\mathbb{P}\left(X_{\tau\wedge T}=LJ_2\right)&=\mathbb{P}\left(X_{\tau\wedge T}=LJ_2,T\geq\tau\right)\\ &=\mathbb{P}\left(X_\tau=LJ_2\right)-\mathbb{P}\left(X_\tau=LJ_2,T<\tau\right)\\ &\geq\mathbb{P}\left(X_\tau=LJ_2\right)-\mathbb{P}\left(T<\tau\right)\\ &\geq\frac{J_1-J_0}{J_2\mathsf{e}^{T\alpha}-J_0}-\left(\frac{J_2}{J_0}\mathsf{e}^{T\alpha}-\frac{J_1}{J_0}\right)\frac{L}{\zeta_0^{\frac{1}{2}}\sigma_{\mathsf{I}}}T^{-\frac{1}{2}},\end{aligned}$$

which concludes the proof. □

The inequality (9.2.7) provides a tool to establish a lower bound to the probability of rise of the L^1-norm of u_α^{I}. In fact, under the assumption that $LJ_2=X_{\tau\wedge T}$, we can obtain the following:

$$LJ_2=X_{\tau\wedge T}=\exp\left(-\alpha\left(T-\tau\wedge T\right)\right)\left|\left|u_\alpha^{\mathsf{I}}(\cdot,\tau\wedge T)\right|\right|_1\leq\sup_{0\leq t\leq T}\left|\left|u_\alpha^{\mathsf{I}}(\cdot,t)\right|\right|_1.$$

This entails that

$$\frac{J_1-J_0}{J_2\mathsf{e}^{T\alpha}-J_0}-\left(\frac{J_2}{J_0}\mathsf{e}^{T\alpha}-\frac{J_1}{J_0}\right)\frac{L}{\zeta_0^{\frac{1}{2}}\sigma_{\mathsf{I}}}T^{-\frac{1}{2}}\leq\mathbb{P}\left(LJ_2\leq\sup_{0\leq t\leq T}\left|\left|u_\alpha^{\mathsf{I}}(\cdot,t)\right|\right|_1\right),\tag{9.2.10}$$

which yields a further step towards the construction of a lower bound to the probability of the onset of turbulence. In fact, such a bound is carried over to the mild solution of (9.1.1) in the next corollary. Since the left-hand side can be negative for large values of T, the assumptions $\alpha\ll 1$ or $L\ll\sqrt{\zeta_0}\sigma_{\mathsf{I}}$ are required to ensure positivity for large intervals in time.

Corollary 9.2.3. *(a) Assume that q, the mild solution of* (9.1.1) *with Itô noise, satisfies $0<q(x,t)\leq 2$ for any $x\in[0,L]$ and $t\in[0,T]$. Furthermore, set the initial conditions such that*

$$0<J_0\mathsf{e}^{-T\alpha}<\frac{||q_0||_1}{L}\mathsf{e}^{-T\alpha}<\frac{||q_0||_1}{L}<J_2.$$

Then, it follows that

$$\frac{J_1-J_0}{J_2\mathsf{e}^{T}-J_0}-\left(\frac{J_2}{J_0}\mathsf{e}^{T}-\frac{J_1}{J_0}\right)\frac{L}{\zeta_0^{\frac{1}{2}}\sigma_{\mathsf{I}}}T^{-\frac{1}{2}}\leq\mathbb{P}\left(LJ_2\leq\sup_{0\leq t\leq T}||q(\cdot,t)||_1\right).$$

(b) Consider q, the mild solution of (9.1.1) *with Itô noise that satisfies*

$$0 < J_0 e^{-T\alpha} < \frac{||q_0||_1}{L} e^{-T\alpha} < \frac{||q_0||_1}{L} < J_2 < 2.$$

The following inequality holds:

$$\sup_{0\le t\le T}\left(\frac{J_1-J_0}{J_2 e^t - J_0} - \left(\frac{J_2}{J_0}e^t - \frac{J_1}{J_0}\right)\frac{L}{\zeta_0^{\frac{1}{2}}\sigma_I}t^{-\frac{1}{2}}\right) \le \mathbb{P}\left(J_2 \le \sup_{0\le t\le T}||q(\cdot,t)||_\infty\right). \tag{9.2.11}$$

Proof. The first statement follows directly from (9.2.10) for $\alpha = 1$ and Lemma 9.1.1 (a). In fact, since $q(x,t) \le 2$ for all $x \in [0,L]$ and $t \in [0,T]$, we obtain

$$\mathbb{P}\left(LJ_2 \le \sup_{0\le t\le T}\left|\left|u_1^{\mathsf{I}}(\cdot,t)\right|\right|_1\right) \le \mathbb{P}\left(LJ_2 \le \sup_{0\le t\le T}||q(\cdot,t)||_1\right).$$

Similarly to the latter case, (9.2.10) for $\alpha = 1$, Hölder's inequality and Lemma 9.1.1 (c) imply that

$$\begin{aligned}\frac{J_1-J_0}{J_2 e^T - J_0} - \left(\frac{J_2}{J_0}e^T - \frac{J_1}{J_0}\right)\frac{L}{\zeta_0^{\frac{1}{2}}\sigma_{\mathsf{I}}}T^{-\frac{1}{2}} &\le \mathbb{P}\left(LJ_2 \le \sup_{0\le t\le T}\left|\left|u_1^{\mathsf{I}}(\cdot,t)\right|\right|_1\right)\\ &\le \mathbb{P}\left(J_2 \le \sup_{0\le t\le T}\left|\left|u_1^{\mathsf{I}}(\cdot,t)\right|\right|_\infty\right) = \mathbb{P}\left(v_{J_2}^{\mathsf{I}} \le T\right)\\ &\le \mathbb{P}\left(\tau_{J_2} \le T\right) = \mathbb{P}\left(J_2 \le \sup_{0\le t\le T}||q(\cdot,t)||_\infty\right).\end{aligned}$$

Lastly, we obtain that, for any $T_0 \le T$,

$$\mathbb{P}\left(J_2 \le \sup_{0\le t\le T_0}||q(\cdot,t)||_\infty\right) \le \mathbb{P}\left(J_2 \le \sup_{0\le t\le T}||q(\cdot,t)||_\infty\right),$$

which concludes the proof. □

The statement in Corollary 9.2.3 pertains to the case in which we consider trajectories of q with initial conditions below the saddle state, $q_0 < q_2$, and final conditions between the saddle and the turbulence state, $q_- < J_2 < q_+$, thus indicating turbulence initiation. Moreover, the assumption $q(x,t) \le 2$ for all $x \in [0,L]$ and $t \in [0,T]$ is also not required to obtain the inequality (9.2.11).
In this setting, the lower bound is valid (positive), for large time intervals under the assumption of thin pipes or large noise intensity. Aside from the value J_2 that indicates the transition to turbulence occurrence, the lower bound in (9.2.7) is affected by the choice of J_0. This has further implications on the role of the final time T since the definition of the stopping time τ depends on J_0. However, in (9.2.11), the sign of the lower bound is not affected by the size of the time interval considered and is constant for sufficiently large T. This is reflected by the dissipation towards q_1 in the drift component of the mild solution q. Such a behaviour indicates that the possibility of the initiation of turbulence is less likely after large times. This property is discussed further in Section 9.4.

9.3 Stratonovich noise: Comparison SPDEs in a logarithmic scale

In this section, we set $\sigma_{\mathsf{S}} + \sigma_{\mathsf{R}} > \sigma_{\mathsf{I}} = 0$ when studying (9.1.1). In order to enforce the existence of the strong solution of the system with Stratonovich noise through Theorem 2.2.8, we enforce the following assumptions. For fixed $m \in \mathbb{N}_{>0}$, we assume that

$$\zeta_i = 0, \text{ for } i > m,$$

and that there exists an $i \in \{0, \dots, m\}$ such that $\zeta_i > 0$ and $\langle e_0, b_i \rangle \neq 0$. Adhering to the study of the linearised system as justified in Lemma 9.1.1, we focus on a generalised version of the system (9.1.2). The model

$$\begin{cases} \mathsf{d}u(x,t) = \left(\partial_{xx}^2 u(x,t) - g(x)u(x,t) + \sigma_{\mathsf{R}} u(x,t) \circ F\left(\xi\right)(x,t)\right) \mathsf{d}t + \sigma_{\mathsf{S}} u(x,t) \circ Q^{\frac{1}{2}} \mathsf{d}W_t, \\ \partial_x u(0,t) = \partial_x u(L,t) = 0, \\ u(x,0) = q_0(x), \end{cases} \tag{9.3.1}$$

for $x \in [0, L]$ and $t > 0$, accounts for space-heterogeneity through the inclusion of the non-negative function $g \in \mathcal{H}_1$. Such an assumption follows from the applications in which the cable equation is found, such as climate science, due to the recurrent discrepancies in certain domain regions that can be found in such fields. In the next subsections, we obtain a lower bound to the probability of the turbulence onset for white and red Stratonovich noise, respectively.

9.3.1 White Stratonovich noise

We set $\sigma_{\mathsf{R}} = 0$ in order to study white Stratonovich noise in time in the equation (9.3.1). The following lemma enables the study of the system on a logarithmic scale through the inverse Cole-Hopf transformation, thus obtaining the KPZ equation [99].

Lemma 9.3.1. *Consider $u_g^{\mathsf{S}} = u_g^{\mathsf{S}}(x,t)$, the strong solution of* (9.3.1) *for $x \in [0, L]$ and $t > 0$. Then, $v_g^{\mathsf{S}}(x,t) = v_g^{\mathsf{S}} := \log\left(u_g^{\mathsf{S}}\right)$ is the strong solution of*

$$\begin{cases} \mathsf{d}v_g^{\mathsf{S}}(x,t) = \left(\partial_{xx}^2 v_g^{\mathsf{S}}(x,t) + \left(\partial_x v_g^{\mathsf{S}}(x,t)\right)^2 - g(x)\right) \mathsf{d}t + \sigma_{\mathsf{S}} Q^{\frac{1}{2}} \mathsf{d}W_t, \\ \partial_x v_g^{\mathsf{S}}(0,t) = \partial_x v_g^{\mathsf{S}}(L,t) = 0, \\ v_g^{\mathsf{S}}(x,0) = \log\left(q_0(x)\right), \end{cases} \tag{9.3.2}$$

for $x \in [0, L]$ and $t > 0$.

Proof. Imposing $u_g^{\mathsf{S}} = \exp\left(v_g^{\mathsf{S}}\right)$ in (9.3.1), we obtain

$$\begin{cases} \begin{aligned} \mathsf{d}v_g^{\mathsf{S}}(x,t) &= u_g^{\mathsf{S}}(x,t)^{-1} \circ \mathsf{d}u_g^{\mathsf{S}}(x,t) \\ &= \left(u_g^{\mathsf{S}}(x,t)^{-1} \partial_{xx}^2 u_g^{\mathsf{S}}(x,t) - g(x) u_g^{\mathsf{S}}(x,t)\right) \mathsf{d}t + \left(\sigma_{\mathsf{S}} u_g^{\mathsf{S}}(x,t)^{-1} u_g^{\mathsf{S}}(x,t)\right) \circ Q^{\frac{1}{2}} \mathsf{d}W_t \\ &= \left(\partial_{xx}^2 v_g^{\mathsf{S}}(x,t) + \left(\partial_x v_g^{\mathsf{S}}(x,t)\right)^2 - g(x)\right) \mathsf{d}t + \sigma_{\mathsf{S}} Q^{\frac{1}{2}} \mathsf{d}W_t, \end{aligned} \\ u_g^{\mathsf{S}}(0,t) \partial_x v_g^{\mathsf{S}}(0,t) = u_g^{\mathsf{S}}(L,t) \partial_x v_g^{\mathsf{S}}(L,t) = 0, \\ \exp\left(v_g^{\mathsf{S}}(x,0)\right) = q_0(x). \end{cases}$$

The boundary conditions in (9.3.2) follow from the fact that u_g^{S} and q_0 are, by construction, almost surely positive functions for any $t > 0$. □

The key benefit of the logarithmic perspective is the conversion of noise from a multiplicative form to an additive one. As a consequence, the nature of the drift component in (9.3.1) and (9.3.2) is drastically different. The system (9.3.2) is not linear since a shear deformation term is included, and a linear-in-time flow affects the solution. The lemma to follow aims to simplify the problem further.

Lemma 9.3.2. *Consider v_g^{S}, strong solution of* (9.3.2)*, and $w_g^{\mathsf{S}} = w_g^{\mathsf{S}}(x,t)$, the strong solution of*

$$\begin{cases} \mathsf{d}w_g^{\mathsf{S}}(x,t) = \left(\partial_{xx}^2 w_g^{\mathsf{S}}(x,t) - g(x)\right)\mathsf{d}t + \sigma_{\mathsf{S}} Q^{\frac{1}{2}}\mathsf{d}W_t, \\ \partial_x w_g^{\mathsf{S}}(0,t) = \partial_x w_g^{\mathsf{S}}(L,t) = 0, \\ w_g^{\mathsf{S}}(x,0) = \mathsf{log}\left(q_0(x)\right), \end{cases} \tag{9.3.3}$$

for $x \in [0,L]$ and $t > 0$. Then, $v_g^{\mathsf{S}}(x,t) \geq w_g^{\mathsf{S}}(x,t)$ holds for the same sample of W, for any almost $x \in [0,L]$ and $t > 0$.

Proof. We define $\tilde{w} = v_g^{\mathsf{S}} - w_g^{\mathsf{S}}$. By construction, it solves

$$\begin{cases} \partial_t \tilde{w}(x,t) = \partial_{xx}^2 \tilde{w}(x,t) + \left(\partial_x v_g^{\mathsf{S}}(x,t)\right)^2, \\ \partial_x \tilde{w}(0,t) = \partial_x \tilde{w}(L,t) = 0, \\ \tilde{w}(x,0) \equiv 0. \end{cases}$$

The conclusion of the proof follows the same reasoning as Lemma 9.1.1. □

For the existence of w_g^{S}, we refer to Theorem 2.2.4. System (9.3.3) can be easily observed along the elements of a basis in $\mathcal{H}_1$. In the following lemma, the projections of the strong solution w_g^{S} along the eigenbasis of the Laplacian operator are studied.

Lemma 9.3.3. *Consider w_g^{S}, the strong solution of* (9.3.3) *for $x \in [0,L]$ and $t > 0$. Then, for all $n \in \mathbb{N}$, the scalar product $I_{n,g}(t) := \left\langle e_n, w_g^{\mathsf{S}}(\cdot,t)\right\rangle$ is the strong solution of*

$$\begin{cases} \mathsf{d}I_{n,g}(t) = \left(\lambda_n I_{n,g}(t) - \langle e_n, g\rangle\right)\mathsf{d}t + \sigma_{\mathsf{S}} \displaystyle\sum_{i=0}^{m} \left(\zeta_i^{\frac{1}{2}} \langle e_n, b_i\rangle \mathsf{d}\beta_i(t)\right), \\ I_{n,g}(0) = \langle e_n, \mathsf{log}\left(q_0\right)\rangle, \end{cases} \tag{9.3.4}$$

for any $t > 0$.

Proof. We arbitrarily fix $n \in \mathbb{N}$. Through (9.3.3), we obtain

$$\begin{cases} \mathsf{d}\left\langle e_n, w_g^{\mathsf{S}}(\cdot,t)\right\rangle = \left(\left\langle e_n, \partial_{xx}^2 w_g^{\mathsf{S}}(\cdot,t)\right\rangle - \langle e_n, g\rangle\right)\mathsf{d}t + \sigma_{\mathsf{S}}\left\langle Q^{\frac{1}{2}} e_n, \mathsf{d}W_t\right\rangle \\ \qquad = \left(\lambda_n \left\langle e_n, w_g^{\mathsf{S}}(\cdot,t)\right\rangle - \langle e_n, g\rangle\right)\mathsf{d}t + \sigma_{\mathsf{S}}\left\langle \displaystyle\sum_{i=0}^{m} \zeta_i^{\frac{1}{2}} \langle e_n, b_i\rangle b_i, \mathsf{d}W_t\right\rangle \\ \qquad = \left(\lambda_n \left\langle e_n, w_g^{\mathsf{S}}(\cdot,t)\right\rangle - \langle e_n, g\rangle\right)\mathsf{d}t + \sigma_{\mathsf{S}} \displaystyle\sum_{i=0}^{m} \left(\zeta_i^{\frac{1}{2}} \langle e_n, b_i\rangle \mathsf{d}\beta_i(t)\right), \\ I_{n,g}(0) = \langle e_n, \mathsf{log}\left(q_0\right)\rangle, \end{cases}$$

for $t > 0$, which concludes the proof. □

The previous lemmas in this section describe, in their entirety, a chain of inequalities that constitute a bound from below of the strong solution u_g^{S} of system (9.3.1). This approach is employed in the following theorem to define a bound to the probability of growth in a fixed time of u_g^{S} on regions of the domain.

Theorem 9.3.4. *Under the assumption that u_g^S is the strong solution of* (9.3.1) *for $x \in [0, L]$ and $t > 0$, the following inequality holds for any non-negative function $f \in \mathcal{H}_1$ that is nonzero almost everywhere:*

$$1 - \Phi\left(\frac{||f||_1 \mathit{log}\left(||f||_1^{-1} J'\right) - \left(\left\langle \mathit{e}^{t\partial_{xx}^2} f, \mathit{log}\left(q_0\right)\right\rangle - a_0 \langle e_0, g\rangle t + \sum_{n=1}^{\infty} a_n \frac{\langle e_n, g\rangle}{\lambda_n}\left(1 - \mathit{e}^{t\lambda_n}\right)\right)}{\sigma_S\left(\sum_{i=0}^{m}\zeta_i\left(a_0^2\langle e_0, b_i\rangle^2 t - \sum_{(n_1,n_2)\neq(0,0)} a_{n_1}a_{n_2}\left(\frac{1-\mathit{e}^{t(\lambda_{n_1}+\lambda_{n_2})}}{\lambda_{n_1}+\lambda_{n_2}}\right)\langle e_{n_1}, b_i\rangle\langle e_{n_2}, b_i\rangle\right)\right)^{\frac{1}{2}}}\right)$$
$$\leq \mathbb{P}\left(J' \leq \left\langle f, u_g^S(\cdot, t)\right\rangle\right), \tag{9.3.5}$$

for Φ, the cumulative distribution function of a standard normally distributed random variable, $J' > 0$, and $a_n = \langle e_n, f\rangle$ for any $n \in \mathbb{N}$.

Proof. We know that

$$I_{n,g}(t) = \mathsf{e}^{t\lambda_n} I_{n,g}(0) + \frac{\langle e_n, g\rangle}{\lambda_n}\left(1 - \mathsf{e}^{t\lambda_n}\right) + \sigma_{\mathsf{S}} \sum_{i=0}^{m}\left(\zeta_i^{\frac{1}{2}}\langle e_n, b_i\rangle \int_0^t \mathsf{e}^{(t-s)\lambda_n}\mathsf{d}\beta_i(s)\right)$$

holds for any $n \in \mathbb{N}_{>0}$, and that

$$I_{0,g}(t) = I_{0,g}(0) - \langle e_0, g\rangle t + \sigma_{\mathsf{S}} \sum_{i=0}^{m}\left(\zeta_i^{\frac{1}{2}}\langle e_0, b_i\rangle \beta_i(s)\right).$$

It follows that

$$\mathbb{E}\left(I_{n,g}(t)\right) = \mathsf{e}^{t\lambda_n} I_{n,g}(0) + \frac{\langle e_n, g\rangle}{\lambda_n}\left(1 - \mathsf{e}^{t\lambda_n}\right),$$

for any $n \in \mathbb{N}_{>0}$, and also

$$\mathbb{E}\left(I_{0,g}(t)\right) = I_{0,g}(0) - \langle e_0, g\rangle t.$$

Moreover, from the construction of the systems (9.3.4) and the limit

$$\lim_{n\to\infty} -\frac{\lambda_n}{1+n^2} < \infty,$$

we obtain that

$$\mathbb{E}\left(\sum_{n=0}^{\infty} a_n I_{n,g}(t)\right) = a_0\left(I_{0,g}(0) - \langle e_0, g\rangle t\right) + \sum_{n=1}^{\infty} a_n\left(\mathsf{e}^{t\lambda_n} I_{n,g}(0) + \frac{\langle e_n, g\rangle}{\lambda_n}\left(1 - \mathsf{e}^{t\lambda_n}\right)\right) < \infty.$$

Lévy's continuity Theorem [27, Section 26] implies that $\sum_{n=0}^{\infty} a_n I_{n,g}(t)$ has a Gaussian distribution with variance

$$\begin{aligned}
&\mathsf{Var}\left(\sum_{n=0}^{\infty} a_n I_{n,g}(t)\right) = \mathsf{Var}\left(\left\langle f, w_g^{\mathsf{S}}(\cdot, t)\right\rangle\right) = \sigma_{\mathsf{S}}^2 \int_0^t \left\langle f, \mathsf{e}^{s\partial_{xx}^2} Q \mathsf{e}^{s\partial_{xx}^2} f\right\rangle \mathsf{d}s \\
=&\sigma_{\mathsf{S}}^2 \int_0^t \left\langle \sum_{n_1=0}^{\infty} a_{n_1}\mathsf{e}^{s\lambda_{n_1}} e_{n_1}, Q\sum_{n_2=0}^{\infty} a_{n_2}\mathsf{e}^{s\lambda_{n_2}} e_{n_2}\right\rangle \mathsf{d}s \\
=&\sigma_{\mathsf{S}}^2 \int_0^t \left\langle \sum_{n_1=0}^{\infty}\sum_{i_1=0}^{m} a_{n_1}\mathsf{e}^{s\lambda_{n_1}}\langle e_{n_1}, b_{i_1}\rangle b_{i_1}, \sum_{n_2=0}^{\infty}\sum_{i_2=0}^{m}\zeta_{i_2} a_{n_2}\mathsf{e}^{s\lambda_{n_2}}\langle e_{n_2}, b_{i_2}\rangle b_{i_2}\right\rangle \mathsf{d}s
\end{aligned}$$

$$
\begin{aligned}
=&\sigma_{\mathsf{S}}^2 \int_0^t \sum_{n_1=0}^{\infty} \sum_{n_2=0}^{\infty} \sum_{i=0}^{m} a_{n_1} a_{n_2} \zeta_i \mathsf{e}^{s\left(\lambda_{n_1}+\lambda_{n_2}\right)} \left\langle e_{n_1}, b_i \right\rangle \left\langle e_{n_2}, b_i \right\rangle \mathsf{d}s \\
=&\sigma_{\mathsf{S}}^2 \sum_{i=0}^{m} \zeta_i \left(a_0^2 \left\langle e_0, b_i \right\rangle^2 t - \sum_{(n_1,n_2)\neq(0,0)} a_{n_1} a_{n_2} \left(\frac{1-\mathsf{e}^{t\left(\lambda_{n_1}+\lambda_{n_2}\right)}}{\lambda_{n_1}+\lambda_{n_2}} \right) \left\langle e_{n_1}, b_i \right\rangle \left\langle e_{n_2}, b_i \right\rangle \right),
\end{aligned}
$$

and that

$$
\begin{aligned}
&\mathbb{P}\left(\sum_{n=0}^{\infty} a_n I_{n,g}(t) \geq J'' \right) \\
=&1-\Phi\left(\frac{J'' - \mathbb{E}\left(\sum_{n=0}^{\infty} a_n I_{n,g}(t) \right)}{\left(\mathsf{Var}\left(\sum_{n=0}^{\infty} a_n I_{n,g}(t) \right) \right)^{\frac{1}{2}}} \right) \\
=&1-\Phi\left(\frac{J'' - \left(a_0 \left(I_{0,g}(0) - \left\langle e_0, g \right\rangle t \right) + \sum_{n=1}^{\infty} a_n \left(\mathsf{e}^{t\lambda_n} I_{n,g}(0) + \frac{\left\langle e_n, g \right\rangle}{\lambda_n} \left(1 - \mathsf{e}^{t\lambda_n} \right) \right) \right)}{\sigma_{\mathsf{S}} \left(\sum_{i=0}^{m} \zeta_i \left(a_0^2 \left\langle e_0, b_i \right\rangle^2 t - \sum_{(n_1,n_2)\neq(0,0)} a_{n_1} a_{n_2} \left(\frac{1-\mathsf{e}^{t\left(\lambda_{n_1}+\lambda_{n_2}\right)}}{\lambda_{n_1}+\lambda_{n_2}} \right) \left\langle e_{n_1}, b_i \right\rangle \left\langle e_{n_2}, b_i \right\rangle \right) \right)^{\frac{1}{2}}} \right) \\
=&1-\Phi\left(\frac{J'' - \left(\left\langle \mathsf{e}^{t\partial_{xx}^2} f, w_g^{\mathsf{S}}(\cdot,0) \right\rangle - a_0 \left\langle e_0, g \right\rangle t + \sum_{n=1}^{\infty} a_n \frac{\left\langle e_n, g \right\rangle}{\lambda_n} \left(1 - \mathsf{e}^{t\lambda_n} \right) \right)}{\sigma_{\mathsf{S}} \left(\sum_{i=0}^{m} \zeta_i \left(a_0^2 \left\langle e_0, b_i \right\rangle^2 t - \sum_{(n_1,n_2)\neq(0,0)} a_{n_1} a_{n_2} \left(\frac{1-\mathsf{e}^{t\left(\lambda_{n_1}+\lambda_{n_2}\right)}}{\lambda_{n_1}+\lambda_{n_2}} \right) \left\langle e_{n_1}, b_i \right\rangle \left\langle e_{n_2}, b_i \right\rangle \right) \right)^{\frac{1}{2}}} \right),
\end{aligned}
$$

for $J'' \in \mathbb{R}$. We assume henceforth that $\sum_{n=0}^{\infty} a_n I_{n,g}(t) \geq J''$. We employ, in order, Lemma 9.3.3, Lemma 9.3.2, Jensen's inequality and Lemma 9.3.1 as follows:

$$
\begin{aligned}
&||f||_1 \mathsf{exp}\left(||f||_1^{-1} J'' \right) \leq ||f||_1 \mathsf{exp}\left(||f||_1^{-1} \sum_{n=0}^{\infty} a_n I_{n,g}(t) \right) \\
=&||f||_1 \mathsf{exp}\left(||f||_1^{-1} \left\langle f, w_g^{\mathsf{S}}(\cdot,t) \right\rangle \right) = ||f||_1 \mathsf{exp}\left(||f||_1^{-1} \int_0^L f(x) w_g^{\mathsf{S}}(x,t) \mathsf{d}x \right) \\
\leq&||f||_1 \mathsf{exp}\left(||f||_1^{-1} \int_0^L f(x) v_g^{\mathsf{S}}(x,t) \mathsf{d}x \right) \leq \frac{||f||_1}{||f||_1} \int_0^L f(x) \mathsf{exp}\left(v_g^{\mathsf{S}}(x,t) \right) \mathsf{d}x \\
=&\left\langle f, \mathsf{exp}\left(v_g^{\mathsf{S}}(\cdot,t) \right) \right\rangle = \left\langle f, u_g^{\mathsf{S}}(\cdot,t) \right\rangle.
\end{aligned}
$$

This entails that

$$
\mathbb{P}\left(\sum_{n=0}^{\infty} a_n I_{n,g}(t) \geq J'' \right) \leq \mathbb{P}\left(||f||_1 \mathsf{exp}\left(||f||_1^{-1} J'' \right) \leq \left\langle f, u_g^{\mathsf{S}}(\cdot,t) \right\rangle \right).
$$

The proof is concluded upon defining $J' = ||f||_1 \mathsf{exp}\left(||f||_1^{-1} J'' \right)$. □

Theorem 9.3.4 provides a lower bound to the probability of the onset of u_g^{S} under the assumption of heterogeneity in space, induced by the term g in (9.3.1). The bound highly depends on the choice of the function f, upon which the strong solution u_g^{S} is projected. While this function defines the observable and

can, therefore, be assumed to be known in applications, the shape of the function g is also required to compute the bound numerically.
In the next corollary, we assume $g \equiv 1$ in order to extend the statement of Theorem 9.3.4 to the study of q, the strong solution of system (9.1.1). The results provide a lower bound to the local initiation of turbulence in q.

Corollary 9.3.5. *Under the assumption that q, strong solution of* (9.1.1)*, satisfies $0 < q(x,t) \leq 2$ for any $x \in [0,L]$ and $t \in [0,T]$, the following inequality holds for any non-negative function $f \in \mathcal{H}_1$ that is nonzero almost everywhere:*

$$1 - \min_{0\leq t\leq T} \Phi\left(\frac{||f||_1 \log\left(||f||_1^{-1} J'\right) - \left\langle e^{t\partial_{xx}^2} f, \log\left(q_0\right)\right\rangle + a_0 L^{\frac{1}{2}} t}{\sigma_S\left(\sum_{i=0}^{m} \zeta_i \left(a_0^2 \left\langle e_0, b_i\right\rangle^2 t - \sum_{(n_1,n_2)\neq(0,0)} a_{n_1} a_{n_2} \left(\frac{1-e^{t(\lambda_{n_1}+\lambda_{n_2})}}{\lambda_{n_1}+\lambda_{n_2}}\right) \left\langle e_{n_1}, b_i\right\rangle \left\langle e_{n_2}, b_i\right\rangle\right)\right)^{\frac{1}{2}}}\right)$$
$$\leq \mathbb{P}\left(J' \leq \sup_{0\leq t\leq T} \langle f, q(\cdot,t)\rangle\right),$$

for Φ, the cumulative distribution function of a standard normally distributed random variable, $a_n = \langle e_n, f\rangle$ for any $n \in \mathbb{N}$, $g = L^{\frac{1}{2}} e_0 \equiv 1$ and $J' > 0$.

Proof. For any $t \in [0,T]$, we employ Lemma 9.1.1 to obtain

$$\mathbb{P}\left(J' \leq \left\langle f, u_g^{\mathsf{S}}(\cdot,t)\right\rangle\right) \leq \mathbb{P}\left(J' \leq \langle f, q(\cdot,t)\rangle\right) \leq \mathbb{P}\left(J' \leq \sup_{0\leq t\leq T} \langle f, q(\cdot,t)\rangle\right).$$

This implies that

$$\max_{0\leq t\leq T} \mathbb{P}\left(J' \leq \left\langle f, u_g^{\mathsf{S}}(\cdot,t)\right\rangle\right) \leq \mathbb{P}\left(J' \leq \sup_{0\leq t\leq T} \langle f, q(\cdot,t)\rangle\right).$$

The statement of Theorem 9.3.4 concludes the proof. □

Similarly to Corollary 9.2.3 (b), we discuss in the corollary to follow the rise of turbulence on the whole domain.

Corollary 9.3.6. *For q, strong solution of* (9.1.1) *for any $x \in [0,L]$ and $t \in [0,T]$, the following inequality holds:*

$$1 - \min_{0\leq t\leq T} \Phi\left(\frac{L^{\frac{1}{2}}}{\sigma_S\left(\sum_{i=0}^{m} \zeta_i \left\langle e_0, b_i\right\rangle^2\right)^{\frac{1}{2}}} \left(t^{-\frac{1}{2}} \left(\log\left(J\right) - L^{-1} \int_0^L \log\left(q_0(x)\right) dx\right) + t^{\frac{1}{2}}\right)\right)$$
$$\leq \mathbb{P}\left(J \leq \sup_{0\leq t\leq T} ||q(\cdot,t)||_\infty\right),$$

for Φ, the cumulative distribution function of a standard normally distributed random variable and $0 < J < 2$.

Proof. We consider inequality (9.3.5) for $g = f = L^{\frac{1}{2}} e_0 \equiv 1$ and $J' = LJ$. This choice of $f \in \mathcal{H}_1$ implies that

$$\left\langle f, u_1^{\mathsf{S}}(\cdot,t)\right\rangle = ||u_1^{\mathsf{S}}(\cdot,t)||_1,$$

for any $t > 0$. Therefore, we obtain that

$$1 - \min_{0\leq t\leq T} \Phi\left(\frac{L\log\left(J\right) - \int_0^L \log\left(q_0(x)\right)\mathsf{d}x + Lt}{\sigma_{\mathsf{S}}\left(Lt\right)^{\frac{1}{2}}\left(\sum_{i=0}^{m}\zeta_i\left\langle e_0, b_i\right\rangle^2\right)^{\frac{1}{2}}}\right) \leq \mathbb{P}\left(LJ \leq \sup_{0\leq t\leq T}||u_1^{\mathsf{S}}(\cdot,t)||_1\right).$$

Lastly, we employ Hölder's inequality and Lemma 9.1.1 in

$$\mathbb{P}\left(LJ \leq \sup_{0\leq t\leq T}||u_1^{\mathsf{S}}(\cdot,t)||_1\right) \leq \mathbb{P}\left(J \leq \sup_{0\leq t\leq T}||u_1^{\mathsf{S}}(\cdot,t)||_\infty\right) \leq \mathbb{P}\left(J \leq \sup_{0\leq t\leq T}||q(\cdot,t)||_\infty\right),$$

which proves the statement. □

Corollary 9.3.6 does not require the upper bound $q \leq 2$ assumption imposed in Corollary 9.3.5. Thus enabling a more direct application of the estimate. The corollaries are further compared in Section 9.4 along with Corollary 9.2.3.

9.3.2 Red Stratonovich noise

In the previous subsection, we introduce an approach for the estimation of a lower bound to the probability of jump in (9.3.1) under the assumption of white Stratonovich noise, i.e., $\sigma_{\mathsf{S}} > \sigma_{\mathsf{R}} = 0$. Conversely, we consider in the remainder part of the section the red noise assumption, i.e., $\sigma_{\mathsf{R}} > \sigma_{\mathsf{S}} = 0$. The red noise influence can be interpreted in different manners depending on the operator F and the adapted process $\xi = \xi(x,t)$ [134, 160, 161, 179]. We consider the strong solution of

$$\begin{cases} \mathsf{d}\xi(x,t) = -\kappa\xi(x,t)\mathsf{d}t + \sigma_\xi Q^{\frac{1}{2}}\mathsf{d}W_t', \\ \xi(x,0) \equiv 0, \end{cases} \tag{9.3.6}$$

for $\kappa > 0$, $\sigma_\xi > 0$, $x \in [0,L]$ and $t \geq 0$. For simplicity of notation, the noise W_t' is cylindrical, adapted, and independent from W_t. Such an Ornstein-Uhlenbeck process enables the construction of q, the strong solution of (9.1.1), and of $u_g^{\mathsf{R}} = u_g^{\mathsf{R}}(x,t)$, the strong solution of (9.3.1) for $x \in [0,L]$ and $t \geq 0$. We define then the inverse Cole-Hopf transform $v_g^{\mathsf{R}} := \log\left(u_g^{\mathsf{R}}\right)$. Since the noise is of Stratonovich type and we are considering strong solutions of the involved systems (Theorem 2.2.4 and Theorem 2.2.8), the process is the strong solution of

$$\begin{cases} \partial_t v_g^{\mathsf{R}}(x,t) = \partial_{xx}^2 v_g^{\mathsf{R}}(x,t) + \left(\partial_x v_g^{\mathsf{R}}(x,t)\right)^2 - g(x) + \sigma_{\mathsf{R}} \circ F(\xi)(x,t), \\ \partial_x v_g^{\mathsf{R}}(0,t) = \partial_x v_g^{\mathsf{R}}(L,t) = 0, \\ v_g^{\mathsf{R}}(x,0) = \log\left(q_0(x)\right), \end{cases}$$

for $x \in [0,L]$ and $t \geq 0$. Such a statement can be proven following the steps in the proof of Lemma 9.3.1 on the couple

$$\begin{pmatrix} v_g^{\mathsf{R}}(x,t) \\ \xi(x,t) \end{pmatrix} = \begin{pmatrix} \log\left(u_g^{\mathsf{R}}(x,t)\right) \\ \xi(x,t) \end{pmatrix}.$$

Similarly, we note that the inequality

$$v_g^{\mathsf{R}}(x,t) \geq w_g^{\mathsf{R}}(x,t)$$

holds for $w_g^{\mathsf{R}} = w_g^{\mathsf{R}}(x,t)$, the strong solution of

$$\begin{cases} \partial_t w_g^{\mathsf{R}}(x,t) = \partial_{xx}^2 w_g^{\mathsf{R}}(x,t) - g(x) + \sigma_{\mathsf{R}} F(\xi)(x,t), \\ \partial_x w_g^{\mathsf{R}}(0,t) = \partial_x w_g^{\mathsf{R}}(L,t) = 0, \\ w_g^{\mathsf{R}}(x,0) = \log\left(q_0(x)\right), \end{cases} \tag{9.3.7}$$

following the reasoning of the proof in Lemma 9.3.2. We then focus on two interpretations of red noise influence. For $F = \mathrm{Id}$, the identity operator on $\mathcal{H}_1$, the systems (9.3.6) and (9.3.7) can be rewritten as

$$\begin{cases} \mathsf{d}\begin{pmatrix} w_g^{\mathsf{R}}(x,t) \\ \xi(x,t) \end{pmatrix} = \left(\begin{pmatrix} \partial_{xx}^2 & \sigma_{\mathsf{R}} \\ 0 & -\kappa \end{pmatrix} \begin{pmatrix} w_g^{\mathsf{R}}(x,t) \\ \xi(x,t) \end{pmatrix} - \begin{pmatrix} g(x) \\ 0 \end{pmatrix} \right) \mathsf{d}t + \begin{pmatrix} 0 & 0 \\ 0 & \sigma_\xi Q^{\frac{1}{2}} \end{pmatrix} \begin{pmatrix} \mathsf{d}W_t \\ \mathsf{d}W_t' \end{pmatrix}, \\ w_g^{\mathsf{R}}(x,0) = \log\left(q_0(x)\right), \\ \xi(x,0) \equiv 0; \end{cases} \tag{9.3.8}$$

for $F = \partial_t$, they can be interpreted as

$$\begin{cases} \mathsf{d}\begin{pmatrix} w_g^{\mathsf{R}}(x,t) \\ \xi(x,t) \end{pmatrix} = \left(\begin{pmatrix} \partial_{xx}^2 & -\kappa\sigma_{\mathsf{R}} \\ 0 & -\kappa \end{pmatrix} \begin{pmatrix} w_g^{\mathsf{R}}(x,t) \\ \xi(x,t) \end{pmatrix} - \begin{pmatrix} g(x) \\ 0 \end{pmatrix} \right) \mathsf{d}t + \begin{pmatrix} 0 & \sigma_{\mathsf{R}}\sigma_\xi Q^{\frac{1}{2}} \\ 0 & \sigma_\xi Q^{\frac{1}{2}} \end{pmatrix} \begin{pmatrix} \mathsf{d}W_t \\ \mathsf{d}W_t' \end{pmatrix}, \\ w_g^{\mathsf{R}}(x,0) = \log\left(q_0(x)\right), \\ \xi(x,0) \equiv 0, \end{cases} \tag{9.3.9}$$

for $x \in [0,L]$ and $t \geq 0$. We focus first on (9.3.8), whose noise term behaves similarly to that studied in Chapter 6; the systems, although qualitatively different, can be studied in a similar manner. In fact, the turbulence system (9.1.1) corresponding to the parameters and operator F associated to (9.3.8) displays additive red noise in $\mathcal{H}_1 \times \mathcal{H}_1$, which entails that the system (9.1.1) has a null Itô-Stratonovich correction term (Subsection 2.2.4). Conversely, for parameters and operator F corresponding to (9.3.9), the noise in system (9.1.1) is interpreted in the Stratonovich sense to implement the chain rule, in contrast to Itô's lemma [40], further below. In Appendix G, the system (9.1.1) is converted to the Itô perspective for the cases covered in the chapter. The equations are simulated in Figure 9.2, where the initiation of turbulence is observed under different assumptions through the TAMS algorithm. The results corresponding to (9.3.9) are displayed at the end of the subsection, discussed in Section 9.4 and proven in [24, Appendix B].
We indicate with $\mathcal{D}\left(\partial_{xx}^2\right)$ the domain of ∂_{xx}^2, which is dense in $\mathcal{H}_1$ for the assumed boundary conditions. We define the linear operator

$$A := \begin{pmatrix} \partial_{xx}^2 & \sigma_{\mathsf{R}} \\ 0 & -\kappa \end{pmatrix} : \mathcal{D}\left(\partial_{xx}^2\right) \times \mathcal{H}_1 \to \mathcal{H}_1 \times \mathcal{H}_1,$$

and A^* the adjoint operator in respect to $\mathcal{H}_1 \times \mathcal{H}_1$. In the mild solution form, the system (9.3.8) is solved by

$$\begin{pmatrix} w_g^{\mathsf{R}}(x,t) \\ \xi(x,t) \end{pmatrix} = \mathsf{e}^{tA} \begin{pmatrix} \log\left(q_0(x)\right) \\ 0 \end{pmatrix} + \int_0^t \mathsf{e}^{sA} \begin{pmatrix} -g(x) \\ 0 \end{pmatrix} \mathsf{d}s + \int_0^t \mathsf{e}^{(t-s)A} \begin{pmatrix} 0 & 0 \\ 0 & \sigma_\xi Q^{\frac{1}{2}} \end{pmatrix} \begin{pmatrix} \mathsf{d}W_s \\ \mathsf{d}W_s' \end{pmatrix}.$$

The covariance operator

$$V_t^{\mathsf{w}} := \begin{pmatrix} V_t^I & V_t^{II} \\ V_t^{III} & V_t^{IV} \end{pmatrix},$$

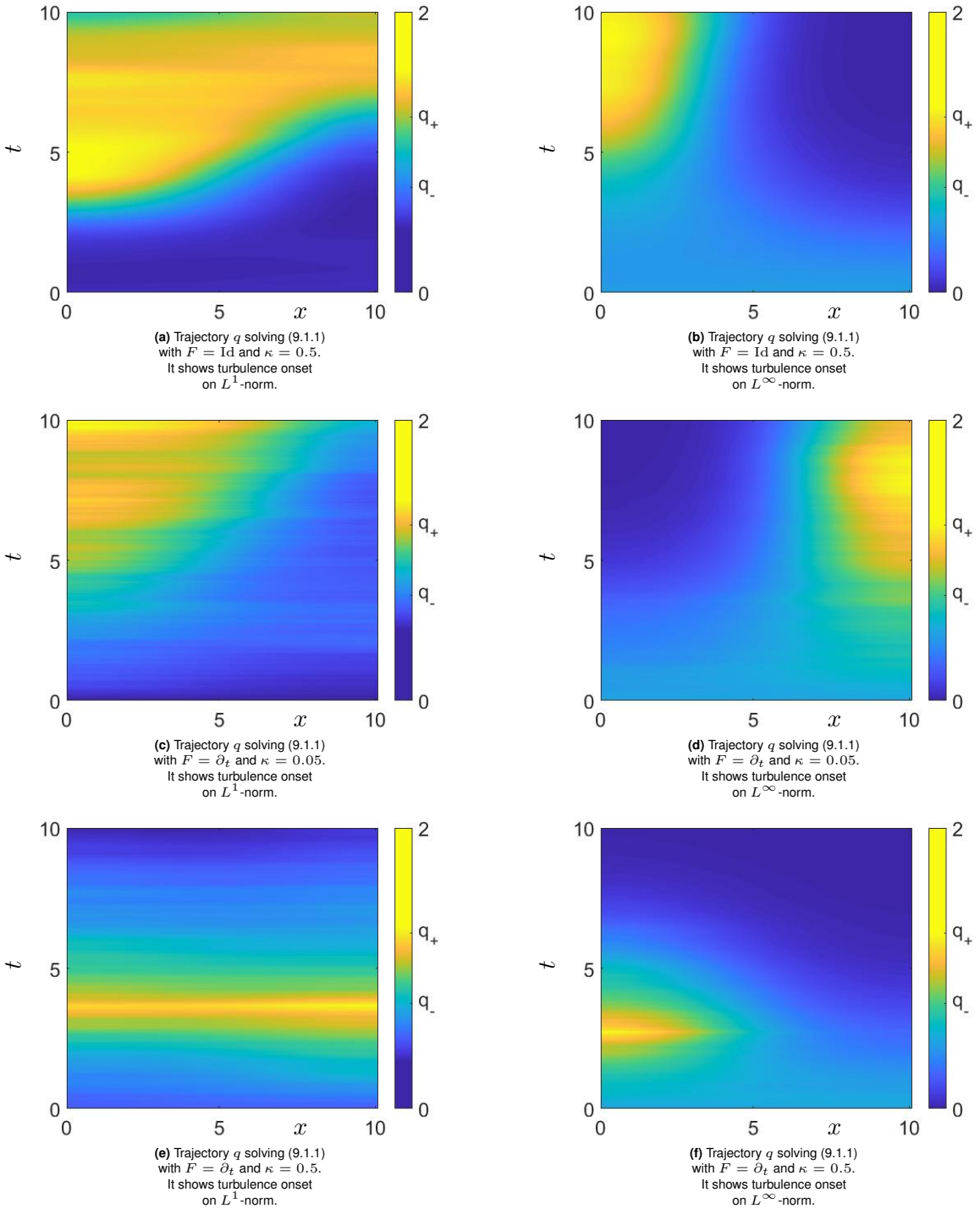

(a) Trajectory q solving (9.1.1) with $F = \mathrm{Id}$ and $\kappa = 0.5$. It shows turbulence onset on L^1-norm.

(b) Trajectory q solving (9.1.1) with $F = \mathrm{Id}$ and $\kappa = 0.5$. It shows turbulence onset on L^∞-norm.

(c) Trajectory q solving (9.1.1) with $F = \partial_t$ and $\kappa = 0.05$. It shows turbulence onset on L^1-norm.

(d) Trajectory q solving (9.1.1) with $F = \partial_t$ and $\kappa = 0.05$. It shows turbulence onset on L^∞-norm.

(e) Trajectory q solving (9.1.1) with $F = \partial_t$ and $\kappa = 0.5$. It shows turbulence onset on L^1-norm.

(f) Trajectory q solving (9.1.1) with $F = \partial_t$ and $\kappa = 0.5$. It shows turbulence onset on L^∞-norm.

Fig. 9.2 Panels (a) and (b) show trajectories of variable q, solution of (9.1.1), indicating the turbulence onset event under additive red noise (see Appendix G), $1.5 = \sigma_{\mathsf{R}} > \sigma_{\mathsf{I}} = \sigma_{\mathsf{S}} = 0$ and $F = \mathrm{Id}$; conversely, in (c)-(f) we consider Stratonovich red noise (see Appendix G), $0.5 = \sigma_{\mathsf{R}} > \sigma_{\mathsf{I}} = \sigma_{\mathsf{S}} = 0$ and $F = \partial_t$. The rare events are computed via the TAMS algorithm, similarly to Figure 9.1. We set the perturbation intensity of ξ, solution of (9.3.6), as $\sigma_\xi = 0.1$ and its dissipation value is indicated under each subfigure. The other parameters are taken as in Figure 9.1. In (a), (c) and (e) we display the rise of $||q||_1$ to the value $q_+ L$, whereas in (b), (d) and (f) we capture the rise of $||q||_\infty$ to the value q_+.
The parameter κ is associated solely with the dissipation of ξ in the case of additive red noise. This is in contrast with the case $F = \partial_t$, where it also indicates the intensity of a nonlinear perturbation term in (9.1.1). In (c) and (d), the solution resembles the case of Stratonovich white noise, which corresponds to $\kappa = 0$; whereas in (e) and (f), κ assumes a higher value and the solution leaves the turbulent state in a short timescale.

associated to the solution of the system at time $t > 0$, satisfies the finite-time Lyapunov equation [64, Lemma 2.45],

$$AV_t^{\mathsf{W}} + V_t^{\mathsf{W}} A^* = \mathsf{e}^{tA} \begin{pmatrix} 0 & 0 \\ 0 & \sigma_\xi^2 Q \end{pmatrix} \mathsf{e}^{tA^*} - \begin{pmatrix} 0 & 0 \\ 0 & \sigma_\xi^2 Q \end{pmatrix}. \tag{9.3.10}$$

For simplicity, we assume that $-\kappa$ is not an eigenvalue of ∂^2_{xx}. The semigroup e^{tA} is then defined as

$$\mathsf{e}^{tA} = \begin{pmatrix} \mathsf{e}^{t\partial^2_{xx}} & \sigma_{\mathsf{R}} t \int_0^1 \mathsf{e}^{ts\partial^2_{xx}} \mathsf{e}^{-t(1-s)\kappa} \mathsf{d}s \\ 0 & \mathsf{e}^{-t\kappa} \end{pmatrix} = \begin{pmatrix} \mathsf{e}^{t\partial^2_{xx}} & \sigma_{\mathsf{R}} \mathrm{R}\left(\partial^2_{xx}+\kappa\right)\left(\mathsf{e}^{t\partial^2_{xx}} - \mathsf{e}^{-t\kappa}\right) \\ 0 & \mathsf{e}^{-t\kappa} \end{pmatrix}$$

and its adjoint, in respect to the $\mathcal{H}_1 \times \mathcal{H}_1$ scalar product, is

$$\left(\mathsf{e}^{tA}\right)^* = \mathsf{e}^{tA^*} = \begin{pmatrix} \mathsf{e}^{t\partial^2_{xx}} & 0 \\ \sigma_{\mathsf{R}} \mathrm{R}\left(\partial^2_{xx}+\kappa\right)\left(\mathsf{e}^{t\partial^2_{xx}} - \mathsf{e}^{-t\kappa}\right) & \mathsf{e}^{-t\kappa} \end{pmatrix}.$$

Solving (9.3.10) implies that

$$\begin{aligned} V_t^{II} &= \sigma_{\mathsf{R}}\sigma_\xi^2 \mathrm{R}\left(\partial^2_{xx}-\kappa\right)\left(\mathsf{e}^{-t\kappa}\mathrm{R}\left(\partial^2_{xx}+\kappa\right)\left(\mathsf{e}^{t\partial^2_{xx}}-\mathsf{e}^{-t\kappa}\right) - \frac{1-\mathsf{e}^{-2t\kappa}}{2\kappa}\right) Q, \\ V_t^{III} &= \sigma_{\mathsf{R}}\sigma_\xi^2 Q\left(\mathsf{e}^{-t\kappa}\mathrm{R}\left(\partial^2_{xx}+\kappa\right)\left(\mathsf{e}^{t\partial^2_{xx}}-\mathsf{e}^{-t\kappa}\right) - \frac{1-\mathsf{e}^{-2t\kappa}}{2\kappa}\right)\mathrm{R}\left(\partial^2_{xx}-\kappa\right), \\ V_t^{IV} &= \frac{\sigma_\xi^2}{2\kappa}\left(1-\mathsf{e}^{-2t\kappa}\right) Q, \end{aligned}$$

and that the equation

$$\begin{aligned} \partial^2_{xx} V_t^I + V_t^I \partial^2_{xx} = &-\sigma_{\mathsf{R}}^2\sigma_\xi^2\Bigg(\mathrm{R}\left(\partial^2_{xx}-\kappa\right)\left(\mathsf{e}^{-t\kappa}\mathrm{R}\left(\partial^2_{xx}+\kappa\right)\left(\mathsf{e}^{t\partial^2_{xx}}-\mathsf{e}^{-t\kappa}\right) - \frac{1-\mathsf{e}^{-2t\kappa}}{2\kappa}\right) Q \\ &+ Q\left(\mathsf{e}^{-t\kappa}\mathrm{R}\left(\partial^2_{xx}+\kappa\right)\left(\mathsf{e}^{t\partial^2_{xx}}-\mathsf{e}^{-t\kappa}\right) - \frac{1-\mathsf{e}^{-2t\kappa}}{2\kappa}\right)\mathrm{R}\left(\partial^2_{xx}-\kappa\right) \\ &+ \mathrm{R}\left(\partial^2_{xx}+\kappa\right)\left(\mathsf{e}^{t\partial^2_{xx}}-\mathsf{e}^{-t\kappa}\right) Q\, \mathrm{R}\left(\partial^2_{xx}+\kappa\right)\left(\mathsf{e}^{t\partial^2_{xx}}-\mathsf{e}^{-t\kappa}\right)\Bigg) \end{aligned} \tag{9.3.11}$$

holds. For $(n_1, n_2) \in \mathbb{N}\times\mathbb{N}$, we label $p_{n_1,n_2} = \langle e_{n_1}, Q e_{n_2}\rangle$. For $(n_1,n_2) \neq (0,0)$, the equation (9.3.11) entails the definition of

$$\begin{aligned} \gamma_{n_1,n_2} &:= \left\langle e_{n_1}, V_t^I e_{n_2}\right\rangle \\ &= -\frac{\sigma_{\mathsf{R}}^2\sigma_\xi^2 p_{n_1,n_2}}{(\lambda_{n_1}+\lambda_{n_2})}\Bigg(\frac{1}{-\lambda_{n_1}+\kappa}\left(-\frac{\mathsf{e}^{-t\kappa}\left(\mathsf{e}^{t\lambda_{n_1}}-\mathsf{e}^{-t\kappa}\right)}{\lambda_{n_1}+\kappa} + \frac{1-\mathsf{e}^{-2t\kappa}}{2\kappa}\right) \\ &\quad + \frac{1}{-\lambda_{n_2}+\kappa}\left(\frac{\mathsf{e}^{-t\kappa}\left(\mathsf{e}^{t\lambda_{n_2}}-\mathsf{e}^{-t\kappa}\right)}{\lambda_{n_2}+\kappa} + \frac{1-\mathsf{e}^{-2t\kappa}}{2\kappa}\right) - \frac{\left(\mathsf{e}^{t\lambda_{n_1}}-\mathsf{e}^{-t\kappa}\right)\left(\mathsf{e}^{t\lambda_{n_2}}-\mathsf{e}^{-t\kappa}\right)}{(\lambda_{n_1}+\kappa)(\lambda_{n_2}+\kappa)}\Bigg) \\ &= -\frac{\sigma_{\mathsf{R}}^2\sigma_\xi^2 p_{n_1,n_2}}{(\lambda_{n_1}+\lambda_{n_2})}\Bigg(\frac{-\lambda_{n_1}-\lambda_{n_2}+2\kappa}{2\kappa(\lambda_{n_1}-\kappa)(\lambda_{n_2}-\kappa)} - \mathsf{e}^{t\left(\lambda_{n_1}+\lambda_{n_2}\right)}\frac{1}{(\lambda_{n_1}+\kappa)(\lambda_{n_2}+\kappa)} \\ &\quad + \mathsf{e}^{t\left(\lambda_{n_1}+\kappa\right)}\frac{\lambda_{n_1}+\lambda_{n_2}}{\left(\lambda_{n_1}^2-\kappa^2\right)(\lambda_{n_2}+\kappa)} \\ &\quad + \mathsf{e}^{t\left(\lambda_{n_2}+\kappa\right)}\frac{\lambda_{n_1}+\lambda_{n_2}}{(\lambda_{n_1}+\kappa)\left(\lambda_{n_2}^2-\kappa^2\right)} + \mathsf{e}^{-2t\kappa}\frac{\lambda_{n_1}+\lambda_{n_2}}{2\kappa(\lambda_{n_1}+\kappa)(\lambda_{n_2}+\kappa)}\Bigg). \end{aligned} \tag{9.3.12}$$

We consider then

$$V_t^{\mathsf{w}} = \sigma_\xi^2 \int_0^t \mathsf{e}^{sA} \begin{pmatrix} 0 & 0 \\ 0 & Q \end{pmatrix} \mathsf{e}^{sA^*} \mathsf{d}s,$$

which implies that

$$\begin{aligned} \gamma_{0,0} &= \left\langle \begin{pmatrix} e_0 \\ 0 \end{pmatrix}, V_t^{\mathsf{w}} \begin{pmatrix} e_0 \\ 0 \end{pmatrix} \right\rangle_{\mathcal{H}_1 \times \mathcal{H}_1} = \left\langle e_0, V_t^I e_0 \right\rangle \\ &= \sigma_{\mathsf{R}}^2 \sigma_\xi^2 \int_0^t \left\langle e_0, \mathrm{R}\left(\partial_{xx}^2 + k\right) \left(\mathsf{e}^{s\partial_{xx}^2} - \mathsf{e}^{-s\kappa}\right) Q \, \mathrm{R}\left(\partial_{xx}^2 + k\right) \left(\mathsf{e}^{s\partial_{xx}^2} - \mathsf{e}^{-s\kappa}\right) e_0 \right\rangle \mathsf{d}s \qquad (9.3.13) \\ &= \frac{\sigma_{\mathsf{R}}^2 \sigma_\xi^2 p_{0,0}}{\kappa^2} \left(t - 2\frac{1 - \mathsf{e}^{-t\kappa}}{\kappa} + \frac{1 - \mathsf{e}^{-2t\kappa}}{2\kappa} \right). \end{aligned}$$

In the theorem to follow, we discuss the lower bound of the probability of rise of u_g^{R}, similarly to Theorem 9.3.4.

Theorem 9.3.7. *Assume u_g^R the strong solution of* (9.3.1) *for $x \in [0, L]$ and $t > 0$. Then the following inequality holds for any non-negative function $f \in \mathcal{H}_1$ that is nonzero almost everywhere:*

$$\begin{aligned} &1 - \Phi \left(\frac{J'' - \left(\left\langle \mathsf{e}^{t\partial_{xx}^2} f, \log\left(q_0\right) \right\rangle - a_0 \left\langle e_0, g \right\rangle t + \sum_{n=1}^{\infty} a_n \frac{\langle e_n, g \rangle}{\lambda_n} \left(1 - \mathsf{e}^{t\lambda_n}\right) \right)}{\left(\sum_{(n_1,n_2) \in \mathbb{N}^2} \left(a_{n_1} a_{n_2} \gamma_{n_1,n_2}\right) \right)^{\frac{1}{2}}} \right) \\ \leq &\mathbb{P}\left(J' \leq \left\langle f, u_g^R(\cdot, t) \right\rangle \right), \qquad (9.3.14) \end{aligned}$$

for Φ, the cumulative distribution function of a standard normally distributed random variable, $J' > 0$, $a_n = \langle e_n, f \rangle$ for any $n \in \mathbb{N}$ and $\{\gamma_{n_1,n_2}\}_{(n_1,n_2) \in \mathbb{N} \times \mathbb{N}}$ as defined in (9.3.12) *and in* (9.3.13)*.*

Proof. The proof follows the same steps as in Theorem 9.3.4, which we describe here in a more condensed manner. The pairing $\begin{pmatrix} w_g^{\mathsf{R}}(x,t) \\ \xi(x,t) \end{pmatrix}$, strong solution of (9.3.8), has a Gaussian distribution in the space $\mathcal{H}_1 \times \mathcal{H}_1$. In particular, we obtain

$$\mathbb{E}\begin{pmatrix} w_g^{\mathsf{R}}(x,t) \\ \xi(x,t) \end{pmatrix} = \mathsf{e}^{tA} \begin{pmatrix} \log\left(q_0(x)\right) \\ 0 \end{pmatrix} + \int_0^t \mathsf{e}^{sA} \begin{pmatrix} -g(x) \\ 0 \end{pmatrix} \mathsf{d}s = \mathsf{e}^{t\partial_{xx}^2} \log\left(q_0(x)\right) - \int_0^t \mathsf{e}^{s\partial_{xx}^2} g(x) \mathsf{d}s$$

and its covariance operator is

$$\sigma_{\mathsf{R}}^2 \int_0^t \mathsf{e}^{sA} \begin{pmatrix} 0 & 0 \\ 0 & Q \end{pmatrix} \mathsf{e}^{sA^*} \mathsf{d}s = \sigma_{\mathsf{R}}^2 \mathsf{e}^{-2t} \begin{pmatrix} t^2 \int_0^1 \mathsf{e}^{ts\left(\partial_{xx}^2 + \mathrm{Id}\right)} \mathsf{d}s Q \int_0^1 \mathsf{e}^{ts\left(\partial_{xx}^2 + \mathrm{Id}\right)} \mathsf{d}s & t \int_0^1 \mathsf{e}^{ts\left(\partial_{xx}^2 + \mathrm{Id}\right)} \mathsf{d}s Q \\ tQ \int_0^1 \mathsf{e}^{ts\left(\partial_{xx}^2 + \mathrm{Id}\right)} \mathsf{d}s & Q \end{pmatrix}.$$

Setting $f \in \mathcal{H}_1$, it follows that

$$\mathbb{P}\left(\left\langle f, w_g^{\mathsf{R}} \right\rangle \geq J'' \right) = 1 - \Phi \left(\frac{J'' - \left\langle f, \mathsf{e}^{t\partial_{xx}^2} \log\left(q_0\right) - \int_0^t \mathsf{e}^{s\partial_{xx}^2} g \mathsf{d}s \right\rangle}{\langle f, V^I f \rangle^{\frac{1}{2}}} \right)$$

$$= 1 - \Phi\left(\frac{J'' - \left(\left\langle \mathsf{e}^{t\partial_{xx}^2} f, w_g^{\mathsf{R}}(\cdot,0)\right\rangle - a_0\left\langle e_0, g\right\rangle t + \sum_{n=1}^{\infty} a_n \frac{\langle e_n, g\rangle}{\lambda_n}\left(1 - \mathsf{e}^{t\lambda_n}\right)\right)}{\left(\sum_{(n_1,n_2)\in\mathbb{N}^2}\left(a_{n_1}a_{n_2}\gamma_{n_1,n_2}\right)\right)^{\frac{1}{2}}}\right),$$

for $J'' \in \mathbb{R}$. We assume that $\left\langle f, w_g^{\mathsf{R}}\right\rangle \geq J''$ and employ Jensen's inequality to obtain

$$\begin{aligned}
||f||_1 \mathsf{exp}\left(||f||_1^{-1} J''\right) &\leq ||f||_1 \mathsf{exp}\left(||f||_1^{-1}\left\langle f, w_g^{\mathsf{R}}\right\rangle\right) = ||f||_1 \mathsf{exp}\left(||f||_1^{-1}\int_0^L f(x) w_g^{\mathsf{R}}(x,t)\mathsf{d}x\right) \\
&\leq ||f||_1 \mathsf{exp}\left(||f||_1^{-1}\int_0^L f(x) v_g^{\mathsf{R}}(x,t)\mathsf{d}x\right) \leq \frac{||f||_1}{||f||_1}\int_0^L f(x)\mathsf{exp}(v_g^{\mathsf{R}}(x,t))\mathsf{d}x \\
&= \left\langle f, \mathsf{exp}\left(v_g^{\mathsf{R}}(\cdot,t)\right)\right\rangle = \left\langle f, u_g^{\mathsf{R}}(\cdot,t)\right\rangle.
\end{aligned}$$

We set $J' = ||f||_1 \mathsf{exp}\left(||f||_1^{-1} J''\right)$, which implies the statement. □

The lower bound (9.3.14) justifies the following corollary, whose proof is equivalent to those in Corollary 9.3.5 and Corollary 9.3.6. Its statement is discussed in Section 9.4.

Corollary 9.3.8. *In the following statements, we refer to Φ as the cumulative distribution function of a standard normally distributed random variable.*

(a) Assume that q, strong solution of (9.1.1)*, satisfies $0 < q(x,t) \leq 2$ for any $x \in [0,L]$ and $t \in [0,T]$. Then, the following inequality holds for any non-negative function $f \in \mathcal{H}_1$ that is nonzero almost everywhere:*

$$\begin{aligned}
&1 - \min_{0\leq t\leq T} \Phi\left(\frac{||f||_1 \mathit{log}\left(||f||_1^{-1} J'\right) - \left\langle \mathit{e}^{t\partial_{xx}^2} f, \mathit{log}\left(q_0\right)\right\rangle + \left\langle f, e_0\right\rangle L^{\frac{1}{2}} t}{\left(\sum_{(n_1,n_2)\in\mathbb{N}^2}\left(a_{n_1}a_{n_2}\gamma_{n_1,n_2}\right)\right)^{\frac{1}{2}}}\right) \\
\leq &\mathbb{P}\left(J' \leq \sup_{0\leq t\leq T}\left\langle f, q(\cdot,t)\right\rangle\right),
\end{aligned}$$

for $J' > 0$, $a_n = \langle e_n, f\rangle$ for any $n \in \mathbb{N}$ and $\{\gamma_{n_1,n_2}\}_{(n_1,n_2)\in\mathbb{N}\times\mathbb{N}}$ as defined in (9.3.12) *and in* (9.3.13)*.*

(b) For q, strong solution of (9.1.1) *for any $x \in [0,L]$ and $t \in [0,T]$, the following inequality holds*

$$\begin{aligned}
&1 - \min_{0\leq t\leq T} \Phi\left(\frac{L^{\frac{1}{2}}\kappa}{\sigma_R \sigma_\xi p_{0,0}^{\frac{1}{2}}} \frac{t^{\frac{1}{2}}\left(t^{-\frac{1}{2}}\left(\mathit{log}\left(J\right) - L^{-1}\int_0^L \mathit{log}\left(q_0(x)\right)\mathit{d}x\right) + t^{\frac{1}{2}}\right)}{\left(t - 2\frac{1-\mathit{e}^{-t\kappa}}{\kappa} + \frac{1-\mathit{e}^{-2t\kappa}}{2\kappa}\right)^{\frac{1}{2}}}\right) \\
=&1 - \min_{0\leq t\leq T} \Phi\left(\frac{L^{\frac{1}{2}}}{\gamma_{0,0}^{\frac{1}{2}}}\left(\mathit{log}\left(J\right) - L^{-1}\int_0^L \mathit{log}\left(q_0(x)\right)\mathit{d}x + t\right)\right) \qquad (9.3.15) \\
\leq &\mathbb{P}\left(J \leq \sup_{0\leq t\leq T} ||q(\cdot,t)||_\infty\right),
\end{aligned}$$

for $0 < J < 2$.

Remark 9.3.9. The system (9.3.8) has a strong solution with variable w_g^{R} characterised by a positive autocorrelation [161], in contrast to (9.3.9). Another core difference in the models is that, for $g \equiv 0$, the

covariance of the strong solution along e_0 diverges in (9.3.8) in the time limit (see Chapter 6), whereas it converges [134] in (9.3.9). Although the models differ greatly, the lower bounds can be obtained through similar methods [24, Appendix B]. Furthermore, for $\kappa > 0$, the statement in Theorem 9.3.7 holds for w_g^{R} defined in the system (9.3.9) by setting the constants

$$\begin{aligned}\gamma_{n_1,n_2} = &- \frac{\sigma_{\mathsf{R}}^2\sigma_\xi^2 p_{n_1,n_2}}{(\lambda_{n_1}+\lambda_{n_2})}\left(\frac{2\lambda_{n_1}\lambda_{n_2}-(\lambda_{n_1}+\lambda_{n_2})\,\kappa}{2\,(\lambda_{n_1}-\kappa)\,(\lambda_{n_2}-\kappa)} - \mathsf{e}^{t(\lambda_{n_1}+\lambda_{n_2})}\frac{\lambda_{n_1}\lambda_{n_2}}{(\lambda_{n_1}+\kappa)\,(\lambda_{n_2}+\kappa)}\right.\\ &- \mathsf{e}^{t(\lambda_{n_1}+\kappa)}\frac{\kappa\lambda_{n_1}\,(\lambda_{n_1}+\lambda_{n_2})}{\left(\lambda_{n_1}^2-\kappa^2\right)(\lambda_{n_2}+\kappa)} - \mathsf{e}^{t(\lambda_{n_2}+\kappa)}\frac{\kappa\lambda_{n_2}\,(\lambda_{n_1}+\lambda_{n_2})}{(\lambda_{n_1}+\kappa)\left(\lambda_{n_2}^2-\kappa^2\right)}\\ &\left.+\,\mathsf{e}^{-2t\kappa}\frac{\kappa\,(\lambda_{n_1}+\lambda_{n_2})}{2\,(\lambda_{n_1}+\kappa)\,(\lambda_{n_2}+\kappa)}\right),\end{aligned} \tag{9.3.16}$$

for $(n_1,n_2)\in\mathbb{N}\times\mathbb{N}\setminus(0,0)$, and

$$\gamma_{0,0} = \sigma_{\mathsf{R}}^2\sigma_\xi^2 p_{0,0}\frac{1-\mathsf{e}^{-2t\kappa}}{2\kappa}, \tag{9.3.17}$$

and assuming, for simplicity, that $-\kappa$ is not an eigenvalue of the Laplacian. For system assumptions associated with (9.3.9), the statement in Corollary 9.3.8 (a) is also equivalent, with the updated constants $\{\gamma_{n_1,n_2}\}_{(n_1,n_2)\in\mathbb{N}\times\mathbb{N}}$ shown in (9.3.16) and (9.3.17). In contrast, the corresponding inequality to (9.3.15) is

$$\begin{aligned}&1-\min_{0\le t\le T}\Phi\left(\frac{(2\kappa L)^{\frac{1}{2}}}{\sigma_{\mathsf{R}}\sigma_\xi p_{0,0}^{\frac{1}{2}}}\frac{t^{\frac{1}{2}}}{(1-\mathsf{e}^{-2t\kappa})^{\frac{1}{2}}}\left(t^{-\frac{1}{2}}\left(\log(J)-L^{-1}\int_0^L\log\left(q_0(x)\right)\mathsf{d}x\right)+t^{\frac{1}{2}}\right)\right)\\ &=1-\min_{0\le t\le T}\Phi\left(\frac{L^{\frac{1}{2}}}{\gamma_{0,0}^{\frac{1}{2}}}\left(\log(J)-L^{-1}\int_0^L\log\left(q_0(x)\right)\mathsf{d}x+t\right)\right)\le\mathbb{P}\left(J\le\sup_{0\le t\le T}||q(\cdot,t)||_\infty\right),\end{aligned} \tag{9.3.18}$$

for $0<J<2$ and $\gamma_{0,0}$ defined in (9.3.17).

9.4 Comparison of methods

In the previous sections, we study lower bounds to the probability of turbulence onset in system (9.1.1) under different noise assumptions. Namely, we consider time-white noise in the Itô sense, in Section 9.2, and time-white or time-red noise in the Stratonovich sense, in Section 9.3. Throughout the chapter, the noise is assumed to be white in space along fixed modes. The techniques employed in the two sections differ in nature. Nonetheless, they manage to capture similar characteristics of the system.

First, we discuss the rise of turbulence under Itô noise. Lemma 9.2.1 and Lemma 9.2.2 are based on methods introduced in [163, 164]. The key idea is to counter the drift effect on the solution of (9.1.2) by applying a convolution operator through the fundamental solution of the cable equation, reserved in time. A stark difference with the assumptions in [163, 164] is that their work studies the heat equation, i.e., $\alpha = 0$. In fact, under strong linear drift dissipation, the left-hand side term in (9.2.11) can be negative, even for large values of T, thus rendering the inequality trivial. This is in contrast with [163], where the lower bound increases with T. In [163, 164], a second lower bound is obtained and employed to prove the blow-up of the mild solution in finite time through an iterative method. The iteration step is based on rescaling the space interval. Once again, the method is not equivalent under the assumption $\alpha > 0$ as the second rescaling affects the linear dissipation and does not return the initial system, thus affecting the iteration at each step (see [163, Lemma 2.6, Proposition 3.2, Section 4]).

We note that the lower bounds in Corollary 9.2.3 are also valid for q mild solution of (9.1.1) under white Stratonovich noise. In fact, we set $u_1^{\mathsf{S}} = u_1^{\mathsf{S}}(x,t)$ the mild solution of (9.1.2) for $\hat{\sigma} = \sigma_{\mathsf{S}} > \sigma_{\mathsf{I}} = \sigma_{\mathsf{R}} = 0$ and $u_1^{\mathsf{I}} = u_1^{\mathsf{I}}(x,t)$ the mild solution of (9.1.2) for $\hat{\sigma} = \sigma_{\mathsf{I}} > \sigma_{\mathsf{S}} = \sigma_{\mathsf{R}} = 0$. We then study $\hat{u} = u_1^{\mathsf{S}} - u_1^{\mathsf{I}}$. By

assuming Q to be trace-class and by the definition of the Itô-Stratonovich correction term in ([14, 88] and Subsection 2.2.4), it is the mild solution of

$$\begin{cases} \mathrm{d}\hat{u}(x,t) = \left(\partial_{xx}^2 \hat{u}(x,t) - \hat{u}(x,t) + u^{\mathsf{I}}(x,t) \dfrac{\hat{\sigma}^2}{2} \displaystyle\sum_{i=0}^{\infty} \zeta_i b_i(x)^2 \right) \mathrm{d}t + \hat{\sigma} \hat{u}(x,t) Q^{\frac{1}{2}} \mathrm{d}W_t, \\ \partial_x \hat{u}(0,t) = \partial_x \hat{u}(L,t) = 0, \\ \hat{u}(x,0) \equiv 0. \end{cases}$$

Following the steps in the proof of Lemma 9.1.1, it is implied that $u_1^{\mathsf{S}} \geq u_1^{\mathsf{I}}$ almost surely. Moreover, we know that $v_J^{\mathsf{S}} \leq v_J^{\mathsf{I}}$ holds.

The methods in Section 9.2 are applied to the mild solutions of the considered stochastic partial differential equations. Conversely, although in Section 9.3 the noise is assumed in Stratonovich sense, the use of Itô's Lemma through the inverse Cole-Hopf transformation requires the study of strong solutions. In order to satisfy the existence of such a solution, the noise is assumed to perturb the system along a finite number of modes, then affected by the multiplication term in the noise intensity (Theorem 2.2.8). Similar results to those in Section 9.3 can also be proven in an equivalent manner under Itô noise assumptions, yet, on a logarithmic scale, an additional negative term appears in the KPZ equation [99]. For instance, under the assumption of white noise, the system obtained in correspondence to (9.3.2) is

$$\begin{cases} \mathrm{d}v_g^{\mathsf{I}}(x,t) = \left(\partial_{xx}^2 v_g^{\mathsf{I}}(x,t) + \left(\partial_x v_g^{\mathsf{I}}(x,t) \right)^2 - g(x) - \dfrac{\sigma_{\mathsf{I}}^2}{2} \displaystyle\sum_{i=0}^{m} \zeta_i b_i(x)^2 \right) \mathrm{d}t + \sigma_{\mathsf{I}} Q^{\frac{1}{2}} \mathrm{d}W_t, \\ \partial_x v_g^{\mathsf{I}}(0,t) = \partial_x v_g^{\mathsf{I}}(L,t) = 0, \\ v_g^{\mathsf{I}}(x,0) = \log\left(q_0(x)\right). \end{cases}$$

Then, the step in Lemma 9.3.2 implies the discard of the nonlinear shear deformation non-negative term, but not of the term $-\frac{\sigma_{\mathsf{I}}^2}{2} \sum_{i=0}^{m} \zeta_i b_i(x)^2$, which has to be included in the moving average of Theorem 9.3.4, Corollary 9.3.5 and Corollary 9.3.6.

Although the lower bounds in Section 9.3 are always positive, they are characterised by severely different behaviours in time. The section contains results that manage to study the initiation of turbulence in certain regions of the domain in Corollary 9.3.5 and Corollary 9.3.8. Nevertheless, we focus on the description of jumps in the L^∞-norm, which are easier to observe. In Corollary 9.3.6, the sum of two terms in the argument of the function Φ defines the nature of the bound. In fact, the term $t^{-\frac{1}{2}}$, multiplied by a positive parameter dependent on initial conditions, refers to the effect of the noise to enable the possibility of a jump, thus decreasing with t the argument in the distribution function. Conversely, the term $t^{\frac{1}{2}}$ takes into account the effect of the drift component, constant in time, which hinders the transition on long times. The clash of these effects implies that at

$$t^* = \log(J) - L^{-1} \int_0^L \log\left(q_0(x)\right) \mathrm{d}x$$

the lower bound to the probability of jump at height J in the L^1-norm reaches its peak, which is maintained for longer times for the statement in the proof of Corollary 9.2.3. A similar behaviour is observed in Corollary 9.2.3, where the best opportunity of occurrence of jump is captured.

We consider in Subsection 9.3.2 red noise in time. We note that, in previous cases, the initiation of turbulence is not a memoryless process since it is affected already by its initial state. The inclusion of red noise in the sense (9.3.8) is justified by its relevance in climate application [160, 161] and the positive autocorrelation of the system in logarithmic scale along the direction e_0. The inequality (9.3.15) in Corollary

9.3.8 (b) resembles the statement in Corollary 9.3.6, but the parameter κ assumes a twofold role: it is proportional to the term

$$\frac{L^{\frac{1}{2}}\kappa}{\sigma_{\mathsf{R}}\sigma_{\xi}p_{0,0}^{\frac{1}{2}}} \tag{9.4.1}$$

and appears in the term

$$\frac{t^{\frac{1}{2}}}{\left(t-2\frac{1-\mathsf{e}^{-t\kappa}}{\kappa}+\frac{1-\mathsf{e}^{-2t\kappa}}{2\kappa}\right)^{\frac{1}{2}}}=\left(\frac{t}{\int_0^t\left(1-\mathsf{e}^{-s\kappa}\right)^2\mathsf{d}s}\right)^{\frac{1}{2}}>1, \tag{9.4.2}$$

due to its dissipative role in (9.3.6). Both perspectives indicate that $\kappa>0$ hinders the jump with respect to the white noise assumption, but their effects differ. In fact, increasing κ leads to an increase in (9.4.1) and a decrease in (9.4.2). Nonetheless, the concept of a best opportunity to jump before being fully controlled by the drift is visible since, for fixed $\kappa>0$, the limit of (9.4.2) in $t\to+\infty$ is finite. Nevertheless, the limit of (9.4.2) in $t\to 0$ is infinite, indicating a smaller probability of jump on short times in comparison to white noise in time. Lastly, we notice that the limit $\kappa=0$ implies $\gamma_{0,0}=\sigma_{\mathsf{R}}^2\sigma_{\xi}^2p_{0,0}\frac{t^3}{3}$, which means that the lower bound is a definitely strictly increasing function in t.
At the end of Subsection 9.3.2, we consider an alternative type of red noise, as discussed in [134]. The role of κ is different from the previous case. In fact, κ indicates both the dissipativity in (9.3.6) and is related to the off-diagonal entry in the linear drift term [24, Appendix B]. The term in (9.3.18),

$$\frac{t^{\frac{1}{2}}}{\left(\frac{1-\mathsf{e}^{-2t\kappa}}{2\kappa}\right)^{\frac{1}{2}}}=\left(\frac{t}{\int_0^t\mathsf{e}^{-2s\kappa}\mathsf{d}s}\right)^{\frac{1}{2}} \tag{9.4.3}$$

is finite in $t\to 0$ and infinite in $t\to+\infty$. This translates to a similar behaviour to the lower bound with the assumption of white noise in Corollary 9.3.5 on small timescales and a smaller lower bound to the probability of jump on large timescales t. This results from the interplay between the dissipativity in the Ornstein-Uhlenbeck process defined in (9.3.6) and the dissipativity in (9.3.1). In this case, increasing $\kappa>0$ indicates in (9.4.3) the decrease in the bound of jump at a fixed time. The limit $\kappa=0$ is equivalent to the time-white noise assumption in Subsection 9.3.1.

9.5 Summary

In this chapter, we establish lower bounds for the probability of turbulence initiation in a simplified model of plane Couette flow. The phenomenon is modelled through an SPDE on an interval under various forms of multiplicative Gaussian noise. The simulation of similar systems leads to the study of other rare events in the pipe flow [91, 92]. The application of equivalent algorithms shows the possibility of such an occurrence, whose probability has not been estimated analytically so far. Central to our approach is the comparison between the linearised and original models, starting with a rigorous treatment of Itô white noise. Using the fundamental solution of the cable equation under Neumann or periodic boundary conditions, we counter the drift term and obtain an observable in the form of a martingale. The bound is then described following techniques employed in the study of finite-time blow-up of the mild solution of the stochastic heat equation [163, 164].
Expanding this framework, we employ logarithmic-scale comparison methods to address systems perturbed by time-white Stratonovich noise, time-red additive noise, and time-red Stratonovich noise, with the latter two modelled through coupling with Ornstein–Uhlenbeck processes. This approach requires different assumptions on the noise term to ensure the existence of a strong solution for the model. Our analysis reveals that, whereas the lower bounds vary across noise types, they consistently reflect a key dynamical

feature: the probability of turbulence onset in a fixed time declines beyond an optimal jumping time. This property is implied by the invariance of the linearised model under a suitable rescaling of the solution.

10 Computation of Instantons

Rare event methods based on sampling rely on biasing techniques to increase the likelihood of a rare event, such as importance splitting techniques (AMS and TAMS [45, 46, 142] for example). In this chapter, we consider the noise strength to be infinitesimally small. This puts us in the purview of Freidlin-Wentzell theory of large deviations [86], meaning that both the limiting event probability scaling and its most likely pathway of occurrence are rigorously predictable and available in a sampling-free and deterministic manner. Obtaining the most likely pathway through numerical methods provides insights into the physical mechanism of the transition as such a trajectory often crosses between two different deterministic basins of attraction. If the transition is achieved on a large timescale, this is usually referred to as an instanton. The analytic properties of the corresponding solution have been described for certain SDEs [38, 209], and the suitable technique involved in its numerical description usually depends on the particular model [28, 96, 126]. Especially challenging is the assumption of non-white noise, which can be found in many applications, such as privacy risk management [35]. This chapter is based on the content of [22] and focuses on the numerical study of white-in-time Gaussian but degenerate noise, which forces only specific components of the system. This type of noise is fairly generically assumed in many scientific situations, where stochasticity is inserted to model a subset of unknown or unknowable degrees of freedom [30]. For example, one would force only small or large-scale structures in fluid turbulence [75], or only surface freshwater influx or wind stresses in ocean modelling ([10] and Chapter 5). We observe that the coexistence between multistability and degenerate noise poses a challenge to numerical algorithms to compute the most likely transition trajectory, even more so if the noise is multiplicative.

10.1 Freidlin-Wentzell theory

In this section, we introduce Freidlin-Wentzell theory [86] and its application to SPDEs. For initial condition $\bar{u}_0 \in \mathcal{H}_1 = L^2(\mathcal{X}_1)$, deterministic drift term $b : \mathcal{H}_1 \to \mathcal{H}_1$, noise diffusion operator $\sigma : \mathcal{H}_1 \to \mathcal{H}_1$ and W a cylindrical Wiener process, we assume (Chapter 2) that there exists a mild solution u^ε of the system

$$\begin{cases} \mathsf{d}u^\varepsilon(x,t) = b\left(u^\varepsilon(x,t)\right)\mathsf{d}t + \sqrt{\varepsilon}\sigma\left(u^\varepsilon(x,t)\right)\mathsf{d}W(x,t), & x \in \mathcal{X}_1,\ t \geq 0, \\ u^\varepsilon(x,0) = \bar{u}_0(x), & x \in \mathcal{X}_1. \end{cases}$$

For a fixed time $T > 0$, we introduce the action functional

$$I_T(\phi) = \inf_{g \in \mathcal{J}_T} \frac{1}{2}\int_0^T ||\dot{g}(s)||^2 \mathsf{d}s,$$

for

$$\mathcal{J}_T = \left\{ g : [0,T] \to \mathcal{H}^1 :\ \phi(t) = \bar{u}_0 + \int_0^t b(\phi(s))\mathsf{d}s + \int_0^t \sigma(\phi(s))\dot{g}(s)\mathsf{d}s,\ t \leq T \right\},$$

which quantifies the effect of the noise on the solution path ϕ in the time interval $[0,T]$. As discussed in [86], under the assumption of small noise intensity $0 < \varepsilon \ll 1$, the following exponential estimate holds

$$\log\left(\mathbb{P}\left(\sup_{t\in[0,T]} ||u^\varepsilon(t) - \phi(t)||^2 < \delta\right)\right) \propto -\varepsilon^{-1} I_T(\phi),$$

for small enough $\delta > 0$. It follows that, in the limit $\varepsilon \to 0$, the most likely paths ϕ minimise the action functional. For rare transitions between metastable states [96, 176], particular importance is given to paths in

$$\mathfrak{C} := \{\phi \in C([0,T]) \mid \phi(0) = \bar{u}_0, \phi(T) = \bar{u}_T\},$$

for $\bar{u}_0, \bar{u}_T \in \mathcal{H}_1$ in disjoint deterministically invariant subsets of $\mathcal{X}_1$. Under the assumption of small noise intensity, paths that cross the two states are unlikely by construction. For example, this is the case of the elements in $\mathfrak{C}$ for $\bar{u}_0$ and $\bar{u}_T$ in different basins of attraction. For $\varepsilon \to 0$ and fixed states $\bar{u}_0, \bar{u}_T \in \mathcal{H}_1$, the instanton $\bar{\phi}$ is the most likely solution u^ε such that $\phi \in \mathfrak{C}$, and equivalently, it satisfies

$$\bar{\phi} = \operatorname*{argmin}_{\phi \in \mathfrak{C}} I_T(\phi), \tag{10.1.1}$$

and solves the Freidlin-Wentzell minimisation problem. The nature of the noise is defined by the noise diffusion operator σ and the noise covariance $a := \sigma\sigma^*$. If there exist $u, v \in \mathcal{H}_1$ and $v \not\equiv 0$, such that $\sigma(u)v = 0$, then the noise is degenerate. We then define the Hamiltonian functional

$$H(\phi, \theta) = \langle b(\phi), \theta \rangle + \frac{1}{2}\langle \theta, a(\phi)\theta \rangle$$

for θ called the conjugate momentum of ϕ. The instanton solves the corresponding Hamilton equations [96]

$$\begin{cases} \dot{\phi} = \partial_\theta H(\phi, \theta) \quad = b(\phi) + a(\phi)\theta, \\ \dot{\theta} = -\partial_\phi H(\phi, \theta) = -\partial_\phi \left(b(\phi)\right)\theta - \dfrac{1}{2}\theta\partial_\phi \left(a(\phi)\right)\theta. \end{cases}$$

The first Hamilton equation indicates that the weighted conjugate variable $\sigma(\phi)^*\theta$ can be interpreted as the optimal noise on the instanton path. However, in the case of degenerate noise, it is clear that its role is more subtle. In particular, we know that in this case there must be modes $v \in \mathcal{H}_1$ that remain unforced regardless of the choice of θ. In other words, while it remains true that $\sigma^*(\phi)\theta$ is the optimal noise, the mapping between noise and trajectory ϕ is no longer one-to-one: there exist trajectories ϕ that cannot be realised by any value of the noise.

This fact stands in the way of applying traditional methods for computing large deviation minimisers, such as the minimum action method (MAM) [77, 212] and its geometric counterpart [95, 108, 194]. Such methods obtain the optimal transition path of the Lagrangian optimisation problem via relaxation or gradient descent, which necessitates inverting the noise covariance matrix $a(\phi)$. In other words, methods that rely on optimising the path instead of the noise are inadequate in the presence of degenerate noise and non-invertible covariance matrices. On the other hand, methods based on the Hamiltonian formalism, as introduced above, do not suffer from the same shortcomings as they circumvent inverting the noise covariance by considering the Legendre transform of the Lagrangian optimisation problem in the form of the Hamilton equations. Corresponding methods have been employed successfully in the presence of degenerate noise even for high-dimensional systems [94, 96, 181]. Unfortunately, with the notable exception of [210], these approaches are in general incapable of dealing with metastability, which always implies nonconvexity of the rate function, leading to nonuniqueness of the boundary conditions of the adjoint variable [3].

In the following, we propose to unify these two approaches by simultaneously applying the adjoint state method (allowing us to consider degenerate noise), while also convexifying the problem through the application of the augmented Lagrangian method [167] or penalisation of the endpoint constraint (see also the equivalent idea of the generalised canonical ensemble in statistical mechanics [58]). This combination allows us to deal with metastability and degenerate noise simultaneously in the study of high-dimensional and complex systems such as SPDEs.

10.2 Adjoint state method

The adjoint state method is a well-known technique for the solution of constained minimisation problems [169]. Its application to the action minimisation problem is easily justifiable and analysable when realising that the (10.1.1) can be interpreted as the minimisation of the $L^2(a, \mathcal{X}_1)$-cost of the noise under a functional constraint enforcing all degrees of freedom of the path in $\mathcal{J}_T$, both the stochastically forced and the deterministic ones.[1] Concretely, we define the variables ϕ, θ and introduce the adjoint state variable, or the Lagrange multiplier, μ. Such variables assume values in $\mathcal{H}_1$ for any $t \in [0, T]$. Further, the endpoint constraint is enforced through a penalty parameter $\lambda > 0$. The cost function is then constructed as follows,

$$J(\phi, \theta, \mu, \lambda) = \underbrace{\frac{1}{2}\int_0^T ||\sigma^*(\phi)\theta||^2 \mathrm{d}t}_{\text{Weighted action}} + \underbrace{\int_0^T \left\langle \mu, \dot{\phi} - \partial_\theta H(\phi, \theta) \right\rangle \mathrm{d}t}_{\text{First Hamilton equation enforcer}} + \frac{1}{2}\underbrace{\lambda ||\mathrm{F}\left(\phi(T) - \bar{u}_T\right)||^2}_{\text{Penalty term}}. \tag{10.2.1}$$

The first term in (10.2.1) is the actual cost of the stochastic forcing, appropriately weighted by the noise covariance $\sigma^*(\phi)$. The second term employs the adjoint trajectory $\mu(t)$ to enforce the first Hamilton's equation, which yields the unique path $\phi(t)$ caused by the noise $\sigma^*(\phi)\theta$. Finally, the last term enforces the endpoint constraint of the path via a penalty term. The linear operator F is employed as a filter to capture characteristics of the final condition $\bar{u}_T$. With this, we observe that the method corresponds to a Lagrange Multiplier Penalty method [167] in path space.

In the upcoming examples, it is assumed to be the identity operator Id or a multiplication operator. The cost function is iteratively minimised, for example via gradient descent or quasi-Newton method, until the partial derivatives of J with respect to ϕ, θ, and μ have norms below a pre-chosen threshold. Each iteration is accomplished in accordance with the steps to follow.

1. We enforce $\partial_\mu J = 0$, i.e.

$$\partial_\mu J = \underbrace{\dot{\phi} - \partial_\theta H(\phi, \theta)}_{\text{First Hamilton equation}} = \dot{\phi} - b(\phi) - \sigma(\phi)\sigma^*(\phi)\theta,$$

   by solving the first Hamilton equation, for which $\phi = \bar{u}_0$ is chosen as the initial condition. The variable θ assumes the role of the conjugate momentum of ϕ. For our SPDE-examples, this is solved through the mild solution formula, in the eigenbasis of the Laplacian, while for SDEs we employ the implicit Euler-Maruyama method (see Chapter 2 and Chapter 3).

2. Next, we enforce $\partial_\phi J = 0$, i.e.

$$\partial_\phi J = \underbrace{-\dot{\mu} - \partial_\phi H(\phi, \mu)}_{\text{Second Hamilton equation}} + \underbrace{\frac{1}{2}\partial_\phi \left(\left(\sigma\left(\phi\right)\left(\theta - \mu\right)\right)^2 \right)}_{\text{Error term}} + \underbrace{\delta_T \lambda\, \mathrm{F}^*\, \mathrm{F}\left(\phi - \bar{u}_T\right)}_{\text{Final condition enforcer}}.$$

   Such a constraint is equivalent to solving the second Hamilton equation, with μ in the role of the conjugate variable and with an error term. The equation is solved backward in time and initialised as $\mu(T) = \lambda\left(\phi(T) - \bar{u}_T\right)$. Such a final condition in the adjoint state variables aims to enforce the targeted final condition in the path variable $F\phi(T) = F\bar{u}_T$. Similarly to the previous step, the numerical computation of the SPDEs is resolved through the mild solution formula in the eigenbasis of the Laplacian with corresponding boundary conditions. The SDEs are solved through the implicit Euler-Maruyama method and $\mathrm{F} = \mathrm{Id}$.

3. Lastly, we compute $\partial_\theta J$, i.e.

$$\partial_\theta J = a\left(\phi\right)\left(\theta - \mu\right) = \sigma(\phi)\sigma^*(\phi)\left(\theta - \mu\right).$$

[1] We consider the $L^2(a, \mathcal{X}_1)$ space as the set of functions f such that $\sigma^*(\phi)f$ is in $L^2(\mathcal{X}_1)$. In fact, such a space depends on the state of the trajectory ϕ.

This gradient is guaranteed to be a descent direction of the cost function (10.2.1) in the space of θ-variables from the construction of a. Consequently, it can be used to update the variable θ, in our case through the Limited Memory Broyden–Fletcher–Goldfarb–Shanno (L-BFGS) method [167].

The iteration is halted as the norm of $\partial_\theta J$ is less than a fixed tolerance value, $tol > 0$. At the actual minimiser, we have $\partial_\theta J(\phi, \theta, \mu, \lambda) = 0$ and it is implied that $\sigma^*(\phi)(\theta - \mu) = 0$. Therefore, the error term in the second step is null, and the Lagrange multiplier μ solves the first Hamilton equation in the first step. This implies that the couple (ϕ, μ) solves the Hamilton equations and that ϕ is the instanton of the SPDE under initial condition $\phi(0) = \bar{u}_0$ and final condition $\mathrm{F}\,\phi(T) = \mathrm{F}\,\bar{u}_T$. Furthermore, this implies that the optimal noise can be read off as $\sigma^*(\phi)\mu(t)$ at convergence.

The optimisation problem presented above can be solved for any assumed transition time $T > 0$. Generally, though, the optimisation problem is harder to solve for long time intervals. First, this is because long time intervals necessitate a larger number of numerical timesteps and degrees of freedom to optimise. Second, and more importantly, in a metastable system, the most likely transition will generally involve a localised-in-time jump from one state to the other (hence the name 'instanton'). Because of this, for long time intervals, the optimisation problem is generally very insensitive to time-translations: the Freidlin-Wentzell action of an earlier or later jump is almost identical, leading to flat directions in the cost functional that involve many degrees of freedom and are thus hard to correct for, even with quasi-Newton methods. On the other hand, this phenomenologically implies that the optimisation procedure will rather rapidly converge to the correct transition path, and from then on only very slowly to the correct transition time.

10.3 Applications

In this section, we demonstrate the applicability and efficiency of the above method for the computation of transition pathways in stochastic complex systems with degenerate noise. In particular, we consider systems of increasing complexity, starting with a toy SDE model of a two-dimensional double-well with degenerate noise, then considering the Allen-Cahn reaction diffusion SPDE, forced only through the boundary in Subsection 10.3.2, and the Gierer-Meinhardt SPDE for pattern formation with multiplicative degenerate noise in Subsection 10.3.3. Afterwards, we focus on SPDEs of advection-reaction-diffusion type involving formation of moving spikes, including the spatially extended FitzHugh-Nagumo model with additive degenerate noise in Subsection 10.3.4, and lastly the Barkley model for turbulence proliferation in pipe flow with multiplicative degenerate noise in Subsection 10.3.5.

10.3.1 Two-dimensional SDE with degenerate multiplicative noise

We want to consider the non-standard question on how a noise-induced transition between the two metastable fixed points is achieved in the most likely way in the small degenerate noise limit, $\varepsilon \to 0$. For $u = (x_1, x_2) \in \mathbb{R}^2$, the SDE

$$\mathrm{d}u^\varepsilon = \mathrm{d}\begin{pmatrix} x_1 \\ x_2 \end{pmatrix} = \begin{pmatrix} 2x_2 - (x_1 + x_2)^3 \\ 2x_1 - (x_1 + x_2)^3 \end{pmatrix} \mathrm{d}t + \sqrt{\varepsilon} \begin{pmatrix} (x_1 - x_2 + 0.2) \\ 0 \end{pmatrix} \mathrm{d}W_t \tag{10.3.1}$$

represents diffusion in a double-well potential on the main diagonal $x_1 = x_2$. It has two deterministically stable solutions at $(x_1, x_2) = u_\pm = \pm(0.5, 0.5)$ and a saddle $(x_1, x_2) = (0, 0)$. The noise is multiplicative and chosen in order to assume a higher intensity for (x_1, x_2) distant from a chosen region in $\mathbb{R}^2$. In particular, it vanishes completely on the line $x_2 = x_1 + 0.2$. Furthermore, we only exert stochastic forcing on the x_1-component of the equation. Since the transition necessitates a change in both the x_1 and x_2 component, but only x_1 is fluctuating, we expect a non-trivial transition trajectory that makes optimal use of the coupling terms. The situation is depicted in Figure 10.1a, where we display the deterministic dynamics as streamlines, all three fixed points (two stable and one saddle) as white markers, as well as the noise

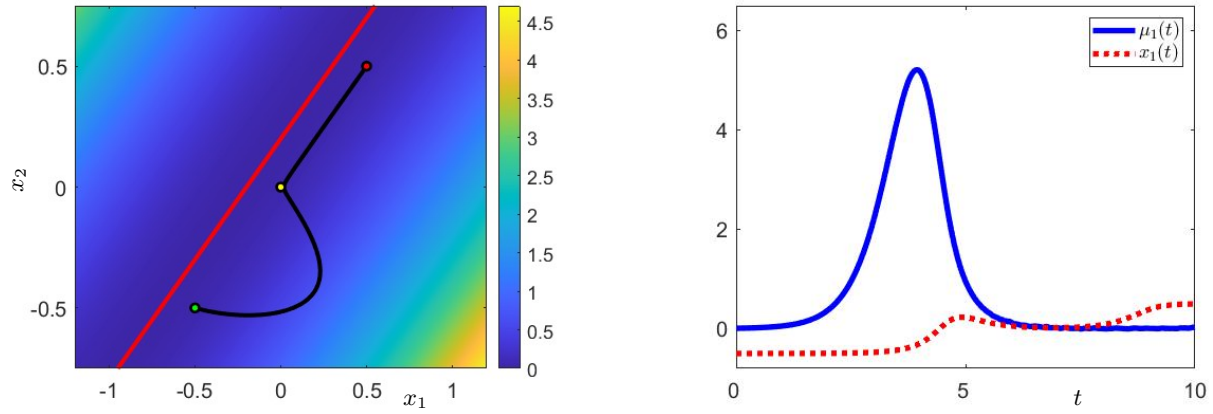

(a) Instanton of (10.3.1) connecting two wells through degenerate noise

(b) Forcing exerted by the noise on a component of (10.3.1)

Fig. 10.1 (a) Instanton (solid line) for the transition between the two stable attractors of the dynamics (10.3.1) (streamlines). The shading refers to the strength of the multiplicative noise, $a(x_1, x_2)$, with a dashed line at $a(x_1, x_2) = 0$. The markers indicate the initial point $\bar{u}_0$, the saddle, and the final point $\bar{u}_T$. (b) Lagrange multiplier $\mu_1(t)$ adjoint to the optimal noise (solid blue), and first component of the minimiser, $x_1(t)$ (dashed red), with respect to time. The figures are obtained for $\lambda = 5$ and $tol = 10^{-4}$.

strength as shading, with a dashed line marking the points where the noise vanishes. The instanton, as minimiser of the Freidlin-Wentzell action (10.1.1), for $\bar{u}_0 = u_-$, $\bar{u}_T = u_+$ and $T = 10$, is depicted as solid line. It is clear that the noise leads the solution against the flow in a nontrivial and curved way because noise is available solely on the x_1-component, nonetheless it uses the deterministic dynamics to approach the saddle. Once crossing the separatrix at the saddle point, the instanton can relax deterministically into the opposite stable fixed point. Figure 10.1b shows the functional Lagrange multiplier $\mu_1(t)$ as a function of time in blue. In this context, the Lagrange multiplier can be interpreted as the optimal noise driving the transition. Stochasticity is only needed to perform the uphill portion of the dynamics, up until the saddle is reached at approximately $t = 7$. After that, the path relaxes deterministically towards $\bar{u}_T$ in the proximity to the saddle, and we have $\mu_1(t) = 0$ for $t > 7$. The $x_1(t)$ component is shown in dashed red for comparison.

10.3.2 One-dimensional Allen-Cahn model with boundary additive noise

The second example covers the one-dimensional Allen-Cahn model on an interval $\mathcal{X}_1 = [0, \pi]$. We employ stochastic forcing through Neumann boundary conditions. Concretely, at $x = 0$ we consider white Neumann boundary noise and at $x = \pi$ we set homogeneous Neumann conditions. For the model

$$\begin{cases} \mathrm{d}u^\varepsilon(x,t) = (\partial_x^2 u^\varepsilon(x,t) + \alpha u^\varepsilon(x,t) - u^\varepsilon(x,t)^3)\mathrm{d}t, \\ \partial_x u^\varepsilon(0,t) = \sqrt{\varepsilon}\sigma_0 \dot{W}_t, \\ \partial_x u^\varepsilon(\pi,t) = 0, \end{cases} \tag{10.3.2}$$

with $x \in \mathcal{X}_1$ and $t \geq 0$, we follow the analytic results from [63] to obtain the instanton for the transitions between the two spatially homogeneous stable fixed points $\bar{u}_0 \equiv -\sqrt{\alpha}$, $\bar{u}_T \equiv \sqrt{\alpha}$, $T = 20$, for the choice $\alpha = 1.5$ and $\sigma_0 = 0.5$. The solution of the system is

$$u^\varepsilon(\cdot,t) = \mathrm{e}^{\Delta_\mathrm{N} t}\bar{u}_0 + \int_0^t \mathrm{e}^{\Delta_\mathrm{N}(t-s)}\left(\alpha u^\varepsilon(\cdot,s) - u^\varepsilon(\cdot,s)^3\right)\mathrm{d}s + (\Delta_\mathrm{N} + \mathrm{Id})\int_0^t \mathrm{e}^{\Delta_\mathrm{N}(t-s)} D\mathrm{d}W_s,$$

for any $t \geq 0$, where Δ_N is the Laplacian with homogeneous Neumann boundary conditions in $\mathcal{X}_1$ and W is a scalar Wiener process. Lastly, $D : \mathbb{R} \to \mathcal{H}_1$ satisfies

$$D(c_1)(x) = -\frac{\cosh(\pi - x)}{\sinh(\pi)} c_1$$

for any $c_1 \in \mathbb{R}$. We also denote as $D^* : \mathcal{H}_1 \to \mathbb{R}$ the operator

$$D^*(\varphi) = -\frac{1}{\sinh(\pi)} \int_0^\pi \cosh(\pi - x)\varphi(x)\mathrm{d}x$$

for any $\varphi \in \mathcal{H}_1$. It follows that the covariance operator is

$$a = (\Delta_{\mathrm{N}} + 1)\, DD^*\, (\Delta_{\mathrm{N}} + 1)\,.$$

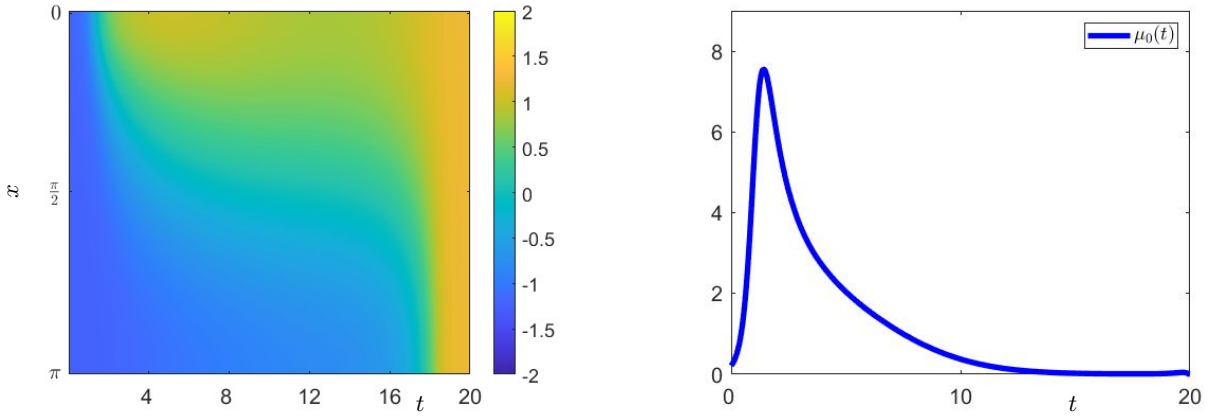

(a) Instanton of (10.3.2) connecting two flat stable states through boundary noise

(b) Noise exerted on an extreme of $\mathcal{X}_1$ to induce the rare transition on the entire domain of (10.3.2)

Fig. 10.2 (a) Instanton for the transition between $\bar{u}_0 \equiv -\sqrt{\alpha}$ to $\bar{u}_T \equiv \sqrt{\alpha}$ with random Neumann boundary condition at $x = 0$. First, the noise drags the solution towards the saddle by generating an influx at $x = 0$. After reaching a saddle, at approximately $t = 15$, the trajectory relaxes deterministically into the other stable solution $\bar{u}_T \equiv \sqrt{\alpha}$. (b) The effect of the optimal noise is described by the Lagrange multiplier $\mu_0(t)$, which only acts on the portion before reaching the saddle. The results are obtained for $\lambda = 200$, $\mathrm{F} = \mathrm{Id}$ and $tol = 10^{-3}$.

This is all the information needed to compute the large deviation minimiser for the boundary-noise induced transition between $\bar{u}_0$ and $\bar{u}_T$. Figure 10.2a displays the instanton ϕ in space and time: starting at $\bar{u}_0 \equiv -\sqrt{\alpha}$, the stochastic forcing generates an influx at $x = 0$ that is just enough to push the system towards the saddle configuration at approximately $t = 15$. In Figure 10.2b, we see the Lagrange multiplier $\mu_0(t)$ associated with the noise exerted on the solution on $x = 0$. The optimal noise is concentrated close to $t = 0$ and is approximately zero on the "downhill" portion for $15 < t \leq T$, as expected.

10.3.3 Spike merging in Gierer-Meinhardt model with degenerate multiplicative noise

The reaction-diffusion Gierer-Meinhardt model [200] finds applications in biology, such as in the pattern formation of stripes on seashells. We consider the one-dimensional version on the interval $\mathcal{X}_1 = [0, 1]$ with homogeneous Neumann boundary conditions,

$$\begin{cases} \mathrm{d}u^\varepsilon = \begin{pmatrix} \mathrm{d}A \\ \mathrm{d}H \end{pmatrix} = \begin{pmatrix} d_A^2 \partial_x^2 A - A + \frac{A^2}{H} \\ \frac{1}{\tau}\left(d_H \partial_x^2 H - H + A^2\right) \end{pmatrix} \mathrm{d}t + \sqrt{\varepsilon}\sigma_0 \begin{pmatrix} 0 \\ H \end{pmatrix} \mathrm{d}W_t, \\ \partial_x A(0,t) = \partial_x A(1,t) = \partial_x H(0,t) = \partial_x H(1,t) = 0, \end{cases} \tag{10.3.3}$$

for $t \geq 0$. The Gierer-Meinhardt model is known to display steady solutions characterised by spikes on the variables $A \geq 0$, the so-called "activator", and $H \geq 0$, the "inhibitor". The number of spikes present in a stable solution depends on the diffusivity constants $d_A, d_H > 0$. Moreover, the stability of the flat solution $A = H \equiv 1$, depends on the timescale $\tau > 0$. We are interested in the effect of noise-induced spike merging, i.e., the stochasticity transforming a pair of spikes into a single spike. Following [4, 124, 205], we consider the effect of degenerate multiplicative noise that forces the component H only, leaving A to act solely under the influence of H. In the figures to follow, we display the instanton that describes the merge of two spikes in time interval $[0, T] = [0, 200]$ and for $d_A = 0.06$, $d_H = 0.04$, $\tau = 0.5$ and $\sigma_0 = 0.5$.

In Figure 10.3a, we display the initial conditions $\bar{u}_0$ with light colours, and the final conditions $\bar{u}_T$ in dark colours. The steady solutions $\bar{u}_0$ and $\bar{u}_T$ are obtained numerically following [200, Chapter 2.1] and their stability is proven by [200, Remark 4.4].

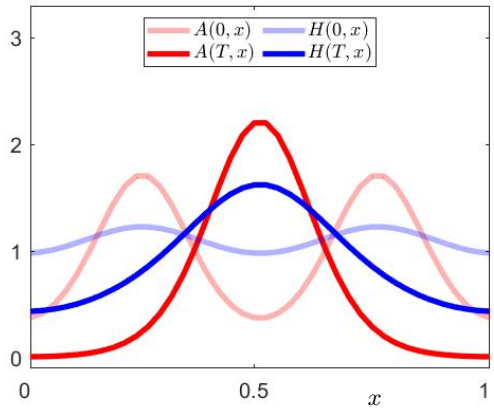

(a) Initial and final states associated with the merging of two spikes in the system (10.3.3)

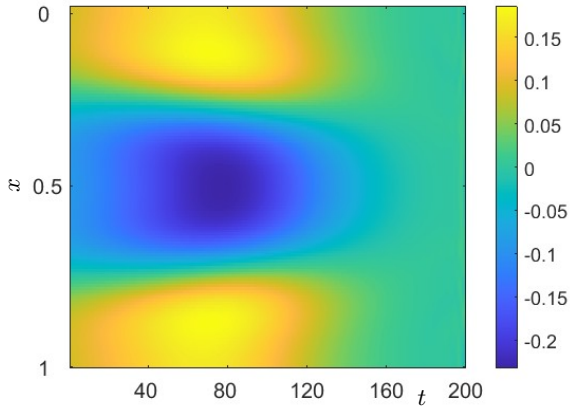

(b) Noise forcing, $H\mu_H$, exerted on the inhibitor component within the instanton of (10.3.3)

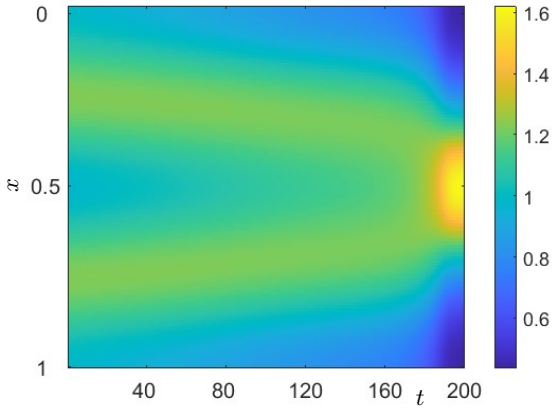

(c) Inhibitor component, H, within the instanton of (10.3.3) displaying the spike merging event

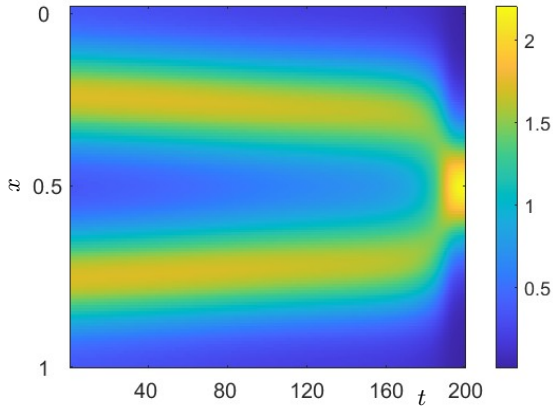

(d) Activator component, A, within the instanton of (10.3.3) showing the spike merging event

Fig. 10.3 (a) Initial (light) and final (dark) conditions of the instanton, transitioning from the stable two-spike configuration to the stable one-spike configuration. Here, the inhibitor H is depicted in blue, and the activator A in red. (b) Optimal noise $H\mu_H$ on the inhibitor component. The optimal noise is only needed to transiently move the peaks closer together, so that afterwards, the gap closes deterministically. Panels (c) and (d) show the inhibitor and activator components of the instanton, respectively. The two components display the merging of the spikes at similar times. The figures have been obtained with the parameters $\lambda = 20$, $\mathrm{F} = \mathrm{Id}$ and $tol = 10^{-4}$.

In Figure 10.3a, the forced component H is shown in blue, and the activator A is indicated in red, for the initial conditions (light colour) and final conditions (dark colour). In Figure 10.3b, the optimal noise is displayed as $H\mu_H$, for μ_H the Lagrange multiplier associated with the differential equation of H. It is apparent that the noise prioritises shifting the spikes closer together and, afterwards, when a critical distance is achieved at roughly $t = 150$, the instanton approaches $\bar{u}_T$ deterministically. In Figure 10.3c and in Figure 10.3d, the components H and A are shown, respectively. As the instanton approaches $\bar{u}_T$ in a deterministic manner, the merge of the two spikes occurs simultaneously in the inhibitor and the activator components.

10.3.4 Pulse initiation in FitzHugh-Nagumo model with degenerate additive noise

The reaction-diffusion FitzHugh-Nagumo model is often employed in the simulation of electric impulses through nerve axons [80, 118]. It displays a behaviour qualitatively similar to the Hodgkin-Huxley model [110], despite being composed of significantly simpler equations. The reaction-diffusion model on the real line is

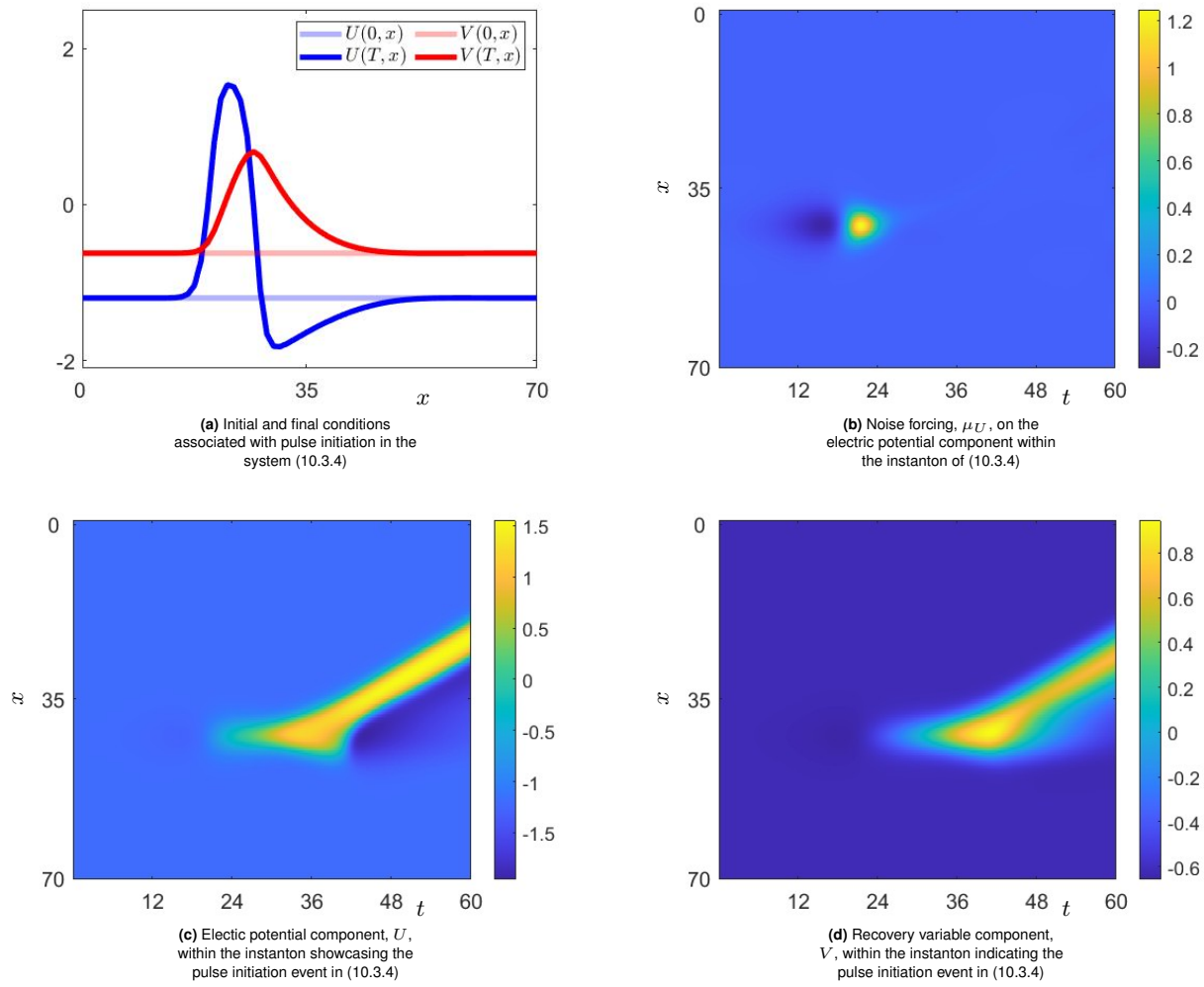

(a) Initial and final conditions associated with pulse initiation in the system (10.3.4)

(b) Noise forcing, μ_U, on the electric potential component within the instanton of (10.3.4)

(c) Electic potential component, U, within the instanton showcasing the pulse initiation event in (10.3.4)

(d) Recovery variable component, V, within the instanton indicating the pulse initiation event in (10.3.4)

Fig. 10.4 (a) The initial, $\bar{u}_0$, and final, $\bar{u}_T$, conditions in light and dark lines, respectively. The forced component, U, is displayed in blue, and V is indicated in red. (b) The Lagrange multiplier is shown and indicates the effect of the noise in the pulse initiation. Panels (c) and (d) show the pulse initiation on the U and V components, respectively. The figures are obtained for parameters $\lambda = 0.5$ and $tol = 5\ 10^{-4}$ and with periodic boundary conditions. The filter on the final condition is $\mathrm{F} = \mathrm{Id}$.

characterised by travelling pulse solutions, whose properties have been extensively studied [98, 178]. In the current subsection, we construct an instanton for the model

$$\mathrm{d}u^{\varepsilon} = \begin{pmatrix} \mathrm{d}U \\ \mathrm{d}V \end{pmatrix} = \begin{pmatrix} \nu_1 \partial_x^2 U + U - U^3 - V \\ \nu_2 \partial_x^2 V + \delta\,(U - \gamma_1 V + \gamma_2) \end{pmatrix} \mathrm{d}t + \sqrt{\varepsilon}\sigma_0 \begin{pmatrix} 1 \\ 0 \end{pmatrix} \mathrm{d}W_t, \tag{10.3.4}$$

the reaction-diffusion FitzHugh-Nagumo model with additive noise on variable U, following the example of [79]. We associate the component U to the electric potential and V with a recovery variable. The instanton describes the noise-induced initiation of a pulse, a well-studied event [116]. Note that in (10.3.4), only the electric potential is subject to additive Gaussian stochastic noise, while the recovery variable is left unforced. The parameters are set as $T = 60$, $\nu_1 = 1$, $\nu_2 = 0.1$, $\delta = 0.08$, $\gamma_1 = 0.8$, $\gamma_2 = 0.7$ and $\sigma_0 = 0.5$. The spatially homogeneous initial condition $\bar{u}_0 \approx (-1.19941, -0.62426)^T$ (absence of a pulse) and final condition $\bar{u}_T$ (pulse present) are chosen from [26, Example 2.4]. They are displayed in Figure 10.4a in light and dark lines, respectively. The forced component U is indicated in blue, and the term V is shown in red. The stability of $\bar{u}_0$ can be easily computed, and the stability of the travelling wave of frame $\bar{u}_T$ is obtained in [26, Example 3.7]. In Figure 10.4b, the Lagrange multiplier, μ_U, associated with the first equation in the model, is displayed. The noise provides first a small negative push to the flat solution $\bar{u}_0$ in a concentrated region and, secondly, initiates the pulse through an input of larger magnitude. Then, it directs the pulse

in the same direction along which $\bar{u}_T$ travels. In fact, the travelling wave mirrored in space to the pulse associated with $\bar{u}_T$ is also a stable solution of the system. Lastly, the instanton converges deterministically to $\bar{u}_T$. In Figure 10.4c and in Figure 10.4d, the perturbed component U and the component V are shown in contour plots, respectively. The creation of the pulse appears to be close to simultaneous in the terms. Furthermore, the negative bell in the tail of the pulse in the term U arises in a deterministic manner. Note that the pulse solution is only a fixed point in a reference frame of its movement speed, while our equations are defined in the stationary reference frame. For this reason, the instanton, as a solution to the optimisation problem, automatically initiates the pulse at a sufficient distance to allow it to travel to its pre-chosen endpoint.

10.3.5 Puff splitting in Barkley model with degenerate multiplicative noise

As the final, and from a numerical perspective, most complex example, we take the Barkley model for the evolution of turbulent puffs in pipe flow. It is defined by coupled SPDEs on the real line with degenerate multiplicative noise,

$$\mathsf{d}u^{\varepsilon} = \begin{pmatrix} \mathsf{d}q \\ \mathsf{d}v \end{pmatrix} = \begin{pmatrix} d_q \partial_x^2 q + \xi_2 \partial_x q + q\left(v + r - 1 - (r+\delta)(q-1)^2\right) \\ \left(-\xi_1 + \xi_2\right)\partial_x v + \varepsilon_1(1-v) - \varepsilon_2 v q \end{pmatrix} \mathsf{d}t + \sqrt{\varepsilon}\sigma_0 \begin{pmatrix} q \\ 0 \end{pmatrix} \mathsf{d}W_t. \tag{10.3.5}$$

The system describes the evolution of turbulence in shear flows through a long pipe [12], extended in x-direction. The variable $q \geq 0$ indicates the turbulent kinetic energy, as difference of the transverse velocity components to the laminar background profile. The variable v in turn describes the centerline velocity. The model is normalised such that the centerline velocity is 0 in the presence of strong turbulence, and 1 for the laminar flow. The parameters $\varepsilon_1 > 0$ and $\varepsilon_2 > 0$ define the attractivity of such states. Furthermore, the real parameters ξ_1 and ξ_2 indicate the advection velocity in v and define the moving reference frame, respectively. The variable $r > 0$ represents the fluid Reynolds number. Phenomenologically, this model always allows for the spatially homogeneous laminar flow $(q, v) = (0, 1)$ to be stable at any Reynolds number, representing the fact that in transitional pipe flow the laminar solution of the Navier-Stokes equation remains linearly stable. The stochastic forcing models the chaotic nature of turbulent flow, and is hence chosen to act on q only, and proportional to q itself. Consequently, the laminar solution exhibits no noise at all and is hence an absorbing state. At sufficiently high Reynolds numbers, the system additionally exhibits turbulent puff solutions in the form of localised travelling packets with $q > 0$, similarly to what occurs in actual pipe flow. They are long-lived in nature and linearly stable in the model. Crucially, stochasticity may force the turbulent puff to either decay into laminar flow, or alternatively, split into two independent, separated turbulent puffs. Above a critical Reynolds number r_c, puff splitting dominates puff decay, and turbulence proliferates in the pipe [12, 13, 91].

Our aim is to capture the puff splitting process [87] by computing the split instanton, the noise-induced transition from a single puff into two. Here, the noise generates a second puff splitting off from an existing one, on the interval $[0, 150]$ with periodic boundary conditions. Note that, in contrast to the model in Subsection 10.3.4, a puff cannot be created in a completely laminar region, since there the stochastic forcing is necessarily identically zero. This makes this model particularly difficult to handle, as the noise is not only inactive on the whole v-field, but dynamically inactive for q in most of the domain as well.
The parameters are taken as $d_q = 0.5$, $r = 0.6$, $\delta = 0.1$ and $\sigma_0 = 0.5$. In order to describe the centerline velocity, we have chosen the values $\varepsilon_1 = 0.1$ and $\varepsilon_2 = 0.2$. Lastly, the parameters $\xi_1 = \xi_2 = 0.8$ refer to the advection speed and the moving reference frame. The Barkley model is considered with the initial condition $\bar{u}_0$, at time $t = 0$, which is a puff obtained as a converging solution from an initial bell-shaped state. The initial condition is shown in Figure 10.5a in a light blue line for the perturbed component q and a light red line for v. The final condition is obtained as follows. We label the single puff states as $\bar{u}^{\mathsf{s}}_{70} = (q^{\mathsf{s}}_{70}, v^{\mathsf{s}}_{70})^T$ the state at $t = 70$ and as $\bar{u}^{\mathsf{s}}_T$ the state at $t = T = 100$. We define as $\mathfrak{R}_c$ the rotation operator with a shift of value c in the right direction on the interval $[0, 150]$ with periodic boundary conditions. To construct the double puff state $\bar{u}_T = \bar{u}^{\mathsf{d}}_T$, we observe again the Barkley model with new initial conditions

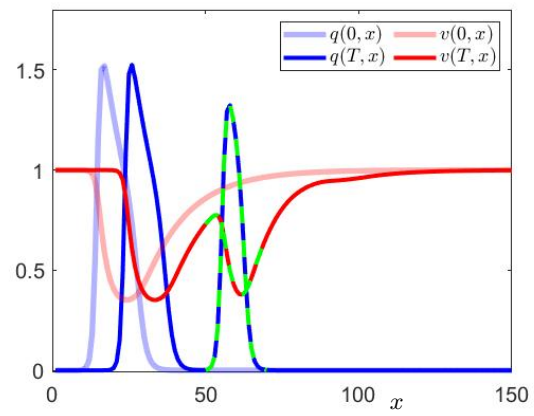

(a) Initial and final states associated a puff splitting event in (10.3.5), highlighting the filtered region

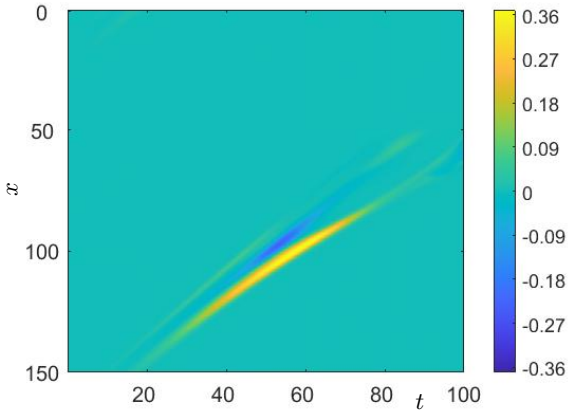

(b) Noise forcing, $q\mu_q$, exerted on the turbulence component of the instanton in the system (10.3.5)

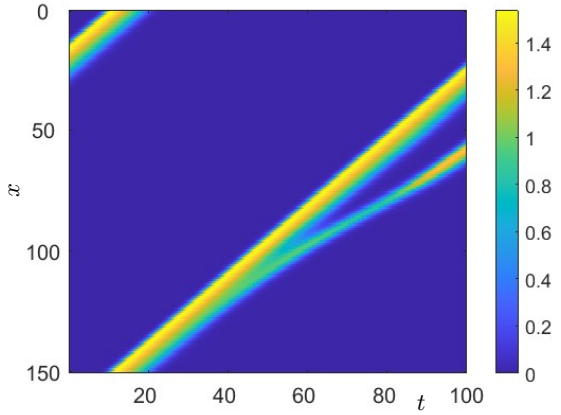

(c) Turbulence component, q, within the instanton associated to the puff splitting event in (10.3.5)

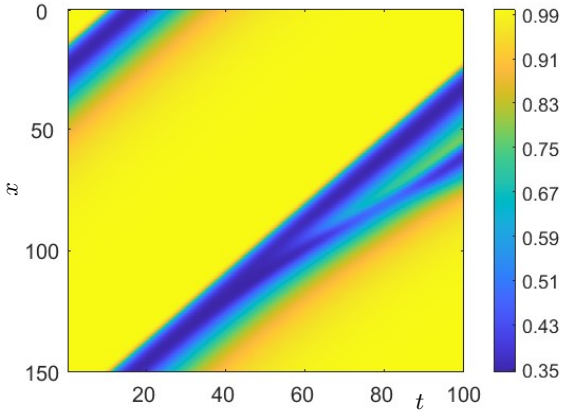

(d) Centerline velocity, v, within the instanton capturing the puff splitting event in (10.3.5)

Fig. 10.5 (a) The initial, light, and final, dark, conditions of the instanton. The enforced final condition, on $\mathcal{X}_{\mathsf{F}} = [50, 70]$, is shown in dashed green. The blue lines are associated with the forced component q and the red lines to v. The state $\bar{u}_0$ is a state of a stable travelling wave of the model , whereas $\bar{u}_T$ is not the frame of a travelling wave. Panel (b) displays $q\mu_q$, which indicates the optimal noise that defines the instanton. Figures (c) and (d) show the puff-splitting event for the components q and v, respectively. The figures are obtained for parameters $\lambda = 200$ and $tol = 10^{-2}$.

$\bar{u}^{\mathsf{d}}_{70} = \left(q^{\mathsf{d}}_{70}, v^{\mathsf{d}}_{70}\right)^T = \left(q^{\mathsf{s}}_{70} + \mathfrak{R}_{\frac{150}{7}} q^{\mathsf{s}}_{70}, v^{\mathsf{s}}_{70} + \mathfrak{R}_{\frac{150}{7}} v^{\mathsf{s}}_{70} - 1\right)^T$ at $t = 70$. The final condition $\bar{u}^{\mathsf{d}}_T$ is defined as the state of the solution of the system at time $t = T$. Its shape corresponds to a leading and a second well-separated trailing puff, as shown in Figure 10.5a in dark lines. The component q is shown in blue, and v is indicated in red. The state $\bar{u}^{\mathsf{d}}_{70}$ is chosen to obtain a realistic sustainable double puff state in $\bar{u}_T = \bar{u}^{\mathsf{d}}_T$. Furthermore, at time $T = 100$, the position of the higher puff in $\bar{u}^{\mathsf{d}}_T$ is qualitatively similar to the location of the puff shown in the state $\bar{u}^{\mathsf{s}}_T$ on the interval with periodic boundary conditions. A filter is chosen in order to capture the shape of the second puff in $\bar{u}_T$. Therefore, we choose $\mathrm{F} = \mathbb{1}_{\mathcal{X}_{\mathsf{F}}}$, the multiplication operator for the indicator function with support on $\mathcal{X}_{\mathsf{F}} = [50, 70]$. The dashed green lines indicate the enforced structure in the penalty method.

In Figure 10.5b, the optimal noise is described by $q\mu_q$, for μ_q that indicates the Lagrange multiplier for the first differential equation in the system. The conjugate variable can be interpreted to cause the following: first, it elongates the tail of the original puff into a wider object; second, for $t \in [40, 60]$, it generates a laminar gap to cut the elongated puff into two, deep enough to result in a split; afterward, weak final stochastic adjustments are made to meet the final locations of the two puffs. The adjustments are further justified by the fact that $\bar{u}_T$ is not the frame of a steady travelling wave. The instanton describing a puff splitting event is shown in Figure 10.5c and in Figure 10.5d, which display the components q and v,

respectively, in contour plots. Similarly to the previous examples, the splitting event appears to happen simultaneously on both terms, despite the degeneracy of the noise.

10.4 Summary

We introduce a method to compute instantons, large deviations minimisers, for metastable SPDEs in the presence of degenerate noise. We demonstrate the applicability of the method for various example problems of increasing complexity, culminating in the computation of the turbulent puff splitting instanton in the Barkley model, a system that describes the behaviour of regions of turbulence in a long pipe. Further applications of the algorithm are spike merging in the Gierer-Meinhardt model, with multiplicative noise on the inhibitor component, and pulse creation in the FitzHugh-Nagumo model, with additive noise on the electric potential component. The implementation of the algorithm enables the construction of the most likely paths under degenerate noise and boundary noise.

11 Conclusion and Outlook

The main topic of this thesis is the construction and development of early-warning signs for abrupt transitions. It focuses on the analytic and numerical study of fast-slow SPDE models, to incorporate minor perturbations as noise terms and spatial dissipation through the deterministic component. Such trends align with various phenomena in climate science, which is the principal application of this work. In order to predict tipping phenomena, we track a critical manifold, following a stable solution under the change of a critical parameter. As the state loses stability, we discuss the approach to such a threshold, which corresponds to a codimension-1 bifurcation. This dissertation includes two main parts, distinguishing between the study of bifurcation-induced tipping and noise-induced tipping. Nonetheless, as discussed in the Introduction (Chapter 1), such concepts are entwined and sometimes equated in applications. Consequently, the results discussed in each part are relevant to both types of tipping.

The first part extends well-known signals on box models to SPDEs with additive noise. These capture the critical slowing down effect, descriptive of the approach to a bifurcation threshold. To construct such observables, we rely on the linearisation of the model and study the fast subsystem. This is justified by the assumption that trajectories stay close to the slow manifold of a stable solution of the deterministic model and that the slow component is almost stationary (approximated by a parameter) in comparison with the fast variable. The most studied early-warning signal throughout the part is the time-asymptotic (auto)covariance. We describe the rate of divergence of the observable for the linearised system with purely discrete spectrum and how it is affected by the nature of the additive Gaussian noise. Through the study of a space-heterogeneous Chafee-Infante equation, we find sufficient assumptions for the construction of the signal in the case of a Q-Wiener process that does not share all eigenfunctions with the linear drift operator. Such a hyperbolic rate resembles standard results in SDEs but relies on strong assumptions about the model. In order to describe the applicability of such an instrument, we test it on cases in which it exhibits different behaviour. We address first the case of the linear drift operator characterised by a purely continuous spectrum. By the employment of a tool operator, we describe the rate of the signal in the case of analytic multiplication operators in the drift for multidimensional domains. We then extend the results to applied models through the use of Fourier transforms. Under such spectral assumptions, we observe a hindered scaling law of the signal and, in some instances, a complete silencing of the early-warning sign. Secondly, we consider models with a linear drift operator with purely generalised discrete spectrum. In such a case, the rate of divergence of the observable is enhanced depending on the algebraic multiplicity of the most sensitive eigenvalue. In conclusion, such an early-warning sign requires a deep understanding of the drift operator of the corresponding model in order to be properly applied. Throughout the analysis, we have enforced different parameters, such as the noise intensity, to be constant. In case this assumption is not fulfilled, the scaling law would be further affected by the noise intensity. The risk of addressing false early-warning signals depends on the reliability of the model and on the observation of the correct phenomenon. Equivalent rates of divergence are obtained under the assumption of red Gaussian noise, as suggested by Hasselmann's paradigm. Furthermore, the case of a generalised discrete spectrum has been extended to the assumption of boundary noise. Such a result has been applied to a Boussinesq model to predict the approach to two different bifurcation thresholds, while underscoring the need in applications for ensuring the fulfilment of analytic assumptions through numerical approaches.

A recurring problem in the observation of real climate observations is missing data. In the case of SPDEs, the knowledge of a trajectory in certain regions of the domain can be collected through the projection on functions with corresponding support. In this thesis, we find that the highest scaling law of the time-asymptotic (auto)covariance is observed along a large family of functions in the case of non-degenerate noise. Therefore, an increase in variance can be registered without prior knowledge of the eigenfunctions

of the drift operator. Such a property is not shared by the exponential growth of the autocovariance, which is another standard early-warning sign in SDEs. In fact, it needs to be observed along the most sensible simple eigenfunction, if existent, to assume an equivalent growth.
The linearisation of the original model is a reliable technique for a critical parameter that is distant from the bifurcation threshold. As such, the discussed early-warning signs are less valid in their proximity. Furthermore, in the case of small gaps between the most sensible eigenvalues, such as the case of the Laplace operator in large domains, the growth of the observable can be delayed. In addition, in multistable systems, the trajectory can escape the basin of attraction in finite time and the variance would not be correctly estimated through ergodic theory. While the finite-time Lyapunov exponents require shorter trajectory intervals than other observables, in the space-heterogeneous stochastic Chafee-Infante equation its peak value changes sign at a supercritical pitchfork bifurcation, serving as an early-warning signal. The rate of convergence to zero is reciprocal to that displayed by the time-asymptotic variance. In fact, both methods rely on a Frechét derivative and are therefore deeply connected. Nonetheless, the latest observable is computed through the derivation of the unique (singleton) random attractor, a stochastic object.

In conclusion, the reliability of early-warning signs for B-tipping depends on the properties of the model and on the insights provided by the trajectory. Furthermore, their validity is hindered by the multistability of the system and the possibility of a noise-driven transition prior to the bifurcation crossing. In such instances, early-warning signs for N-tipping aim to capture the probability of a jump in a given timescale and the nature of the corresponding phenomenon. In this thesis, we obtain estimates of the probability of exit from a neighbourhood of a stable steady state for the non-autonomous space-heterogeneous Chafee-Infante equation and a band-free plane Couette flow model with multiplicative noise. The first is achieved through an analytic Galerkin method and a Bernstein-type inequality. From such an upper bound, further moment estimates are computed. The second estimation is obtained through martingale properties of the solution and Jensen-type inequalities. In alignment with Hasselmann's paradigm, we extended the last results to different types of red Gaussian noise.
In order to study the steps that describe a rare event transition forced by weak noise, we employ numerical techniques that rely on large deviation theory and the Hamiltonian perspective. The instanton, which is the most likely path that indicates a rare phenomenon, is obtained via the state adjoint method by minimising a cost functional comprising a weighted action, a Hamiltonian constraint, and a penalty enforcing the desired final state. The numerical iterative method has been applied to models in biology, medicine, and fluid mechanics. The resulting trajectory describes the natural response of the deterministic system to the noise perturbation; the algorithm also provides further insight into the most sensitive stages of the transition and the noise realisation that drives the instanton.

Overall, we have described and extended the use of early-warning signs to SPDEs. Controversially, most signals for B-tipping are more relevant far from the bifurcation thresholds, whereas those related to N-tipping find more use in its proximity. While an exceptional research topic would be the development of methods that capture the structure of geometric early-warning signs, such as the quasipotential or the committor function, another promising further step in research would be a score function for the reliability of a signal. Novel directions can be the construction of signals for SPDEs and B-tipping under different noise assumptions, such as multiplicative noise and Lévy additive noise. The estimation of the probability of critical transitions is also currently case-dependent. While improvement on their computation is useful, the description of general approaches that are applicable to a wide family of SPDEs would find broader applications. Finally, the numerical estimation of metastable transitions benefits from the incorporation of machine learning techniques in the search for geometric early-warning signs. Iterative algorithms to compute the committor function [51] and the instanton [119, 120] are showing promising results.
While the employment of the observables requires deep knowledge of the models, the field is ever-expanding. The contribution of this thesis lies in advancing the theoretical and numerical understanding of early-warning signals within complex systems, as well as demonstrating their applicability across a range of model scenarios. By refining detection techniques and providing insights into the conditions under which early-warning signals are most reliable, this work supports more effective forecasting of critical transitions in both climate and engineered systems.

Bibliography

[1] I. Adan and J. Resing. “Simple analysis of a fluid queue driven by an M/M/1 queue”. In: *Queueing Syst.* 22 (1996), pp. 171–174.

[2] S. Agmon. “On the eigenfunctions and on the eigenvalues of general elliptic boundary value problems”. In: *Comm. Pure Appl. Math.* 15.2 (1962), pp. 119–147.

[3] M. Alqahtani and T. Grafke. “Instantons for rare events in heavy-tailed distributions”. In: *J. Phys. A* 54.17 (Apr. 2021), p. 175001. ISSN: 1751-8121. DOI: 10.1088/1751-8121/abe67b.

[4] K. Antwi-Fordjour, S. Kim, and M. Nkashama. “Global analysis of the shadow Gierer-Meinhardt system with general linear boundary conditions in a random environment”. In: *arXiv preprint arXiv: 1907.10122* (2019).

[5] V. I. Arnold et al. *Dynamical systems V: bifurcation theory and catastrophe theory*. Vol. 5. Springer Science & Business Media, 2013.

[6] Y. Asgari, M. Ghaemi, and M. G. Mahjani. “Pattern formation of the FitzHugh-Nagumo model: cellular automata approach”. In: *Iran. J. Chem. Chem. Eng.* (2011).

[7] P. Ashwin et al. “Tipping Points in Open Systems: Bifurcation, Noise-Induced and Rate-Dependent Examples in the Climate System”. In: *Philos. Trans. R. Soc. A* 370.1962 (2012), pp. 1166–1184. DOI: 10.1098/rsta.2011.0306.

[8] P. Ashwin et al. “Early warning skill, extrapolation and tipping for accelerating cascades”. In: *Proc. R. Soc. A.* 481.20250405 (2025).

[9] S. Baars, F. W. Wubs, and H. Dijkstra. *Transiflow*. Feb. 17, 2024. URL: https://github.com/BIMAU/transiflow.

[10] S. Baars et al. “Continuation of probability density functions using a generalized Lyapunov approach”. In: *J. Comput. Phys.* 336 (2017), pp. 627–643.

[11] M. Bär, E. Meron, and C. Utzny. “Pattern formation on anisotropic and heterogeneous catalytic surfaces”. In: *Chaos* 12.1 (2002), pp. 204–214.

[12] D. Barkley. “Modeling the transition to turbulence in shear flows”. In: *J. Phys. Conf. Ser.* Vol. 318. 3. IOP Publishing. 2011, p. 032001.

[13] D. Barkley. “Theoretical perspective on the route to turbulence in a pipe”. In: *J. Fluid Mech.* 803 (2016), P1.

[14] I. F. Barna et al. “Analytic self-similar solutions of the Kardar-Parisi-Zhang interface growing equation with various noise term”. In: *arXiv preprint arXiv:1904.01838* (2019).

[15] R. Bastiaansen, H. A. Dijkstra, and A. S. von der Heydt. “Fragmented tipping in a spatially heterogeneous world”. In: *Environ. Res. Lett.* 17.4 (2022), p. 045006.

[16] N. Berglund and B. Gentz. “Pathwise description of dynamic pitchfork bifurcations with additive noise”. In: *Probab. Theory Relat. Fields* 122.3 (2002), pp. 341–388.

[17] N. Berglund and B. Gentz. *Noise-induced phenomena in slow-fast dynamical systems: a sample-paths approach*. Springer Science & Business Media, 2006.

[18] N. Berglund and B. Gentz. “Sharp estimates for metastable lifetimes in parabolic SPDEs: Kramers’ law and beyond”. In: *Electron. J. Probab.* 18 (2013), pp. 1–58.

[19] N. Berglund and R. Nader. “Stochastic resonance in stochastic PDEs”. In: *Stoch. Partial Differ. Equ.* (2022), pp. 1–40.

[20] P. Bernuzzi, H. Dijkstra, and C. Kuehn. “Warning Signs for Boundary Noise and Their Application to an Ocean Boussinesq Model”. In: *Phys. D: Nonlinear Phenom.* 470 (2024), p. 134391. ISSN: 01672789. DOI: 10.1016/j.physd.2024.134391.

[21] P. Bernuzzi, A. F. S. Düx, and C. Kuehn. “Early Warning Signs for SPDEs with Continuous Spectrum”. In: *Eur. J. Appl. Math.* (2024), pp. 1–40. ISSN: 0956-7925, 1469-4425. DOI: 10.1017/S0956792524000330.

[22] P. Bernuzzi and T. Grafke. “Large Deviation Minimizers for Stochastic Partial Differential Equations with Degenerate Noise”. In: *Multiscale Model. Simul.* 23.3 (2025), pp. 1274–1288.

[23] P. Bernuzzi and C. Kuehn. “Bifurcations and Early-Warning Signs for SPDEs with Spatial Heterogeneity”. In: *J. Dyn. Differ. Equ.* (2023), pp. 1–45.

[24] P. Bernuzzi and C. Kuehn. “Probability of Transition to Turbulence in a Reduced Stochastic Model of Pipe Flow”. In: *arXiv preprint arXiv:2503.00987* (2025).

[25] P. Bernuzzi, C. Kuehn, and A. Morr. “Critical Slowing Down in Bifurcating Stochastic Partial Differential Equations with Red Noise”. In: *arXiv preprint arXiv:2504.06198* (2025).

[26] W.-J. Beyn, D. Otten, and J. Rottmann-Matthes. “Computation and stability of traveling waves in second order evolution equations”. In: *SIAM J. Numer. Anal.* 56.3 (2018), pp. 1786–1817.

[27] P. Billingsley. *Probability and measure*. John Wiley & Sons, 2017.

[28] K. Bisewski, D. Crommelin, and M. Mandjes. “Rare event simulation for steady-state probabilities via recurrency cycles”. In: *Chaos* 29.3 (2019).

[29] D. Blömker, M. Hairer, and G. Pavliotis. “Modulation equations: Stochastic bifurcation in large domains”. In: *Comm. Math. Phys.* 258 (2005), pp. 479–512.

[30] D. Blömker et al. “Numerical study of amplitude equations for SPDEs with degenerate forcing”. In: *Int. J. Comput. Math.* 89.18 (2012), pp. 2499–2516.

[31] A. Blumenthal, M. Engel, and A. Neamţu. “On the pitchfork bifurcation for the Chafee–Infante equation with additive noise”. In: *Probab. Theory Relat. Fields* 187.3 (2023), pp. 603–627.

[32] N. Boers. “Observation-based early-warning signals for a collapse of the Atlantic Meridional Overturning Circulation”. In: *Nat. Clim. Change* 11.8 (2021), pp. 680–688.

[33] N. Boers and M. Rypdal. “Critical slowing down suggests that the western Greenland Ice Sheet is close to a tipping point”. In: *Proc. Natl. Acad. Sci. U.S.A.* 118.21 (2021), e2024192118.

[34] C. Boettiger and R. Batt. “Bifurcation or state tipping: assessing transition type in a model trophic cascade”. In: *J. Math. Biol.* 80 (2020), pp. 143–155.

[35] A. Borovykh et al. “Privacy Risk for anisotropic Langevin dynamics using relative entropy bounds”. In: *arXiv preprint arXiv:2302.00766* (2023).

[36] A. Bowers and N. J. Kalton. *An introductory course in functional analysis*. New York, United States of America: Springer, 2014.

[37] A. J. Bray. “Theory of phase-ordering kinetics”. In: *Adv. Phys.* 51.2 (2002), pp. 481–587.

[38] M. Breden and C. Kuehn. “Rigorous validation of stochastic transition paths”. In: *J. Math. Pures Appl.* 131 (2019), pp. 88–129.

[39] T. Brett et al. “Detecting Critical Slowing down in High-Dimensional Epidemiological Systems”. In: *PLOS Comput. Biol.* 16.3 (2020), pp. 1–19. DOI: 10.1371/journal.pcbi.1007679.

[40] Z. Brzeźniak et al. “Itô’s formula in UMD Banach spaces and regularity of solutions of the Zakai equation”. In: *J. Differ. Equ.* 245.1 (2008), pp. 30–58.

[41] J. Burke and E. Knobloch. “Homoclinic snaking: structure and stability”. In: *Chaos* 17.3 (2007).

[42] J. Burke and E. Knobloch. “Snakes and ladders: localized states in the Swift–Hohenberg equation”. In: *Phys. Rev. A* 360.6 (2007), pp. 681–688.

[43] T. Caraballo, J. A. Langa, and J. C. Robinson. “Stability and random attractors for a reaction-diffusion equation with multiplicative noise”. In: *Discrete Contin. Dyn. Syst.* 6.4 (2000), p. 875.

[44] T. Caraballo et al. “The effect of noise on the Chafee-Infante equation: a nonlinear case study”. In: *Proc. Amer. Math. Soc.* 135.2 (2007), pp. 373–382.

[45] F. Cerou and A. Guyader. “Adaptive multilevel splitting for rare event analysis”. In: *Stochastic Anal. Appl.* 25.2 (2007), pp. 417–443. ISSN: 0736-2994. DOI: 10.1080/07362990601139628.

[46] F. Cérou, A. Guyader, and M. Rousset. “Adaptive multilevel splitting: Historical perspective and recent results”. In: *Chaos* 29.4 (Apr. 2019), p. 043108. ISSN: 1054-1500. DOI: 10.1063/1.5082247.

[47] S. Cerrai. *Second order PDE's in finite and infinite dimension: a probabilistic approach*. Springer, 2001.

[48] P. Cessi. “A simple box model of stochastically forced thermohaline flow”. In: *J. Phys. Oceanogr.* 24.9 (1994), pp. 1911–1920.

[49] P. Cessi and W. R. Young. “Multiple equilibria in two-dimensional thermohaline circulation”. In: *J. Fluid Mech.* 241 (1992), pp. 291–309.

[50] N. Chafee and E. F. Infante. “A bifurcation problem for a nonlinear partial differential equation of parabolic type”. In: *Appl. Anal.* 4.1 (1974), pp. 17–37.

[51] R. R. Chapman, P. Ashwin, and R. A. Wood. “Quantifying tipping behavior: Geometric early warnings and quasipotentials for a box model of AMOC”. In: *Chaos* 35.2 (2025).

[52] D. Chua and Y. M. Goh. “Poisson model of construction incident occurrence”. In: *J. Constr. Eng. Manag.* 131.6 (2005), pp. 715–722.

[53] I. Chueshov and P.-A. Vuillermot. “Non-random invariant sets for some systems of parabolic stochastic partial differential equations”. In: *Stoch. Anal. Appl.* 22.6 (2004), pp. 1421–1486.

[54] I. D. Chueshov and M. Scheutzow. “Inertial manifolds and forms for stochastically perturbed retarded semilinear parabolic equations”. In: *J. Dyn. Differ. Equ.* 13.2 (2001), pp. 355–380.

[55] F. Cordoni and L. D. Persio. “Optimal control for the stochastic FitzHugh-Nagumo model with recovery variable”. In: *Evolution Equations and Control Theory* 7.4 (2018), pp. 571–585. DOI: 10.3934/eect.2018027. URL: https://www.aimsciences.org/article/id/f54262f6-5f6e-4de5-9fb2-2cec29958334.

[56] F. Cordoni and L. D. Persio. “Optimal Control of the FitzHugh–Nagumo Stochastic Model with Nonlinear Diffusion”. In: *Appl. Math. Optim.* (2021), pp. 1–22.

[57] I. Corwin. “Exactly solving the KPZ equation”. In: *arXiv preprint arXiv:1804.05721* (2018).

[58] M. Costeniuc et al. “The Generalized Canonical Ensemble and Its Universal Equivalence with the Microcanonical Ensemble”. In: *J. Stat. Phys.* 119.5 (June 2005), pp. 1283–1329. ISSN: 1572-9613. DOI: 10.1007/s10955-005-4407-0.

[59] E. Cotilla-Sanchez, P. D. Hines, and C. M. Danforth. “Predicting critical transitions from time series synchrophasor data”. In: *IEEE Trans. Smart grid* 3.4 (2012), pp. 1832–1840. DOI: 10.1109/TSG.2012.2213848.

[60] M. G. Crandall and P. H. Rabinowitz. “Bifurcation from simple eigenvalues”. In: *J. Funct. Anal.* 8.2 (1971), pp. 321–340.

[61] H. Crauel. “White noise eliminates instability”. In: *Arch. Math.* 75.6 (2000), pp. 472–480.

[62] M. Crichton. *Jurassic park: A novel*. Vol. 1. Ballantine Books, 2012.

[63] G. Da Prato. “Evolution equations with white-noise boundary conditions”. In: *Stochastics* 42.3-4 (1993), pp. 167–182.

[64] G. Da Prato. *Kolmogorov equations for stochastic PDEs*. Springer Science & Business Media, 2004.

[65] G. Da Prato and J. Zabczyk. *Stochastic equations in infinite dimensions*. Cambridge university press, 2014.

[66] G. Da Prato, J. Zabczyk, and J. Zabczyk. *Ergodicity for infinite dimensional systems*. Vol. 229. Cambridge University Press, 1996.

[67] G. Da Prato et al. *Functional analytic methods for evolution equations*. Springer Science & Business Media, 2004.

[68] A. Debussche. “Hausdorff dimension of a random invariant set”. In: *J. Math. Pures Appl.* 77.10 (1998), pp. 967–988.

[69] A. Debussche, M. Högele, and P. Imkeller. *The dynamics of nonlinear reaction-diffusion equations with small Lévy noise*. Vol. 2085. Springer, 2013.

[70] P. Deift and R. Killip. “On the Absolutely Continuous Spectrum of One-Dimensional Schrödinger Operators with Square Summable Potentials”. In: *Comm. Math. Phys.* 203 (1999), pp. 341–347.

[71] H. A. Dijkstra. “On the structure of cellular solutions in Rayleigh–Bénard–Marangoni flows in small-aspect-ratio containers”. In: *J. Fluid Mech.* 243 (1992), pp. 73–102.

[72] H. A. Dijkstra and M. J. Molemaker. “Symmetry breaking and overturning oscillations in thermohaline-driven flows”. In: *J. Fluid Mech.* 331 (1997), pp. 169–198.

[73] P. Ditlevsen and S. Johnsen. “Tipping points: early warning and wishful thinking”. In: *Geophys. Res. Lett.* 37 (2010), p. 19703.

[74] P. Ditlevsen and S. Ditlevsen. “Warning of a forthcoming collapse of the Atlantic meridional overturning circulation”. In: *Nat. Commun.* 14.1 (2023), pp. 1–12.

[75] Z. Dong and X.-h. Peng. “Ergodicity of the 2D Navier-Stokes equations with degenerate multiplicative noise”. In: *Acta Math. Appl. Sin.* 34.1 (2018), pp. 97–118.

[76] T. A. Driscoll, N. Hale, and L. N. Trefethen. *Chebfun guide*. Pafnuty Publications, Oxford, 2014.

[77] W. E, W. Ren, and E. Vanden-Eijnden. “Minimum action method for the study of rare events”. In: *Commun. Pure Appl. Math.* 57.5 (May 2004), pp. 637–656. ISSN: 1097-0312. DOI: 10.1002/cpa.20005.

[78] D. E. Edmunds and W. D. Evans. *Elliptic differential operators and spectral analysis*. Springer, 2018.

[79] K. Eichinger, M. V. Gnann, and C. Kuehn. “Multiscale analysis for traveling-pulse solutions to the stochastic FitzHugh–Nagumo equations”. In: *Ann. Appl. Probab.* 32.5 (2022), pp. 3229–3282.

[80] B. Ermentrout and D. H. Terman. *Mathematical foundations of neuroscience*. Vol. 35. Springer, 2010.

[81] L. C. Evans. *Partial differential equations*. Vol. 19. American Mathematical Society, 1997.

[82] W. G. Faris and G. Jona-Lasinio. “Large fluctuations for a nonlinear heat equation with noise”. In: *J. Phys. A Math. Theor.* 15.10 (1982), p. 3025.

[83] N. Fenichel. “Geometric singular perturbation theory for ordinary differential equations”. In: *J. Differ. Equ.* 31.1 (1979), pp. 53–98.

[84] F. Flandoli and U. Pappalettera. “2D Euler equations with Stratonovich transport noise as a large-scale stochastic model reduction”. In: *J. Nonlinear Sci.* 31.1 (2021), p. 24.

[85] N. P. Foukal and L. Chafik. “Consensus around a common definition of Atlantic overturning will promote progress”. In: *Oceanography* 37.3 (2024), pp. 10–15.

[86] M. I. Freidlin and A. D. Wentzell. *Random Perturbations of Dynamical Systems*. Springer, 1998.

[87] A. Frishman and T. Grafke. "Mechanism for turbulence proliferation in subcritical flows". In: *Proc. R. Soc. A* 478.2265 (Sept. 2022), p. 20220218. DOI: 10.1098/rspa.2022.0218.

[88] C. W. Gardiner. "Handbook of stochastic methods for physics, chemistry and the natural sciences". In: *Springer series in synergetics* (1985).

[89] P. Gates and H. Tong. "On Markov chain modeling to some weather data". In: *J. Appl. Meteorol. Climatol.* 15.11 (1976), pp. 1145–1151.

[90] M. Gnann, C. Kuehn, and A. Pein. "Towards sample path estimates for fast-slow SPDEs". In: *Euro. J. Appl. Math.* 30.5 (2019), pp. 1004–1024.

[91] S. Gomé, L. S. Tuckerman, and D. Barkley. "Extreme events in transitional turbulence". In: *Philos. Trans. R. Soc. A* 380.2226 (2022), p. 20210036.

[92] S. Gomé et al. "Phase Transition to Turbulence via Moving Fronts". In: *Phys. Rev. Lett.* 132.26 (2024), p. 264002.

[93] K. Gowda and C. Kuehn. "Early-warning signs for pattern-formation in stochastic partial differential equations". In: *Commun. Nonlinear Sci. Numer. Simul.* 22.1-3 (2015), pp. 55–69.

[94] T. Grafke et al. "Arclength Parametrized Hamilton's Equations for the Calculation of Instantons". In: *Multiscale Model. Simul.* 12.2 (Jan. 2014), pp. 566–580. ISSN: 1540-3459. DOI: 10.1137/130939158.

[95] T. Grafke, T. Schäfer, and E. Vanden-Eijnden. "Long Term Effects of Small Random Perturbations on Dynamical Systems: Theoretical and Computational Tools". In: *Recent Progress and Modern Challenges in Applied Mathematics, Modeling and Computational Science*. Fields Institute Communications. Springer, New York, NY, 2017, pp. 17–55. ISBN: 978-1-4939-6968-5. DOI: 10.1007/978-1-4939-6969-2_2.

[96] T. Grafke and E. Vanden-Eijnden. "Numerical computation of rare events via large deviation theory". In: *Chaos* 29.6 (2019).

[97] J. Guckenheimer and P. Holmes. *Nonlinear oscillations, dynamical systems, and bifurcations of vector fields*. Vol. 42. Springer Science & Business Media, 2013.

[98] J. Guckenheimer and C. Kuehn. "Homoclinic orbits of the FitzHugh-Nagumo equation: The singular-limit". In: *SIAM Journal on Applied Dynamical Systems* 9.1 (2010), pp. 138–153. DOI: 10.1137/090758404. eprint: https://doi.org/10.1137/090758404. URL: https://doi.org/10.1137/090758404.

[99] M. Hairer. "Solving the KPZ equation". In: *Ann. Math.* (2013), pp. 559–664.

[100] B. C. Hall. *Quantum theory for mathematicians*. Springer, 2013.

[101] P. Hänggi and P. Jung. "Colored Noise in Dynamical Systems". In: *Advances in Chemical Physics*. John Wiley & Sons, Ltd, 1994. ISBN: 978-0-470-14148-9. DOI: 10.1002/9780470141489.ch4.

[102] P. Hänggi et al. "Can Colored Noise Improve Stochastic Resonance?" In: *J. Stat. Phys.* 70.1 (1993), pp. 25–47. DOI: 10.1007/BF01053952.

[103] A. Hariz et al. "Swift-Hohenberg equation with third-order dispersion for optical fiber resonators". In: *Phys. Rev. A* 100.2 (2019), p. 023816.

[104] K. Hasselman. "Stochastic climate model. Part I: Theory". In: *Tellus* 28 (1976), pp. 289–305.

[105] D. Henry. *Geometric theory of semilinear parabolic equations*. Vol. 840. Springer, 2006.

[106] E. Hernández-Garcia et al. "Noise and pattern selection in the one-dimensional Swift-Hohenberg equation". In: *Phys. D* 61.1-4 (1992), pp. 159–165.

[107] J. P. Hespanha et al. "Forecasting COVID-19 cases based on a parameter-varying stochastic SIR model". In: *Annu. rev. Control* 51 (2021), pp. 460–476.

[108] M. Heymann and E. Vanden-Eijnden. “Pathways of maximum likelihood for rare events in nonequilibrium systems: application to nucleation in the presence of shear”. In: *Phys. Rev. Lett.* 100.14 (2008), p. 140601.

[109] D. J. Higham. “An algorithmic introduction to numerical simulation of stochastic differential equations”. In: *SIAM rev.* 43.3 (2001), pp. 525–546. DOI: 10.1137/S0036144500378302.

[110] A. L. Hodgkin and A. F. Huxley. “A quantitative description of membrane current and its application to conduction and excitation in nerve”. In: *J. Physiol.* 117.4 (1952), p. 500.

[111] M. A. Högele. *Metastability of the Chafee-Infante Equation with small heavy-tailed Lévy Noise*. Humboldt-Universität zu Berlin, Mathematisch-Naturwissenschaftliche Fakultät II, 2011.

[112] P. Hohenberg and J. Swift. “Effects of additive noise at the onset of Rayleigh-Bénard convection”. In: *Phys. Rev. A* 46.8 (1992), p. 4773.

[113] D. D. Holm. “Stochastic Modelling in Fluid Dynamics: Itô vs Stratonovich”. In: *Proc. R. Soc. A.* 476.20190812 (2020).

[114] M. Hoshino, Y. Inahama, and N. Naganuma. “Stochastic complex Ginzburg-Landau equation with space-time white noise”. In: *Electron. J. Probab.* 22 (2017), pp. 1–68.

[115] F. Hummel, S. Jelbart, and C. Kuehn. “Geometric blow-up of a dynamic Turing instability in the Swift-Hohenberg equation”. In: *J. Differ. Equ.* 427 (2025), pp. 219–309.

[116] I. Idris. *Initiation of excitation waves*. The University of Liverpool (United Kingdom), 2008.

[117] A. Intissar and J.-K. Intissar. “Functional Analysis and Spectral Theory for Non-Selfadjoint Compact Operators with Applications to Gribov-Intissar’s Operators and other concrete operators & Exercises with detailed Solutions”. In: Jan. 2019, pp. 249–331.

[118] E. M. Izhikevich. *Dynamical systems in neuroscience*. MIT press, 2007.

[119] V. Jacques-Dumas, R. M. van Westen, and H. A. Dijkstra. “Estimation of AMOC Transition Probabilities Using a Machine Learning–Based Rare-Event Algorithm”. In: *Artif. Intell. Earth Syst.* 3.4 (2024), e240002.

[120] V. Jacques-Dumas et al. “Data-driven methods to estimate the committor function in conceptual ocean models”. In: *Nonlinear Process. Geophys.* 30.2 (2023), pp. 195–216.

[121] A. James, M. J. Plank, and A. M. Edwards. “Assessing Lévy walks as models of animal foraging”. In: *J. R. Soc. Interface* 8.62 (2011), pp. 1233–1247.

[122] S. Jelbart and C. Kuehn. “A formal geometric blow-up method for pattern forming systems”. In: *Topics in Multiple Time Scale Dynamics*. Vol. 806. American Mathematical Society, 2024, pp. 49–86.

[123] H.-C. Kao, C. Beaume, and E. Knobloch. “Spatial localization in heterogeneous systems”. In: *Phys. Rev. E* 89.1 (2014), p. 012903.

[124] J. Kelkel and C. Surulescu. “On a stochastic reaction–diffusion system modeling pattern formation on seashells”. In: *J. Math. Biol.* 60 (2010), pp. 765–796.

[125] R. Z. Khas’minskii. “Ergodic properties of recurrent diffusion processes and stabilization of the solution to the Cauchy problem for parabolic equations”. In: *Theory Probab. Appl.* 5.2 (1960), pp. 179–196.

[126] Y. Khoo, J. Lu, and L. Ying. “Solving for high-dimensional committor functions using artificial neural networks”. In: *Res. Math. Sci.* 6 (2019), pp. 1–13.

[127] E. Korotyaev and N. Saburova. “On continuous spectrum of magnetic Schrödinger operators on periodic discrete graphs”. In: *arXiv preprint arXiv:2101.05571* (2021).

[128] K. Koss et al. “Fractal Brownian Motion of Colloidal Particles in Plasma”. In: *Plasma Phys. Rep.* 49.1 (2023), pp. 57–64.

[129] L. Kramer and W. Pesch. “Convection instabilities in nematic liquid crystals”. In: *Annu. Rev. Fluid Mech.* 27.1 (1995), pp. 515–539.

[130] C. Kuehn. “Scaling of saddle-node bifurcations: degeneracies and rapid quantitative changes”. In: *J. Phys. A* 42.4 (2008), pp. 9–17. DOI: 10.1088/1751-8113/42/4/045101.

[131] C. Kuehn. *Multiple time scale dynamics*. Vol. 191. Springer, 2015.

[132] C. Kuehn. “Numerical Continuation and SPDE Stability for the 2D Cubic-Quintic Allen–Cahn Equation”. In: *SIAM-ASA J. Uncertain. Quantif.* 3.1 (2015), pp. 762–789.

[133] C. Kuehn. *PDE Dynamics: An Introduction*. Vol. 23. SIAM, 2019.

[134] C. Kuehn, K. Lux, and A. Neamţu. “Warning Signs for Non-Markovian Bifurcations: Colour Blindness and Scaling Laws”. In: *Proc. R. Soc. A: Math. Phys. Eng. Sci.* 478.2259 (2022). DOI: 10.1098/rspa.2021.0740.

[135] C. Kuehn and F. Romano. “Scaling laws and warning signs for bifurcations of SPDEs”. In: *European J. Appl. Math.* 30.5 (2019), pp. 853–868.

[136] L. D. Landau and E. M. Lifshitz. *Fluid Mechanics: Volume 6*. Vol. 6. Elsevier, 1987.

[137] I. Lasiecka. “Unified theory for abstract parabolic boundary problems—a semigroup approach”. In: *Appl. Math. Optim.* 6.1 (1980), pp. 287–333.

[138] J. Lega, J. Moloney, and A. Newell. “Swift-Hohenberg equation for lasers”. In: *Phys. Rev. Lett.* 73.22 (1994), p. 2978.

[139] J. Lega, J. Moloney, and A. Newell. “Universal description of laser dynamics near threshold”. In: *Phys. D* 83.4 (1995), pp. 478–498.

[140] T. M. Lenton. “Early warning of climate tipping points”. In: *Nat. Clim. Change* 1.4 (2011), pp. 201–209.

[141] T. Lenton et al. “Early warning of climate tipping points from critical slowing down: comparing methods to improve robustness”. In: *Phil. Trans. R. Soc. A* 370.1962 (2012), pp. 1185–1204.

[142] T. Lestang et al. “Computing return times or return periods with rare event algorithms”. In: *J. Stat. Mech.: Theory Exp.* 2018.4 (2018), p. 043213.

[143] Z. Liu, P. Gu, and T. L. Delworth. “Strong Red Noise Ocean Forcing on Atlantic Multidecadal Variability Assessed from Surface Heat Flux: Theory and Application”. In: *J. Clim.* 36.1 (2023), pp. 55–80. DOI: 10.1175/JCLI-D-22-0063.1.

[144] G. J. Lord, C. E. Powell, and T. Shardlow. *An introduction to computational stochastic PDEs*. Vol. 50. Cambridge University Press, 2014.

[145] E. N. Lorenz. “Deterministic Nonperiodic Flow 1”. In: *Universality in Chaos, 2nd edition*. Routledge, 2017, pp. 367–378.

[146] A. Lunardi. *Interpolation theory*. Vol. 16. Springer, 2018.

[147] Q. Luo, Y. Gong, and C. Jia. “Stability of gene regulatory networks with Lévy noise”. In: *Sci. China Inf. Sci* 60 (2017), pp. 1–13.

[148] H. M’F et al. “Pattern selection in the generalized Swift-Hohenberg model”. In: *Phys. Rev. E* 51.3 (1995), p. 2046.

[149] O. Malcai et al. “Theoretical analysis and simulations of the generalized Lotka-Volterra model”. In: *Phy. Rev. E* 66.3 (2002), p. 031102.

[150] R. R. Marathe and S. M. Ryan. “On the validity of the geometric Brownian motion assumption”. In: *Eng. Econ.* 50.2 (2005), pp. 159–192.

[151] *MATLAB version 9.12.0.1884302 (R2022a)*. The Mathworks, Inc. Natick, Massachusetts, 2021.

[152] P. E. McSharry, L. A. Smith, and L. Tarassenko. “Prediction of epileptic seizures: are nonlinear methods relevant?” In: *Nat. Med.* 9.3 (2003), pp. 241–242. ISSN: 1546-170X. DOI: 10.1038/nm0303-241.

[153] O. Mehling, K. Bellomo, and J. von Hardenberg. “Centennial-scale variability of the Atlantic meridional overturning circulation in CMIP6 models shaped by Arctic–North Atlantic interactions and sea ice biases”. In: *Geophys. Res. Lett.* 51.20 (2024), e2024GL110791.

[154] C. Meisel and C. Kuehn. “Scaling Effects and Spatio-Temporal Multilevel Dynamics in Epileptic Seizures”. In: *PLoS One* 7.2 (2012), pp. 1–11. DOI: 10.1371/journal.pone.0030371.

[155] F. Mezzadri. “How to generate random matrices from the classical compact groups”. In: *arXiv preprint math-ph/0609050* (2006).

[156] D. Middleton. “On the detection of stochastic signals in additive normal noise–I”. In: *IEEE Trans. Inf. Theory* 3.2 (2003), pp. 86–121.

[157] M. S. Miguel and J. M. Sancho. “Multiplicative Ornstein Uhlenbeck Noise in Nonequilibrium Phenomena”. In: *Stochastic Nonlinear Systems in Physics, Chemistry, and Biology*. Ed. by L. Arnold and R. Lefever. Springer Berlin Heidelberg, 1981, pp. 137–150. ISBN: 978-3-642-68038-0. DOI: 10.1007/978-3-642-68038-0{_}13.

[158] M. Milošević and R. Geurts. “The Ginzburg-Landau theory in application”. In: *Phys. C* 470.19 (2010), pp. 791–795.

[159] F. Mormann et al. “Seizure prediction: the long and winding road”. In: *Brain* 130.2 (2006), pp. 314–333. ISSN: 0006-8950. DOI: 10.1093/brain/awl241.

[160] A. Morr and N. Boers. “Detection of approaching critical transitions in natural systems driven by red noise”. In: *Phys. Rev. X* 14.2 (2024), p. 021037.

[161] A. Morr, D. Kreher, and N. Boers. “Red noise in continuous-time stochastic modelling”. In: *R. Soc. Open Sci.* 12.8 (2025), p. 250573.

[162] C. Mueller. “Long time existence for the heat equation with a noise term”. In: *Probab. Theory Relat. Fields* 90 (1991), pp. 505–517.

[163] C. Mueller. “The critical parameter for the heat equation with a noise term to blow up in finite time”. In: *Ann. Probab.* 28.4 (2000), pp. 1735–1746.

[164] C. Mueller and R. Sowers. “Blowup for the heat equation with a noise term”. In: *Probab. Theory Relat. Fields* 97.3 (1993), pp. 287–320.

[165] M. A. Munoz. “Multiplicative noise in non-equilibrium phase transitions: A tutorial”. In: *arXiv preprint cond-mat/0303650* (2003).

[166] M. Newman, P. D. Sardeshmukh, and C. Penland. “Stochastic Forcing of the Wintertime Extratropical Flow”. In: *J. Atmos. Sci.* 54.3 (1997), pp. 435–455. DOI: 10.1175/1520-0469(1997)054<0435:SFOTWE>2.0.CO;2.

[167] J. Nocedal and S. J. Wright. *Numerical optimization*. Springer, 1999.

[168] E. O’Sullivan, K. Mulchrone, and S. Wieczorek. “Rate-induced tipping to metastable zombie fires”. In: *Proc. R. Soc. Lond.A* 479.2275 (2023), p. 20220647.

[169] R.-E. Plessix. “A review of the adjoint-state method for computing the gradient of a functional with geophysical applications”. In: *Geophys. J. Int.* 167.2 (2006), pp. 495–503.

[170] Y. Pomeau and P. Manneville. “Wavelength selection in cellular flows”. In: *Phys. Lett. A* 75.4 (1980), pp. 296–298.

[171] Y. Pomeau. “Front motion, metastability and subcritical bifurcations in hydrodynamics”. In: *Phys. D: Nonlinear Phenom.* 23.1-3 (1986), pp. 3–11.

[172] Y. Pomeau. “The transition to turbulence in parallel flows: a personal view”. In: *C. R. Méc* 343.3 (2015), pp. 210–218.

[173] J. Poschel. *Inverse spectral theory*. Academic Press, 1987.

[174] D. Revuz and M. Yor. *Continuous martingales and Brownian motion*. Vol. 293. Springer Science & Business Media, 2013.

[175] S. Rinaldi and S. Muratori. “Slow-fast limit cycles in predator-prey models”. In: *Ecol. Model.* 61.3-4 (1992), pp. 287–308.

[176] J. Rolland, F. Bouchet, and E. Simonnet. “Computing transition rates for the 1-D stochastic Ginzburg–Landau–Allen–Cahn equation for finite-amplitude noise with a rare event algorithm”. In: *J. Stat. Phys.* 162 (2016), pp. 277–311.

[177] M. Salins. “Solutions to the stochastic heat equation with polynomially growing multiplicative noise do not explode in the critical regime”. In: *arXiv preprint arXiv:2309.04330* (2023).

[178] B. Sandstede. “Stability of multiple-pulse solutions”. In: *Trans. Am. Math. Soc.* 350.2 (1998), pp. 429–472.

[179] P. Sardeshmukh, C. Penland, and M. Newman. “Drifts induced by multiplicative red noise with application to climate”. In: *EPL* 63.4 (2003), p. 498.

[180] M. Scheffer et al. “Catastrophic shifts in ecosystems”. In: *Nature* 413.6856 (2001), pp. 591–596. DOI: 10.1038/35098000.

[181] E. Simonnet. “Computing non-equilibrium trajectories by a deep learning approach”. In: *J. Comput. Phys.* 491 (Oct. 2023), p. 112349. ISSN: 0021-9991. DOI: 10.1016/j.jcp.2023.112349.

[182] K. Slyman and C. K. Jones. “Rate and noise-induced tipping working in concert”. In: *Chaos* 33.1 (2023).

[183] J. Soons, T. Grafke, and H. A. Dijkstra. “Optimal transition paths for amoc collapse and recovery in a stochastic box model”. In: *J. Phys. Oceanogr.* 54.12 (2024), pp. 2537–2552.

[184] J. Soons, T. Grafke, and H. A. Dijkstra. “Most likely noise-induced tipping of the overturning circulation in a two-dimensional Boussinesq fluid model”. In: *J. Fluid Mech.* 1009 (2025), A53. DOI: 10.1017/jfm.2025.248.

[185] S. Spielberg et al. *Jurassic park*. A. Mondadori, 1993.

[186] J. M. Steele. “Kingman’s subadditive ergodic theorem”. In: *Annales de l’IHP Probabilités et statistiques*. Vol. 25. 1. 1989, pp. 93–98.

[187] H. Stommel. “Thermohaline convection with two stable regimes of flow”. In: *Tellus* 13.2 (1961), pp. 224–230.

[188] J. Swift and P. C. Hohenberg. “Hydrodynamic fluctuations at the convective instability”. In: *Phys. Rev. A* 15.1 (1977), p. 319.

[189] A. N. Tikhonov. “Systems of differential equations containing small parameters in the derivatives”. In: *Mat. Sb.* 73.3 (1952), pp. 575–586.

[190] H. C. Tuckwell. “Random perturbations of the reduced Fitzhugh-Nagumo equation”. In: *Phys. Scr.* 46.6 (1992), p. 481.

[191] K. Twardowska. “An approximation theorem of Wong-Zakai type for nonlinear stochastic partial differential equations”. In: *Stoch. Anal. Appl.* 13.5 (1995), pp. 601–626.

[192] K. Twardowska and A. Nowak. “On the relation between the Itô and Stratonovich integrals in Hilbert spaces”. In: *Ann. Math. Sil.* Vol. 18. 2004, pp. 49–63.

[193] H. Uecker. *Numerical continuation and bifurcation in Nonlinear PDEs*. SIAM, 2021.

[194] E. Vanden-Eijnden and M. Heymann. “The geometric minimum action method for computing minimum energy paths”. In: *Jour. Chem. Phys.* 128 (2008), p. 061103.

[195] A. Veldman and K. Rinzema. “Playing with nonuniform grids”. In: *J. Engrg. Math.* 26.1 (1992), pp. 119–130.

[196] J. B. Walsh. “An introduction to stochastic partial differential equations”. In: *Lect. Notes Math.* (1986), pp. 265–439.

[197] B. Wang. “Random attractors for the stochastic FitzHugh–Nagumo system on unbounded domains”. In: *Nonlinear Anal. Theory Methods Appl.* 71.7-8 (2009), pp. 2811–2828.

[198] H. Wang, Y. Yu, and G. Wen. “Dynamical Analysis of the Lorenz-84 Atmospheric Circulation Model”. In: *J. Appl. Math.* 2014.1 (2014), p. 296279.

[199] P. Wang, D. Castellana, and H. A. Dijkstra. “Improvements to the use of the Trajectory-Adaptive Multilevel Sampling algorithm for the study of rare events”. In: *Nonlinear Process. Geophys.* 28.1 (2021), pp. 135–151.

[200] J. Wei and M. Winter. *Mathematical aspects of pattern formation in biological systems*. Vol. 189. Springer Science & Business Media, 2013.

[201] H. H. Weiss. “The SIR model and the foundations of public health”. In: *Materials matematics* (2013), pp. 0001–17.

[202] R. M. van Westen, M. Kliphuis, and H. A. Dijkstra. “Physics-based early warning signal shows that AMOC is on tipping course”. In: *Sci. Adv.* 10.6 (2024), eadk1189.

[203] S. Wieczorek, C. Xie, and P. Ashwin. “Rate-induced tipping: Thresholds, edge states and connecting orbits”. In: *Nonlinearity* 36.6 (2023), p. 3238.

[204] A. Winfree. “Heart muscle as a reaction–diffusion medium: The roles of electric potential diffusion, activation front curvature, and anisotropy”. In: *Int. J. Bifurc. Chaos Appl. Sci. Eng.* 7.03 (1997), pp. 487–526.

[205] M. Winter et al. “The dynamics of the stochastic shadow Gierer–Meinhardt system”. In: *J. Differ. Equ.* 260.1 (2016), pp. 84–114.

[206] R. Wu et al. “Turing and Hopf bifurcation of Gierer-Meinhardt activator-substrate model”. In: (2017).

[207] N. Wunderling et al. “Climate tipping point interactions and cascades: A review”. In: *Earth Syst. Dyn.* 15.1 (2024), pp. 41–74.

[208] H.-w. Xi, J. D. Gunton, and J. Viñals. “Spiral-pattern formation in Rayleigh-Bénard convection”. In: *Phys. Rev. E* 47 (5 May 1993), R2987–R2990. DOI: 10.1103/PhysRevE.47.R2987. URL: https://link.aps.org/doi/10.1103/PhysRevE.47.R2987.

[209] G. Xu, G. Lin, and J. Liu. “Rare-Event Simulation for the Stochastic Korteweg–de Vries Equation”. In: *SIAM/ASA J. Uncertain. Quantificat.* 2.1 (2014), pp. 698–716.

[210] R. Zakine and E. Vanden-Eijnden. “Minimum-Action Method for Nonequilibrium Phase Transitions”. In: *Phys. Rev. X* 13.4 (Dec. 2023), p. 041044. ISSN: 2160-3308. DOI: 10.1103/PhysRevX.13.041044.

[211] L. Zhang. “The completeness of generalized eigenfunctions of a discrete operator”. In: *J. Math. Anal. Appl.* 261.1 (2001), pp. 241–253.

[212] X. Zhou, W. Ren, and W. E. “Adaptive minimum action method for the study of rare events”. In: *J. Chem. Phys.* 128 (2008), p. 104111.

[213] C. Zimmerman et al. “Slowed response of Atlantic meridional overturning circulation not a robust signal of collapse”. In: *Geophys. Res. Lett.* 52.2 (2025), e2024GL112415.

Appendices

The following appendices are extracted from publications by the author. In detail, Appendix A, Appendix B and Appendix C result from [23]. Among them, Appendix A provides an asymptotic spectral comparison between the Laplacian and a family of Schrödinger operators, addressing the synchronisation of their eigenfunctions in an L^∞-norm and Appendix B includes a lemma for the $\mathcal{W}^{1,2}$-continuity of the solution of a space-heterogeneous SPDE. Moreover, Appendix D and Appendix E include the proofs of Theorem 4.2.5 and Theorem 4.2.7, respectively. Such theorems employ Appendix F, which describes a scaling law in Chapter 4 and [21]. Lastly, Appendix G illustrates the SPDEs discussed in Chapter 9 and [24] in Itô sense.

A Appendix: Properties of the Schrödinger operator

The Schrödinger operator $A := \Delta - g$ inherits important properties from the Laplacian operator under the assumption of Dirichlet boundary conditions and $g \in L^\infty(\mathcal{X}_1)$ almost-everywhere positive. Firstly, the system

$$\begin{cases} Au = -w \\ u(\cdot,t)|_{\mathcal{X}_0} = 0, \quad \forall t \geq 0 \end{cases} \tag{A.1}$$

admits unique weak solutions in $\mathcal{W}^{1,2}(\mathcal{X}_1)$ for any $w \in \mathcal{H}_1$. In fact, they satisfy

$$\langle (-A)u, v\rangle = \langle \nabla u, \nabla v\rangle + \langle u, gv\rangle = \langle w, v\rangle, \quad \forall v \in \mathcal{W}^{1,2}(\mathcal{X}_1).$$

From the Poincaré Inequality, there exist $c, c' > 0$ so that

$$\begin{aligned} ||v||^2_{\mathcal{W}^{1,2}(\mathcal{X}_1)} = -\langle v, \Delta v\rangle \leq -\langle v, \Delta v\rangle + \langle v, gv\rangle = -\langle v, Av\rangle =: ||v||_A \\ \leq ||v||^2_{\mathcal{W}^{1,2}(\mathcal{X}_1)} + ||g||_\infty ||v||^2_{\mathcal{W}^{1,2}(\mathcal{X}_1)} \leq c\Big(||v||^2_{\mathcal{W}^{1,2}(\mathcal{X}_1)} + ||v||^2_{\mathcal{W}^{1,2}(\mathcal{X}_1)}\Big) \leq c'||v||_{\mathcal{W}^{1,2}(\mathcal{X}_1)} \end{aligned}$$

for any $v \in \mathcal{W}^{1,2}(\mathcal{X}_1)$. Therefore, the spaces $\mathcal{W}^{1,2}(\mathcal{X}_1) = \mathcal{D}((-\Delta)^{\frac{1}{2}})$ and $\mathcal{D}((-A)^{\frac{1}{2}})$ are the same in the sense that the norms on which they are defined are equivalent.
The existence and uniqueness of the weak solutions of (A.1) are implied by the fact that the map

$$v \mapsto \langle w, v\rangle = \langle (-A)u, v\rangle$$

is continuous in $\mathcal{W}^{1,2}(\mathcal{X}_1)$ with norm $||\cdot||_A$:

$$|\langle w, v\rangle| \leq ||w||\ ||v|| \leq c||w||\ ||v||_{\mathcal{W}^{1,2}(\mathcal{X}_1)} \leq c||w||\ ||v||_A, \tag{A.2}$$

for a constant $c > 0$. We can then use Riesz Theorem [36] to assert that there exists a unique $u \in \mathcal{W}^{1,2}(\mathcal{X}_1)$ that satisfies

$$\langle \nabla u, \nabla v\rangle + \langle u, gv\rangle = \langle w, v\rangle$$

for any $v \in \mathcal{W}^{1,2}(\mathcal{X}_1)$. Defining the inverse of $-A$, the operator $(-A)^{-1} : \mathcal{H}_1 \to \mathcal{W}^{1,2}(\mathcal{X}_1)$, we have shown that the system (A.1) admits an unique solution $(-A)^{-1}w = u \in \mathcal{W}^{1,2}(\mathcal{X}_1)$ for any $w \in \mathcal{H}_1$. From the Rellich-Kondrachov Theorem [81] and the fact that $(-A)^{-1} : \mathcal{H}_1 \to \mathcal{H}_1$ is a self-adjoint compact operator, its eigenfunctions form a basis in $\mathcal{H}_1$. Moreover, since $(-A)^{-1}$ is the inverse of A, they share the same

eigenfunctions $\{e_k\}_{k\in\mathbb{N}_{>0}}$. We label as e_k the eigenfunction of $(-A)^{-1}$ corresponding to the eigenvalue η_k for any $k \in \mathbb{N}_{>0}$ and we set $\{\eta_k\}_{k\in\mathbb{N}_{>0}}$ to be a decreasing sequence. From

$$\langle \nabla(-A)^{-1}w, \nabla v\rangle + \langle (-A)^{-1}w, gv\rangle = \langle w, v\rangle,$$

by taking $v, w = e_k \in \mathcal{W}^{1,2}(\mathcal{X}_1)$ for any $k \in \mathbb{N}_{>0}$ we obtain

$$\eta_k\Big(\langle \nabla e_k, \nabla e_k\rangle + \langle e_k, g\, e_k\rangle\Big) = \langle e_k, e_k\rangle$$

and, therefore, η_k is strictly positive. By construction, we have proven that the eigenvalues of A, the family $\{\lambda_k\}_{k\in\mathbb{N}_{>0}}$, are strictly negative.

An in-depth description of the asymptotic behaviour of the eigenfunctions and eigenvalues of A can be found in [173, Theorem 2.4]. In order to address it, we consider $\left\{\lambda'_k, e'_k\right\}_{k\in\mathbb{N}_{>0}}$ that define the spectral decomposition of Δ as described in Chapter 3. Then, the rate

$$\left|\lambda_k - \lambda'_k + \int_0^L g(x)\mathsf{d}x\right|^2 + \left|\left|e_k - e'_k\right|\right|_\infty + \frac{1}{k}\left|\left|\frac{\mathsf{d}}{\mathsf{d}x}e_k - \frac{\mathsf{d}}{\mathsf{d}x}e'_k\right|\right|_\infty = \mathcal{O}\Big(\frac{1}{k}\Big) \tag{A.3}$$

indicates that, for high indexes k, the influence of the heterogeneity on space induced by g on the respective modes becomes less relevant and A behaves similarly to $\Delta - \int_0^L g(x)\mathsf{d}x$ along such directions.

Lastly, another important property of A is $\lambda_k < \lambda_{k+1}$ for $k \in \mathbb{N}_{>0}$, i.e., the eigenvalues are simple ([173, Theorem 2.2]).

B Appendix: Operator theory

In the current appendix, we consider methods and results by [65] and definitions from [78]. Our goal is to show the continuity in $\mathcal{W}^{1,2}(\mathcal{X}_1)$ of the mild solution of (3.0.1). It addresses the assumption of synchronisation of the spectrum of the linear drift operator with the covariance operator. Such a case provides a generalisation to the systems perturbed by additive noise in [65, Chapter 5].

We note that the Schrödinger operator $A = \Delta - g$ generates by the Hille-Yosida Theorem 2.1.2 a $\mathcal{C}_0$-semigroup on $\mathcal{H}_1$. Such a property is employed in the following lemma, which is a generalisation of [65, Lemma 5.19].

Lemma B.1. *Set $d_0 \in \mathbb{N}_{>0}$ and $d_1 \in \mathbb{N}$. Assume that there exists $\{\rho^{j_2}_{j_1}\}_{j_1,j_2\in\mathbb{N}_{>0}} \subset [0,1]$, a dual indexed sequence, such that the eigenfunctions $\{b_j\}_{j\in\mathbb{N}_{>0}}$ and the eigenvalues $\{\zeta_j\}_{j\in\mathbb{N}_{>0}}$ of Q satisfy the following properties:*

(B1) *for all $0 < j_2 \le d_0$, $b_{j_2} = \sum\limits_{j_1\le d_0} \rho^{j_2}_{j_1} e'_{j_1}$;*

(B2) *for all $d_0 < j_2$, $b_{j_2} = \sum\limits_{\{|j_1-j_2|\le d_1, j_1>d_0\}} \rho^{j_2}_{j_1} e'_{j_1}$;*

(B3) *there exists $\gamma > 0$ for which $\sum\limits_{j=1}^{\infty} \zeta_j(-\lambda'_{j+d_1})^\gamma < +\infty$.*

Then, for

$$w_\Delta(x,t) := \sum_{k=1}^{\infty}\sqrt{\zeta_k}\sum_{n=1}^{\infty}\rho^k_n e'_n(x)\int_0^t e^{-\lambda'_n(t-t_1)}\mathsf{d}\beta_k(t_1), \tag{B.1}$$

for $t \ge 0$, $x \in [0,L]$ and $\{\beta_k\}_{k\in\mathbb{N}_{>0}}$ a family of independent Wiener processes, the following estimations hold: there exists $C_1 > 0$ such that

$$\mathbb{E}|\nabla(w_\Delta(x,t) - w_\Delta(x',t))|^2 \le C_1|x-x'|^2, \tag{B.2}$$

$$\mathbb{E}|\nabla(w_\Delta(x,t)-w_\Delta(x,t'))|^2 \le C_1|t-t'|^2, \tag{B.3}$$

for all $t,t' \ge 0$ *and for all* $x,x' \in [0,L]$.

Proof. For simplicity, we define $\{\lambda'_{-j}\}_{j\in\mathbb{N}}$ as $\lambda_{-j} := \lambda_1$ for any $j \in \mathbb{N}$. Before proving the well-posedness of $\nabla w_\Delta(\cdot,t)$ in $L^2(\Omega,\mathcal{F},\mathbb{P};\mathcal{H}_1)$ for any $t>0$, we introduce tools that are employed further in the proof. First is the existence of $C>0$ for which $|e'_k(x)| \le C$ and $|\nabla e'_k(x)| \le C\sqrt{-\lambda'_k}$ for all $x \in [0,L]$ and $k \in \mathbb{N}_{>0}$. Another useful tool is the fact that $\sum_{j=1}^{\infty}\zeta_j(-\lambda'_{j+d_1})^\gamma < +\infty$ implies, for monotonicity and order of divergence of λ'_k in respect to k, that $\sum\limits_{j=1}^{\infty}\zeta_j(-\lambda'_{j+d_1})^\epsilon < +\infty$ for any $\epsilon \le \gamma$.

We now prove that the outer series that defines $\nabla w_\Delta(\cdot,t)$ converges in $L^2(\Omega,\mathcal{F},\mathbb{P};\mathcal{H}_1)$ for any $t>0$. In order to achieve that, we use $0 \le \rho_{j_1}^{j_2} \le 1$ for all j_1, j_2 and Ito's isometry:

$$\begin{aligned}
&\mathbb{E}\left|\sum_{k=k_1}^{k_2}\sqrt{\zeta_k}\sum_{n=1}^{\infty}\rho_n^k\nabla e'_n(x)\int_0^t \mathsf{e}^{\lambda'_n(t-t_1)}\mathsf{d}\beta_k(t_1)\right|^2\\
\le& C^2\sum_{k=k_1}^{k_2}\zeta_k\sum_{n,m}|\rho_n^k\rho_m^k|\sqrt{-\lambda'_n}\sqrt{-\lambda'_m}\int_0^t \mathsf{e}^{(\lambda'_n+\lambda'_m)(t-t_1)}\mathsf{d}t_1\\
=& -C^2\sum_{k=k_1}^{k_2}\zeta_k\sum_{n,m}|\rho_n^k\rho_m^k|\frac{\sqrt{-\lambda'_n}\sqrt{-\lambda'_m}}{\lambda'_n+\lambda'_m}\\
\le& -C^2\left(\sum_{k=k_1}^{d_0}\zeta_k\sum_{n,m\le d_0}\frac{\sqrt{-\lambda'_n}\sqrt{-\lambda'_m}}{\lambda'_n+\lambda'_m}+\sum_{k=d_0+1}^{k_2}\zeta_k\sum_{|n-k|\le d_1,|m-k|\le d_1}\frac{\sqrt{-\lambda'_n}\sqrt{-\lambda'_m}}{\lambda'_n+\lambda'_m}\right)\\
\le& C^2\left(\sum_{k=k_1}^{d_0}\zeta_k d_0^2\frac{\lambda'_{d_0}}{2\lambda'_1}+\sum_{k=d_0+1}^{k_2}\zeta_k(2d_1+1)^2\frac{\lambda'_{k+d_1}}{2\lambda'_{k-d_1}}\right) \le \frac{C^2}{2\lambda'_1}\min_{j\in\{d_0,1+2d_1\}}\{\lambda'_j j^2\}\sum_{k=1}^{\infty}\zeta_k<\infty,
\end{aligned}$$

which holds for the definition of $\{\lambda'_j\}_j$. The proof for the estimate (B.2) is the following:

$$\begin{aligned}
&\mathbb{E}|\nabla(w_\Delta(x,t)-w_\Delta(x',t))|^2\\
\le&\sum_{k=1}^{\infty}\zeta_k\sum_{n,m}|\rho_n^k\rho_m^k|\sqrt{-\lambda'_n}\sqrt{-\lambda'_m}|e''_n(x)-e''_n(x')||e''_m(x)-e''_m(x')|\int_0^t \mathsf{e}^{(\lambda'_n+\lambda'_m)(t-t_1)}\mathsf{d}t_1,
\end{aligned}$$

by defining $e''_k(x) = \sqrt{\frac{2}{L}}\cos\left(\frac{\pi k}{L}x\right)$, for all $k \in \mathbb{N}_{>0}$ and $x \in \mathcal{X}_1$. Since $|\nabla e''_k(x)| \le C\sqrt{-\lambda'_k}$, we can obtain through Lagrange's theorem

$$|e''_k(x)-e''_k(x')| \le 2^{1-2\epsilon}C(-\lambda'_k)^\epsilon|x-x'|^{2\epsilon}, \tag{B.4}$$

for all $x,x' \in [0,L]$, $\epsilon \le \frac{1}{2}$ and $k \in \mathbb{N}_{>0}$. In particular, (B.4) holds for $\epsilon = \frac{\gamma}{4}$. Then,

$$\begin{aligned}
&\mathbb{E}|\nabla(w_\Delta(x,t)-w_\Delta(x',t))|^2 \le -2^{2-\gamma}C^2\sum_{k=1}^{\infty}\zeta_k\sum_{n,m}|\rho_n^k\rho_m^k|\frac{(-\lambda'_n)^{\frac{2+\gamma}{4}}(-\lambda'_m)^{\frac{2+\gamma}{4}}}{\lambda'_n+\lambda'_m}|x-x'|^\gamma\\
\le& -2^{2-\gamma}C^2\left(d_0^2\sum_{k=1}^{d_0}\zeta_k\frac{(-\lambda'_{d_0})^{1+\frac{\gamma}{2}}}{2\lambda'_1}+(1+2d_1)^2\sum_{k=d_0+1}^{\infty}\zeta_k\frac{(-\lambda'_{k+d_1})^{1+\frac{\gamma}{2}}}{2\lambda'_{k-d_1}}\right)|x-x'|^\gamma\\
\le& 2^{1-\gamma}\frac{C^2}{\lambda'_1}\min_{j\in\{d_0,1+2d_1\}}\{\lambda'_j j^2\}\left(\sum_{k=1}^{d_0}\zeta_k(-\lambda'_{d_0})^{\frac{\gamma}{2}}+\sum_{k=d_0+1}^{\infty}\zeta_k(-\lambda'_{k+d_1})^{\frac{\gamma}{2}}\right)|x-x'|^\gamma.
\end{aligned}$$

For $t > t' > 0$, the inequality (B.3) is the result of

$$\begin{aligned}
&\mathbb{E}|\nabla(w_\Delta(x,t) - w_\Delta(x,t'))|^2 \\
\leq& C^2 \sum_{k=1}^{\infty} \zeta_k \sum_{n,m} |\rho_n^k \rho_m^k| \sqrt{-\lambda'_n}\sqrt{-\lambda'_m} \Bigg(\int_{t'}^{t} \mathsf{e}^{(\lambda'_n+\lambda'_m)(t-t_1)} \mathsf{d}t_1 \\
&+ \int_0^{t'} |\mathsf{e}^{\lambda'_n(t-t_1)} - \mathsf{e}^{\lambda'_n(t'-t_1)}||\mathsf{e}^{\lambda'_m(t-t_1)} - \mathsf{e}^{\lambda'_m(t'-t_1)}| \mathsf{d}t_1 \Bigg).
\end{aligned}$$

The first term is controlled as follows:

$$\begin{aligned}
&C^2 \sum_{k=1}^{\infty} \zeta_k \sum_{n,m} |\rho_n^k \rho_m^k| \sqrt{-\lambda'_n}\sqrt{-\lambda'_m} \int_{t'}^{t} \mathsf{e}^{(\lambda'_n+\lambda'_m)(t-t_1)} \mathsf{d}t_1 \\
=& - C^2 \sum_{k=1}^{\infty} \zeta_k \sum_{n,m} |\rho_n^k \rho_m^k| \frac{\sqrt{-\lambda'_n}\sqrt{-\lambda'_m}}{\lambda'_n + \lambda'_m} \left(1 - \mathsf{e}^{(\lambda'_n+\lambda'_m)(t-t')}\right)
\end{aligned}$$

and, by the fact that for all $\epsilon \in [0,1]$ there exists a $c_\epsilon > 0$ that satisfies $|\mathsf{e}^{-t} - \mathsf{e}^{-t'}| \leq c_\epsilon |t-t'|^\epsilon$ for all $t, t' \geq 0$,

$$\begin{aligned}
&C^2 \sum_{k=1}^{\infty} \zeta_k \sum_{n,m} |\rho_n^k \rho_m^k| \sqrt{-\lambda'_n}\sqrt{-\lambda'_m} \int_{t'}^{t} \mathsf{e}^{(\lambda'_n+\lambda'_m)(t-t_1)} \mathsf{d}t_1 \\
&\leq c_\gamma C^2 \sum_{k=1}^{\infty} \zeta_k \sum_{n,m} |\rho_n^k \rho_m^k| \frac{\sqrt{-\lambda'_n}\sqrt{-\lambda'_m}}{(-\lambda'_n - \lambda'_m)^{1-\gamma}} |t-t'|^\gamma \\
&\leq c_\gamma \frac{C^2}{2\lambda'_1} \min_{j \in \{d_0, 1+2d_1\}} \{\lambda'_j\} \left(\sum_{k=1}^{d_0} \zeta_k \sum_{n,m \leq d_0} (-\lambda'_n - \lambda'_m)^\gamma + \sum_{k=d_0+1}^{\infty} \zeta_k \sum_{|n-k| \leq d_1, |m-k| \leq d_1} (-\lambda'_n - \lambda'_m)^\gamma \right) |t-t'|^\gamma \\
&\leq c_\gamma \frac{2^{\gamma-1} C^2}{\lambda'_1} \min_{j \in \{d_0, 1+2d_1\}} \{\lambda'_j j^2\} \left(\sum_{k=1}^{d_0} \zeta_k (-\lambda'_{d_0})^\gamma + \sum_{k=d_0+1}^{\infty} \zeta_k (-\lambda'_{k+d_1})^\gamma \right) |t-t'|^\gamma.
\end{aligned}$$

The second term is studied similarly:

$$\begin{aligned}
&C^2 \sum_{k=1}^{\infty} \zeta_k \sum_{n,m} |\rho_n^k \rho_m^k| \sqrt{-\lambda'_n}\sqrt{-\lambda'_m} \int_0^{t'} \left(\mathsf{e}^{\lambda'_n(t-t_1)} - \mathsf{e}^{\lambda'_n(t'-t_1)}\right)\left(\mathsf{e}^{\lambda'_m(t-t_1)} - \mathsf{e}^{\lambda'_m(t'-t_1)}\right) \mathsf{d}t_1 \\
\leq& C^2 \sum_{k=1}^{\infty} \zeta_k \sum_{n,m} |\rho_n^k \rho_m^k| \sqrt{-\lambda'_n}\sqrt{-\lambda'_m} \\
&\times \int_0^{t'} \Big(\mathsf{e}^{\lambda'_n(t-t_1) - \lambda'_m(t-t_1)} - \mathsf{e}^{\lambda'_n(t'-t_1) + \lambda'_m(t-t_1)} \\
&- \mathsf{e}^{\lambda'_n(t-t_1) + \lambda'_m(t'-t_1)} + \mathsf{e}^{\lambda'_n(t'-t_1) + \lambda'_m(t'-t_1)} \Big) \mathsf{d}t_1 \\
=& - C^2 \sum_{k=1}^{\infty} \zeta_k \sum_{n,m} |\rho_n^k \rho_m^k| \frac{\sqrt{-\lambda'_n}\sqrt{-\lambda'_m}}{\lambda'_n + \lambda'_m} \\
&\times \Big(\mathsf{e}^{\lambda'_n t - \lambda'_n t' + \lambda'_m t - \lambda'_m t'} - \mathsf{e}^{\lambda'_n t + \lambda'_m t} - \mathsf{e}^{\lambda'_m t - \lambda'_m t'} + \mathsf{e}^{\lambda'_n t' + \lambda'_m t} \\
&- \mathsf{e}^{\lambda'_n t - \lambda'_n t'} + \mathsf{e}^{\lambda'_n t + \lambda'_m t'} + 1 - \mathsf{e}^{-\lambda'_n t' - \lambda'_m t'} \Big)
\end{aligned}$$

$$
\begin{aligned}
&\leq - C^2 \sum_{k=1}^{\infty} \zeta_k \sum_{n,m} |\rho_n^k \rho_m^k| \frac{\sqrt{-\lambda'_n}\sqrt{-\lambda'_m}}{\lambda'_n + \lambda'_m} \\
&\quad \times \Big(|\mathsf{e}^{\lambda'_n t - \lambda'_n t' + \lambda'_m t - \lambda'_m t'} - \mathsf{e}^{\lambda'_m t - \lambda'_m t'}| + |1 - \mathsf{e}^{\lambda'_n t - \lambda'_n t'}| \\
&\quad + |\mathsf{e}^{\lambda'_n t + \lambda'_m t'} - \mathsf{e}^{\lambda'_n t + \lambda'_m t}| + |\mathsf{e}^{\lambda'_n t' + \lambda'_m t} - \mathsf{e}^{\lambda'_n t' + \lambda'_m t'}| \Big) \\
&\leq - 2C^2 c_\gamma |t - t'|^\gamma \sum_{k=1}^{\infty} \zeta_k \sum_{n,m} |\rho_n^k \rho_m^k| \frac{\sqrt{-\lambda'_n}\sqrt{-\lambda'_m}}{\lambda'_n + \lambda'_m} \left((-\lambda'_n)^{\frac{\gamma}{2}} + (-\lambda'_m)^{\frac{\gamma}{2}} \right) \\
&\leq - 2C^2 c_\gamma |t - t'|^\gamma \\
&\quad \times \left(\sum_{k=1}^{d_0} \zeta_k \sum_{n,m \leq d_0} \frac{\sqrt{-\lambda'_n}\sqrt{-\lambda'_m}}{\lambda'_n + \lambda'_m} \left((-\lambda'_n)^{\frac{\gamma}{2}} + (-\lambda'_m)^{\frac{\gamma}{2}} \right) \right. \\
&\quad \left. + \sum_{k=d_0+1}^{\infty} \zeta_k \sum_{|n-k| \leq d_1, |m-k| \leq d_1} \frac{\sqrt{-\lambda'_n}\sqrt{-\lambda'_m}}{\lambda'_n + \lambda'_m} \left((-\lambda'_n)^{\frac{\gamma}{2}} + (-\lambda'_m)^{\frac{\gamma}{2}} \right) \right) \\
&\leq c_\gamma \frac{C^2}{\lambda'_1} |t - t'|^\gamma \min_{j \in \{d_0, 1+2d_1\}} \{\lambda'_j j^2\} \left(\sum_{k=1}^{d_0} \zeta_k (-\lambda'_{d_0})^{\frac{\gamma}{2}} + \sum_{k=d_0+1}^{\infty} \zeta_k (-\lambda'_{k+d_1})^{\frac{\gamma}{2}} \right),
\end{aligned}
$$

for which the symbol $\times$ is used as the product operation for readability. □

Having proven the previous lemma, we can use Theorem 2.2.3 to state that w_Δ, defined in (B.1), admits a version with continuous paths in $\mathcal{W}^{1,2}(\mathcal{X}_1)$. Through the fact that the Laplacian operator satisfies Theorem 2.1.2, we can imply from [65, Theorem 5.27] that $w_A : \mathcal{X}_1 \times [0,T] \to L^2(\Omega, \mathcal{F}, \mathbb{P})$, defined as

$$
w_A(x,t) := \sum_{k=1}^{\infty} \sqrt{\zeta_k} \sum_{n=1}^{\infty} \rho_n^k e_n(x) \int_0^t \mathsf{e}^{\lambda'_n (t - t_1)} \mathsf{d}\beta_k(t_1), \quad \forall t > 0 \quad \text{and} \quad x \in \mathcal{X}_1, \tag{B.5}
$$

admits a version continuous in $\mathcal{W}^{1,2}(\mathcal{X}_1)$ as well. From such results, Theorem 2.2.5 and Theorem 2.2.6 imply the existence and uniqueness of the mild solution of (3.0.1) that is $\mathbb{P}$-almost surely in the space $\mathcal{C}([0,+\infty); \mathcal{W}^{1,2}(\mathcal{X}_1))$ if $u_0 \in \mathcal{W}^{1,2}(\mathcal{X}_1)$. Finally, Theorem 2.2.6 leads to the existence of a unique mild solution of (3.0.1),

$$
u \in L^2(\Omega \times (0,T); \mathcal{W}^{1,2}(\mathcal{X}_1)) \cap L^2(\Omega, \mathcal{F}, \mathbb{P}; \mathcal{C}([0,T]; \mathcal{H}_1))
$$

for all $T > 0$.

Remark. In Chapter 3, we use Lemma B.1 for $d_1 = 0$, which is sufficient to guarantee great freedom on a finite number of eigenfunctions of Q.

The lemma can be generalised in different aspects. In fact, the choice of the space on which the continuity of the solution of (3.0.1) is sought depends on γ. For instance, under the assumption that $-1 < \gamma < 0$, the continuity of the paths of w_Δ in $\mathcal{H}_1$ can be proven in an equivalent manner. We note also that, tracking the same steps of the proof of Lemma B.1, the continuity in $\mathcal{W}^{1,2}(\mathcal{X}_1)$ of $w_A : \mathcal{X}_1 \times [0,T] \to L^2(\Omega, \mathcal{F}, \mathbb{P})$, defined in (B.5), can be proven in the case in which the properties (B1), (B2) and (B3) were to be assumed in relation to the eigenfunctions and eigenvalues of A, instead of those of Δ, i.e.,

(B1') $b_{j_2} = \sum_{j_1 \leq d_0} \rho_{j_1}^{j_2} e_{j_1}$, for all $0 < j_2 \leq d_0$;

(B2') $b_{j_2} = \sum_{\{|j_1 - j_2| \leq d_1, j_1 > d_0\}} \rho_{j_1}^{j_2} e_{j_1}$, for all $d_0 < j_2$;

(B3') there exists $\gamma > 0$ for which $\sum_{j=1}^{\infty} \zeta_j (-\lambda_{j+d_1})^\gamma < +\infty$.

This is implied by (A.3). Lastly, assuming instead of the properties (B1) and (B2) the scaling

$$||e_k - b_k|| = \mathcal{O}\Big(\frac{1}{k}\Big)$$

and Q to be only trace class, then the continuity of w_A in $\mathcal{W}^{s,2}(\mathcal{X}_1)$ can be shown for $0 < s < 1$.

C Appendix: Parseval–Plancherel identity on Hilbert spaces

This appendix provides a formal justification for the observation of the trajectories of (3.0.1) and (3.1.1) along eigenmodes of Laplace operator in Chapter 3. Such a perspective enables the construction of an early-warning sign for B-tipping. We set the Hilbert space $\mathcal{H}$ with basis $\{\phi_j\}_{j\in\mathbb{N}_{>0}}$, scalar product $\langle\cdot,\cdot\rangle_{\mathcal{H}}$ and $f_1, f_2 \in \mathcal{H}$. By definition of a basis, we know that the sequences $\left\{ f_n^k := \sum_{j=1}^{n} \langle f_k, \phi_j\rangle_{\mathcal{H}}\phi_j \right\}_{n\in\mathbb{N}_{>0}}$ converge strongly in the norm defined by the scalar product, $||\cdot||_{\mathcal{H}}$, to $f_k = \sum_{j=1}^{\infty} \langle f_k, \phi_j\rangle_{\mathcal{H}}\phi_j$, for $k \in \{1, 2\}$. It is then well known and easy to prove the following consequence:

$$\begin{aligned} |\langle f_n^1, f_n^2\rangle_{\mathcal{H}} - \langle f_1, f_2\rangle_{\mathcal{H}}| &\leq |\langle f_n^1 - f_1, f_n^2\rangle_{\mathcal{H}}| + |\langle f_1, f_n^2 - f_2\rangle_{\mathcal{H}}| \\ &\leq ||f_n^1 - f_1||_{\mathcal{H}}\, ||f_n^2||_{\mathcal{H}} + ||f_n^2 - f_2||_{\mathcal{H}}\, ||f_1||_{\mathcal{H}} \\ &\leq \max\Big\{||f_1||_{\mathcal{H}}, ||f_2||_{\mathcal{H}}\Big\}\Big(||f_n^1 - f_1||_{\mathcal{H}} + ||f_n^2 - f_2||_{\mathcal{H}}\Big) \underset{n\to\infty}{\to} 0. \end{aligned} \tag{C.1}$$

By definition

$$\begin{aligned} \langle f_n^1, f_n^2\rangle_{\mathcal{H}} &= \Big\langle \sum_{j_1=1}^{n} \langle f_1, \phi_{j_1}\rangle_{\mathcal{H}}\phi_{j_1}, \sum_{j_2=1}^{n} \langle f_2, \phi_{j_2}\rangle_{\mathcal{H}}\phi_{j_2} \Big\rangle_{\mathcal{H}} \\ &= \sum_{j_1=1}^{n}\sum_{j_2=1}^{n} \langle f_1, \phi_{j_1}\rangle_{\mathcal{H}}\langle f_2, \phi_{j_2}\rangle_{\mathcal{H}}\langle \phi_{j_1}, \phi_{j_2}\rangle_{\mathcal{H}} = \sum_{j=1}^{n} \langle f_1, \phi_j\rangle_{\mathcal{H}}\langle f_2, \phi_j\rangle_{\mathcal{H}}. \end{aligned} \tag{C.2}$$

Combining (C.1) and (C.2), we obtain

$$\langle f_1, f_2\rangle_{\mathcal{H}} = \sum_{j=1}^{\infty} \langle f_1, \phi_j\rangle_{\mathcal{H}}\langle f_2, \phi_j\rangle_{\mathcal{H}}.$$

D Appendix: Proof of Theorem 4.2.5

The following proof justifies the description of the scaling law of the upper bound presented in Theorem 4.2.5, and its results are summarised in Table 4.3. The proof is based upon a splitting of the upper bound into two summands, labelled as $\mathfrak{A}$ and $\mathfrak{B}$, the first of which is studied similarly to the methods employed in the proof of Theorem 4.1.1.

Proof Theorem 4.2.5. Up to permutation of indices, we assume $i_2 \geq i_1 \geq 1$ for simplicity. We also set $\varepsilon = 1$, up to rescaling of the space variable x and subsequently of $\mathcal{X}_1$. Lemma 4.2.3 implies for a positive constant $C > 0$ that

$$\langle g, V_\infty^{\mathsf{w}} g\rangle \leq \frac{1}{C}\int_0^1\int_0^1 \frac{1}{x_1^{i_1}x_2^{i_2} - p}\,\mathrm{d}x_2\mathrm{d}x_1 = \frac{-1}{Cp}\int_0^1\int_0^1 \frac{1}{\Big(x_1(-p)^{-\frac{1}{2i_1}}\Big)^{i_1}\Big(x_2(-p)^{-\frac{1}{2i_2}}\Big)^{i_2} + 1}\,\mathrm{d}x_2\mathrm{d}x_1.$$

For convenience, we write $q = -p > 0$. Through integration by substitution with $y_n := x_n q^{-\frac{1}{2i_n}}$ for $n \in \{1,2\}$, we obtain that

$$\begin{aligned}\langle g, V_\infty^{\mathsf{w}} g\rangle &\leq \frac{1}{Cq}\int_0^1\int_0^1 \frac{1}{\left(x_1 q^{-\frac{1}{2i_1}}\right)^{i_1}\left(x_2 q^{-\frac{1}{2i_2}}\right)^{i_2}+1}\,\mathsf{d}y_2\mathsf{d}y_1 \\ &= \frac{1}{C}q^{-1+\frac{1}{2}\left(\frac{1}{i_1}+\frac{1}{i_2}\right)}\int_0^{q^{-\frac{1}{2i_1}}}\int_0^{q^{-\frac{1}{2i_2}}}\frac{1}{y_1^{i_1}y_2^{i_2}+1}\,\mathsf{d}y_2\mathsf{d}y_1.\end{aligned} \tag{D.1}$$

We evaluate the integral by substituting $z = \frac{1}{y_1^{i_1}y_2^{i_2}+1}$ to get

$$\begin{aligned}\langle g, V_\infty^{\mathsf{w}} g\rangle \leq& \frac{1}{C}q^{-1+\frac{1}{2}\left(\frac{1}{i_1}+\frac{1}{i_2}\right)}\int_0^{q^{-\frac{1}{2i_1}}}\int_0^{q^{-\frac{1}{2i_2}}}\frac{1}{y_1^{i_1}y_2^{i_2}+1}\,\mathsf{d}y_2\,\mathsf{d}y_1 \\ =& \frac{1}{C}q^{-1+\frac{1}{2}\left(\frac{1}{i_1}+\frac{1}{i_2}\right)}\int_0^{q^{-\frac{1}{2i_1}}}\int_{\frac{1}{y_1^{i_1}q^{-\frac{1}{2}}+1}}^1 z z^{-2}\frac{1}{i_2}\left(\frac{1}{z}-1\right)^{\frac{1}{i_2}-1} y_1^{-\frac{i_1}{i_2}}\,\mathsf{d}z\,\mathsf{d}y_1 \\ =& \frac{1}{C}q^{-1+\frac{1}{2}\left(\frac{1}{i_1}+\frac{1}{i_2}\right)}\int_0^{q^{-\frac{1}{2i_1}}}\left(\frac{q^{-\frac{1}{2i_2}}}{y_1^{i_1}q^{-\frac{1}{2}}+1}+\int_{\frac{1}{y_1^{i_1}q^{-\frac{1}{2}}+1}}^1\left(\frac{1}{z}-1\right)^{\frac{1}{i_2}} y_1^{-\frac{i_1}{i_2}}\,\mathsf{d}z\right)\mathsf{d}y_1 \\ =& \underbrace{\frac{1}{C}\,q^{-1+\frac{1}{2i_1}}\int_0^{q^{-\frac{1}{2i_1}}}\frac{1}{y_1^{i_1}q^{-\frac{1}{2}}+1}\,\mathsf{d}y_1}_{\mathfrak{A}} \\ &+ \underbrace{\frac{1}{C}\,q^{-1+\frac{1}{2}\left(\frac{1}{i_1}+\frac{1}{i_2}\right)}\int_0^{q^{-\frac{1}{2i_1}}}\int_{\frac{1}{y_1^{i_1}q^{-\frac{1}{2}}+1}}^1\left(\frac{1}{z}-1\right)^{\frac{1}{i_2}} y_1^{-\frac{i_1}{i_2}}\,\mathsf{d}z\,\mathsf{d}y_1}_{\mathfrak{B}}.\end{aligned} \tag{D.2}$$

In the following, we first analyse $\mathfrak{A}$ before evaluating the order of divergence of $\mathfrak{B}$. Moreover, the choice of i_1 and i_2 dictates the rate of the upper bound, as seen above. Hence, we consider different cases corresponding to the choice of values of i_1 and i_2, whose numbering is displayed in Table 4.3.

◊ Scaling law of $\mathfrak{A}$ in Cases 1 and 3.
Note that the order of $\mathfrak{A}$ is independent of i_2, which simplifies the study of its scaling law. We start by discussing $\mathfrak{A}$ for $i_2 \geq i_1 > 1$. Through the substitution $y_1' = y_1 q^{-\frac{1}{2i_1}}$, it follows that

$$\mathfrak{A} = q^{-1+\frac{1}{i_1}}\int_0^{q^{-\frac{1}{i_1}}}\frac{1}{y_1'^{i_1}+1}\,\mathsf{d}y_1'.$$

As already established in (4.1.6), the integral is converging for $p \to 0^-$, and therefore we find a rate of divergence for the first summand given by

$$\Theta_p\left((-p)^{-1+\frac{1}{i_1}}\right) \tag{D.3}$$

for $p \to 0^-$ and $i_2 \geq i_1 > 1$.

◊ Scaling law of $\mathfrak{A}$ in Cases 2 and 4.
Next, we consider $\mathfrak{A}$ assuming that $i_2 \geq i_1 = 1$. Through the same substitutions addressed in the previous case, we get

$$\mathfrak{A} = \int_0^{q^{-1}} \frac{1}{y_1' + 1} \, \mathrm{d}y_1' = \log\left(q^{-1} + 1\right).$$

This component diverges for q approaching zero from above. For $i_2 \geq i_1 = 1$, it follows that

$$\Theta_p\left(\log\left((-p)^{-1}\right)\right) = \Theta_p\left(-\log\left(-p\right)\right) \tag{D.4}$$

is the rate of divergence for p approaching zero from below.

♦ Scaling law of $\mathfrak{B}$ in Case 1.
We consider the case $i_2 > i_1 > 1$. In regard to $\mathfrak{B}$, our first goal is to switch integrals for more convenient computation. Through Fubini's Theorem, we obtain

$$\begin{aligned}
\mathfrak{B} &= q^{-1+\frac{1}{2}\left(\frac{1}{i_1}+\frac{1}{i_2}\right)} \int_{\frac{1}{q^{-1}+1}}^{1} \int_{\left(\frac{1}{z}-1\right)^{\frac{1}{i_1}} q^{\frac{1}{2i_1}}}^{q^{-\frac{1}{2i_1}}} \left(\frac{1}{z} - 1\right)^{\frac{1}{i_2}} y_1^{-\frac{i_1}{i_2}} \, \mathrm{d}y_1 \, \mathrm{d}z \\
&= q^{-1+\frac{1}{2}\left(\frac{1}{i_1}+\frac{1}{i_2}\right)} \int_{\frac{1}{q^{-1}+1}}^{1} \left(\frac{1}{z} - 1\right)^{\frac{1}{i_2}} \left[\frac{1}{\left(1 - \frac{i_1}{i_2}\right)} y_1^{-\frac{i_1}{i_2}+1}\right]_{\left(\frac{1}{z}-1\right)^{\frac{1}{i_1}} q^{\frac{1}{2i_1}}}^{q^{-\frac{1}{2i_1}}} \mathrm{d}z \\
&= \frac{q^{-1+\frac{1}{2}\left(\frac{1}{i_1}+\frac{1}{i_2}\right)}}{1 - \frac{i_1}{i_2}} \int_{\frac{1}{q^{-1}+1}}^{1} \left(\frac{1}{z} - 1\right)^{\frac{1}{i_2}} \left(q^{\frac{1}{2i_2}-\frac{1}{2i_1}} - \left(\frac{1}{z} - 1\right)^{\frac{1}{i_1}-\frac{1}{i_2}} q^{\frac{1}{2i_1}-\frac{1}{2i_2}}\right) \mathrm{d}z \\
&= \left(1 - \frac{i_1}{i_2}\right)^{-1} \left(q^{-1+\frac{1}{i_2}} \int_{\frac{1}{q^{-1}+1}}^{1} \left(\frac{1}{z} - 1\right)^{\frac{1}{i_2}} \mathrm{d}z - q^{-1+\frac{1}{i_1}} \int_{\frac{1}{q^{-1}+1}}^{1} \left(\frac{1}{z} - 1\right)^{\frac{1}{i_1}} \mathrm{d}z\right).
\end{aligned} \tag{D.5}$$

By substitution with $z' = \frac{1}{z} - 1$, we obtain

$$\mathfrak{B} = \left(1 - \frac{i_1}{i_2}\right)^{-1} \left(q^{-1+\frac{1}{i_2}} \int_0^{q^{-1}} \frac{z'^{\frac{1}{i_2}}}{(z'+1)^2} \, \mathrm{d}z' - q^{-1+\frac{1}{i_1}} \int_0^{q^{-1}} \frac{z'^{\frac{1}{i_1}}}{(z'+1)^2} \, \mathrm{d}z'\right). \tag{D.6}$$

Given $i_2 > i_1 > 1$, the integrals in (D.6) can be uniformly bounded for any $q > 0$. Consequently, we find that the rate of divergence of $\mathfrak{B}$ is given by

$$\Theta_p\left(q^{-1+\frac{1}{i_2}}\right) - \Theta_p\left(q^{-1+\frac{1}{i_1}}\right) = \Theta_p\left((-p)^{-1+\frac{1}{i_2}}\right) - \Theta_p\left((-p)^{-1+\frac{1}{i_1}}\right) = \Theta_p\left((-p)^{-1+\frac{1}{i_2}}\right)$$

as p approaches zero from below. From (D.2), we get the rate of divergence of the upper bound as

$$\Theta_p\left((-p)^{-1+\frac{1}{i_1}}\right) + \Theta_p\left((-p)^{-1+\frac{1}{i_2}}\right) = \Theta_p\left((-p)^{-1+\frac{1}{i_2}}\right),$$

for $i_2 > i_1 > 1$.

♦ Scaling law of $\mathfrak{B}$ in Case 2.
We suppose now that $i_2 > i_1 = 1$. We can follow the steps in the case above, up to (D.6). We then note that

$$\int_0^{q^{-1}} \frac{z'}{(z'+1)^2} \, \mathrm{d}z' = \log\left(q^{-1} + 1\right) + \frac{1}{q^{-1}+1} - 1. \tag{D.7}$$

Therefore, we obtain that $\mathfrak{B}$ diverges with rate

$$\Theta_p\left((-p)^{-1+\frac{1}{i_2}}\right) - \Theta_p\left(\log((-p)^{-1})\right) = \Theta_p\left((-p)^{-1+\frac{1}{i_2}}\right),$$

for $p \to 0^-$. Combining this result with equation (D.4) we obtain for $i_2 > i_1 = 1$ an overall rate of divergence of order

$$\Theta_p\left(-\log(-p)\right) + \Theta_p\left((-p)^{-1+\frac{1}{i_2}}\right) = \Theta_p\left((-p)^{-1+\frac{1}{i_2}}\right).$$

- Scaling law of $\mathfrak{B}$ in Case 3.
  For the third case we consider $\mathfrak{B}$ with $i_2 = i_1 = i > 1$, for which we get

$$\begin{aligned}
\mathfrak{B} &= q^{-1+\frac{1}{i}} \int_{\frac{1}{q^{-1}+1}}^{1} \int_{\left(\frac{1}{z}-1\right)^{\frac{1}{i}} q^{\frac{1}{2i}}}^{q^{-\frac{1}{2i}}} \left(\frac{1}{z}-1\right)^{\frac{1}{i}} y_1^{-1}\, \mathrm{d}y_1\, \mathrm{d}z \\
&= q^{-1+\frac{1}{i}} \int_{\frac{1}{q^{-1}+1}}^{1} \left(\frac{1}{z}-1\right)^{\frac{1}{i}} \left(\log\left(q^{-\frac{1}{2i}}\right) - \log\left(\left(\frac{1}{z}-1\right)^{\frac{1}{i}} q^{\frac{1}{2i}}\right)\right) \mathrm{d}z \\
&= q^{-1+\frac{1}{i}} \left(-\frac{\log(q)}{i} \int_{\frac{1}{q^{-1}+1}}^{1} \left(\frac{1}{z}-1\right)^{\frac{1}{i}} \mathrm{d}z - \frac{1}{i} \int_{\frac{1}{q^{-1}+1}}^{1} \left(\frac{1}{z}-1\right)^{\frac{1}{i}} \log\left(\frac{1}{z}-1\right) \mathrm{d}z\right).
\end{aligned}$$

  Again, we substitute $z' = \frac{1}{z} - 1$ to get

$$\mathfrak{B} = q^{-1+\frac{1}{i}} \left(-\frac{\log(q)}{i} \int_0^{q^{-1}} \frac{z'^{\frac{1}{i}}}{(z'+1)^2}\, \mathrm{d}z' - \frac{1}{i} \int_0^{q^{-1}} \frac{z'^{\frac{1}{i}} \log(z')}{(z'+1)^2}\, \mathrm{d}z'\right). \tag{D.8}$$

  The integrals in (D.8) are uniformly bounded for any $q > 0$ due to $i > 1$. Equation (D.8) implies that $\mathfrak{B}$ assumes, in this case, rate of divergence

$$\Theta_p\left(-(-p)^{-1+\frac{1}{i}}\log(-p)\right) + \Theta_p\left((-p)^{-1+\frac{1}{i}}\right) = \Theta_p\left(-(-p)^{-1+\frac{1}{i}}\log(-p)\right)$$

  for $p \to 0^-$.
  From (D.2) and (D.3), we get that the rate of divergence of the upper bound is

$$\Theta_p\left((-p)^{-1+\frac{1}{i}}\right) + \Theta_p\left(-(-p)^{-1+\frac{1}{i}}\log(-p)\right) = \Theta_p\left(-(-p)^{-1+\frac{1}{i}}\log(-p)\right).$$

- Scaling law of $\mathfrak{B}$ in Case 4.
  In the last case, we suppose that $i_2 = i_1 = i = 1$. Consequently, (D.8) assumes the form

$$\begin{aligned}
\mathfrak{B} &= -\log(q) \int_0^{q^{-1}} \frac{z'}{(z'+1)^2}\, \mathrm{d}z' - \int_0^{q^{-1}} \frac{z'\log(z')}{(z'+1)^2}\, \mathrm{d}z' \qquad \text{(D.9)} \\
&= -\log(q)\left(\log(q^{-1}+1) + \frac{1}{q^{-1}+1} - 1\right) - \int_0^{q^{-1}} \frac{z'\log(z')}{(z'+1)^2}\, \mathrm{d}z'.
\end{aligned}$$

  We obtain therefore from (D.9) and (F.3), in Appendix F, that the two leading terms in $\mathfrak{B}$ diverge respectively as $\log^2(q)$ and as $-\frac{1}{2}\log^2(q)$. Hence, we know that the divergence of $\mathfrak{B}$ assumes rate

$$\Theta_p\left(\log^2(-p)\right) \quad \text{for } p \to 0^-.$$

Combining such a result with the rate of divergence of $\mathfrak{A}$ in (D.4), we obtain

$$\Theta_p\left(-\log(-p)\right) + \Theta_p\left(\log^2(-p)\right) = \Theta_p\left(\log^2(-p)\right) \quad \text{for } p \to 0^-,$$

as an overall upper bound for $i_2 = i_1 = 1$.

□

E Appendix: Proof of Theorem 4.2.7

The subsequent proof validates the description of the rate of divergence of the upper bound discussed in Theorem 4.2.7. The approach is similar to the one involved in the proof of Theorem 4.2.5 as the upper bound is split into two summands, called $\mathfrak{C}$ and $\mathfrak{D}$. The first summand is studied similarly to the upper bound in the stated proof for the two-dimensional case. The scaling laws of the summands are summarised in Table 4.4.

Proof Theorem 4.2.7. Lemma 4.2.3 implies that

$$\langle g, V_\infty^{\mathsf{w}} g\rangle \leq \frac{\sigma^2}{2C}\int_0^\varepsilon\int_0^\varepsilon\int_0^\varepsilon \frac{1}{x_1^{i_1}x_2^{i_2}x_3^{i_3}-p}\,\mathrm{d}x_3\,\mathrm{d}x_2\,\mathrm{d}x_1$$

for a constant $C > 0$ and any $p < 0$. As in the two-dimensional case, we employ $q = -p > 0$ and we fix $\varepsilon = 1$, up to rescaling of the spatial variable x. Up to permutation of the indices, we consider $i_3 \geq i_2 \geq i_1 \geq 1$, thus excluding the cases described in Remark 4.2.4.

We follow a similar computation of the integral as in Theorem 4.2.5. First, we study it in the coordinates $y_n = x_n q^{-\frac{1}{3i_n}}$ for all $n \in \{1,2,3\}$ and then we substitute y_3 with $z = \frac{1}{y_1^{i_1}y_2^{i_2}y_3^{i_3}+1}$ to obtain

$$\begin{aligned}
&\int_0^1\int_0^1\int_0^1 \frac{1}{x_1^{i_1}x_2^{i_2}x_3^{i_3}+q}\,\mathrm{d}x_3\,\mathrm{d}x_2\,\mathrm{d}x_1\\
=&q^{-1+\frac{1}{3}\left(\frac{1}{i_1}+\frac{1}{i_2}+\frac{1}{i_3}\right)}\int_0^{q^{-\frac{1}{3i_1}}}\int_0^{q^{-\frac{1}{3i_2}}}\int_0^{q^{-\frac{1}{3i_3}}} \frac{1}{y_1^{i_1}y_2^{i_2}y_3^{i_3}+1}\,\mathrm{d}y_3\,\mathrm{d}y_2\,\mathrm{d}y_1\\
=&q^{-1+\frac{1}{3}\left(\frac{1}{i_1}+\frac{1}{i_2}+\frac{1}{i_3}\right)}\int_0^{q^{-\frac{1}{3i_1}}}\int_0^{q^{-\frac{1}{3i_2}}}\int_{\frac{1}{y_1^{i_1}y_2^{i_2}q^{-\frac{1}{3}}+1}}^1 zz^{-2}\frac{1}{i_3}\left(\frac{1}{z}-1\right)^{\frac{1}{i_3}-1} y_1^{-\frac{i_1}{i_3}}y_2^{-\frac{i_2}{i_3}}\,\mathrm{d}z\,\mathrm{d}y_2\,\mathrm{d}y_1.
\end{aligned}$$

Through integration by parts on the inner integral, it follows that

$$\begin{aligned}
&\int_0^1\int_0^1\int_0^1 \frac{1}{x_1^{i_1}x_2^{i_2}x_3^{i_3}+q}\,\mathrm{d}x_3\,\mathrm{d}x_2\,\mathrm{d}x_1\\
=&\underbrace{q^{-1+\frac{1}{3}\left(\frac{1}{i_1}+\frac{1}{i_2}\right)}\int_0^{q^{-\frac{1}{3i_1}}}\int_0^{q^{-\frac{1}{3i_2}}} \frac{1}{y_1^{i_1}y_2^{i_2}q^{-\frac{1}{3}}+1}\,\mathrm{d}y_2\,\mathrm{d}y_1}_{\mathfrak{C}}\\
&+\underbrace{q^{-1+\frac{1}{3}\left(\frac{1}{i_1}+\frac{1}{i_2}+\frac{1}{i_3}\right)}\int_0^{q^{-\frac{1}{3i_1}}}\int_0^{q^{-\frac{1}{3i_2}}}\int_{\frac{1}{y_1^{i_1}y_2^{i_2}q^{-\frac{1}{3}}+1}}^1 \left(\frac{1}{z}-1\right)^{\frac{1}{i_3}} y_1^{-\frac{i_1}{i_3}}y_2^{-\frac{i_2}{i_3}}\,\mathrm{d}z\,\mathrm{d}y_2\,\mathrm{d}y_1}_{\mathfrak{D}}.
\end{aligned} \tag{E.1}$$

We study each summand independently as in Theorem 4.2.5. Further, we distinguish between different choices of values for i_n for $n \in \{1,2,3\}$. We find the scaling laws of $\mathfrak{C}$, $\mathfrak{D}$, and the overall upper bound for each case. The numbering of the cases is reported in Table 4.4.

◊ Scaling law of $\mathfrak{C}$ in Cases 1 - 8.
We assume $i_1, i_2, i_3 > 0$. We substitute the variables in the integral with $y_n' = y_n q^{-\frac{1}{6i_n}}$ for $n \in \{1,2\}$ to have

$$\begin{aligned} &q^{-1+\frac{1}{3}\left(\frac{1}{i_1}+\frac{1}{i_2}\right)} \int_0^{q^{-\frac{1}{3i_1}}} \int_0^{q^{-\frac{1}{3i_2}}} \frac{1}{\left(y_1 q^{-\frac{1}{6i_1}}\right)^{i_1}\left(y_2 q^{-\frac{1}{6i_2}}\right)^{i_2}+1}\,\mathrm{d}y_2\,\mathrm{d}y_1 \\ =&q^{-1+\frac{1}{2}\left(\frac{1}{i_1}+\frac{1}{i_2}\right)} \int_0^{q^{-\frac{1}{2i_1}}} \int_0^{q^{-\frac{1}{2i_2}}} \frac{1}{y_1'^{i_1} y_2'^{i_2}+1}. \end{aligned}$$

We note that this expression is equivalent to the integral given by (D.1), as i_3 does not affect such a rate of divergence. Consequently, we have proven the divergence of $\mathfrak{C}$ for different choices of i_1, i_2 and that its corresponding rate is displayed in Table 4.3.

♦ Scaling law of $\mathfrak{D}$ in Case 1.
Next, we continue analysing the component $\mathfrak{D}$ of (E.1). First, we assume that $i_3 > i_2 > i_1 > 1$.
We change the order of integrals through Fubini's Theorem, placing the integral on z in the outer position and obtaining

$$\begin{aligned} &q^{-1+\frac{1}{3}\left(\frac{1}{i_1}+\frac{1}{i_2}+\frac{1}{i_3}\right)} \int_0^{q^{-\frac{1}{3i_1}}} \int_0^{q^{-\frac{1}{3i_2}}} \int_{\frac{1}{y_1^{i_1} y_2^{i_2} q^{-\frac{1}{3}}+1}}^1 \left(\frac{1}{z}-1\right)^{\frac{1}{i_3}} y_1^{-\frac{i_1}{i_3}} y_2^{-\frac{i_2}{i_3}}\,\mathrm{d}z\,\mathrm{d}y_2\,\mathrm{d}y_1 \qquad \text{(E.2)} \\ =&q^{-1+\frac{1}{3}\left(\frac{1}{i_1}+\frac{1}{i_2}+\frac{1}{i_3}\right)} \int_{\frac{1}{q^{-1}+1}}^1 \int_{\left(\frac{1}{z}-1\right)^{\frac{1}{i_1}} q^{\frac{2}{3i_1}}}^{q^{-\frac{1}{3i_1}}} \int_{\left(\frac{1}{z}-1\right)^{\frac{1}{i_2}} q^{\frac{1}{3i_2}} y_1^{-\frac{i_1}{i_2}}}^{q^{-\frac{1}{3i_2}}} \left(\frac{1}{z}-1\right)^{\frac{1}{i_3}} y_1^{-\frac{i_1}{i_3}} y_2^{-\frac{i_2}{i_3}}\,\mathrm{d}y_2\,\mathrm{d}y_1\,\mathrm{d}z. \end{aligned}$$

Since $i_3 > i_2$, it follows that

$$\begin{aligned} &\left(-\frac{i_2}{i_3}+1\right)\mathfrak{D} \\ =&q^{-1+\frac{1}{3}\left(\frac{1}{i_1}+\frac{1}{i_2}+\frac{1}{i_3}\right)} \int_{\frac{1}{q^{-1}+1}}^1 \int_{\left(\frac{1}{z}-1\right)^{\frac{1}{i_1}} q^{\frac{2}{3i_1}}}^{q^{-\frac{1}{3i_1}}} \left(\frac{1}{z}-1\right)^{\frac{1}{i_3}} y_1^{-\frac{i_1}{i_3}} \left[y_2^{-\frac{i_2}{i_3}+1}\right]_{y_2=\left(\frac{1}{z}-1\right)^{\frac{1}{i_2}} q^{\frac{1}{3i_2}} y_1^{-\frac{i_1}{i_2}}}^{q^{-\frac{1}{3i_2}}} \mathrm{d}y_1\,\mathrm{d}z \\ =&\underbrace{q^{-1+\frac{1}{3i_1}+\frac{2}{3i_3}} \int_{\frac{1}{q^{-1}+1}}^1 \left(\frac{1}{z}-1\right)^{\frac{1}{i_3}} \int_{\left(\frac{1}{z}-1\right)^{\frac{1}{i_1}} q^{\frac{2}{3i_1}}}^{q^{-\frac{1}{3i_1}}} y_1^{-\frac{i_1}{i_3}}\,\mathrm{d}y_1\,\mathrm{d}z}_{\mathfrak{D}.\mathrm{I}} \qquad \text{(E.3)} \\ &\underbrace{-q^{-1+\frac{1}{3i_1}+\frac{2}{3i_2}} \int_{\frac{1}{q^{-1}+1}}^1 \left(\frac{1}{z}-1\right)^{\frac{1}{i_2}} \int_{\left(\frac{1}{z}-1\right)^{\frac{1}{i_1}} q^{\frac{2}{3i_1}}}^{q^{-\frac{1}{3i_1}}} y_1^{-\frac{i_1}{i_2}}\,\mathrm{d}y_1\,\mathrm{d}z}_{\mathfrak{D}.\mathrm{II}}. \end{aligned}$$

From $i_3 > i_1$, we know that $\mathfrak{D}$.I is equal to

$$\begin{aligned}&\Big(-\frac{i_1}{i_3}+1\Big)^{-1}\left(q^{-1+\frac{1}{i_3}}\int_{\frac{1}{q^{-1}+1}}^{1}\left(\frac{1}{z}-1\right)^{\frac{1}{i_3}}\,\mathrm{d}z - q^{-1+\frac{1}{i_1}}\int_{\frac{1}{q^{-1}+1}}^{1}\left(\frac{1}{z}-1\right)^{\frac{1}{i_1}}\,\mathrm{d}z\right) \qquad \text{(E.4)}\\ =&\Big(-\frac{i_1}{i_3}+1\Big)^{-1}\Bigg(\underbrace{q^{-1+\frac{1}{i_3}}\int_0^{q^{-1}}\frac{z'^{\frac{1}{i_3}}}{(z'+1)^2}\,\mathrm{d}z'}_{\mathfrak{D}.\mathrm{I}.1} - \underbrace{q^{-1+\frac{1}{i_1}}\int_0^{q^{-1}}\frac{z'^{\frac{1}{i_1}}}{(z'+1)^2}\,\mathrm{d}z'}_{\mathfrak{D}.\mathrm{I}.2}\Bigg),\end{aligned}$$

with $z' = \frac{1}{z} - 1$. Equivalently, since $i_2 > i_1$, the summand $\mathfrak{D}$.II is equal to

$$\Big(-\frac{i_1}{i_2}+1\Big)^{-1}\Bigg(\underbrace{q^{-1+\frac{1}{i_2}}\int_0^{q^{-1}}\frac{z'^{\frac{1}{i_2}}}{(z'+1)^2}\,\mathrm{d}z'}_{\mathfrak{D}.\mathrm{II}.1} - \underbrace{q^{-1+\frac{1}{i_1}}\int_0^{q^{-1}}\frac{z'^{\frac{1}{i_1}}}{(z'+1)^2}\mathrm{d}z'}_{\mathfrak{D}.\mathrm{II}.2}\Bigg).$$

For $i_1, i_2, i_3 > 1$, the integrals in $\mathfrak{D}$.I.1, $\mathfrak{D}$.I.2, $\mathfrak{D}$.II.1 and $\mathfrak{D}$.II.2 are uniformly bounded for any $q > 0$. Hence, the rate of divergence of $\mathfrak{D}$ is

$$\Theta_p\left((-p)^{-1+\frac{1}{i_3}}\right) - \Theta_p\left((-p)^{-1+\frac{1}{i_1}}\right) - \Theta_p\left((-p)^{-1+\frac{1}{i_2}}\right) + \Theta_p\left((-p)^{-1+\frac{1}{i_1}}\right) = \Theta_p\left((-p)^{-1+\frac{1}{i_3}}\right).$$

Combining the rates of $\mathfrak{C}$ and $\mathfrak{D}$, we prove the divergence, for $i_3 > i_2 > i_1 > 1$, of the upper bound with a scaling law

$$\Theta_p\left((-p)^{-1+\frac{1}{i_2}}\right) + \Theta_p\left((-p)^{-1+\frac{1}{i_3}}\right) = \Theta_p\left((-p)^{-1+\frac{1}{i_3}}\right).$$

♦ Scaling law of $\mathfrak{D}$ in Case 2.
Next, we consider the case $i_3 > i_2 = i_1 = i > 1$. We can follow the same argumentation of the previous case until (E.4) and prove that

$$\mathfrak{D}.\mathrm{I} = \Big(-\frac{i}{i_3}+1\Big)^{-1}\Big(\mathfrak{D}.\mathrm{I}.1 - \mathfrak{D}.\mathrm{I}.2\Big).$$

In this case, summand $\mathfrak{D}$.II is equal to

$$\begin{aligned}&q^{-1+\frac{1}{i}}\int_{\frac{1}{q^{-1}+1}}^{1}\left(\frac{1}{z}-1\right)^{\frac{1}{i}}\int_{\left(\frac{1}{z}-1\right)^{\frac{1}{i}}q^{\frac{2}{3i}}}^{q^{-\frac{1}{3i}}} y_1^{-1}\,\mathrm{d}y_1\,\mathrm{d}z\\ =&-\frac{1}{i}q^{-1+\frac{1}{i}}\int_{\frac{1}{q^{-1}+1}}^{1}\left(\frac{1}{z}-1\right)^{\frac{1}{i}}\left(\log(q)+\log\left(\frac{1}{z}-1\right)\right)\mathrm{d}z \qquad \text{(E.5)}\\ =&-\frac{1}{i}\underbrace{q^{-1+\frac{1}{i}}\log(q)\int_0^{q^{-1}}\frac{z'^{\frac{1}{i}}}{(z'+1)^2}\mathrm{d}z}_{\mathfrak{D}.\mathrm{II}.3} - \frac{1}{i}\underbrace{q^{-1+\frac{1}{i}}\int_0^{q^{-1}}\frac{z'^{\frac{1}{i}}\log(z')}{(z'+1)^2}\mathrm{d}z}_{\mathfrak{D}.\mathrm{II}.4}.\end{aligned}$$

The integrals in $\mathfrak{D}$.II.3 and $\mathfrak{D}$.II.4 are uniformly bounded for any $q > 0$, therefore the rate of divergence of $\mathfrak{D}$.II is $\Theta_p\left(-(-p)^{1+\frac{1}{i}}\log(-p)\right)$. The rate assumed by $\mathfrak{D}$ is

$$\Theta_p\left((-p)^{-1+\frac{1}{i_3}}\right) - \Theta_p\left(-(-p)^{-1+\frac{1}{i}}\log(-p)\right) = \Theta_p\left((-p)^{-1+\frac{1}{i_3}}\right).$$

Overall, we find the rate of the upper bound in the case $i_3 > i_2 = i_1 > 1$ to be

$$\Theta_p\left(-(-p)^{-1+\frac{1}{i_2}}\log(-p)\right) + \Theta_p\left((-p)^{-1+\frac{1}{i_3}}\right) = \Theta_p\left((-p)^{-1+\frac{1}{i_3}}\right).$$

- Scaling law of $\mathfrak{D}$ in Case 3.
  Next, we consider the case $i_3 = i_2 > i_1 > 1$. We observe again equation (E.2) and label $i_3 = i_2 = i$ to obtain that

$$
\begin{aligned}
& q^{-1+\frac{1}{3}\left(\frac{1}{i_1}+\frac{2}{i}\right)} \int_{\frac{1}{q^{-1}+1}}^{1} \int_{\left(\frac{1}{z}-1\right)^{\frac{1}{i_1}} q^{\frac{2}{3i_1}}}^{q^{-\frac{1}{3i_1}}} \int_{\left(\frac{1}{z}-1\right)^{\frac{1}{i}} q^{\frac{1}{3i}} y_1^{-\frac{i_1}{i}}}^{q^{-\frac{1}{3i}}} \left(\frac{1}{z}-1\right)^{\frac{1}{i}} y_1^{-\frac{i_1}{i}} y_2^{-1} \, \mathrm{d}y_2 \, \mathrm{d}y_1 \, \mathrm{d}z \\
=& q^{-1+\frac{1}{3}\left(\frac{1}{i_1}+\frac{2}{i}\right)} \log\left(q^{-\frac{1}{3i}}\right) \int_{\frac{1}{q^{-1}+1}}^{1} \int_{\left(\frac{1}{z}-1\right)^{\frac{1}{i_1}} q^{\frac{2}{3i_1}}}^{q^{-\frac{1}{3i_1}}} \left(\frac{1}{z}-1\right)^{\frac{1}{i}} y_1^{-\frac{i_1}{i}} \, \mathrm{d}y_1 \, \mathrm{d}z \\
& - q^{-1+\frac{1}{3}\left(\frac{1}{i_1}+\frac{2}{i}\right)} \int_{\frac{1}{q^{-1}+1}}^{1} \int_{\left(\frac{1}{z}-1\right)^{\frac{1}{i_1}} q^{\frac{2}{3i_1}}}^{q^{-\frac{1}{3i_1}}} \left(\frac{1}{z}-1\right)^{\frac{1}{i}} y_1^{-\frac{i_1}{i}} \log\left(\left(\frac{1}{z}-1\right)^{\frac{1}{i}} q^{\frac{1}{3i}} y_1^{-\frac{i_1}{i}}\right) \mathrm{d}y_1 \, \mathrm{d}z \\
=& \underbrace{-\frac{2}{3i} q^{-1+\frac{1}{3}\left(\frac{1}{i_1}+\frac{2}{i}\right)} \log(q) \int_{\frac{1}{q^{-1}+1}}^{1} \int_{\left(\frac{1}{z}-1\right)^{\frac{1}{i_1}} q^{\frac{2}{3i_1}}}^{q^{-\frac{1}{3i_1}}} \left(\frac{1}{z}-1\right)^{\frac{1}{i}} y_1^{-\frac{i_1}{i}} \, \mathrm{d}y_1 \, \mathrm{d}z}_{\mathfrak{D}.\mathrm{III}} \\
& \underbrace{- \frac{1}{i} q^{-1+\frac{1}{3}\left(\frac{1}{i_1}+\frac{2}{i}\right)} \int_{\frac{1}{q^{-1}+1}}^{1} \int_{\left(\frac{1}{z}-1\right)^{\frac{1}{i_1}} q^{\frac{2}{3i_1}}}^{q^{-\frac{1}{3i_1}}} \left(\frac{1}{z}-1\right)^{\frac{1}{i}} \log\left(\frac{1}{z}-1\right) y_1^{-\frac{i_1}{i}} \, \mathrm{d}y_1 \, \mathrm{d}z}_{\mathfrak{D}.\mathrm{IV}} \\
& \underbrace{+ \frac{i_1}{i} q^{-1+\frac{1}{3}\left(\frac{1}{i_1}+\frac{2}{i}\right)} \int_{\frac{1}{q^{-1}+1}}^{1} \int_{\left(\frac{1}{z}-1\right)^{\frac{1}{i_1}} q^{\frac{2}{3i_1}}}^{q^{-\frac{1}{3i_1}}} \left(\frac{1}{z}-1\right)^{\frac{1}{i}} y_1^{-\frac{i_1}{i}} \log(y_1) \, \mathrm{d}y_1 \, \mathrm{d}z}_{\mathfrak{D}.\mathrm{V}} .
\end{aligned}
\tag{E.6}
$$

  First, we evaluate $\mathfrak{D}.\mathrm{III}$ by integrating with respect to y_1. Since $i > i_1$, we get that $\mathfrak{D}.\mathrm{III}$ is equal to

$$
\begin{aligned}
& \left(-\frac{i_1}{i}+1\right)^{-1} \log(q) \left(q^{-1+\frac{1}{i}} \int_{\frac{1}{q^{-1}+1}}^{1} \left(\frac{1}{z}-1\right)^{\frac{1}{i}} \mathrm{d}z - q^{-1+\frac{1}{i_1}} \int_{\frac{1}{q^{-1}+1}}^{1} \left(\frac{1}{z}-1\right)^{\frac{1}{i_1}} \mathrm{d}z \right) \\
=& \left(-\frac{i_1}{i}+1\right)^{-1} \left(\underbrace{q^{-1+\frac{1}{i}} \log(q) \int_0^{q^{-1}} \frac{z'^{\frac{1}{i}}}{(z'+1)^2} \, \mathrm{d}z'}_{\mathfrak{D}.\mathrm{III}.1} - \underbrace{q^{-1+\frac{1}{i_1}} \log(q) \int_0^{q^{-1}} \frac{z'^{\frac{1}{i_1}}}{(z'+1)^2} \, \mathrm{d}z'}_{\mathfrak{D}.\mathrm{III}.2} \right).
\end{aligned}
\tag{E.7}
$$

  Since $i, i_1 > 1$, the integrals in $\mathfrak{D}.\mathrm{III}.1$ and in $\mathfrak{D}.\mathrm{III}.2$ are uniformly bounded for $q > 0$. The rate of divergence of $\mathfrak{D}.\mathrm{III}$ is therefore $-\Theta_p\left(-q^{1-\frac{1}{i}} \log(q)\right)$.
  Through a similar approach, we note that $\mathfrak{D}.\mathrm{IV}$ corresponds to

$$
\left(-\frac{i_1}{i}+1\right)^{-1} \left(\underbrace{q^{-1+\frac{1}{i}} \int_0^{q^{-1}} \frac{z'^{\frac{1}{i}} \log(z)}{(z'+1)^2} \, \mathrm{d}z'}_{\mathfrak{D}.\mathrm{IV}.1} - \underbrace{q^{-1+\frac{1}{i_1}} \int_0^{q^{-1}} \frac{z'^{\frac{1}{i_1}} \log(z)}{(z'+1)^2} \, \mathrm{d}z'}_{\mathfrak{D}.\mathrm{IV}.2} \right).
$$

  The rate of divergence of $\mathfrak{D}.\mathrm{IV}$ is $\Theta_p\left(q^{1-\frac{1}{i}}\right)$ because the integrals in $\mathfrak{D}.\mathrm{IV}.1$ and $\mathfrak{D}.\mathrm{IV}.2$ are uniformly bounded for $q > 0$ since $i, i_1 > 1$.
  Lastly, through integration by parts we obtain that $\mathfrak{D}.\mathrm{V}$ is equal to

$$
\left(-\frac{i_1}{i}+1\right)^{-1} q^{-1+\frac{1}{i}} \log\left(q^{-\frac{1}{3i_1}}\right) \int_{\frac{1}{q^{-1}+1}}^{1} \left(\frac{1}{z}-1\right)^{\frac{1}{i}} \mathrm{d}z
$$

$$
\begin{aligned}
&- \Big(-\frac{i_1}{i}+1\Big)^{-2} q^{-1+\frac{1}{i}} \int_{\frac{1}{q^{-1}+1}}^{1} \left(\frac{1}{z}-1\right)^{\frac{1}{i}} \mathsf{d}z \\
&- \Big(-\frac{i_1}{i}+1\Big)^{-1} q^{-1+\frac{1}{i_1}} \int_{\frac{1}{q^{-1}+1}}^{1} \left(\frac{1}{z}-1\right)^{\frac{1}{i_1}} \log\left(\left(\frac{1}{z}-1\right)^{\frac{1}{i_1}} q^{\frac{2}{3i_1}}\right) \mathsf{d}z \\
&+ \Big(-\frac{i_1}{i}+1\Big)^{-2} q^{-1+\frac{1}{i_1}} \int_{\frac{1}{q^{-1}+1}}^{1} \left(\frac{1}{z}-1\right)^{\frac{1}{i_1}} \mathsf{d}z \\
=& - \Big(-\frac{i_1}{i}+1\Big)^{-2} \underbrace{q^{-1+\frac{1}{i}} \int_0^{q^{-1}} \frac{z'^{\frac{1}{i}}}{(z'+1)^2}\, \mathsf{d}z'}_{\mathfrak{D}.\mathrm{V}.1} \\
&+ \Big(-\frac{i_1}{i}+1\Big)^{-2} \underbrace{q^{-1+\frac{1}{i_1}} \int_0^{q^{-1}} \frac{z'^{\frac{1}{i_1}}}{(z'+1)^2}\, \mathsf{d}z'}_{\mathfrak{D}.\mathrm{V}.2} \\
&- \Big(-\frac{i_1}{i}+1\Big)^{-1} \frac{1}{3i_1} \underbrace{q^{-1+\frac{1}{i}} \log(q) \int_0^{q^{-1}} \frac{z'^{\frac{1}{i}}}{(z'+1)^2}\, \mathsf{d}z'}_{\mathfrak{D}.\mathrm{V}.3} \\
&- \Big(-\frac{i_1}{i}+1\Big)^{-1} \frac{2}{3i_1} \underbrace{q^{-1+\frac{1}{i_1}} \log(q) \int_0^{q^{-1}} \frac{z'^{\frac{1}{i_1}}}{(z'+1)^2}\, \mathsf{d}z'}_{\mathfrak{D}.\mathrm{V}.4} \\
&- \Big(-\frac{i_1}{i}+1\Big)^{-1} \frac{1}{i_1} \underbrace{q^{-1+\frac{1}{i_1}} \int_0^{q^{-1}} \frac{z'^{\frac{1}{i_1}} \log(z')}{(z'+1)^2}\, \mathsf{d}z'}_{\mathfrak{D}.\mathrm{V}.5}.
\end{aligned}
\tag{E.8}
$$

The rate of divergence of $\mathfrak{D}$.V is $\Theta_p\left(-q^{-1+\frac{1}{i}}\log(q)\right)$, since the integrals in (E.8) are uniformly bounded for $q>0$. Overall, the rate assumed by $\mathfrak{D}$ is

$$
\Theta_p\left(-q^{1-\frac{1}{i}}\log(q)\right) - \Theta_p\left(q^{1-\frac{1}{i}}\right) + \Theta_p\left(-q^{-1+\frac{1}{i}}\log(q)\right) = \Theta_p\left(-q^{-1+\frac{1}{i}}\log(q)\right).
$$

We find the rate of divergence for the upper bound in the case $i_3=i_2>i_1>1$ given by

$$
\Theta_p\left((-p)^{-1+\frac{1}{i_2}}\right) + \Theta_p\left(-(-p)^{-1+\frac{1}{i_3}}\log(-p)\right) = \Theta_p\left(-(-p)^{-1+\frac{1}{i_3}}\log(-p)\right).
$$

♦ Scaling law of $\mathfrak{D}$ in Case 4.
We suppose now that $i_3=i_2=i_1>1$. We trace the previous case until equation (E.6) and label $i=i_3=i_2=i_1$. Therefore, $\mathfrak{D}$.III is equal to

$$
\begin{aligned}
&q^{-1+\frac{1}{i}}\log(q) \int_{\frac{1}{q^{-1}+1}}^{1} \int_{\left(\frac{1}{z}-1\right)^{\frac{1}{i}} q^{\frac{2}{3i}}}^{q^{-\frac{1}{3i}}} \left(\frac{1}{z}-1\right)^{\frac{1}{i}} y_1^{-1}\, \mathsf{d}y_1\, \mathsf{d}z \\
=& -\frac{1}{i} q^{-1+\frac{1}{i}} \log^2(q) \int_{\frac{1}{q^{-1}+1}}^{1} \left(\frac{1}{z}-1\right)^{\frac{1}{i}} \mathsf{d}z \\
&-\frac{1}{i} q^{-1+\frac{1}{i}} \log(q) \int_{\frac{1}{q^{-1}+1}}^{1} \left(\frac{1}{z}-1\right)^{\frac{1}{i}} \log\left(\frac{1}{z}-1\right) \mathsf{d}z
\end{aligned}
\tag{E.9}
$$

$$= -\frac{1}{i}\underbrace{q^{-1+\frac{1}{i}}\log^2(q)\int_0^{q^{-1}}\frac{z'^{\frac{1}{i}}}{(z'+1)^2}\,\mathrm{d}z'}_{\mathfrak{D}.\mathrm{III}.3} - \frac{1}{i}\underbrace{q^{-1+\frac{1}{i}}\log(q)\int_0^{q^{-1}}\frac{z'^{\frac{1}{i}}\log(z')}{(z'+1)^2}\,\mathrm{d}z}_{\mathfrak{D}.\mathrm{III}.4}.$$

Since $i > 1$, the integrals in the right-hand side of (E.9) are uniformly bounded for any $q > 0$. Therefore, the rate of divergence of $\mathfrak{D}$.III is $-\Theta_p\left(q^{-1+\frac{1}{i}}\log^2(q)\right)$. Similarly, the summand $\mathfrak{D}$.IV assumes value

$$\begin{aligned}
&q^{-1+\frac{1}{i}}\int_{\frac{1}{q^{-1}+1}}^{1}\int_{\left(\frac{1}{z}-1\right)^{\frac{1}{i}}q^{\frac{2}{3i}}}^{q^{-\frac{1}{3i}}}\left(\frac{1}{z}-1\right)^{\frac{1}{i}}\log\left(\frac{1}{z}-1\right)y_1^{-1}\,\mathrm{d}y_1\,\mathrm{d}z\\
=&-\frac{1}{i}q^{-1+\frac{1}{i}}\log(q)\int_{\frac{1}{q^{-1}+1}}^{1}\left(\frac{1}{z}-1\right)^{\frac{1}{i}}\log\left(\frac{1}{z}-1\right)\mathrm{d}z \qquad \text{(E.10)}\\
&-\frac{1}{i}q^{-1+\frac{1}{i}}\int_{\frac{1}{q^{-1}+1}}^{1}\left(\frac{1}{z}-1\right)^{\frac{1}{i}}\log^2\left(\frac{1}{z}-1\right)\mathrm{d}z\\
=&-\frac{1}{i}\underbrace{q^{-1+\frac{1}{i}}\log(q)\int_0^{q^{-1}}\frac{z'^{\frac{1}{i}}\log(z')}{(z'+1)^2}\,\mathrm{d}z'}_{\mathfrak{D}.\mathrm{IV}.3} - \frac{1}{i}\underbrace{q^{-1+\frac{1}{i}}\int_0^{q^{-1}}\frac{z'^{\frac{1}{i}}\log^2(z')}{(z'+1)^2}\,\mathrm{d}z'}_{\mathfrak{D}.\mathrm{IV}.4}.
\end{aligned}$$

Again, since $i > 1$, the integrals in the right-hand side of (E.10) are uniformly bounded for any $q > 0$ and the rate of divergence of $\mathfrak{D}$.IV is in this case $\Theta_p\left(-q^{-1+\frac{1}{i}}\log(q)\right)$.
Lastly, the summand $\mathfrak{D}$.V is corresponds to

$$\begin{aligned}
&q^{-1+\frac{1}{i}}\int_{\frac{1}{q^{-1}+1}}^{1}\int_{\left(\frac{1}{z}-1\right)^{\frac{1}{i}}q^{\frac{2}{3i}}}^{q^{-\frac{1}{3i}}}\left(\frac{1}{z}-1\right)^{\frac{1}{i}}y_1^{-1}\log(y_1)\,\mathrm{d}y_1\mathrm{d}z\\
=&\frac{1}{2}q^{-1+\frac{1}{i}}\log^2(q^{-\frac{1}{3i}})\int_{\frac{1}{q^{-1}+1}}^{1}\left(\frac{1}{z}-1\right)^{\frac{1}{i}}\mathrm{d}z - \frac{1}{2}q^{-1+\frac{1}{i}}\int_{\frac{1}{q^{-1}+1}}^{1}\left(\frac{1}{z}-1\right)^{\frac{1}{i}}\log^2\left(\left(\frac{1}{z}-1\right)^{\frac{1}{i}}q^{\frac{2}{3i}}\right)\mathrm{d}z\\
=&-\frac{1}{6i^2}q^{-1+\frac{1}{i}}\log^2(q)\int_{\frac{1}{q^{-1}+1}}^{1}\left(\frac{1}{z}-1\right)^{\frac{1}{i}}\mathrm{d}z\\
&-\frac{2}{3i^2}q^{-1+\frac{1}{i}}\log(q)\int_{\frac{1}{q^{-1}+1}}^{1}\left(\frac{1}{z}-1\right)^{\frac{1}{i}}\log\left(\frac{1}{z}-1\right)\mathrm{d}z \qquad \text{(E.11)}\\
&-\frac{1}{2i^2}q^{-1+\frac{1}{i}}\int_{\frac{1}{q^{-1}+1}}^{1}\left(\frac{1}{z}-1\right)^{\frac{1}{i}}\log^2\left(\frac{1}{z}-1\right)\mathrm{d}z\\
=&-\frac{1}{6i^2}\underbrace{q^{-1+\frac{1}{i}}\log^2(q)\int_0^{q^{-1}}\frac{z'^{\frac{1}{i}}}{(z'+1)^2}\mathrm{d}z'}_{\mathfrak{D}.\mathrm{V}.6} - \frac{2}{3i^2}\underbrace{q^{-1+\frac{1}{i}}\log(q)\int_0^{q^{-1}}\frac{z'^{\frac{1}{i}}\log(z')}{(z'+1)^2}\mathrm{d}z'}_{\mathfrak{D}.\mathrm{V}.7}\\
&-\frac{1}{2i^2}\underbrace{q^{-1+\frac{1}{i}}\int_0^{q^{-1}}\frac{z'^{\frac{1}{i}}\log^2(z')}{(z'+1)^2}\mathrm{d}z'}_{\mathfrak{D}.\mathrm{V}.8}.
\end{aligned}$$

Since $i > 1$, the integrals in the right-hand side of (E.11) are uniformly bounded for any $q > 0$ and the rate of divergence of $\mathfrak{D}$.V is in this case $-\Theta_p\left(q^{-1+\frac{1}{i}}\log^2(q)\right)$.

Observing (E.6), (E.9) and (E.11), we note that the leading terms of $\mathfrak{D}$ are $\frac{2}{3i^2}\mathfrak{D}.\text{III}.3$ and $-\frac{1}{6i^2}\mathfrak{D}.\text{V}.6$. Therefore, $\mathfrak{D}$ is characterised by the same rate of divergence as

$$\frac{2}{3i^2}\mathfrak{D}.\text{III}.3 - \frac{1}{6i^2}\mathfrak{D}.\text{V}.6 = \frac{1}{2i^2}q^{-1+\frac{1}{i}}\log^2(q)\int_0^{q^{-1}}\frac{z'^{\frac{1}{i}}}{(z'+1)^2}\,\mathrm{d}z' = \Theta_p\left(q^{-1+\frac{1}{i}}\log^2(q)\right).$$

Combining both summands $\mathfrak{C}$ and $\mathfrak{D}$, we obtain the rate of the upper bound as

$$\Theta_p\left(-(-p)^{-1+\frac{1}{i_2}}\log(-p)\right) + \Theta_p\left((-p)^{-1+\frac{1}{i}}\log^2(-p)\right) = \Theta_p\left((-p)^{-1+\frac{1}{i}}\log^2(-p)\right)$$

for $i_3 = i_2 = i_1 > 1$.

- Scaling law of $\mathfrak{D}$ in Case 5.
  In the next case, we consider $i_3 > i_2 > i_1 = 1$. We can follow the same steps as in the computation of the scaling law of $\mathfrak{D}$ in Case 1, but we note that the integrals in $\mathfrak{D}.\text{I}.2$ and $\mathfrak{D}.\text{II}.2$ diverge as $\Theta_p\left(\log\left(q^{-1}\right)\right)$ due to (D.7). The rate of divergence of $\mathfrak{D}$ is therefore

$$\Theta_p\left(q^{-1+\frac{1}{i_3}}\right) - \Theta_p\left(-\log(q)\right) - \Theta_p\left(q^{-1+\frac{1}{i_2}}\right) + \Theta_p\left(-\log(q)\right) = \Theta_p\left(q^{-1+\frac{1}{i_3}}\right)$$

  and the rate of the upper bound in the case $i_3 > i_2 > i_1 = 1$ is

$$\Theta_p\left((-p)^{-1+\frac{1}{i_2}}\right) + \Theta_p\left((-p)^{-1+\frac{1}{i_3}}\right) = \Theta_p\left((-p)^{-1+\frac{1}{i_3}}\right).$$

- Scaling law of $\mathfrak{D}$ in Case 6.
  We assume that $i_3 > i_2 = i_1 = 1$ and proceed as in the previous case as we prove that the rate of divergence of $\mathfrak{D}.\text{I}$ is

$$\Theta_p\left(q^{-1+\frac{1}{i_3}}\right) - \Theta_p\left(-\log(q)\right) = \Theta_p\left(q^{-1+\frac{1}{i_3}}\right).$$

  We can then follow the same approach as in the computation of the scaling law of $\mathfrak{D}$ in Case 2 and study the summands in (E.5). Inserting $i_2 = i_1 = i = 1$, we know, from (D.7), that the rate of divergence assumed by $\mathfrak{D}.\text{II}.3$ is $-\Theta_p\left(\log^2(q)\right)$. We also know, from (F.1) in Appendix F, that the rate of $\mathfrak{D}.\text{II}.4$ is $\Theta_p\left(\log^2(q)\right)$. Hence, we can state that $\mathfrak{D} = \Theta_p\left(q^{-1+\frac{1}{i_3}}\right)$, and in the case $i_3 > i_2 = i_1 = 1$ that the rate of divergence of the upper bound is

$$\Theta_p\left(\log^2(-p)\right) + \Theta_p\left((-p)^{-1+\frac{1}{i_3}}\right) = \Theta_p\left((-p)^{-1+\frac{1}{i_3}}\right).$$

- Scaling law of $\mathfrak{D}$ in Case 7.
  We now consider $i_3 = i_2 > i_1 = 1$. We follow the same approach employed in the computation of the scaling law of $\mathfrak{D}$ in Case 3 and set $i_3 = i_2 = i$. We obtain that, due to (D.7) and (F.1),

$$\begin{aligned}
&\mathfrak{D}.\text{III}.1 = -\Theta_p\left(-q^{1-\frac{1}{i}}\log(q)\right), && \mathfrak{D}.\text{III}.2 = -\Theta_p\left(\log^2(q)\right), && \mathfrak{D}.\text{IV}.1 = \Theta_p\left(q^{1-\frac{1}{i}}\right),\\
&\mathfrak{D}.\text{IV}.2 = \Theta_p\left(\log^2(q)\right), && \mathfrak{D}.\text{V}.1 = \Theta_p\left(q^{1-\frac{1}{i}}\right), && \mathfrak{D}.\text{V}.2 = \Theta_p\left(-\log(q)\right),\\
&\mathfrak{D}.\text{V}.3 = -\Theta_p\left(-q^{1-\frac{1}{i}}\log(q)\right), && \mathfrak{D}.\text{V}.4 = -\Theta_p\left(\log^2(q)\right), && \mathfrak{D}.\text{V}.5 = \Theta_p\left(\log^2(q)\right)
\end{aligned}$$

  hold. The rate of divergence of $\mathfrak{D}$ is then

$$\begin{aligned}
&\Theta_p\left(-q^{1-\frac{1}{i}}\log(q)\right) - \Theta_p\left(\log^2(q)\right) - \Theta_p\left(q^{1-\frac{1}{i}}\right) + \Theta_p\left(\log^2(q)\right) - \Theta_p\left(q^{1-\frac{1}{i}}\right)\\
&+ \Theta_p\left(-\log(q)\right) + \Theta_p\left(-q^{1-\frac{1}{i}}\log(q)\right) + \Theta_p\left(\log^2(q)\right) - \Theta_p\left(\log^2(q)\right) = \Theta_p\left(-q^{1-\frac{1}{i}}\log(q)\right).
\end{aligned}$$

Combining the results on the scaling law of $\mathfrak{C}$ and of $\mathfrak{D}$, we observe that the rate of divergence of the upper bound is

$$\Theta_p\left((-p)^{-1+\frac{1}{i_2}}\right)+\Theta_p\left(-(-p)^{-1+\frac{1}{i_3}}\log(-p)\right)=\Theta_p\left(-(-p)^{-1+\frac{1}{i_3}}\log(-p)\right),$$

for $i_3=i_2>i_1=1$.

- Scaling law of $\mathfrak{D}$ in Case 8.
  The last case for which we evaluate $\mathfrak{D}$ assumes $i_3=i_2=i_1=1$. Following the same steps of the computation of the scaling law of $\mathfrak{D}$ in Case 4, we obtain (E.9), (E.10) and (E.11). We know, from (D.7) and (F.3) in Appendix F, that $\mathfrak{D}.\mathrm{III}.3$, $\mathfrak{D}.\mathrm{IV}.4$, $\mathfrak{D}.\mathrm{V}.6$, and $\mathfrak{D}.\mathrm{V}.8$ diverge with rate $\Theta_p\left(-\log^3(q)\right)$ and that $\mathfrak{D}.\mathrm{III}.4$, $\mathfrak{D}.\mathrm{IV}.3$, $\mathfrak{D}.\mathrm{V}.7$ as $-\Theta_p\left(-\log^3(q)\right)$.
  From (D.7), (F.2) and (F.3), we get the rate of divergence of the summand $\mathfrak{D}$ as

$$\begin{aligned}&\frac{2}{3}\mathfrak{D}.\mathrm{III}.3+\frac{2}{3}\mathfrak{D}.\mathrm{III}.4+\mathfrak{D}.\mathrm{IV}.3+\mathfrak{D}.\mathrm{IV}.4-\frac{1}{6}\mathfrak{D}.\mathrm{V}.6-\frac{2}{3}\mathfrak{D}.\mathrm{V}.7-\frac{1}{2}\mathfrak{D}.\mathrm{V}.8\\&=\left(\frac{2}{3}-\frac{2}{3}\frac{1}{2}-\frac{1}{2}+\frac{1}{3}-\frac{1}{6}+\frac{2}{3}\frac{1}{2}-\frac{1}{2}\frac{1}{3}\right)\Theta_p\left(-\log^3(q)\right)=\Theta_p\left(-\log^3(q)\right)\end{aligned}$$

  Conclusively, in the case $i_3=i_2=i_1=1$ we find that $\langle g,V_\infty^{\mathsf{w}}g\rangle$ has an upper bound with rate of divergence

$$\Theta_p\left(\log^2(-p)\right)+\Theta_p\left(-\log^3(-p)\right)=\Theta_p\left(-\log^3(-p)\right).$$

□

F Appendix: Scaling law of a tool integral

This appendix describes a scaling law included in the proofs of Theorem 4.2.5 and Theorem 4.2.7 in Chapter 4. For $q>0$ and $m\in\mathbb{N}\cup\{0\}$,

$$\int_0^{q^{-1}}\frac{z'\log^m(z')}{(z'+1)^2}\,\mathrm{d}z'=\Theta\left((-\log(q))^{m+1}\right)\tag{F.1}$$

holds true by considering

$$\lim_{q\to0^+}\int_0^{q^{-1}}\frac{z'\log^m(z')}{(z'+1)^2}\,\mathrm{d}z'=\int_0^{n}\frac{z'\log^m(z')}{(z'+1)^2}\,\mathrm{d}z'+\lim_{q\to0^+}\int_n^{q^{-1}}\frac{z'\log^m(z')}{(z'+1)^2}\,\mathrm{d}z',$$

with $n>0$. Whereas the first integral is finite for any finite $n>0$, we find that, in the limit $z'\to+\infty$, $\frac{z'\log^m(z')}{(z'+1)^2}$ behaves equivalently to $\frac{\log^m(z')}{z'}$ since

$$\lim_{z'\to\infty}\frac{(z'+1)^{-2}z'\log^m(z')}{z'^{-1}\log^m(z')}=1.\tag{F.2}$$

We then study the integral

$$\int_n^{q^{-1}}\frac{\log^m(z')}{z'}\,\mathrm{d}z'=\left[\frac{1}{m+1}\log^{m+1}(z')\right]_n^{q^{-1}}=\frac{1}{m+1}\log^{m+1}(q^{-1})-\frac{1}{m+1}\log^{m+1}(n),$$

which concludes the proof. Lastly, we note that

$$\lim_{q\to 0^+} \frac{1}{\frac{1}{m+1}\log^{m+1}(q^{-1})} \int_0^{q^{-1}} \frac{z' \log^m(z')}{(z'+1)^2}\, \mathrm{d}z' = 1. \tag{F.3}$$

G Appendix: Turbulence from the Itô noise perspective

Throughout Chapter 9, system (9.1.1) is studied under different noise and parameter assumptions. In this appendix, we address various cases and translate them to the Itô noise perspective through the Itô-Stratonovich correction term [88, 192]. The boundary conditions are assumed Neumann homogeneous, and the initial condition is set at $q(x,0) = q_0(x)$ for $x \in [0, L]$.

- In Section 9.2, the noise is assumed to be white and in Itô sense, i.e., $\sigma_\mathsf{S} = \sigma_\mathsf{R} = 0$. The system studied is characterised, therefore, by the form

  $$\mathrm{d}q(x,t) = \left(\partial_{xx}^2 q(x,t) - q(x,t) + (r+1)q(x,t)^2(2-q(x,t))\right)\mathrm{d}t + \sigma_\mathsf{I} q(x,t) Q^{\frac{1}{2}} \mathrm{d}W_t,$$

  for $x \in [0, L]$ and $t > 0$.

- In Subsection 9.3.1, the noise is assumed white and in Stratonovich sense, i.e., $\sigma_\mathsf{I} = \sigma_\mathsf{R} = 0$. The first equation in (9.1.1) with Itô noise is then

  $$\begin{aligned}\mathrm{d}q(x,t) = &\left(\partial_{xx}^2 q(x,t) - q(x,t) + (r+1)q(x,t)^2(2-q(x,t)) + \frac{\sigma_\mathsf{S}^2}{2} q(x,t) \sum_{i=0}^{m} \left(\zeta_i b_i(x)^2\right)\right)\mathrm{d}t \\ &+ \sigma_\mathsf{S} q(x,t) Q^{\frac{1}{2}} \mathrm{d}W_t.\end{aligned}$$

- In Subsection 9.3.2, we discuss the effect of red in time Stratonovich noise on the turbulence system, i.e., $\sigma_\mathsf{R} > \sigma_\mathsf{I} = \sigma_\mathsf{S} = 0$. The variable q is coupled to the Ornstein-Uhlenbeck process, the solution of (9.3.6), depending on the choice of the operator F. In (9.3.8), we set $F = \mathrm{Id}$. Then, the first equation in (9.1.1) coupled with (9.3.6) can be interpreted as

  $$\begin{aligned}\mathrm{d}\begin{pmatrix} q(x,t) \\ \xi(x,t)\end{pmatrix} = &\begin{pmatrix} \partial_{xx}^2 q(x,t) - q(x,t) + (r+1)q(x,t)^2(2-q(x,t)) + \sigma_\mathsf{R} q(x,t)\xi(x,t) \\ -\kappa\xi \end{pmatrix}\mathrm{d}t \\ &+ \begin{pmatrix} 0 & 0 \\ 0 & \sigma_\xi Q^{\frac{1}{2}} \end{pmatrix}\begin{pmatrix} \mathrm{d}W_t \\ \mathrm{d}W_t' \end{pmatrix}.\end{aligned}$$

  The noise is additive in $\mathcal{H}_1 \times \mathcal{H}_1$, which implies that the Itô-Stratonovich correction term is null and the equation is equivalent regardless of the interpretation of the noise.

- In Remark 9.3.9, we discuss the lower bound to the probability of initiation of turbulence under Stratonovich red noise defined by $F = \partial_t$. The equation defining the behaviour of the variables q and ξ in time is, therefore,

  $$\begin{aligned}\mathrm{d}\begin{pmatrix} q(x,t) \\ \xi(x,t)\end{pmatrix} = &\begin{pmatrix} \partial_{xx}^2 q(x,t) - q(x,t) + (r+1)q(x,t)^2(2-q(x,t)) \\ -\kappa\xi \end{pmatrix}\mathrm{d}t \\ &+ \begin{pmatrix} \sigma_\mathsf{R} q(x,t) \\ 0 \end{pmatrix} \circ \mathrm{d}\xi(x,t) + \begin{pmatrix} 0 & 0 \\ 0 & \sigma_\xi Q^{\frac{1}{2}} \end{pmatrix}\begin{pmatrix} \mathrm{d}W_t \\ \mathrm{d}W_t' \end{pmatrix}\end{aligned}$$

$$= \begin{pmatrix} \partial_{xx}^2 q(x,t) - q(x,t) + (r+1)q(x,t)^2(2-q(x,t)) - \sigma_{\mathsf{R}}\kappa q(x,t)\xi(x,t) \\ -\kappa\xi \end{pmatrix} \mathsf{d}t$$
$$+ \begin{pmatrix} q(x,t) & 0 \\ 0 & 1 \end{pmatrix} \circ \begin{pmatrix} 0 & \sigma_{\mathsf{R}}\sigma_\xi Q^{\frac{1}{2}} \\ 0 & \sigma_\xi Q^{\frac{1}{2}} \end{pmatrix} \begin{pmatrix} \mathsf{d}W_t \\ \mathsf{d}W_t' \end{pmatrix},$$

with noise in the Stratonovich sense. Indicating with $*$ the adjoint operator in $\mathcal{H}_1 \times \mathcal{H}_1$, the operator

$$\begin{pmatrix} 0 & \sigma_{\mathsf{R}}\sigma_\xi Q^{\frac{1}{2}} \\ 0 & \sigma_\xi Q^{\frac{1}{2}} \end{pmatrix} \begin{pmatrix} 0 & \sigma_{\mathsf{R}}\sigma_\xi Q^{\frac{1}{2}} \\ 0 & \sigma_\xi Q^{\frac{1}{2}} \end{pmatrix}^* = \sigma_\xi^2 \begin{pmatrix} 0 & \sigma_{\mathsf{R}} Q^{\frac{1}{2}} \\ 0 & Q^{\frac{1}{2}} \end{pmatrix} \begin{pmatrix} 0 & 0 \\ \sigma_{\mathsf{R}} Q^{\frac{1}{2}} & Q^{\frac{1}{2}} \end{pmatrix} = \sigma_\xi^2 \begin{pmatrix} \sigma_{\mathsf{R}}^2 Q & \sigma_{\mathsf{R}} Q \\ \sigma_{\mathsf{R}} Q & Q \end{pmatrix}$$

is characterised by a purely discrete spectrum, composed by $\{\Lambda_i, \Lambda_i'\}_{i\in\mathbb{N}}$. These eigenvalues are defined as

$$\Lambda_i := \left(1+\sigma_{\mathsf{R}}^2\right)\sigma_\xi^2\zeta_i \qquad \text{and} \qquad \Lambda_i' := 0,$$

for all $i \in \mathbb{N}$. The corresponding eigenbasis in $\mathcal{H}_1 \times \mathcal{H}_1$ is composed by

$$B_i(x) := \left(1+\sigma_{\mathsf{R}}^2\right)^{-\frac{1}{2}} \begin{pmatrix} \sigma_{\mathsf{R}} b_i(x) \\ b_i(x) \end{pmatrix} \qquad \text{and} \qquad B_i'(x) := \left(1+\sigma_{\mathsf{R}}^2\right)^{-\frac{1}{2}} \begin{pmatrix} b_i(x) \\ -\sigma_{\mathsf{R}} b_i(x) \end{pmatrix},$$

for all $i \in \mathbb{N}$ and $x \in [0, L]$. The equation defining q and ξ is, then,

$$\mathsf{d}\begin{pmatrix} q(x,t) \\ \xi(x,t) \end{pmatrix} = \begin{pmatrix} \partial_{xx}^2 q(x,t) - q(x,t) + (r+1)q(x,t)^2(2-q(x,t)) - \sigma_{\mathsf{R}}\kappa q(x,t)\xi(x,t) \\ -\kappa\xi \end{pmatrix} \mathsf{d}t$$
$$+ \frac{1}{2\left(1+\sigma_{\mathsf{R}}^2\right)} \begin{pmatrix} q(x,t)\partial_q\left(q(x,t)\right) \sum_{i=0}^m \left(\Lambda_i \sigma_{\mathsf{R}}^2 b_i(x)^2 + \Lambda_i' b_i(x)^2\right) \\ \partial_\xi\left(1\right) \sum_{i=0}^m \left(\Lambda_i b_i(x)^2 + \Lambda_i' \sigma_{\mathsf{R}}^2 b_i(x)^2\right) \end{pmatrix} \mathsf{d}t$$
$$+ \begin{pmatrix} q(x,t) & 0 \\ 0 & 1 \end{pmatrix} \begin{pmatrix} 0 & \sigma_{\mathsf{R}}\sigma_\xi Q^{\frac{1}{2}} \\ 0 & \sigma_\xi Q^{\frac{1}{2}} \end{pmatrix} \begin{pmatrix} \mathsf{d}W_t \\ \mathsf{d}W_t' \end{pmatrix}$$
$$= \begin{pmatrix} \partial_{xx}^2 q(x,t) - q(x,t) + (r+1)q(x,t)^2(2-q(x,t)) - \sigma_{\mathsf{R}}\kappa q(x,t)\xi(x,t) \\ -\kappa\xi \end{pmatrix} \mathsf{d}t$$
$$+ \begin{pmatrix} \frac{\sigma_{\mathsf{R}}^2\sigma_\xi^2}{2} q(x,t) \sum_{i=0}^m \left(\zeta_i b_i(x)^2\right) \\ 0 \end{pmatrix} \mathsf{d}t + \begin{pmatrix} q(x,t) & 0 \\ 0 & 1 \end{pmatrix} \begin{pmatrix} 0 & \sigma_{\mathsf{R}}\sigma_\xi Q^{\frac{1}{2}} \\ 0 & \sigma_\xi Q^{\frac{1}{2}} \end{pmatrix} \begin{pmatrix} \mathsf{d}W_t \\ \mathsf{d}W_t' \end{pmatrix},$$

with noise interpreted in Itô sense.